

Rare-Earth-Metal Alkylidene Chemistry

DISSERTATION

der Mathematisch-Naturwissenschaftlichen Fakultät
der Eberhard Karls Universität Tübingen
zur Erlangung des Grades eines
Doktors der Naturwissenschaften
(Dr. rer. nat.)

vorgelegt von
M. Sc. Verena M. Birkelbach
aus Forchheim

Tübingen
2019

Gedruckt mit Genehmigung der Mathematisch-Naturwissenschaftlichen Fakultät der Eberhard Karls Universität Tübingen.

Tag der mündlichen Qualifikation:

20.12.2019

Dekan:

Prof. Dr. Wolfgang Rosenstiel

1. Berichterstatter:

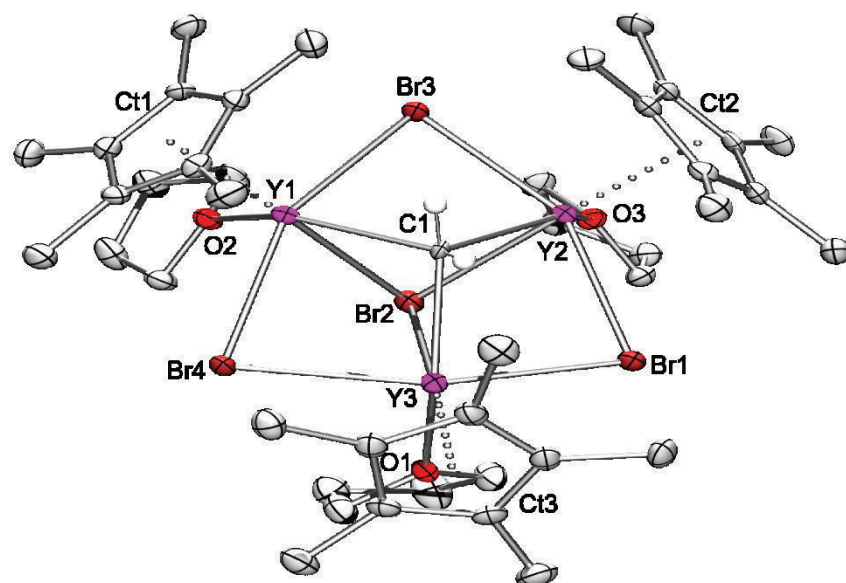
Prof. Dr. Reiner Anwander

2. Berichterstatter:

Prof. Dr. Doris Kunz

Rare-Earth-Metal Alkylidene Chemistry

Verena M. Birkelbach



In Memoriam

Ottmar Birkelbach

07.03.1954 - 11.02.2019

Preface

The following PhD thesis consists of a survey on the chemistry of rare-earth-metal methyl and methyldene complexes, a summary of the main results, and original scientific papers. The work has been carried out at the Institut für Anorganische Chemie of the Eberhard Karls Universität Tübingen, Germany, over the period from November 2015 to November 2019 under the supervision of Prof. Dr. Reiner Anwander. Funding has been gratefully received from the Deutsche Forschungsgemeinschaft (DFG).

Parts of this thesis have been presented at international and national conferences as poster contributions.

Acknowledgements

First of all, I would like to express my gratitude to my supervisor Prof. Dr. **Reiner** Anwander. Thank you for accepting me, a foreigner, in your high standard synthesis laboratory without any reservations, your helpful guidance, and the very interesting research topic for this thesis. Thank you for the opportunities to attend international and national conferences for the successful exchange with other researchers.

Special thanks go to Dr. Cäcilia (**Cili**) Maichle-Mössmer for all crystal structure determinations and her helpful discussions. Further thanks to Dr. **Dorothea** Schädle for her advice and proof reading my papers and this thesis.

My thanks also go to Dr. **Klaus** Eichele and Kristina (**Krissi**) Strohmaier for maintaining the high standard equipment, as well as their help in all aspects regarding NMR spectroscopy. Further thanks go to Wolfgang Bock (**Herr Bock**) for performing elemental analyses, even with highly fluorinated samples.

Thanks to the staff of the metal, electronics and glass workshops for manufacturing and repairing lab equipment. I further thank **Tobias** Wolf and especially **Elke** Niquet for their help, support and their friendly and always helpful nature.

Many thanks to **Sabine** Ehrlich for all her administrative work and to **Nadja** Wattering for all the desperately needed IT help.

I also would like to thank my current and former coworkers of the Anwander group. Special thanks go to **Uwe** Bayer, **Lorenz** Bock, **Alexandros** Mortis, and Dr. **Daniel** Werner for all the funny moments with you, the nice atmosphere you create, and for all the discussions, whether chemistry related or not. Thank you, Dr. **Renita** Thim, for your support, your friendship and your words of encouragement when needed. It was a pleasure to work and share a glovebox with you! Further thanks go to **Damir** Barisic, **Martin** Bonath, **Denis** Burghardt, **Dennis** A. Buschmann, **Dominic** Diether, Dr. **Christoph** O. Hollfelder, **Markus** Katzenmayer, **Felix** Kracht, **Lars** Kuckuk, **Jakob** Lebon, Dr. **Yucang** Liang, Dr. **Leilei** Luo, **Eric** Moinet, **Theresa** Rieser, Dr. **David** Schneider, **Andrea** Sonström, **Georgios** Spiridopoulos, Dr. **Christoph** Stuhl, **Simon** Trzmiel, Dr. **Benjamin** Wolf, and **Xin** Ning for the very supportive and friendly atmosphere in the lab.

My special thanks go to **Uwe** Bayer, thank you for being both: the best colleague someone could wish for and my love. You make it so easy to spend work and private life with you because of your wonderful character. Thank you for your love and support every day!

Last but not least, gebührt meiner Familie ein ganz besonders großes Dankeschön. Vor allem will ich mich bei meinen **Eltern** (Irmgard und Ottmar) bedanken für ihre finanzielle Unterstützung, die mir mein Studium erst ermöglicht hat, aber noch viel wichtiger möchte ich mich für ihre uneingeschränkte Unterstützung und ihre aufbauenden Worte bedanken. Bei meiner Schwester **Johanna** und meinem Bruder **Benedikt** möchte ich mich für ihre lustige Art bedanken, mit der sie mich immer wieder zum Lachen bringen.

Contents

Preface	I
Acknowledgements	II
Contents	III
Abbreviations	IV
Summary	V
Zusammenfassung	VII
Publications	IX
Personal Contribution	X
Objective of this Thesis	XI
A. Methyl and Alkylidene Complexes of the Rare-Earth Metals	1
1 Metal Carbene vs. Alkylidene Complexes	2
2 Reactive Ln(III) Methyl Complexes	4
3 Historical Overview of Rare-Earth-Metal Alkylidenes	7
4 Ln–C(Alkylidene) Bond Lengths	14
5 Reactivity of Rare-Earth-Metal Alkylidenes	17
5.1 Pincer-Type Rare-Earth-Metal Alkylidenes	17
5.2 Multimetallic and TEBBE-like Rare-Earth-Metal Alkylidenes	18
5.3 Monometallic Donor-Stabilized Rare-Earth-Metal Alkylidenes	22
B. Summary of the Main Results	25
1 Rare-Earth-Metal Complexes as Precursors for Alkylidenes	26
2 Mixed Methyl/Aryloxy Rare-Earth-Metal Complexes	30
3 Cp-Supported Rare-Earth-Metal Methylidene Complexes	33
C. Unpublished Results	37
Synthesis of (CNC)-Pincer Rare-Earth-Metal Complexes	38
D. Bibliography	57
E. Publications	
F. Appendix	

Abbreviations

18c6	1,4,7,10,13,16-hexaoxacyclooctadecane	Me	Methyl
Ar	Aryl	Mes	Mesityl
Bn	Benzyl	<i>N</i> -nacnac	<i>N</i> -donor-functionalized nacnac MeC(NDipp)CHC(Me)(NC H ₂ CH ₂ NR ₂)
<i>n</i> -BuLi	<i>n</i> -Butyllithium	Nacnac	1,3-diketiminato
<i>t</i> Bu	<i>tert</i> -Butyl	NMR	Nuclear Magnetic Resonance
Cp	Cyclopentadienyl	NTf ₂	trifluoromethanesulfonimide
Cp*	C ₅ Me ₅	OTf	triflate
Cp'	C ₅ Me ₄ SiMe ₃	Ph	Phenyl
DEPT	Distortionless Enhancement by Polarization Transfer	<i>i</i> Pr	<i>iso</i> -Propyl
Dipp	<i>Diisopropylphenyl</i>	pz	pyrazolyl
dmap	4-dimethylaminopyridine	RT	ambient (Room) temperature
dmpz	dimethylpyrazolyl	thf	tetrahydrofuran
Do	Donor	TMS	trimethylsilyl
DRIFT	Diffuse Reflectance Infrared Fourier Transform	Tp ^{<i>t</i>Bu,Me}	tris(3- <i>tert</i> -butyl-5-methyl-pyrazolyl)borato
EA	Elemental Analysis	HSQC	Heteronuclear Single Quantum Coherence
equiv.	equivalent	HMBC	Heteronuclear Multiple Bond Correlation
<i>et al.</i>	<i>et alii</i> or <i>et aliae</i>		
LA	LEWIS Acid		
Ln	rare-earth metal (Sc, Y, La - Lu)		
M	Metal		

Summary

In contrast to well-established transition metal alkylidene complexes, stabilization of rare-earth-metal alkylidene complexes is still challenging. Methylidene complexes attracted great research interest due to their reactivity in organic transformations. Despite this fact, the chemistry of the rare-earth-metal variants is still unexplored.

In a first approach for the generation of terminal rare-earth-metal methylidene complexes stabilized by a super bulky tris(pyrazolyl)borato ligand, reactive mixed methyl/triflate and methyl/alkyl complexes $\text{Tp}^{t\text{Bu},\text{Me}}\text{LnMe}(\text{R})$ ($\text{Ln} = \text{Y}, \text{Lu}$; $\text{R} = \text{OTf}, \text{NTf}_2, \text{alkyl}$) were investigated. Reaction of $\text{Tp}^{t\text{Bu},\text{Me}}\text{LuMe}_2$ or $\text{Tp}^{t\text{Bu},\text{Me}}\text{YMe}(\text{AlMe}_4)$ with Me_3SiOTf or $\text{Me}_3\text{SiNTf}_2$ led to the successful isolation of $\text{Tp}^{t\text{Bu},\text{Me}}\text{LnMe}(\text{OTf})$ or $\text{Tp}^{t\text{Bu},\text{Me}}\text{LnMe}(\text{NTf}_2)$, respectively. Attempted reactions with the WITTIG reagent $\text{H}_2\text{C}=\text{PPh}_3$ showed no reactivity towards leaving group abstraction. Further effort led to the formation of $\text{Tp}^{t\text{Bu},\text{Me}}\text{LnX}_2$ ($\text{X} = \text{Cl}, \text{I}$) and especially mixed $\text{Tp}^{t\text{Bu},\text{Me}}\text{LuMeCl}$ for its application in salt metathesis protocols with KBn and $\text{LiCH}_2\text{SiMe}_3$ and the successful formation of $\text{Tp}^{t\text{Bu},\text{Me}}\text{LuMe}(\text{R})$ ($\text{R} = \text{CH}_2\text{C}_6\text{H}_5, \text{CH}_2\text{SiMe}_3$). However, even at elevated temperatures no abstraction of either methane, toluene or SiMe_4 , but rather C–H-bond activation at the ligand backbone was observed.

Further interest in reactive terminal methyl complexes led to investigations on the stability of mixed methyl aryloxy compounds $\text{Tp}^{t\text{Bu},\text{Me}}\text{LnMe}(\text{OAr})$ ($\text{Ln} = \text{Y}, \text{Lu}$; $\text{OAr} = \text{OC}_6\text{H}_3\text{Me}_{2-2,6}, \text{OC}_6\text{H}_3\text{Pr}_{2-2,6}, \text{OC}_6\text{H}_2\text{tBu}_{2-2,6-\text{Me}-4}, \text{OC}_6\text{H}_3(\text{CF}_3)_{2-3,5}$). The desired rare-earth-metal methyl complexes were obtained by applying salt metathesis as well as protonolysis approaches with $\text{Tp}^{t\text{Bu},\text{Me}}\text{LuMe}_2$ and $\text{Tp}^{t\text{Bu},\text{Me}}\text{LnMe}(\text{AlMe}_4)$ and the respective KOAr or HOAr .

Exchange of the ligand system led to the generation of silylamide stabilized reactive rare-earth-metal complexes $(\text{Me}_x\text{Ph}_y\text{Si})_2\text{NLn}(\text{AlMe}_4)_2$ ($\text{Ln} = \text{Y}, \text{Lu}$, $x = 0-2$, $y = 3-x$) which showed intramolecular C–H-bond activation to afford rare-earth-metal complexes supported by (CNC)-pincer ligands.

Successful isolation of various mixed trimetallic halogenido/methylidene rare-earth-metal complexes $(\text{Cp}^{\text{R}})_3\text{Ln}_3(\mu\text{-X})_3(\mu_3\text{-X})(\mu_3\text{-CH}_2)(\text{thf})_3$ ($\text{Ln} = \text{Y}, \text{La}$; $\text{X} = \text{Cl}, \text{Br}, \text{I}$; $\text{Cp}^{\text{R}} = \text{C}_5\text{Me}_5, \text{C}_5\text{Me}_4\text{SiMe}_3$) was achieved *via* donor-induced tetramethylaluminate cleavage and further C–H-bond activation of $[(\text{Cp}^{\text{R}})\text{Ln}(\text{AlMe}_4)_y(\text{X})_z]_x$. Reactivity tests with carbonylic substrates revealed a behavior analogous to the TEBBE reagent and therefore those complexes can be

considered as SCHROCK-type nucleophilic carbenes. Furthermore, the methyldiene rare-earth-metal complexes were active in the polymerization of δ -valerolactone.

Zusammenfassung

Im Gegensatz zu Übergangsmetall-Alkyliden-Komplexen ist die Stabilisierung von Seltenerdmetall-Alkylidenen immer noch eine Herausforderung. Methyliden-Komplexe fallen vor allem durch ihre Reaktivität in der Umwandlung organischer Gruppen auf. Ungeachtet dessen ist die Chemie der Seltenerdmetall-Analoga immer noch nahezu unerforscht.

In einem ersten Ansatz zur Synthese von terminalen Seltenerdmetall-Methyliden-Komplexen, stabilisiert durch einen sterisch anspruchsvollen Tris(pyrazolylborato) Liganden, wurden gemischte Methyl/Triflat und Methyl/Alkyl Komplexe $\text{Tp}^{\text{tBu,Me}}\text{LnMe}(\text{R})$ ($\text{Ln} = \text{Y, Lu}$; $\text{R} = \text{OTf, NTf}_2, \text{Alkyl}$) untersucht. Die Reaktion von $\text{Tp}^{\text{tBu,Me}}\text{LuMe}_2$ und $\text{Tp}^{\text{tBu,Me}}\text{YMe}(\text{AlMe}_4)$ mit Me_3SiOTf oder $\text{Me}_3\text{SiNTf}_2$ führte zu der Isolierung von einerseits $\text{Tp}^{\text{tBu,Me}}\text{LnMe}(\text{OTf})$ sowie $\text{Tp}^{\text{tBu,Me}}\text{LnMe}(\text{NTf}_2)$. Versuche, diese mit dem WITTIG Reagenz $\text{H}_2\text{C}=\text{PPh}_3$ umzusetzen um eine Abspaltung der Abgangsgruppe zu erzielen, zeigten keine Reaktivität dahingehend. Durch weitere Anstrengungen gelang die Synthese von $\text{Tp}^{\text{tBu,Me}}\text{LnX}_2$ ($\text{X} = \text{Cl, I}$) und vor allem $\text{Tp}^{\text{tBu,Me}}\text{LuMeCl}$. So gelang die Umsetzung mit KBn und $\text{LiCH}_2\text{SiMe}_3$ in einer Salzmetathese-Reaktion zu $\text{Tp}^{\text{tBu,Me}}\text{LuMe}(\text{R})$ ($\text{R} = \text{CH}_2\text{C}_6\text{H}_5, \text{CH}_2\text{SiMe}_3$). Auch erhöhte Temperaturen führten nicht zur Abstraktion des Alkans und der Bildung des anvisierten Alkylidens.

Weiteres Interesse an der Chemie von reaktiven Methyl-Komplexen führte zu Untersuchungen über gemischte Methyl/Aryloxid Verbindungen $\text{Tp}^{\text{tBu,Me}}\text{LnMe}(\text{OAr})$ ($\text{Ln} = \text{Y, Lu}$; $\text{OAr} = \text{OC}_6\text{H}_3\text{Me}_2\text{-2,6, OC}_6\text{H}_3\text{iPr}_2\text{-2,6, OC}_6\text{H}_2\text{tBu}_2\text{-2,6-Me-4, OC}_6\text{H}_3(\text{CF}_3)_2\text{-3,5}$). Um die erwünschten Verbindungen zu erhalten, wurden sowohl Salzmetathese- als auch Protonolyse-Protokolle mit $\text{Tp}^{\text{tBu,Me}}\text{LuMe}_2$ und $\text{Tp}^{\text{tBu,Me}}\text{LnMe}(\text{AlMe}_4)$ und den entsprechenden Phenolderivaten angewandt.

Durch die Verwendung eines anderen Ligandensystems gelang die Synthese von weiteren Silylamid-stabilisierten Seltenerdmetallkomplexen $(\text{Me}_x\text{Ph}_y\text{Si})_2\text{NLn}(\text{AlMe}_4)_2$ ($\text{Ln} = \text{Y, Lu}$, $x = 0\text{-}2$, $y = 3\text{-}x$), die durch intramolekulare C–H-Bindungsaktivierung (CNC)-Pincer Komplexe generierten.

Die erfolgreiche Isolierung von verschiedenen gemischten trimetallischen Halogenid/Methyliden Komplexen $(\text{Cp}^{\text{R}})_3\text{Ln}_3(\mu\text{-X})_3(\mu_3\text{-X})(\mu_3\text{-CH}_2)(\text{thf})_3$ ($\text{Ln} = \text{Y, La}$; $\text{X} = \text{Cl, Br, I}$; $\text{Cp}^{\text{R}} = \text{C}_5\text{Me}_5, \text{C}_5\text{Me}_4\text{SiMe}_3$) konnte durch Donor-induzierte Tetramethylaluminatspaltung gefolgt von C–H-Bindungsaktivierung erzielt werden. Reaktivitätstests mit Substraten, die eine Carbonyl-Funktionalität tragen, zeigten Reaktivitäten ähnlich dem TEBBE Reagenz, weswegen

diese Methyliden-Komplexe als nukleophile Carbene des SCHROCK-Typs eingestuft werden können. Zudem wurden die Seltenerdmetall-Methyliden-Komplexe erfolgreich in der Polymerisation von δ -Valerolacton getestet.

Publications

Publications incorporated into this thesis

- Paper I** Potential Precursors for Terminal Methylidene Rare-Earth-Metal Complexes Supported by a Superbulky Tris(pyrazolyl)borato Ligand
V. M. Birkelbach, R. Thim, C. Stuhl, C. Maichle-Mössmer, R. Anwander
Chem. Eur. J. **2019**, *25*, 14711-14720
<https://doi.org/10.1002/chem.201903606>
- Paper II** Mixed Methyl Aryloxy Rare-Earth-Metal Complexes Stabilized by a Superbulky Tris(pyrazolyl)borato Ligand
V. M. Birkelbach, C. Stuhl, C. Maichle-Mössmer, R. Anwander
Organometallics **2019**, *38*, 4485-4496
<https://doi.org/10.1021/acs.organomet.9b00631>
- Paper III** Elucidation of Cyclopentadienyl-Supported Rare-Earth-Metal Methylidene Complexes: Scope of Coligands and Tebbe olefination
V. M. Birkelbach, H. M. Dietrich, C. Stuhl, C. Maichle-Mössmer, R. Anwander
manuscript

Poster presentations

- Poster I** Cp-stabilized Homometallic Rare-Earth-Metal Complexes
V. M. Birkelbach, C. Stuhl, C. Maichle-Mössmer, R. Anwander
XXVIII. Tage der Seltenen Erden, Tübingen, Germany, *October 4-6, 2017*.
- Poster II** Rare-Earth-Metal Mixed Halide Methylidene Complexes: Synthesis and Reactivity
V. M. Birkelbach, C. Stuhl, C. Maichle-Mössmer, R. Anwander
43rd International Conference on Coordination Chemistry ICCS, Sendai, Japan, *July 30-August 4, 2018*.
- Poster III** Rare-Earth-Metal Mixed Halide Methylidene Complexes: Synthesis and Reactivity
V. M. Birkelbach, C. Stuhl, C. Maichle-Mössmer, R. Anwander
6th International Workshop on Transition Metal Clusters IWTMC, Tübingen, Germany, *September 5-7, 2018*.
- Poster IV** Potential Precursors for Terminal Methylidene Rare-Earth-Metal Complexes
V. M. Birkelbach, C. Stuhl, C. Maichle-Mössmer, R. Anwander
19. Vortragstagung f. Anorg. Chemie der Fachgruppen der Wöhler-Vereinigung u. Festkörperchemie u. Materialforschung, Regensburg, Germany, *September 24-27, 2018*.

Personal Contribution

Paper I:

All reactions and analyses described were planned and conducted by myself (except $\text{Tp}^{\text{tBu,Me}}\text{LuMeCl}$). Analyses include one-dimensional (^1H , $^{13}\text{C}\{^1\text{H}\}$, $^{19}\text{F}\{^1\text{H}\}$, $^{11}\text{B}\{^1\text{H}\}$, $^{29}\text{Si}\{^1\text{H}\}$ DEPT-45), two-dimensional (^1H - ^{13}C HSQC, ^1H - ^{13}C HMBC) NMR spectroscopic methods, and DRIFT spectroscopy. Manuscript writing was also done by me. The synthesis of $\text{Tp}^{\text{tBu,Me}}\text{LuMeCl}$ was planned by Dr. Renita Thim.

Elemental analyses were performed by Wolfgang Bock. The structural analyses by single crystal X-ray diffraction were performed by Dr. Cécilia Maichle-Mössmer and Dr. Christoph Stuhl.

Paper II:

All reactions and analyses described were planned and conducted by myself. Analyses include one-dimensional (^1H , $^{13}\text{C}\{^1\text{H}\}$, $^{11}\text{B}\{^1\text{H}\}$, $^{19}\text{F}\{^1\text{H}\}$), two-dimensional (^1H - ^{13}C HSQC, ^1H - ^{13}C HMBC, ^1H - ^{89}Y HSQC) NMR spectroscopic methods, and DRIFT spectroscopy. Manuscript writing was also done by me.

Elemental analyses were performed by Wolfgang Bock. The structural analyses by single crystal X-ray diffraction were performed by Dr. Cécilia Maichle-Mössmer and Dr. Christoph Stuhl.

Paper III:

All reactions and analyses described were planned and conducted by myself. Analyses include one-dimensional (^1H , $^{13}\text{C}\{^1\text{H}\}$), two-dimensional (^1H - ^{13}C HSQC, ^1H - ^{13}C HMBC, ^1H - ^{89}Y HSQC) NMR spectroscopic methods, and DRIFT spectroscopy. Manuscript writing was also done by me. The synthesis of precursors $[(\text{C}_5\text{Me}_5)\text{Ln}(\text{AlMe}_4)\text{X}]_2$ and $[(\text{C}_5\text{Me}_5)_3\text{La}_3(\text{AlMe}_4)_2\text{X}_4]_2$ was planned by Dr. H. Martin Dietrich.

Elemental analyses were performed by Wolfgang Bock. The structural analyses by single crystal X-ray diffraction were performed by Dr. Cécilia Maichle-Mössmer and Dr. Christoph Stuhl.

Objective of this Thesis

The main emphasis of this thesis is to develop new synthesis strategies for the formation of rare-earth-metal methyl or methylidene complexes.

Chapter A of this thesis gives a brief overview of the classification of carbene or alkylidene complexes in general. Further emphasis is put on rare-earth-metal methyl complexes as precursors in rare-earth-metal alkylidene chemistry. The development of rare-earth-metal alkylidene complexes are given in a historical overview with all structurally characterized alkylidene complexes and their respective Ln–C(alkylidene) bond lengths. Additionally, the differences in reactivity are displayed for the afore presented rare-earth-metal alkylidene complexes.

In **Chapter B** the main results of this thesis are presented. The emphasis is put on the following aspects:

- Synthesis of Methyl Complexes as Potential Precursors for Terminal Methylidenes
- Synthesis and Reactivity of Mixed Methyl/Aryloxy Rare-Earth-Metal Complexes
- Mixed Halogenido/Methylidene Rare-Earth-Metal Complexes: Synthesis and Reactivity

Chapter C contains a manuscript with unpublished results about (*CNC*)-pincer-like rare-earth-metal complexes

Chapter E is a compilation of publications and a manuscript to be submitted.

A

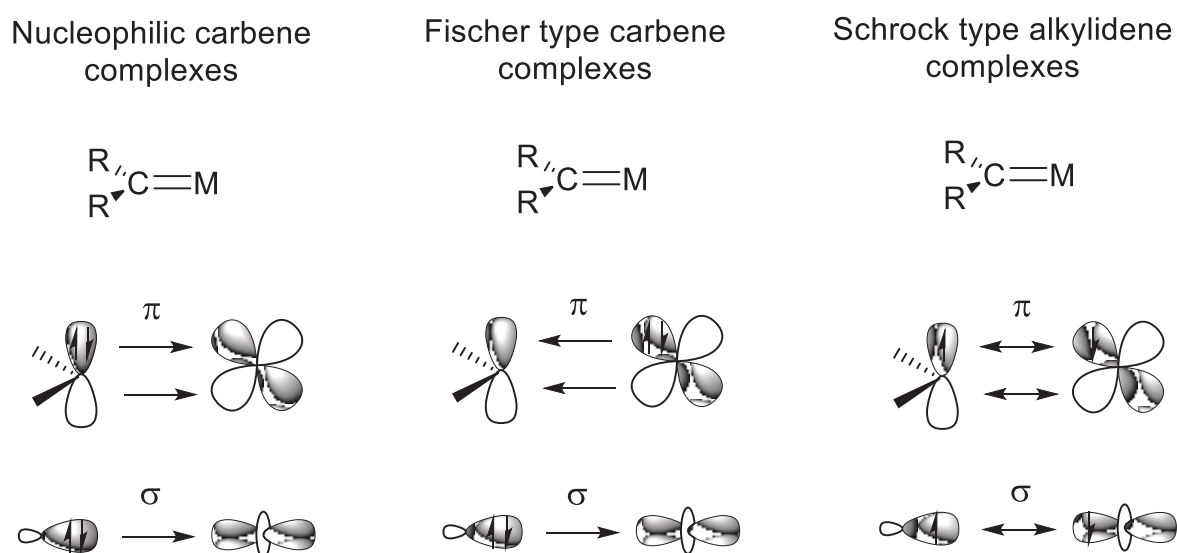
**Methyl and Alkylidene
Complexes of the Rare-
Earth Metals**

1 Metal Carbene vs. Alkylidene Complexes

In general, carbene complexes can be best described as divalent carbon species coordinated to a metal center *via* a formal carbon metal double bond. Deeper insights into the bonding situation and the electro- or nucleophilicity of the respective carbon or metal fragment leads to the classification into three different types of transition metal carbene complexes (Scheme 1):^[1]

Nucleophilic carbene complexes,^[1d-f, 2] where the four electrons of the formal M=C double bond are solely provided by the ligand system (Scheme 1, left). R represents electron withdrawing groups to stabilize the nucleophilic carbene unit with the electron deficient metal center. Therefore, the bonding situation is best described as dative bond from a strong σ -donor ligand. Representatives for this class are pincer-like bis(phosphorous)-stabilized carbene complexes formed from geminal dianions and the metal cation.^[1d-f, 2]

FISCHER-type carbene complexes,^[1a, f, g, 2] or singlet carbene complexes bear an electrophilic carbon species with R representing heteroatoms (Scheme 1, middle). The double-bond situation shows a σ -type electron donation from the carbene and π -type back bonding of the d-orbitals of the metal. Mainly, such complexes are accessible for late transition metals in low oxidation states. The synthesis of FISCHER-type carbenes can be achieved through *e.g.* addition of lithium alkyls to M-CO and subsequent alkylation or protonation of acyl complexes.^[1a, f, g, 2]



Scheme 1. Classification of the different carbene complexes and their bonding modes (Scheme adopted and slightly modified from ref. [1f]).

SCHROCK-type alkylidene complexes,^[1c, g, 2] or triplet carbene complexes feature a nucleophilic CR_2^{2-} unit with R representing hydrogen and alkyl substituents and a metal center in a formal high oxidation state (Scheme 1, right). The double bond character results from the σ - and π -bonding with two single electrons each from the metal center as well as the carbene moiety. Furthermore, SCHROCK alkylidene complexes can be generated, *e.g.* from deprotonation of alkyl groups or trapping reactions of free carbenes.^[1c, g, 2]

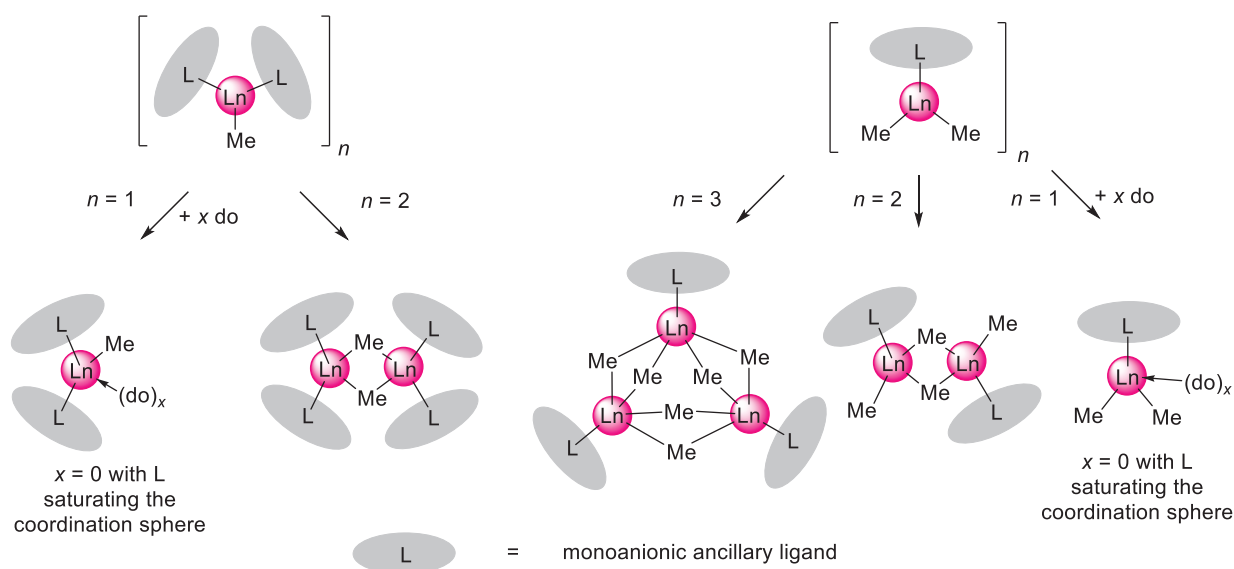
The reactivity of these different types of carbene complexes strongly varies, for example, FISCHER carbene complexes with their electrophilic carbene moiety can be utilized in *e.g.* addition reactions of nucleophiles like amines or lithium alkyls for the generation of other carbenes, synthesis of carbocycles, carbene transfer reactions, or benzanullation reactions, whereas the nucleophilic carbene unit of the SCHROCK alkylidene complex can be used in metathesis reactions or even more importantly in WITTIG-type alkylidene transfer reactions.^[1g, 2]

Although the bonding situation of transition-metal alkylidene complexes cannot be directly transferred to rare-earth-metal chemistry (rare-earth metals cannot stabilize the carbonic moiety by back donation and feature a mainly ionic bonding situation which is described in the next paragraph), the analogy to transition metal alkylidene complexes is justified, due to the similarities in their reactivity.

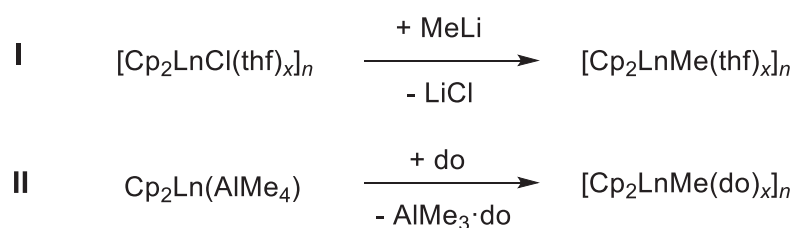
In the following, we will mainly focus on SCHROCK-type alkylidene rare-earth-metal complexes. Interestingly, despite the numerous examples of transition-metal alkylidene complexes, lanthanide alkylidene complexes are still elusive.^[3] This can mainly be attributed to an energetic orbital mismatch between the f-element metal center and the orbitals of the C-based alkylidene.^[4] Rare-earth metals are most stable in the oxidation state +III (Ln^{3+}), which is due to their electronic configuration, *e.g.* Sc $[\text{Ar}]3d^14s^2$, Y $[\text{Kr}]4d^15s^2$, La $[\text{Xe}]5d^16s^2$, and Lu $[\text{Xe}]4f^{14}5d^16s^2$ and the consequence of a closed valence shell with the loss of three electrons. Due to the fact that 4f orbitals have a smaller radial extension compared to the orbitals of the Ln^{3+} metal center, the overlap with the ligand orbitals is restricted. Therefore, the impact of this energetic orbital mismatch results in a predominantly ionic bond between the metal center and the alkylidene moiety and further the chemistry is defined by electrostatic and steric factors.

2 Reactive Ln(III) Methyl Complexes

One approach for the successful synthesis of rare-earth-metal alkylidenes is the intended C–H-bond activation of reactive $[\text{LLnR}_2]$ ($\text{R} = \text{alkyl}$) precursors stabilized by the ancillary monoanionic ligand L .^[5] Already in the late 70s, SCHUMANN reported on the successful synthesis of $\text{Li}_3\text{LnMe}_6(\text{tmeda})_3$.^[6] However, it was the discovery of WATSON and BERCAW in the 80s that $\text{Ln}-\text{CH}_3$ moieties are capable of methane activation.^[7] In 2005 and later in 2019 further efforts from our group led to the discovery of very reactive homoleptic unsolvated LnMe_3 (Sc , Y , Ho , Lu) accessible through donor-induced aluminate-cleavage from the respective $\text{Ln}(\text{AlMe}_4)_3$.^[8] Due to this very reactive nature, the synthesis of discrete rare-earth-metal methyl bonds is still challenging and especially unsolvated, non-ate rare-earth-metal complexes are considered as most reactive.^[9] The reactivity of these complexes is attributed to their composition: rare-earth metals $\text{Ln}(\text{III})$ with large ionic radii (for six-coordinated Ln^{3+} , e.g. La^{3+} 1.032 Å, Y^{3+} 0.900 Å, Lu^{3+} 0.861 Å, Sc^{3+} 0.745 Å)^[10] and the methyl ligand with its enhanced basicity causing an ionic bonding situation.^[11] Despite this, different structural motifs are known for the formation of homometallic ligand-stabilized rare-earth-metal methyl complexes, for instance $[\text{L}_2\text{LnMe}]_x$ or $[\text{LLnMe}_2]_x$ (Scheme 2). Crucial for the accessibility of these systems is the stabilizing effect of the monoanionic ligand L or the introduction of external donors. Therefore, it is not surprising, that many homometallic $[\text{L}_2\text{LnMe}]_n$ complexes ($n = 1, 2$) have been structurally characterized, mainly supported by cyclopentadienyl derivatives, e.g.



Scheme 2. Previously reported structural motifs adapted by $[\text{LLnMe}_2]_n$ and $[\text{L}_2\text{LnMe}]_n$ rare-earth-metal complexes.

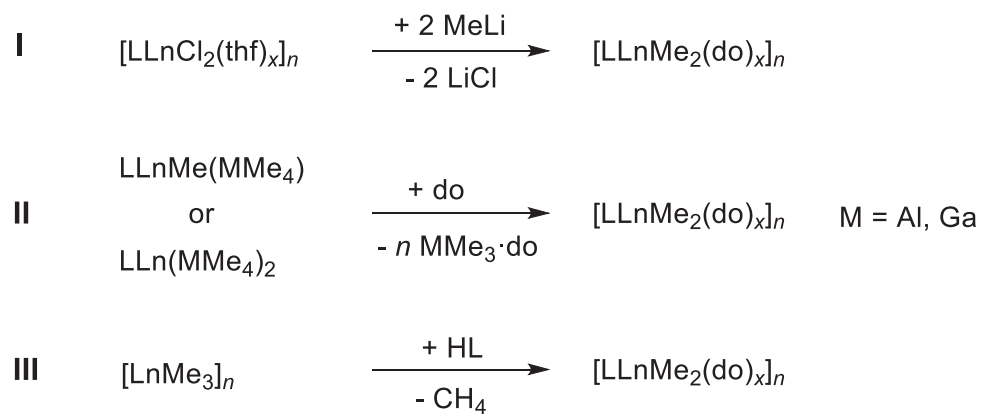


Scheme 3. Synthesis pathway to methyl complexes with the general composition $[\text{Cp}_2\text{LnMe}]_n$.

unsubstituted $[\text{Cp}_2\text{LnMe}]_2$ ($\text{Ln} = \text{Y}, \text{Yb}$; $\text{Cp} = \text{C}_5\text{H}_5$),^[12] monomeric ($n = 1$) $\text{Cp}_2\text{YbMe}(\text{thf})$,^[13] or alkyl-substituted Cp complexes $[\text{Cp}^{\text{Me}}_2\text{YMe}]_2$ ($\text{Cp}^{\text{Me}} = \text{C}_5\text{H}_3(\text{Me})_{2-1,3}$),^[14] $[\text{Cp}^*\text{LnMe}]_x$ ($n = 1$ for Sc, $n = 2$ for Lu; $\text{Cp}^* = \text{C}_5\text{Me}_5$),^[15] $[\text{Cp}^{i\text{Pr}}_2\text{LuMe}]_2$ ($\text{Cp}^{i\text{Pr}} = \text{C}_5\text{Me}_4i\text{Pr}$),^[16] $[\text{Cp}^{t\text{Bu}}_2\text{LnMe}]_2$ ($\text{Ln} = \text{Ce}, \text{Nd}, \text{Tb}$; $\text{Cp}^{t\text{Bu}} = \text{C}_5\text{Me}_4t\text{Bu}$),^[17] as well as various silyl derivatives $[\text{Cp}'_2\text{LnMe}]_2$ ($\text{Ln} = \text{Y}, \text{Sm}$; $\text{Cp}' = \text{C}_5\text{Me}_4\text{SiMe}_3$),^[18] $[\text{Cp}^{\text{SiMe}_3}_2\text{LnMe}]_2$ ($\text{Ln} = \text{Nd}, \text{Sm}$; $\text{Cp}^{\text{SiMe}_3} = \text{C}_5\text{Me}_3(\text{SiMe}_3)_{2-1,3}$),^[18a] $[\text{Cp}^{\text{SiEt}_3}_2\text{LnMe}]_2$ ($\text{Ln} = \text{Y}, \text{Sm}, \text{Lu}$; $\text{Cp}^{\text{SiEt}_3} = \text{C}_5\text{Me}_3(\text{SiEt}_3)_{2-1,3}$).^[19] Two different synthesis pathways are known for the generation of these $[\text{Cp}_2\text{LnMe}]_n$ derivatives (Scheme 3): Path **I** is widely used and displays a salt-metathesis approach utilizing a $[\text{Cp}_2\text{LnCl}]_n$ precursor for the reaction with a methylating agent like MeLi. Path **II** shows the donor-cleavage of $\text{Cp}_2\text{Ln}(\text{AlMe}_4)$, a so-called “alkyl in disguise” due to the stabilizing effect on the methyl group from the trimethylaluminum.^[20] The introduced donor solvent then forms the LEWIS acid-base pair $\text{AlMe}_3 \cdot \text{do}$ to generate the terminal methyl group.

Particular challenging is the kinetic stabilization of discrete dimethyl Ln(III) derivatives of the type $[\text{LLnMe}_2]_n$ which strongly depends on the steric bulk of the ancillary ligand L.^[11] Mainly, Cp-based dimethyl complexes display methyl-bridged dimerized and oligomerized solid-state structural motifs, e.g. $[\text{Cp}'\text{ScMe}_2]_2$,^[21] $[\text{Cp}'\text{LnMe}_2]_3$ ($\text{Ln} = \text{Tm}, \text{Lu}$),^[5b] and $[\text{Cp}^*\text{LnMe}_2]_3$ ($\text{Ln} = \text{Y}, \text{Ho}, \text{Dy}, \text{Tb}, \text{Lu}$).^[9a, 22] In contrast to this, sterically demanding *N*-coordinating ligands gave access to monometallic complexes $[\text{LLnMe}_2]$ evidenced by X-ray structure analysis, for example $\{(\text{Dipp})\text{NC}(t\text{Bu})\text{CHC}(t\text{Bu})\text{N}(\text{Dipp})\}\text{ScMe}_2$ ($\text{Dipp} = \text{C}_6\text{H}_3i\text{Pr}_{2-2,6}$),^[23] $\{1-(\text{NDipp})-2-(\text{PPh}_2=\text{NAr})\text{C}_6\text{H}_4\}\text{ScMe}_2$,^[24] $\text{Tp}^{t\text{Bu},\text{Me}}\text{LnMe}_2$ ($\text{Ln} = \text{Ho}, \text{Lu}$; $\text{Tp}^{t\text{Bu},\text{Me}} = \text{tris}(\text{pyrazolyl-}t\text{Bu-3-Me-5})\text{borato}$),^[11, 25] and further *N*- or *P*-donor supported 2- $\{\text{NDippC}(\text{Ph})\text{NC}_6\text{H}_4\text{CH}=\text{NDipp}\}\text{ScMe}_2$,^[26] $\text{N}(2\text{-}i\text{Pr}_2\text{-4-methylphenyl})_2\text{ScMe}_2$,^[27] and $\{\text{MeC}(\text{NDipp})\text{CHC}(\text{Me})\text{N}(\text{CH}_2)_2\text{N}(\text{Me})(\text{CH}_2)_2\text{NMe}_2\}\text{YMe}_2$.^[28] If the coordination sphere is not completely saturated from the bulky ancillary ligand, introduction of external donors can give rise to monometallic complexes as $\text{Cp}^*\text{ScMe}_2(\text{OP}t\text{Bu}_3)$,^[29] $\{\text{N}(\text{SiMe}_3)(\text{Dipp})\}\text{LuMe}_2(\text{thf})_2$,^[5c] and $\{(\text{Dipp})\text{NC}(\text{Me})\text{CHC}(\text{Me})\text{N}(\text{Dipp})\}\text{ScMe}_2(\text{thf})$.^[23] In addition to synthesis strategies **I** and **II** toward $[\text{Cp}_2\text{LnMe}]_n$ complexes, $[\text{LLnMe}_2]_n$ complexes

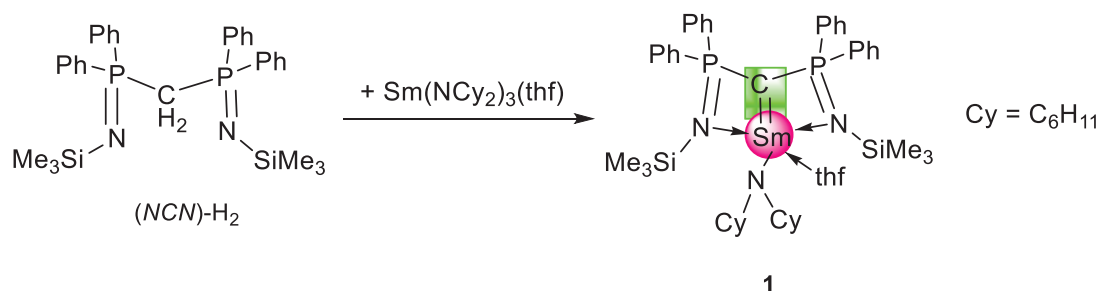
can also be accessed from the donor-cleavage of a weaker LEWIS acid stabilizing the alkyl (Scheme 4, Path **II**, Ga) and further, *via* protonolysis reactions of $[\text{LnMe}_3]_n$ precursors with HL (Scheme 4, Path **III**). With respect to rare-earth-metal alkylidene formation, monometallic^[5c] or trimetallic^[5b, 22b] $[\text{LLnMe}_2(\text{do})_x]_n$ were already proven to be suitable starting materials.



Scheme 4. Synthesis pathway to methyl complexes with the general composition $[\text{LLnMe}_2]$.

3 Historical Overview of Rare-Earth-Metal Alkylidenes

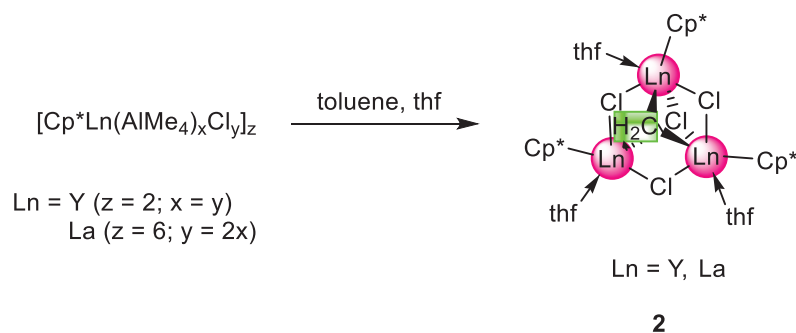
Already in the late 70s, SCHUMANN reported on the synthesis of lutetium and erbium alkylidenes $[\text{Li}(\text{do})_x][\text{Ln}(\text{CH}_2\text{SiMe}_3)_2(\text{CHSiMe}_3)]_n$ via a silane elimination protocol.^[30] He substantiated his findings with NMR spectroscopic analysis as well as elemental analysis, however, there was no structural elucidation. Despite this great achievement, it lasted almost 30 years until CAVELL in 2000 succeeded in the formation of the first structurally characterized rare-earth-metal alkylidene $\{\text{C}(\text{Ph}_2\text{P}=\text{NSiMe}_3)_2\}\text{Sm}(\text{NCy}_2)(\text{thf})$ **1** with a pincer-like structural motif by reacting the protonated ligand $(\text{NCN})\text{-H}_2$ with the homoleptic samarium amide precursor (Scheme 5).^[31] Crystal structure analysis revealed a very short bond length for the Sm–C(alkylidene) bond with 2.467(4) Å (all bond lengths mentioned in this chapter are given in Table 1 in chapter 4). Shortly after this discovery, similar samarium and thulium alkylidene complexes such as $[\{(\text{Ph}_2\text{P}=\text{S})_2\text{C}\}\text{LnI}]_2$ (Ln = Sm, Tm) were found from the dilithiated (SCS)-pincer-type ligand and $\text{LnI}_3(\text{thf})_x$ with bond lengths for Ln–C(alkylidene) of 2.371(6) Å and 2.325(5) Å, respectively. Further efforts led to ionic $[\{(\text{Ph}_2\text{P}=\text{S})_2\text{C}_2\text{Ln}][\text{Li}(\text{thf})_4]$ bis(carbene) complexes with bond lengths of 2.491(5) and 2.507(5) Å for samarium as well as 2.368(3) and 2.423(9) Å for thulium developed by LE FLOCH.^[32] Even though comparison of these complexes with a hypervalent geminal dianionic *P*-stabilized ligand set and a trivalent metal center to other rare-earth-metal complexes bearing a nucleophilic CH_2^{2-} moiety seems difficult, reactivity studies have proven similar trends toward carbonylic functionalities. So the analogy to SCHROCK alkylidene complexes allows for their position in this chapter. Further details on their reactivity will be given in chapter 5.



Scheme 5. Synthesis of the first structurally characterized bis(iminophosphorano) samarium complex.

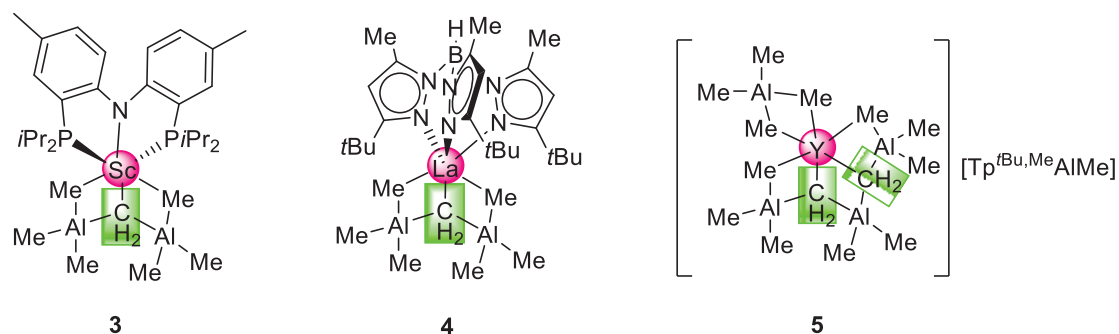
In 2006, our group successfully utilized the donor-induced aluminate-cleavage and C–H-bond activation of a Cp*-stabilized heterobimetallic precursor $[\text{Cp}^*\text{Ln}(\text{AlMe}_4)_x\text{Cl}_y]_z$ (Ln = Y: $z = 2$, $y = x$; Ln = La: $z = 6$, $y = 2x$) for the synthesis of a trimetallic rare-earth-metal nucleophilic methylidene complexes $\text{Cp}^*_3\text{Ln}_3(\mu\text{-Cl})_3(\mu_3\text{-Cl})(\mu_3\text{-CH}_2)(\text{thf})_3$ (Ln = Y, La) **2** with bridging

chlorido ligands (Scheme 6).^[33] The core of this methylidene cluster adopts a distorted hexagonal bipyramidal geometry with the striking methylidene unit bridging the three lanthanide metal centers. Bond lengths for the methylidene and the rare-earth-metal centers range from 2.424(2) to 2.450(2) Å for yttrium and 2.537(3) to 2.635(3) Å for lanthanum.^[33]



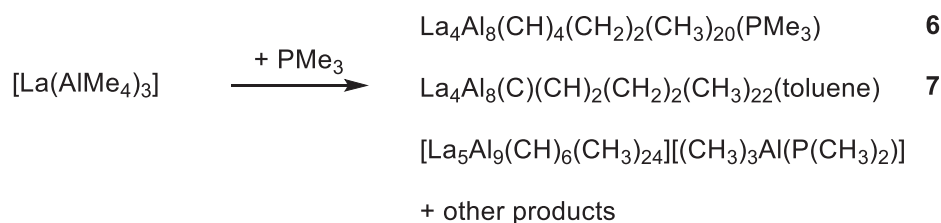
Scheme 6. Synthesis of the first trimetallic rare-earth-metal methylidene complexes.

Only two years later in 2008, a new structural motif was discovered independently from our group and MINDIOLA and coworkers, namely LEWIS-acid stabilized rare-earth-metal complexes of the type $[\text{LLn}(\text{CH}_2)(\text{AlMe}_3)_2]$ (Scheme 7). The striking feature of these complexes is the similarity to the TEBBE reagent $\text{Cp}_2\text{Ti}(\text{CH}_2)\text{ClAlMe}_2$. The group of MINDIOLA utilized a (*PNP*)-pincer ligand ($\text{PNP} = \text{N}[2\text{-}i\text{Pr}_2\text{-4-methylphenyl}]_2$) for the reaction of the rare-earth-metal precursor (*PNP*) ScMe_2 with trimethylaluminum to form **3** featuring a Sc–C(alkylidene) bond length of 2.317(2) Å.^[27] Our group showed that the reaction of the superbulky tris(pyrazolyl)borato ligand $\text{KTp}^{\text{tBu,Me}}$ in a salt-metathetical approach with $\text{La}(\text{AlMe}_4)_3$ also led to a TEBBE-like lanthanum complex **4** with a La–C(methylidene) bond of 2.519(2) Å.^[34] Another LEWIS-acid stabilized methylidene was also achieved by our group from the protonolysis reaction of $\text{HTp}^{\text{tBu,Me}}$ with $\text{Y}(\text{AlMe}_4)_3$ and gave ionic $[\text{Tp}^{\text{tBu,Me}}\text{AlMe}][\text{Y}(\text{AlMe}_4)\{(\text{CH}_2)\text{AlMe}_3\}_2(\text{AlMe}_2)]$ **5** (Y–CH₂: 2.344(8), 2.411(9) Å).^[20]



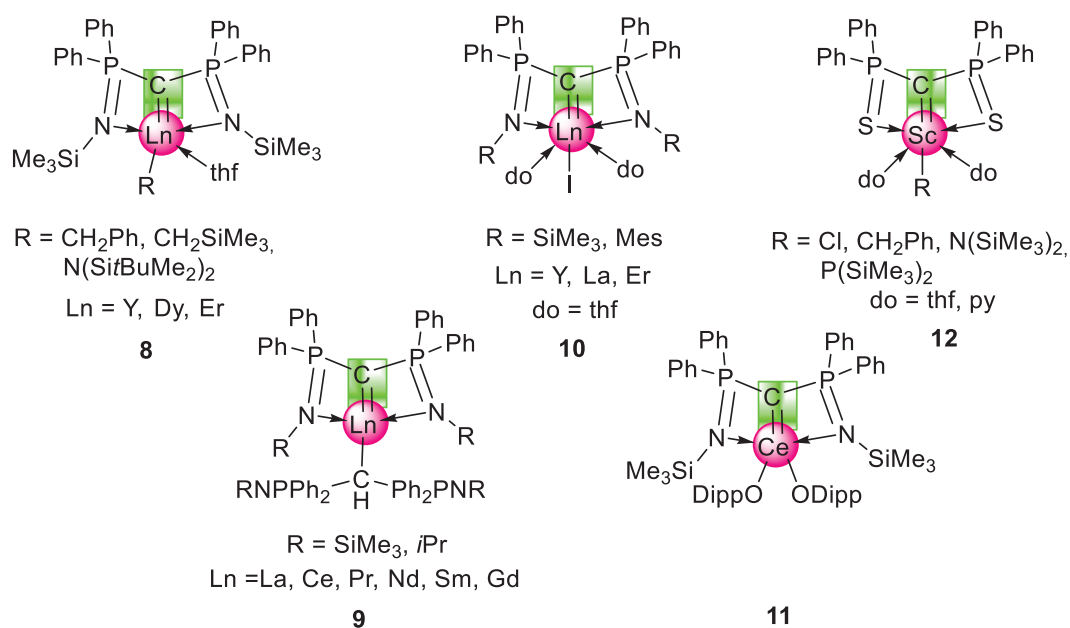
Scheme 7. TEBBE-like rare-earth-metal methylidene complexes.

On the way to donor-solvent free complexes $[\text{LnMe}_3]_n$ via the reaction of $\text{La}(\text{AlMe}_4)_3$ with donors as PMe_3 , our group observed lanthanum clusters containing, amongst methylidyne and carbide also methylene moieties (Scheme 8).^[35] This occurred through multiple C–H-bond activations by implementation of donors and gave methylene cluster compounds **6** and **7** with $\text{La–C}(\text{CH}_2)$ bond lengths between 2.549(7) and 2.889(7) Å.



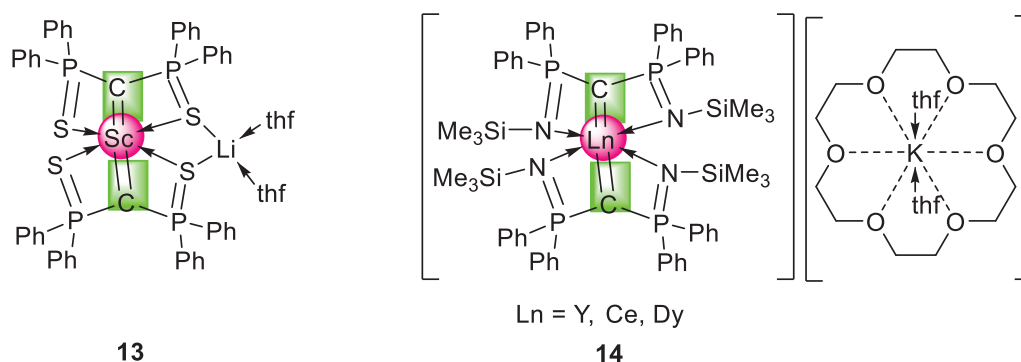
Scheme 8. Snapshots of the stepwise aluminate cleavage of $[\text{La}(\text{AlMe}_4)_3]$.

In 2008 and up to now follow-up chemistry on CAVELLS discoveries led to similar alkylidene complexes found by LITTLE and LE FLOCH (Scheme 9, **8–11**) implementing a (*NCN*)-pincer system with N–SiMe_3 ($\text{NCN}^{\text{SiMe}_3}$) or $\text{N–}i\text{Pr}$ ($\text{NCN}^{i\text{Pr}}$) groups.^[36] Several structural motifs containing (*NCN*)-supported rare-earth-metal alkyl (Ln–C : **8–Y** ^{CH_2Ph} 2.357(3) Å, **8–Y** ^{CH_2SiMe_3} 2.406(3) Å, **8–Y** ^{$\text{N}(\text{Si}^i\text{BuMe}_2)_2$} 2.357(3) Å, **8–Er** ^{CH_2Ph} 2.339(4) Å), di(pincer) (Ln–C : **9–La** ^{SiMe_3} 2.512(2) Å, **9–Ce** ^{SiMe_3} 2.472(4) Å, **9–Pr** ^{SiMe_3} 2.458(5) Å, **9–Sm** ^{SiMe_3} 2.40(2) Å, **9–Gd** ^{SiMe_3} 2.406(2) Å, **9–Nd** ^{$i\text{Pr}$} 2.592(3) Å) and halide complexes (Ln–C : **10–Y** ^{SiMe_3} 2.356(3) Å, **10–La** ^{Mes} 2.5284 Å, **10–Er** ^{SiMe_3} 2.322(2) Å) were elucidated.^[36]



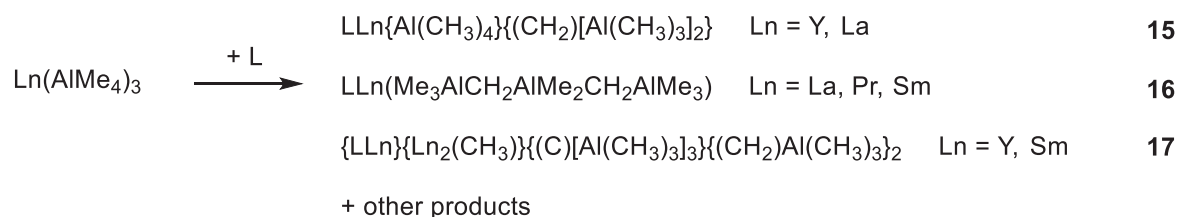
Scheme 9. Structural motifs of rare-earth-metal pincer-type alkylidene complexes.

In 2013, LIDDLE and coworkers found the Ce(IV)-alkylidene **11** (2.441(5) Å) through oxidation of the respective Ce(III)-di(alkoxy) precursor and further Ce(IV) di(carbene) $\{(\text{Ph}_2\text{P}=\text{NSiMe}_3)_2\text{C}\}_2\text{Ce}$ (2.385(2)-2.399(3) Å) *via* oxidation with AgBPh_4 .^[36h, 37] Structurally elucidated complexes for Sc with the (SCS)-pincer ligand set were found by MÉZAILLES in 2015 with $\{(\text{Ph}_2\text{P}=\text{S})_2\text{C}\}\text{Sc}(\text{R})(\text{do})_x$ **12** and complex $\{(\text{Ph}_2\text{P}=\text{S})_2\text{C}\}\text{Sc}\{\text{CH}(\text{S}=\text{PPh}_2)_2\}$ similar to **9** with Sc–C(alkylidene) bond lengths between 2.200(3)-2.225(3) Å.^[38] Furthermore, rare ionic bis(methandiide) complexes $[\{(\text{Ph}_2\text{P}=\text{S})_2\text{C}\}_2\text{Sc}][\text{Li}(\text{thf})_2]$ **13** (2.212(8)-2.243(8) Å) and $[\{(\text{Ph}_2\text{P}=\text{S})_2\text{C}\}_2\text{Ln}][\text{K}(\text{18c6})(\text{thf})_2]$ **14** (Ce: 2.385(2), 2.399(3) Å; Dy: 2.433(6), 2.434(6) Å) expanded the series of di(carbene) complexes found by LE FLOCH in the early 21st century (Scheme 10).^[37-39]



Scheme 10. Ionic bis(methandiide) complexes.

Similar to our approach in 2008, MITZEL found methylidene clusters through the reaction of homoleptic tris(tetramethylaluminates) $\text{Ln}(\text{AlMe}_4)_3$ with different bulky neutral *N*-donor ligands *L*.^[40] Here, through steric pressure the system was forced to release methane and to generate **15**, **16**, and **17** amongst other methyl and methylidyne complexes. Despite the different ligand systems, the bond lengths for each metal center, respectively, are all in the same range, namely for yttrium 2.367(5)-2.452(5) Å, for lanthanum 2.491(3)-2.549(2) Å, for praseodymium 2.436(3)-2.489(5) Å, and for samarium 2.408(4)-2.515(4) Å.

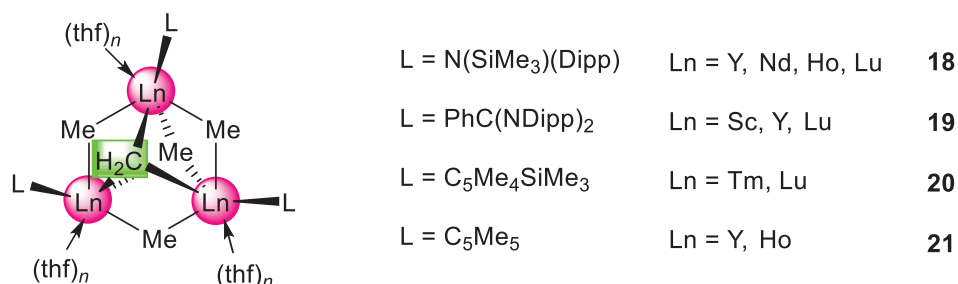


L = (R)NCH₂N(R)CH₂N(R)CH₂ with R = Me (TMTAC), *i*Pr (TiPTAC) or *t*Bu (TfBTAC)

Scheme 11. Different rare-earth-metal methylidene clusters stabilized by neutral *N*-donor ligands.

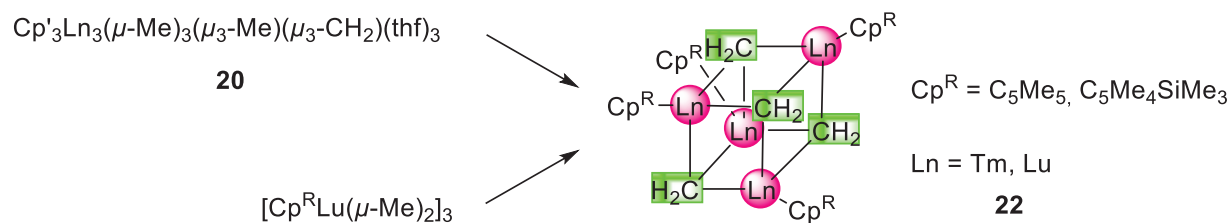
Isochronal to these discoveries, the working group of HOU succeeded in the synthesis of the first heterobimetallic rare-earth-metal transition-metal complex.^[41] They utilized an yttrium polyhydride complex for the reaction with $\text{Cp}^*\text{Ir}(\text{CO})_2$ and generated $\text{Cp}'_4\text{Y}_4(\text{H})_2(\text{O})_2(\text{CH}_3)(\text{CH}_2)\text{Hlr}(\text{Cp}^*)$ with a bridging methylidene $\text{Ir}-\text{CH}_2-\text{Y}$ moiety. The $\text{Y}-\text{C}(\text{CH}_2)$ bond lengths are 2.520(1) and 2.567(1) Å, slightly elongated compared to yttrium alkylidene complexes presented so far.

Between 2010 and 2019 several trimetallic mixed methyl/methylidene complexes $\text{L}_3\text{Ln}_3(\mu\text{-Me})_3(\mu_3\text{-Me})(\mu_3\text{-CH}_2)(\text{thf})_n$ with different stabilizing *C*- or *N*-coordinating monoanionic ancillary ligands *L* were found. As mentioned in Chapter 2, those complexes **18-21** were obtained by utilizing C–H-bond activation protocols of $[\text{LLnMe}_2]_n$ precursors (complexes depicted in Scheme 12).^[5, 22b, 42] This structural motif is isostructural to complexes **2** with bond lengths for the rare-earth-metal center and the bridging methylidene between 2.283(4) (shortest bond length for **21-Y**) and 2.505(8) Å (longest distance for **18-Nd**).^[5, 22b, 42] Complex **19-Y** is not structurally characterized, but is mentioned for completeness.



Scheme 12. Mixed methyl/methylidene rare-earth-metal complexes.

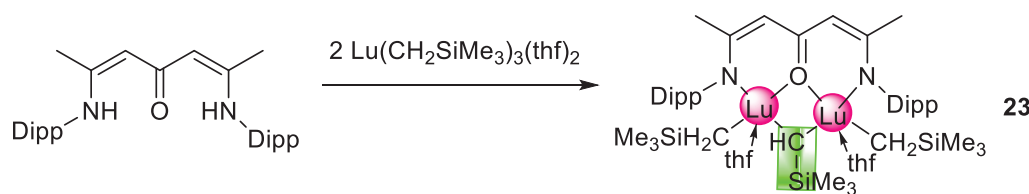
Further heating of complex **20** then led to tetrametallic cubane-like rare-earth-metal methylidenes **22** with four “ $\text{Cp}'\text{Ln}(\mu_3\text{-CH}_2)$ ” units (Scheme 13). Additionally, these clusters can be generated from the $[\text{Cp}'\text{Lu}(\mu\text{-Me})_2]_3$ precursors *via* multiple C–H-bond activation and release of methane. In comparison to **20** (av. 2.49(1) Å), the $\text{Lu}-\text{C}(\text{CH}_2)$ bond lengths are slightly decreased for cubane-like **22-Lu^{Cp'}** (2.32(1)-2.41(1) Å) and **22-Lu^{Cp*}** (2.333(4)-2.396(4) Å).^[5b, 43] The same trend can be found for the thulium congener (**20-Tm**: 2.330(5)-2.365(5) Å, **22-Tm^{Cp'}**: 2.319(5)-2.424(5) Å).^[5b] It is noteworthy, that similarly to heating $[\text{Cp}^*\text{LuMe}_2]_3$ for the formation of **22-Lu^{Cp*}**, the thermolysis of complex $[\text{Cp}^*\text{YMe}_2]_3$ led to hexametallc mixed methyl/methylidene complex $\text{Cp}^*_6\text{Y}_6\text{Me}_4(\text{CH}_2)_4$ with a wide range of $\text{Y}-\text{C}$ bond lengths (2.46(1)-2.61(1) Å). This is due to issues in differentiation between methyl and methylidene units in the solid state structure determination.^[22b]



Scheme 13. Synthesis pathways for cubane-like rare-earth-metal complexes.

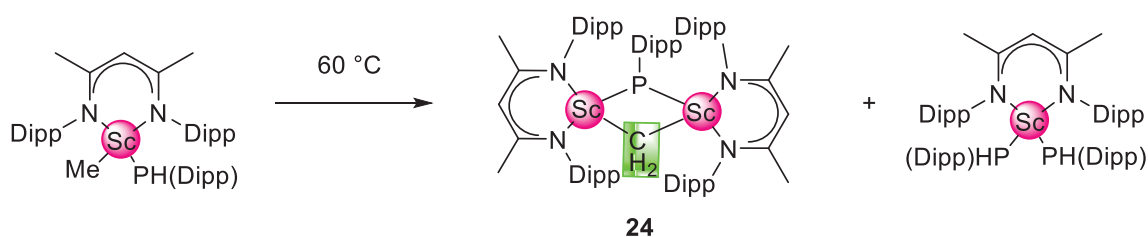
Also in 2011, DIACONESCU and coworkers found a ferrocenediamine-stabilized scandium-aluminum methylidene from the reaction of the scandium precursor ($\text{NN}^{\text{fc}}\text{Sc}(\text{L})$) with AlMe_3 ($\text{NN}^{\text{fc}} = 1,10\text{-fc}(\text{NSi}t\text{BuMe}_2)_2$) with L as the tridentate imidazole-imine-amido ligand and a Sc–C(alkylidene) bond length of 2.692(2) Å.^[44] This bond length is slightly elongated in comparison to other Sc–alkylidene bonds (*cf.* **3**, **19-Sc**), a trend which was also observed for heterobimetallic $\text{Cp}'_4\text{Y}_4(\text{H})_2(\text{O})_2(\text{CH}_3)(\text{CH}_2)\text{Hlr}(\text{Cp}^*)$.^[41]

Some years later, CUI successfully brought back the chemistry of SCHUMANN from the 70s: Through application of a thermolysis protocol on $\text{Lu}(\text{CH}_2\text{SiMe}_3)_3(\text{thf})_2$ and the efficient $\alpha\text{-H}$ abstraction, the first four-coordinate methandiide alkyl lutetium complex **23** was obtained.^[45] Accordingly, $\text{Lu}(\text{CH}_2\text{SiMe}_3)_3(\text{thf})_2$ was reacted with a protonated $\beta\text{-oxo-}\delta\text{-diimino}$ ligand ($\text{BODDI-H}_2 = (\text{Dipp})\text{NC}(\text{Me})\text{CHCOCH}(\text{Me})\text{N}(\text{Dipp})$) for the release of silane (Scheme 14). XRD measurements revealed a relatively short bond length for the Lu–CH(SiMe₃) moiety with 2.309(6) Å.



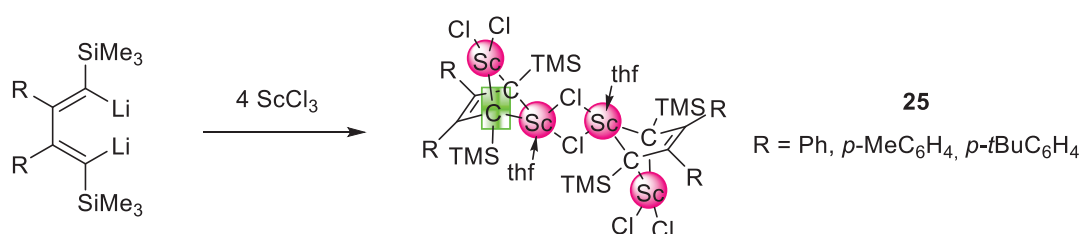
Scheme 14. Synthesis of four-coordinate methandiide lutetium complex.

Shortly after, CHEN and coworkers found that dimerization and thermal decomposition of a scandium methyl phosphide precursor led to diphosphide complex ($\text{Dipp-nacnac}\text{Sc}\{\text{PH}(\text{Dipp})\}$) and the mixed methylidene/phosphinidene complex **24** with Sc–C(CH₂) bond lengths of 2.193(3) and 2.232(3) Å (Scheme 15).^[46] Similar to the achievements of CUI (complex **23**), the working group of CHEN also synthesized an alkylidene bridged bimetallic complex bearing a neutral tris(pyrazolyl)methanide (CTp) ligand, namely $(\text{CTp}^{\text{Me},\text{Me}})_2\text{Lu}_2(\text{CHSiMe}_3)(\text{dmpz})_2$ with a Lu–C(alkylidene) bond length of 2.300(6) Å.^[47]



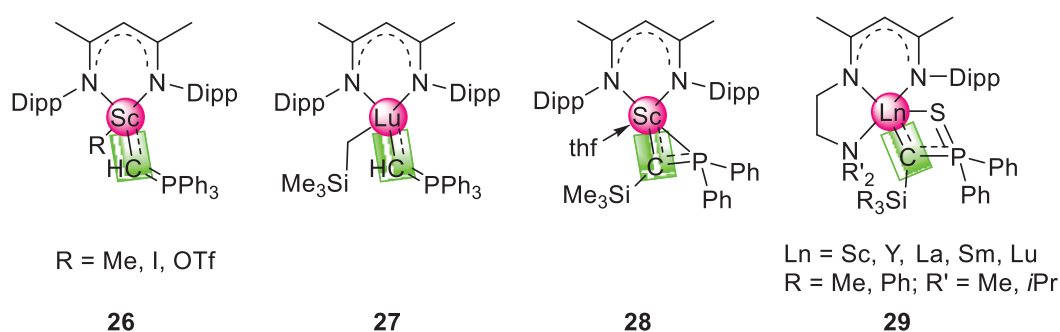
Scheme 15. Synthesis of mixed methylidene/phosphinidene complex **24**.

In 2017, the group of ZHANG reported on the synthesis of the first bridged scandium bis(alkylidene) **25** from 1,4-dilithio-1,3-butadienes and ScCl_3 *via* scandacyclopentadiene and scandacyclopentadiene (Scheme 16).^[48]



Scheme 16. Formation of bridged bis(alkylidene) scandium complexes. For the sake of readability only one alkylidene moiety is highlighted.

Only recently, a series of different monometallic phosphinoalkylidenes **26**, **27**, and **28**, as well as silyl-thiophosphinoyl-alkylidene rare-earth-metal complexes **29** were discovered through stabilization by β -ketiminato ligands as Dipp-nacnac or tridentate *N*-nacnac (Scheme 17).^[49] Some of these complexes display the shortest bond lengths for a $\text{Ln}-\text{C}(\text{alkylidene})$ for the respective metal known up to now, *e.g.* **26-Sc^I** with 2.044(5) Å, **29-La^{Ph}** with 2.465(2) Å, **29-Sm^{Me}** with 2.296(2) Å, and **27-Lu** with 2.19(1) Å. Complex **29-Sc^{Me}** (with $R' = i\text{Pr}$) is not structurally characterized, however it is mentioned for completeness and discussions about its reactivity in chapter 5.3.



Scheme 17. Different monometallic alkylidene rare-earth-metal complexes.

4 Ln–C(Alkylidene) Bond Lengths

Table 1 shows an overview of structurally characterized rare-earth-metal alkylidene complexes and their corresponding Ln–C(alkylidene) bond lengths.

Table 1. Rare-earth-metal alkylidene complexes and their corresponding Ln–C(alkylidene) bond lengths [Å].

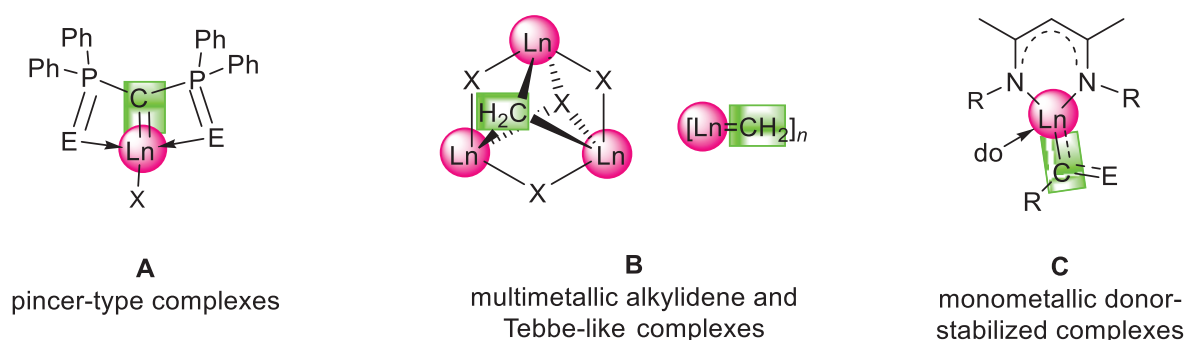
Alkylidene Complex	Ln–C(alkylidene) bond length [Å]	ref.
Sc		
(PNP)Sc(CH ₂)(AlMe ₃) ₂ 3	2.317(2)	[27]
(SCS)Sc[N(SiMe ₃) ₂](thf) 12-Sc^{N(SiMe₃)₂}	2.247(2)	[38]
(SCS)Sc[P(SiMe ₃) ₂](py) ₂ 12-Sc^{P(SiMe₃)₂}	2.200(3), 2.225(3)	[38]
(SCS)Sc[CH(S=PPh ₂) ₂](thf)	2.204(4)	[38]
[(SCS) ₂ Sc][Li(thf) ₂] 13	2.212(8)-2.243(8)	[38]
(PhC(NDipp)) ₂ Sc ₃ (μ-Me) ₃ (μ ₃ -Me)(μ ₃ -CH ₂)(thf) ₃ 19-Sc	av. 2.367	[42a]
fc(Me ₂ Al) ₂ CH ₂ Sc(NSi ^{<i>t</i>} BuMe ₂) ₂ AlMe ₂	2.692(2)	[44]
(Dipp-nacnac)Sc(CH ₂)(PDipp)Sc(Dipp-nacnac) 24	2.193(3)-2.232(3)	[46]
(Dipp-nacnac)Sc(CHPPh ₃)Me 26-Sc^{Me}	2.105(2)	[49a]
(Dipp-nacnac)Sc(CHPPh ₃)I 26-Sc^I	2.044(5)	[49a]
(Dipp-nacnac)Sc(CHPPh ₃)(OTf) 26-Sc^{OTf}	2.060(3)	[49a]
(Dipp-nacnac)ScC(SiMe ₃)(PPh ₂) 28-Sc	2.089(3)	[49b]
Y		
Cp [*] ₃ Y ₃ (μ-Cl) ₃ (μ ₃ -Cl)(μ ₃ -CH ₂)(thf) ₃ 2-Y	2.424(2)-2.450(2)	[33]
[Tp ^{<i>t</i>} Bu,MeAlMe][Y(AlMe ₄){(CH ₂)AlMe ₃ } ₂ (AlMe ₂) ₂] 5	2.344(8), 2.411(9)	[20]
(NCN ^{SiMe₃})Y(CH ₂ Ph)(thf) 8-Y^{CH₂Ph}	2.357(3)	[36a]
(NCN ^{SiMe₃})Y(CH ₂ SiMe ₃)(thf) 8-Y^{CH₂SiMe₃}	2.406(3)	[36d]
(NCN ^{SiMe₃})Y(N(Si ^{<i>t</i>} BuMe ₂) ₂)(thf) 8-Y^{N(Si^{<i>t</i>}BuMe₂)₂}	2.357(3)	[36f]
(NCN ^{SiMe₃})Y(I)(thf) ₂ 10-Y^{SiMe₃}	2.356(3)	[36e]
(TiPTAC)Y{Al(CH ₃) ₄ }{(CH ₂)[Al(CH ₃) ₄] ₂ } 15-Y^{iPr}	2.376(3)	[40b]
(TMTAC)Y{Y ₂ (CH ₃)}{C[Al(CH ₃) ₃] ₃ }{CH ₂ Al(CH ₃) ₃] ₂ 17-Y^{Me}	2.367(5), 2.452(5)	[40a]
{Cp [*] ₄ Y ₄ (H) ₂ (O) ₂ }(CH ₃)(CH ₂)Hlr(Cp [*])	2.520(1), 2.567(1)	[41]
[SiMe ₃ (Dipp)N] ₃ Y ₃ (μ-Me) ₃ (μ ₃ -Me)(μ ₃ -CH ₂)(thf) ₃ 18-Y	2.345(5)-2.424(4)	[5a]
Cp [*] ₃ Y ₃ (μ-Me) ₃ (μ ₃ -Me)(μ ₃ -CH ₂)(thf) ₂ 21-Y	2.283(4)-2.477(3)	[22b]
Cp [*] ₆ Y ₆ Me ₄ (CH ₂) ₄	2.46(1)-2.61(1)	[43]
(N-nacnac)Y[C(SiMe ₃)(SPPH ₂)] 29-Y^{Me}	2.256(3)	[49c]
(N-nacnac)Y[C(SiPh ₃)(SPPH ₂)] 29-Y^{Ph}	2.316(2)	[49c]

La		
$\text{Cp}^*_3\text{La}_3(\mu\text{-Cl})_3(\mu_3\text{-Cl})(\mu_3\text{-CH}_2)(\text{thf})_3$ 2-La	2.537(3)-2.635(3)	[33]
$\text{Tp}^{i\text{Bu,Me}}\text{La}(\text{CH}_2)(\text{AlMe}_3)_2$ 4	2.519(2)	[34]
$\text{La}_4\text{Al}_8(\text{CH})_4(\text{CH}_2)_2(\text{CH}_3)_{20}(\text{PMe}_3)$ 6	2.588(4)-2.629(4)	[35]
$\text{La}_4\text{Al}_8(\text{C})(\text{CH})_2(\text{CH}_2)_2(\text{CH}_3)_{22}(\text{toluene})$ 7	2.549(7)-2.889(7)	[35]
$(\text{NCN}^{\text{SiMe}_3})\text{La}[\text{CH}(\text{Ph}_2\text{P}=\text{NSiMe}_3)_2]$ 9-La^{SiMe3}	2.512(2)	[36b]
$(\text{NCN}^{\text{Mes}})\text{LaI}(\text{thf})_3$ 10-La^{Mes}	2.5284	[36g]
$(\text{TMTAC})\text{La}\{\text{Al}(\text{CH}_3)_4\}\{(\text{CH}_2)[\text{Al}(\text{CH}_3)_4]_2\}$ 15-La^{Me}	2.549(2)	[40a]
$(\text{TiPTAC})\text{La}(\text{Me}_3\text{AlCH}_2\text{AlMe}_2\text{CH}_2\text{AlMe}_3)$ 16-La^{iPr}	2.521(4), 2.542(4)	[40d]
$(\text{TiBTAC})\text{La}(\text{Me}_3\text{AlCH}_2\text{AlMe}_2\text{CH}_2\text{AlMe}_3)$ 16-La^{tBu}	2.491(3), 2.502(3)	[40d]
$(N\text{-nacnac})\text{La}[\text{C}(\text{SiPh}_3)(\text{SPPH}_2)]$ 29-La^{Ph}	2.465(2)	[49c]
Ce		
$(\text{NCN}^{\text{SiMe}_3})\text{Ce}[\text{CH}(\text{Ph}_2\text{P}=\text{NSiMe}_3)_2]$ 9-Ce^{SiMe3}	2.472(4)	[36b]
$(\text{NCN}^{\text{SiMe}_3})\text{Ce}(\text{ODipp})_2$ 11	2.441(5)	[36h]
$\{(\text{Ph}_2\text{P}=\text{NSiMe}_3)_2\text{C}\}_2\text{Ce}$	2.385(2)-2.399(3)	[37]
$[\{(\text{Ph}_2\text{P}=\text{S})_2\text{C}\}_2\text{Ce}][\text{K}(\text{18c6})(\text{thf})_2]$ 14-Ce	2.385(2), 2.399(3)	[37]
Pr		
$(\text{NCN}^{\text{SiMe}_3})\text{Pr}[\text{CH}(\text{Ph}_2\text{P}=\text{NSiMe}_3)_2]$ 9-Pr^{SiMe3}	2.458(5)	[36b]
$(\text{TMTAC})\text{Pr}(\text{Me}_3\text{AlCH}_2\text{AlMe}_2\text{CH}_2\text{AlMe}_3)$ 16-Pr^{Me}	2.456(6), 2.489(5)	[40d]
$(\text{TiBTAC})\text{Pr}(\text{Me}_3\text{AlCH}_2\text{AlMe}_2\text{CH}_2\text{AlMe}_3)$ 16-Pr^{tBu}	2.436(3), 2.459(3)	[40d]
Nd		
$(\text{NCN}^{i\text{Pr}})\text{Nd}[\text{CH}(\text{Ph}_2\text{P}=\text{NiPr})_2]$ 9-Nd^{iPr}	2.592(3)	[36c]
$\{\text{SiMe}_3(\text{Dipp})\text{N}\}_3\text{Nd}_3(\mu\text{-Me})_3(\mu_3\text{-Me})(\mu_3\text{-CH}_2)(\text{thf})_3$ 18-Nd	2.425(7)-2.505(8)	[5c]
Sm		
$(\text{NCN}^{\text{SiMe}_3})\text{Sm}(\text{NCy}_2)(\text{thf})$ 1	2.467(4)	[31]
$[(\text{SCS})\text{Sm}]_2$	2.371(6)	[32a]
$[(\text{SCS})_2\text{Sm}][\text{Li}(\text{thf})_4]$	2.491(5), 2.507(5)	[32a]
$(\text{NCN}^{\text{SiMe}_3})\text{Sm}[\text{CH}(\text{Ph}_2\text{P}=\text{NSiMe}_3)_2]$ 9-Sm	2.40(2)	[36b]
$(\text{TMTAC})\text{Sm}(\text{Me}_3\text{AlCH}_2\text{AlMe}_2\text{CH}_2\text{AlMe}_3)$ 16-Sm^{Me}	2.426(5), 2.441(5)	[40a]
$(\text{TiPTAC})\text{Sm}(\text{Me}_3\text{AlCH}_2\text{AlMe}_2\text{CH}_2\text{AlMe}_3)$ 16-Sm^{iPr}	2.464(8)	[40c]
$(\text{TMTAC})\text{Sm}\{\text{Sm}_2\text{CH}_3\}\{\text{C}[\text{Al}(\text{CH}_3)_3]_3\text{CH}_2\text{Al}(\text{CH}_3)_3\}_2$ 17-Sm^{Me}	2.408(4), 2.515(4)	[40a]
$(N\text{-nacnac})\text{Sm}[\text{C}(\text{SiMe}_3)(\text{SPPH}_2)]$ 29-Sm^{Me}	2.296(2)	[49c]
$(N\text{-nacnac})\text{Sm}[\text{C}(\text{SiPh}_3)(\text{SPPH}_2)]$ 29-Sm^{Ph}	2.357(4)	[49c]
Gd		
$(\text{NCN}^{\text{SiMe}_3})\text{Gd}[\text{CH}(\text{Ph}_2\text{P}=\text{NSiMe}_3)]$ 9-Gd^{SiMe3}	2.406(2)	[36b]

Dy		
[{(Ph ₂ P=S) ₂ C ₂ Ce}[K(18c6)(thf) ₂] 14-Dy	2.434(6), 2.433(6)	[39]
Ho		
{SiMe ₃ (Dipp)N} ₃ Ho ₃ (μ-Me) ₃ (μ ₃ -Me)(μ ₃ -CH ₂)(thf) ₃ 18-Ho	2.36(1)-2.43(1)	[5c]
Cp* ₃ Ho ₃ (μ-Me) ₃ (μ ₃ -Me)(μ ₃ -CH ₂)(thf) ₂ 21-Ho	2.275(4)-2.468(4)	[22a]
Er		
(NCN ^{SiMe₃})Er(CH ₂ Ph)(thf) 8-Er^{CH₂Ph}	2.339(4)	[36b]
(NCN ^{SiMe₃})ErI(thf) ₂ 10-Er^{SiMe₃}	2.322(2)	[36c]
Tm		
[(SCS)TmI] ₂	2.325(5)	[32b]
[(SCS) ₂ Tm][Li(thf) ₄]	2.423(9), 2.368(3)	[32b]
Cp* ₃ Tm ₃ (μ-Me) ₃ (μ ₃ -Me)(μ ₃ -CH ₂)(thf) ₃ 20-Tm	2.330(5)-2.365(5)	[5b]
[Cp* ₃ Tm(μ ₃ -CH ₂) ₄] 22-Tm^{Cp*}	2.319(5)-2.424(5)	[5b]
Lu		
{SiMe ₃ (Dipp)N} ₃ Lu ₃ (μ-Me) ₃ (μ ₃ -Me)(μ ₃ -CH ₂)(thf) ₃ 18-Lu	2.310(5)-2.383(5)	[5a]
(PhC(NDipp) ₂) ₃ Lu ₃ (μ-Me) ₃ (μ ₃ -Me)(μ ₃ -CH ₂)(thf) ₃ 19-Lu	2.371(9)-2.381(8)	[42a]
Cp* ₃ Lu ₃ (μ-Me) ₃ (μ ₃ -Me)(μ ₃ -CH ₂)(thf) ₃ 20-Lu^{Cp*}	av. 2.49(1)	[5b]
[Cp* ₃ Lu(μ ₃ -CH ₂) ₄] 22-Lu^{Cp*}	2.333(4)-2.396(4)	[43]
[Cp* ₃ Lu(μ ₃ -CH ₂) ₄] 22-Lu^{Cp*}	2.32(1)-2.41(1)	[5b]
(BODDI)Lu ₂ (CH ₂ SiMe ₃) ₂ (CHSiMe ₃)(thf) ₂ 23	2.309(6)	[45]
(CTp ^{Me, Me}) ₂ Lu ₂ (CHSiMe ₃)(dmpz) ₂	2.300(6)	[47]
(Dipp-nacnac)Lu(CHPh ₃)(CH ₂ SiMe ₃) 27-Lu	2.19(1)	[49a]
(N-nacnac)Lu[C(SiMe ₃)(SPh ₂)] 29-Lu^{Me}	2.204(3)	[49c]
(N-nacnac)Lu[C(SiPh ₃)(SPh ₂)] 29-Lu^{Ph}	2.245(3)	[49c]

5 Reactivity of Rare-Earth-Metal Alkylidenes

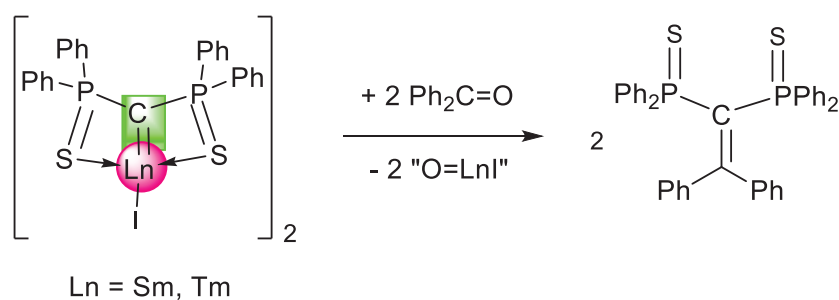
The reactivity of rare-earth-metal alkylidenes is a result of the highly nucleophilic character of the $R'RC^{2-}$ unit. For better comparison of the different types of rare-earth-metal alkylidene complexes and thereof the various reactivity observed, the alkylidenes mentioned in chapter 3 will be subclassified in three different categories, according to their reactivity towards different substrates. This chapter will solely focus on reactivity of alkylidene complexes, excluding *e.g.* ligand-based reduction as observed for complex **25**.^[48]



Scheme 18. Subclassification of the different alkylidene rare-earth-metal complexes according to their reactivity.

5.1 Pincer-Type Rare-Earth-Metal Alkylidenes

Since the rare-earth-metal alkylidene chemistry was still in its infancy when CAVELL made his discoveries about pincer-like rare-earth-metal alkylidenes in 2000, the electronic nature and the reactivity of the alkylidene still needed to be evaluated. Naturally, first attempts wanted to point out reactivity similar to transition metal based SCHROCK-type nucleophilic carbene complexes and therefore, LE FLOCH attempted the reaction of $[\{ (\text{Ph}_2\text{P}=\text{S})_2\text{C} \} \text{SmI}]_2$ with benzophenone and succeeded in the formation of the respective olefin representing WITTIG-type reactivity.^[32a]

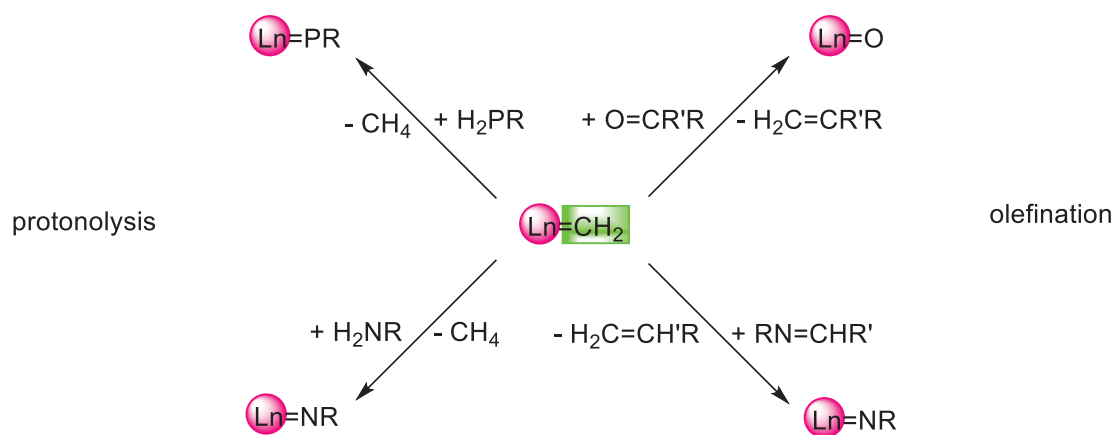


Scheme 19. WITTIG-type reactivity of pincer-like rare-earth-metal complexes.

Since then, it appeared, that the reactivity of a hypervalent phosphorus-stabilized geminal dianion coordinated to a metal center is comparable to other, *e.g.* multimetallic rare-earth-metal alkylidene complexes and their reactivity similar to the TEBBE reagent. Later, MÉZAILLES also proved this reactivity for the thulium congener $[\{(Ph_2P=S)_2C\}TmI]_2$.^[32b] Furthermore, $10-Y^{SiMe_3}$ was shown to convert $SCNtBu$ into the respective olefin $(Ph_2P=NSiMe_3)_2C=CNtBu$, however, amines as $DippNH_2$ revealed only addition to the $Y-C$ double bond.^[50] It is noteworthy that complexes with alkyl groups R instead of the halogenido ligand did not undergo these displacement reactions with the alkylidene moiety, however, they add Ph_2CO to the respective alkyl R . The same reactivity was observed with azoderivatives $RN=NR$.^[36a, 51] Similar to $[\{(Ph_2P=S)_2C\}SmI]_2$, the tetravalent cerium analog $\{(Ph_2P=NSiMe_3)_2C\}Ce(ODipp)_2$ **11** was found to undergo also WITTIG-type reactions with carbonyl functionalities as in benzaldehyde, and others.^[36h] As the reactivity of pincer-like rare-earth-metal alkylidene complexes is not the main emphasis of this thesis, we like to refer to other references for further interests in this particular chemistry.^[50, 52]

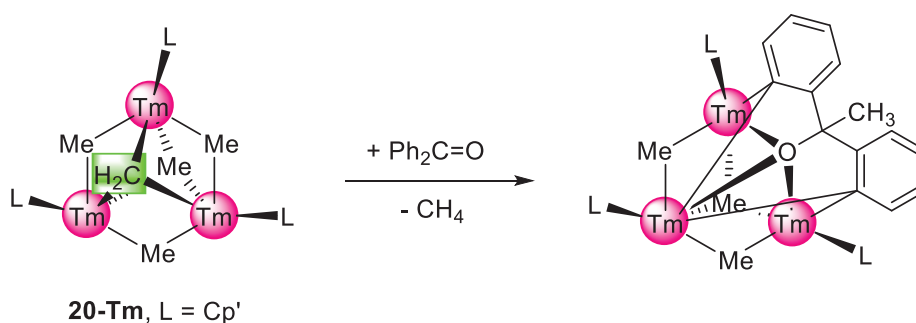
5.2 Multimetallic and TEBBE-like Rare-Earth-Metal Alkylidenes

Since the reactivity of the rare-earth-metal alkylidenes is mainly controlled by the nucleophilic character and the expected double bond character of the $M=CRR'$ moiety, reagents with polarized unsaturated bonds like $R'RC=O$ seemed promising for proving reactivity according to SCHROCK-type alkylidenes. Interestingly, complexes mentioned in chapter 3 undergo olefination reactions with various carbonyl compounds (*e.g.* 9-fluorenone, benzophenone, benzaldehyde, and cyclohexanone). For instance, TEBBE-like rare-earth-metal complexes **3**,^[27]



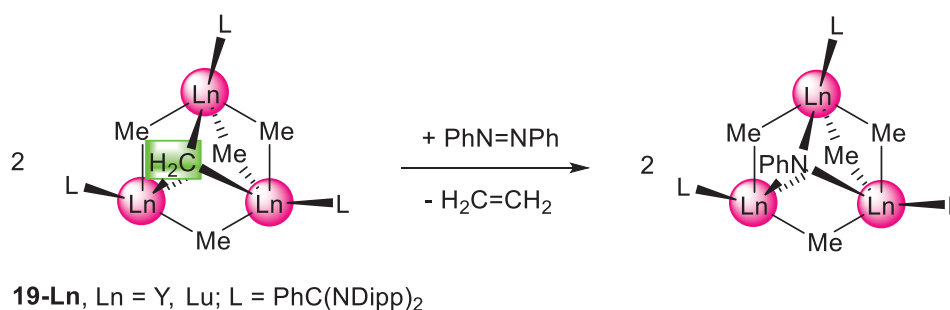
Scheme 20. Protonolysis and olefination reactivity of rare-earth-metal alkylidene complexes. For the sake of readability, a methylidene moiety is shown, although also alkylidene moieties as in complex **23** are known to convert for example, carbonylic substrates.

4,^[34] trimetallic complexes with μ_3 -bridging CH_2^{2-} such as **2-Ln**,^[33] **18-Ln**,^[5a, c] **19-Ln**,^[42] cubane-like **22-Ln**,^[5b] and also the methandiide lutetium complex **23**^[45] showed good conversion of the carbonylic functionality to the respective olefin (Scheme 20, top right). Different to this, no C=O bond cleavage was observed for the addition of benzophenone to **20-Tm** but the selective addition to the methyldiene moiety and further double C–H-bond activation of the phenyl groups of the benzophenone (Scheme 21).^[5b]



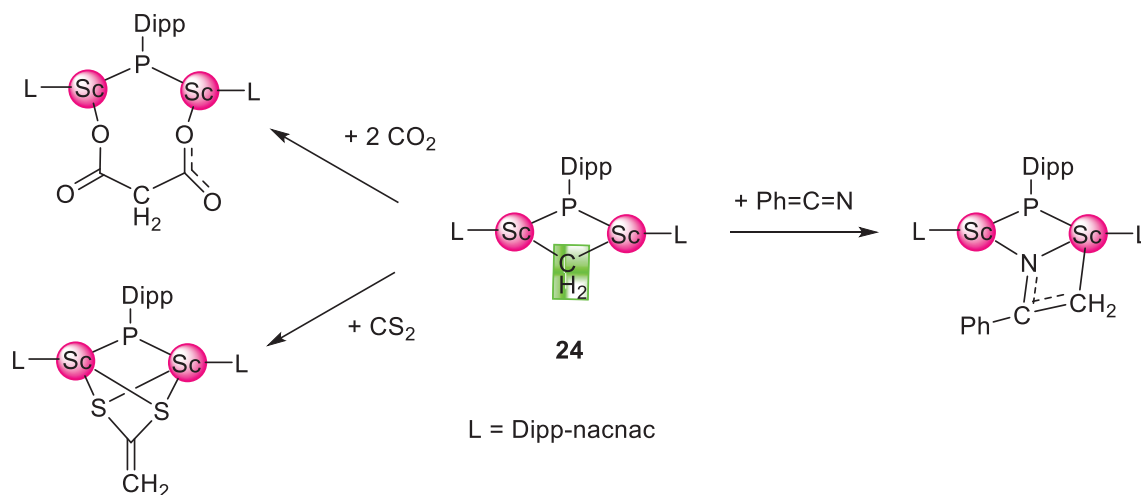
Scheme 21. Addition reaction of benzophenone to **20-Tm**.

It is only plausible that rare-earth-metal methyldiene complexes were tested in the cleavage of other unsaturated bonds as C=N and N=N. The investigation into the olefination capability of **19-Ln** showed conversion of azobenzene to ethene *via* N=N- followed by C=N-bond cleavage (Scheme 22).^[53] Furthermore, these complexes are capable of converting *N*-methylethaniline to the respective rare-earth-metal imide complexes (Scheme 20, bottom right). The bimetallic lutetium methandiide complex (BODDI)Lu₂(CH₂SiMe₃)₂(CHSiMe₃)(thf)₂ **23** was also treated with PhN=C=O and insertion into the Lu–CH₂ bond was observed.^[45] The same Lu–C bond cleavage was also found for complexes **23** and **24** reacted with triple bonds as in isocyanide *t*BuNC as isoelectronic analog to CO.^[45-46]



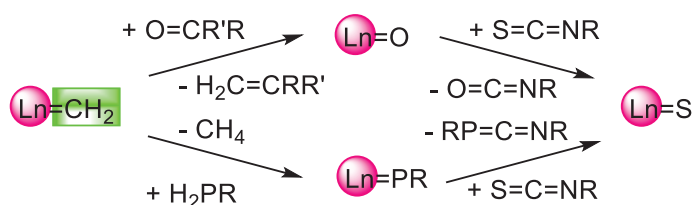
Scheme 22. N=N-bond cleavage of azobenzene with **19-Ln**.

Scandium complex **24** is further capable of nucleophilic addition reactions with benzonitrile for the monoaddition product (Scheme 23, right), activation of two CO₂ molecules for a [CH₂(CO₂)₂]²⁻ anion bridging the metal centers, as well as the reaction with CS₂ forming a ethene dithiolate scandium complex (Scheme 23, left).



Scheme 23. Reactivity of complex **24** towards CO₂, CS₂, and benzonitrile.

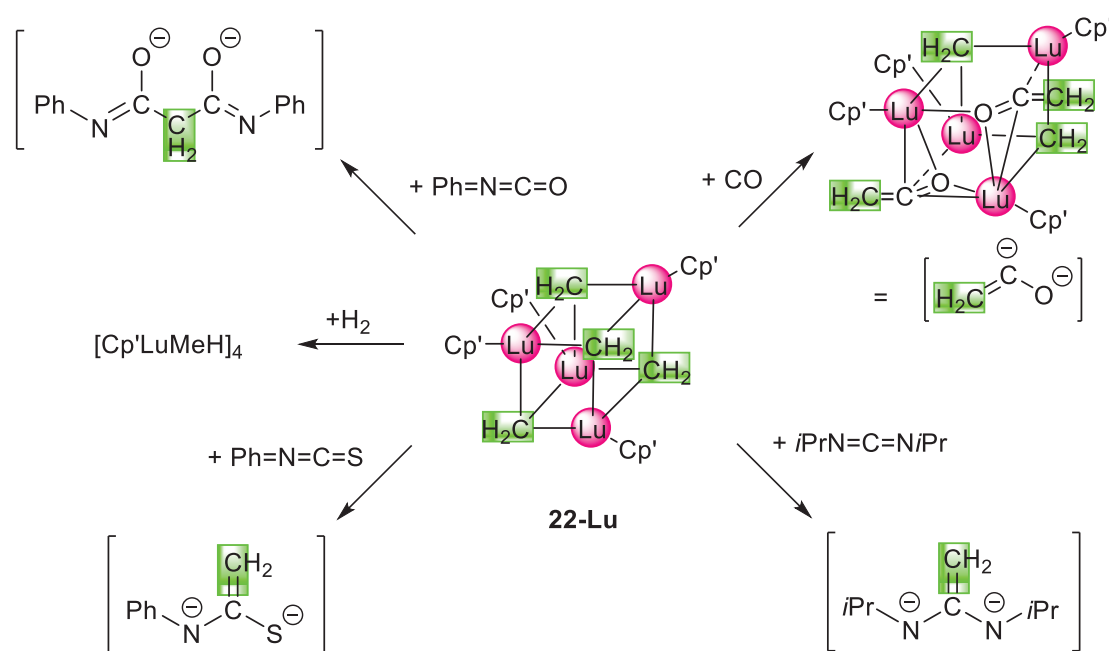
It is noteworthy that rare-earth-metal Ln=S bonds can also be achieved with complexes **19-Ln**, however, a two-step reaction is involved: CH₂²⁻ → O²⁻ → S²⁻[^{42b}] or CH₂²⁻ → P²⁻ → S²⁻[⁵⁴] (Scheme 24).



Scheme 24. Schematic presentation of the two-step-reaction for the generation of Ln=S bonds.

Additionally, rare-earth-metal methylidene complexes can also be utilized in protonolysis reactions with H₂NR or H₂PR for the generation of imide or phosphinidene compounds (Scheme 20, left). The H–N-bond cleavage of complexes **19-Ln** (Ln = Y, Lu) and **23** *e.g.* with H₂NDipp were successful.^[45, 53] Attempting protonolysis reactions with **3** and H₂NDipp, however, did not lead to the respective imide but gave the addition product, a methyl/amine complex.^[27] Reactivity studies involving **19-Ln** (Ln = Y, Lu) and PhPH₂ showed good conversion to a rare mixed methyl phosphinidene complex (PhC(NDipp)₂)₃Ln₃(μ-Me)₃(μ₃-Me)(μ₃-PPh).^[54]

In addition to the reactivity discussed already, the unique reactivity of cubane-like **22-Lu** as a rare-earth-metal representative with solely “ $\text{Ln}=\text{CH}_2$ ” units is of major interest. As mentioned before, complexes **22-Ln** are capable of WITTIG-type olefinations (Scheme 20, top right). Further, the lutetium complex also exhibits reactivity toward CO (insertion of CO into the Lu– CH_2 bond) for the formation of an intermediate acyl species and further rearrangement to a bis(ketene dianion) lutetium methylidene complex (Scheme 25, top right, the structure of the CO-inserted complex as well as the newly generated $\text{CH}_2\text{CO}^{2-}$ unit is depicted).^[55] The reaction of **22-Lu** with one equivalent of a carbodiimide favors the formation of ethylene diamido lutetium complex in an addition reaction (Scheme 25, bottom right).^[55] Similarly, the reaction toward unsaturated C=S bonds as in phenylisothiocyanate yielded in an ethylene amido thiolate (Scheme 25, bottom left).^[55] Reaction of **22-Lu** with four equivalents of phenylisocyanate led to a malonodiimide lutetium methylidene complex with two equivalents of the C=O unsaturated substrate added to the CH_2^{2-} unit (Scheme 25, top left).^[55] Hydrogenolysis attempts showed conversion to the respective hydride/methyl complex $[\text{Cp}'\text{LnHMe}]_4$ as one of the few examples of mixed methyl/hydride rare-earth-metal complexes (Scheme 25, middle left). Here, also the selective protonolysis of solely one methylidene group was achieved.^[56]



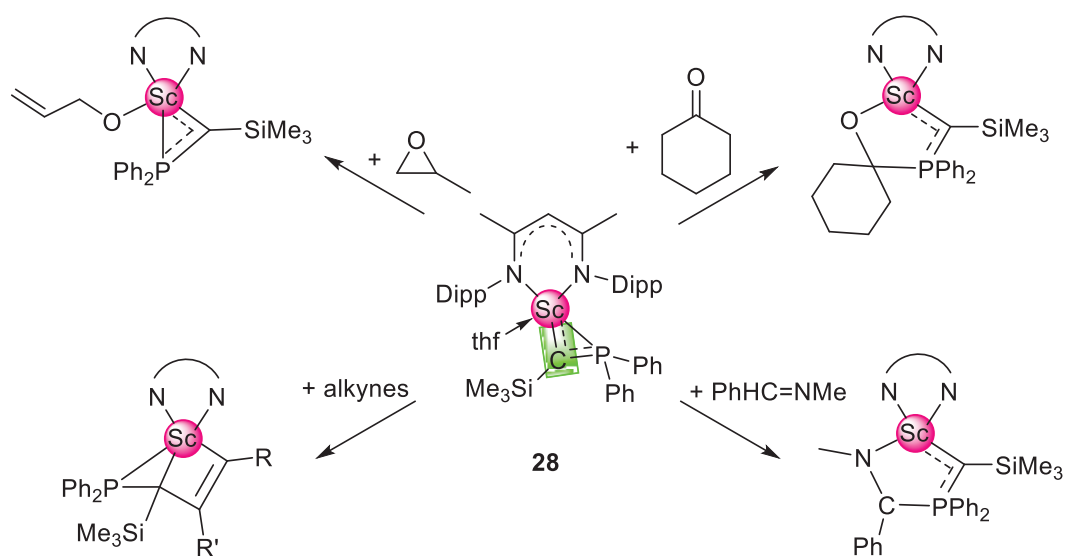
Scheme 25. Reactivity of **22-Lu** toward phenylisocyanate, CO, carbodiimide $i\text{PrNCNiPr}$, phenylisothiocyanate, and dihydrogen. For improved readability only the generated organic fragment is depicted.

For all pathways showing reactions with unsaturated bonds in Scheme 25, one or respectively two (for CO and PHNCO) methylidene moieties react with the introduced substrate, however,

the cluster integrity of the remaining “LLn=CH₂” units with the four rare-earth metal centers and the remaining bridging methyldiene units is retained.

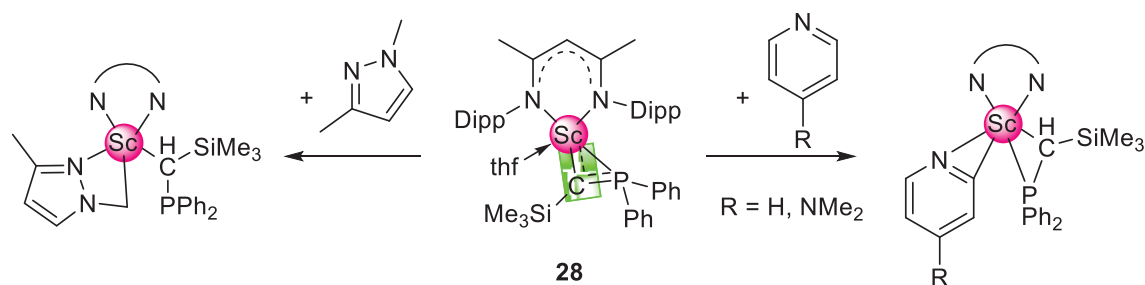
5.3 Monometallic Donor-Stabilized Rare-Earth-Metal Alkylidenes

Different to the typically observed WITTIG-type reactivity of the rare-earth-metal alkylidene complexes (chapter 5.2), the recently developed monometallic rare-earth-metal alkylidenes **26-29** do not show olefination reactions with unsaturated C=O bonds, however, addition reactions were observed for **28** (Scheme 26, top right).^[57] Reaction of **28** with benzyldenemethanamine led to insertion into the Sc–P bond and addition of the amine (Scheme 26, bottom right).^[57] The reaction with different sterically demanding alkynes gave scandacycloalkenes in a cycloaddition reaction (Scheme 26, left bottom).^[57] Additionally, the reaction of propylene oxide (Scheme 26, top left) as well as 3,5-dimethylisoxazole or pinacolborane (not depicted but analogous) with complex **28** led to C–O-, C–N-, and C–B-bond cleavage, respectively, and to Sc–O-bond formation due to the high oxophilicity of the rare-earth metal.^[57]



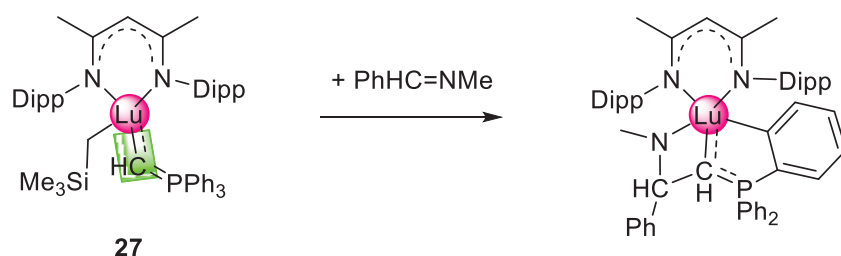
Scheme 26. Exemplary reactivity of **28** towards propylene oxide, cyclohexanone, benzyldenemethanamine, and alkynes. The Dipp-nacnac ligand is abbreviated in the products for better readability.

Supplemental to the reactivity shown in Scheme 26, complex **28** also undergoes C–H-bond activation of pyridine derivatives, and pyrazoles (Scheme 27).^[49b]



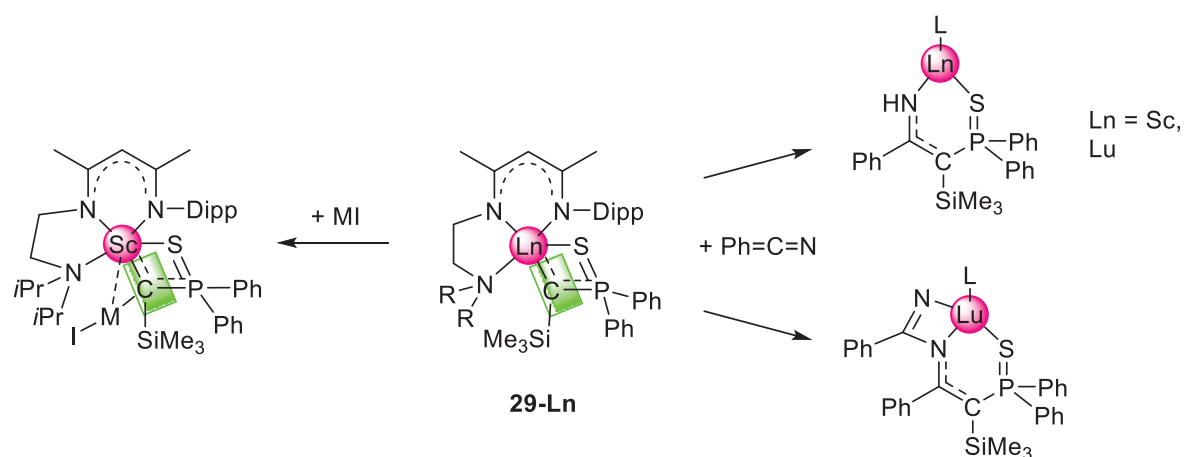
Scheme 27. Reactivity of complex **28** with pyridine derivatives and pyrazoles.

It is noteworthy that contrary to the reactivity of complex **28**, monometallic complex **27** reacts with benzylidenemethanamine under addition to the Lu–C bond including C–H-bond activation of one phenyl group (Scheme 28).^[49a]



Scheme 28. Reactivity observed for complex **27** with benzylidenemethanamine.

Further, heterobimetallic complexes with copper and silver (M) were achieved by the reaction of **29-Ln** with MI as well as different motifs for the cycloaddition of benzonitril (Scheme 29).^[49c, d]



Scheme 29. Generation of heterobimetallic rare-earth-metal transition-metal complexes (left) and different cycloaddition reactions with benzonitrile (right). For better readability the *N*-nacnac ligand is shown as L.

B

Summary of the Main Results

1 Rare-Earth-Metal Complexes as Precursors for Alkylidenes

In transition-metal chemistry, common protocols for the formation of alkylidenes are the abstraction of a leaving group followed by deprotonation of a hydrocarbyl fragment as it was found for the generation of $(\text{PN})_2\text{Ti}(\text{CH}_2)$ ($\text{PN} = (\text{N}(2\text{-}(\text{diisopropylphosphino})\text{-4-methylphenyl})\text{-2,4,6-trimethylanilide})$) by MINDIOLA and co-workers^[58] and moreover, thermolysis and alkane elimination, e.g. for PETASIS' reagent $\text{Cp}_2\text{Ti}(\text{CH}_3)_2$ as well as $\text{Cp}_2\text{Ti}(\text{R})(\text{CH}_2\text{SiMe}_3)$ ($\text{R} = \text{Me}, \text{CH}_2\text{SiMe}_3$).^[59] Here, the reactive alkylidene moiety $\text{Cp}_2\text{Ti}(\text{CHR})$ is generated *in situ* at elevated temperatures. Heteroleptic rare-earth-metal complexes suitable to adopt this concept still need to be developed.

Similar to the above mentioned PN ligand, the $\text{Tp}^{\text{tBu,Me}}$ ligand ($\text{Tp}^{\text{tBu,Me}} = \text{tris}(3\text{-tert-butyl-5-methyl-pyrazolyl})\text{borato}$) represents a very bulky tridentate ligand potentially suitable for the stabilization of terminal alkylidene complexes and their reactive precursors. Mixed Me/OTf complexes **A**_{L_n} and **C**, as well as bis(triflate) complexes **B** and **D** were synthesized from $\text{Tp}^{\text{tBu,Me}}\text{LnMe}(\text{AlMe}_4)^{[20]}$ ($\text{Ln} = \text{Y}, \text{Lu}$) or $\text{Tp}^{\text{tBu,Me}}\text{LuMe}_2^{[25]}$ by applying a silane-elimination protocol (Figures S1 and S2).^[60] It is noteworthy that all obtained yttrium complexes show decomposition at ambient temperature, however, the lutetium analogs withstand even temperatures up to 50 °C. Treatment of all heteroleptic complexes **A**_{L_n} and **C** with the WITTIG reagent $\text{H}_2\text{C}=\text{PPh}_3$ did not give reactivity analogous to transition-metal chemistry, however, elevated temperatures only led to C–H-bond activation of the *t*Bu moieties of the ancillary

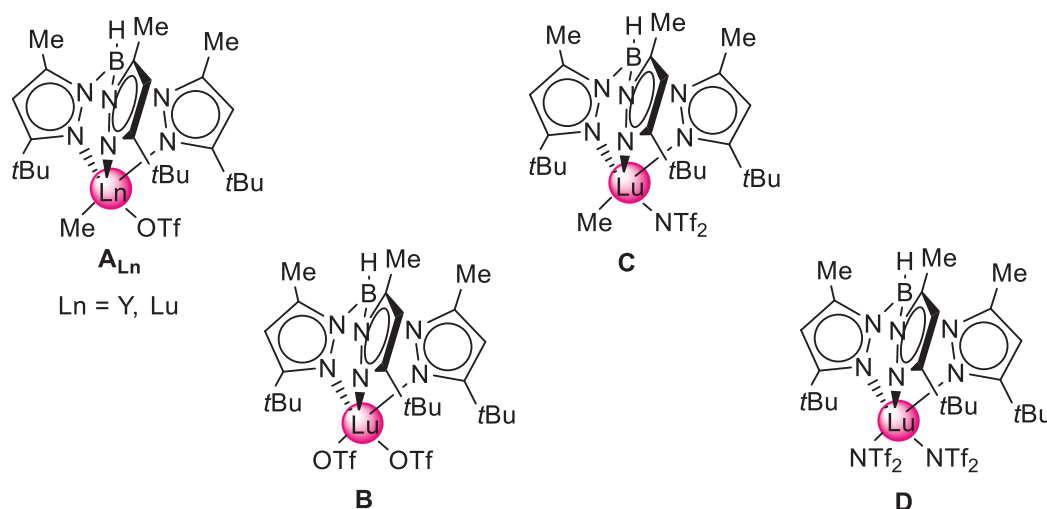


Figure S1. Heteroleptic methyl, triflate, and triflimide rare-earth-metal complexes stabilized by $\text{Tp}^{\text{tBu,Me}}$.

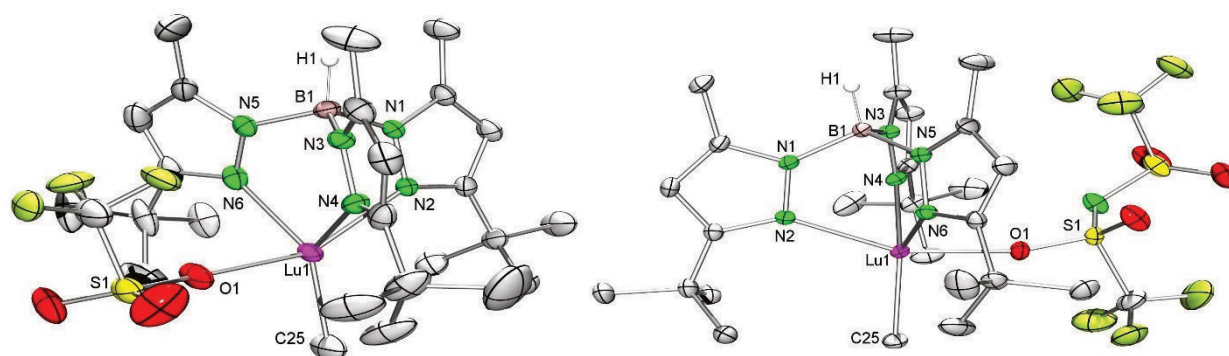
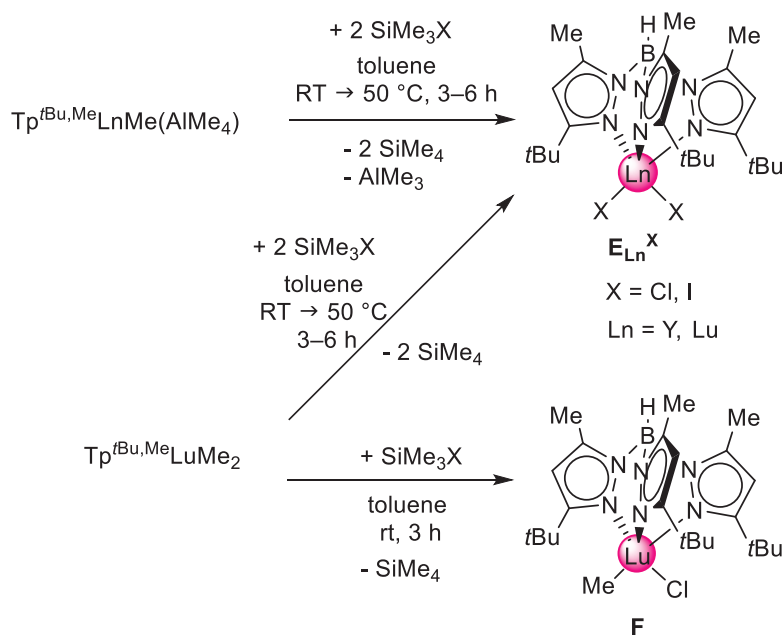


Figure S2. Solid-state structures of Tp^{tBu,Me}LuMeOTf (A_{Lu}) and Tp^{tBu,Me}LuMeNTf₂ (C).

ligand. Nonetheless, these very reactive mixed Me/OTf or Me/NTf₂ structural motives have not yet been found for Tp-supported rare-earth-metal complexes (**Paper I**).^[61]

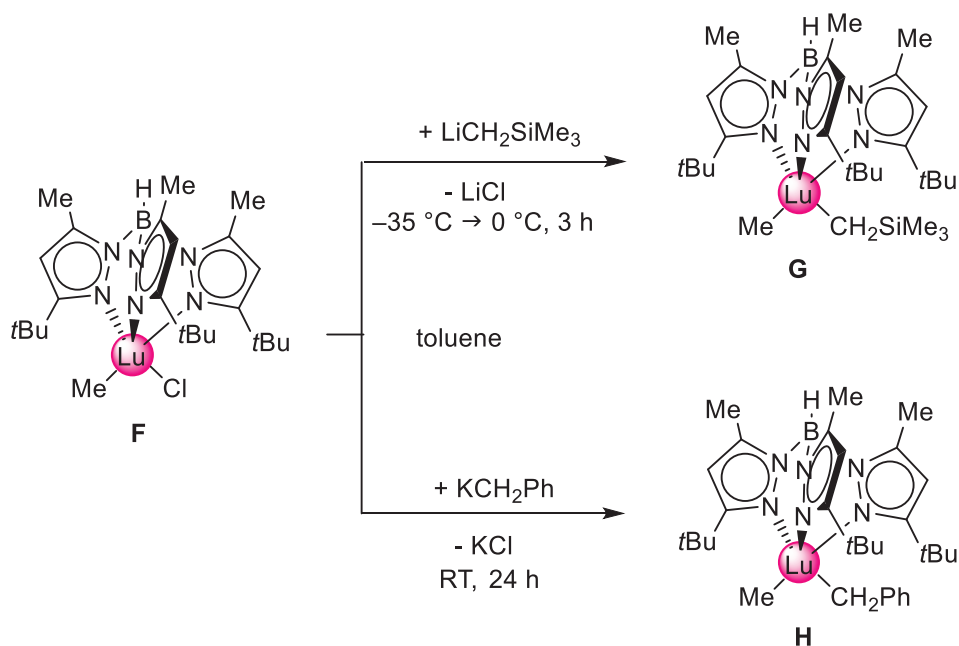
As described before, another concept of targeting alkylidenes originates from mixed methyl/alkyl complexes capable of intramolecular elimination of methane or alkanes by thermolysis or treatment with strong donor ligands.^[59] Therefore, mixed precursors were established by treatment of Tp^{tBu,Me}LnMe(AlMe₄) as well as Tp^{tBu,Me}LuMe₂ with mild halogenido transfer reagents SiMe₃X (X = Cl, I) for the generation of bis(halide) and mixed methyl/halide complexes. Hence, the isolation of mixed methyl/chloride complex **F** succeeded (Scheme S1).



Scheme S1. Heteroleptic methyl, triflate, triflimido, and halogenido rare-earth-metal complexes stabilized by the Tp^{tBu,Me} ligand.

Additionally, other mixed methyl/halogenido combinations were found to undergo ligand scrambling and therefore bis(halide) complexes E_{Ln}^X could be isolated (**Paper I**). It is noteworthy that the isolation of heteroleptic halide complexes with the tris(pyrazolyl)borato ligand is known to be complicated due to B–N-bond cleavage.^[62] Additionally, tests for TEBBE-like complexes with E_{Ln}^{Cl} and two equiv. of $AlMe_3$ led to unidentified complicated reaction mixtures, mainly followed by ligand degradation.

Aiming at rare-earth-metal complexes similar to the PETASIS reagent, the reactivity of $Tp^{tBu,Me}LuMe_2$ in olefination reactions with 9-fluorenone at 50 °C was assessed, however, only the respective alkoxide species was found. In another approach, mixed alkyl complexes were synthesized by utilizing **F** in salt-metathesis reactions with $LiCH_2SiMe_3$ and KCH_2Ph to afford complexes **G** and **H** (Scheme S2, Figure S3). Here, careful adjustment of the reaction conditions is crucial, since especially the reaction of **F** in combination with lithium salts at ambient temperatures favors the undesired formation of $LiTp^{tBu,Me}$. In contrast to this, the formation of **H** needed prolonged reaction times.



Scheme S2. Synthesis of $Tp^{tBu,Me}LuMe(CH_2SiMe_3)$ (**G**, left) and $Tp^{tBu,Me}LuMe(CH_2Ph)$ (**H**, right).

The examination of the thermolysis capability of the di(alkyl) complexes **G** and **H** revealed that **G** is already slowly decomposing at ambient temperature. Unfortunately, an intramolecular C–H-bond activation of the ancillary ligand was observed.^[63] Regardless, complex **H** is more stable at ambient temperature, but shows the same degradation process at 40 °C. The attempted

donor-induced alkane elimination with the introduction of *N*- or *O*-donors (DMAP or THF) under mild conditions, however, failed.

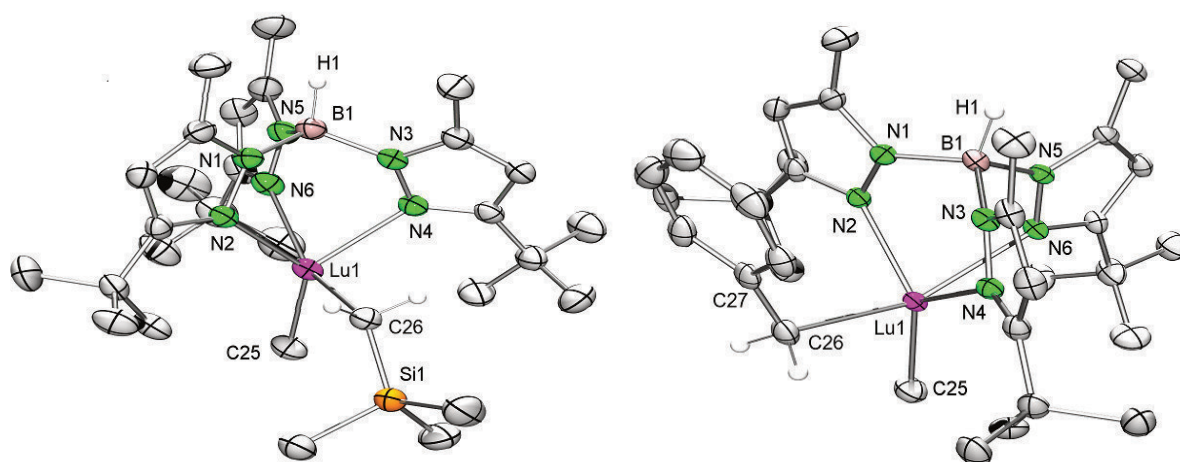


Figure S3. Crystal structures of $\text{Tp}^{\text{tBu,Me}}\text{LuMe}(\text{CH}_2\text{SiMe}_3)$ (**G**, left) and $\text{Tp}^{\text{tBu,Me}}\text{LuMe}(\text{CH}_2\text{Ph})$ (**H**, right).

The successful isolation of these heteroleptic methyl/triflato, methyl/triflimido, bis(halide), methyl/chlorido, and mixed alkyl complexes supported by the $\text{Tp}^{\text{tBu,Me}}$ ligand spurred the interest in the steric effects of this ligand set and its flexibility to bear sterically demanding co-ligands. In order to determine the steric shielding by the bulky tris(pyrazolyl)borato ligand, the mathematically exact cone angles were calculated for structurally characterized heteroleptic lutetium complexes as depicted in Table S1 (**Paper I**).^[64] It was found that the very exclusive trigonal bipyramidal geometry around the metal centers gave similar cone angles. This finding revealed that the scorpionate ligand adapts only slightly to the steric demand of the co-ligands.

Table S1. Overview of mathematically exact calculated cone angles θ [°] of **A_{Lu}**, **C**, **E_{Lu}^I**, **F**, **G**, and **H**.

	A_{Lu}	C	E_{Lu}^I	F	G	H
θ	278.0 / 280.9	280.4	278.2	278.9	277.1	277.3

Nevertheless, the calculated cone angles show a noticeable trend where the mixed alkyl complexes **G** and **H** involve the smallest cone angle, followed by the halogenido-containing complexes **E_{Lu}^I** and **F**. Moreover, the most flexible and most weakly coordinating triflato and triflimido ligands allow for the largest cone angles of the ancillary ligand.

2 Mixed Methyl/Aryloxy Rare-Earth-Metal Complexes

The chemistry of rare-earth-metal methyl or alkyl compounds is considered to be extremely challenging due to the very reactive nature of the Ln–C(alkyl) (R = alkyl) bond, which is indicated by the large orbital energy mismatch between the rare-earth metals and the alkyl fragment.^[9c, 11, 15a, 65] One objective of this work was to investigate these very reactive and elusive compounds with the introduction of a stabilizing environment and consequently the formation of heteroleptic rare-earth-metal compounds bearing one methyl group. This could be achieved through the utilization of the very bulky monoanionic Tp ligand as well as the introduction of various aryloxy ligands.

First, examination of the performance of the reactive precursor $\text{Tp}^{\text{tBu,Me}}\text{LuMe}_2$ ^[25] in protonolysis reactions toward HOAr (Ar = $\text{C}_6\text{H}_3\text{Me}_2$ -2,6; $\text{C}_6\text{H}_3\text{iPr}_2$ -2,6; $\text{C}_6\text{H}_3(\text{CF}_3)_2$ -3,5, $\text{C}_6\text{H}_3\text{tBu}_2$ -2,6-Me-4) was elucidated (Figures S4-S6). Interestingly, the steric demand of the

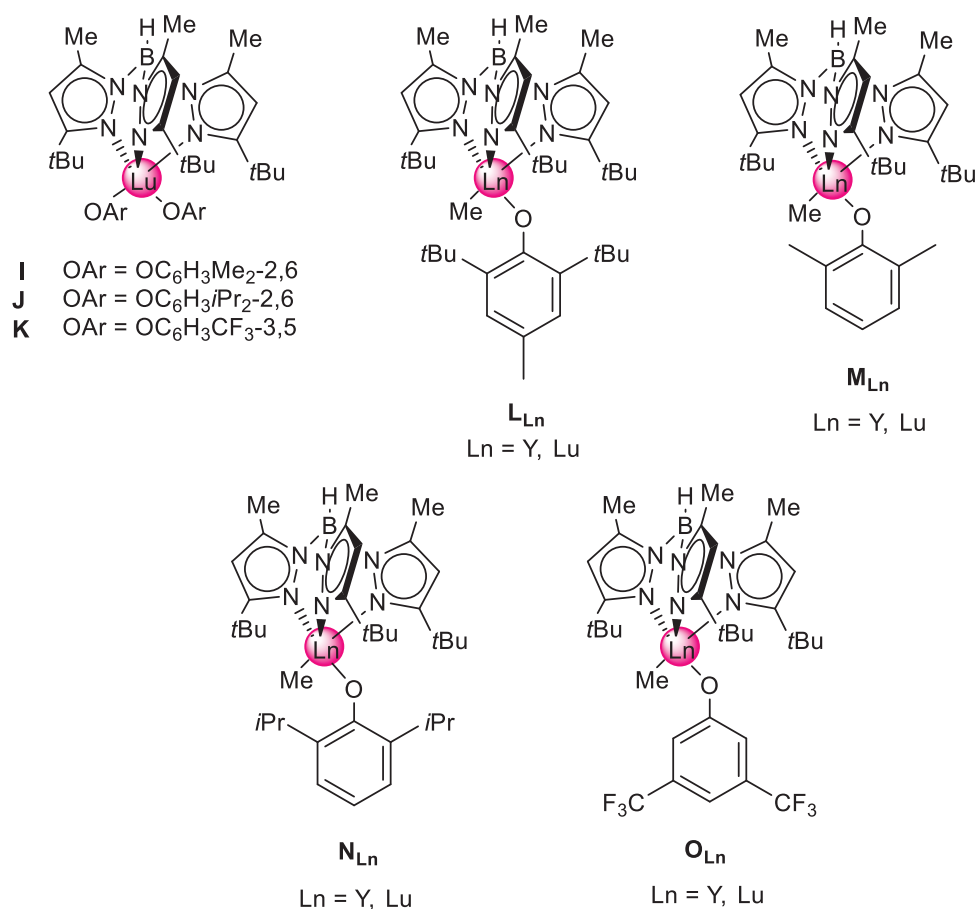


Figure S4. Mononuclear $\text{Tp}^{\text{tBu,Me}}\text{Ln}(\text{OAr})_2$ (**I**, **J**, **K**, left) and mixed methyl/aryloxy $\text{Tp}^{\text{tBu,Me}}\text{LuMe}(\text{OAr})$ (**L_{Ln}**, **M_{Ln}**, **N_{Ln}**, **O_{Ln}**, middle and right).

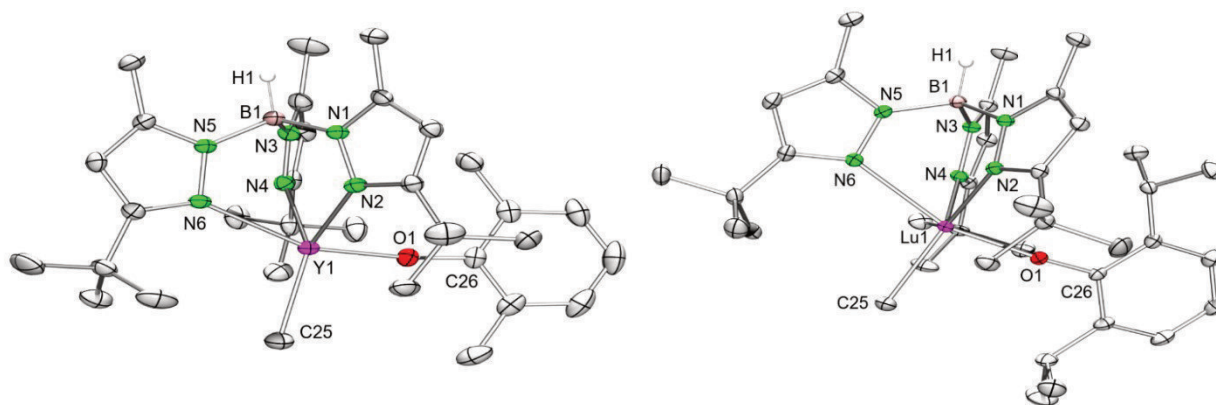


Figure S5. Crystal structures of $\text{Tp}^{t\text{Bu},\text{Me}}\text{YMe}(\text{OC}_6\text{H}_3\text{Me}_{2-2,6})$ (M_Y , left) and $\text{Tp}^{t\text{Bu},\text{Me}}\text{LuMe}(\text{OC}_6\text{H}_3i\text{Pr}_{2-2,6})$ (N_Lu , right).

introduced aryloxo ligand controls the formation of either bis(aryloxo) compounds **I**, **J**, and **K** or, with increased steric bulk in 2- and 6-position, the mixed methyl/aryloxo complex L_Ln . Subsequently, a salt-metathetical approach was chosen starting with $\text{Tp}^{t\text{Bu},\text{Me}}\text{LnMe}(\text{AlMe}_4)^{[20]}$ ($\text{Ln} = \text{Y}, \text{Lu}$) to access smaller aryloxides and yttrium analogs (**Paper II**).^[66] It was found that optimization of the reaction conditions is crucial and fast degradation proceeds with B–N-bond cleavage of the ancillary Tp ligand, if not prevented by lower temperature (especially for **L**_Y and **O**_Y, the latter with the electron-deficient aryloxo ligand), underlining the reactive nature of the Ln–Me bond. Interestingly, the striking structural similarities between L_Lu , M_Ln , N_Ln , and O_Ln determined by XRD mainly result from the κ_3 -coordination of the Tp ligand causing the routinely observed distorted trigonal bipyramidal geometry around the different metal centers (Figures S5 and S6).

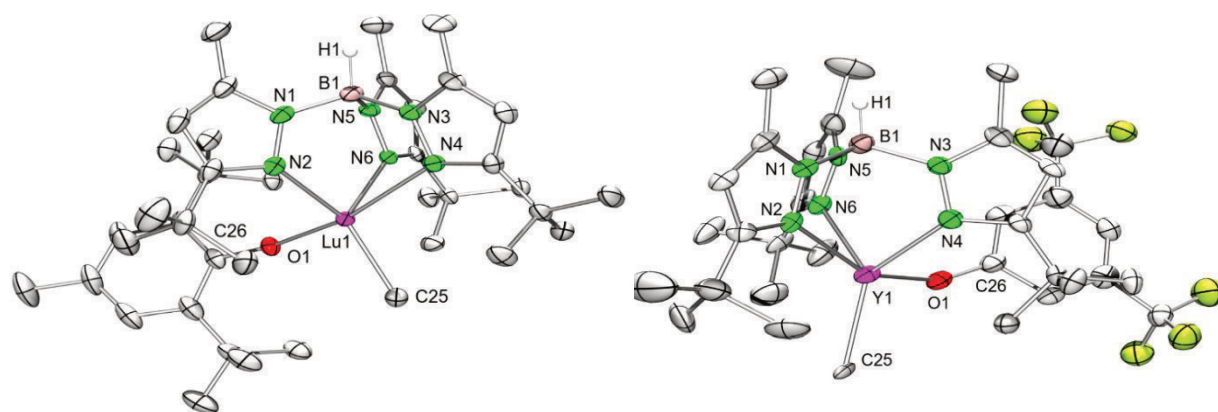


Figure S6. Crystal structures of $\text{Tp}^{t\text{Bu},\text{Me}}\text{LuMe}(\text{OC}_6\text{H}_2t\text{Bu}_{2-2,6}\text{CH}_3\text{-4})$ (L_Lu , left) and $\text{Tp}^{t\text{Bu},\text{Me}}\text{LuMe}\{\text{OC}_6\text{H}_3(\text{CF}_3)_{2-3,5}\}$ (O_Y , right).

To gain further insight into the reactivity of these terminal methyl moieties, the performance of L_Ln in isoprene polymerization was exemplarily examined as well as its thermal stability. Noteworthy, the addition of DMAP during the protonolysis reaction of the precursor

$\text{Tp}^{t\text{Bu},\text{Me}}\text{LnMe}(\text{AlMe}_4)$ and $\text{HOC}_6\text{H}_3t\text{Bu}_{2,6}\text{-Me-4}$, the ionic species \mathbf{P}_{Ln} is formed (Figure S7). Unfortunately, complexes \mathbf{P}_{Ln} are not active as single-component catalyst in isoprene polymerization. The thermal stability of \mathbf{L}_{Y} was examined, revealing that the heteroleptic complex decomposes at ambient temperatures to an ill-defined product mixture *via* B–N-bond cleavage of the ancillary ligand. Interestingly, the Lu congener \mathbf{L}_{Lu} is inert up to 60 °C however, at elevated temperatures intramolecular C–H-bond activation of the ligand *t*Bu groups with the Lu–Me moiety occurs. To conclude, the feasibility to isolate heteroleptic methyl/aryloxy complexes strongly depends on the precursor. Furthermore, the thermal stability of all generated complexes depends on the rare-earth metal (lutetium more stable than yttrium) as well as on the introduced aryloxy ligand: $\text{C}_6\text{H}_3\text{Me}_{2,6}$ with the most stabilizing effect, whereas very bulky and electron-deficient methyl/aryloxy complexes decompose readily at elevated temperatures (**Paper II**).

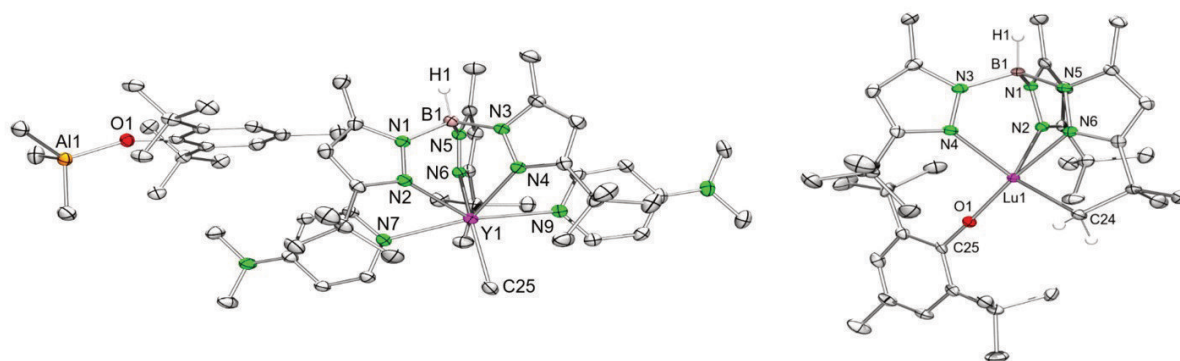


Figure S7. Crystal structures of $[\text{Tp}^{t\text{Bu},\text{Me}}\text{YMe}][\text{Me}_3\text{AlOC}_6\text{H}_3t\text{Bu}_{2,6}\text{-Me-4}]$ (\mathbf{P}_{Y} , left) and $(\text{Tp}^{(t\text{Bu-H})/(t\text{Bu})_2,\text{Me}}\text{Lu}(\text{OC}_6\text{H}_2t\text{Bu}_{2,6}\text{-Me-4}))(\text{Tp}^{(t\text{Bu-H})/(t\text{Bu})_2,\text{Me}} = \text{hydrobis}(3\text{-Me-5-}t\text{Bu-pyrazolyl})\{\mu\text{-}(3\text{-Me-5-Me}_2\text{C-CH}_2\text{pyrazolyl})\}\text{borato})$ (\mathbf{Q}_{Lu} , right).

Subsequently, the sterical aspects of the introduced aryloxy ligand *via* calculation of the mathematically exact cone angle accessible *via* X-ray structure analyses were investigated.^[64] The $\text{Tp}^{t\text{Bu},\text{Me}}$ complexes adopt a trigonal bipyramidal geometry and hence, similar cone angles were determined with regard of the metal center (Table S2, **Paper II**). Interestingly, for the Y complexes methyl groups in 2- and 6-position of the aryl ligand demand the cone to open more than *i*Pr groups or the CF_3 groups in 3- and 5-position ($\mathbf{M}_{\text{Y}} < \mathbf{N}_{\text{Y}} < \mathbf{O}_{\text{Y}}$). A similar trend was observed for the Lu congener ($\mathbf{M}_{\text{Lu}} < \mathbf{L}_{\text{Lu}} < \mathbf{N}_{\text{Lu}} < \mathbf{O}_{\text{Lu}}$).

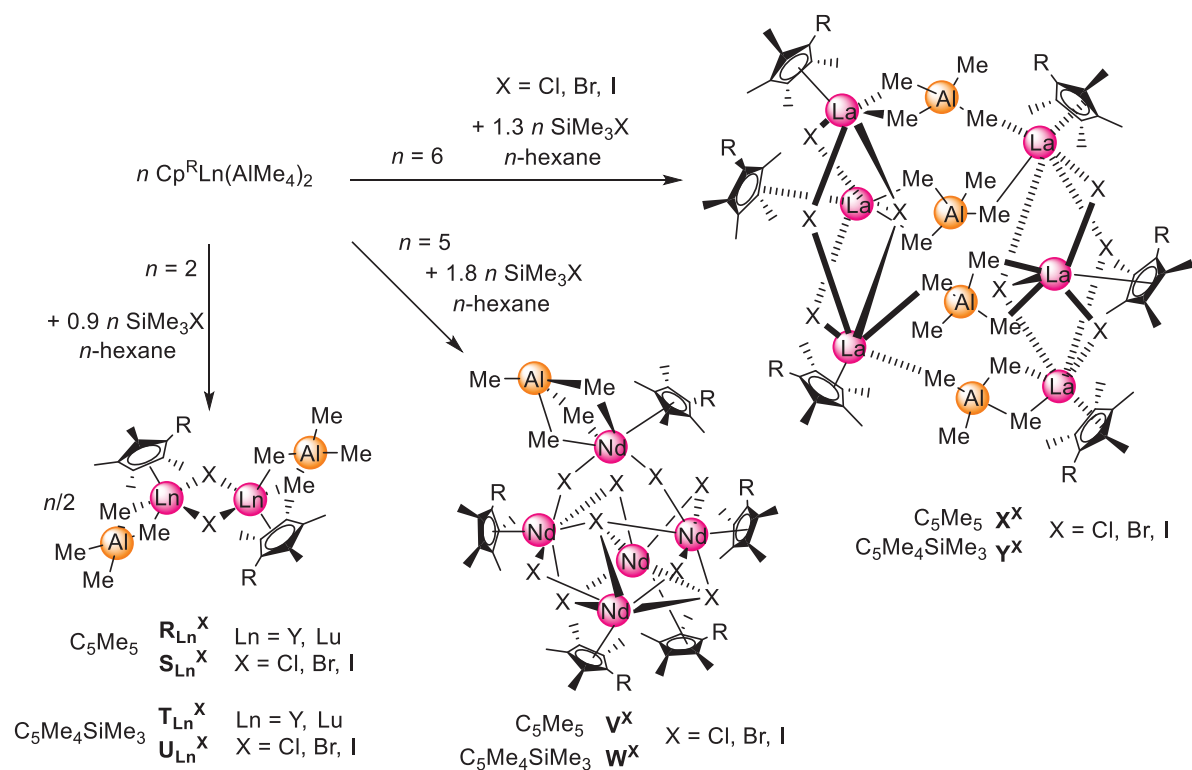
Table S2. Overview of mathematically exact calculated cone angles θ [°] of **I**, **J**, **K**, \mathbf{L}_{Ln} , \mathbf{M}_{Ln} , \mathbf{N}_{Ln} , \mathbf{O}_{Ln} , \mathbf{P}_{Y} , and \mathbf{Q}_{Lu} .

		I	J	K	\mathbf{L}_{Ln}	\mathbf{M}_{Ln}	\mathbf{N}_{Ln}	\mathbf{O}_{Ln}	\mathbf{P}_{Y}	\mathbf{Q}_{Lu}
θ	Y					273.9	276.1	278.6	276.8	
	Lu	276.1	272.5	280.4	278.1	276.1	279.2	280.3		286.3

3 Cp-Supported Rare-Earth-Metal Methylidene Complexes

In comparison to transition-metal-alkylidene chemistry, the chemistry of rare-earth-metal variants has been only scarcely explored.^[3a, c] Despite this, alkylidene chemistry increasingly gained interest due to its importance in synthetic organic chemistry for the olefination of carbonylic substrates as featured by the WITTIG or the TEBBE reagent.^[67] Further utilization of the nucleophilic CH_2^{2-} unit allows for successful metathesis reactions.^[67d, 68] Nonetheless, the synthesis of rare-earth-metal alkylidenes represents a particular challenge and requires a stabilizing environment by the chosen ligand system, *e.g.* as it is provided by Cp ligands. In previous studies the syntheses of rare-earth-metal methylidene complexes from $\text{X}^-/\text{AlMe}_4^-$ cluster compounds by donor-induced alkylaluminato cleavage followed by alkane elimination have been elaborated.^[33, 69]

A rational approach toward these mixed $\text{X}^-/\text{AlMe}_4^-$ clusters is the reaction of different $(\text{Cp}^{\text{R}})\text{Ln}(\text{AlMe}_4)_2$ ^[70] ($\text{Ln} = \text{Y, La, Nd, Lu}$; $\text{Cp}^{\text{R}} = \text{C}_5\text{Me}_5, \text{C}_5\text{Me}_4\text{SiMe}_3$) with mild halogenido transfer reagents SiMe_3X ($\text{X} = \text{Cl, Br, I}$). It is noteworthy that the nuclearity of the clusters is metal-size dependent.



Scheme S3. Synthesis of mixed halogenido/aluminato rare-earth-metal clusters ($\text{R}_{\text{Ln}}^{\text{X}}$, $\text{S}_{\text{Ln}}^{\text{X}}$, $\text{T}_{\text{Ln}}^{\text{X}}$, $\text{U}_{\text{Ln}}^{\text{X}}$, V^{X} , W^{X} , X^{X} , Y^{X}).

More precisely, tetrametallic complexes $[(Cp^R)Ln(AlMe_4)(\mu-X)]_2$ (R_{Ln}^X , S_{Ln}^X , T_{Ln}^X , U_{Ln}^X) are formed for smaller rare-earth metals as yttrium and lutetium, as well as hexa- or decametallal cluster compounds of the type $(Cp^R)_5Nd_5(AlMe_4)(\mu_3-X)_3(\mu-X)_6$ (V^X , W^X) and $[(Cp^R)_3La_3(AlMe_4)_2(\mu-X)_4]_2$ (X^X , Y^X) for larger rare-earth metals, respectively (Scheme S3, Figure S8 left). The intended introduction of pseudo-halogenido ligands as the triflate ligand did not lead to decametallal clusters for lanthanum due to the different coordination possibilities of the triflate moiety, however, complex $(C_5Me_5)_3La_3(\mu-OTf)_3(\mu_3-OTf)_2(AlMe_4)(thf)_2$ **Z** with μ^2 - as well as μ^3 -bridging triflate ligands was observed.

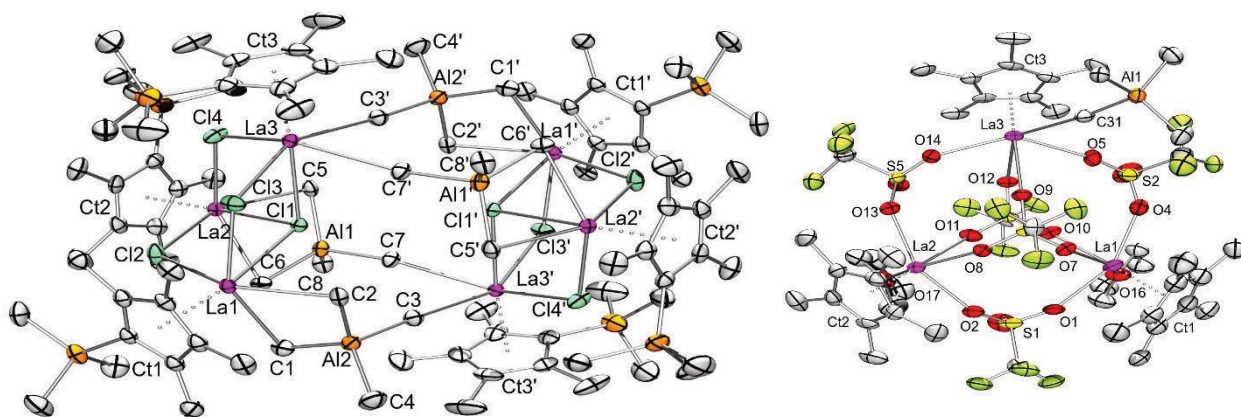


Figure S8. Crystal structures of $[(C_5Me_4SiMe_3)_3La_3(AlMe_4)_2(\mu-Cl)_4]_2$ (**Y^{Cl}**, left) and $(C_5Me_5)_3La_3(\mu-OTf)_3(\mu_3-OTf)_2(AlMe_4)(thf)_2$ (**Z**, right).

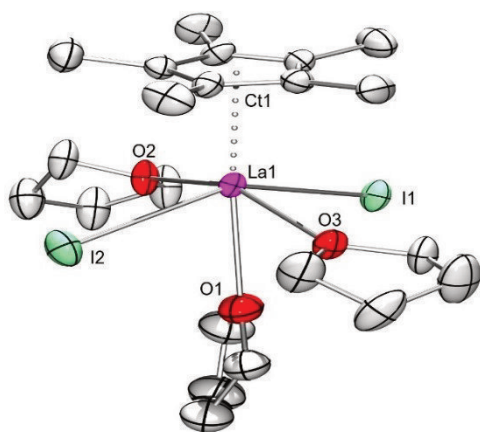
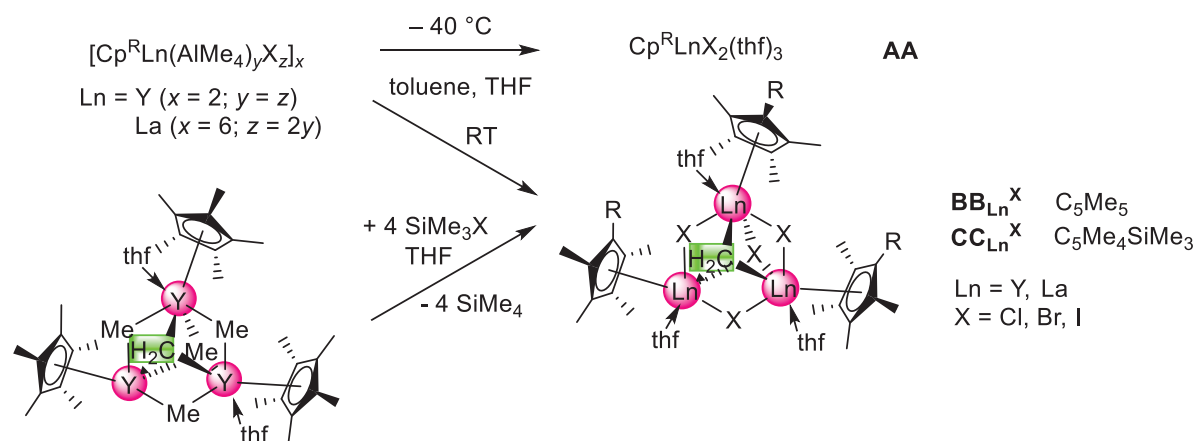


Figure S9. Solid-state structure of $(C_5Me_5)LaI_2(thf)_3$ (**AA**).

The THF-induced cleavage of the yttrium and lanthanum complexes led to the formation of trimetallic cluster compounds **BB** and **CC** with three μ_2 -bridging halogenido ligands, one μ_3 -bridging halogenido and one μ_3 -bridging methylidene in apical positions (Scheme S4, Figure S10). Similar complexes $(L)_3Ln_3(\mu-Me)_3(\mu_3-Me)(\mu_3-CH_2)(thf)_3$ developed by our group showed the same striking trimetallic structural motif.^[5a, c] It is noteworthy that careful adjustment of the reaction conditions is crucial, and temperatures below ambient temperature



Scheme S4. Low-temperature product $Cp^R LnX_2(thf)_3$ (**AA**) and mixed halogenido/methylidene rare-earth-metal complexes (BB_{Ln}^X , CC_{Ln}^X).

can lead to formation of bis(halogenido) rare-earth-metal complexes (Cp^R) $LnX_2(thf)_3$ (e.g. **AA** in Scheme S4, Figure S9). Additionally, mixed methyl/methylidene yttrium complexes^[22b] can undergo a Me/X exchange when reacted with the halogenido transfer reagent $SiMe_3X$. However, reaction with $HOCH_2tBu$ showed protonolysis of the methylidene as well as the methyl groups and therefore, bimetallic complex $[(C_5Me_5)Y(OCH_2tBu)_2]_2$ (**DD**) (Figure S11) was obtained.

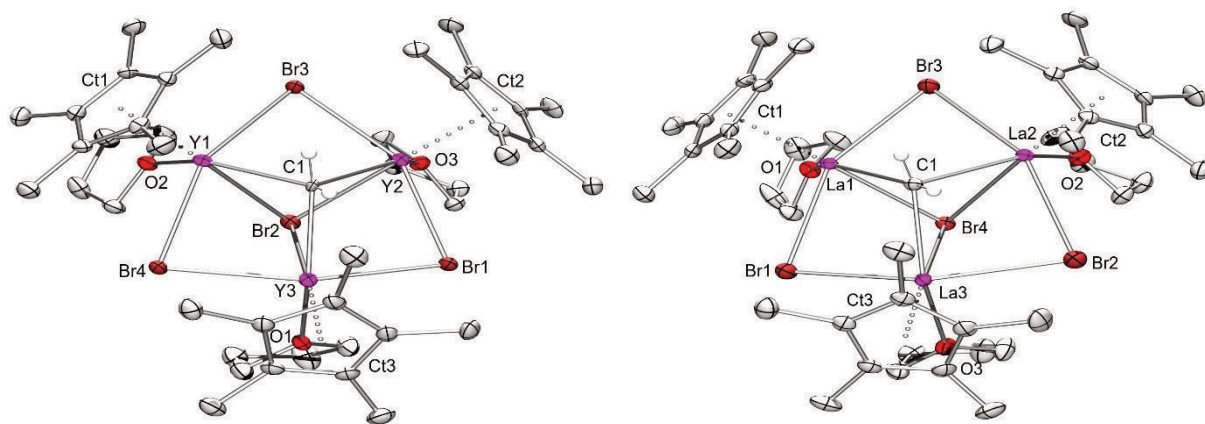


Figure S10. Crystal structures of $(C_5Me_5)_3Y_3(\mu-Br)_3(\mu_3-Br)(\mu_3-CH_2)(thf)_3$ (BB_{Y}^{Br} , left) and $(C_5Me_5)_3La_3(\mu-Br)_3(\mu_3-Br)(\mu_3-CH_2)(thf)_3$ (BB_{La}^{Br} , right).

Unfortunately, complexes with yttrium as metal center and bridging iodido ligands cannot be obtained. Our strong interest to examine the performance of the isolated complexes in olefination reactions gave rise to tests with various carbonylic substrates (Table S3, **Paper III**). NMR spectroscopic investigations of the reaction between the methylidene complexes BB_{Ln}^X

or $\text{CC}_{\text{Ln}}^{\text{X}}$ and 9-fluorenone, benzaldehyde, and cyclohexanone proved that the complexes showed performance in WITTIG-type reactions, however the sterical demand of iodido-bridging complexes affects the conversion of the sterically more demanding carbonylic derivatives. Nonetheless, the reactivity of *e.g.*, $\text{BB}_{\text{Y}}^{\text{X}}$ and $\text{CC}_{\text{Y}}^{\text{X}}$ were found to be as efficient as the TEBBE reagent. Although the structural elucidation of the TEBBE reagent $\text{Cp}_2\text{Ti}(\mu\text{-CH}_2)(\mu\text{-Cl})\text{AlMe}_2$ co-crystallized with 48 % of side product $\text{Cp}_2\text{Ti}(\mu\text{-Cl})_2\text{AlMe}_2$ was already accomplished by MINDIOLA and Co-workers,^[71] successful solid-state structure determination showed decreasing amount of side product to solely 6 % (Figure S11).

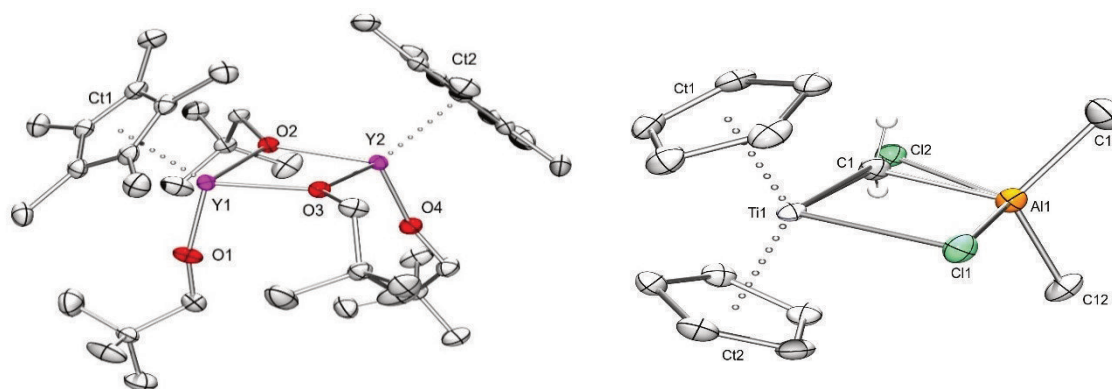


Figure S11. Crystal structures of complex $[(\text{C}_5\text{Me}_5)\text{Y}(\text{OCH}_2t\text{Bu})_2]_2$ (**DD**, left) and the TEBBE reagent $\text{Cp}_2\text{Ti}(\mu\text{-CH}_2)(\mu\text{-Cl})\text{AlMe}_2$ co-crystallized with side product $\text{Cp}_2\text{Ti}(\mu\text{-Cl})_2\text{AlMe}_2$ (right).

Additionally, most mixed halogenido/methylidene rare-earth-metal complexes showed reactivity in the polymerization δ -valerolactone for the formation of biodegradable poly(valerolactone) in moderate to high yields.

Table S3. Methylidene-transfer and reactivity in the polymerization of δ -valerolactone of rare-earth-metal methylidene complexes $\text{BB}_{\text{Ln}}^{\text{X}}$, and $\text{CC}_{\text{Ln}}^{\text{X}}$ in comparison to the methylidene transfer of the TEBBE reagent [%].^[P] yields of polymerization; **A**: 9-fluorenone, **B**: benzaldehyde, **C**: cyclohexanone, **D**: δ -valerolactone

	Y				La						Ti
	C ₅ Me ₅		C ₅ Me ₄ SiMe ₃		C ₅ Me ₅		C ₅ Me ₄ SiMe ₃				TEBBE
	BB _Y ^X		CC _Y ^X		BB _{La} ^X		CC _{La} ^X				
Cl	Br	Cl	Br	Cl	Br	I	Cl	Br	I		
A	>99	>99	>99	>99	62	95	0	62	44	0	>99
B	>99	>99	>99	>99	53	57	59	64	72	78	>99
C	>99	>99	>99	>99	62	85	55	>99	>99	>99	>99
D	76 ^[P]	86 ^[P]	60 ^[P]	51 ^[P]	67 ^[P]	87 ^[P]	23 ^[P]	88 ^[P]	85 ^[P]	70 ^[P]	>99

C

Unpublished Results

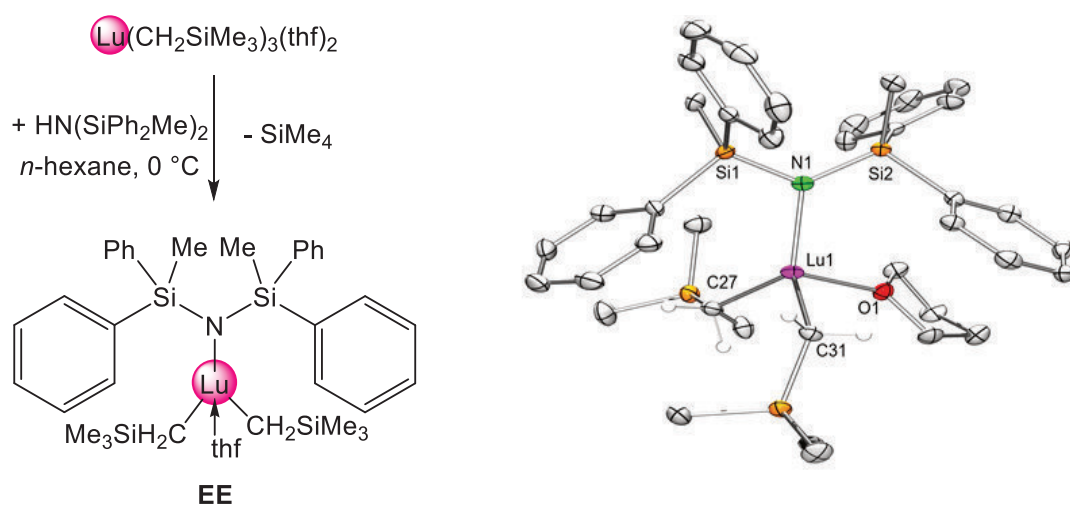
Synthesis of (CNC)-Pincer Rare-Earth-Metal Complexes

Introduction

Typically, tridentate (CNC)-pincer complexes are bis(NHC)-incorporated (NHC = N-heterocyclic carbene) monoanionic ligand systems with strong electron-donating ylidene carbon atoms for the stabilization of the Ln(III) metal center.^[72] The synthesis of (CNC)-pincer rare-earth-metal complexes from Ln alkyl complexes supported by bulky silylamido ligands through double intramolecular C–H-bond activation to afford “naked” (CNC)Ln(thf)_x as potential pincer-like analogue has gained less attention. Moreover, those complexes could reveal interesting reactivity in alkyldiene and imide chemistry as well as their utilization in polymerization reactions.

Results and Discussion

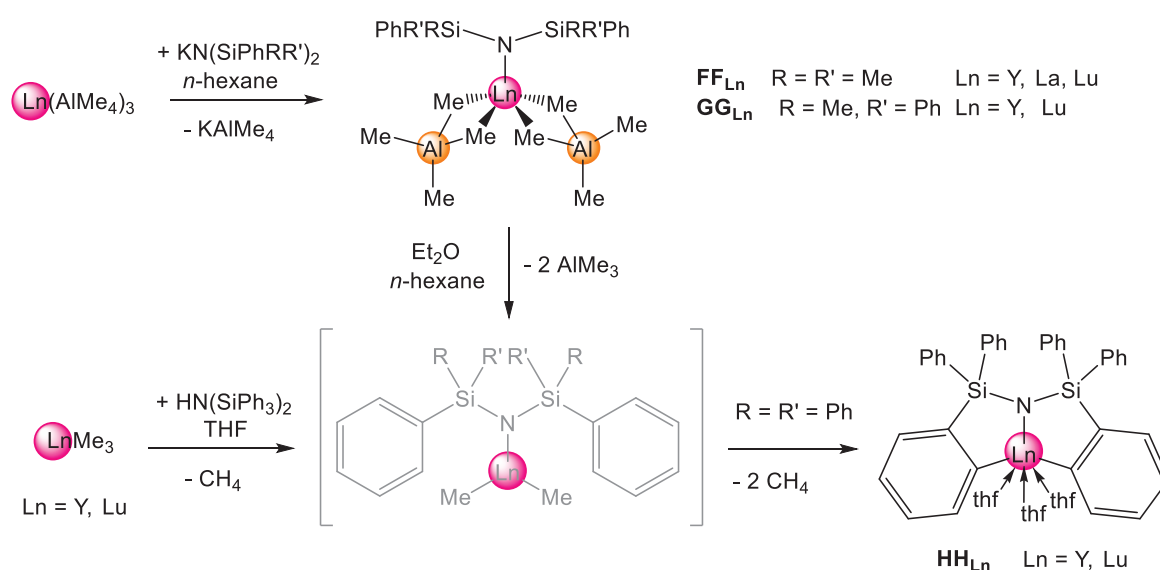
We entered this research field with the synthesis of a silylamido-stabilized bis(neosilyl) complex (MePh₂Si)₂NLu(CH₂SiMe₃)₂(thf) **EE**. This was achieved from the respective neosilyl precursor Lu(CH₂SiMe₃)₃(thf)₂ by application of a SiMe₄-elimination protocol. XRD analysis of **EE** revealed a tetrahedral coordination geometry around the metal with coordination of one THF molecule to saturate the coordination sphere (Scheme UPR1). The Lu–N(amido) distance is 2.215(6) Å and is slightly elongated compared to homoleptic Lu[N(SiMe₃)₂]₃ (2.191(5) Å).^[73] The Lu–C(neosilyl) bond lengths (2.330(6) Å, 2.323(7) Å) are in the same range as for the precursor Lu(CH₂SiMe₃)(thf)₂ (2.314(18)-2.344(18) Å)^[74] and complex Tp^{tBu,Me}LuMe(CH₂SiMe₃) (2.372(2) Å)^[60] (G, Paper I).



Scheme UPR1. Silylamido-supported rare-earth-metal bis(neosilyl) complexes (left) and crystal structure of **EE** (right).

Due to the highly reactive nature of the CH_2SiMe_3 moiety, fast decomposition proceeded concomitant with the release of SiMe_4 . Therefore, lutetium complexes form only under mild reaction conditions with temperatures below ambient temperature. Similar approaches towards the yttrium congener were not successful, however, lower temperatures might guide the way to bis(neosilyl) complexes of yttrium.

The next target was the synthesis of different silylamido-supported rare-earth-metal bis(aluminate) complexes (Scheme UPR2, FF_{Ln} , GG_{Ln}). A salt-metathesis approach was successfully utilized, starting from the homoleptic rare-earth-metal aluminate and the respective potassium silylamide. It is noteworthy that reactions involving the sterically most demanding ligand $\text{KN}(\text{SiPh}_3)_2$ did not show any conversion with $\text{Ln}(\text{AlMe}_4)_3$. With addition of donors like Et_2O to FF_{Ln} and GG_{Ln} , $[\text{LLnMe}_2]$ was observed in NMR-scale-reactions for lutetium and yttrium complexes, however no di(methyl) complex could be isolated. As further interest lies in the generation of these reactive rare-earth-metal methyl complexes, treatment of LnMe_3 with the sterically most demanding $\text{HN}(\text{SiPh}_3)_2$ in THF was accomplished. Instant gas formation was observed and NMR-spectroscopic analysis showed C–H-bond activation, however, the absence of peaks for the expected $\text{Ln}-\text{CH}_3$ moieties. Further investigations led to the conclusion, that double C–H-bond activation of both phenyl groups occurred (Scheme UPR2, HH_{Ln}). Most presumably, complex $[(\text{Ph}_3\text{Si})_2\text{NLnMe}_2]$ is formed *in situ*, and the proximity of the methyl groups allowed for instant *ortho*-metalation of the phenyl ligand back bone and to the unintended but serendipitous formation of a rare-earth-metal (CNC)-pincer-like system.



Scheme UPR2. Synthetic approaches toward amido-supported and (CNC)-pincer rare-earth-metal complexes FF_{Ln} , GG_{Ln} , and HH_{Ln} .

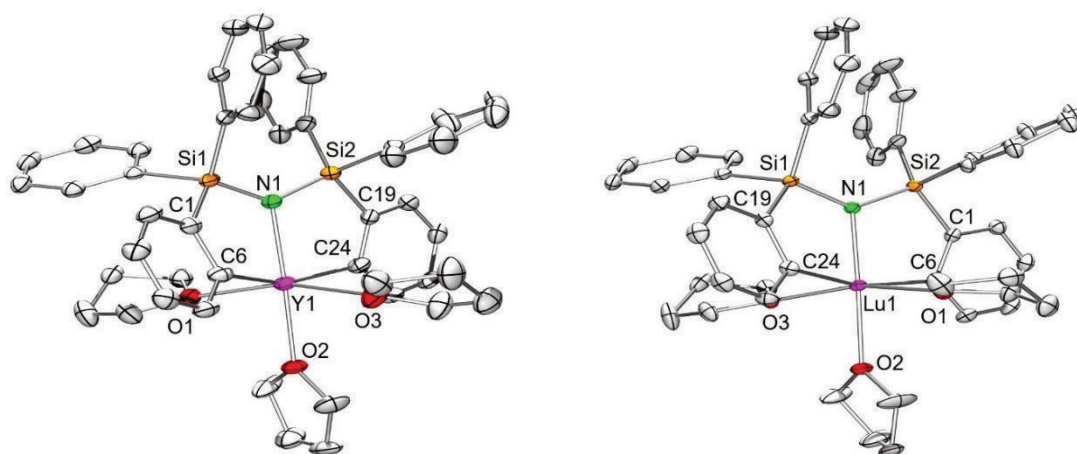


Figure UPR2. Crystal structures of **HH_Y** and **HH_{Lu}**.

X-ray structure analysis of **HH_{Ln}** revealed a distorted octahedral coordination geometry around the rare-earth-metal centers accomplished by the (CNC)-pincer ligand and three additional THF molecules. The Ln–N bond lengths are elongated compared to **EE** (**HH_Y**: 2.303(2) Å; **HH_{Lu}**: 2.236(1) Å). For **HH_Y** this can be explained as a metal-size effect, for **HH_{Lu}** it nicely demonstrates the constraint geometry for the lutetacycle and how the ligand system adapts. The Ln–O distances are similar in accordance with the different ionic radii of the rare-earth metals (**HH_Y**: 2.336(2)–2.392(2) Å; **HH_{Lu}**: 2.2757(12)–2.3450(12) Å). The same trend is observed for the Ln–C bond lengths (**HH_Y**: 2.485(3), 2.487(3) Å; **HH_{Lu}**: 2.433(2), 2.436(2) Å).

First approaches toward terminal monometallic rare-earth-metal imido complexes by reacting **HH_Y** with aniline H₂NC₆H₃-Me-2,6 showed conversion to the respective amide complex. Therefore, further investigations and thermolysis or LEWIS-base induced protonolysis might give access to scarce rare-earth-metal imide complexes.

Experimental Section

General Considerations. All operations were performed with rigorous exclusion of air and water by using standard Schlenk, high-vacuum, and glovebox techniques (MBraun 200B; <0.1 ppm O₂, <0.1 ppm H₂O). Solvents were purified by using Grubbs columns (MBraun SPS, solvent purification system) and stored inside a glovebox. [D₆]benzene was obtained from Sigma-Aldrich, degassed and dried over NaK alloy for two days and filtered prior to use. [D₈]thf was obtained from Sigma-Aldrich, stirred over NaK alloy, and distilled. The NMR spectra of air- and moisture-sensitive compounds were recorded by using J. Young valve NMR tubes on a Bruker AVII+500 spectrometer (¹H, 500.00 MHz, ¹³C, 125.72 MHz, ⁸⁹Y 24.496 MHz), a Bruker AVII+400 spectrometer (¹H, 400.13 MHz, ¹³C, 100.61 MHz) and on a Bruker AVII+300 spectrometer (¹H, 300.00 MHz, ²⁹Si, 59.59 MHz). DRIFT spectra were recorded on a Thermo Fisher Scientific NICOLET 6700 FTIR spectrometer using a DRIFT chamber with dry KBr/sample mixture and KBr windows; IR (DRIFT) data were converted by using the Kubelka-Munk refinement. Elemental analyses were performed on an Elementar Vario MICRO Cube.

(MePh₂Si)₂NLu(CH₂SiMe₃)₂(thf) (EE): A solution of Lu(CH₂SiMe₃)₃(thf)₂ (50.0 mg, 0.0861 mmol) in *n*-hexane (1 mL) was added to a stirred solution of HN(SiPh₂Me)₂ (35.0 mg, 0.0861 mmol) in *n*-hexane (1 mL). The reaction mixture was stirred for 2 h at 0 °C and concentrated *in vacuo*. Colorless crystals were obtained from a saturated solution at –40 °C (42.0 mg, 0.0506 mmol, 59 %). ¹H NMR (400 MHz, [D₆]benzene, 26 °C): δ = 7.85–7.82 (m,

8H, Ar-H), 7.25-7.21 (m, 8H, Ar-H), 7.18-7.12 (m, 4H, Ar-H), 3.21 (br s, 4H, thf), 0.89 (m, 4H, thf), 0.70 (s, 6H, Si-CH₃), 0.26 (s, 18H, CH₂Si(CH₃)₃), -0.73 (s, 4H, CH₂Si(CH₃)₃) ppm. IR (KBr): $\tilde{\nu}$ = 3388 (vw), 3130 (vw), 3062 (w), 3019 (vw), 3008 (vw), 2995 (vw), 2950 (w), 2890 (vw), 2846 (vw), 2806 (vw), 1959 (vw), 1903 (vw), 1889 (vw), 1824 (vw), 1587 (vw), 1482 (vw), 1454 (vw), 1427 (m), 1406 (vw), 1377 (vw), 1326 (vw), 1303 (vw), 1259 (w), 1249 (w), 1237 (w), 1185 (vw), 1163 (w), 1153 (w), 1105 (s), 1065 (vw), 1030 (w), 1000 (w), 980 (s), 927 (m), 885 (m), 800 (vs), 787 (m), 738 (vs), 718 (m), 703 (s), 676 (w), 665 (vw), 647 (vw), 507 (w), 500 (w), 483 (w), 470 (w), 460 (m), 429 (vw), 424 (vw), 418 (w), 406 (vw) cm⁻¹; elemental analysis calcd (%) for C₃₈H₅₆LuNOSi₄: C 54.98, H 6.80, N 1.69; C 55.28, H 6.01, N 2.26.

(Me₂PhSi)₂NY(AlMe₄)₂ (FF_V): A solution of Y(AlMe₄)₃ (200 mg, 0.571 mmol) in *n*-hexane (5 mL) was added to a stirred suspension of KN(SiPhMe₂)₂ (185 mg, 0.572 mmol) in *n*-hexane (10 mL). The reaction mixture was stirred overnight at ambient temperatures. The precipitate was allowed to settle and the solution was separated *via* filtration. The solid was washed with *n*-hexane (3 x 5 ml), the collected solutions were combined, and concentrated *in vacuo*. Colorless crystals were obtained from a saturated solution at -40 °C (200 mg, 0.365 mmol, 64 %). ¹H NMR (400 MHz, [D₆]benzene, 26 °C): δ = 7.63-7.61 (m, 4H, Ar-H), 7.21-7.17 (m, 4H, Ar-H), 7.11-7.07 (m, 2H, Ar-H), 0.36 (s, 12H, Si-CH₃), -0.37 (d, ²J(YH) = 2.5 Hz, 24H, Al-CH₃) ppm. ¹³C{¹H}c NMR (101 MHz, [D₆]benzene, 26 °C): δ 137.8 (Ar-C1), 136.7 (Ar-C3,5), 131.9 (Ar-C4), 130.2 (Ar-C2,5), 3.2 (Si-CH₃), 2.1 (Al-CH₃) ppm. ²⁹Si{¹H} dept45 NMR (60 MHz, [D₆]benzene, 26 °C): δ -13.3 ppm. ⁸⁹Y NMR (from ¹H-⁸⁹Y HSQC, 25 MHz, [D₆]benzene, 26 °C): δ = 451 ppm; IR (KBr): $\tilde{\nu}$ = 3085 (vw), 3067 (vw), 3050 (vw), 3017 (vw), 3006 (vw), 2997 (vw), 2947 (w), 2927 (w), 2888 (w), 2819 (vw), 2795 (vw), 1583 (vw), 1560 (vw), 1486 (vw), 1425 (w), 1315 (vw), 1305 (vw), 1291 (vw), 1254 (m), 1214 (w), 1188 (m), 1109 (m), 1094 (m), 937 (w), 845 (s), 824 (s), 791 (s), 776 (s), 745 (s), 730 (vs), 715 (vs), 702 (vs), 692 (vs), 648 (w), 632 (w), 608 (w), 575 (s), 557 (m), 547 (m), 540 (m), 486 (m), 474 (m), 460 (w), 450 (w), 402 (s) cm⁻¹; elemental analysis calcd (%) for C₂₄H₄₆Al₂NSi₂Y: C 52.63, H 8.47, N 2.56; C 52.86, H 8.75, N 2.63.

(Me₂PhSi)₂NLa(AlMe₄)₂ (FF_{La}): A solution of La(AlMe₄)₃ (200 mg, 0.500 mmol) in *n*-hexane was added to a stirred suspension of KN(SiPhMe₂)₂ (162 mg, 0.501 mmol) in *n*-hexane. The reaction mixture was stirred overnight at ambient temperatures. The precipitate was allowed to settle and the solution was separated *via* filtration. The solid was washed with *n*-hexane (3 x 5 ml), the collected solutions were combined, and concentrated *in vacuo*. Colourless crystals were obtained from a saturated solution at -40 °C (160 mg, 0.292 mmol, 58 %). ¹H NMR (400 MHz, [D₆]benzene, 26 °C): δ = 7.64-7.62 (m, 4H, Ar-H), 7.23-7.19 (m, 4H, Ar-H), 7.10-7.05 (m, 2H, Ar-H), 0.29 (s, 12H, Si-CH₃), -0.41 (s, 24H, Al-CH₃) ppm. ¹³C{¹H} NMR (63 MHz, [D₆]benzene, 26 °C): δ 136.3 (Ar-C1), 136.0 (Ar-C3,5), 132.5 (Ar-C4), 131.4 (Ar-C2,5), 5.3 (Al-CH₃), 2.5 (Si-CH₃) ppm. ²⁹Si{¹H} dept45 NMR (60 MHz, [D₆]benzene, 26 °C): δ -15.4 ppm; IR (KBr): $\tilde{\nu}$ = 3067 (vw), 2999 (vw), 2949 (w), 2921 (w), 2885 (w), 2883 (w), 2779 (w), 1585 (vw), 1485 (8vw), 1446 (vw), 1426 (w), 1309 (vw), 1252 (m), 1202 (w), 1191 (w), 1104 (m), 1030 (vw), 999 (m), 987 (m), 844 (s), 823 (m), 790 (s), 776 (s), 725 (vs), 705 (vs), 692 (vs), 600 (s), 581 (s), 546 (m), 518 (w), 487 (m), 482 (m), 473 (s), 447 (m), 419 (w), 410 (vw) cm⁻¹; elemental analysis calcd (%) for C₂₄H₄₆Al₂LaNSi₂: C 48.23, H 7.76, N 2.34; C 48.61, H 7.83, N 2.44.

(Me₂PhSi)₂NLu(AlMe₄)₂ (FF_{Lu}): A solution of Lu(AlMe₄)₃ (200 mg, 0.458 mmol) in *n*-hexane was added to a stirred suspension of KN(SiPhMe₂)₂ (149 mg, 0.460 mmol) in *n*-hexane. The reaction mixture was stirred overnight at ambient temperatures. The precipitate was allowed to settle and the solution was separated *via* filtration. The solid was washed with *n*-hexane (3 x 5 ml), the collected solutions were combined, and concentrated *in vacuo*. Colorless crystals were obtained from a saturated solution at -40 °C (180 mg, 0.284 mmol, 62 %). ¹H NMR (400 MHz, [D₆]benzene, 26 °C): δ = 7.63-7.61 (m, 4H, Ar-H), 7.21-7.17 (m, 4H, Ar-H), 7.11-7.07 (m, 2H, Ar-H), 0.36 (s, 12H, Si-CH₃), -0.37 (s, 24H, Al-CH₃) ppm. ¹³C{¹H} NMR (101 MHz, [D₆]benzene, 26 °C): δ 137.7 (Ar-C1), 137.1 (Ar-C3,5), 131.8 (Ar-C4), 129.8 (Ar-C2,5), 3.5 (Si-CH₃), 3.2 (Al-CH₃) ppm. ²⁹Si{¹H} dept45 NMR (60 MHz, [D₆]benzene, 26 °C): δ -11.5 ppm; IR (KBr): $\tilde{\nu}$ = 3067 (vw), 3050 (vw), 3016 (vw), 2926 (w), 2891 (w), 1583 (vw), 1485 (vw), 1425 (w), 1315 (vw), 1253 (m), 1218 (w), 1191 (w), 1109 (w), 1094 (w), 1029 (vw), 954 (m), 950 (m), 937 (m), 841 (m), 823 (s), 792 (s), 783 (s), 770 (m), 751 (s), 742 (s), 727 (vs), 719 (vs), 710 (s), 696 (vs), 686 (s), 678 (m), 659 (w), 646 (w), 608 (w), 594 (m), 575 (m), 542 (m), 530 (m), 518 (m), 488 (vw), 476 (m), 463 (m), 446 (m), 434 (s), 414 (m), 407 (vw) cm⁻¹; elemental analysis calcd (%) for C₂₄H₄₆Al₂LuNSi₂: C 45.49, H 7.32, N 2.21; C 45.63, H 7.56, N 2.30.

(MePh₂Si)₂NY(AlMe₄)₂ (GG_V): A solution of Y(AlMe₄)₃ (100 mg, 0.285 mmol) in *n*-hexane was added to a stirred suspension of KN(SiPh₂Me)₂ (128 mg, 0.285 mmol) in *n*-hexane. The reaction mixture was stirred overnight at ambient temperatures. The precipitate was allowed to settle and the solution was separated *via* filtration. The solid was washed with *n*-hexane (3 x 5 ml), the collected solutions were combined, and concentrated *in vacuo*. Colourless crystals were obtained from a saturated solution at -40 °C (96.0 mg, 0.143 mmol, 50 %). ¹H NMR (400 MHz, [D₆]benzene, 26 °C): δ = 7.72-7.70 (m, 8H, Ar-H), 7.20-7.16 (m, 8H, Ar-H), 7.14-7.10 (m, 4H, Ar-H), 0.63 (s, 6H, Si-CH₃), -0.31 (d, ²J(YH) = 2.4 Hz, 24H, Al-CH₃) ppm. ¹³C{¹H} NMR (63 MHz, [D₆]benzene,

26 °C): δ 137.9 (Ar-C1), 136.6 (Ar-C3,5), 130.9 (Ar-C4), 129.1 (Ar-C2,5), 2.5 (Al-CH₃), 2.3 (Si-CH₃) ppm. ²⁹Si{¹H} dept45 NMR (60 MHz, [D₆]benzene, 26 °C): δ -18.4 ppm. ⁸⁹Y NMR (from ¹H-⁸⁹Y HSQC, 25 MHz, [D₆]benzene, 26 °C): δ = 445 ppm; IR (KBr): $\tilde{\nu}$ = 3128 (vw), 3063 (w), 3051 (w), 3017 (w), 3000 (w), 2926 (w), 2888 (w), 2821 (vw), 2787 (vw), 1960 (vw), 1893 (vw), 1829 (vw), 1586 (vw), 1483 (vw), 1426 (m), 1303 (vw), 1217 (w), 1190 (w), 1159 (vw), 1104 (s), 1064 (vw), 1029 (w), 998 (w), 961 (s), 860 (vw), 801 (s), 787 (s), 769 (m), 735 (vs), 670 (vs), 650 (w), 587 (m), 574 (m), 544 (m), 529 (m), 503 (s), 489 (s), 458 (s), 418 (vw) cm⁻¹.

(MePh₂Si)₂NLu(AlMe₄)₂ (GG_{Lu}): A solution of Lu(AlMe₄)₃ (100 mg, 0.229 mmol) in *n*-hexane was added to a stirred suspension of KN(SiPh₂Me)₂ (103 mg, 0.230 mmol) in *n*-hexane. The reaction mixture was stirred overnight at ambient temperatures. The precipitate was allowed to settle and the solution was isolated *via* filtration. The solid was washed with *n*-hexane (3 x 5 ml), the collected solutions were combined, and concentrated *in vacuo*. Colourless crystals were obtained from a saturated solution at -40 °C (135 mg, 0.178 mmol, 78 %). ¹H NMR (400 MHz, [D₆]benzene, 26 °C): δ = 7.73-7.71 (m, 8H, Ar-H), 7.20-7.18 (m, 8H, Ar-H), 7.14-7.10 (m, 4H, Ar-H), 0.67 (s, 6H, Si-CH₃), -0.10 (s, 24H, Al-CH₃) ppm; ¹³C{¹H} NMR (63 MHz, [D₆]benzene, 26 °C): δ 137.9 (Ar-C1), 136.6 (Ar-C3,5), 130.8 (Ar-C4), 128.9 (Ar-C2,5), 2.6 (Si-CH₃), 2.2 (Al-CH₃) ppm.

(Ph₂SiC₆H₅)₂NY(thf)₃ (HH_Y): A solution of HN(SiPh₃)₂ (199 mg, 0.373 mmol) in thf (5 mL) was added to a stirred suspension of YMe₃ (50.0 mg, 0.373 mmol) in toluene (5 mL) at ambient temperature. The suspension was allowed to stir for additional 12 h at 40 °C. The reaction mixture changed from white to orange-red. The solution was filtered and concentrated *in vacuo*. Orange crystals were obtained from a saturated solution in thf/toluene at -40 °C (262 mg, 0.313 mmol 84 %). ¹H NMR (400 MHz, [D₈]thf, 26 °C): δ = 7.63-7.61 (m, 2H, Ar-H), 7.28-7.25 (m, 8H, Ar-H), 7.20-7.19 (m, 2H, Ar-H), 7.02-6.98 (m, 4H, Ar-H), 6.92-6.88 (m, 8H, Ar-H), 6.87-6.83 (m, 2H, Ar-H), 6.80-6.76 (m, 2H, Ar-H), 3.58 (s, thf), 1.72 (s, thf) ppm. ¹³C{¹H} NMR (63 MHz, [D₈]thf, 26 °C): δ 199.4 (d, ¹J(YC) = 43 Hz, Y-C2), 155.4 (Si-C1), 144.6 (Si-C7), 137.0 (Ar-C8,12), 136.1 (Ar-C3), 134.0 (Ar-C6), 127.5 (Ar-C10), 126.7 (Ar-C9,11), 125.2 (Ar-C4), 123.8 (Ar-C5), 67.2 (thf), 25.3 (thf) ppm. ²⁹Si{¹H} dept45 NMR (60 MHz, [D₈]thf, 26 °C): δ -25.8 ppm. ⁸⁹Y NMR (from ¹H-⁸⁹Y HSQC, 25 MHz, [D₈]thf, 26 °C): δ = 567 ppm; IR (KBr): $\tilde{\nu}$ = 3062 (w), 3014 (w), 2934 (w), 2872 (w), 2785 (vw), 1584 (vw), 1483 (vw), 1457 (vw), 1426 (w), 1407 (vw), 1294 (vw), 1259 (vw), 1232 (vw), 1213 (vw), 1183 (vw), 1154 (vw), 1100 (s), 1071 (m), 1033 (m), 1008 (s), 918 (w), 861 (m), 782 (vw), 729 (s), 700 (vs), 674 (w), 655 (m), 635 (w), 620 (vw), 578 (vw), 555 (m), 536 (w), 518 (vs), 503 (w), 484 (s), 451 (w), 435 (w) cm⁻¹; elemental analysis calcd (%) for C₄₈H₅₂NO₃Si₂Y: C 68.96, H 6.27, N 1.68; C 67.83, H 6.28, N 1.63.

(Ph₂SiC₆H₅)₂NLu(thf)₃ (HH_{Lu}): A solution of HN(SiPh₃)₂ (121 mg, 0.227 mmol) in thf (5 mL) was added to a stirred suspension of LuMe₃ (50.0 mg, 0.227 mmol) in toluene (5 mL) at ambient temperature. The suspension was allowed to stir for additional 12 h at 40 °C. The reaction mixture changed from white to orange-red. The solution was filtered and concentrated *in vacuo*. Yellow crystals were obtained from a saturated solution in thf/toluene at -40 °C (174 mg, 0.189 mmol 83 %). ¹H NMR (400 MHz, [D₈]thf, 26 °C): δ = 7.66-7.64 (m, 2H, Ar-H), 7.29-7.26 (m, 10H, Ar-H), 7.02-6.98 (m, 4H, Ar-H), 6.94-6.88 (m, 10H, Ar-H), 6.81-6.77 (m, 2H, Ar-H), 3.58 (s, thf), 1.72 (s, thf) ppm. ¹³C{¹H} NMR (63 MHz, [D₈]thf, 26 °C): δ 207.3 (Lu-C2), 155.4 (Si-C1), 144.5 (Si-C7), 137.2 (Ar-C3), 136.8 (Ar-C8,12), 134.2 (Ar-C6), 127.4 (Ar-C10), 126.6 (Ar-C9,11), 125.5 (Ar-C4), 123.6 (Ar-C5), 67.2 (thf), 25.3 (thf) ppm. ²⁹Si{¹H} dept45 NMR (60 MHz, [D₆]benzene, 26 °C): δ -26.2 ppm; IR (KBr): $\tilde{\nu}$ = 3062 (w), 3015 (m), 2992 (m), 2934 (w), 2889 (w), 1483 (vw), 1473 (vw), 1456 (vw), 1427 (m), 1408 (vw), 1294 (vw), 1259 (vw), 1214 (vw), 1183 (vw), 1100 (s), 1072 (m), 1033 (m), 1017 (vs), 918 (w), 860 (m), 738 (s), 731 (vs), 700 (vs), 674 (w), 657 (m), 635 (w), 556 (m), 518 (vs), 504 (w), 485 (s), 451 (w), 436 (w) cm⁻¹.

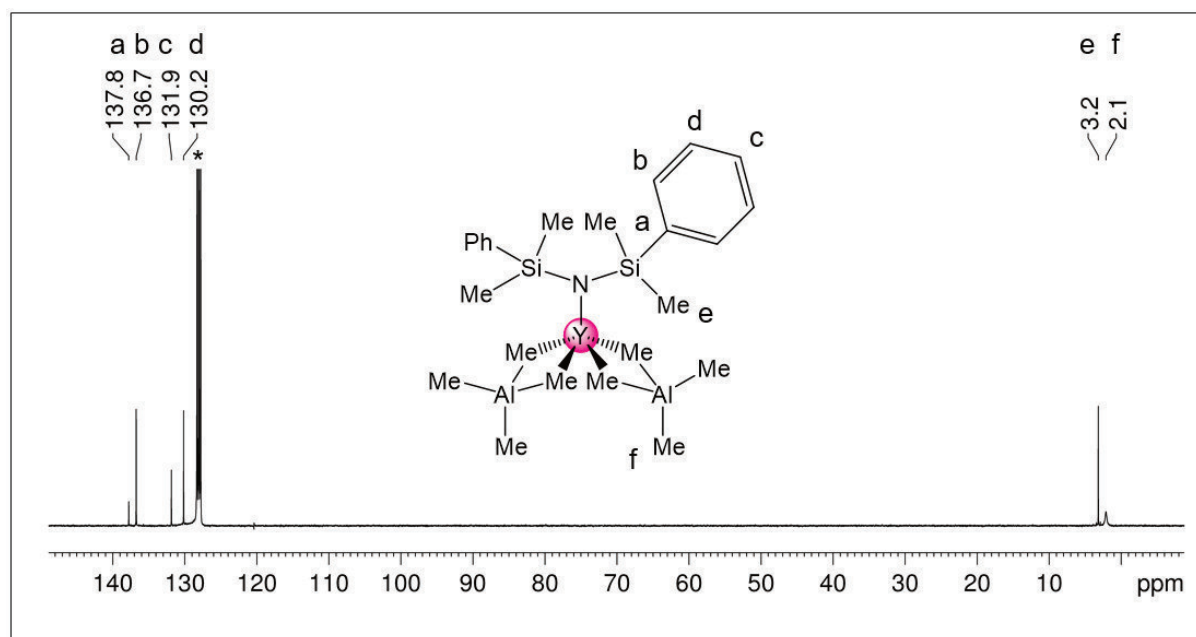


Figure UPR3. ^{13}C NMR spectrum (101 MHz, $[\text{D}_6]$ benzene) of complex FF_Y at 26 °C.

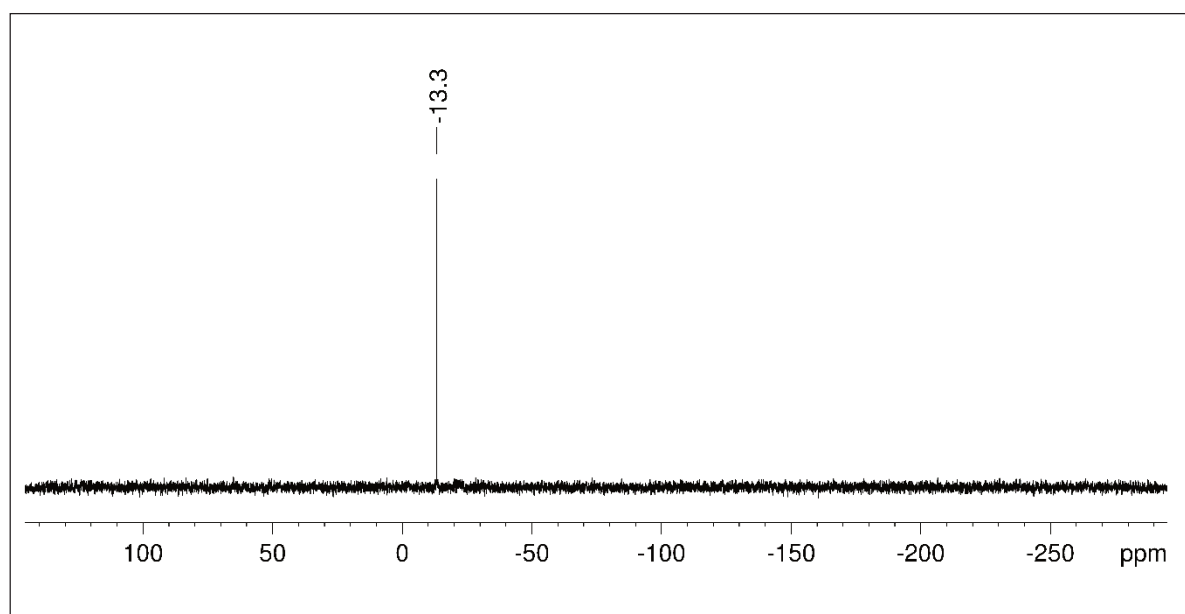


Figure UPR4. $^{29}\text{Si}\{^1\text{H}\}$ -dept NMR spectrum (60 MHz, $[\text{D}_6]$ benzene) of complex FF_Y at 26 °C.

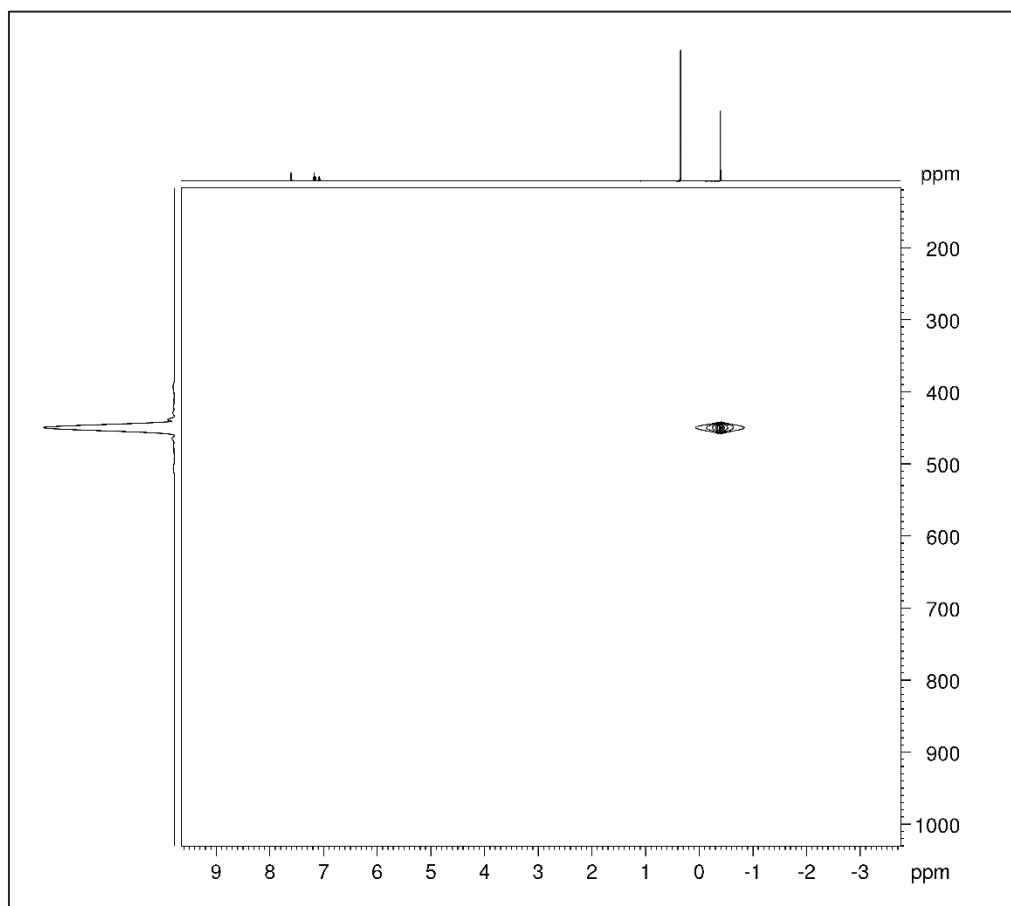


Figure UPR5. ^1H - ^{89}Y HSQC NMR spectrum (25 MHz, $[\text{D}_6]$ benzene) of complex FF_Y at 26 °C.

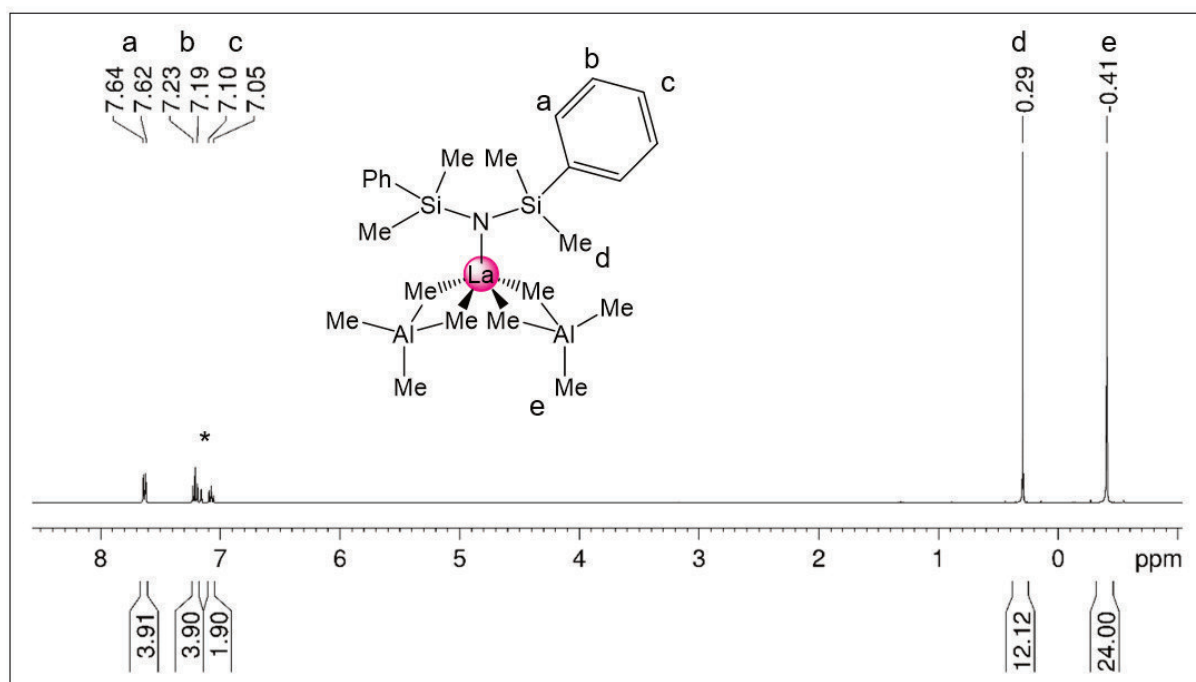


Figure UPR6. ^1H NMR spectrum (400 MHz, $[\text{D}_6]$ benzene) of complex FF_{La} at 26 °C.

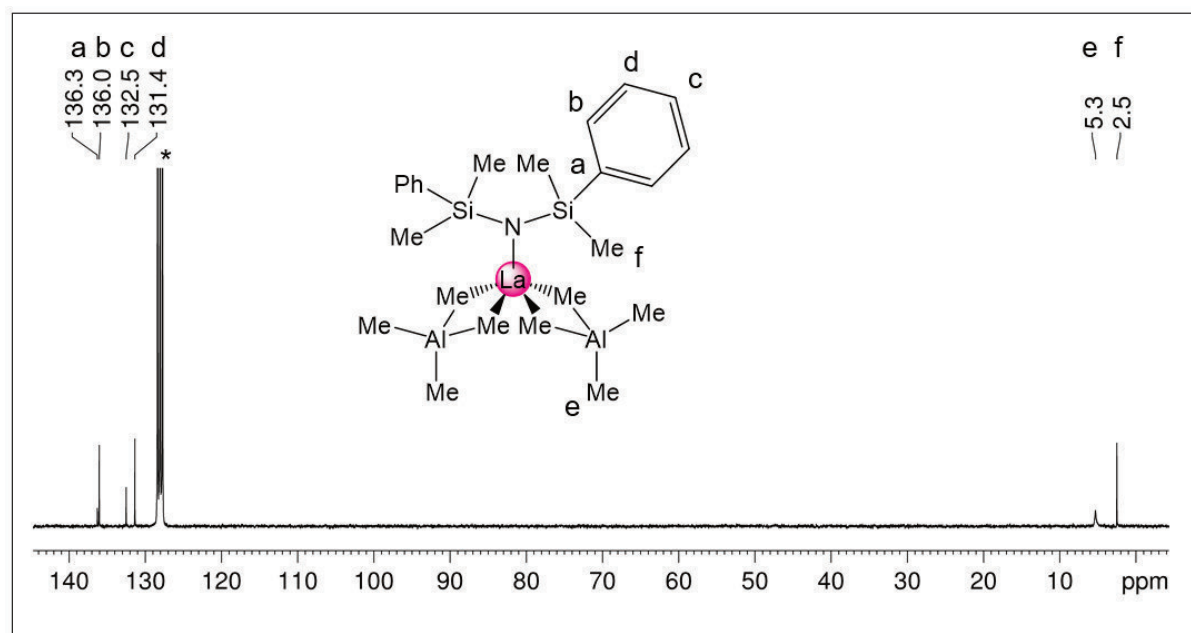


Figure UPR7. $^{13}\text{C}\{^1\text{H}\}$ NMR spectrum (101 MHz, $[\text{D}_6]\text{benzene}$) of complex **FFLa** at 26 °C.

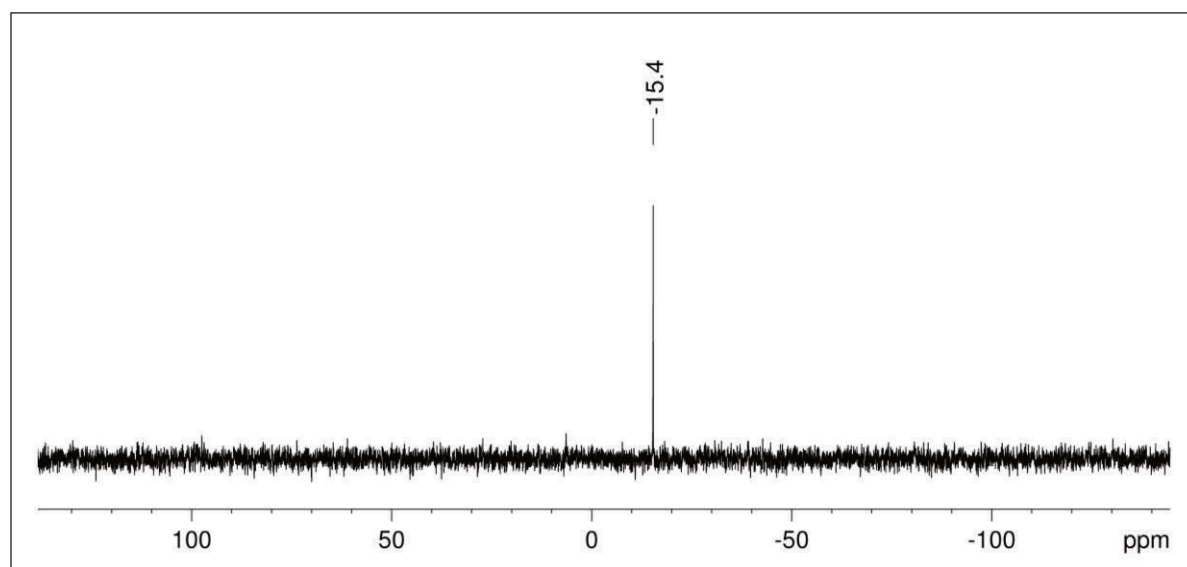


Figure UPR8. $^{29}\text{Si}\{^1\text{H}\}$ -dept NMR spectrum (60 MHz, $[\text{D}_6]\text{benzene}$) of complex **FFLa** at 26 °C.

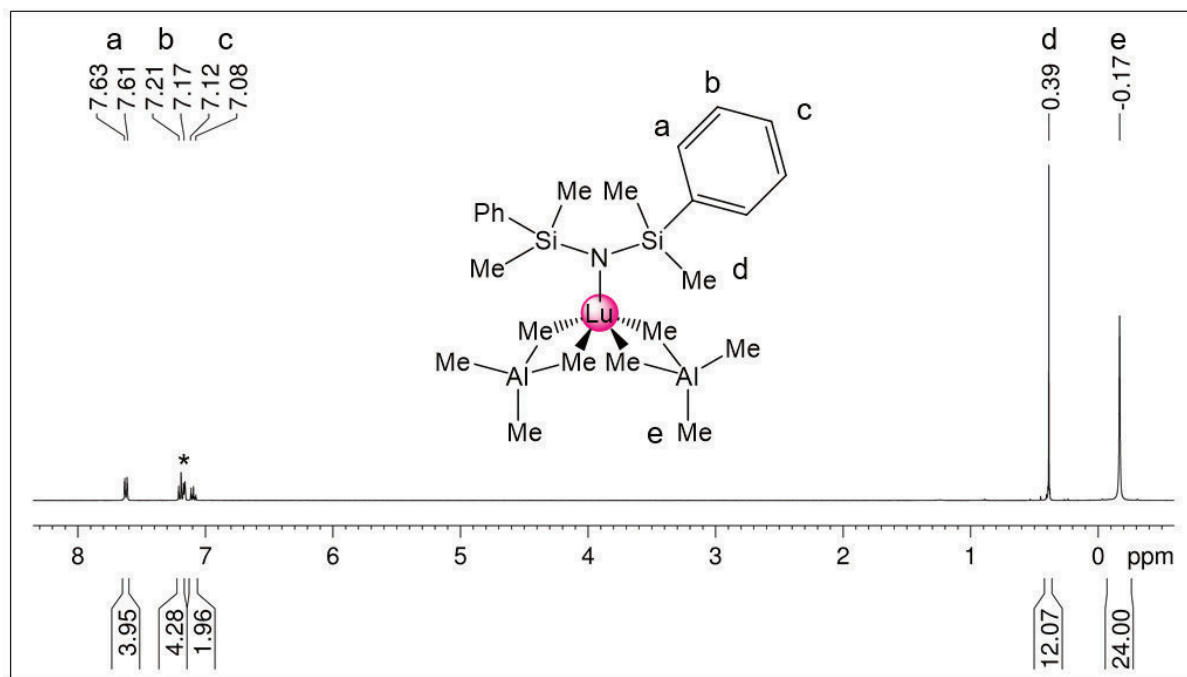


Figure UPR9. ^1H NMR spectrum (400 MHz, $[\text{D}_6]\text{benzene}$) of complex FF_{Lu} at 26 °C.

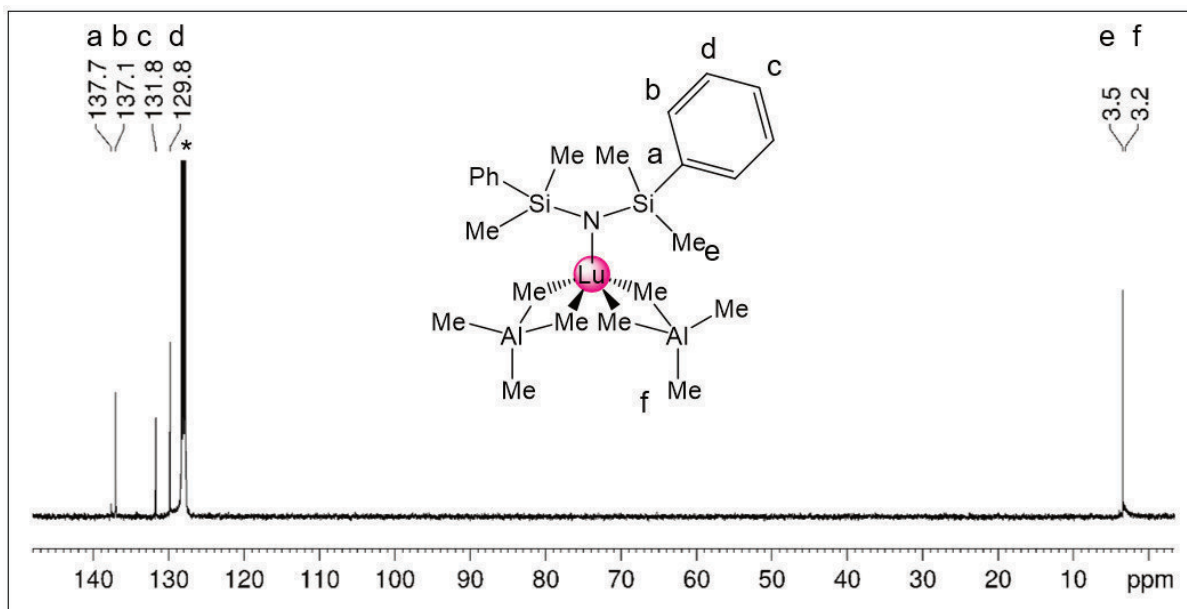


Figure UPR10. $^{13}\text{C}\{^1\text{H}\}$ NMR spectrum (101 MHz, $[\text{D}_6]\text{benzene}$) of complex FF_{Lu} at 26 °C.

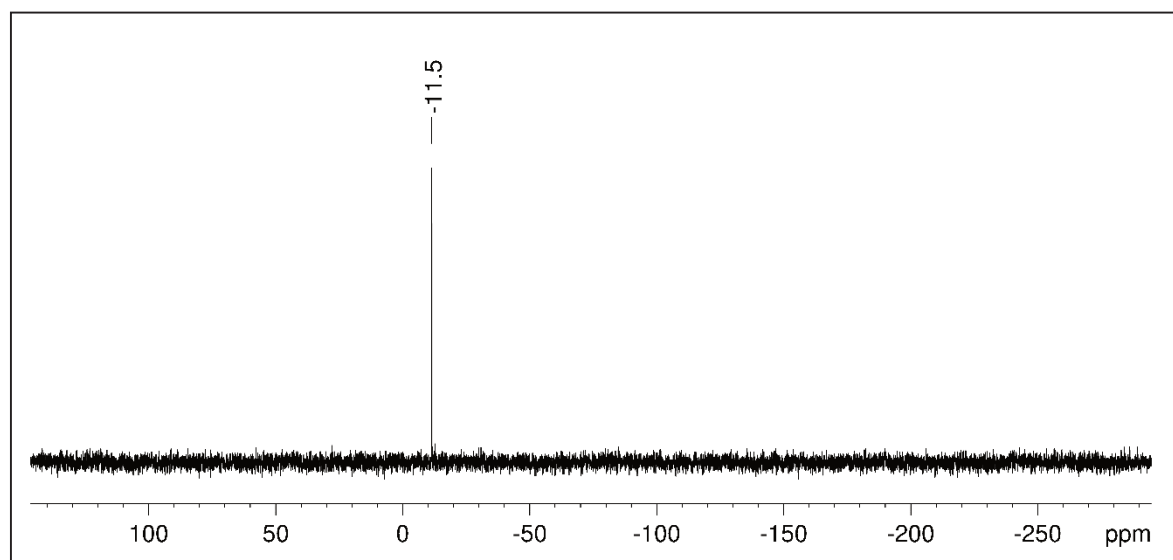


Figure UPR11. $^{29}\text{Si}\{^1\text{H}\}$ -dept NMR spectrum (60 MHz, $[\text{D}_6]$ benzene) of complex **FFLu** at 26 °C.

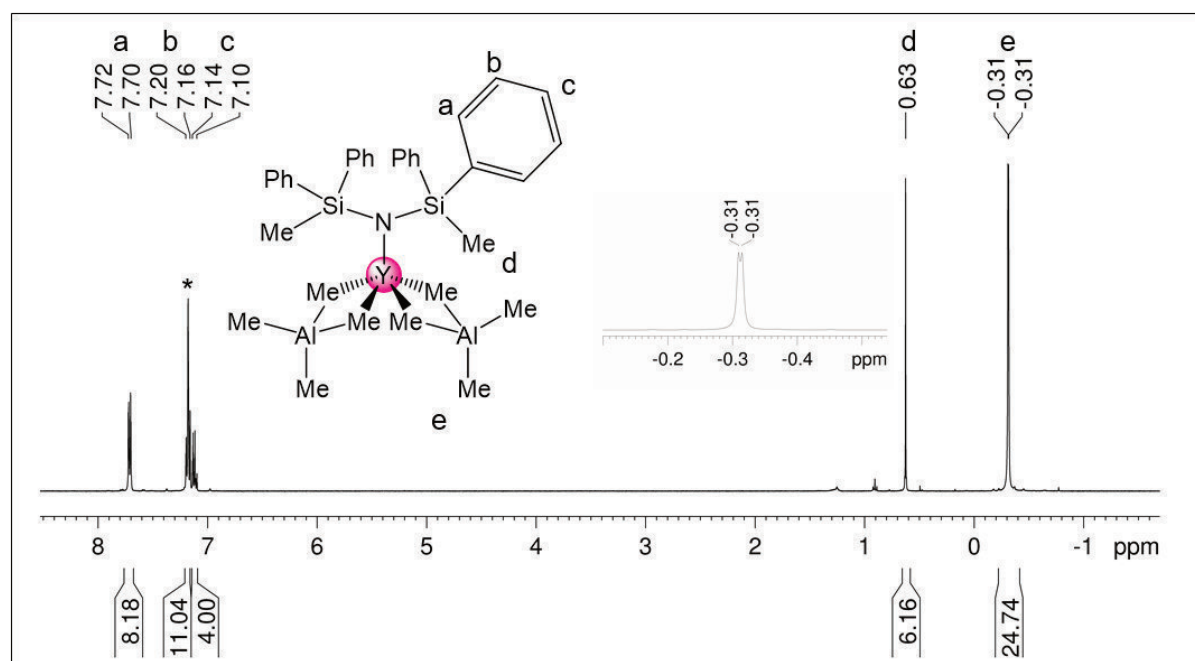


Figure UPR12. ^1H NMR spectrum (400 MHz, $[\text{D}_6]$ benzene) of complex **GGy** at 26 °C.

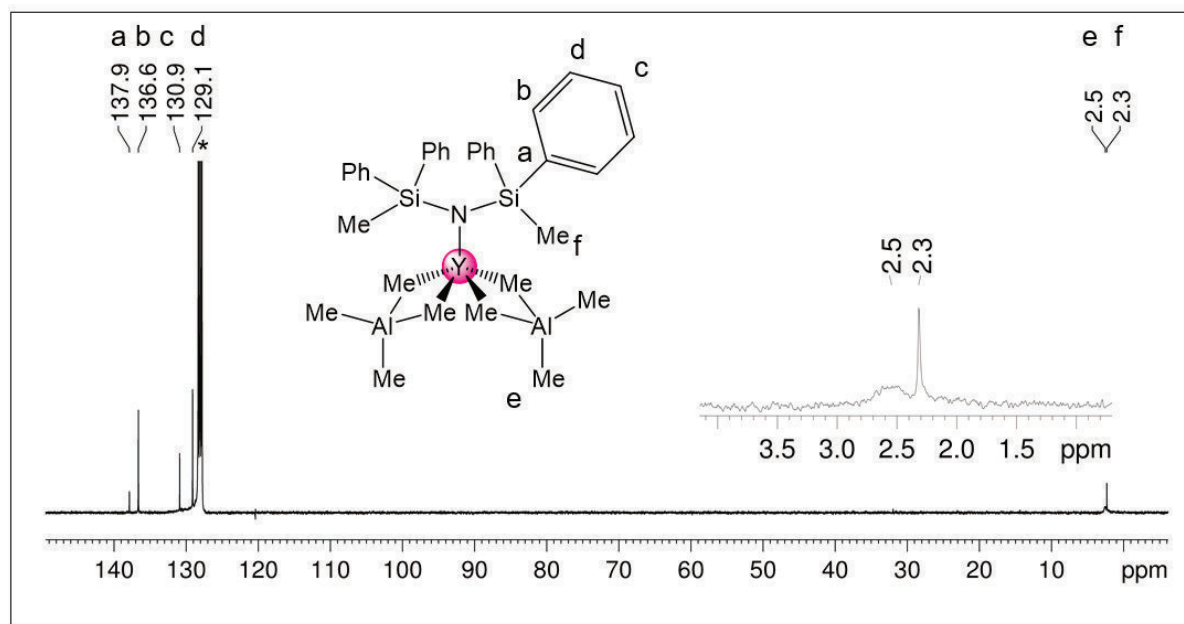


Figure UPR13. $^{13}\text{C}\{^1\text{H}\}$ NMR spectrum (101 MHz, $[\text{D}_6]\text{benzene}$) of complex **GGy** at 26 °C.

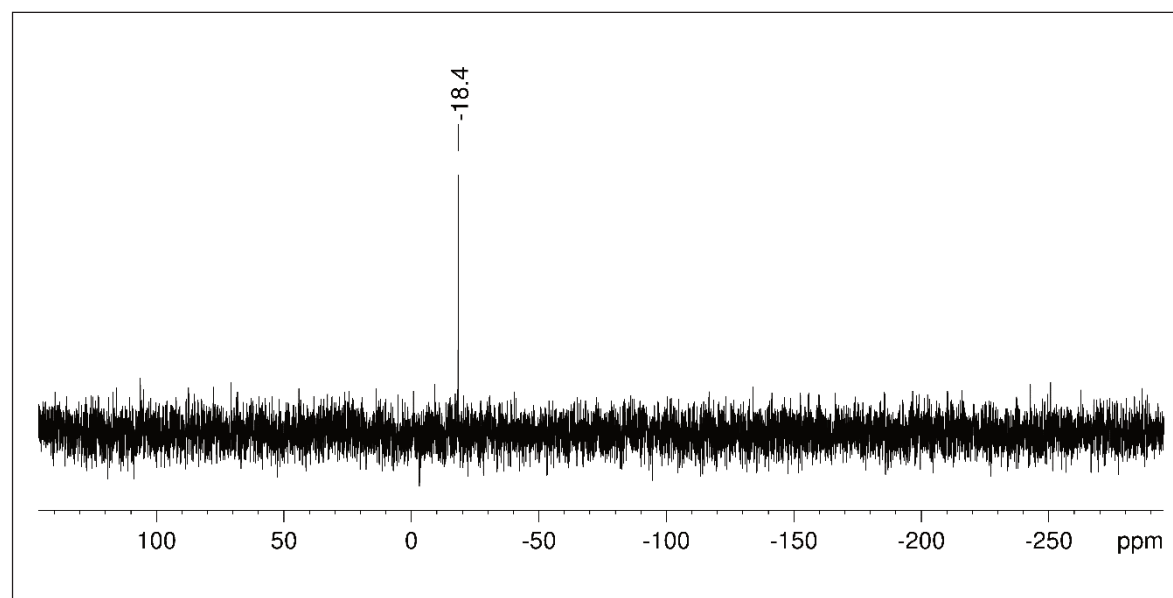


Figure UPR14. $^{29}\text{Si}\{^1\text{H}\}$ -dept NMR spectrum (60 MHz, $[\text{D}_6]\text{benzene}$) of complex **GGy** at 26 °C.

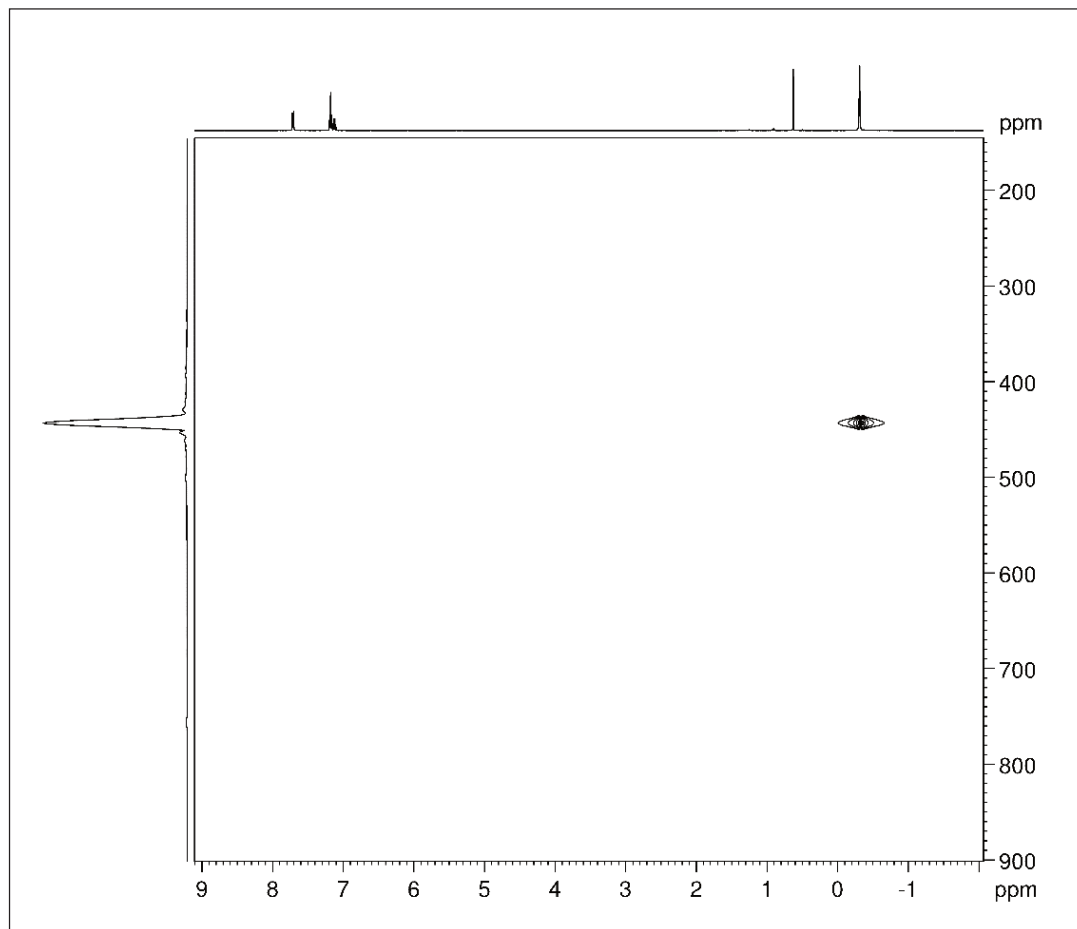


Figure UPR15. ^1H - ^{89}Y HSQC NMR spectrum (25 MHz, $[\text{D}_6]$ benzene) of complex GG_Y at 26 °C.

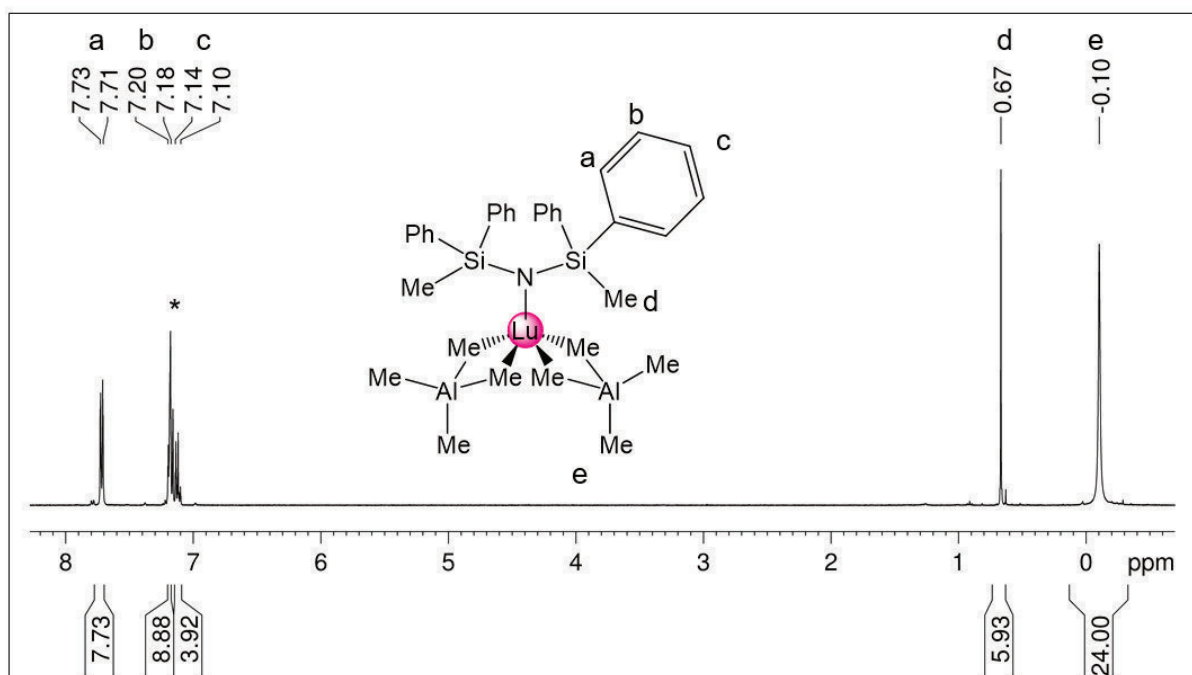


Figure UPR16. ^1H NMR spectrum (400 MHz, $[\text{D}_6]$ benzene) of complex GG_Lu at 26 °C.

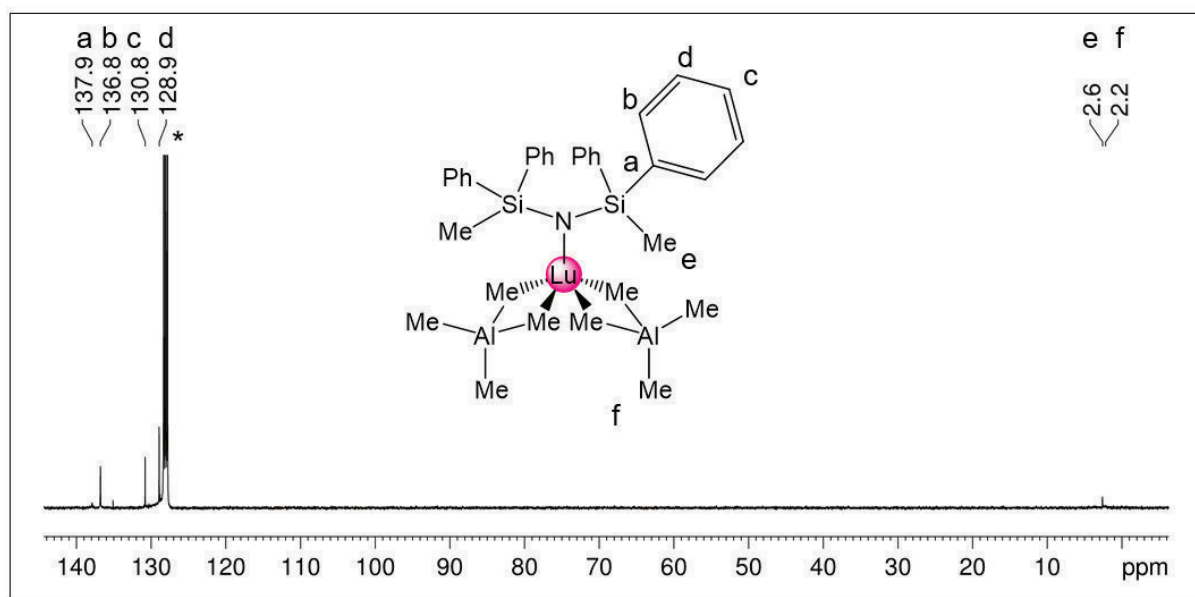


Figure UPR17. ¹³C{¹H} NMR spectrum (101 MHz, [D₆]benzene) of complex **GG_{Lu}** at 26 °C.

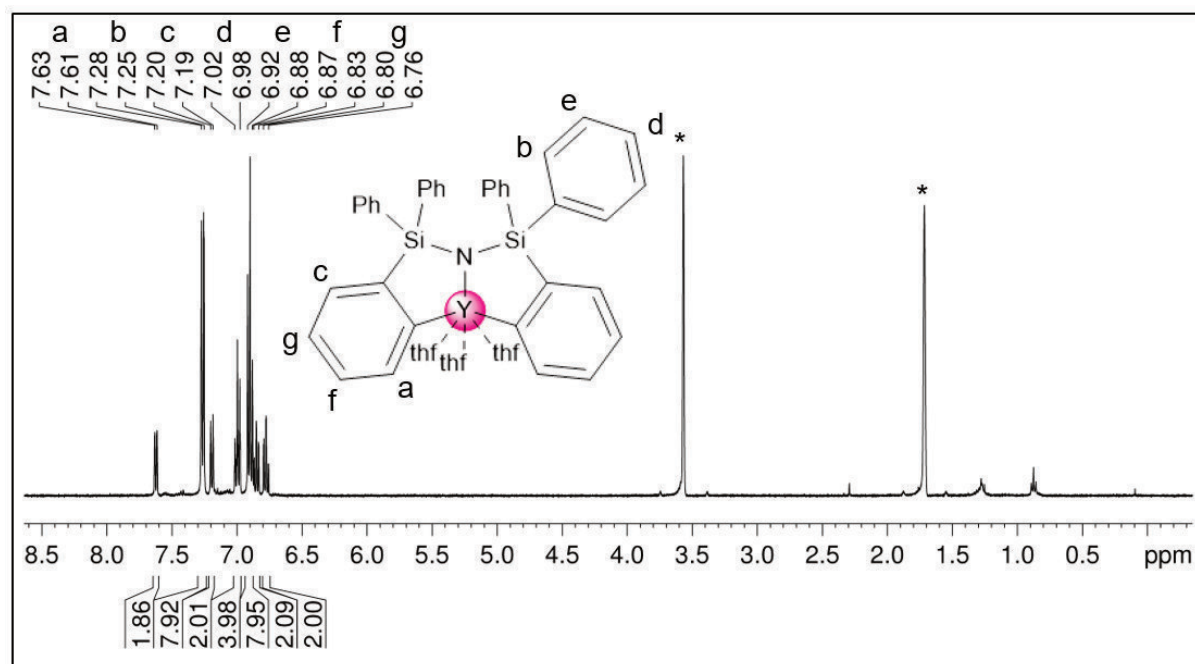


Figure UPR18. ¹H NMR spectrum (400 MHz, [D₈]thf) of complex **HH_Y** at 26 °C with traces of *n*-hexane.

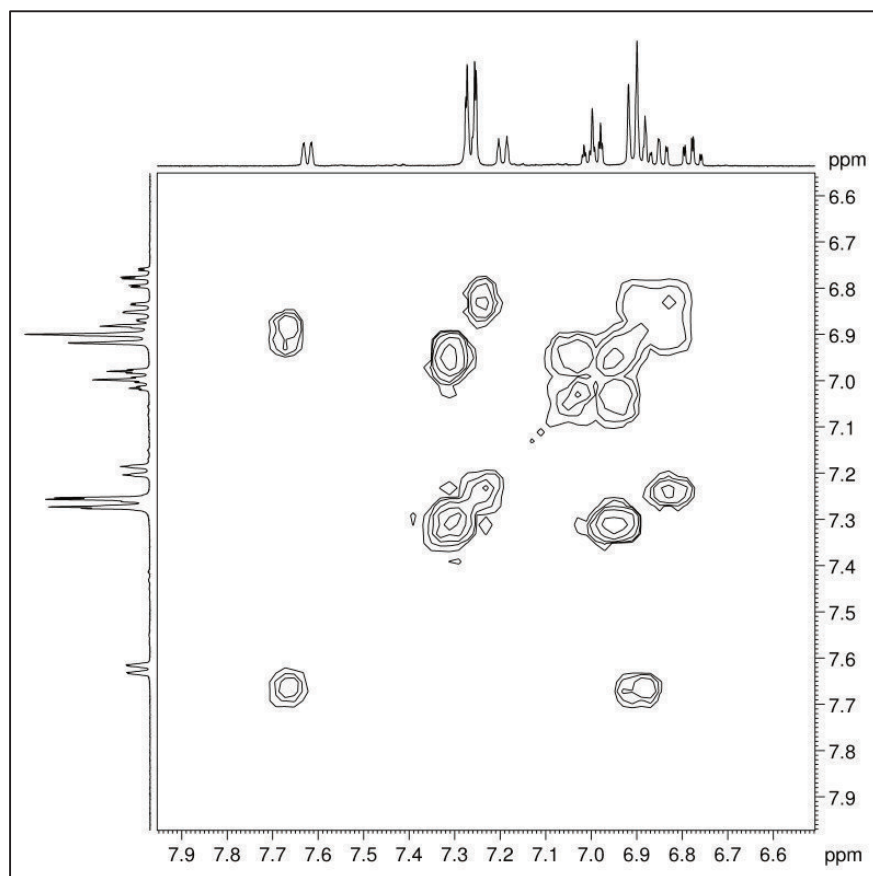


Figure UPR19. ^1H - ^1H COSY NMR spectrum (400 MHz, $[\text{D}_8]\text{thf}$) of complex HH_V at 26 °C.

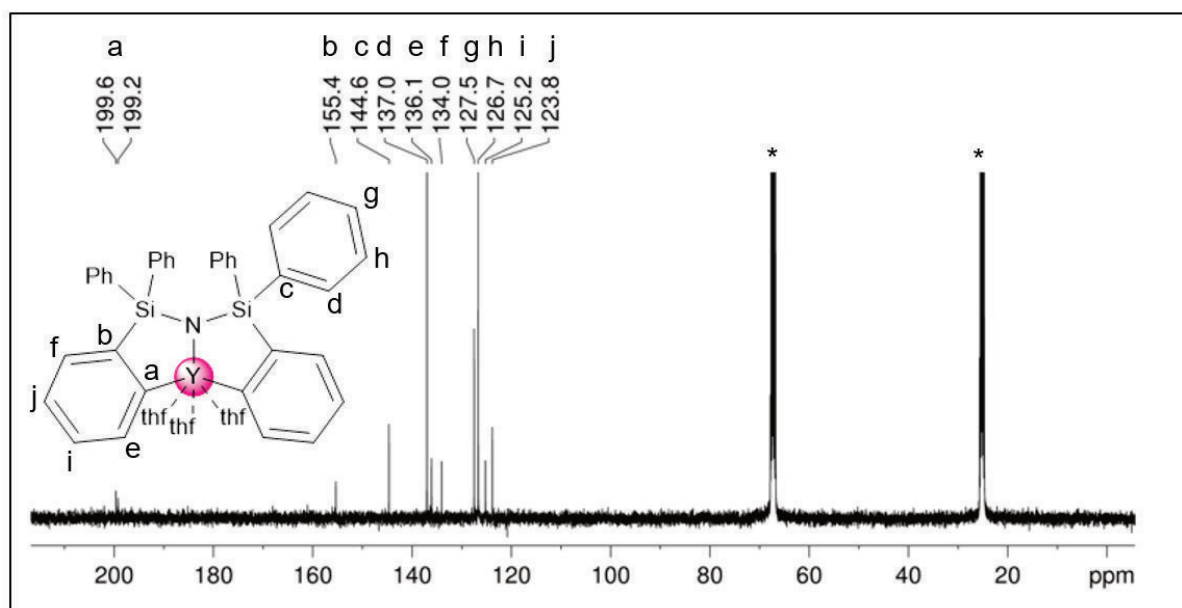


Figure UPR20. $^{13}\text{C}\{^1\text{H}\}$ NMR spectrum (101 MHz, $[\text{D}_8]\text{thf}$) of complex HH_V at 26 °C.

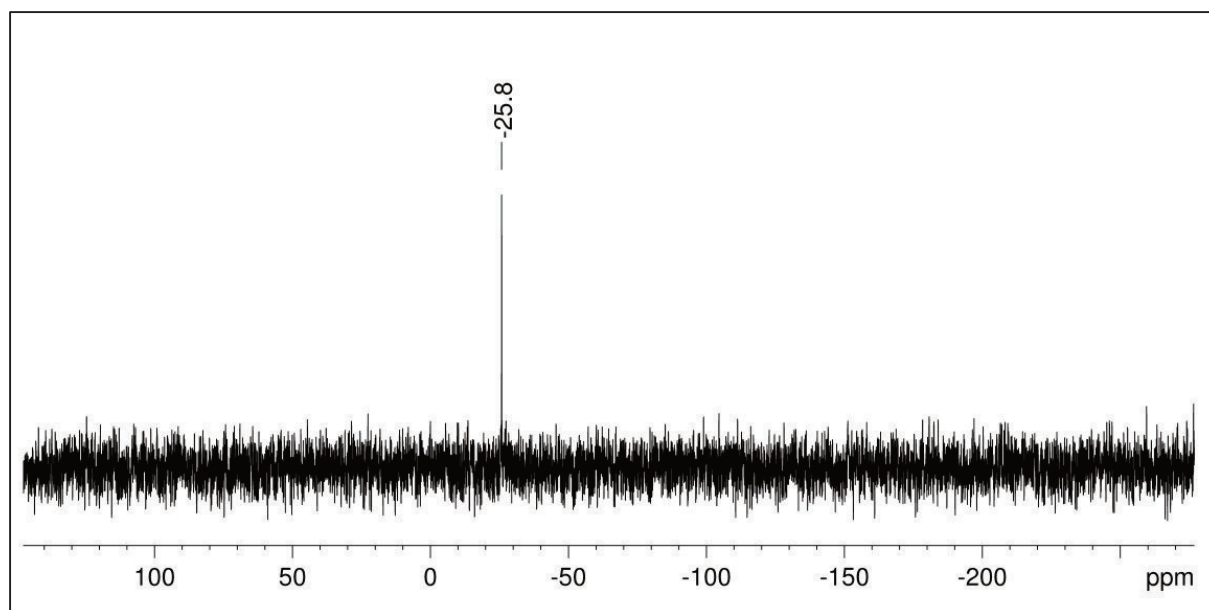


Figure UPR21. $^{29}\text{Si}\{^1\text{H}\}$ -dept NMR spectrum (60 MHz, $[\text{D}_8]\text{thf}$) of complex HH_Y at 26 °C.

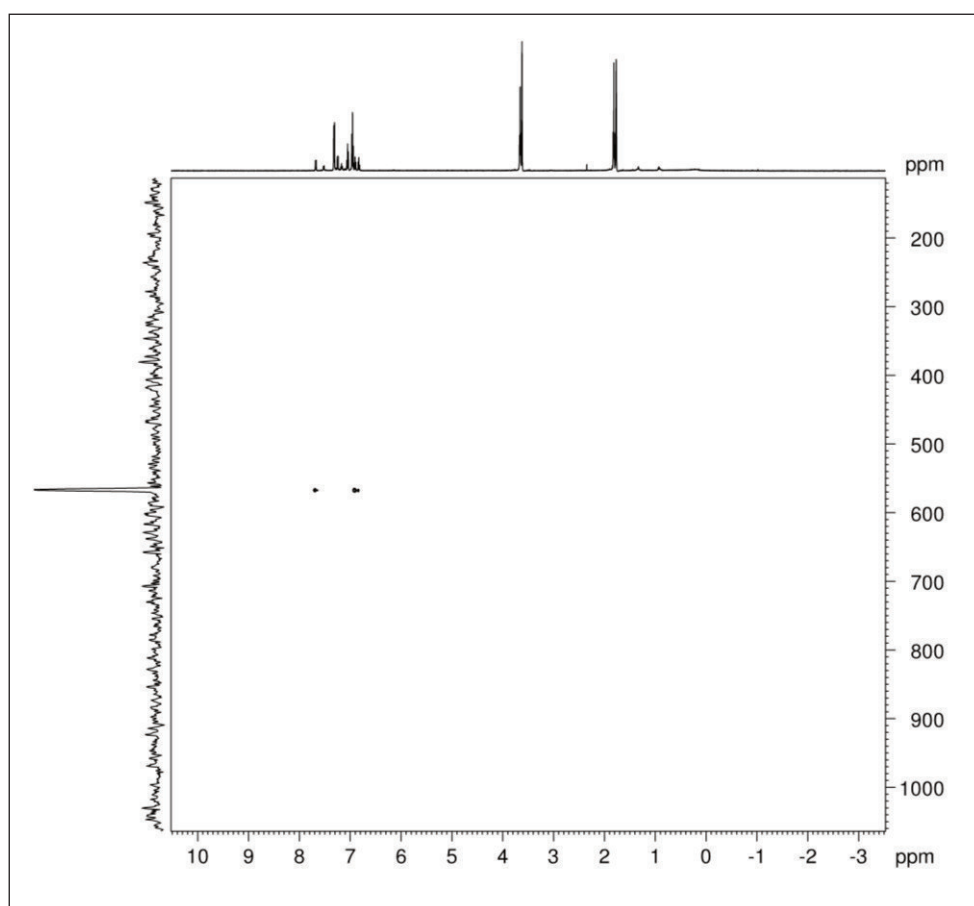


Figure UPR22. ^1H - ^{89}Y HSQC NMR spectrum (25 MHz, $[\text{D}_8]\text{thf}$) of complex HH_Y at 26 °C.

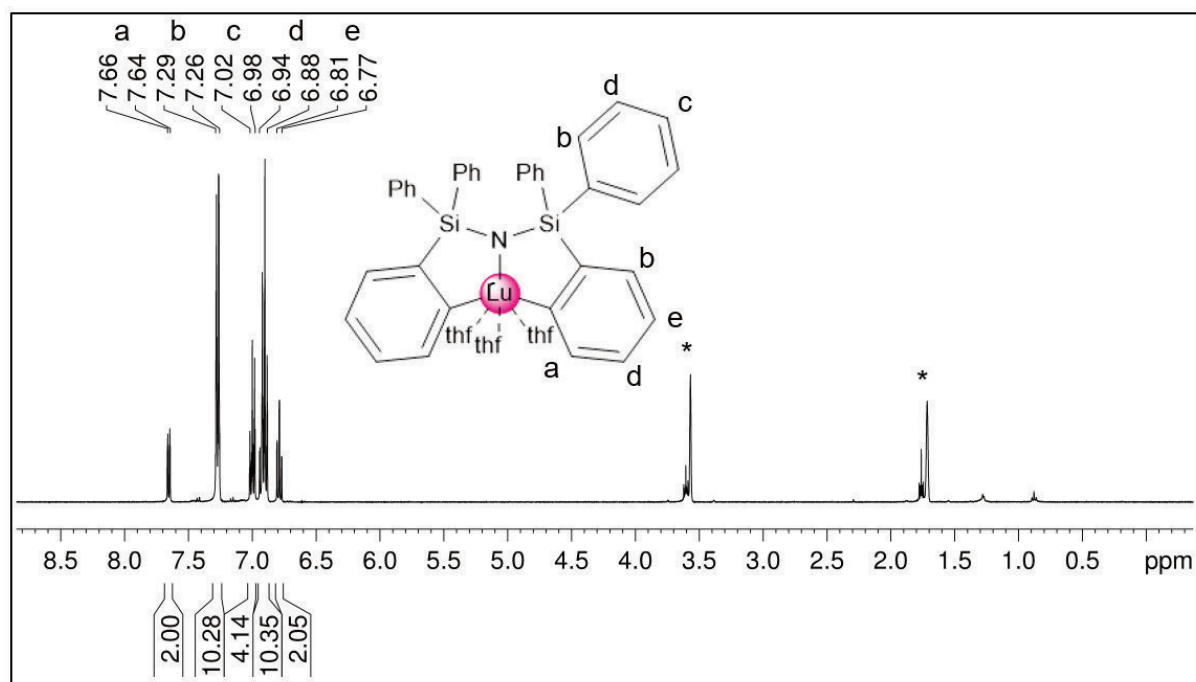


Figure UPR23. ^1H NMR spectrum (400 MHz, $[\text{D}_8]\text{thf}$) of complex HH_{Lu} at 26 °C with traces of *n*-hexane.

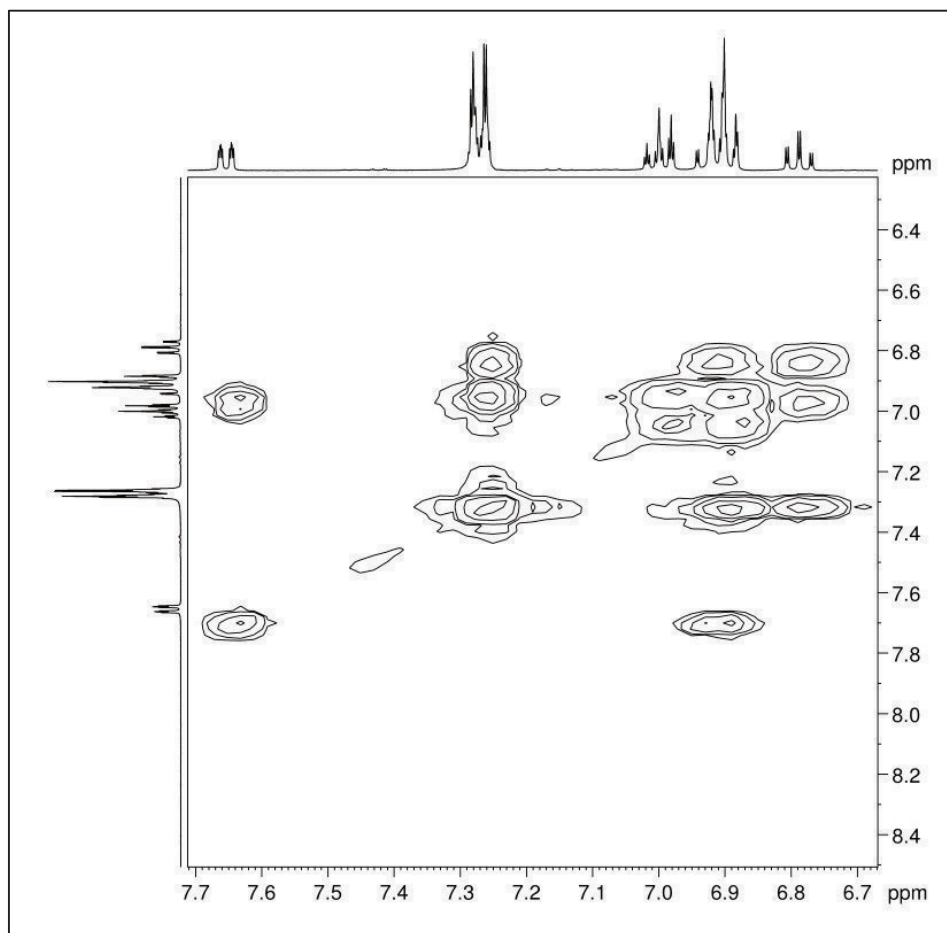


Figure UPR24. ^1H - ^1H COSY NMR spectrum (400 MHz, $[\text{D}_8]\text{thf}$) of complex HH_{Lu} at 26 °C.

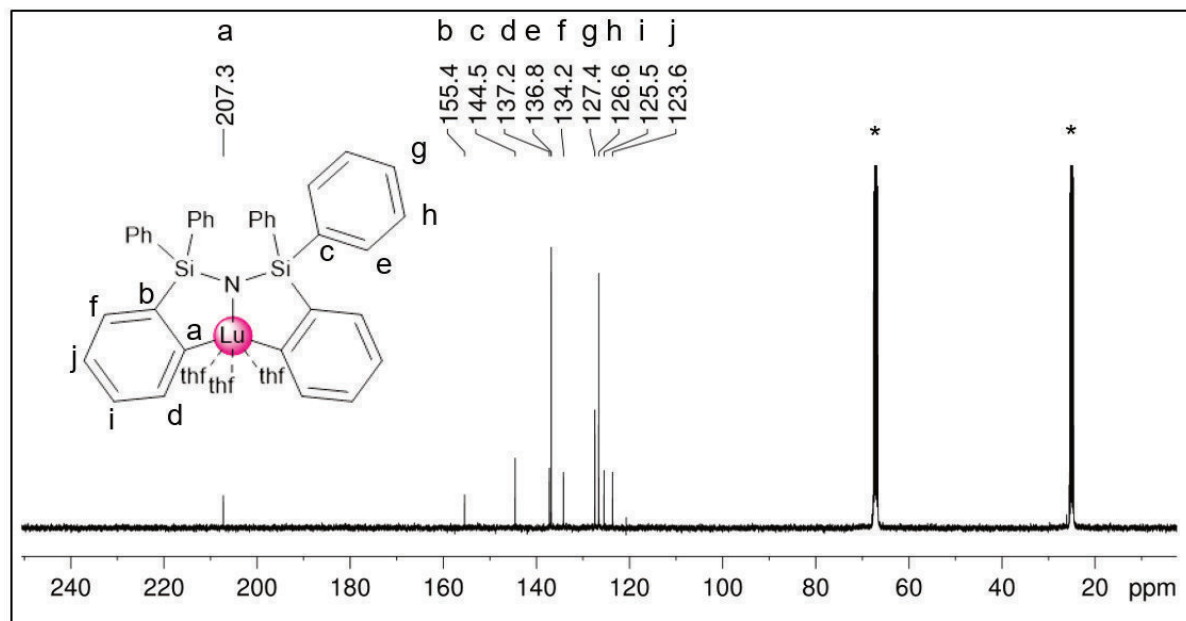


Figure UPR25. $^{13}\text{C}\{^1\text{H}\}$ NMR spectrum (101 MHz, $[\text{D}_8]\text{thf}$) of complex HHLu at 26 °C.

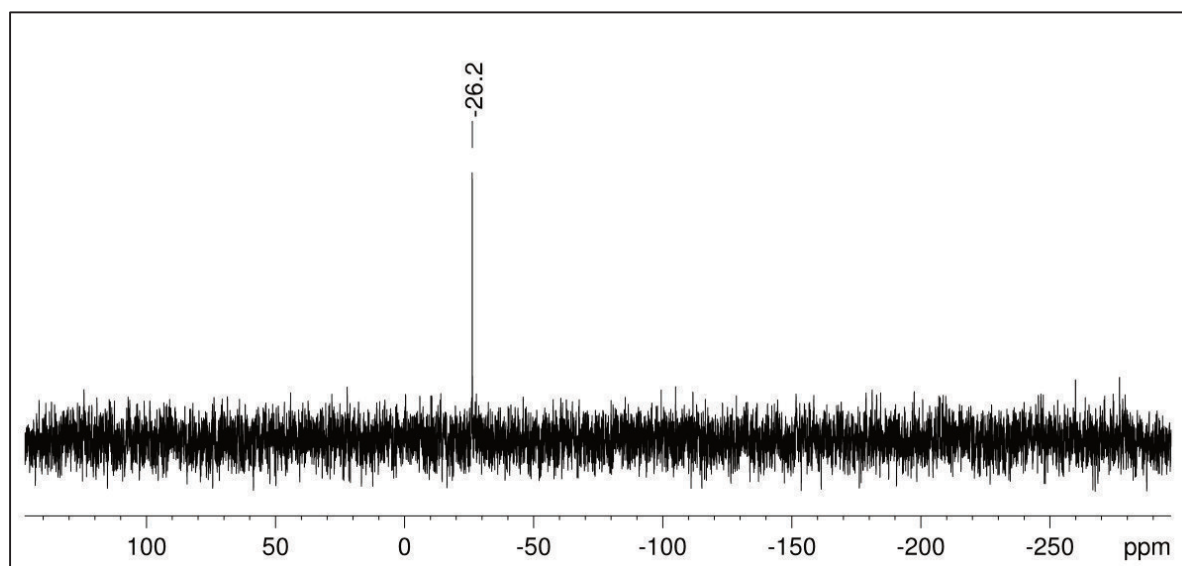


Figure UPR26. $^{29}\text{Si}\{^1\text{H}\}$ -dept NMR spectrum (60 MHz, $[\text{D}_8]\text{thf}$) of complex HHLu at 26 °C.

Table S1. Comprehensive crystallographic data for compounds **EE**, **HH_Y**, and **HH_{Lu}**.

	EE	HH_Y	HH_{Lu}
formula	C ₇₆ H ₁₁₂ Lu ₂ N ₂ O ₂ Si ₈	C ₅₅ H ₆₀ NO ₃ Si ₂ Y	C ₅₅ H ₆₀ NO ₃ Si ₂ Lu
M [g mol ⁻¹]	1660.33	928.13	1014.19
crystal system	monoclinic	monoclinic	monoclinic
space group	<i>P</i> 2 ₁	<i>P</i> 2 ₁ / <i>c</i>	<i>P</i> 2 ₁ / <i>c</i>
a [Å]	10.3066(8)	11.715(5)	11.7435(9)
b [Å]	40.211(3)	12.156(6)	12.0158(9)
c [Å]	10.6985(8)	34.014(16)	34.138(3)
α [°]	90	90	90
β [°]	114.5430(10)	97.892(12)	97.3510(10)
γ [°]	90	90	90
V [Å ³]	4033.3(5)	4798(4)	4777.5(6)
Z	2	4	4
T [K]	100(2)	100(2)	100(2)
ρ _{calcd} [g cm ⁻³]	1.367	1.285	1.410
μ [mm ⁻¹]	2.595	1.309	2.161
F (000)	1704	1952	2080
Θ range [°]	5.06 to 21.54	1.209 to 28.281	1.992 to 30.109
total reflns	112281	55510	105907
unique reflns	23356	11901	14060
R _{int}	0.0862	0.0681	0.0421
observed reflns (I>2σ)	23356	8806	12870
Data/restraints/parameter	23356 / 1 / 828	11901 / 124 / 598	14060 / 258 / 675
R1/wR2 (I>2σ) ^[a]	0.0440 / 0.0964	0.0560 / 0.1087	0.0225 / 0.0488
R1/wR2 (all data) ^[a]	0.0520 / 0.1011	0.0863 / 0.1179	0.0262 / 0.0500
GOF ^[a]	0.988	1.082	1.073
largest diff. peak and hole [e Å ⁻³]	6.977 and -1.029	0.993 and -0.753	0.765 and -1.173

[a] R1 = $\Sigma(|F_o| - |F_c|) / \Sigma|F_o|, F_o > 4\sigma(F_o)$. wR2 = $\{\Sigma[w(F_o^2 - F_c^2)^2] / \Sigma[w(F_o^2)^2]\}^{1/2}$.

D

Bibliography

- [1] a) E. O. Fischer, A. Maasböl, *Angew. Chem. Int. Ed.* **1964**, *3*, 580-581; b) T. M. Trnka, R. H. Grubbs, *Acc. Chem. Res.* **2001**, *34*, 18-29; c) R. R. Schrock, *Chem. Rev.* **2002**, *102*, 145-180; d) F. E. Hahn, M. C. Jahnke, *Angew. Chem. Int. Ed.* **2008**, *47*, 3122-3172; *Angew. Chem.* **2008**, *120*, 3166-3216; e) K. H. Dötz, J. Stendel, *Chem. Rev.* **2009**, *109*, 3227-3274; f) M. Ephritikhine, *Compt. Rend. Chim.* **2013**, *16*, 391-405; g) G. Bertrand, *Carbene Chemistry - from fleeting intermediates to powerful reagents* **2002**, Marcel Dekker, Inc.
- [2] C. Elschenbroich, *Organometallchemie, 6. überarbeitete Auflage* **2008**, B. G. Teubner Verlag / GWV Fachverlage GmbH, Wiesbaden 2008, 308-323.
- [3] a) J. Kratsch, P. W. Roesky, *Angew. Chem. Int. Ed.* **2014**, *53*, 376-383; *Angew. Chem.* **2014**, *126*, 384-391; b) J. Scott, D. J. Mindiola, *Dalton Trans.* **2009**, 8463-8472; c) O. T. Summerscales, J. C. Gordon, *RSC Adv.* **2013**, *3*, 6682-6692.
- [4] G. R. Giesbrecht, J. C. Gordon, *Dalton Trans.* **2004**, 2387-2393.
- [5] a) M. Zimmermann, D. Rauschmaier, K. Eichele, K. W. Törnroos, R. Anwänder, *Chem. Commun.* **2010**, *46*, 5346-5348; b) W. X. Zhang, Z. Wang, M. Nishiura, Z. Xi, Z. Hou, *J. Am. Chem. Soc.* **2011**, *133*, 5712-5715; c) D. Schädle, M. Meermann-Zimmermann, C. Maichle-Mössmer, C. Schädle, K. W. Törnroos, R. Anwänder, *Dalton Trans.* **2015**, *44*, 18101-18110.
- [6] H. Schumann, J. Müller, *Angew. Chem.* **1978**, *90*, 307-308.
- [7] P. L. Watson, *J. Am. Chem. Soc.* **1983**, *105*, 6491-6493.
- [8] a) H. M. Dietrich, G. Raudaschl-Sieber, R. Anwänder, *Angew. Chem. Int. Ed.* **2005**, *44*, 5303-5306; *Angew. Chem.* *117*, 5437-5440; b) D. Barisic, D. Diether, C. Maichle-Mössmer, R. Anwänder, *J. Am. Chem. Soc.* **2019**, *141*, 13931-13940.
- [9] a) H. M. Dietrich, H. Grove, K. W. Törnroos, R. Anwänder, *J. Am. Chem. Soc.* **2006**, *128*, 1458-1459; b) A. D. Sadow, T. D. Tilley, *J. Am. Chem. Soc.* **2003**, *125*, 7971-7977; c) P. L. Watson, G. W. Parshall, *Acc. Chem. Res.* **2002**, *18*, 51-56; d) T. Ziegler, E. Folga, A. Berces, *J. Am. Chem. Soc.* **1993**, *115*, 636-646; e) M. E. Thompson, J. E. Bercaw, *Pure Appl Chem* **1984**, *56*, 1-11; f) P. J. Davidson, M. F. Lappert, R. Pearce, *Chem. Rev.* **1976**, *76*, 219-242; g) M. Zimmermann, R. Anwänder, *Chem. Rev.* **2010**, *110*, 6194-6259.
- [10] R. D. Shannon, *Acta Crystallogr. Sect. A* **1976**, *32*, 751-767.
- [11] M. Zimmermann, R. Litlabø, K. W. Törnroos, R. Anwänder, *Organometallics* **2009**, *28*, 6646-6649.
- [12] J. Holton, M. F. Lappert, D. G. H. Ballard, R. Pearce, J. L. Atwood, W. E. Hunter, *J. Chem. Soc., Dalton Trans.* **1979**, 54-61.
- [13] W. J. Evans, R. Dominguez, T. P. Hanusa, *Organometallics* **1986**, *5*, 263-270.
- [14] W. J. Evans, D. K. Drummond, T. P. Hanusa, R. J. Doedens, *Organometallics* **1987**, *6*, 2279-2285.

- [15] a) W. J. Evans, J. M. Perotti, J. W. Ziller, *J. Am. Chem. Soc.* **2005**, *127*, 3894-3909; b) M. E. Thompson, S. M. Baxter, A. R. Bulls, B. J. Burger, M. C. Nolan, B. D. Santarsiero, W. P. Schaefer, J. E. Bercaw, *J. Am. Chem. Soc.* **1987**, *109*, 203-219.
- [16] H. Schumann, M. R. Keitsch, J. Winterfeld, S. Mühle, G. A. Molander, *J. Organomet. Chem.* **1998**, *559*, 181-190.
- [17] a) A. Z. Voskoboynikov, I. N. Parshina, A. K. Shestakova, K. P. Butin, I. P. Beletskaya, L. a. G. Kuz'mina, J. A. K. Howard, *Organometallics* **1997**, *16*, 4041-4055; b) S. D. Stults, R. A. Andersen, A. Zalkin, *J. Organomet. Chem.* **1993**, *462*, 175-182; c) Q. Shen, Y. Cheng, Y. Lin, *J. Organomet. Chem.* **1991**, *419*, 293-298.
- [18] a) Y. Satoh, N. Ikitake, Y. Nakayama, S. Okuno, H. Yasuda, *J. Organomet. Chem.* **2003**, *667*, 42-52; b) H. Schumann, M. R. Keitsch, J. Demtschuk, G. A. Molander, *J. Organomet. Chem.* **1999**, *582*, 70-82.
- [19] H. Schumann, M. R. Keitsch, S. H. Mühle, *Z. Anorg. Allg. Chem.* **2002**, *628*, 1311-1318.
- [20] M. Zimmermann, J. Takats, G. Kiel, K. W. Törnroos, R. Anwander, *Chem. Commun.* **2008**, *5*, 612-614.
- [21] D. Robert, T. P. Spaniol, J. Okuda, *Eur. J. Inorg. Chem.* **2008**, 2801-2809.
- [22] a) C. O. Hollfelder, M. Meermann-Zimmermann, G. Spiridopoulos, D. Werner, K. W. Törnroos, C. Maichle-Mössmer, R. Anwander, *Molecules* **2019**, *24*; b) C. O. Hollfelder, L. N. Jende, H. M. Dietrich, K. Eichele, C. Maichle-Mössmer, R. Anwander, *Chem. Eur. J.* **2019**, *25*, 7298-7302.
- [23] P. G. Hayes, W. E. Piers, L. W. M. Lee, L. K. Knight, M. Parvez, M. R. J. Elsegood, W. Clegg, *Organometallics* **2001**, *20*, 2533-2544.
- [24] K. D. Conroy, W. E. Piers, M. Parvez, *J. Organomet. Chem.* **2008**, *693*, 834-846.
- [25] D. Schädle, C. Maichle-Mössmer, C. Schädle, R. Anwander, *Chem. Eur. J.* **2015**, *21*, 662-670.
- [26] J. Zhou, L. Xiang, J. Guo, X. Leng, Y. Chen, *Chem. Eur. J.* **2017**, *23*, 5424-5428.
- [27] J. Scott, H. Fan, B. F. Wicker, A. R. Fout, M. H. Baik, D. J. Mindiola, *J. Am. Chem. Soc.* **2008**, *130*, 14438-14439.
- [28] J. Zhou, J. Chu, Y. Zhang, G. Yang, X. Leng, Y. Chen, *Angew. Chem. Int. Ed.* **2013**, *52*, 4243-4246; *Angew. Chem.* **2013**, *125*, 4337-4340.
- [29] L. D. Henderson, G. D. MacInnis, W. E. Piers, M. Parvez, *Can. J. Chem.* **2004**, *82*, 162-165.
- [30] H. Schumann, J. Müller, *J. Organomet. Chem.* **1979**, *169*, C1-C4.
- [31] K. Aparna, M. Ferguson, R. G. Cavell, *J. Am. Chem. Soc.* **2000**, *122*, 726-727.

- [32] a) T. Cantat, F. Jaroschik, F. Nief, L. Ricard, N. Mezailles, P. Le Floch, *Chem. Commun.* **2005**, 5178-5180; b) T. Cantat, F. Jaroschik, L. Ricard, P. Le Floch, F. Nief, N. Mézailles, *Organometallics* **2006**, *25*, 1329-1332.
- [33] H. M. Dietrich, K. W. Törnroos, R. Anwander, *J. Am. Chem. Soc.* **2006**, *128*, 9298-9299.
- [34] R. Litlabø, M. Zimmermann, K. Saliu, J. Takats, K. W. Törnroos, R. Anwander, *Angew. Chem. Int. Ed.* **2008**, *47*, 9560-9564; *Angew. Chem.* **2008**, *120*, 9702-9706.
- [35] L. C. Gerber, E. Le Roux, K. W. Tornroos, R. Anwander, *Chem. Eur. J.* **2008**, *14*, 9555-9564.
- [36] a) D. P. Mills, O. J. Cooper, J. McMaster, W. Lewis, S. T. Liddle, *Dalton Trans.* **2009**, 4547-4555; b) A. J. Wooles, D. P. Mills, W. Lewis, A. J. Blake, S. T. Liddle, *Dalton Trans.* **2010**, 500-510; c) A. Buchard, A. Auffrant, L. Ricard, X. F. Le Goff, R. H. Platel, C. K. Williams, P. Le Floch, *Dalton Trans.* **2009**, 10219-10222; d) S. T. Liddle, J. McMaster, J. C. Green, P. L. Arnold, *Chem. Commun.* **2008**, 1747-1749; e) D. P. Mills, A. J. Wooles, J. McMaster, W. Lewis, A. J. Blake, S. T. Liddle, *Organometallics* **2009**, *28*, 6771-6776; f) F. Ortu, M. Gregson, A. J. Wooles, D. P. Mills, S. T. Liddle, *Organometallics* **2017**, *36*, 4584-4590; g) A. J. Wooles, O. J. Cooper, J. McMaster, W. Lewis, A. J. Blake, S. T. Liddle, *Organometallics* **2010**, *29*, 2315-2321; h) M. Gregson, E. Lu, J. McMaster, W. Lewis, A. J. Blake, S. T. Liddle, *Angew. Chem. Int. Ed.* **2013**, *52*, 13016-13019; *Angew. Chem.* **2013**, *125*, 13254-13257.
- [37] M. Gregson, E. Lu, D. P. Mills, F. Tuna, E. J. McInnes, C. Hennig, A. C. Scheinost, J. McMaster, W. Lewis, A. J. Blake, A. Kerridge, S. T. Liddle, *Nature Commun.* **2017**, *8*, 14137.
- [38] M. Fustier, X.-F. Le Goff, M. Lutz, J. C. Slootweg, N. Mézailles, *Organometallics* **2014**, *34*, 63-72.
- [39] M. Gregson, N. F. Chilton, A. M. Ariciu, F. Tuna, I. F. Crowe, W. Lewis, A. J. Blake, D. Collison, E. J. L. McInnes, R. E. P. Winpenny, S. T. Liddle, *Chem. Sci.* **2016**, *7*, 155-165.
- [40] a) A. Venugopal, I. Kamps, D. Bojer, R. J. Berger, A. Mix, A. Willner, B. Neumann, H. G. Stammler, N. W. Mitzel, *Dalton Trans.* **2009**, 5755-5765; b) D. Bojer, A. Venugopal, A. Mix, B. Neumann, H. G. Stammler, N. W. Mitzel, *Chem. Eur. J.* **2011**, *17*, 6248-6255; c) D. Bojer, B. Neumann, H. G. Stammler, N. W. Mitzel, *Chem. Eur. J.* **2011**, *17*, 6239-6247; d) D. Bojer, B. Neumann, H. G. Stammler, N. W. Mitzel, *Eur. J. Inorg. Chem.* **2011**, 3791-3796.
- [41] Y. Takenaka, T. Shima, J. Baldamus, Z. Hou, *Angew. Chem. Int. Ed.* **2009**, *48*, 7888-7891; *Angew. Chem.* **2009**, *121*, 8028-8031.
- [42] a) J. Hong, L. Zhang, X. Yu, M. Li, Z. Zhang, P. Zheng, M. Nishiura, Z. Hou, X. Zhou, *Chem. Eur. J.* **2011**, *17*, 2130-2137; b) J. Hong, H. Tian, L. Zhang, X. Zhou, I. Del Rosal, L. Weng, L. Maron, *Angew. Chem. Int. Ed.* **2018**, *57*, 1062-1067; *Angew. Chem.* **2018**, *130*, 1074-1079.
- [43] L. N. Jende, *PhD Thesis* **2015**.
- [44] W. Huang, C. T. Carver, P. L. Diaconescu, *Inorg. Chem.* **2011**, *50*, 978-984.

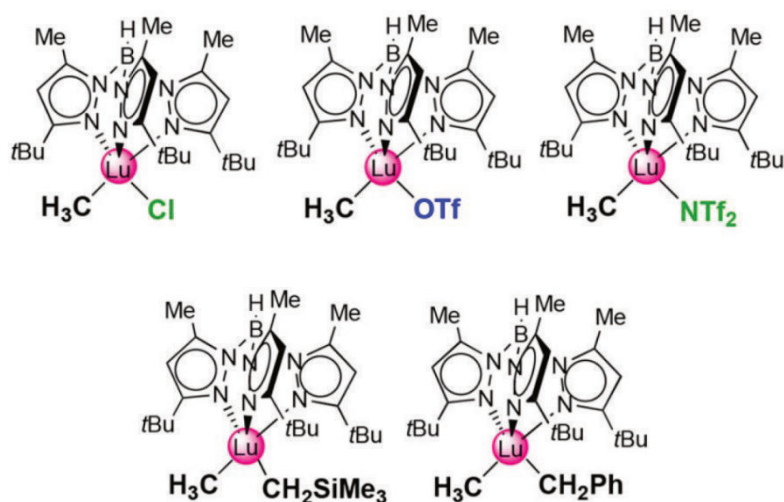
- [45] S. Li, M. Wang, B. Liu, L. Li, J. Cheng, C. Wu, D. Liu, J. Liu, D. Cui, *Chem. Eur. J.* **2014**, *20*, 15493-15498.
- [46] J. Zhou, T. Li, L. Maron, X. Leng, Y. Chen, *Organometallics* **2015**, *34*, 470-476.
- [47] T. Li, G. Zhang, J. Guo, S. Wang, X. Leng, Y. Chen, *Organometallics* **2016**, *35*, 1565-1572.
- [48] W. Ma, C. Yu, Y. Chi, T. Chen, L. Wang, J. Yin, B. Wei, L. Xu, W. X. Zhang, Z. Xi, *Chem. Sci.* **2017**, *8*, 6852-6856.
- [49] a) W. Mao, L. Xiang, L. Maron, X. Leng, Y. Chen, *J. Am. Chem. Soc.* **2017**, *139*, 17759-17762; b) W. Mao, L. Xiang, C. Alvarez Lamsfus, L. Maron, X. Leng, Y. Chen, *J. Am. Chem. Soc.* **2017**, *139*, 1081-1084; c) C. Wang, W. Mao, L. Xiang, Y. Yang, J. Fang, L. Maron, X. Leng, Y. Chen, *Chem. Eur. J.* **2018**, *24*, 13903-13917; d) C. Wang, L. Xiang, Y. Yang, J. Fang, L. Maron, X. Leng, Y. Chen, *Chem. Eur. J.* **2018**, *24*, 5637-5643.
- [50] D. P. Mills, W. Lewis, A. J. Blake, S. T. Liddle, *Organometallics* **2013**, *32*, 1239-1250.
- [51] a) S. T. Liddle, D. P. Mills, A. J. Wooles, *Chem. Soc. Rev.* **2011**, *40*, 2164-2176; b) D. P. Mills, L. Soutar, W. Lewis, A. J. Blake, S. T. Liddle, *J. Am. Chem. Soc.* **2010**, *132*, 14379-14381.
- [52] M. Fustier-Boutignon, N. Mézailles, *Topics in Organometallic Chemistry, vol 47. Stable Geminal Dianions as Precursors for Gem-Diorganometallic and Carbene Complexes* **2014**, *47*, 63-127.
- [53] J. Hong, L. Zhang, K. Wang, Y. Zhang, L. Weng, X. Zhou, *Chem. Eur. J.* **2013**, *19*, 7865-7873.
- [54] K. Wang, G. Luo, J. Hong, X. Zhou, L. Weng, Y. Luo, L. Zhang, *Angew. Chem. Int. Ed. Engl.* **2014**, *53*, 1053-1056; *Angew. Chem.* **2014**, *126*, 1071-1074.
- [55] T. Li, M. Nishiura, J. Cheng, Y. Li, Z. Hou, *Chem. Eur. J.* **2012**, *18*, 15079-15085.
- [56] T. Li, M. Nishiura, J. Cheng, W. Zhang, Y. Li, Z. Hou, *Organometallics* **2013**, *32*, 4142-4148.
- [57] W. Mao, L. Xiang, C. A. Lamsfus, L. Maron, X. Leng, Y. Chen, *Chin. J. Chem.* **2018**, *36*, 904-908.
- [58] L. N. Grant, S. Ahn, B. C. Manor, M. H. Baik, D. J. Mindiola, *Chem. Commun.* **2017**, *53*, 3415-3417.
- [59] a) N. A. Petasis, E. I. Bzowej, *J. Am. Chem. Soc.* **1990**, *112*, 6392-6394; b) N. A. Petasis, S. P. Lu, E. I. Bzowej, D. K. Fu, J. P. Staszewski, I. Akritopoulou-Zanze, M. A. Patane, Y. H. Hu, *Pure Appl Chem* **1996**, *68*, 667-670.
- [60] V. M. Birkelbach, R. Thim, C. Stuhl, C. Maichle-Mössmer, R. Anwänder, *Chem. Eur. J.* **2019**, *25*, 14711-14720.

- [61] a) S.-Y. Liu, G. H. Maunder, A. Sella, M. Stevenson, D. A. Tocher, *Inorg. Chem.* **1996**, *35*, 76-81; b) R. J. H. Clark, S. Y. Liu, G. H. Maunder, A. Sella, M. R. J. Elsegood, *J. Chem. Soc., Dalton Trans.* **1997**, 2241-2247.
- [62] a) F. A. Kunrath, O. L. Casagrande, L. Toupet, J.-F. Carpentier, *Polyhedron* **2004**, *23*, 2437-2445; b) N. Marques, A. Sella, J. Takats, *Chem. Rev.* **2002**, *102*, 2137-2160.
- [63] M. Bonath, C. O. Hollfelder, D. Schädle, C. Maichle-Mössmer, P. Sirsch, R. Anwänder, *Eur. J. Inorg. Chem.* **2017**, 4683-4692.
- [64] C. Stuhl, C. Maichle-Mössmer, R. Anwänder, *Chem. Eur. J.* **2018**, *24*, 14254-14268.
- [65] D. M. P. Mingos, R. H. Crabtree, *Comprehensive Organometallic Chemistry III* **2006**, Vol. 4.01.
- [66] V. M. Birkelbach, C. Stuhl, C. Maichle-Mössmer, R. Anwänder, *Organometallics* **2019**, *38*, 4485-4496.
- [67] a) F. N. Tebbe, G. W. Parshall, G. S. Reddy, *J. Am. Chem. Soc.* **1978**, *100*, 3611-3613; b) J. Holton, M. F. Lappert, R. Pearce, P. I. W. Yarrow, *Chem. Rev.* **1983**, *83*, 135-201; c) R. R. Schrock, A. H. Hoveyda, *Angew. Chem. Int. Ed.* **2003**, *42*, 4592-4633; *Angew. Chem.* **2003**, *115*, 38, 4740-4782; d) R. H. Grubbs, *Tetrahedron* **2004**, *60*, 7117-7140.
- [68] J. D. Meinhart, E. V. Anslyn, R. H. Grubbs, *Organometallics* **1989**, *8*, 583-589.
- [69] H. M. Dietrich, O. Schuster, K. W. Törnroos, R. Anwänder, *Angew. Chem. Int. Ed.* **2006**, *45*, 4858-4863; *Angew. Chem.* **2006**, *18*, 4977.
- [70] a) M. Zimmermann, K. W. Törnroos, H. Sitzmann, R. Anwänder, *Chem. Eur. J.* **2008**, *14*, 7266-7277; b) H. M. Dietrich, C. Zapilko, E. Herdtweck, R. Anwänder, *Organometallics* **2005**, *24*, 5767-5771.
- [71] R. Thompson, E. Nakamaru-Ogiso, C.-H. Chen, M. Pink, D. J. Mindiola, *Organometallics* **2013**, *33*, 429-432.
- [72] a) X. Gu, L. Zhang, X. Zhu, S. Wang, S. Zhou, Y. Wei, G. Zhang, X. Mu, Z. Huang, D. Hong, F. Zhang, *Organometallics* **2015**, *34*, 4553-4559; b) X. Gu, X. Zhu, Y. Wei, S. Wang, S. Zhou, G. Zhang, X. Mu, *Organometallics* **2014**, *33*, 2372-2379.
- [73] G. Scarel, C. Wiemer, M. Fanciulli, I. L. Fedushkin, G. K. Fukin, G. A. Domrachev, Y. Lebedinskii, A. Zenkevich, G. Pavia, *Z. Anorg. Allg. Chem.* **2007**, *633*, 2097-2103.
- [74] H. Schumann, D. M. M. Freckmann, S. Dechert, *Z. Anorg. Allg. Chem.* **2002**, *628*, 2422-2426.

E

Publications

Potential Precursors for Terminal Methylidene Rare-Earth-Metal Complexes Supported by a Superbulky Tris(pyrazolyl)borato Ligand



<https://doi.org/10.1002/chem.201903606>

reprinted with permission from

Chem. Eur. J. **2019**, *25*, 14711-14720

License Number 4701980158697

Rare-Earth Metals | Hot Paper

Potential Precursors for Terminal Methylidene Rare-Earth-Metal Complexes Supported by a Superbulky Tris(pyrazolyl)borato Ligand

Verena M. Birkelbach, Renita Thim, Christoph Stuhl, Cäcilia Maichle-Mössmer, and Reiner Anwander*^[a]

Abstract: A series of solvent-free heteroleptic terminal rare-earth-metal alkyl complexes stabilized by a superbulky tris(pyrazolyl)borato ligand with the general formula $[\text{Tp}^{\text{fBu,Me}}\text{LnMeR}]$ have been synthesized and fully characterized. Treatment of the heterobimetallic mixed methyl/tetramethylaluminum compounds $[\text{Tp}^{\text{fBu,Me}}\text{LnMe}(\text{AlMe}_4)]$ ($\text{Ln} = \text{Y}, \text{Lu}$) with two equivalents of the mild halogenido transfer reagents SiMe_3X ($\text{X} = \text{Cl}, \text{I}$) gave $[\text{Tp}^{\text{fBu,Me}}\text{LnX}_2]$ in high yields. The addition of only one equivalent of SiMe_3Cl to $[\text{Tp}^{\text{fBu,Me}}\text{LuMe}(\text{AlMe}_4)]$ selectively afforded the desired mixed methyl/chloride complex $[\text{Tp}^{\text{fBu,Me}}\text{LuMeCl}]$. Further reactivity studies of $[\text{Tp}^{\text{fBu,Me}}\text{LuMeCl}]$ with LiR or KR ($\text{R} = \text{CH}_2\text{Ph}, \text{CH}_2\text{SiMe}_3$) through salt metathesis led to the monomeric

mixed-alkyl derivatives $[\text{Tp}^{\text{fBu,Me}}\text{LuMe}(\text{CH}_2\text{SiMe}_3)]$ and $[\text{Tp}^{\text{fBu,Me}}\text{LuMe}(\text{CH}_2\text{Ph})]$, respectively, in good yields. The SiMe_4 elimination protocols were also applicable when using SiMe_3X featuring more weakly coordinating moieties (here $\text{X} = \text{OTf}, \text{NTf}_2$). X-ray structure analyses of this diverse set of new $[\text{Tp}^{\text{fBu,Me}}\text{LnMeR/X}]$ compounds were performed to reveal any electronic and steric effects of the varying monoanionic ligands R and X , including exact cone-angle calculations of the tridentate tris(pyrazolyl)borato ligand. Deeper insights into the reactivity of these potential precursors for terminal alkylidene rare-earth-metal complexes were gained through NMR spectroscopic studies.

Introduction

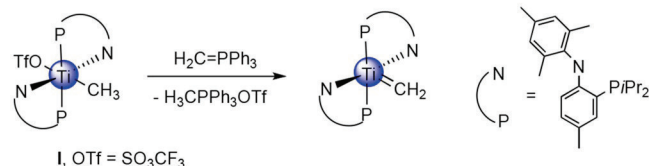
Terminal transition-metal carbene and alkylidene complexes are of fundamental importance in organometallic chemistry/catalysis and organic synthesis.^[1] In contrast, discrete terminal rare-earth-metal (Ln) alkylidene complexes of the type $\text{LLn}[\text{=CR}_2]$ ($\text{R} = \text{H}$ or hydrocarbon substituent; $\text{L} =$ monoanionic ancillary ligand) have remained elusive,^[2] which is mainly attributed to the dominance of $\text{Ln}-\text{C}$ ionic bonding and hence pronounced tendency for intermetallic bridging.^[3] Notwithstanding, such bridging alkylidene moieties were accessed in mixed methyl/methylidene,^[4] methyl/chloride,^[5] cubane-like methylidene complexes,^[6] and the first four-coordinate methandiide alkyl lutetium complex.^[7] Also, Lewis acid-stabilized^[8] or pincer-like rare-earth-metal alkylidene complexes^[9] have been reported. Recent advances in the latter areas are represented by the syntheses of the first bridged bis-alkylidene scandium complex,^[10] a non-pincer-type monometallic phosphinoalkylidene

scandium complex,^[11] and silyl-thiophosphinoyl alkylidene as well as phosphinomethylidene rare-earth-metal compounds.^[12] By nature, higher-valent transition-metal chemistry draws upon alternative approaches to access terminal alkylidenes. For example, in 2017, Mindaola and co-workers isolated the first terminal titanium methylidene complex $[(\text{PN})_2\text{Ti}(\text{=CH}_2)]$ by treating $[(\text{PN})_2\text{Ti}(\text{CH}_3)(\text{OTf})]$ (**I**, $\text{PN} = (N-(2-(\text{diisopropylphosphino})-4\text{-methylphenyl})-2,4,6\text{-trimethylanilide})$) with the Wittig reagent $\text{H}_2\text{C}=\text{PPh}_3$. This protocol involves the abstraction of the weakly coordinating OTf group ($\text{OTf} =$ trifluoromethanesulfonato, also triflate or SO_3CF_3) and formation of the reactive $\text{Ti}=\text{CH}_2$ moiety (Scheme 1, path **A**).^[13] Another prominent example in transition-metal methylidene chemistry is the reaction behavior of $[\text{Cp}_2\text{Ti}(\text{CH}_2\text{R})_2]$ (**II**, $\text{Cp} = \text{C}_5\text{H}_5$, $\text{R} = \text{H}, \text{SiMe}_3, \text{Ph}$) during thermolysis.^[14] Petasis et al. found this compound to be an olefination agent for carbonylic derivatives. Therefore, terminal alkylidenes $[\text{Cp}_2\text{Ti}(\text{=CHR})]$ were proposed as reaction intermediates (Scheme 1, path **B**), similar to the effective methylenating species of the Tebbe reagent.^[15] Although Petasis et al. could not confirm their proposal by X-ray diffraction analysis (neither did Tebbe et al.), methane elimination during thermolysis and further reactivity studies substantiated their proposal of an intermediate methylidene moiety. Additionally, mixed alkyl titanocenes, for example, $[\text{Cp}_2\text{Ti}(\text{CH}_3)(\text{CH}_2\text{SiMe}_3)]$ ^[14a] showed the ability of olefination during exposure to higher temperatures. Crucially, all the aforementioned titanium(IV) alkylidene chemistry proceeds at a relatively small Ti^{IV} center supported by two

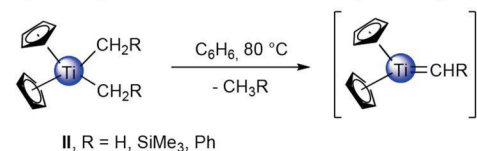
[a] V. M. Birkelbach, Dr. R. Thim, Dr. C. Stuhl, Dr. C. Maichle-Mössmer, Prof. Dr. R. Anwander
Institut für Anorganische Chemie, Eberhard Karls Universität Tübingen
Auf der Morgenstelle 18, 72076 Tübingen (Germany)
E-mail: reiner.anwander@uni-tuebingen.de
Homepage: <http://uni-tuebingen.de/syncat-anwander>

Supporting information and the ORCID identification number(s) for the author(s) of this article can be found under:
<https://doi.org/10.1002/chem.201903606>

Synthesis path A: Abstraction of leaving group followed by deprotonation



Synthesis path B: Alkane elimination through thermolysis



Scheme 1. Synthesis approaches in titanium alkylidene chemistry. **Path A** displays the formation of a terminal methylidene through abstraction of a weakly coordinating OTf group and introduction of the CH_2 group utilizing the Wittig reagent. **Path B** shows the proposed intermediate for the thermolysis and alkane/toluene elimination of dialkyl titanocenes.

monoanionic stabilizing ligands. Only recently, Okuda and co-workers reported on the structural elucidation of the anionic complex $[\text{Li}(\text{Me}_3\text{TACD})\text{Ti}(\text{CHSiMe}_3)(\text{CH}_2\text{SiMe}_3)_2]$ ($\text{Me}_3\text{TACD} = 1,4,7\text{-trimethyl-1,4,7,10-tetraazacyclododecane}$).^[16] Inspired by this transition-metal alkylidene chemistry, and in particular that of titanium, our group investigated the feasibility of rare-earth-metal variants of Mindiola's and Petasis' starting compounds, for example, $[\text{Ln}(\text{CH}_3)(\text{OTf})]$ and $[\text{Ln}(\text{CH}_3)\text{R}]$ ($\text{R} = \text{alkyl}$, $\text{L} = \text{monoanionic ancillary ligand}$). Herein, we present different reaction schemes for the synthesis of the targeted heteroleptic complexes and further reactivity studies for their utilization in rare-earth-metal alkylidene chemistry.

Results and Discussion

In search of potential precursors for terminal Ln^{III} alkylidene chemistry we focused on monomeric compounds $[\text{Tp}^{\text{tBu,Me}}\text{LnMe}(\text{AlMe}_4)]$ ($\text{Ln} = \text{Y, Lu}$)^[17] and $[\text{Tp}^{\text{tBu,Me}}\text{LuMe}_2]$ ^[18] supported by the superbulky scorpionate ligand $\text{Tp}^{\text{tBu,Me}}$ (hydrotris(3-*tert*-butyl-5-methylpyrazolyl)borato).^[19] Importantly, Piers et al. and Takats and co-workers reported similar complexes featuring $[\text{Tp}^{\text{R,Me}}\text{Sc}(\text{CH}_2\text{SiMe}_3)_2(\text{THF})_x]$ ($\text{R} = \text{Me}$, $x = 1$; $\text{R} = \text{tBu}$, $x = 0$),^[20] $[\text{Tp}^{\text{Me,Me}}\text{Ln}(\text{CH}_2\text{SiMe}_3)_2(\text{THF})]$ ($\text{Ln} = \text{Y, Nd, Sm, Yb, Lu}$),^[21] $[\text{Tp}^{\text{tBu,Me}}\text{Ln}(\text{CH}_2\text{SiMe}_3)_2]$ ($\text{Ln} = \text{Y, Yb, Lu}$),^[21] $[\text{Tp}^{\text{tPr,tPr}}\text{Ln}(\text{CH}_2\text{SiMe}_3)_2(\text{THF})]$ ($\text{Ln} = \text{Y, Lu}$)^[22] obtained from $[\text{Ln}(\text{CH}_2\text{SiMe}_3)_3(\text{THF})_x]$ either by protonolysis with $\text{HTp}^{\text{R,R}}$ or reaction with $\text{TiTp}^{\text{R,R}}$.

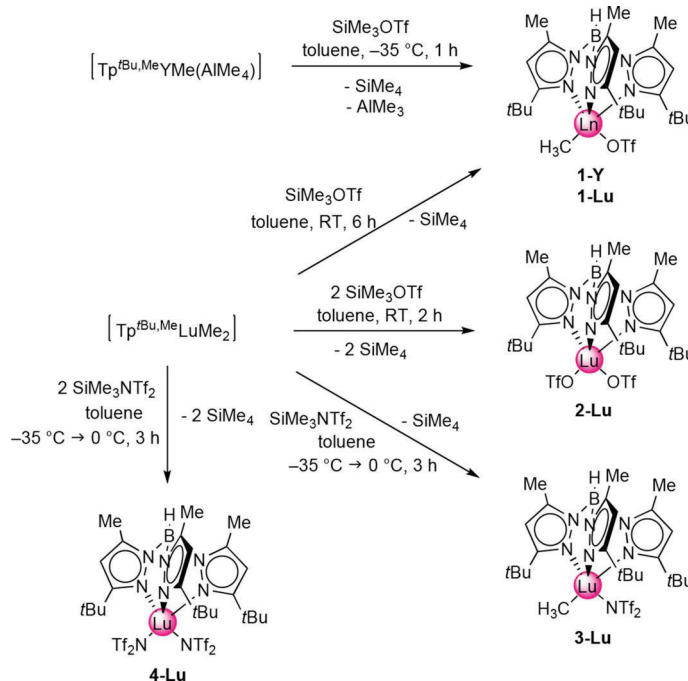
"Half-sandwich" triflate complexes

In accordance to Scheme 1/path A/complex I, we anticipated the introduction of trifluoromethanesulfonato (OTf) or the even weaker coordinating trifluoromethanesulfonimido ($\text{N}(\text{SO}_2\text{CF}_3)_2$ or NTf_2) ligands to be feasible through mild trimethylsilyl-based transfer reagents SiMe_3X ($\text{X} = \text{OTf, NTf}_2$). Therefore, the scorio-

nate-supported hydrocarbyl complexes $[\text{Tp}^{\text{tBu,Me}}\text{YMe}(\text{AlMe}_4)]$ and $[\text{Tp}^{\text{tBu,Me}}\text{LuMe}_2]$ were treated with one or two equivalents of SiMe_3X , respectively, in toluene (Scheme 2).

In particular, given that the yttrium derivatives are extremely temperature sensitive, careful adjustment of the reaction conditions was required to afford complexes $[\text{Tp}^{\text{tBu,Me}}\text{LnMe}(\text{OTf})]$ ($\text{Ln} = \text{Y, Lu}$, **1-Y**; **1-Lu**), $[\text{Tp}^{\text{tBu,Me}}\text{Lu}(\text{OTf})_2]$ (**2-Lu**), $[\text{Tp}^{\text{tBu,Me}}\text{LnMe}(\text{NTf}_2)]$ (**3-Lu**), and $[\text{Tp}^{\text{tBu,Me}}\text{Ln}(\text{NTf}_2)_2]$ (**4-Lu**). The ambient-temperature ^1H NMR spectra of the diamagnetic compounds **1-4** showed only one set of signals for the pyrazolyl groups of the $\text{Tp}^{\text{tBu,Me}}$ ligand with chemical shifts similar to those of the starting compounds (spectral data are presented in the Supporting Information). This indicates a highly fluxional behavior, which is in accordance with previous studies on complex $[\text{Tp}^{\text{tBu,Me}}\text{LuMe}(\text{AlMe}_4)]$.^[17] However, these previous studies also reported that similar complexes behave differently at lower temperatures, with the pyrazolyl rings revealing a 2:1 splitting in the ^1H NMR spectra in accordance with the C_s symmetry of these complexes in the solid state.^[17] For **1-Lu** and **3-Lu**, the Lu-bound Me groups gave sharp singlets at $\delta = 0.39$ and 0.14 ppm, respectively.

The ambient-temperature ^1H NMR spectrum of **1-Y** in C_6D_6 showed a broadened signal at $\delta = 0.26$ ppm for the terminal methyl moiety, not indicative of any Y–H coupling. To further investigate this behavior, a low-temperature ^1H NMR spectroscopy study was carried out (Figure S2 in the Supporting Information). Due to solubility issues in toluene at temperatures below 20°C and rapid decomposition of complex **1-Y** in THF, a few drops of $[\text{D}_8]\text{THF}$ were added to a precooled solution of **1-Y** in $[\text{D}_8]\text{toluene}$. Remarkably, the chosen NMR solvent "mix-



Scheme 2. Synthesis pathways toward mixed methyl/triflate complexes $[\text{Tp}^{\text{tBu,Me}}\text{LnMe}(\text{OTf})]$ ($\text{Ln} = \text{Y, Lu}$), the mixed methyl/trifluoromethanesulfonimide complex $[\text{Tp}^{\text{tBu,Me}}\text{LuMe}(\text{NTf}_2)]$, bis(triflate) complex $[\text{Tp}^{\text{tBu,Me}}\text{Lu}(\text{OTf})_2]$, and bis(triflimide) complex $[\text{Tp}^{\text{tBu,Me}}\text{Lu}(\text{NTf}_2)_2]$.

ture" showed a strong influence on the chemical shift of the Y–Me moiety at low temperature, revealing a doublet at $\delta = -0.13$ ppm ($^2J(Y-H) = 1.5$ Hz) markedly shifted to higher fields compared with **1-Y** in $[D_6]benzene$ ($\delta = 0.26$ ppm, Figure S1, Supporting Information). The $^1H-^{89}Y$ HSQC NMR spectrum of **1-Y** at $0^\circ C$ shows a cross peak at $\delta = 515$ ppm on the ^{89}Y NMR scale (Figure 1), which is shifted to higher field in comparison

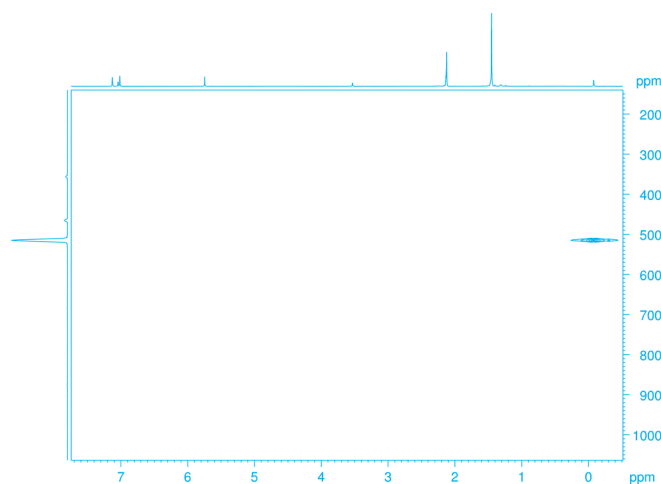


Figure 1. $^1H-^{89}Y$ HSQC NMR spectrum (24.5 MHz, $[D_8]toluene$ and a few drops of $[D_3]THF$) of complex $[Tp^{tBu,Me}YMe(OTf)]$ (**1-Y**) at $0^\circ C$.

to precursor $[Tp^{tBu,Me}YMe(AlMe_3)]$ ($\delta = 798$ ppm).^[18] The ^{13}C NMR spectra of the fluorine-containing complexes **1-Lu**, **2-Lu**, **3-Lu**, and **4-Lu** showed one set of signals for the $Tp^{tBu,Me}$ ligand but ^{13}C resonances of the CF_3 groups could not be detected, which is consistent with already reported compounds.^[23] Notwithstanding, the presence of OTf and NTf_2 moieties was unambiguously evidenced by ^{19}F NMR spectroscopy revealing one

sharp resonance at $\delta = -78.0, -78.1, -77.5, -77.9,$ and -76.9 ppm each for complexes **1-Y**, **1-Lu**, **2-Lu**, **3-Lu**, and **4-Lu**, respectively.

X-ray crystallographic structure determinations were performed on **1-Lu**, **3-Lu**, and **4-Lu** (Figure 2, Table 1). The fivefold-coordinated lutetium centers of the methyl complexes $[Tp^{tBu,Me}LuMeX]$ ($X = OTf$, **1-Lu**; NTf_2 , **3-Lu**) adopt a distorted trigonal-bipyramidal coordination geometry. Moreover, the typically observed κ^3 coordination of the ancillary ligand is adopted. In comparison with the reactant $[Tp^{tBu,Me}LuMe_2]$,^[24] the Lu–N(pz) (pz = pyrazolyl) bond lengths (2.339(2)–2.483(2) Å) of the $Tp^{tBu,Me}$ ligand are significantly shortened for **1-Lu** (2.299(3)–2.376(3) Å) and **3-Lu** (2.289(1)–2.328(1) Å); this could be attributable to the bulky electron-withdrawing triflate moieties. As known from literature, OTf^- and NTf_2^- moieties can coordinate in a monodentate, non-bridging (N- or O-wise, the latter was found for **1-Lu** and **3-Lu**) or in a bidentate, bridging fashion.^[25] The Lu–O1 distance for **1-Lu** (2.191(3) Å) is significantly shorter than those reported before for eightfold-coordinated $[CpLu(OTf)_2(THF)_3]$ ^[26] (2.237(4), 2.213(4) Å) and $[Lu(OTf)_3(OPPh_3)_4]$ ^[25a] (2.202(6), 2.232(5) Å) featuring likewise monodentate triflate ligands. Similarly, the Lu–O1 distance in bidentate eightfold-coordinated complex $[(bmpyr)Lu(NTf_2)_4]$ ^[27] (bmpyr = 1-butyl-1-methylpyrrolidinium) (av. 2.30 Å) is elongated compared with that in **3-Lu** (2.243(1) Å). The presence of the electron-withdrawing triflate moieties implies also slightly shorter Lu–C(Me) distances of **1-Lu** (2.327(4) Å) and **3-Lu** (2.323(2) Å) than those in the precursor $[Tp^{tBu,Me}LuMe_2]$ ^[24] (2.364(3)/2.375(2) Å). Despite several achievements on the structural characterization of various Tp-supported Ln–OTf complexes,^[28] mixed Me/OTf and Me/ NTf_2 structural motifs have not yet been identified. So far, the structurally authenticated complexes comprise “sandwich complexes” exclusively, namely sevenfold-coordinated $[(Tp^{Me,Me})_2Nd(OTf)]$ (Nd–O, 2.421(5) Å), sixfold-coordinated $[(Tp^{Me,Me})_2Yb](OTf)$, eightfold-

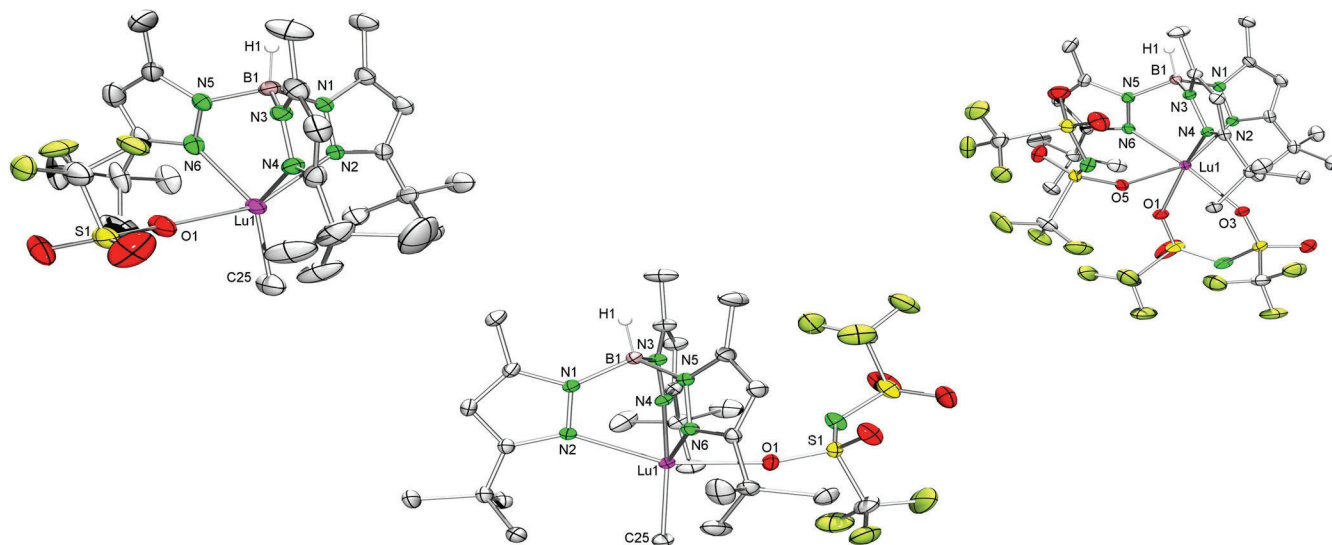


Figure 2. ORTEP representation of the molecular structure of **1-Lu** (left), **3-Lu** (middle), and **4-Lu** (right) with atomic displacement parameters set at the 50% level. Hydrogen atoms except for BH, toluene, and the disorder in one *t*Bu and the SO_2CF_3 group are omitted for clarity. Selected bond lengths are given in Table 1.

Table 1. Selected bond lengths [Å] of **1-Lu**, **3-Lu**, **4-Lu**, **5-Lu**, **6-Lu**, **7-Lu**, **8-Lu**, **9-Lu**.

	1-Lu (X = Me, X' = O)	3-Lu (X = Me, X' = O)	4-Lu (X = X' = O)	5-Lu (X = X' = Cl)	6-Lu (X = X' = I)	7-Lu (X = Me, X' = Cl)	8-Lu (X = Me, X' = CH ₂)	9-Lu (X = Me, X' = CH ₂)
Lu–N2	2.376(3)	2.376(3)	2.311(2)	2.391(6)	2.298(3)	2.313(9)	2.352(2)	2.310(2)
Lu–N4	2.299(3)	2.299(3)	2.3260(2)	2.306(3)	2.293(3)	2.413(1)	2.353(2)	2.323(2)
Lu–N6/N'	2.309(4)	2.309(4)	2.3108(2)	2.306(3)	2.378(3)	2.313(9)	2.487(2)	2.466(2)
Lu–X	2.327(4)	2.323(2)	2.2820(1)/2.2885(1)	2.4916(2)	2.8467(4)	2.393(1)	2.343(2)	2.349(3)
Lu–X'	2.191(3)	2.191(3)	2.2213(1)	2.494(1)	2.8987(4)	2.526(4)	2.372(2)	2.412(3)

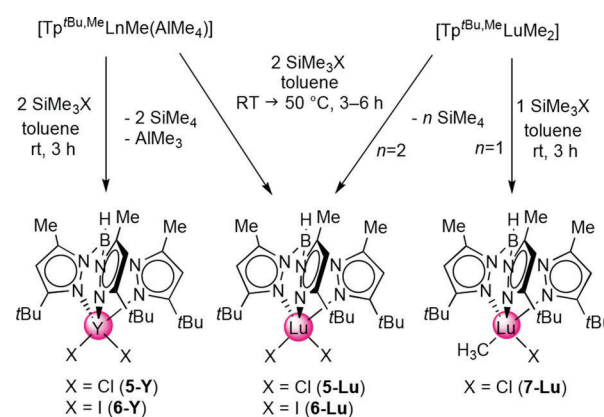
coordinated $[(\text{Tp}^{\text{Me,Me}})_2\text{La}(\text{OTf})(\text{CH}_3\text{CN})]$ (La–O, 2.514(5) Å), and sevenfold-coordinated $[(\text{Tp}^{\text{Me,Me}})_2\text{Nd}(\text{CH}_3\text{CN})_2](\text{OTf})$. All these complexes were synthesized through salt metathesis employing $\text{Ln}(\text{OTf})_3$ and $\text{KTp}^{\text{Me,Me}}$, followed by exposure to donor molecules. Interestingly, complex $[\text{Tp}^{\text{tBu,Me}}\text{Ln}(\text{NTf}_2)_2]$ (**4-Lu**) is sixfold-coordinated by $\text{Tp}^{\text{tBu,Me}}$ (κ^3 -mode) and each one monodentate and bidentate NTf_2 ligand (Figure 2, right). The Lu–O(triflate) distances range from 2.2213(1) to 2.2885(1) Å.

To target the envisaged LnMeX to $\text{Ln}=\text{CH}_2$ transformation (see Scheme 1/path A) complexes $[\text{Tp}^{\text{tBu,Me}}\text{LuMeX}]$ (X = OTf, **1-Lu**; NTf_2 , **3-Lu**) were treated with one equivalent of H_2CPh_3 in $[\text{D}_6]$ benzene. Unfortunately, no reactivity was observed at ambient temperature. Further heating the reaction mixture to 50 °C led to methane elimination through C–H bond activation involving the *t*Bu methyl groups of the ancillary ligand and the Lu–CH₃ moiety, as observed previously.^[17] This intramolecular C–H bond activation could not be prevented by addition of N- or O-donors like 4-dimethylaminopyridine (DMAP) and tetrahydrofuran (THF).

Generation of di(halogenido) and mixed methyl/halogenido and methyl/alkyl complexes

Further efforts to generate Ln^{III} alkydienes led to the idea of targeting mixed methyl/alkyl (Me/R) complexes $[\text{Tp}^{\text{tBu,Me}}\text{LuMeR}]$. The latter might be convertible to the envisaged alkydienes species following a thermal or donor-induced intramolecular elimination of either methane or the respective HR analog to Petasis (see Scheme 1/path B). Note that half-sandwich complexes of the type $[(\text{C}_5\text{Me}_4\text{SiMe}_3)\text{Ln}(\mu_3\text{-CH}_2)]_3$ were previously shown to undergo such reactions affording tetrametallic cuboid clusters $[(\text{C}_5\text{Me}_4\text{SiMe}_3)\text{Ln}(\mu_3\text{-CH}_2)]_4$ (Ln = Tm, Lu).^[6] Preliminary NMR-scale reactivity studies probing the olefination capability of $[\text{Tp}^{\text{tBu,Me}}\text{LuMe}_2]$ toward 9-fluorenone at 50 °C (according to Petasis) indicated the exclusive formation of the respective alkoxide species. Therefore, to evade such preferential nucleophilic attack of the methyl moiety at the carbonyl functionality, the initial formation of an alkydienes species was envisaged. To provide a more versatile platform for further derivatization reactions, the above-mentioned precursors $[\text{Tp}^{\text{tBu,Me}}\text{LnMe}(\text{AlMe}_4)]$ and $[\text{Tp}^{\text{tBu,Me}}\text{LuMe}_2]$ were treated with one equivalent of SiMe_3X (here X = Cl, I) in toluene for the generation of mixed alkyl/halogenido compounds as depicted in Scheme 3.

Unfortunately, for yttrium and the combination Lu/I only the di(halogenido) derivatives $[\text{Tp}^{\text{tBu,Me}}\text{YCl}_2]$ (**5-Y**), $[\text{Tp}^{\text{tBu,Me}}\text{YI}_2]$ (**6-Y**),



Scheme 3. Synthesis pathways toward di(halide) complexes $[\text{Tp}^{\text{tBu,Me}}\text{LnX}_2]$ (Ln = Y, Lu; X = Cl, I) and the mixed methyl/halide complex $[\text{Tp}^{\text{tBu,Me}}\text{LuMeCl}]$.

and $[\text{Tp}^{\text{tBu,Me}}\text{LuI}_2]$ (**6-Lu**) could be isolated, evidencing extensive ligand redistribution. It is noteworthy that the synthesis and isolation of such di(halogenido) “half-sandwich” complexes has been formerly assessed as problematic because of the occurrence of ligand redistribution reactions and B–N bond cleavage (formation of pyrazole adducts), in particular for complexes derived from $\text{Tp}^{\text{Me,Me}}$.^[29] The few monomeric complexes $[\text{Tp}^{\text{R,R}}\text{Ln}(\text{halogenido})_2]$ authenticated by X-ray structure analysis include THF adducts $[(\text{Tp}^{\text{Me,Me}})\text{LnCl}_2(\text{THF})]$ and $[(\text{Tp}^{\text{Me,Me}})_2\text{NdI}_2(\text{THF})]$, as well as N-donor stabilized $[(\text{Tp}^{\text{Me,Me}})_2\text{LnCl}_2(\text{dmpzH})]$,^[30] $[(\text{Tp}^{\text{Me,Me}})_2\text{YCl}_2(1,10\text{-phen})]$, and $[(\text{Tp}^{\text{Me,Me}})_2\text{LaCl}_2(\text{bipy})]$ (dmpzH: dimethylpyrazole, 1,10-phen: 1,10-phenanthroline, bipy: 2,2'-bipyridine).^[31]

Much to our delight, the combination Lu/Cl gave the desired mixed methyl/chloride complex $[\text{Tp}^{\text{tBu,Me}}\text{LuMeCl}]$ (**7-Lu**), in addition to the di(chlorido) derivative $[\text{Tp}^{\text{tBu,Me}}\text{LuCl}_2]$ (**5-Lu**, two-equivalent reaction). All halide complexes exhibit low solubility which facilitated their isolation through crystallization (**5-Y**, **6-Y**, **6-Lu**, **7-Lu**) or precipitation (**5-Lu**) from toluene solutions. Single crystals of **6-Lu** and **7-Lu** were grown from saturated toluene solutions at –35 °C, whereas **5-Lu** was crystallized from THF at –35 °C. The ¹H and ¹³C NMR spectroscopic data for all compounds clearly showed only one set of signals for the pyrazolyl groups of the ancillary ligand. In comparison with **1-Lu** and **3-Lu**, the proton NMR spectrum of **7-Lu** shows a sharp singlet of the Lu–Me moiety located at $\delta = 0.29$ ppm, and hence shifted slightly to lower field. Overall, the Lu–N(pz) (pz = pyrazolyl) bond lengths in **5-Lu**, **6-Lu** and **7-Lu** (Figure 3) are comparable to those found for **1-Lu**, **3-Lu**, and **4-Lu**. The

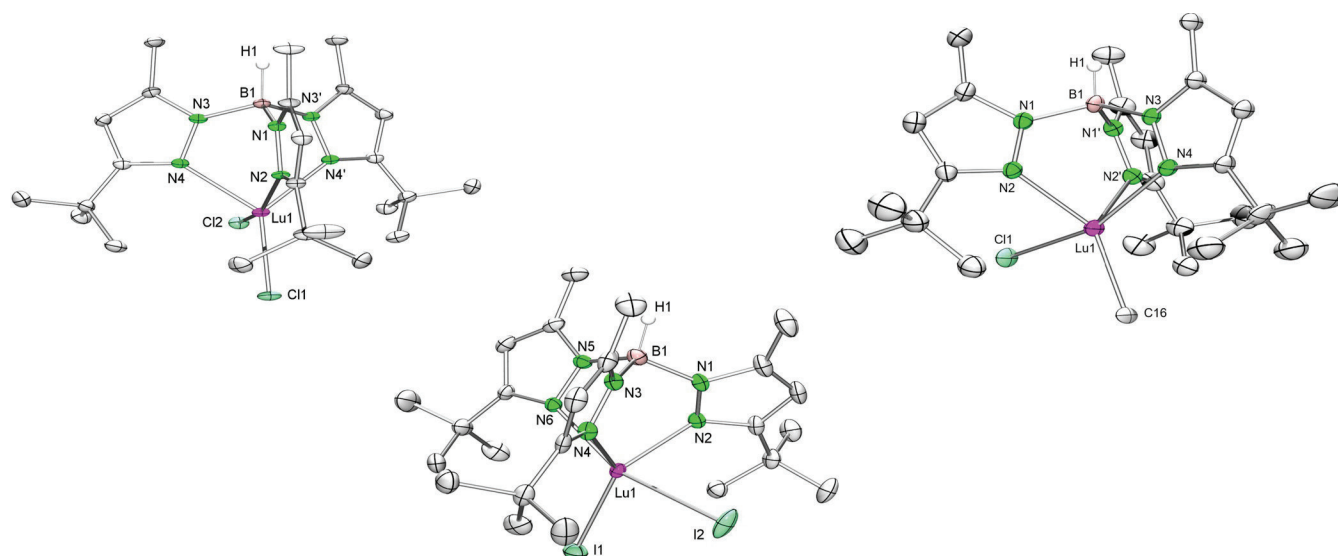


Figure 3. ORTEP representation of the molecular structures of **5-Lu** (left), **6-Lu** (middle), and **7-Lu** (right) with atomic displacement parameters set at the 50% level. Hydrogen atoms except for BH and solvent THF are omitted for clarity. Selected bond lengths are given in Table 1.

Lu–X distances in the di(halogenido) derivatives [$\text{Tp}^{\text{tBu,Me}}\text{LuCl}_2$] (**5-Lu**) and [$\text{Tp}^{\text{tBu,Me}}\text{LuI}_2$] (**6-Lu**) average 2.493 and 2.873 Å, respectively, reflecting the size of the halogenido anion. The Lu–C(methyl) bond length of 2.393(1) Å in **7-Lu** is slightly longer than in [$\text{Tp}^{\text{tBu,Me}}\text{LuMe}_2$]^[24] (2.364(3)/2.375(2) Å) and complexes **1-Lu** and **3-Lu** (see Table 1). Striking is the elongated Lu–Cl bond of 2.526(4) Å in **7-Lu** compared with **5-Lu**, apparently caused by the presence of the methyl ligand.

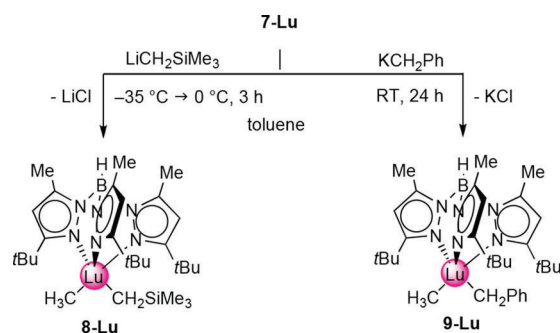
Aiming at mixed methyl/alkyl compounds, the mixed methyl/chloride lutetium complex **7-Lu** was examined in salt-metathesis reactions with different alkali-metal alkyls (Scheme 4). Due to the low solubility of **7-Lu** in other nonpolar solvents and unintended C–H-bond activation in donor solvents, all subsequent reactions were carried out in toluene.

The mixed alkyl complex [$\text{Tp}^{\text{tBu,Me}}\text{LuMe}(\text{CH}_2\text{SiMe}_3)$] (**8-Lu**) was obtained by reacting **7-Lu** with $\text{LiCH}_2\text{SiMe}_3$. Due to the thermal lability of **8-Lu**, the reaction was performed at temperatures below 0 °C. Such low temperatures are also beneficial to the use of Li salts because conducting the involved metathesis reactions at ambient temperature favors the formation of

$\text{LiTp}^{\text{tBu,Me}}$ ^[20] In contrast, the mixed methyl/benzyl complex [$\text{Tp}^{\text{tBu,Me}}\text{LuMe}(\text{CH}_2\text{Ph})$] (**9-Lu**) is thermally stable, but a prolonged reaction time is crucial when reacting **7-Lu** with potassium benzyl. For both mixed bis(alkyl) complexes **8-Lu** and **9-Lu**, the ¹H and ¹³C NMR spectra show only one set of signals for the pyrazolyl groups. The Ln-bound methyl groups appeared as narrow singlets at $\delta = 0.19$ (**8-Lu**) and 0.39 ppm (**9-Lu**). In agreement with literature reports, the methylene moieties of the neosilyl and benzyl ligand feature distinctly shifted signals at $\delta = -0.71$ and 1.63 ppm, respectively, attributable to a strong electronic influence of the SiMe_3/Ph groups.

Complexes **8-Lu** and **9-Lu** were crystallized from saturated toluene solutions at –35 °C and their solid-state structures analyzed by X-ray crystallography (Figure 4). As commonly observed for $\text{Ln}^{\text{III}}\text{-Tp}^{\text{tBu,Me}}$ complexes with coordination number 5, both complexes adopt a distorted trigonal-bipyramidal geometry. The pyrazolyl nitrogen atoms N2 and N4 and the methyl carbon C25 reside in the equatorial plane, whereas the methylene carbon atom C26 and the pyrazolyl nitrogen atom N6 occupy the axial positions. In comparison with complexes **1-Lu** and **3-Lu** the Lu–N(pz) bond lengths are slightly elongated for the mixed alkyl compounds **8-Lu** (2.352(2)–2.487(2) Å) and **9-Lu** (2.310(2)–2.466(2) Å).

Furthermore, the Lu–C(Me) distances of **8-Lu** (2.343(2) Å) and **9-Lu** (2.349(3) Å) lie in between those of **1-Lu/3-Lu** and **7-Lu** (Table 1). In accordance with literature, the Lu–C(neosilyl) bond length of **8-Lu** of 2.372(2) Å is in the same range as detected for $\text{Lu}(\text{CH}_2\text{SiMe}_3)_3(\text{THF})_2$ ^[32] (2.314(18)–2.344(18) Å) and $\text{Tp}^{\text{Me,Me}}\text{Lu}(\text{CH}_2\text{SiMe}_3)_2(\text{THF})$ (2.373(2)–2.379(2) Å).^[21] Other rare solid-state structures of monomeric but heteroleptic Tp-based rare-earth-metal complexes as [$\text{Tp}^{\text{R,R}}\text{Ln}(\text{Danip})(\text{CH}_2\text{SiMe}_3)$] (R = Me or R = H, Ln = Yb, Danip = 2,6-di(*o*-anisyl)phenyl) display similar bond lengths (Yb–C_{ipso}: 2.414(3)–2.438(4)/2.402(4)–2.435(5) Å; Yb–C(neosilyl): 2.379(4)–2.392(4)/2.359(4)–2.368(4) Å) taking into account the metal-ion size.^[33] The Lu–



Scheme 4. Salt-metathesis conversion of methyl/halide complex [$\text{Tp}^{\text{tBu,Me}}\text{LuMeCl}$] (**7-Lu**) to mixed methyl/alkyl compounds [$\text{Tp}^{\text{tBu,Me}}\text{LuMeR}$] (R = CH_2SiMe_3 (**8-Lu**), CH_2Ph (**9-Lu**)).

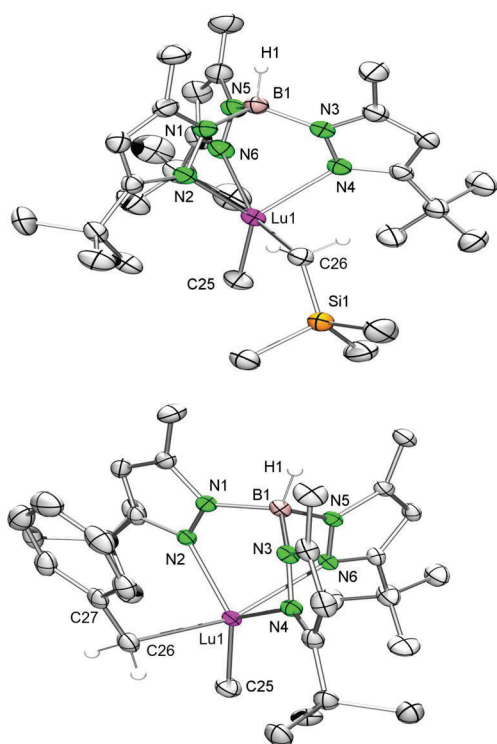


Figure 4. ORTEP representation of the molecular structures of **8-Lu** (top) and **9-Lu** (bottom) with atomic displacement parameters set at the 50% level. Hydrogen atoms except for BH and CH₂ are omitted for clarity. For **9-Lu** the disorder in one *t*Bu group and toluene are omitted for clarity. Selected bond lengths are given in Table 1.

C(benzyl) bond length (2.412(3) Å) in **9-Lu** matches that in Lu(CH₂Ph)₃(THF)₃ (2.404(7)–2.413(5) Å) and Lu(CH₂Ph)₃(THF)₂ (2.380(3)–2.404(3) Å)^[35] but is slightly elongated compared with Cp*Lu(CH₂Ph)₂(THF) (2.378(2)–2.386(2) Å; Cp* = C₅Me₅).^[36] Furthermore, there is no significant secondary interaction between Lu1 and the *ipso* carbon atom C27 for **9-Lu**, as suggested by the Lu1...C27 distance of 3.314 Å and the Lu–C(CH₂)–C27 angle (114.3(2)°). For further comparison, complex [Tp^{Me,Me}Y(CH₂Ph)₂(THF)] was obtained through salt metathesis from [Tp^{Me,Me}YCl₂(THF)₂] and potassium benzyl (Y–C(CH₂)₂ 2.457(8) and 2.418(8) Å, Y–CH₂–C_{*ipso*} 116.4(6) and 130.1(6)°).^[37]

Next, we examined whether complexes **8-Lu** and **9-Lu** are capable of intramolecular deprotonation and alkane elimination (see Scheme 1/path B). As mentioned before, [Tp^{tBu,Me}LuMe(CH₂SiMe₃)] is temperature-sensitive. After one day at ambient temperature, a solution of complex **8-Lu** in [D₆]benzene turned from colorless to yellow. Monitoring this behavior with ¹H NMR spectroscopy revealed degradation of the ancillary ligand as indicated by different new pyrazolyl signals and methane evolution. Further attempts at generating alkylidenes through intramolecular deprotonation led to the use of N- or O-donor molecules such as DMAP or THF, but failed for the same reasons. Although compound **9-Lu** is stable in solution in [D₆]benzene at ambient temperature, heating to 40 °C for 4 h also led to degradation of the ancillary ligand, as did the utilization of various donors. In accordance with other already reported degradation processes, we assume C–H-bond

activation of one *tert*-butyl group or B–N bond cleavage to be responsible for the formation of multiple unidentified metal complexes in these reaction mixtures.^[29b,38] It is also noteworthy, that the di(chlorido) derivative [Tp^{tBu,Me}LuCl₂] (**5-Lu**) does not undergo any “Tebbe-like” reaction with AlMe₃ at ambient temperature, but leads to unidentified complicated reaction mixtures (ancillary ligand degradation) at elevated temperatures (*T* = 50 °C).

In spite of these sobering findings, the successful isolation of mixed alkyl complexes **8-Lu** and **9-Lu** spurred our interest in the evaluation of the steric effects on the ancillary Tp^{tBu,Me} ligand caused by the distinct triflato, halogenido, or alkyl co-ligands. According to a method recently reported by our group, we calculated the exact ligand cone angles Θ° (the procedure is given in the Supporting Information).^[39] According to Allen and co-workers, the term “exact” refers to the acute mathematical solution and does not reflect the accuracy of the input structure itself.^[39b] As a prerequisite for meaningful interpretations, the metal centers should have the same coordination number (CN, here 5) and the same overall charge. A general overview of the determined cone angles is summarized in Table 2.

Table 2. Overview of mathematically exact calculated cone angles Θ° [°] of selected Tp^{tBu,Me}LuMeX or Tp^{tBu,Me}LuMeR (see the Supporting Information for calculations).^[a]

1-Lu	3-Lu	6-Lu	7-Lu	8-Lu	9-Lu
278.0 280.9	280.4	278.2	278.9	277.1	277.3
[a] directly determined from atomic positions.					

The Tp^{tBu,Me} ligand engages in an exclusive trigonal-bipyramidal coordination geometry at the Lu complexes under study, and hence, very similar cone angles (Θ° = 277.1 to 280.9° for CN = 5) were calculated. For **1-Lu**, two different cone angles are displayed due to the respective disorder in one *tert*-butyl group. Nonetheless, the noticeable trend makes complexes with mixed alkyl co-ligands the least sterically demanding, followed by the di(halide) complexes, whereas the weakly coordinating triflato or triflimido moieties allow for the largest cone angles. Another important finding is that the mathematically exact method determines cone angles distinctly higher than those reported for Tp^{tBu,Me} complexes in the literature (Θ° = 244°).^[40] Therefore, further efforts should be expended to build up a library for better comparison.

Conclusions

Aiming at new synthesis protocols for terminal rare-earth-metal alkylidene complexes, we gained access to unprecedented mono-tris(pyrazolyl)borate complexes. Following TMS-elimination protocols by applying complexes [Tp^{tBu,Me}YMe(AlMe₃)] and [Tp^{tBu,Me}LuMe₂] along with SiMe₃X (X = OTf, NTf₂), the superbulky ligand Tp^{tBu,Me} supports the formation of mixed

methyl triflate and mixed methyl triflimide complexes of yttrium and lutetium as new structural motif in rare-earth-metal chemistry. Moreover, similar reactions employing SiMe_3X ($\text{X} = \text{Cl}, \text{I}$) afforded not only unsolvated di(halide) complexes $\text{Tp}^{\text{fBu,Me}}\text{LnX}_2$ but also the mixed methyl/chloride complex $[\text{Tp}^{\text{fBu,Me}}\text{LuMeCl}]$. The latter gave efficient access to mixed alkyl complexes $[\text{Tp}^{\text{fBu,Me}}\text{LuMe}(\text{CH}_2\text{SiMe}_3)]$ and $[\text{Tp}^{\text{fBu,Me}}\text{LuMe}(\text{CH}_2\text{Ph})]$ through salt-metathesis reactions with different alkali-metal salts. Unfortunately, neither reactivity studies utilizing the Wittig reagent nor the attempted thermally-induced intramolecular deprotonation afforded rare-earth-metal alkylidene compounds. It seems that terminal alkylidenes devoid of Lewis acid stabilization are not accessible/isolable in the presence of this very $\text{Tp}^{\text{fBu,Me}}$ ligand, which engages preferably in intramolecular B–N- and C–H-bond activation processes. Ongoing research focuses on tripodal ancillary ligand systems which are less prone to degradation and C–H-bond activation.

Experimental Section

All operations were performed under rigorous exclusion of air and water by using standard Schlenk, high-vacuum, and glovebox techniques (MBraun 200B; <0.1 ppm O_2 , <0.1 ppm H_2O). Solvents were purified by using Grubbs-type columns (MBraun SPS, solvent purification system) and stored inside a glovebox. $[\text{D}_6]\text{Benzene}$ and $[\text{D}_8]\text{toluene}$ were obtained from Sigma–Aldrich and degassed, $[\text{D}_6]\text{benzene}$ was dried over NaK alloy for two days and $[\text{D}_8]\text{toluene}$ was stored over Na. Both were filtered prior to use. $[\text{D}_8]\text{THF}$ was obtained from Sigma–Aldrich, stirred over NaK alloy, and distilled. SiMe_3Cl , trimethylsilyl trifluoromethanesulfonate (Me_3SiOTf), and (trimethylsilyl)methylolithium ($\text{LiCH}_2\text{SiMe}_3$) solutions were purchased from Sigma Aldrich, SiMe_3I and N-(trimethylsilyl)bis(trifluoromethanesulfonyl)imide ($\text{Me}_3\text{SiINTf}_2$) were purchased from ABCR and all chemicals were used as received. Potassium benzyl (KBn),^[41] $[\text{Tp}^{\text{fBu,Me}}\text{YMe}(\text{AlMe}_4)]$,^[17] $[\text{Tp}^{\text{fBu,Me}}\text{LuMe}(\text{AlMe}_4)]$,^[17] and $[\text{Tp}^{\text{fBu,Me}}\text{LuMe}_2]$ ^[18] were synthesized according to literature procedures. The NMR spectra of air- and moisture-sensitive compounds were recorded by using J. Young valve NMR tubes on a Bruker AVII + 400 spectrometer (^1H , 400.13; ^{13}C , 100.61; ^{19}F , 376.31 MHz), on a Bruker AVII + 500 spectrometer (^1H , 500.13; ^{13}C , 125.76; ^{89}Y , 24.51 MHz) and on a Bruker AVII + 250 spectrometer (^1H , 250.00; ^{11}B , 80.21; ^{13}C , 62.86 MHz). IR spectra were recorded on a Thermo Fisher Scientific NICOLET 6700 FTIR spectrometer using a DRIFT chamber with dry KBr/sample mixture and KBr windows; IR (DRIFT) data were converted by using the Kubelka–Munk refinement. Elemental analyses were performed on an Elementar Vario MICRO Cube.

Synthesis and characterization

$[\text{Tp}^{\text{fBu,Me}}\text{YMe}(\text{OTf})]$ (1-Y): A chilled solution of Me_3SiOTf (18.1 mg, 0.0814 mmol) in toluene (2 mL) was added to a precooled solution of $[\text{Tp}^{\text{fBu,Me}}\text{YMe}(\text{AlMe}_4)]$ (50.0 mg, 0.0814 mmol) in toluene (5 mL) at -20°C . The reaction mixture was allowed to stir for 12 h at -20°C . The solution was concentrated in vacuo and stored at -35°C . Crystallization yielded compound **1-Y** (30.0 mg, 0.0443 mmol, 54%) as colorless crystals. ^1H NMR (250 MHz, $[\text{D}_6]\text{benzene}$, 25°C): $\delta = 5.56$ (s, 3H, 4-pz-H), 4.42 (v br d, $^1J(\text{BH}) = 350$ Hz, 1H, BH), 2.01 (s, 9H, pz- CH_3), 1.36 (s, 27H, pz-C(CH_3) $_3$), 0.26 ppm (s, Y- CH_3). ^1H NMR (500 MHz, $[\text{D}_8]\text{toluene}$, 0°C): $\delta = 5.70$ (s, 3H, 4-pz-H), 4.52 (v br d, $^1J(\text{BH}) = 355$ Hz, 1H, BH), 2.07 (s, 9H, pz- CH_3), 1.40 (s, 27H, pz-

$\text{C}(\text{CH}_3$) $_3$), -0.13 ppm (d, $^2J(\text{YH}) = 1.5$ Hz, 3H, Y- CH_3). $^{13}\text{C}\{^1\text{H}\}$ NMR (126 MHz, $[\text{D}_8]\text{toluene}$, 0°C): $\delta = 164.7$ (5-pz-C), 147.0 (3-pz-C), 104.4 (4-pz-C), 32.7 (pz-C(CH_3) $_3$), 31.0 (pz-C(CH_3) $_3$), 25.4 (d, $^2J(\text{YC}) = 22.3$ Hz, Y- CH_3), 13.4 ppm (pz-C(CH_3) $_3$). ^{13}C NMR resonances for the triflate groups were not detected. $^{11}\text{B}\{^1\text{H}\}$ NMR (80 MHz, $[\text{D}_6]\text{benzene}$, 26°C): $\delta = -8.6$ ppm. $^{19}\text{F}\{^1\text{H}\}$ NMR (376 MHz, $[\text{D}_6]\text{benzene}$, 26°C): $\delta = -78.0$ ppm. ^{89}Y NMR (from ^1H - ^{89}Y HSQC, 25 MHz, $[\text{D}_8]\text{toluene}$, 0°C): $\delta = 515$ ppm. IR (KBr): $\tilde{\nu} = 2964$ (w), 2931 (w), 2883 (w), 2873 (w), 2822 (vw), 2577 (B-H, vw), 2248 (vw), 2202 (vw), 2124 (vw), 1764 (vw), 1737 (vw), 1562 (vw), 1536 (w), 1518 (vw), 1501 (w), 1480 (w), 1462 (w), 1428 (w), 1342 (m), 1335 (m), 1282 (s), 1270 (s), 1228 (vs), 1204 (vs), 1171 (m), 1164 (m), 1136 (vw), 1097 (vw), 1053 (s), 1002 (vw), 995 (vw), 960 (vw), 940 (vw), 909 (vw), 892 (vw), 873 (vw), 860 (vw), 850 (vw), 837 (vw), 799 (w), 763 (w), 716 (m), 711 (m), 702 (m), 696 (m), 688 (m), 637 (vs), 586 (vw), 571 (vw), 550 (vw), 512 (w), 480 (vw), 469 (vw), 463 (vw), 431 (vw), 424 cm^{-1} (vw); elemental analysis calcd (%) for $\text{C}_{26}\text{H}_{43}\text{BF}_3\text{N}_6\text{O}_3\text{SY}$: C 46.17, H 6.41, N 12.42; found C 46.98, H 7.80, N 12.95. Due to the high S and F contents no better elemental analysis could be obtained.

$[\text{Tp}^{\text{fBu,Me}}\text{LuMe}(\text{OTf})]$ (1-Lu): A solution of Me_3SiOTf (18.0 mg, 0.0814 mmol) in toluene (2 mL) was added to a solution of $[\text{Tp}^{\text{fBu,Me}}\text{LuMe}_2]$ (50.0 mg, 0.0788 mmol) in toluene (5 mL) at ambient temperature. The reaction mixture was allowed to stir for 2 h. The solution was concentrated in vacuo and stored at -35°C . Crystallization yielded compound **1-Lu** (48.0 mg, 0.0630 mmol, 80%) as colorless crystals. ^1H NMR (250 MHz, $[\text{D}_6]\text{benzene}$, 26°C): $\delta = 5.64$ (s, 3H, 4-pz-H), 4.50 (v br d, $^1J(\text{BH}) = 355$ Hz, 1H, BH), 1.96 (s, 9H, pz- CH_3), 1.44 (s, 27H, pz-C(CH_3) $_3$), 0.39 ppm (s, 3H, Lu- CH_3). $^{13}\text{C}\{^1\text{H}\}$ NMR (63 MHz, $[\text{D}_6]\text{benzene}$, 26°C): $\delta = 166.5$ (5-pz-C), 147.9 (3-pz-C), 104.4 (4-pz-C), 36.6 (Lu- CH_3), 32.5 (pz-C(CH_3) $_3$), 31.1 (pz-C(CH_3) $_3$), 13.1 ppm (pz-C(CH_3) $_3$). ^{13}C NMR resonances for the triflate groups could not be detected. $^{11}\text{B}\{^1\text{H}\}$ NMR (80 MHz, $[\text{D}_6]\text{benzene}$, 26°C): $\delta = -9.2$ ppm. $^{19}\text{F}\{^1\text{H}\}$ NMR (376 MHz, $[\text{D}_6]\text{benzene}$, 26°C): $\delta = -78.1$ ppm. IR (KBr): $\tilde{\nu} = 2964$ (m), 2931 (w), 2910 (w), 2887 (vw), 2866 (vw), 2558 (vw, B-H), 1540 (m), 1477 (w), 1464 (w), 1433 (m), 1382 (vw), 1365 (m), 1351 (s), 1336 (s), 1238 (s), 1206 (vs), 1186 (vs), 1141 (vw), 1070 (m), 1062 (m), 1030 (vs), 1010 (w), 989 (vw), 848 (vw), 840 (vw), 822 (vw), 804 (w), 789 (w), 765 (m), 678 (vw), 660 (vw), 648 (s), 587 (vw), 516 (w), 511 (w), 488 (vw), 413 cm^{-1} (m); elemental analysis calcd (%) for $\text{C}_{26}\text{H}_{42}\text{BF}_3\text{LuN}_6\text{O}_3\text{S}$: C 40.96, H 5.68, N 11.02; found C 41.12, H 5.57, N 10.53.

$[\text{Tp}^{\text{fBu,Me}}\text{Lu}(\text{OTf})_2]$ (2-Lu): A solution of Me_3SiOTf (36.2 mg, 0.163 mmol) in toluene (2 mL) was added to a solution of $[\text{Tp}^{\text{fBu,Me}}\text{LuMe}_2]$ (50.0 mg, 0.0788 mmol) in toluene (5 mL). The reaction mixture was allowed to stir for 4 h at ambient temperature. The solution was concentrated in vacuo and stored at -35°C . Crystallization yielded compound **2-Lu** (50.0 mg, 0.0558 mmol, 71%) as colorless crystals. ^1H NMR (400 MHz, $[\text{D}_6]\text{benzene}$, 26°C): $\delta = 5.51$ (s, 3H, 4-pz-H), 4.61 (v br d, $^1J(\text{BH}) = 115$ Hz, 1H, BH), 1.87 (s, 9H, pz- CH_3), 1.40 ppm (s, 27H, pz-C(CH_3) $_3$). $^{13}\text{C}\{^1\text{H}\}$ NMR (63 MHz, $[\text{D}_6]\text{benzene}$, 26°C): $\delta = 167.1$ (5-pz-C), 148.5 (3-pz-C), 104.8 (4-pz-C), 32.4 (pz-C(CH_3) $_3$), 31.0 (pz-C(CH_3) $_3$), 12.8 ppm (pz-C(CH_3) $_3$). ^{13}C NMR resonances for the triflate groups were not detected. $^{11}\text{B}\{^1\text{H}\}$ NMR (80 MHz, $[\text{D}_6]\text{benzene}$, 26°C): $\delta = -8.3$ ppm. $^{19}\text{F}\{^1\text{H}\}$ NMR (376 MHz, $[\text{D}_6]\text{benzene}$, 26°C): $\delta = -77.5$ ppm. IR (KBr): $\tilde{\nu} = 3138$ (vw), 2963 (w), 2932 (vw), 2849 (vw), 2572 (vw, B-H), 1538 (m), 1480 (w), 1467 (w), 1455 (w), 1434 (m), 1355 (vs), 1350 (vs), 1290 (vw), 1240 (s), 1202 (vs), 1193 (vs), 1167 (s), 1132 (vw), 1076 (w), 1061 (w), 1021 (m), 1004 (vs), 859 (vw), 850 (vw), 839 (vw), 826 (vw), 817 (vw), 804 (w), 765 (w), 677 (vw), 661 (vw), 637 (vs), 589 (vw), 568 (vw), 524 (vw), 508 cm^{-1} (vw); elemental analysis calcd (%) for $\text{C}_{26}\text{H}_{40}\text{BF}_6\text{LuN}_6\text{O}_6\text{S}_2$: C 34.83, H 4.50, N 9.37; found C 34.70, H 4.52, N 9.40.

[Tp^{Bu,Me}LuMe(NTf₂)] (3-Lu): A precooled solution of Me₃SiNTf₂ (56.0 mg, 0.158 mmol) in toluene (5 mL) was added to a precooled solution of [Tp^{Bu,Me}LuMe₂] (100 mg, 0.158 mmol) in toluene (5 mL) at -35 °C. The reaction mixture was allowed to stir for 3 h at 0 °C. The solution was concentrated in vacuo and stored at -35 °C. Crystallization yielded compound **3-Lu** (80.0 mg, 0.0895 mmol, 57%) as colorless crystals. ¹H NMR (250 MHz, [D₆]benzene, 26 °C): δ = 5.66 (s, 3H, 4-pz-H), 4.55 (v br d, ¹J(BH) = 355 Hz, 1H, BH), 2.05 (s, 9H, pz-CH₃), 1.38 (s, 27H, pz-C(CH₃)₃), 0.14 ppm (s, 3H, Lu-CH₃). ¹³C{¹H} NMR (63 MHz, [D₆]benzene, 26 °C): δ = 166.9 (5-pz-C), 148.8 (3-pz-C), 105.1 (4-pz-C), 35.7 (Lu-CH₃), 32.3 (pz-C(CH₃)₃), 31.0 (pz-C(CH₃)₃), 13.0 ppm (pz-C(CH₃)₃). ¹³C NMR resonances for the triflate groups were not detected. ¹¹B{¹H} NMR (80 MHz, [D₆]benzene, 26 °C): δ = -8.3 ppm. ¹⁹F{¹H} NMR (376 MHz, [D₆]benzene, 26 °C): δ = -77.9 ppm. IR (KBr): $\tilde{\nu}$ = 3138 (vw), 3026 (vw), 2968 (m), 2931 (w), 2913 (w), 2863 (w), 2569 (vw, B-H), 1602 (vw), 1537 (m), 1393 (w), 1477 (m), 1465 (m), 1433 (m), 1367 (vs), 1352 (s), 1323 (s), 1208 (vs), 1190 (vs), 1161 (s), 1141 (s), 1122 (s), 1060 (vs), 1030 (m), 988 (w), 848 (vw), 817 (w), 801 (m), 759 (m), 741 (w), 728 (w), 694 (w), 675 (vw), 657 (w), 642 (m), 614 (m), 599 (w), 569 (w), 511 (m), 482 (vw), 465 (vw), 434 cm⁻¹ (w); elemental analysis calcd (%) for C₂₇H₄₃BF₆LuN₇O₄S₂ · x C₇H₈: C 41.43, H 5.21, N 9.95; found C 41.01, H 5.12, N 9.99.

[Tp^{Bu,Me}Lu(NTf₂)₂] (4-Lu): A precooled solution of Me₃SiNTf₂ (56.0 mg, 0.158 mmol) in toluene (5 mL) was added to a precooled solution of [Tp^{Bu,Me}LuMe₂] (50.0 mg, 0.0788 mmol) in toluene (5 mL) at -35 °C. The reaction mixture was allowed to stir for 4 h at 0 °C. The solution was concentrated in vacuo and stored at -35 °C. Crystallization yielded compound **4-Lu** (65.0 mg, 0.0561 mmol, 71%) as colorless crystals. ¹H NMR (250 MHz, [D₆]benzene, 26 °C): δ = 5.74 (s, 3H, 4-pz-H), 4.54 (v br d, ¹J(BH) = 340 Hz, 1H, BH), 2.06 (s, 9H, pz-CH₃), 1.31 ppm (s, 27H, pz-C(CH₃)₃). ¹³C{¹H} NMR (63 MHz, [D₆]benzene, 26 °C): δ = 168.1 (5-pz-C), 150.5 (3-pz-C), 106.9 (4-pz-C), 32.3 (pz-C(CH₃)₃), 30.9 (pz-C(CH₃)₃), 13.3 ppm (pz-C(CH₃)₃). ¹³C NMR resonances for the triflate groups could not be detected. ¹¹B{¹H} NMR (80 MHz, [D₆]benzene, 26 °C): δ = -7.6 ppm. ¹⁹F{¹H} NMR (376 MHz, [D₆]benzene, 26 °C): δ = -76.9 ppm. IR (KBr): $\tilde{\nu}$ = 3149 (vw), 2974 (w), 2936 (w), 2873 (vw), 2569 (vw, B-H), 1544 (m), 1482 (w), 1464 (w), 1422 (w), 1358 (s), 1338 (vs), 1324 (m), 1239 (vs), 1218 (vs), 1193 (vs), 1134 (s), 1119 (s), 1100 (vs), 1055 (m), 1035 (m), 1017 (w), 982 (vw), 928 (vw), 847 (vw), 838 (vw), 824 (w), 806 (w), 767 (w), 743 (w), 681 (vw), 661 (w), 653 (m), 605 (s), 579 (m), 531 (vw), 512 (m), 441 (vw), 426 cm⁻¹ (vw); elemental analysis calcd (%) for C₂₈H₄₀BF₁₂LuN₆O₈S₄: C 29.03, H 3.48, N 9.67; found C 30.12, H 3.49, N 9.27. Due to the high S and F contents no better elemental analysis could be obtained.

[Tp^{Bu,Me}YCl₂] (5-Y): A solution of SiMe₃Cl (18.0 mg, 0.166 mmol) in toluene (5 mL) was added to a solution of [Tp^{Bu,Me}YMe(AlMe₄)] (50.0 mg, 0.0814 mmol) in toluene (5 mL) and stirred for 3 h at ambient temperature. The solution was concentrated in vacuo and stored at -35 °C. Crystallization yielded compound **5-Y** (42.0 mg, 0.0720 mmol, 89%) as colorless crystals. ¹H NMR (250 MHz, [D₈]toluene, 26 °C): δ = 5.56 (s, 3H, 4-pz-H), 4.47 (v br d, ¹J(BH) = 140 Hz, 1H, BH), 1.95 (s, 9H, pz-CH₃), 1.50 ppm (s, 27H, pz-C(CH₃)₃). ¹³C{¹H} NMR (63 MHz, [D₈]toluene, 26 °C): δ = 175.4 (5-pz-C), 147.1 (3-pz-C), 104.0 (4-pz-C), 32.6 (pz-C(CH₃)₃), 31.5 (pz-C(CH₃)₃), 13.1 ppm (pz-C(CH₃)₃). ¹³C{¹H} NMR (63 MHz, [D₈]THF, 26 °C): δ = 166.4 (5-pz-C), 147.6 (3-pz-C), 105.7 (4-pz-C), 33.3 (pz-C(CH₃)₃), 31.5 (pz-C(CH₃)₃), 13.2 ppm (pz-C(CH₃)₃). ¹¹B{¹H} NMR (80 MHz, [D₈]THF, 26 °C): δ = -7.9 ppm. IR (KBr): $\tilde{\nu}$ = 2963 (s), 2928 (w), 2859 (w), 2577 (vw, B-H), 1538 (vs), 1471 (w), 1463 (m), 1435 (s), 1382 (w), 1360 (m), 1346 (s), 1346 (s), 1332 (w), 1241 (w), 1192 (s), 1173 (vs), 1133 (vw), 1121 (vw), 1067 (m), 1064 (m), 1029 (m), 1014 (w), 989 (vw),

847 (vw), 810 (w), 804 (w), 787 (m), 777 (w), 765 (s), 729 (vw), 683 (vw), 677 (vw), 659 (vw), 645 (m), 515 cm⁻¹ (vw); elemental analysis calcd (%) for C₂₄H₄₀BCl₂N₆Y: C 49.42, H 6.91, N 14.41; found C 49.01, H 6.99, N 13.74.

[Tp^{Bu,Me}LuCl₂] (5-Lu): In a pressure tube a solution of SiMe₃Cl (40.0 mg, 0.368 mmol) in toluene (5 mL) was added to a solution of [Tp^{Bu,Me}LuMe₂] (100 mg, 0.158 mmol) in toluene (10 mL) and stirred for 6 h at 50 °C. The formed precipitate was allowed to settle, the supernatant was decanted and the solid washed with *n*-hexane (3 × 2 mL). The precipitate was dried in vacuo to afford **5-Lu** (60.0 mg, 0.0896 mmol, 57%) as a white solid. Single crystals suitable for X-ray diffraction could be obtained by crystallization from a saturated THF solution at -35 °C. ¹H NMR (400 MHz, [D₈]THF, 26 °C): δ = 6.04 (s, 3H, 4-pz-H), 4.83 (v br d, ¹J(BH) = 135 Hz, 1H, BH), 2.38 (s, 9H, pz-CH₃), 1.49 ppm (s, 27H, pz-C(CH₃)₃). ¹³C{¹H} NMR (63 MHz, [D₈]benzene, 26 °C): δ = 166.1 (5-pz-C), 147.0 (3-pz-C), 104.1 (4-pz-C), 32.6 (pz-C(CH₃)₃), 31.0 (pz-C(CH₃)₃), 13.0 ppm (pz-C(CH₃)₃). ¹¹B{¹H} NMR (80 MHz, [D₈]THF, 26 °C): δ = -9.2 ppm. IR (KBr): $\tilde{\nu}$ = 2961 (vs), 2906 (s), 2862 (s), 2550 (w, B-H), 1539 (vs), 1476 (s), 1463 (s), 1424 (vs), 1380 (m), 1356 (vs), 1332 (m), 1295 (vw), 1241 (s), 1192 (vs), 1176 (vs), 1070 (vs), 1028 (s), 1015 (s), 987 (m), 913 (w), 867 (m), 849 (m), 840 (s), 804 (s), 789 (s), 781 (s), 766 (vs), 731 (w), 658 (m), 644 (s), 515 cm⁻¹ (w); elemental analysis calcd (%) for C₂₄H₄₀Bl₂LuN₆: C 43.07, H 6.02, N 12.56; found C 43.32, H 5.99, N 12.39.

[Tp^{Bu,Me}YI₂] (6-Y): A solution of SiMe₃I (33.0 mg, 0.165 mmol) in toluene (5 mL) was added to a solution of [Tp^{Bu,Me}YMe(AlMe₄)] (50.0 mg, 0.0814 mmol) in toluene (5 mL) and stirred for 3 h. The solution was concentrated in vacuo and stored at -35 °C. Crystallization yielded compound **6-Y** (52.0 mg, 0.0679 mmol, 84%) as colorless crystals. ¹H NMR (250 MHz, [D₈]toluene, 26 °C): δ = 5.55 (s, 3H, 4-pz-H), 4.50 (v br d, ¹J(BH) = 130 Hz, 1H, BH), 1.95 (s, 9H, pz-CH₃), 1.54 ppm (s, 27H, pz-C(CH₃)₃). ¹³C{¹H} NMR (63 MHz, [D₈]toluene, 26 °C): δ = 166.6 (5-pz-C), 147.9 (3-pz-C), 104.5 (4-pz-C), 33.1 (pz-C(CH₃)₃), 32.1 (pz-C(CH₃)₃), 13.2 ppm (pz-C(CH₃)₃). ¹¹B{¹H} NMR (80 MHz, [D₈]toluene, 26 °C): δ = -8.7 ppm. IR (KBr): $\tilde{\nu}$ = 2964 (s), 2927 (w), 2863 (vw), 2562 (vw, B-H), 1539 (vs), 1473 (m), 1456 (w), 1430 (vs), 1380 (w), 1364 (m), 1135 (vw), 1124 (vw), 1068 (m), 1061 (m), 1027 (m), 1014 (w), 985 (w), 846 (vw), 825 (vw), 802 (w), 799 (w), 764 (s), 729 (vw), 683 (vw), 674 (vw), 659 (w), 642 (m), 515 (vw), 472 (vw), 440 cm⁻¹ (vw); elemental analysis calcd (%) for C₂₄H₄₀Bl₂N₆Y: C 37.62, H 5.26, N 10.97; found C 37.68, H 5.18, N 11.00.

[Tp^{Bu,Me}LuI₂] (6-Lu): A solution of SiMe₃I (47.0 mg, 0.235 mmol) in toluene (5 mL) was added to a solution of [Tp^{Bu,Me}LuMe₂] (50.0 mg, 0.0788 mmol) in toluene (5 mL) and stirred for 3 h at ambient temperature. The solution was concentrated in vacuo and stored at -35 °C. Crystallization yielded compound **6-Lu** (60.0 mg, 0.0704 mmol, 89%) as colorless crystals. ¹H NMR (250 MHz, [D₈]toluene, 26 °C): δ = 5.60 (s, 3H, 4-pz-H), 4.48 (v br d, ¹J(BH) = 135 Hz, 1H, BH), 1.94 (s, 9H, pz-CH₃), 1.56 ppm (s, 27H, pz-C(CH₃)₃). ¹³C{¹H} NMR (101 MHz, [D₈]toluene, 26 °C): δ = 167.3 (5-pz-C), 148.1 (3-pz-C), 105.0 (4-pz-C), 32.9 (pz-C(CH₃)₃), 31.8 (pz-C(CH₃)₃), 12.9 ppm (pz-C(CH₃)₃). ¹¹B{¹H} NMR (80 MHz, [D₈]toluene, 26 °C): δ = -7.6 ppm. IR (KBr): $\tilde{\nu}$ = 3126 (vw), 2961 (vs), 2928 (w), 2906 (w), 2862 (w), 2553 (vw, B-H), 1541 (vs), 1475 (m), 1463 (w), 1430 (vs), 1381 (w), 1354 (s), 1324 (w), 1242 (w), 1201 (m), 1191 (s), 1171 (vs), 1131 (m), 1065 (vs), 1030 (w), 1024 (w), 1015 (w), 984 (w), 846 (vw), 824 (vw), 804 (m), 794 (m), 762 (s), 729 (vw), 673 (vw), 656 (w), 642 (m), 472 (vw), 412 cm⁻¹ (w); elemental analysis calcd (%) for C₂₄H₄₀Bl₂LuN₆: C 33.83, H 4.73, N 9.86; found C 33.96, H 4.68, N 9.93.

[Tp^{BU₃Me}LuMeCl] (7-Lu): A solution of SiMe₃Cl (34.2 mg, 0.315 mmol) in toluene (5 mL) was added to a solution of [Tp^{BU₃Me}LuMe₂] (200.0 mg, 0.315 mmol) in toluene (10 mL) and stirred for 3 h at ambient temperature. The solvent was evaporated and the remaining white precipitate was washed with cold toluene (3 × 2 mL). The solid was dried in vacuo to afford **7-Lu** (150 mg, 0.231 mmol, 73%). Single crystals suitable for X-ray diffraction could be obtained by crystallization from a saturated THF solution at –35 °C. ¹H NMR (400 MHz, [D₆]THF, 26 °C): δ = 5.98 (s, 3H, 4-pz-H), 4.75 (v br d, ³J(BH) = 135 Hz, 1H, BH), 2.40 (s, 9H, pz-CH₃), 1.48 (s, 27H, pz-C(CH₃)₃), –0.29 ppm (s, 3H, Lu-CH₃). ¹³C{¹H} NMR (63 MHz, [D₆]THF, 26 °C): δ = 166.0 (5-pz-C), 147.6 (3-pz-C), 104.7 (4-pz-C), 35.5 (Lu-CH₃), 32.9 (pz-C(CH₃)₃), 31.0 (pz-C(CH₃)₃), 13.1 ppm (pz-C(CH₃)₃). ¹¹B{¹H} NMR (80 MHz, [D₆]THF, 26 °C): δ = –8.7 ppm. IR (KBr): $\tilde{\nu}$ = 2963 (s), 2953 (s), 2931 (w), 2907 (m), 2861 (w), 2575 (vw, B-H), 1540 (vs), 1474 (m), 1463 (m), 1435 (vs), 1381 (w), 1362 (s), 1351 (s), 1335 (w), 1242 (w), 1193 (s), 1172 (vs), 1123 (w), 1075 (s), 1063 (s), 1030 (m), 1014 (w), 987 (w), 849 (vw), 841 (w), 806 (m), 787 (vs), 777 (m), 765 (vs.), 729 (w), 694 (vw), 677 (w), 660 (w), 645 (s), 515 (w), 492 (vw), 442 (vw), 411 cm^{–1} (m); elemental analysis calcd (%) for C₂₅H₄₃BClLuN₆: C 46.28, H 6.68, N 12.95; found C 45.70, H 6.42, N 12.66.

[Tp^{BU₃Me}LuMe(CH₂SiMe₃)] (8-Lu): A precooled solution of LiCH₂SiMe₃ (14.5 mg, 0.154 mmol) in toluene (5 mL) was added to a precooled solution of [Tp^{BU₃Me}LuMeCl] (100 mg, 0.154 mmol) in toluene (5 mL) at –35 °C. The reaction mixture was allowed to stir for 3 h at 0 °C. The precipitate was filtered off and the solution was concentrated in vacuo and stored at –35 °C. Crystallization yielded compound **8-Lu** (56.0 mg, 0.0799 mmol, 52%) as colorless crystals. ¹H NMR (400 MHz, [D₆]benzene, 26 °C): δ = 5.65 (s, 3H, 4-pz-H), 4.54 (v br d, ³J(BH) = 360 Hz, 1H, BH), 2.06 (s, 9H, pz-CH₃), 1.51 (s, 27H, pz-C(CH₃)₃), 0.23 (s, 18H, SiCH₃), 0.19 (s, 3H, Lu-CH₃), –0.71 ppm (s, 2H, CH₂SiMe₃). ¹³C{¹H} NMR (63 MHz, [D₆]benzene, 26 °C): δ = 165.3 (5-pz-C), 146.7 (3-pz-C), 103.9 (4-pz-C), 37.6 (Lu-CH₂), 32.6 (pz-C(CH₃)₃), 31.9 (Lu-CH₃), 31.4 (pz-C(CH₃)₃), 13.2 (pz-C(CH₃)₃), 4.5 ppm (SiMe₃). ¹¹B{¹H} NMR (80 MHz, [D₆]benzene, 26 °C): δ = –8.2 ppm. ²⁹Si{¹H} dept45 NMR (50 MHz, [D₆]benzene, 26 °C): δ = –0.3 ppm. IR (KBr): $\tilde{\nu}$ = 2960 (vs), 2926 (s), 2866 (m), 2815 (vw), 2552 (vw, B-H), 1540 (vs), 1463 (m), 1432 (s), 1379 (w), 1360 (s), 1334 (w), 1236 (m), 1205 (m), 1195 (m), 1175 (s), 1128 (w), 1071 (m), 1060 (m), 1025 (w), 1013 (w), 985 (w), 894 (w), 872 (s), 854 (m), 816 (w), 806 (w), 791 (m), 766 (m), 743 (w), 731 (w), 717 (w), 675 (vw), 663 (w), 645 (m), 521 (vw), 513 (vw), 473 (vw), 434 (vw), 421 (w), 404 cm^{–1} (m); elemental analysis calcd (%) for C₂₉H₅₄BLuN₆Si: C 49.71, H 7.77, N 11.99; found C 49.73, H 7.65, N 11.73.

[Tp^{BU₃Me}LuMe(CH₂Ph)] (9-Lu): A suspension of KCH₂Ph (20.0 mg, 0.154 mmol) in toluene (5 mL) was added to a solution of [Tp^{BU₃Me}LuMeCl] (100 mg, 0.154 mmol) in toluene (5 mL) and stirred for 24 h at ambient temperature. The reaction mixture was filtered and the solution was concentrated in vacuo and stored at –35 °C. Crystallization yielded compound **9-Lu** (49.0 mg, 0.0695 mmol, 45%) as colorless crystals. ¹H NMR (250 MHz, [D₆]benzene, 26 °C): δ = 6.95 (t, ³J(HH) = 15.5 Hz, 2H, Ar-H), 6.62 (t, ³J(HH) = 15.9 Hz, 1H, Ar-H), 6.35 (d, ²J(HH) = 7.6 Hz, 2H, Ar-H), 5.62 (s, 3H, 4-pz-H), 4.52 (v br d, ¹J(BH) = 147 Hz, 1H, BH), 2.02 (s, 9H, pz-CH₃), 1.63 (s, 2H, CH₂), 1.44 (s, 27H, pz-C(CH₃)₃), 0.39 ppm (s, 3H, Lu-CH₃). ¹³C{¹H} NMR (101 MHz, [D₆]benzene, 26 °C): δ = 164.9 (5-pz-C), 154.3 (Ar-C1), 147.0 (3-pz-C), 127.3 (Ar-C2/C6), 124.5 (Ar-C3/C5), 117.1 (Ar-C4), 103.8 (4-pz-C), 61.0 (Lu-CH₂), 38.2 (Lu-CH₃), 32.3 (pz-C(CH₃)₃), 31.2 (pz-C(CH₃)₃), 13.0 ppm (pz-C(CH₃)₃). ¹¹B{¹H} NMR (80 MHz, [D₆]benzene, 26 °C): δ = –8.3 ppm. IR (KBr): $\tilde{\nu}$ = 3054 (vw), 2999 (vw), 2963 (vs), 2926 (w), 2903 (m), 2864 (w), 2544 (vw, B-H), 1589 (m), 1539 (vs), 1486 (s), 1473 (s), 1431 (vs), 1362 (s), 1356 (s), 1330

(w), 1242 (w), 1218 (m), 1203 (m), 1190 (s), 1164 (s), 1129 (m), 1069 (s), 1057 (m), 1025 (m), 1015 (vw), 984 (w), 929 (s), 864 (w), 848 (vw), 810 (m), 802 (m), 787 (m), 775 (w), 764 (s), 742 (m), 732 (s), 696 (s), 682 (vw), 675 (vw), 661 (vw), 643 (s), 521 (w), 510 (vw), 468 (w), 457 cm^{–1} (w); elemental analysis calcd (%) for C₃₂H₅₀BLuN₆: C 54.55, H 7.15, N 11.93; found C 54.72, H 7.25, N 12.29.

X-ray crystallography and crystal structure determinations

Single crystals of **1-Lu**, **3-Lu**, **4-Lu**, **5-Lu**, **6-Lu**, **7-Lu**, **8-Lu**, and **9-Lu** were grown by standard techniques from saturated solutions in *n*-hexane, toluene or THF at –35 °C as stated in the experimental section. Suitable crystals were collected in a glovebox and coated with Parabar 10312 (previously known as Paratone N, Hampton Research) and fixed on a nylon loop/glass fiber.

X-ray data for compounds of **1-Lu**, **3-Lu**, **4-Lu**, **5-Lu**, **6-Lu**, **7-Lu**, **8-Lu**, and **9-Lu** were collected on a Bruker APEX II DUO instrument equipped with an μ S microfocus sealed tube and QUAZAR optics for MoK α (λ = 0.71073 Å) and CuK α (λ = 1.54184 Å) radiation. The data collection strategy was determined using COSMO^[42] employing ω -scans. Raw data were processed using APEX^[43] and SAINT^[44] corrections for absorption effects were applied using SADABS.^[45] The structures were solved by direct methods and refined against all data by full-matrix least-squares methods on F² using SHELXTL^[46] and ShelXle.^[47] Disorder models were calculated using DSR, a program for refining structures in ShelXle.^[48] All graphics were produced employing ORTEP-3^[49] and POV-Ray.^[50] Further details of the refinement and crystallographic data are listed in Table S1 (Supporting Information) and in the CIF files. CCDC 1945695, 1945696, 1945697, 1945698, 1945699, 1945700, 1945701, 1945702 contain the supplementary crystallographic data for this paper. These data are provided free of charge by The Cambridge Crystallographic Data Centre.

Acknowledgements

We are grateful to the German Science Foundation for support (grant: AN 238/15-2).

Conflict of interest

The authors declare no conflict of interest.

Keywords: alkyls • halides • heteroleptic compounds • rare-earth metals • scorpionates

- [1] a) R. H. Grubbs, *Tetrahedron* **2004**, *60*, 7117–7140; b) T. E. Takeda, *Modern Carbonyl Olefination* **2004**, Wiley-VCH, Weinheim, **2004**; c) N. Calderon, *Acc. Chem. Res.* **1972**, *5*, 127–132; d) Y. Chauvin, *Angew. Chem. Int. Ed.* **2006**, *45*, 3740–3747; *Angew. Chem.* **2006**, *118*, 3824–3831; e) R. R. Schrock, *Acc. Chem. Res.* **1979**, *12*, 98–104; f) W. A. Herrmann, *Angew. Chem. Int. Ed. Engl.* **1982**, *21*, 117–130; *Angew. Chem.* **1982**, *94*, 118–131; g) “Fischer–Tropsch Synthesis: Catalysts and Chemistry”: J. van de Loosdrecht, F. G. Botes, I. M. Ciobica, A. Ferreira, P. Gibson, D. J. Middledy, A. M. Salb, J. L. Visagie, C. J. Weststrate, J. W. Niemantsverdiert in *Comprehensive Inorganic Chemistry II*, 2nd ed. (Eds.: J. Reedijk, K. Poeppelmeier), Elsevier, Amsterdam, **2013**, ch. 7.20.
- [2] D. S. Levine, T. D. Tilley, R. A. Andersen, *Organometallics* **2017**, *36*, 80–88.
- [3] G. R. Giesbrecht, J. C. Gordon, *Dalton Trans.* **2004**, 2387–2393.
- [4] M. Zimmermann, D. Rauschmaier, K. Eichele, K. W. Törnroos, R. Anwander, *Chem. Commun.* **2010**, *46*, 5346–5348.

- [5] H. M. Dietrich, K. W. Törnroos, R. Anwander, *J. Am. Chem. Soc.* **2006**, *128*, 9298–9299.
- [6] W. X. Zhang, Z. Wang, M. Nishiura, Z. Xi, Z. Hou, *J. Am. Chem. Soc.* **2011**, *133*, 5712–5715.
- [7] S. Li, M. Wang, B. Liu, L. Li, J. Cheng, C. Wu, D. Liu, J. Liu, D. Cui, *Chem. Eur. J.* **2014**, *20*, 15493–15498.
- [8] R. Litlabø, M. Zimmermann, K. Saliu, J. Takats, K. W. Törnroos, R. Anwander, *Angew. Chem. Int. Ed.* **2008**, *47*, 9560–9564; *Angew. Chem.* **2008**, *120*, 9702–9706.
- [9] a) K. Aparna, M. Ferguson, R. G. Cavell, *J. Am. Chem. Soc.* **2000**, *122*, 726–727; b) S. T. Liddle, D. P. Mills, A. J. Wooles, *Chem. Soc. Rev.* **2011**, *40*, 2164–2176.
- [10] W. Ma, C. Yu, Y. Chi, T. Chen, L. Wang, J. Yin, B. Wei, L. Xu, W. X. Zhang, Z. Xi, *Chem. Sci.* **2017**, *8*, 6852–6856.
- [11] W. Mao, L. Xiang, C. Alvarez Lamsfus, L. Maron, X. Leng, Y. Chen, *J. Am. Chem. Soc.* **2017**, *139*, 1081–1084.
- [12] W. Mao, L. Xiang, L. Maron, X. Leng, Y. Chen, *J. Am. Chem. Soc.* **2017**, *139*, 17759–17762.
- [13] L. N. Grant, S. Ahn, B. C. Manor, M. H. Baik, D. J. Mendiola, *Chem. Commun.* **2017**, *53*, 3415–3417.
- [14] a) N. A. Petasis, E. I. Bzowej, *J. Am. Chem. Soc.* **1990**, *112*, 6392–6394; b) N. A. Petasis, S. P. Lu, E. I. Bzowej, D. K. Fu, J. P. Staszewski, I. Akritopoulou-Zanze, M. A. Patane, Y. H. Hu, *Pure Appl. Chem.* **1996**, *68*, 667–670.
- [15] F. N. Tebbe, G. W. Parshall, G. S. Reddy, *J. Am. Chem. Soc.* **1978**, *100*, 3611–3613.
- [16] H. Osseili, K. N. Truong, T. P. Spaniol, L. Maron, U. Englert, J. Okuda, *Angew. Chem. Int. Ed.* **2019**, *58*, 1833–1837; *Angew. Chem.* **2019**, *131*, 1847–1851.
- [17] M. Zimmermann, J. Takats, G. Kiel, K. W. Törnroos, R. Anwander, *Chem. Commun.* **2008**, 612–614.
- [18] D. Schädle, C. Maichle-Mössmer, C. Schädle, R. Anwander, *Chem. Eur. J.* **2015**, *21*, 662–670.
- [19] For a similar mixed tetramethylaluminate/methyl complex, see: W. Rong, M. Wang, S. Li, J. Cheng, D. Liu, D. Cui, *Organometallics* **2018**, *37*, 971–978.
- [20] J. Blackwell, C. Lehr, Y. Sun, W. E. Piers, S. D. Pearce-Batchilder, M. J. Zaworotko, J. V. G. Young, *Can. J. Chem.* **1997**, *75*, 702–711.
- [21] J. Cheng, K. Saliu, G. Y. Kiel, M. J. Ferguson, R. McDonald, J. Takats, *Angew. Chem. Int. Ed.* **2008**, *47*, 4910–4913; *Angew. Chem.* **2008**, *120*, 4988–4991.
- [22] J. Cheng, M. J. Ferguson, J. Takats, *J. Am. Chem. Soc.* **2010**, *132*, 2–3.
- [23] D. P. Solowey, T. Kurogi, B. C. Manor, P. J. Carroll, D. J. Mendiola, *Dalton Trans.* **2016**, *45*, 15894–15901.
- [24] M. Zimmermann, R. Litlabø, K. W. Törnroos, R. Anwander, *Organometallics* **2009**, *28*, 6646–6649.
- [25] a) J. Fawcett, A. W. G. Platt, D. R. Russell, *Polyhedron* **2002**, *21*, 287–293; b) A. Babai, S. Pitula, A.-V. Mudring, *Eur. J. Inorg. Chem.* **2010**, 4933–4937.
- [26] H. Schumann, J. A. Meese-Marktscheffel, A. Dietrich, *J. Organomet. Chem.* **1989**, *377*, C5–C8.
- [27] A. Babai, A. V. Mudring, *Dalton Trans.* **2006**, 1828–1830.
- [28] a) S.-Y. Liu, G. H. Maunder, A. Sella, M. Stevenson, D. A. Tocher, *Inorg. Chem.* **1996**, *35*, 76–81; b) R. J. H. Clark, S. Y. Liu, G. H. Maunder, A. Sella, M. R. J. Elsegood, *J. Chem. Soc. Dalton Trans.* **1997**, 2241–2247.
- [29] a) N. Marques, A. Sella, J. Takats, *Chem. Rev.* **2002**, *102*, 2137–2160; b) F. A. Kunrath, O. L. Casagrande, L. Toupet, J.-F. Carpentier, *Polyhedron* **2004**, *23*, 2437–2445.
- [30] a) D. P. Long, A. Chandrasekaran, R. O. Day, P. A. Bianconi, *Inorg. Chem.* **2000**, *39*, 4476–4487; b) C. Apostolidis, A. Carvalho, A. Domingos, B. Kallakopoulos, R. Maier, N. Marques, A. Pires de Matos, J. Rebizant, *Polyhedron* **1998**, *18*, 263–272.
- [31] D. Roitershtein, A. Domingos, L. C. Pereira, J. R. Ascenso, N. Marques, *Inorg. Chem.* **2003**, *42*, 7666–7673.
- [32] H. Schumann, D. M. M. Freckmann, S. Dechert, *Z. Anorg. Allg. Chem.* **2002**, *628*, 2422–2426.
- [33] a) G. W. Rabe, F. A. Riederer, M. Zhang-Preße, A. L. Rheingold, *Inorg. Chim. Acta* **2017**, *457*, 103–106; b) G. W. Rabe, F. A. Riederer, M. Zhang-Preße, G. P. A. Yap, *Inorg. Chim. Acta* **2010**, *364*, 255–258.
- [34] N. Meyer, P. W. Roesky, S. Bambirra, A. Meetsma, B. Hessen, K. Saliu, J. Takats, *Organometallics* **2008**, *27*, 1501–1505.
- [35] K. O. Saliu, J. Takats, R. McDonald, *Acta Crystallogr. E* **2018**, *74*, 88–90.
- [36] R. Thim, H. M. Dietrich, M. Bonath, C. Maichle-Mössmer, R. Anwander, *Organometallics* **2018**, *37*, 2769–2777.
- [37] W. Yi, J. Zhang, F. Zhang, Y. Zhang, Z. Chen, X. Zhou, *Chem. Eur. J.* **2013**, *19*, 11975–11983.
- [38] Å. Domingos, M. R. J. Elsegood, A. C. Hillier, G. Lin, S. Y. Liu, I. Lopes, N. Marques, G. H. Maunder, R. McDonald, A. Sella, J. W. Steed, J. Takats, *Inorg. Chem.* **2002**, *41*, 6761–6768.
- [39] a) C. Stuhl, C. Maichle-Mössmer, R. Anwander, *Chem. Eur. J.* **2018**, *24*, 14254–14268; b) J. A. Bilbrey, A. H. Kazez, J. Locklin, W. D. Allen, *J. Comput. Chem.* **2013**, *34*, 1189–1197.
- [40] S. Trofimenko, J. C. Calabrese, J. S. Thompson, *Inorg. Chem.* **1987**, *26*, 1507–1514.
- [41] P. J. Bailey, R. A. Coxall, C. M. Dick, S. Fabre, L. C. Henderson, C. Herber, S. T. Liddle, D. Lorono-Gonzalez, A. Parkin, S. Parsons, *Chem. Eur. J.* **2003**, *9*, 4820–4828.
- [42] COSMO v. 1.61, Bruker AXS Inc., Madison, WI, **2012**.
- [43] APEX 3 v. 2017.3-0, Bruker AXS Inc., Madison, WI, **2017**.
- [44] SAINT v. 8.38A, Bruker AXS Inc., Madison, WI, **2017**.
- [45] L. Krause, R. Herbst-Irmer, G. M. Sheldrick, D. Stalke, *J. Appl. Crystallogr.* **2015**, *48*, 3–10.
- [46] G. Sheldrick, *Acta Crystallogr. Sect. C* **2015**, *71*, 3–8.
- [47] C. B. Hübschle, G. M. Sheldrick, B. Dittrich, *J. Appl. Crystallogr.* **2011**, *44*, 1281–1284.
- [48] D. Kratzert, J. J. Holstein, I. Krossing, *J. Appl. Crystallogr.* **2015**, *48*, 933–938.
- [49] L. J. Farrugia, *J. Appl. Crystallogr.* **2012**, *45*, 849–854.
- [50] POV-Ray v.3.6, Persistence of Vision Pty. Ltd., POV-Ray Williamstown, Victoria, Australia, **2004**, <http://www.povray.org>.

Manuscript received: August 7, 2019

Accepted manuscript online: September 6, 2019

Version of record online: October 22, 2019

CHEMISTRY

A **European** Journal

Supporting Information

Potential Precursors for Terminal Methylidene Rare-Earth-Metal Complexes Supported by a Superbulky Tris(pyrazolyl)borato Ligand

Verena M. Birkelbach, Renita Thim, Christoph Stuhl, Cécilia Maichle-Mössmer, and Reiner Anwander^{*[a]}

chem_201903606_sm_miscellaneous_information.pdf

Supporting Information

Table of contents

NMR spectroscopy

¹ H NMR, ¹³ C{ ¹ H} NMR, ¹¹ B{ ¹ H} NMR, ¹⁹ F{ ¹ H} NMR spectra of complex 1-Y	Pages S2-S4
¹ H NMR, ¹³ C{ ¹ H} NMR, ¹¹ B{ ¹ H} NMR, ¹⁹ F{ ¹ H} NMR spectra of complex 1-Lu	Pages S4-S6
¹ H NMR, ¹³ C{ ¹ H} NMR, ¹¹ B{ ¹ H} NMR, ¹⁹ F{ ¹ H} NMR spectra of complex 2-Lu	Pages S6-S8
¹ H NMR, ¹³ C{ ¹ H} NMR, ¹¹ B{ ¹ H} NMR, ¹⁹ F{ ¹ H} NMR spectra of complex 3-Lu	Pages S9-S10
¹ H NMR, ¹³ C{ ¹ H} NMR, ¹¹ B{ ¹ H} NMR, ¹⁹ F{ ¹ H} NMR spectra of complex 4-Lu	Pages S10-S12
¹ H NMR, ¹³ C{ ¹ H} NMR, ¹¹ B{ ¹ H} NMR spectra of complex 5-Y	Pages S12-S13
¹ H NMR, ¹³ C{ ¹ H} NMR, ¹¹ B{ ¹ H} NMR spectra of complex 5-Lu	Pages S14-S15
¹ H NMR, ¹³ C{ ¹ H} NMR, ¹¹ B{ ¹ H} NMR spectra of complex 6-Y	Pages S15-S16
¹ H NMR, ¹³ C{ ¹ H} NMR, ¹¹ B{ ¹ H} NMR spectra of complex 6-Lu	Pages S17-S18
¹ H NMR, ¹³ C{ ¹ H} NMR, ¹¹ B{ ¹ H} NMR spectra of complex 7-Lu	Pages S19-S20
¹ H NMR, ¹³ C{ ¹ H} NMR, ¹¹ B{ ¹ H} NMR, ²⁹ Si{ ¹ H} NMR spectra of complex 8-Lu	Pages S20-S21
¹ H NMR, ¹³ C{ ¹ H} NMR, ¹¹ B{ ¹ H} NMR spectra of complex 9-Lu	Pages S22-S23

X-ray structure analyses

Comprehensive crystallographic data for compounds 1-Lu , 2-Lu , 4-Lu , 5-Lu , 6-Lu , 7-Lu , 8-Lu , and 9-Lu	Pages S24-25
---------------------------------------------------------------------------------------------------------------------------------------------------------------------	--------------

Cone-angle analyses

Cone angle calculations	Pages S26-28
Raw data files for cone angle calculation	Pages S29-40

NMR spectroscopy

The solvent residual peaks are marked with an asterisk (*).

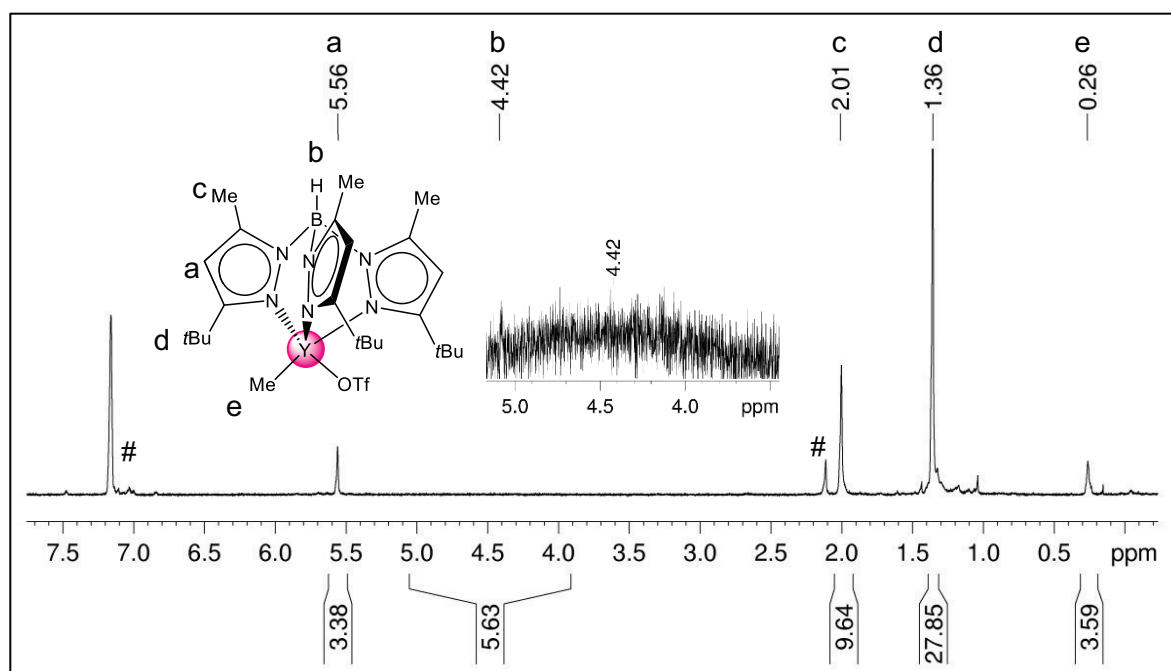


Figure S1. ¹H NMR spectrum (250 MHz, [D₆]benzene of complex [Tp^{tBu,Me}YMe(OTf)] (1-Y) at 26 °C with traces of toluene (#).

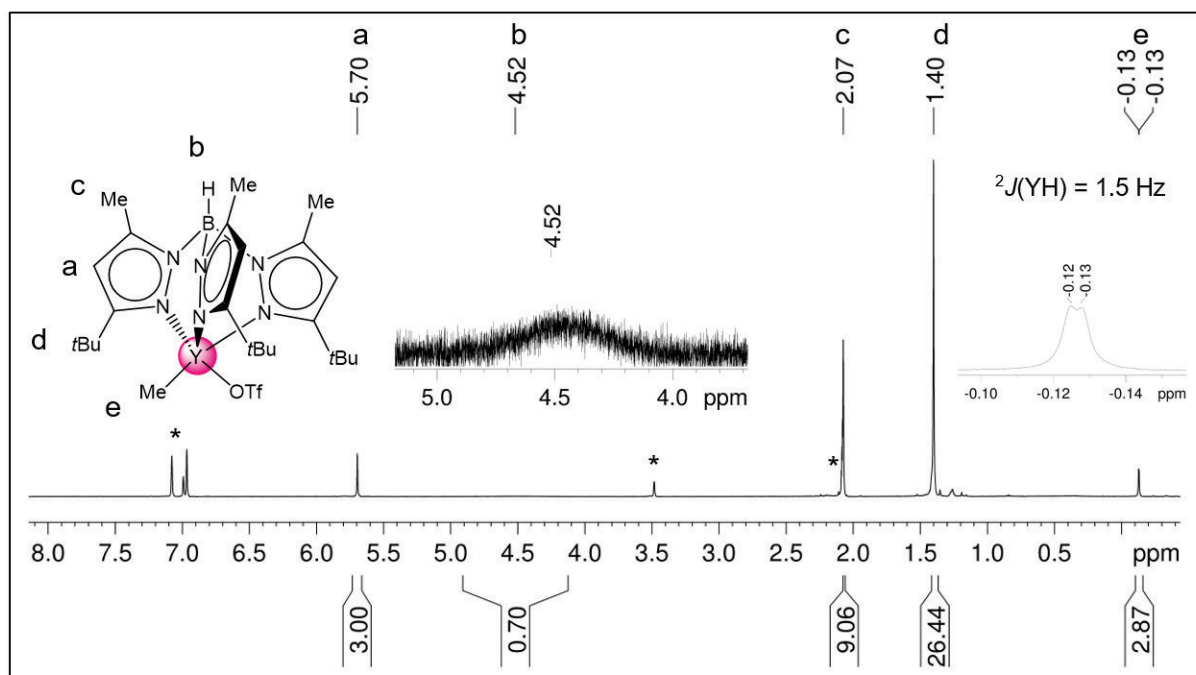


Figure S2. ¹H NMR spectrum (500 MHz, [D₈]toluene and a few drops of [D₈]thf due to solubility issues at lower temperatures) of complex [Tp^{tBu,Me}YMe(OTf)] (1-Y) at 0 °C.

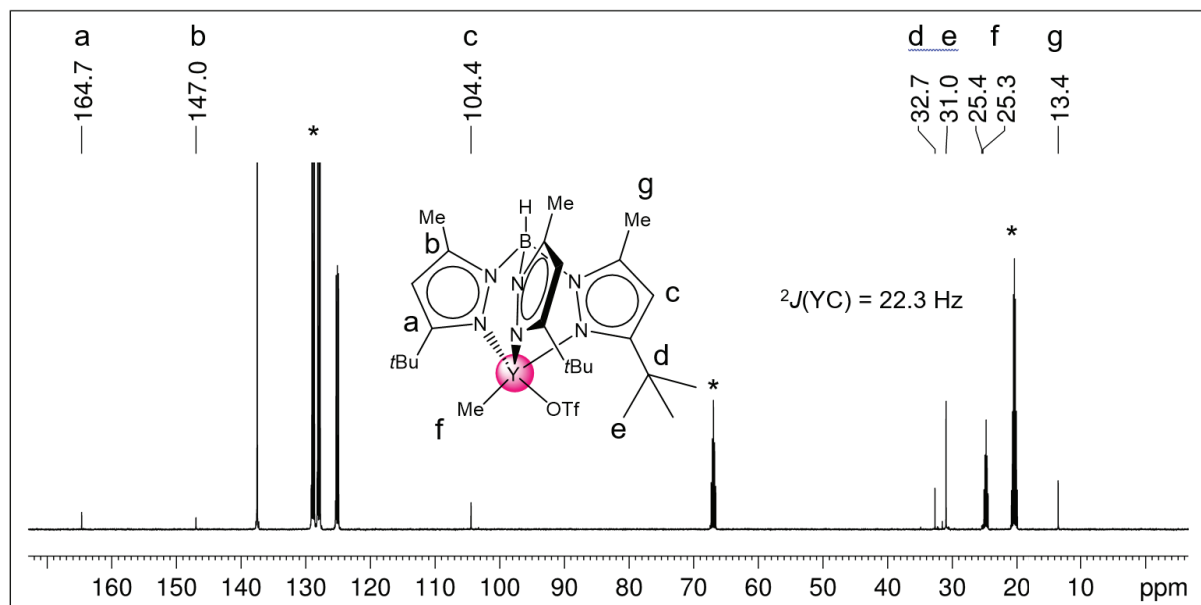


Figure S3. $^{13}\text{C}\{^1\text{H}\}$ NMR spectrum (126 MHz, $[\text{D}_8]$ toluene and a few drops of $[\text{D}_8]$ thf due to solubility issues at lower temperatures) of complex $[\text{Tp}^{\text{tBu,Me}}\text{YMe}(\text{OTf})]$ (**1-Y**) at $0\text{ }^\circ\text{C}$. ^{13}C NMR resonances for the triflate groups could not be detected.

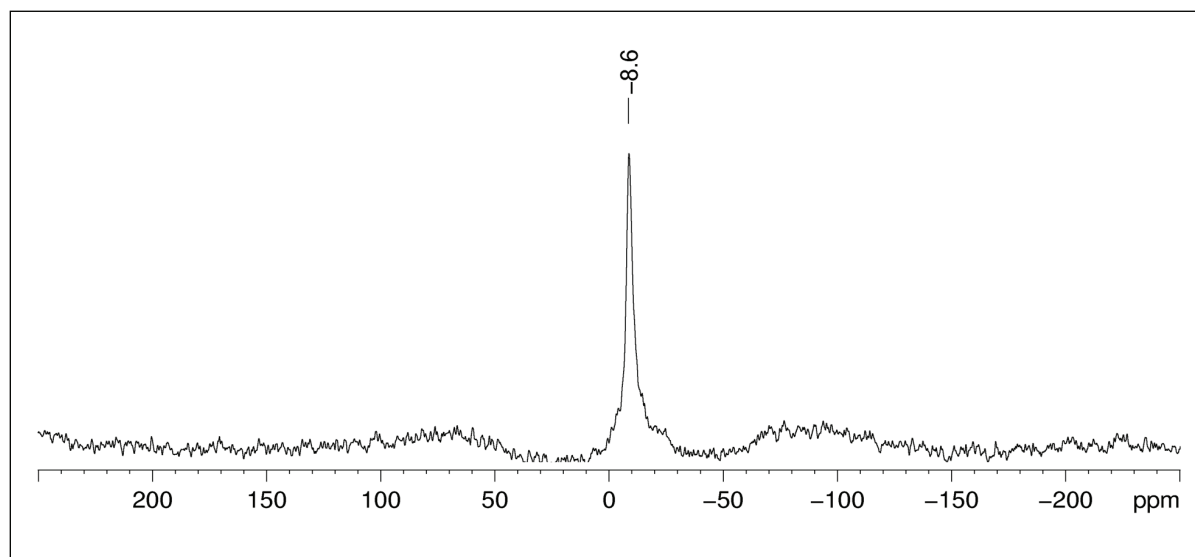


Figure S4. $^{11}\text{B}\{^1\text{H}\}$ NMR spectrum (80 MHz, $[\text{D}_6]$ benzene) of complex $[\text{Tp}^{\text{tBu,Me}}\text{YMe}(\text{OTf})]$ (**1-Y**) at $26\text{ }^\circ\text{C}$.

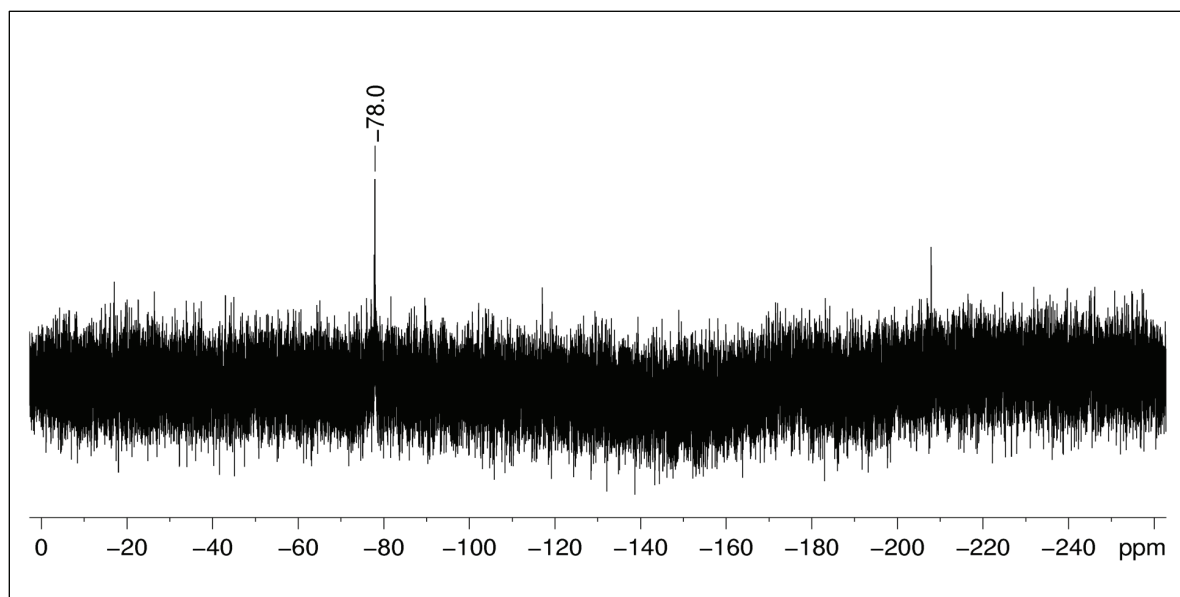


Figure S5. $^{19}\text{F}\{^1\text{H}\}$ NMR spectrum (376 MHz, $[\text{D}_6]$ benzene) of complex $[\text{Tp}^{\text{tBu,Me}}\text{YMe}(\text{OTf})]$ (**1-Y**) at 26 °C.

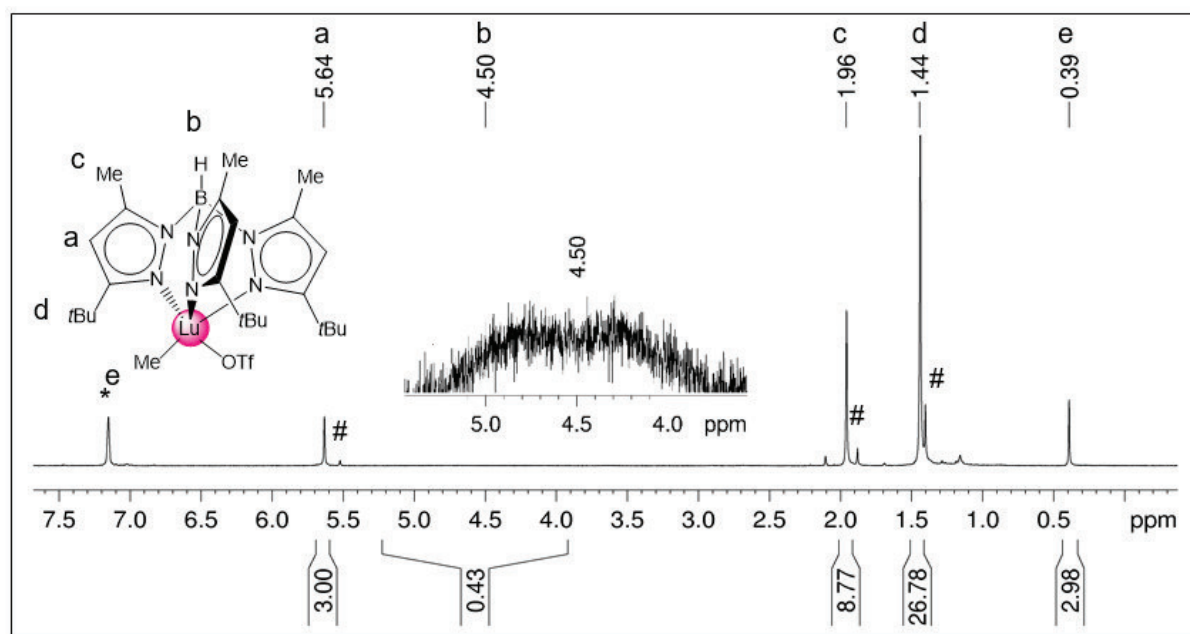


Figure S6. ^1H NMR spectrum (250 MHz, $[\text{D}_6]$ benzene) of complex $[\text{Tp}^{\text{tBu,Me}}\text{LuMe}(\text{OTf})]$ (**1-Lu**) at 26 °C with minor impurities of the reactant $[\text{Tp}^{\text{tBu,Me}}\text{Lu}(\text{OTf})_2]$ (#).

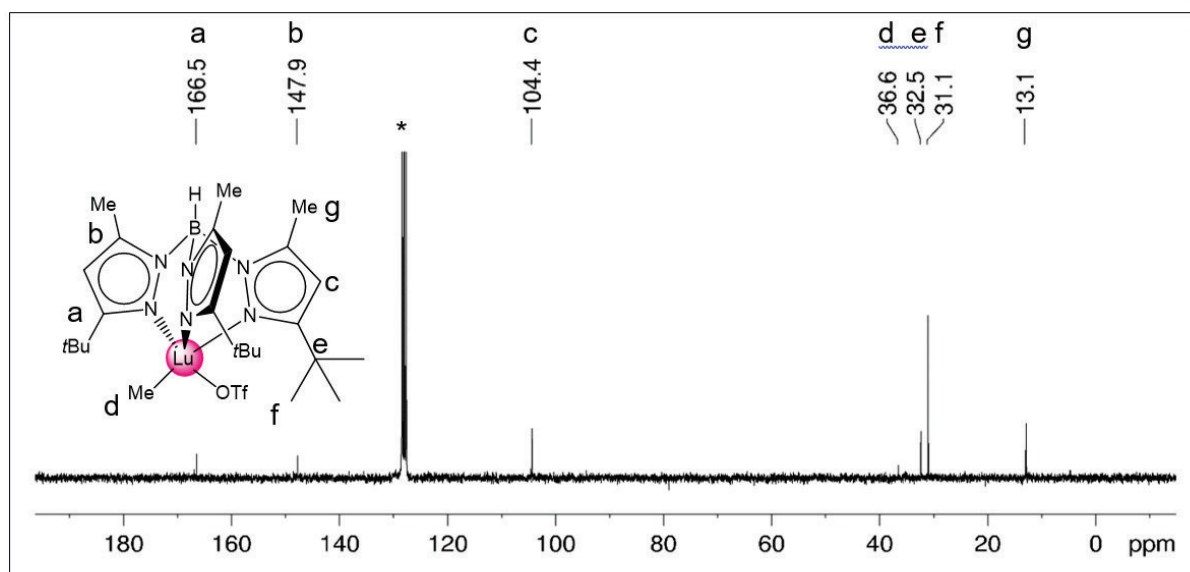


Figure S7. $^{13}\text{C}\{^1\text{H}\}$ NMR spectrum (63 MHz, $[\text{D}_6]$ benzene) of complex $[\text{Tp}^{\text{tBu,Me}}\text{LuMe}(\text{OTf})]$ (**1-Lu**) at 26 °C. ^{13}C NMR resonances for the triflate groups could not be detected.

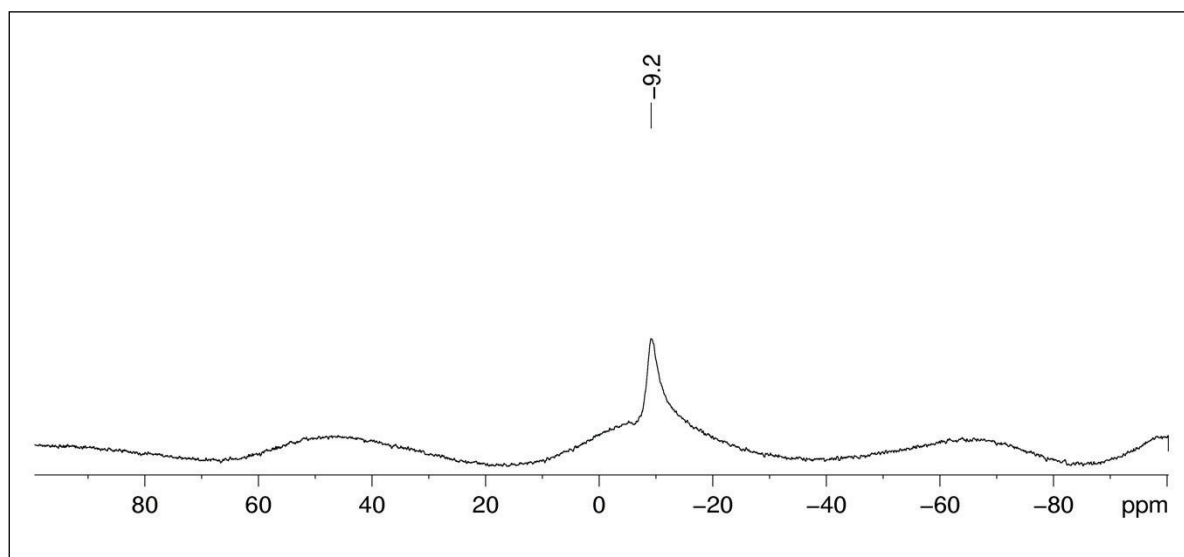


Figure S8. $^{11}\text{B}\{^1\text{H}\}$ NMR spectrum (80 MHz, $[\text{D}_6]$ benzene) of complex $[\text{Tp}^{\text{tBu,Me}}\text{LuMe}(\text{OTf})]$ (**1-Lu**) at 26 °C.

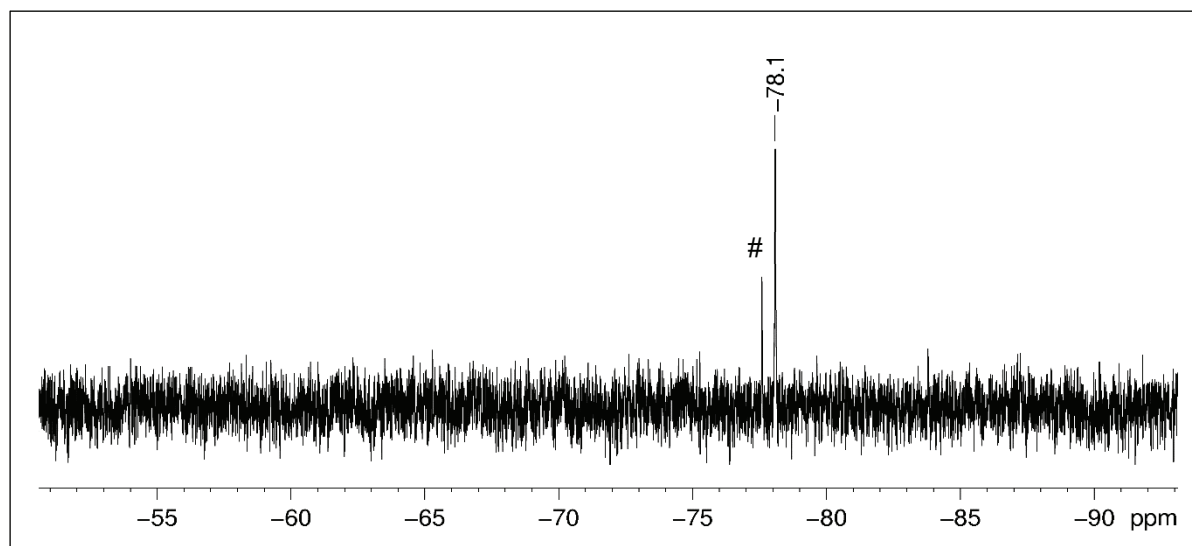


Figure S9. $^{19}\text{F}\{^1\text{H}\}$ NMR spectrum (376 MHz, $[\text{D}_6]$ benzene) of complex $[\text{Tp}^{\text{tBu,Me}}\text{LuMe}(\text{OTf})]$ (**1-Lu**) at 26 °C with minor impurities of $[\text{Tp}^{\text{tBu,Me}}\text{Lu}(\text{OTf})_2]$ (#).

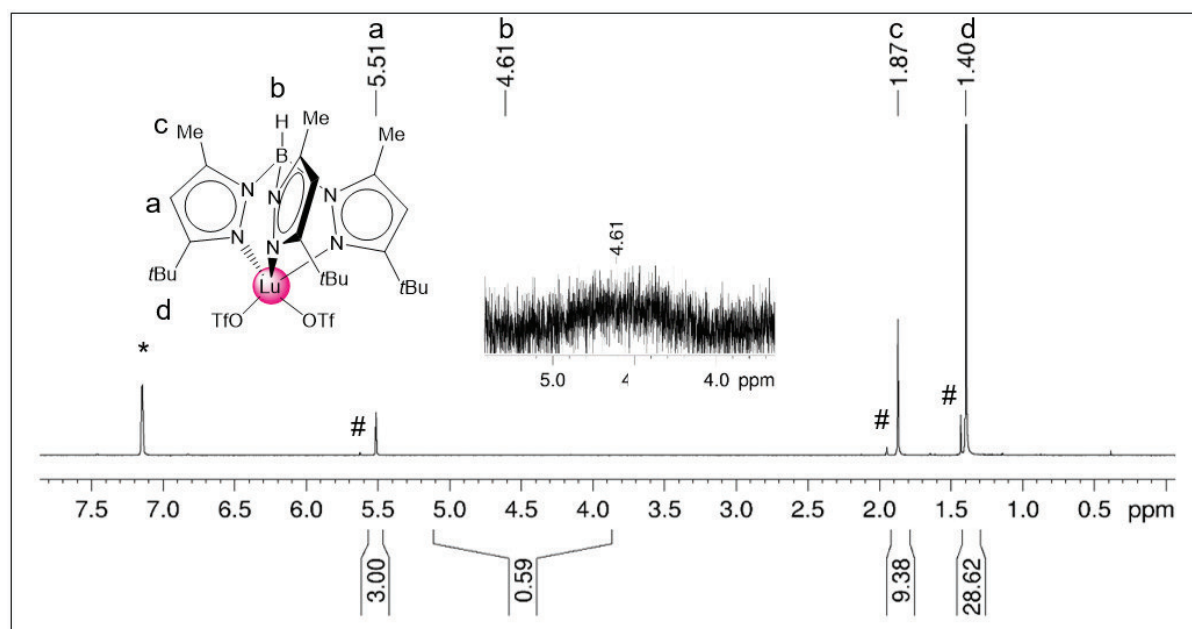


Figure S10. ^1H NMR spectrum (250 MHz, $[\text{D}_6]$ benzene) of complex $[\text{Tp}^{\text{tBu,Me}}\text{Lu}(\text{OTf})_2]$ (**2-Lu**) at 26 °C with minor impurities of $[\text{Tp}^{\text{tBu,Me}}\text{LuMe}(\text{OTf})]$ (#).

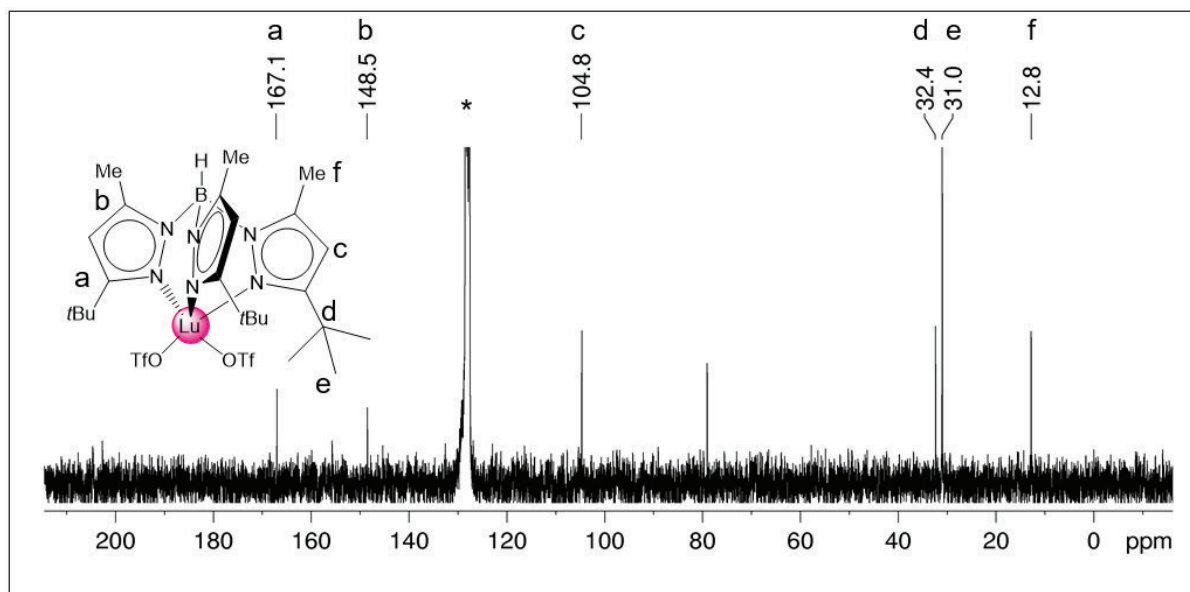


Figure S11. $^{13}\text{C}\{^1\text{H}\}$ NMR spectrum (63 MHz, $[\text{D}_6]$ benzene) of complex $[\text{Tp}^{\text{tBu,Me}}\text{Lu}(\text{OTf})_2]$ (**2-Lu**) at 26 °C. ^{13}C NMR resonances for the triflate groups could not be detected.

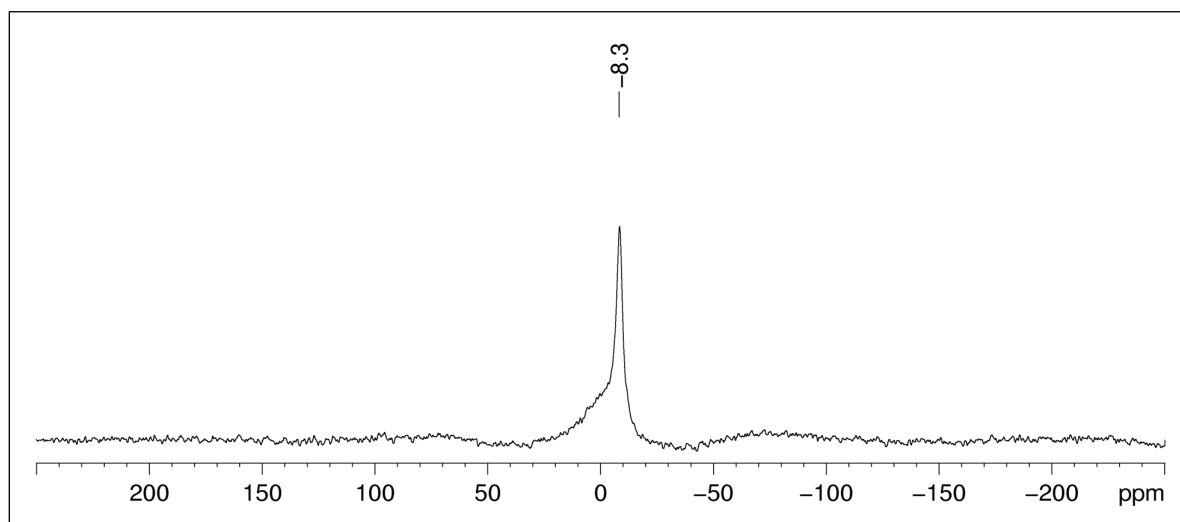


Figure S12. $^{11}\text{B}\{^1\text{H}\}$ NMR spectrum (80 MHz, $[\text{D}_6]$ benzene) of complex $[\text{Tp}^{\text{tBu,Me}}\text{Lu}(\text{OTf})_2]$ (**2-Lu**) at 26 °C.

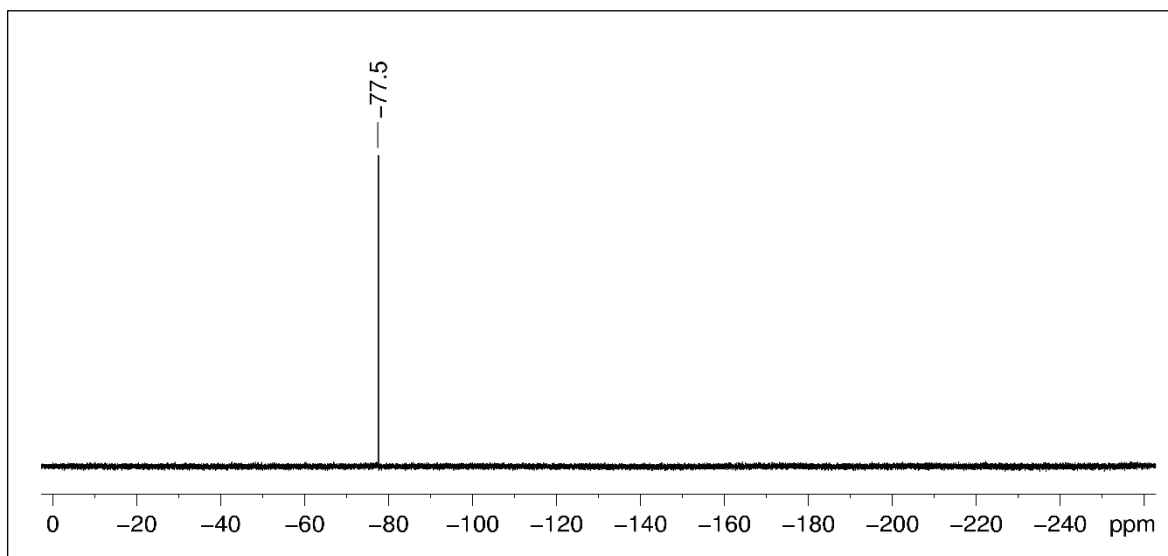


Figure S13. $^{19}\text{F}\{^1\text{H}\}$ NMR spectrum (376 MHz, $[\text{D}_6]$ benzene) of complex $[\text{Tp}^{\text{tBu,Me}}\text{Lu}(\text{OTf})_2]$ (**2-Lu**) at 26 °C.

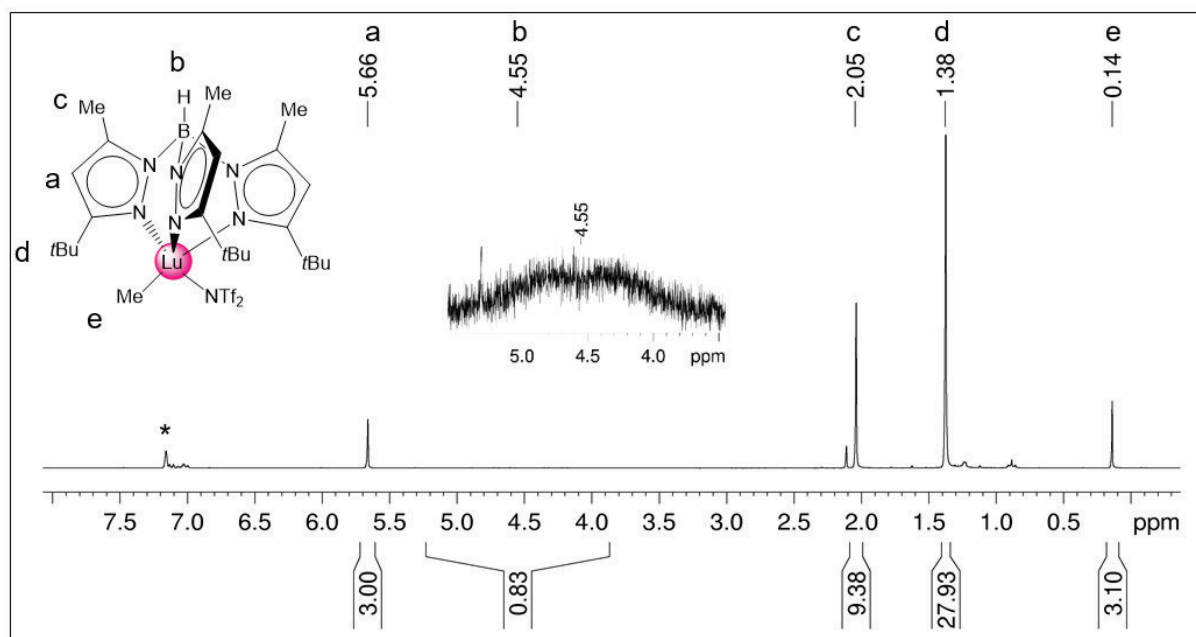


Figure S14. ^1H NMR spectrum (250 MHz, $[\text{D}_6]$ benzene) of complex $[\text{Tp}^{\text{tBu,Me}}\text{LuMe}(\text{NTf}_2)]$ (**3-Lu**) at 26 °C.

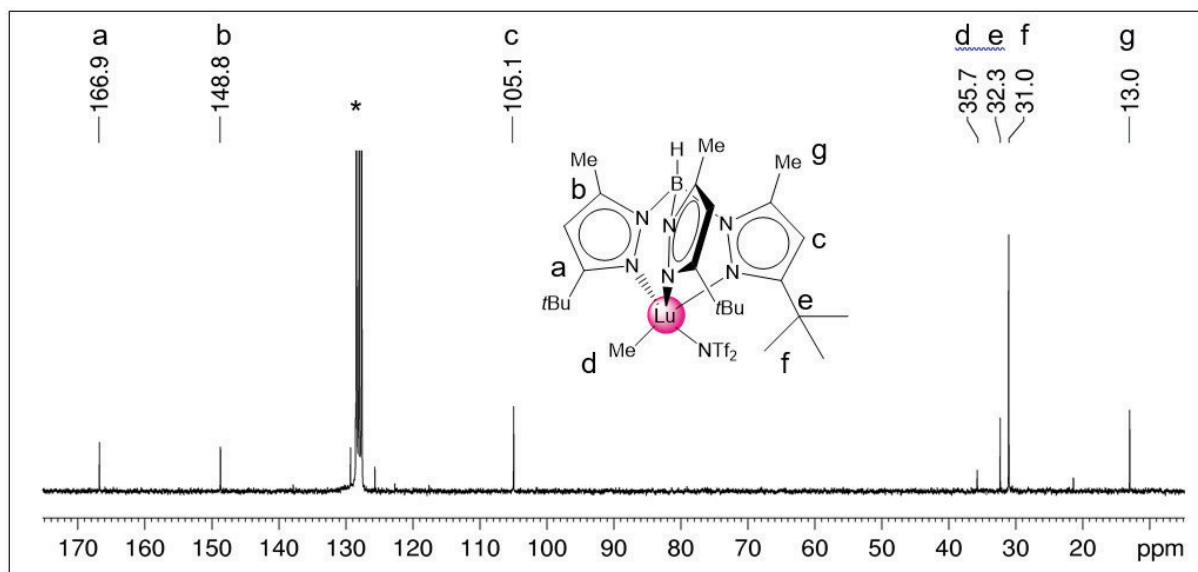


Figure S15. $^{13}\text{C}\{^1\text{H}\}$ NMR spectrum (63 MHz, $[\text{D}_6]$ benzene) of complex $[\text{Tp}^{\text{tBu,Me}}\text{LuMe}(\text{NTf}_2)]$ (**3-Lu**) at 26 °C. ^{13}C NMR resonances for the triflate groups could not be detected.

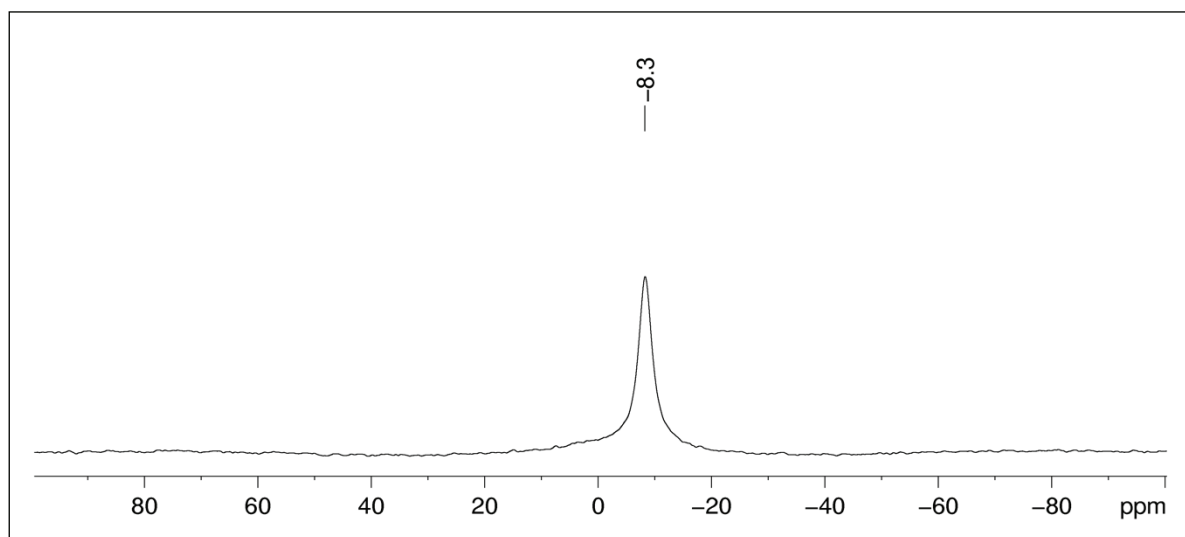


Figure S16. $^{11}\text{B}\{^1\text{H}\}$ NMR spectrum (80 MHz, $[\text{D}_6]$ benzene) of complex $[\text{Tp}^{\text{tBu,Me}}\text{LuMe}(\text{NTf}_2)]$ (**3-Lu**) at 26 °C.

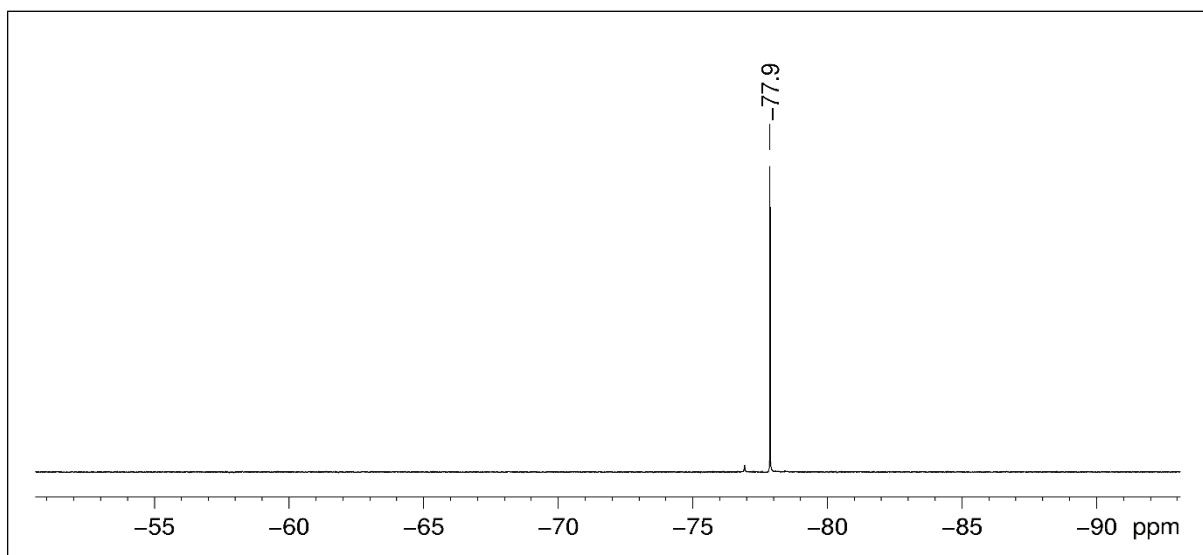


Figure S17. $^{19}\text{F}\{^1\text{H}\}$ NMR spectrum (376 MHz, $[\text{D}_6]$ benzene) of complex $[\text{Tp}^{\text{tBu,Me}}\text{LuMe}(\text{NTf}_2)]$ (**3-Lu**) at 26 °C.

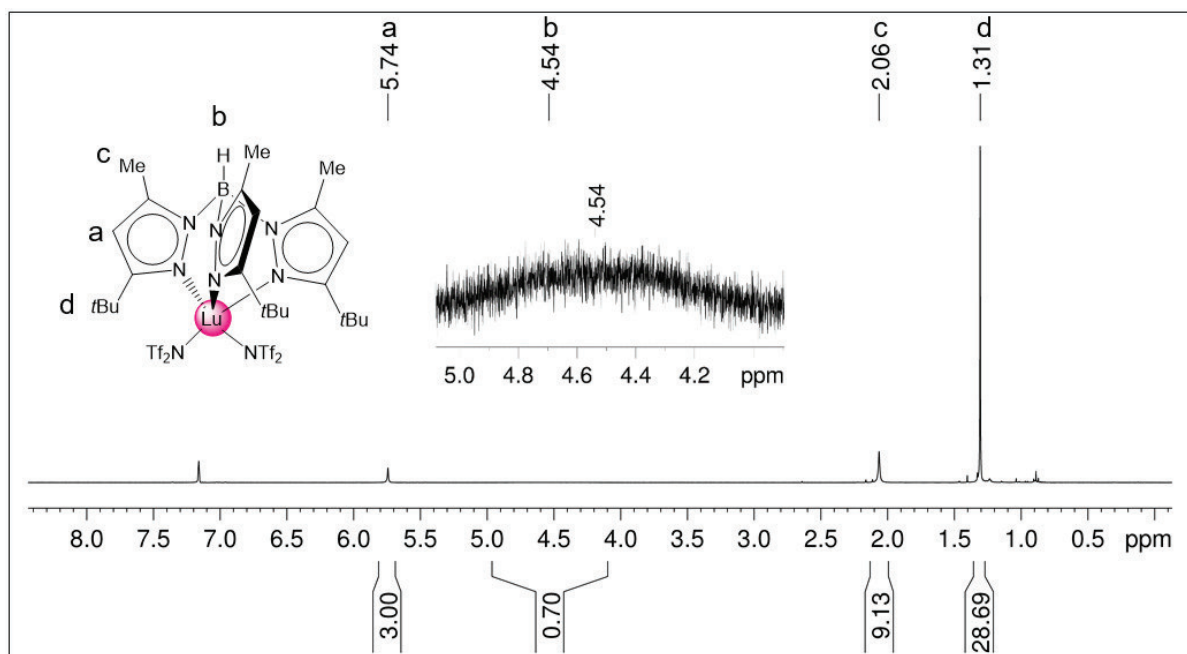


Figure S18. ^1H NMR spectrum (250 MHz, $[\text{D}_6]$ benzene) of complex $[\text{Tp}^{\text{tBu,Me}}\text{Lu}(\text{NTf}_2)_2]$ (**4-Lu**) at 26 °C.

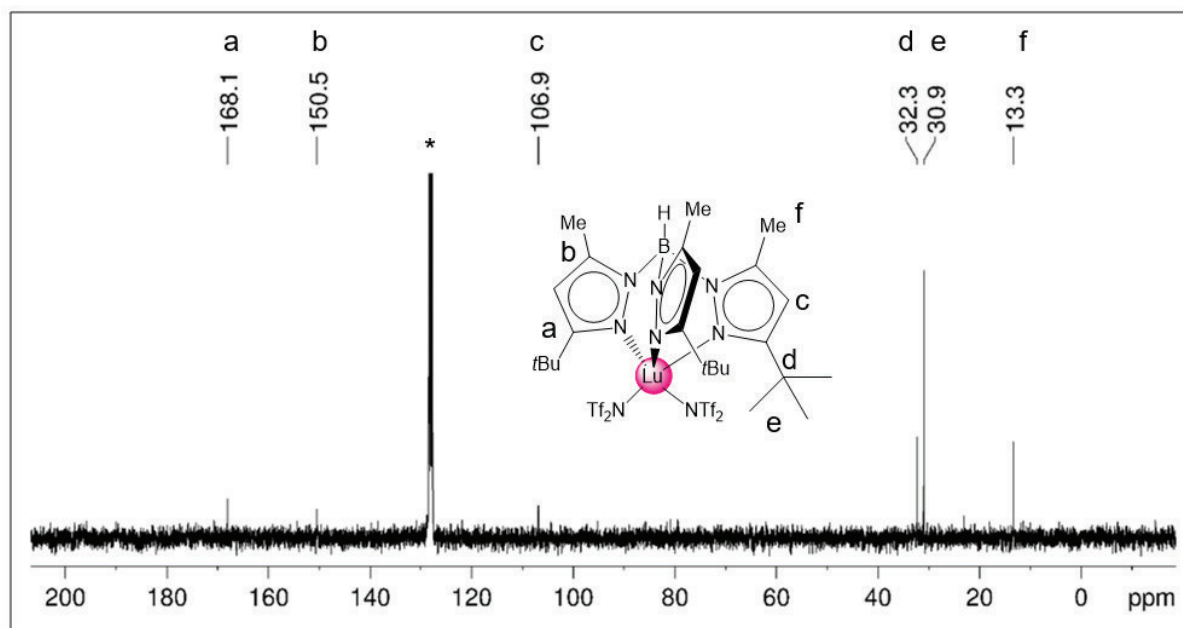


Figure S19. $^{13}\text{C}\{^1\text{H}\}$ NMR spectrum (63 MHz, $[\text{D}_6]\text{benzene}$) of complex $[\text{Tp}^{\text{tBu,Me}}\text{Lu}(\text{NTf}_2)_2]$ (**4-Lu**) at $26\text{ }^\circ\text{C}$. ^{13}C NMR resonances for the triflate groups could not be detected.

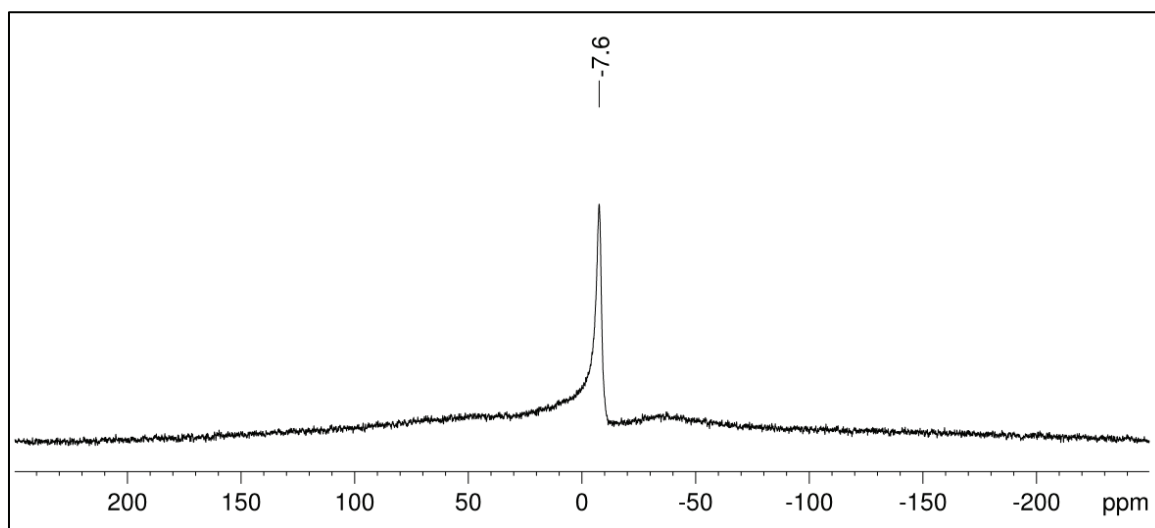


Figure S20. $^{11}\text{B}\{^1\text{H}\}$ NMR spectrum (80 MHz, $[\text{D}_6]\text{benzene}$) of complex $[\text{Tp}^{\text{tBu,Me}}\text{Lu}(\text{NTf}_2)_2]$ (**4-Lu**) at $26\text{ }^\circ\text{C}$.

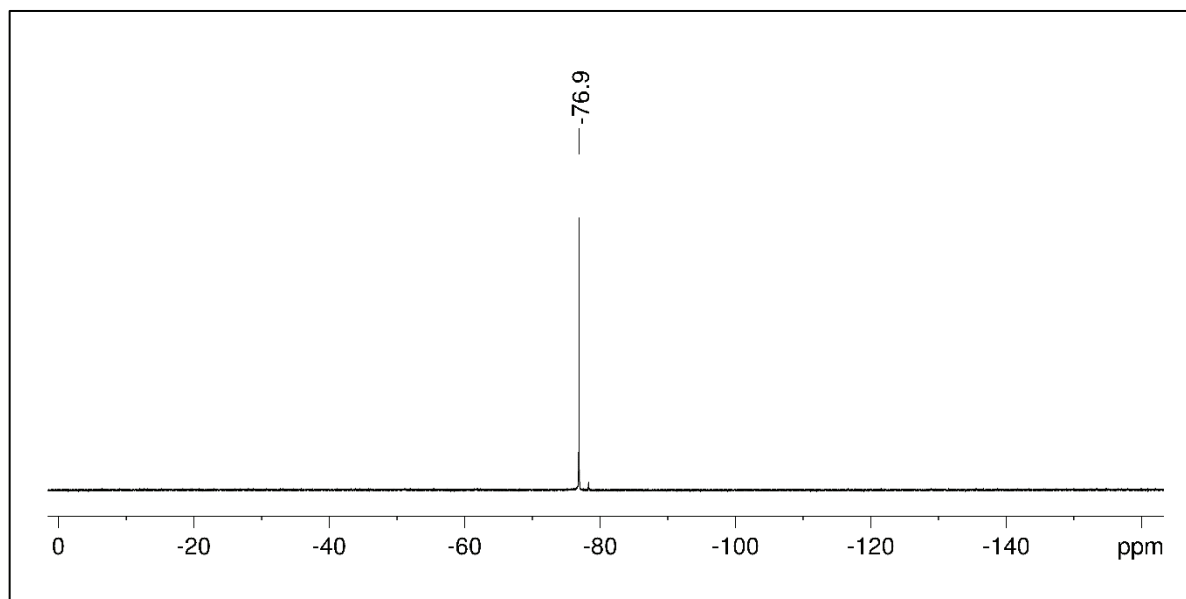


Figure S21. $^{19}\text{F}\{^1\text{H}\}$ NMR spectrum (376 MHz, $[\text{D}_6]$ benzene) of complex $[\text{Tp}^{\text{tBu,Me}}\text{Lu}(\text{NTf}_2)_2]$ (**4-Lu**) at 26 °C.

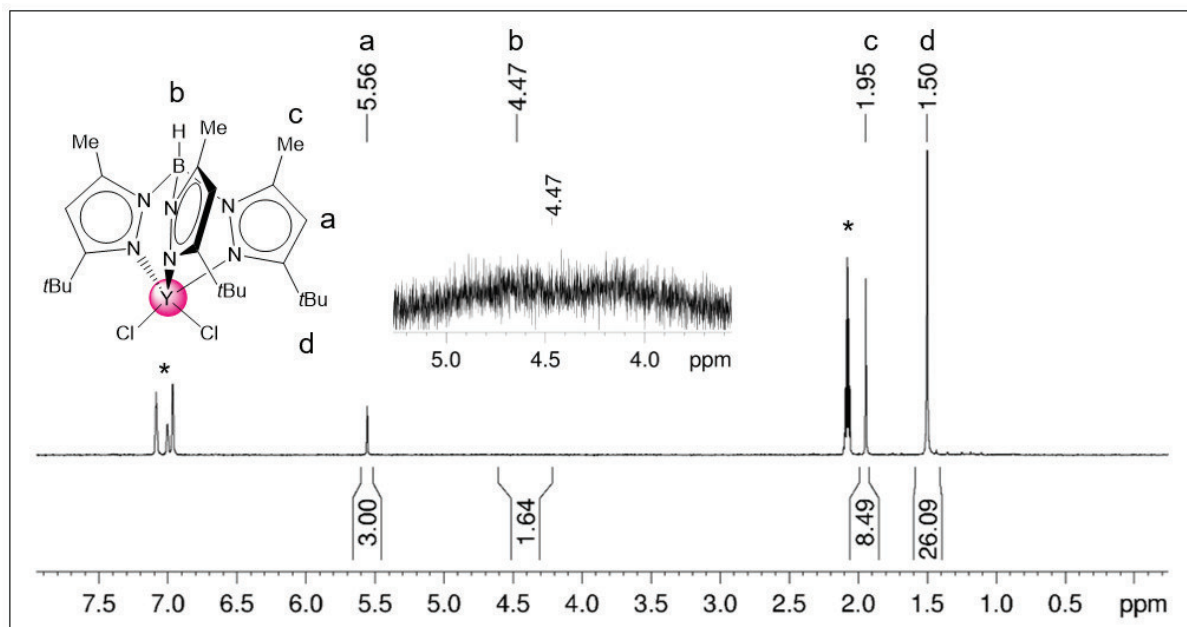


Figure S22. ^1H NMR spectrum (250 MHz, $[\text{D}_8]$ toluene) of complex $[\text{Tp}^{\text{tBu,Me}}\text{YCl}_2]$ (**5-Y**) at 26 °C.

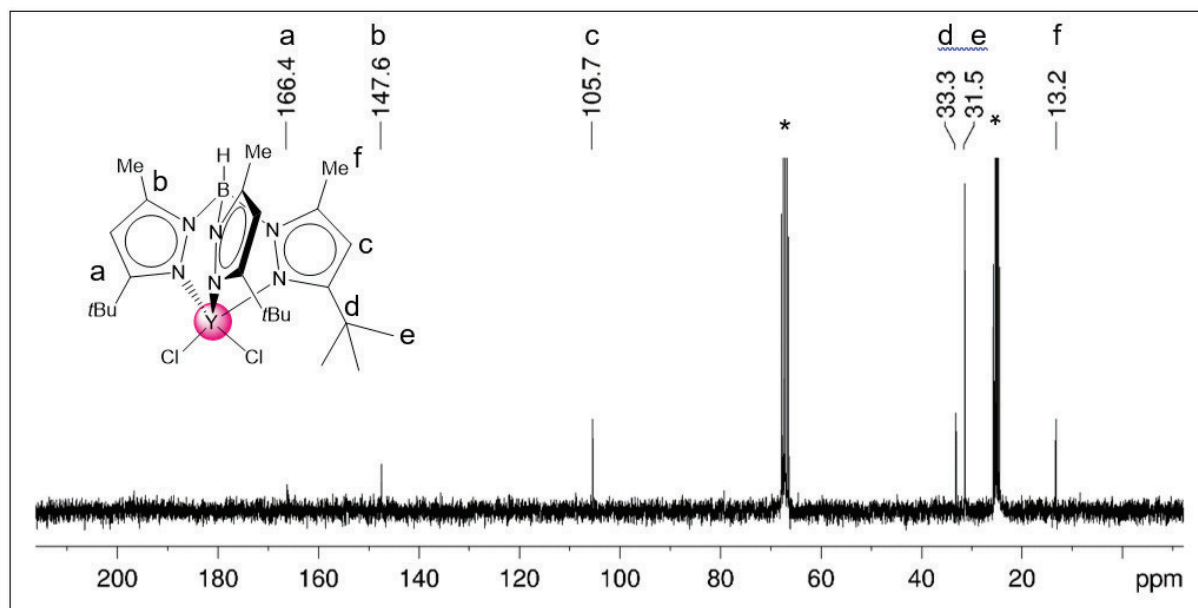


Figure S23. $^{13}\text{C}\{^1\text{H}\}$ NMR spectrum (63 MHz, $[\text{D}_8]\text{thf}$) of complex $[\text{Tp}^{\text{fBu,Me}}\text{YCl}_2]$ (**5-Y**) at 26 °C.

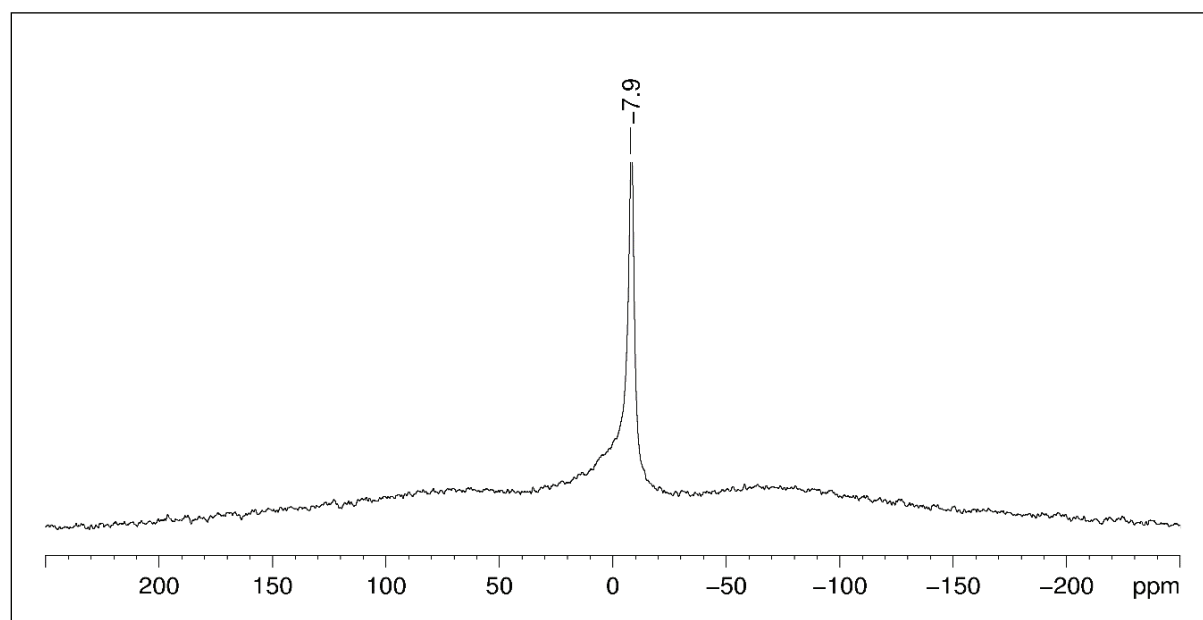


Figure S24. $^{11}\text{B}\{^1\text{H}\}$ NMR spectrum (80 MHz, $[\text{D}_8]\text{thf}$) of complex $[\text{Tp}^{\text{fBu,Me}}\text{YCl}_2]$ (**5-Y**) at 26 °C.

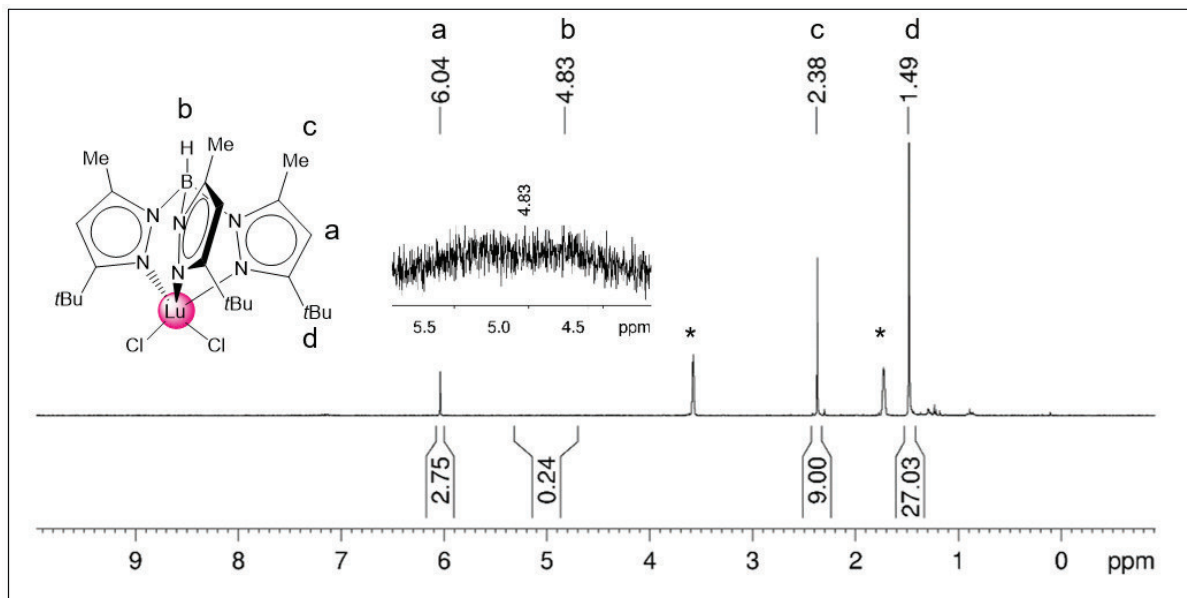


Figure S25. ^1H NMR spectrum (400 MHz, $[\text{D}_8]\text{thf}$) of complex $[\text{Tp}^{\text{tBu,Me}}\text{YLuCl}_2]$ (**5-Lu**) at $26\text{ }^\circ\text{C}$.

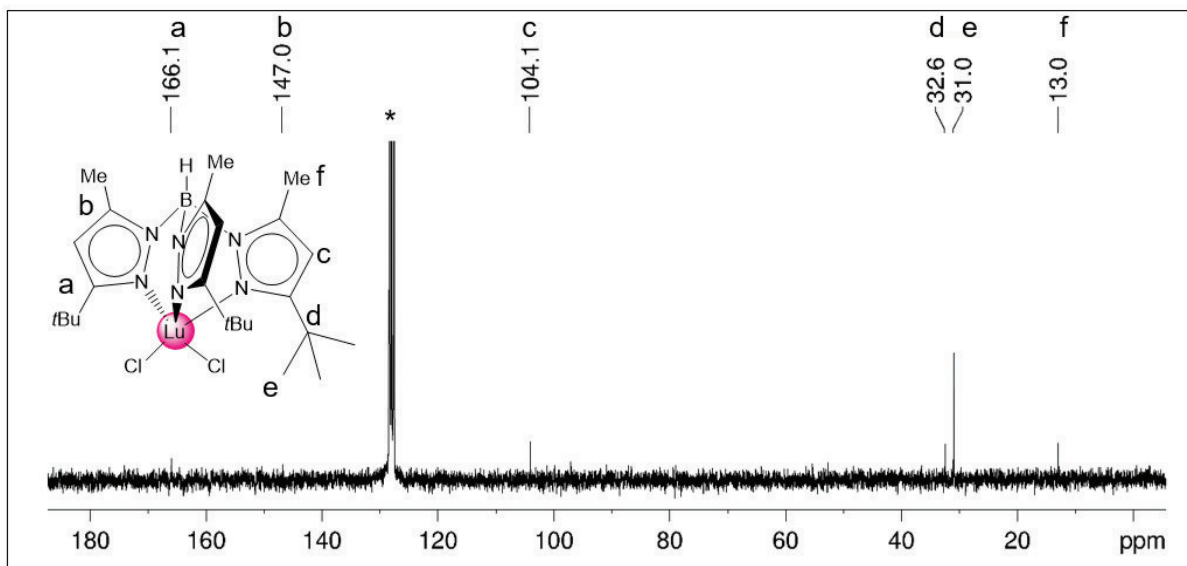


Figure S26. $^{13}\text{C}\{^1\text{H}\}$ NMR spectrum (63 MHz, $[\text{D}_6]\text{benzene}$) of complex $[\text{Tp}^{\text{tBu,Me}}\text{YLuCl}_2]$ (**5-Lu**) at $26\text{ }^\circ\text{C}$.

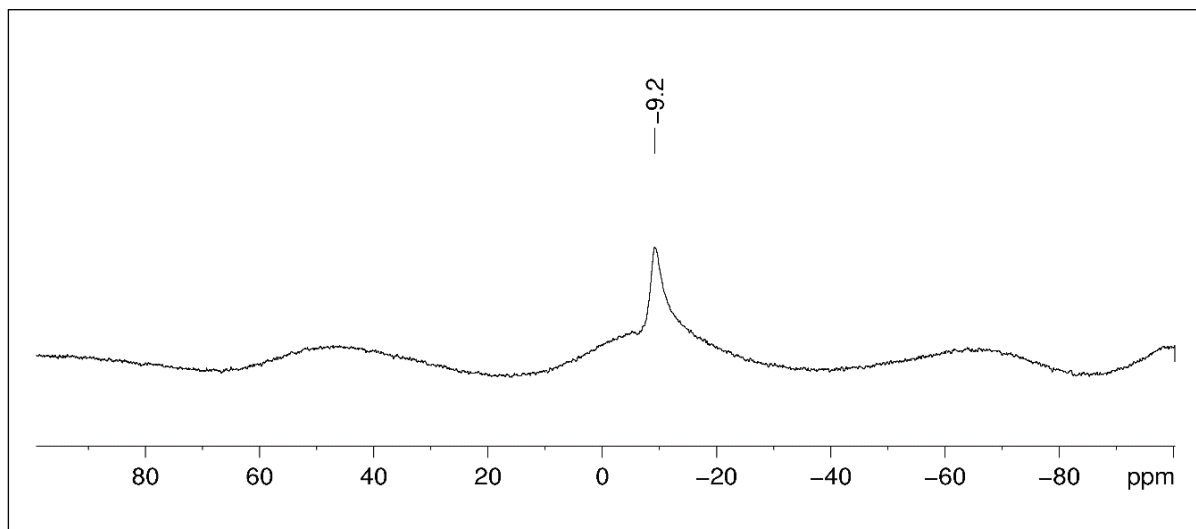


Figure S27. $^{11}\text{B}\{^1\text{H}\}$ NMR spectrum (80 MHz, $[\text{D}_8]\text{thf}$) of complex $[\text{Tp}^{\text{tBu,Me}}\text{YLuCl}_2]$ (**5-Lu**) at 26 °C.

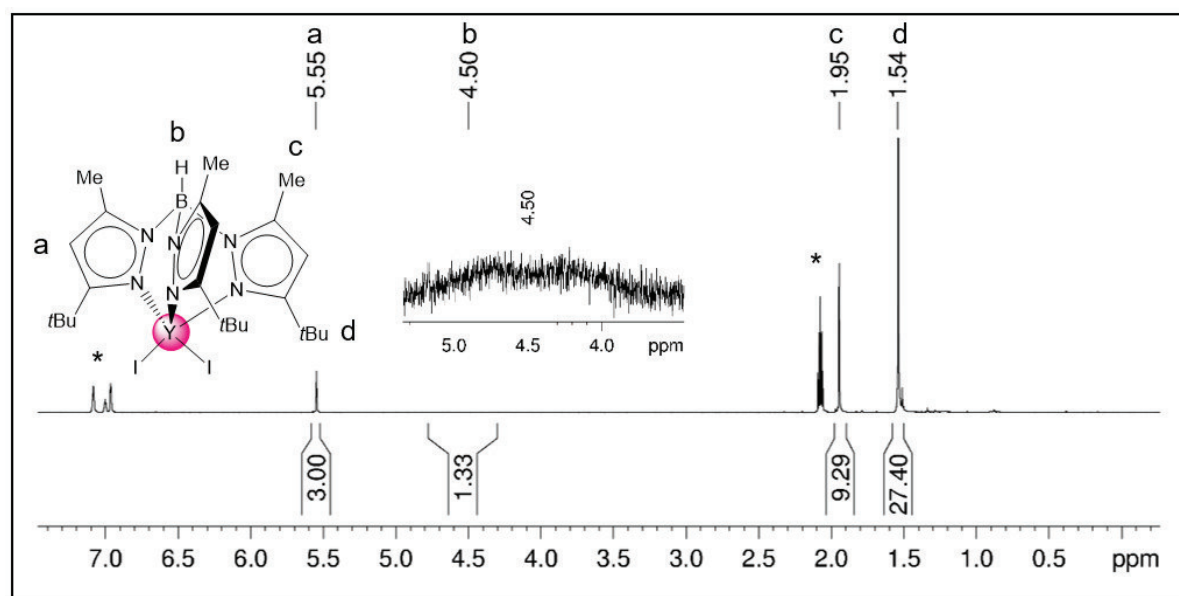


Figure S28. ^1H NMR spectrum (250 MHz, $[\text{D}_8]\text{toluene}$) of complex $[\text{Tp}^{\text{tBu,Me}}\text{YI}_2]$ (**6-Y**) at 26 °C.

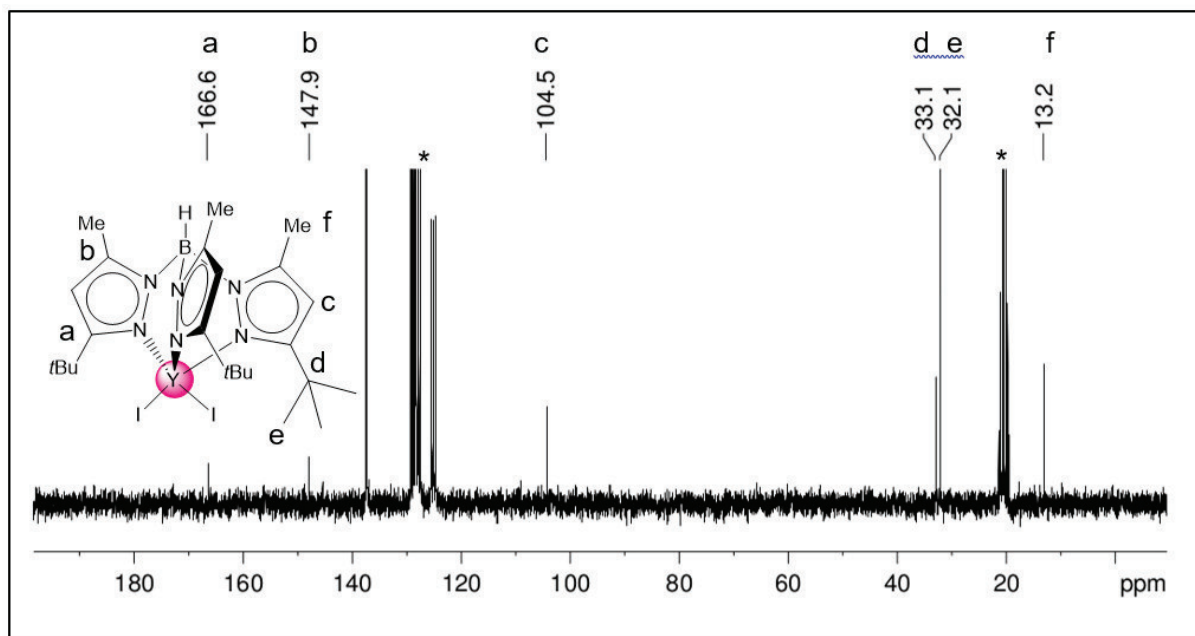


Figure S29. $^{13}\text{C}\{^1\text{H}\}$ NMR spectrum (63 MHz, $[\text{D}_8]\text{toluene}$) of complex $[\text{Tp}^{\text{fBu,Me}}\text{YI}_2]$ (**6-Y**) at $26\text{ }^\circ\text{C}$.

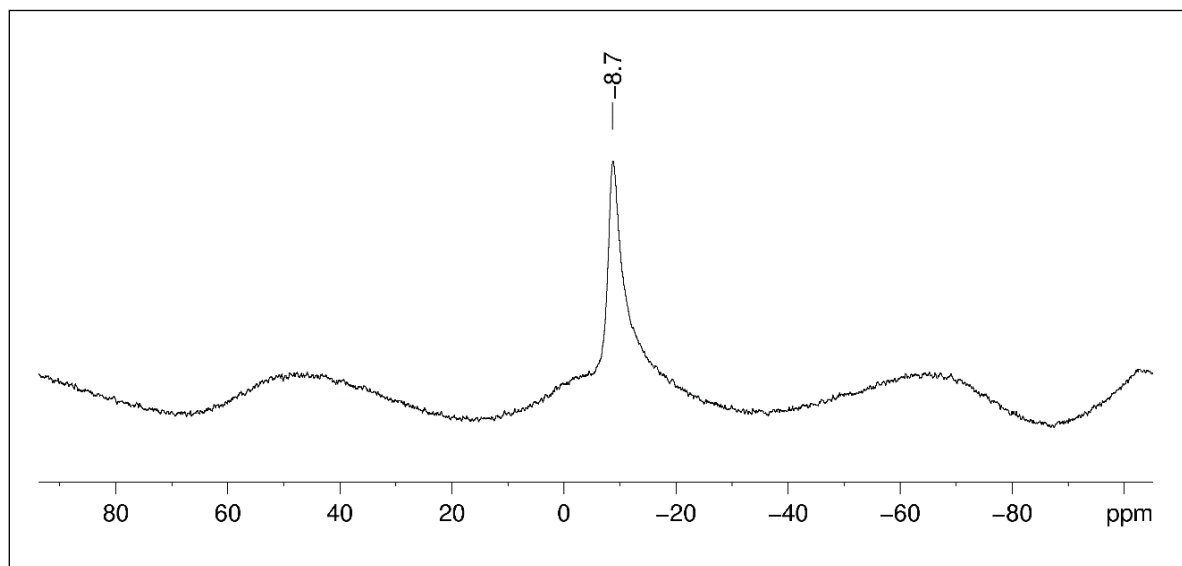


Figure S30. $^{11}\text{B}\{^1\text{H}\}$ NMR spectrum (80 MHz, $[\text{D}_8]\text{toluene}$) of complex $[\text{Tp}^{\text{fBu,Me}}\text{YI}_2]$ (**6-Y**) at $26\text{ }^\circ\text{C}$.

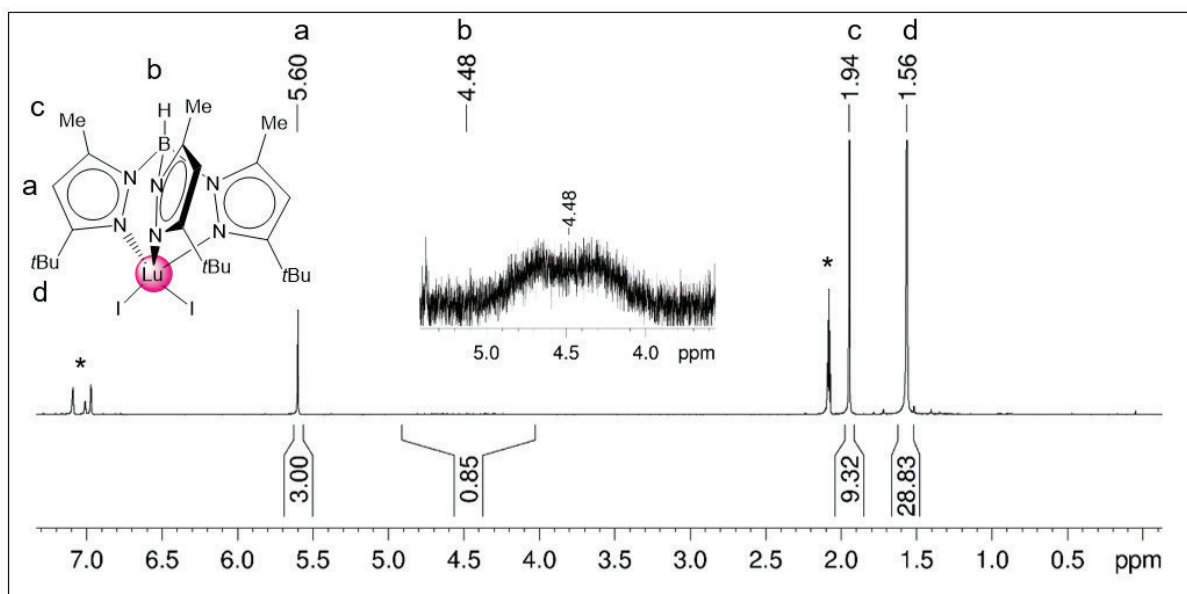


Figure S31. ^1H NMR spectrum (250 MHz, $[\text{D}_8]\text{toluene}$) of complex $[\text{Tp}^{\text{tBu,Me}}\text{Lu}]_2$ (**6-Lu**) at $26\text{ }^\circ\text{C}$.

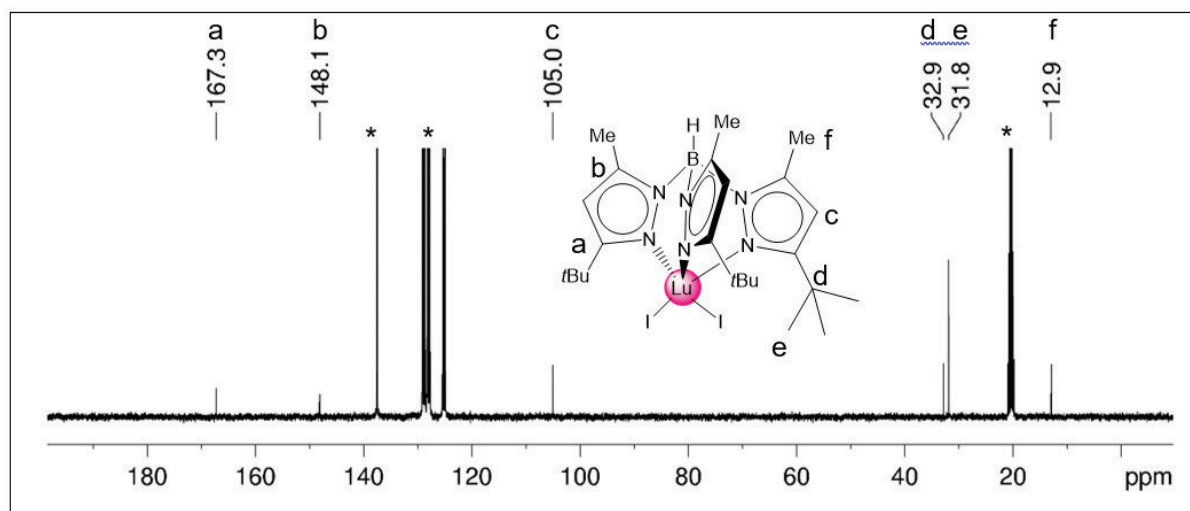


Figure S32. $^{13}\text{C}\{^1\text{H}\}$ NMR spectrum (101 MHz, $[\text{D}_8]\text{toluene}$) of complex $[\text{Tp}^{\text{tBu,Me}}\text{Lu}]_2$ (**6-Lu**) at $26\text{ }^\circ\text{C}$.

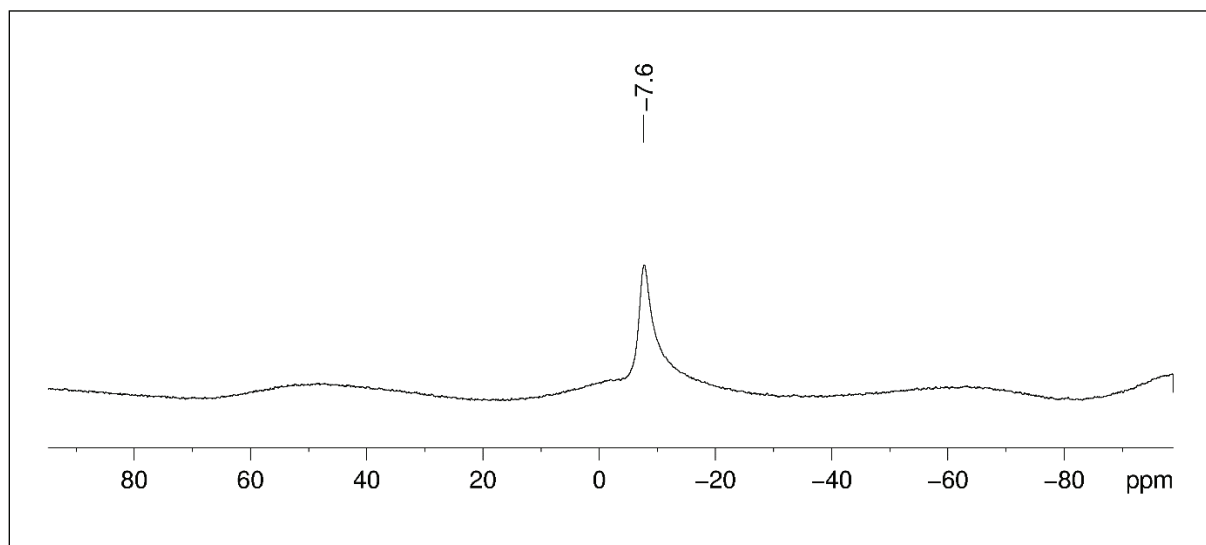


Figure S33. $^{11}\text{B}\{^1\text{H}\}$ NMR spectrum (80 MHz, $[\text{D}_3]$ toluene) of complex $[\text{Tp}^{\text{tBu,Me}}\text{Lu}]_2$ (**6-Lu**) at 26 °C.

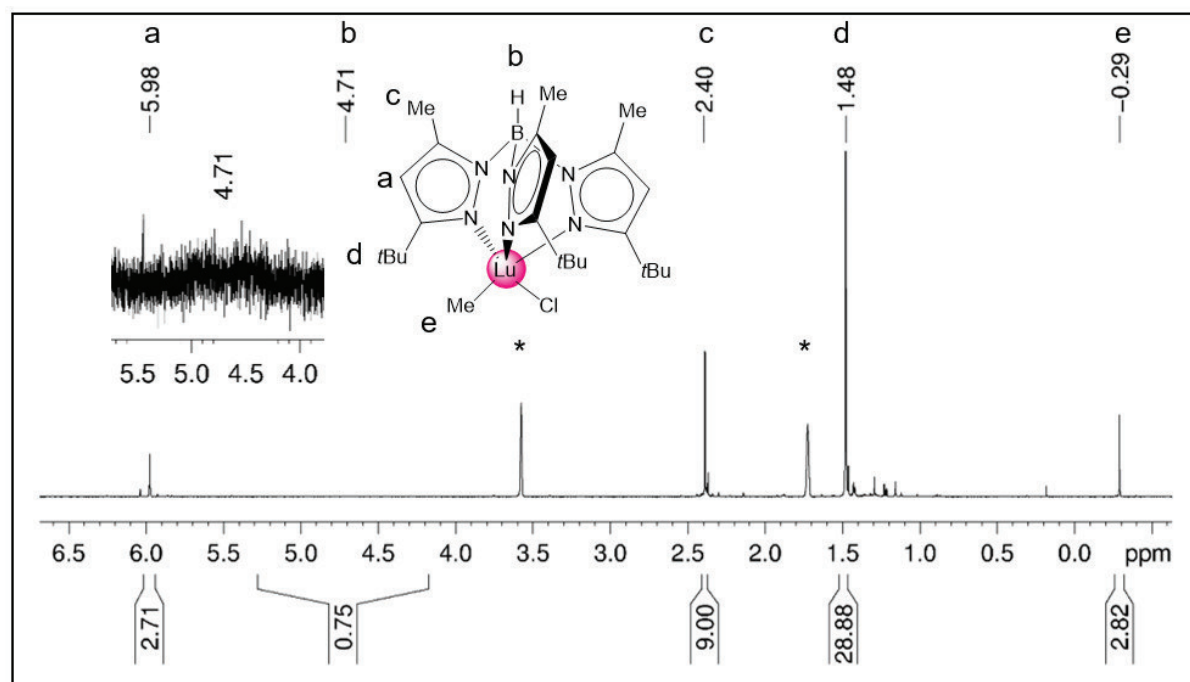


Figure S34. ^1H NMR spectrum (250 MHz, $[\text{D}_3]$ thf) of complex $[\text{Tp}^{\text{tBu,Me}}\text{LuMeCl}]$ (**7-Lu**) at 26 °C.

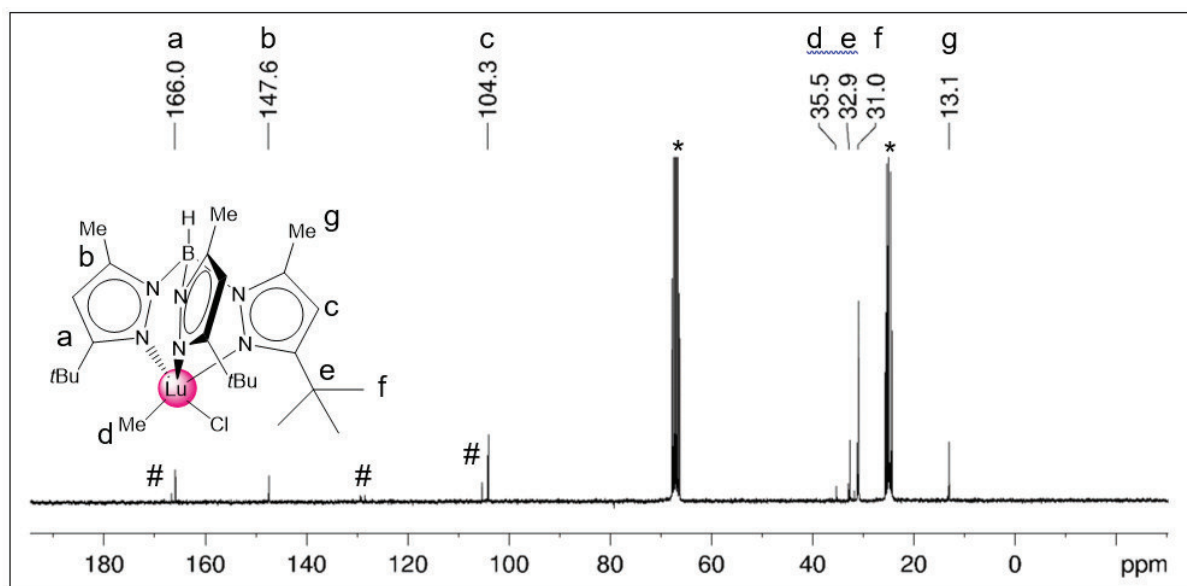


Figure S35. $^{13}\text{C}\{^1\text{H}\}$ NMR spectrum (63 MHz, $[\text{D}_8]\text{thf}$) of complex $[\text{Tp}^{\text{tBu,Me}}\text{LuMeCl}]$ (7-Lu) at 26°C with minor impurities (#) due to decomposition in thf.

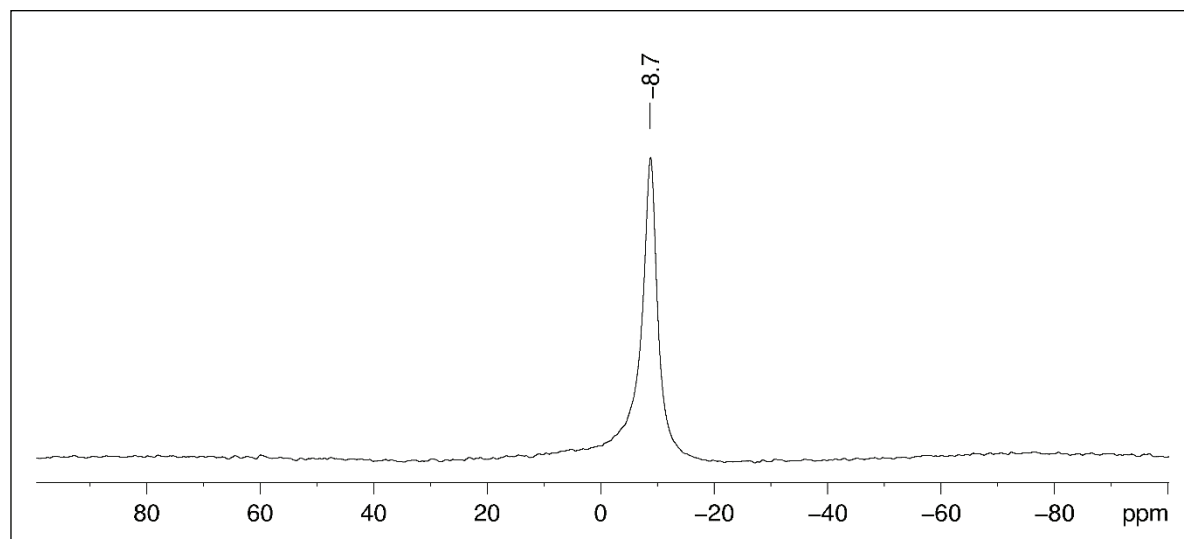


Figure S36. $^{11}\text{B}\{^1\text{H}\}$ NMR spectrum (80 MHz, $[\text{D}_8]\text{thf}$) of complex $[\text{Tp}^{\text{tBu,Me}}\text{LuMeCl}]$ (7-Lu) at 26 °C.

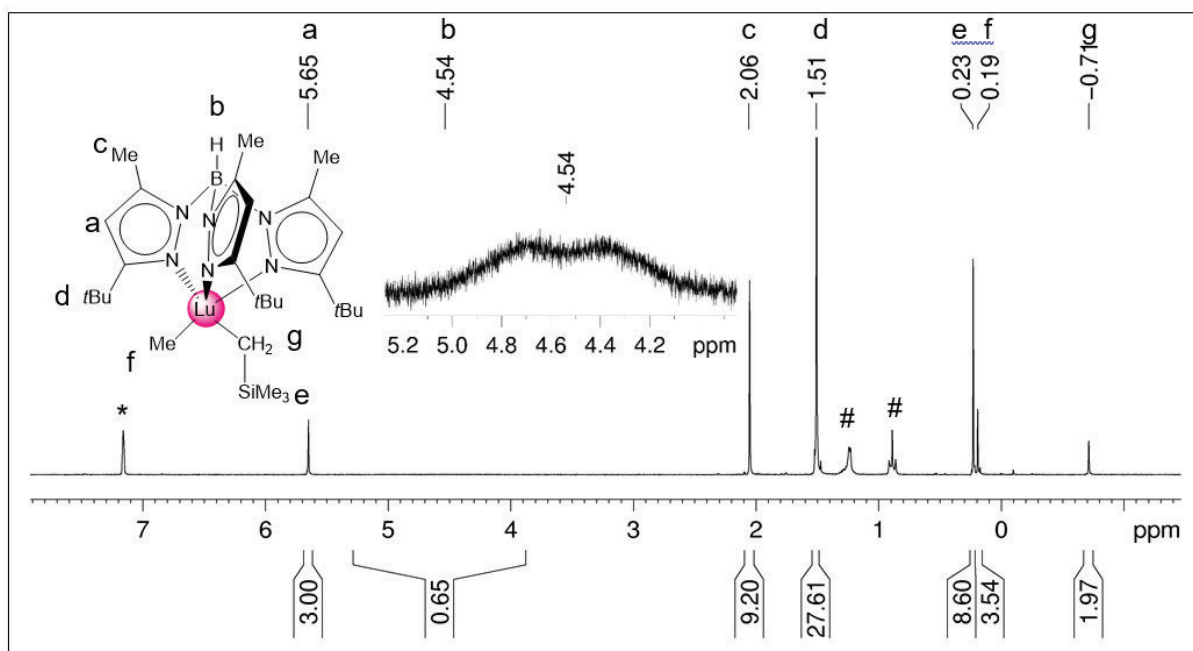


Figure S37. ^1H NMR spectrum (250 MHz, $[\text{D}_6]$ benzene) of complex $[\text{Tp}^{\text{tBu,Me}}\text{LuMe}(\text{CH}_2\text{SiMe}_3)]$ (**8-Lu**) at 26 °C with traces of *n*-hexane (#).

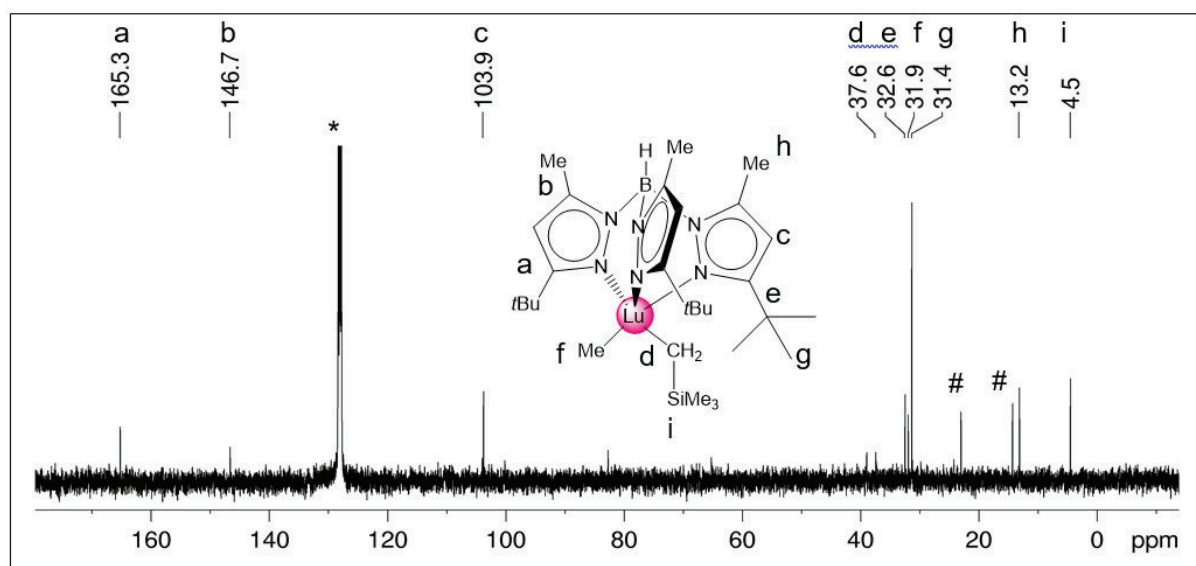


Figure S38. $^{13}\text{C}\{^1\text{H}\}$ NMR spectrum (63 MHz, $[\text{D}_6]$ benzene) of complex $[\text{Tp}^{\text{tBu,Me}}\text{LuMe}(\text{CH}_2\text{SiMe}_3)]$ (**8-Lu**) at 26 °C with traces of *n*-hexane (#).

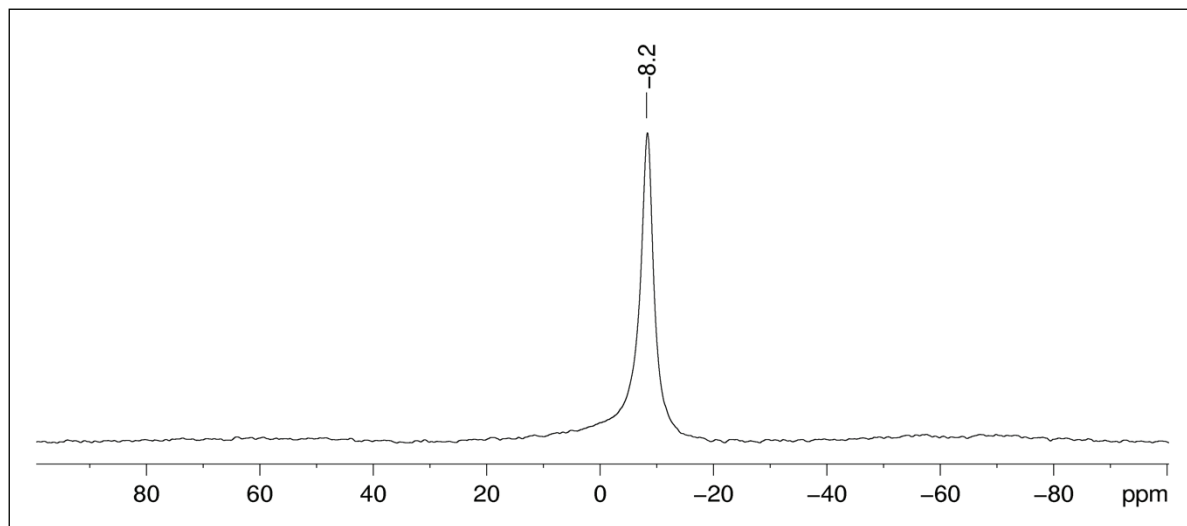


Figure S39. $^{11}\text{B}\{^1\text{H}\}$ NMR spectrum (80 MHz, $[\text{D}_6]$ benzene) of complex $[\text{Tp}^{\text{tBu,Me}}\text{LuMe}(\text{CH}_2\text{SiMe}_3)]$ (**8-Lu**) at 26 °C.

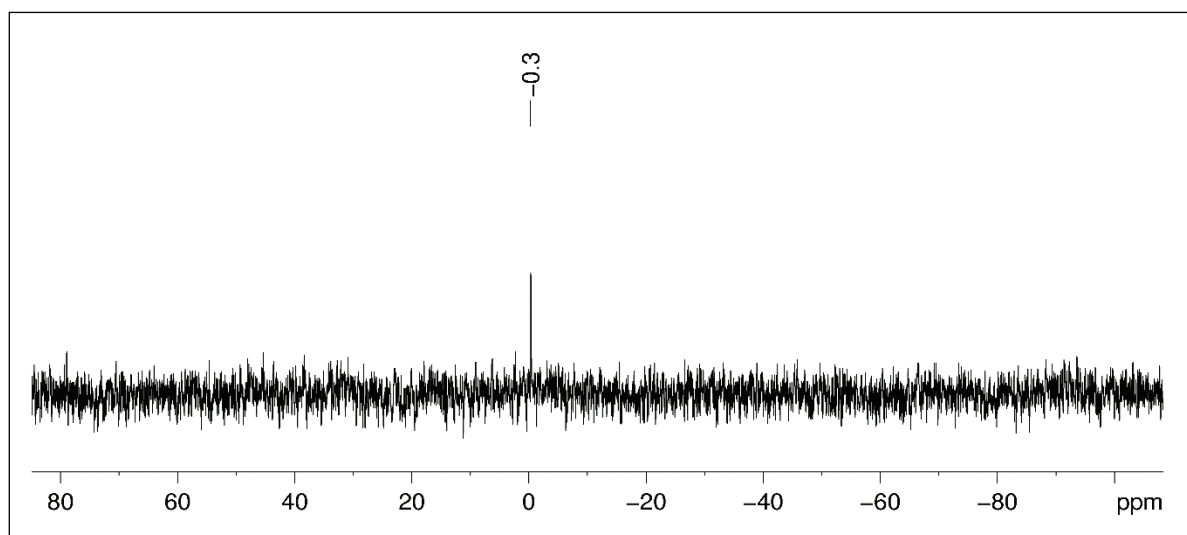


Figure S40. $^{29}\text{Si}\{^1\text{H}\}$ -DEPT45 NMR spectrum (50 MHz, $[\text{D}_6]$ benzene) of complex $[\text{Tp}^{\text{tBu,Me}}\text{LuMe}(\text{CH}_2\text{SiMe}_3)]$ (**8-Lu**) at 26 °C.

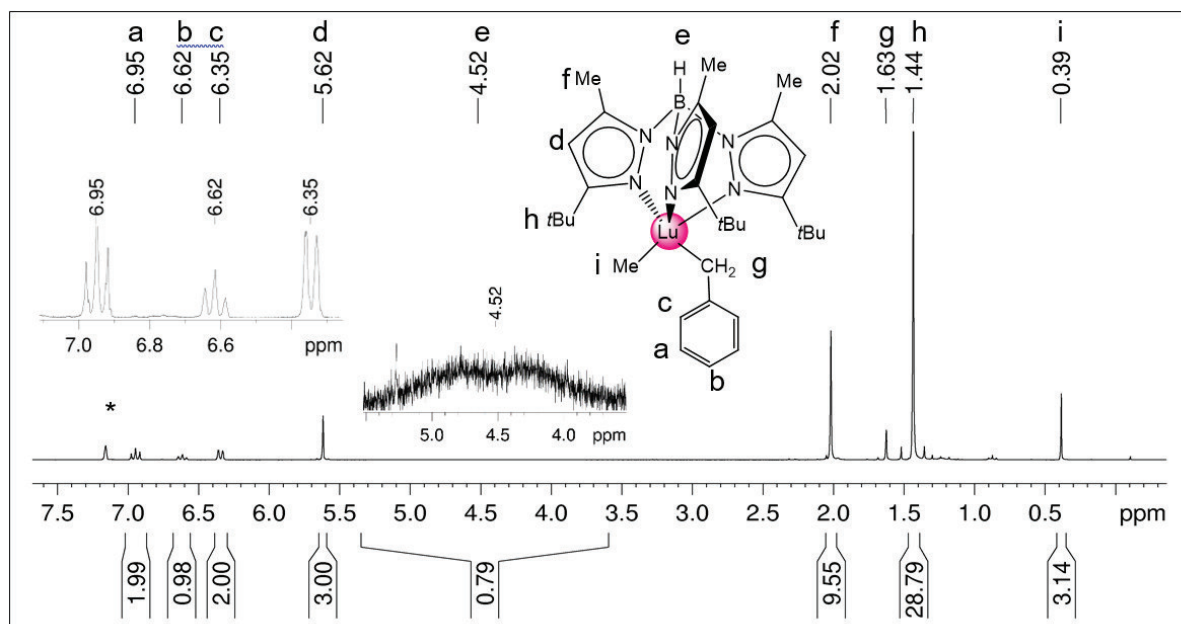


Figure S41. ^1H NMR spectrum (250 MHz, $[\text{D}_6]$ benzene) of complex $[\text{Tp}^{\text{tBu,Me}}\text{LuMe}(\text{CH}_2\text{Ph})]$ (**9-Lu**) at 26 °C.

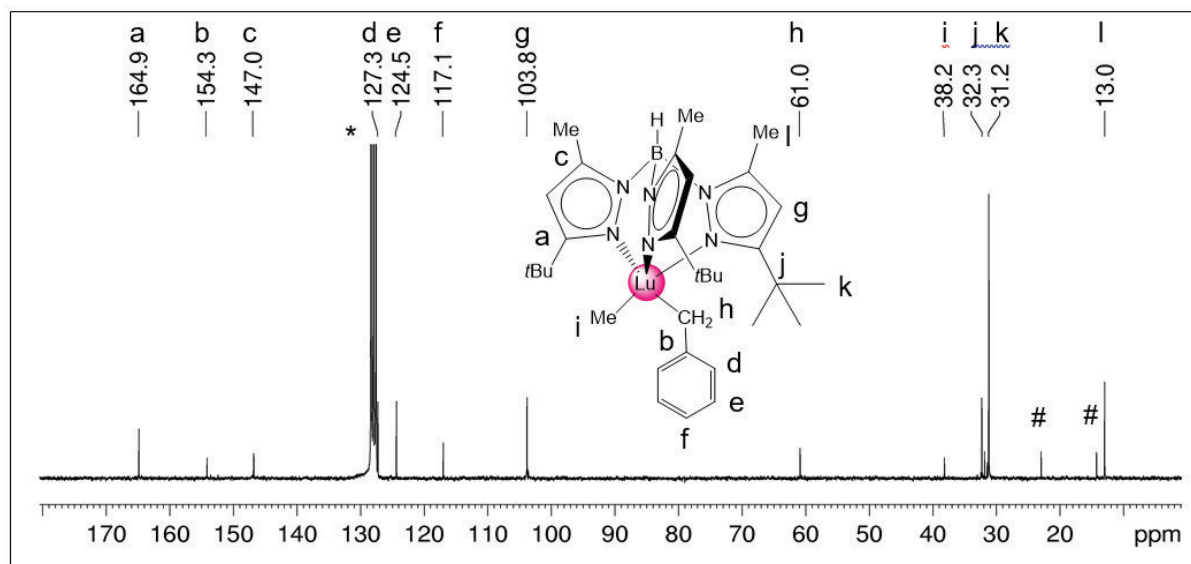


Figure S42. $^{13}\text{C}\{^1\text{H}\}$ NMR spectrum (63 MHz, $[\text{D}_6]$ benzene) of complex $[\text{Tp}^{\text{tBu,Me}}\text{LuMe}(\text{CH}_2\text{Ph})]$ (**9-Lu**) at 26 °C with traces of hexane (#).

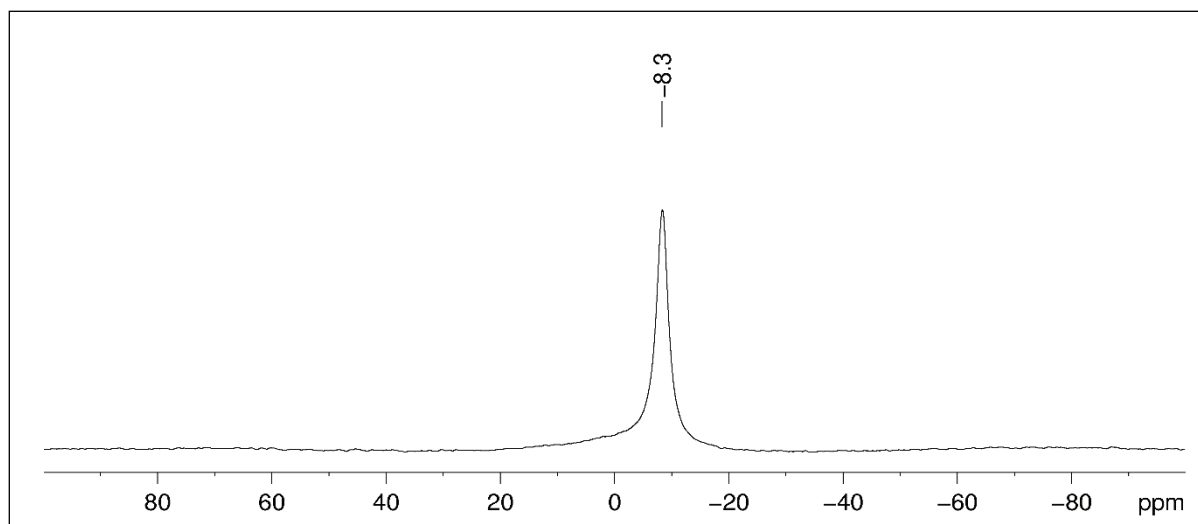


Figure S43. $^{11}\text{B}\{^1\text{H}\}$ NMR spectrum (80 MHz, $[\text{D}_6]$ benzene) of complex $[\text{Tp}^{\text{tBu.Me}}\text{LuMe}(\text{CH}_2\text{Ph})]$ (**9-Lu**) at 26 °C.

X-ray structure analyses

Table S1. Comprehensive crystallographic data for compounds **1-Lu**, **2-Lu**, **4-Lu**, and **5-Lu**

	1-Lu	3-Lu	4-Lu	5-Lu
CCDC	1945695	1945701	1945700	1945696
Formula	C ₂₆ H ₄₃ BF ₃ LuN ₆ O ₃ S	C ₃₄ H ₅₁ BF ₆ LuN ₇ O ₄ S ₂	C ₃₅ H ₄₈ BF ₁₂ Lu N ₈ O ₈ S ₄	C ₃₂ H ₅₆ BCl ₂ LuN ₆ O ₂
M [g mol ⁻¹]	762.50	985.71	1250.83	813.50
Crystal system	Monoclinic	Triclinic	Triclinic	Orthorhombic
Space group	P2 ₁ /n	P $\bar{1}$	P $\bar{1}$	Cmc2 ₁
a [Å]	12.2754(16)	9.8940(3)	12.9270(6)	20.9267(15)
b [Å]	17.658(2)	14.1054(5)	13.7542(6)	9.7844(7)
c [Å]	15.2272(17)	16.1627(6)	14.2033(7)	17.7155(13)
α [°]	90	86.5330(10)	87.4410(10)	90
β [°]	93.699(2)	79.7220(10)	81.360(2)	90
γ [°]	90	76.3470(10)	82.7930(10)	90
V [Å ³]	3293.8(7)	2156.34(13)	2476.1(2)	3627.3(5)
Z	4	2	2	4
T [K]	100(2)	100(2)	100(2)	99(2)
ρ _{calcd} [g cm ⁻³]	1.538	1.518	1.678	1.490
μ [mm ⁻¹]	3.113	2.455	2.262	2.906
F (000)	1536	996	1252	1664
Θ range [°]	1.768 to 27.485	1.281 to 30.189	1.493 to 30.068	1.946 to 30.053
total reflns	48598	65970	106930	39179
unique reflns	7539	12746	14494	5445
R _{int}	0.0784	0.0283	0.0615	0.0544
observed reflns (I > 2σ)	5801	11805	13160	5187
Data/restraints/parameter	7539 / 487 / 494	12746 / 189 / 554	14494 / 397 / 799	5445 / 61 / 235
R1/wR2 (I > 2σ) ^[a]	0.0352 / 0.0718	0.0215 / 0.0505	0.0254 / 0.0594	0.0210 / 0.0469
R1/wR2 (all data) ^[a]	0.0569 / 0.0793	0.0244 / 0.0518	0.0299 / 0.0618	0.0228 / 0.0478
GOF ^[a]	1.046	1.060	1.053	1.038
largest diff. peak and hole [e Å ⁻³]	1.253 and -0.828	2.426 and -0.618	2.101 and -0.638	2.419 and -0.828

[a] $R1 = \sum(|F0| - |Fc|) / \sum|F0|, F0 > 4s(F0)$. $wR2 = \{\sum[w(F02 - Fc2)^2] / \sum[w(F02)^2]\}^{1/2}$.

Table S1 continued. Comprehensive crystallographic data for compounds **6-Lu**, **7-Lu**, **8-Lu**, and **9-Lu**.

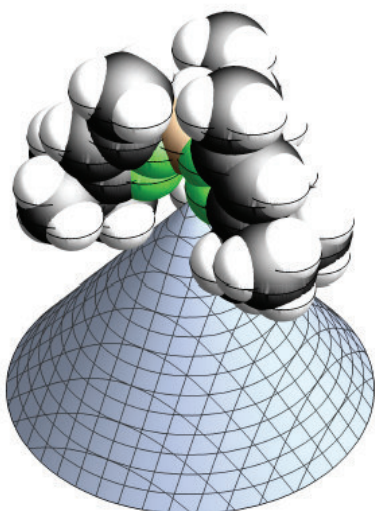
	6-Lu	7-Lu	8-Lu	9-Lu
CCDC	1945699	1945697	1945698	1945702
Formula	C ₂₄ H ₄₀ BI ₂ LuN ₆	C ₂₅ H ₄₂ BCILuN ₆	C ₂₉ H ₅₄ BLuN ₆ Si	C ₃₂ H ₅₀ BLuN ₆ •1/2(C ₇ H ₈)
M [g mol ⁻¹]	852.20	647.87	700.65	750.62
Crystal system	Monoclinic	Orthorhombic	Triclinic	Monoclinic
Space group	P2 ₁ /n	Pnma	P $\bar{1}$	P2 ₁ /n
a [Å]	12.4642(6)	17.9200(18)	11.9871(4)	9.7194(7)
b [Å]	13.2018(7)	16.9031(16)	12.1377(4)	20.3381(15)
c [Å]	19.0586(10)	9.7340(9)	15.4042(5)	18.5754(14)
α [°]	90	90	99.9460(10)	90
β [°]	97.771(2)	90	108.1190(10)	98.5760(10)
γ [°]	90	90	96.9700(10)	90
V [Å ³]	3107.3(3)	2948.5(5)	2061.08(12)	3630.8(5)
Z	4	4	2	4
T [K]	101(2)	173(2)	150(2)	100(2)
ρ _{calcd} [g cm ⁻³]	1.822	1.459	1.129	1.373
μ [mm ⁻¹]	5.143	3.462	2.445	2.750
F (000)	1632	1308	720	1540
Θ range [°]	2.089 to 27.485	2.414 to 28.336	1.427 to 28.700	1.494 to 28.281
total reflns	78632	13206	89956	57404
unique reflns	7119	3749	10644	8999
Rint	0.0567		0.0483	0.0563
observed reflns (I>2σ)	5912	2814	9478	7343
Data/restraints/parameter	7119 / 0 / 323	3749 / 336 / 187	10644 / 0 / 366	8999 / 159 / 483
R1/wR2 (I>2σ) ^[a]	0.0309 / 0.0747	0.0913 / 0.1642	0.0219 / 0.0484	0.0280 / 0.0605
R1/wR2 (all data) ^[a]	0.0407 / 0.0796	0.1254 / 0.1763	0.0274 / 0.0507	0.0381 / 0.0647
GOF ^[a]	1.038	1.278	1.059	1.039
largest diff. peak and hole [e Å ⁻³]	2.973 and -2.205	3.318 and -4.846	2.091 and -0.722	2.504 and -0.750

[a] R1 = $\Sigma(|F_0| - |F_c|) / \Sigma|F_0|$, F0 > 4s(F0). wR2 = $\{\Sigma[w(F_0^2 - F_c^2)^2] / \Sigma[w(F_0^2)^2]\}^{1/2}$.

Cone-angle calculations

To calculate the mathematically exact cone angles a series of .xyz files was generated from the final .cif files with ORTEP. The Mathematica package was downloaded free of charge from <http://www.ccqc.uga.edu/references/software.php>.

The adopted van der Waals radii were $r = 1.20, 1.70, 1.55, 1.52, 1.92, 2.27 \text{ \AA}$ for H, C, N, O, B, Lu in this order.



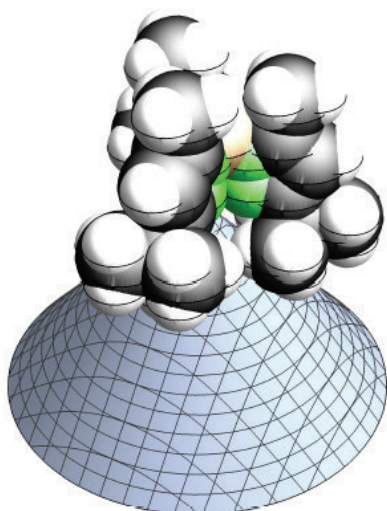
$\text{Tp}^{\text{fBu,Me}}\text{LuMeOTf}_a$ (**1-Lu**)

due to disorder in one *tert*-butyl group two different cone angles were calculated for **1-Lu**

Ligand atoms forming cone = {22, 43, 49}

Cone angle (deg) = 278.007

Cone axis = {-0.316083, 0.800716, -0.508867}

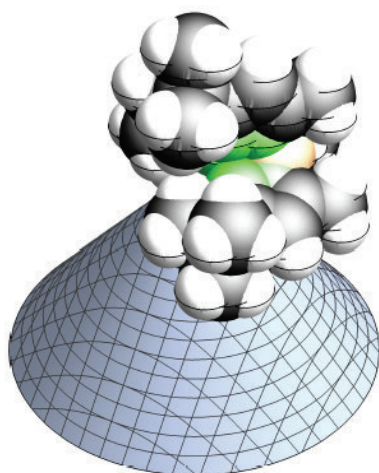


$\text{Tp}^{\text{fBu,Me}}\text{LuMeOTf}_b$ (**1-Lu**)

Ligand atoms forming cone = {11, 34, 51}

Cone angle (deg) = 280.98

Cone axis = {0.162371, 0.909077, 0.383687}

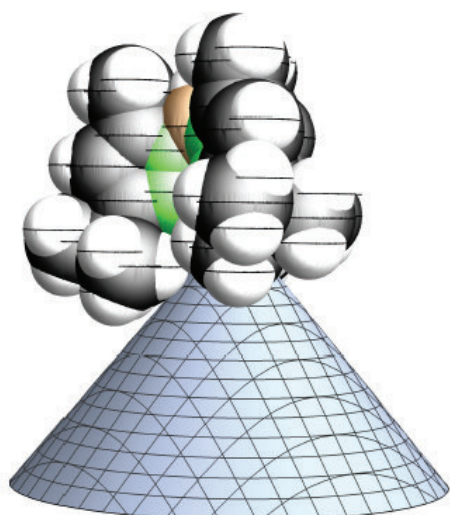


$\text{Tp}^{\text{tBu,Me}}\text{LuMeNTf}_2$ (**2-Lu**)

Ligand atoms forming cone = {37, 42, 53}

Cone angle (deg) = 280.4

Cone axis = {-0.755706, 0.611601, 0.234206}

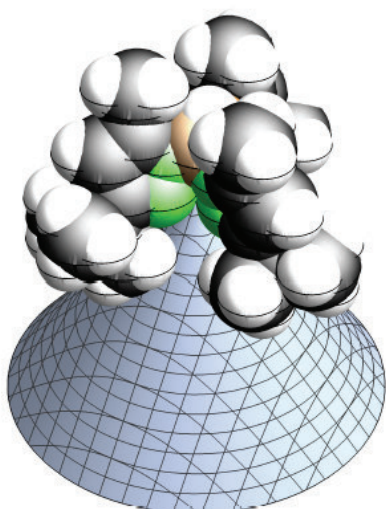


$\text{Tp}^{\text{tBu,Me}}\text{LuI}_2$ (**6-Lu**)

Ligand atoms forming cone = {34, 39, 46}

Cone angle (deg) = 278.17

Cone axis = {-0.143777, 0.94259, 0.301416}

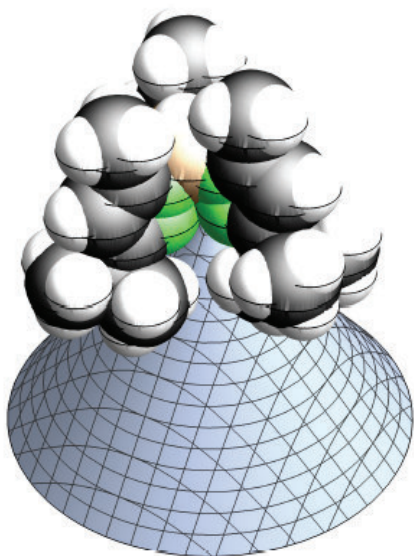


$\text{Tp}^{\text{tBu,Me}}\text{LuMeCl}$ (**7-Lu**)

Ligand atoms forming cone = {35, 45, 56}

Cone angle (deg) = 278.932

Cone axis = {-0.3202, 0.943738, -0.0826429}

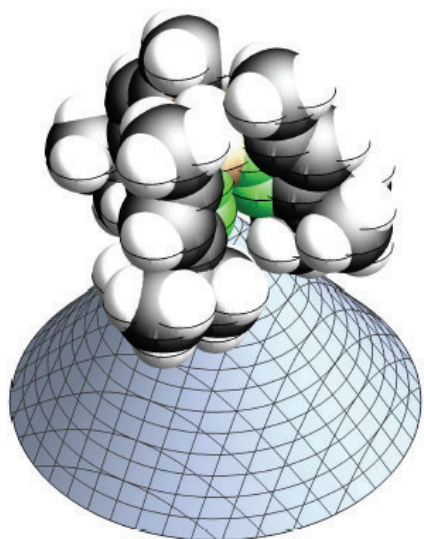


$\text{Tp}^{\text{tBu,Me}}\text{LuMeNeo}$ (**8-Lu**)

Ligand atoms forming cone = {7, 31, 43}

Cone angle (deg) = 277.109

Cone axis = {-0.311522, 0.745404, 0.589344}



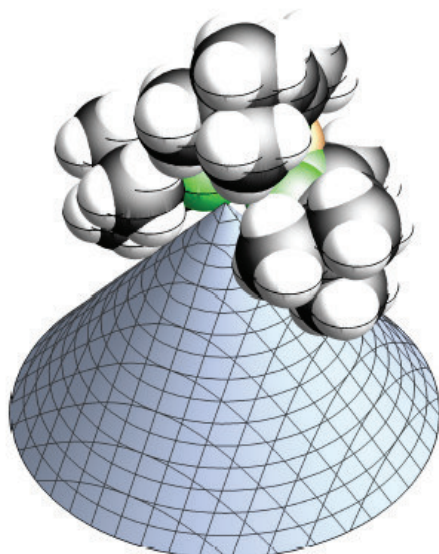
$\text{Tp}^{\text{tBu,Me}}\text{LuMeBn}_a$ (**9-Lu**)

due to disorder in one *tert*-butyl group two different cone angles were calculated for **9-Lu**

Ligand atoms forming cone = {29, 42, 70}

Cone angle (deg) = 277.267

Cone axis = {-0.797352, -0.315855, 0.514262}



$\text{Tp}^{\text{tBu,Me}}\text{LuMeBn}_b$ (**9-Lu**)

Ligand atoms forming cone = {31, 32, 67}

Cone angle (deg) = 277.268

Cone axis = {0.0836185, -0.209561, 0.974214}

Raw Data Files for Cone Angle Calculations

CompexDataBase1.txt

(X1) TptBu,MeLuCl2

1	Lu	-0.36398	-0.36470	-1.55235
2	C	3.70546	-1.32279	-3.30348
3	C	-1.74055	3.63113	-3.19040
4	C	1.81816	-2.74353	-2.49688
5	C	-2.95856	1.60157	-2.39770
6	C	3.13135	-2.07343	-2.08815
7	C	-2.40598	2.96356	-1.97317
8	C	4.13539	-3.15922	-1.67112
9	C	-3.57174	3.85151	-1.51109
10	C	2.91718	-1.12097	-0.94626
11	C	-1.41189	2.81693	-0.85637
12	C	-1.87025	-3.93654	-0.25941
13	C	-3.74781	-2.22864	-0.22042
14	C	3.88177	-0.59254	-0.08289
15	C	-0.95716	3.80916	0.01759
16	C	-2.68715	-2.96827	0.62181
17	C	3.21236	0.19854	0.82490
18	C	-0.08615	3.19899	0.89339
19	C	-1.77299	-1.97891	1.30518
20	C	-3.42012	-3.79831	1.68434
21	C	3.76943	0.97563	1.97688
22	C	0.66101	3.80318	2.04143
23	C	-1.60105	-1.82139	2.68536
24	C	-0.67632	-0.80858	2.85100
25	C	-0.13788	-0.24560	4.11903
26	H	3.82813	-1.95103	-4.04757
27	H	-2.39429	3.70914	-3.91837
28	H	3.08412	-0.61495	-3.57417
29	H	-0.98367	3.08528	-3.48970
30	H	2.00194	-3.44397	-3.15734
31	H	4.56859	-0.92618	-3.06462
32	H	-3.68801	1.73185	-3.03920
33	H	-1.42165	4.52279	-2.94023
34	H	1.21856	-2.07496	-2.88783
35	H	-2.24556	1.07615	-2.81589
36	H	4.25469	-3.79316	-2.40959
37	H	-4.23071	3.92551	-2.23340
38	H	1.39579	-3.14186	-1.70845
39	H	4.99563	-2.74222	-1.45631
40	H	-3.29733	1.12720	-1.61100
41	H	-3.23282	4.74273	-1.28545
42	H	3.79724	-3.63415	-0.88444
43	H	-1.40456	-3.42891	-0.95628
44	H	-3.30225	-1.70269	-0.91687
45	H	-3.99472	3.45373	-0.72264
46	H	-2.47384	-4.58588	-0.67771
47	H	-4.34676	-2.88220	-0.63882
48	H	4.81893	-0.74937	-0.11635
49	H	-1.20227	4.72776	0.00867
50	H	-1.21502	-4.40926	0.29465
51	H	-4.26741	-1.63267	0.35803
52	H	-3.91096	-4.32972	1.32618
53	H	3.55212	1.92460	1.86683
54	H	1.62348	3.67897	1.90688
55	H	4.74260	0.86630	2.00523

56	H	0.46120	4.76084	2.09413
57	H	-2.86954	-4.32525	2.23150
58	H	-3.98400	-3.31149	2.25464
59	H	1.07007	1.12278	2.34745
60	H	3.37904	0.64589	2.81243
61	H	0.38856	3.36615	2.87452
62	H	-2.03472	-2.31382	3.37218
63	H	0.76983	-0.43069	4.16441
64	H	-0.40655	0.63939	4.18884
65	H	-0.57345	-0.73984	4.79369
66	B	0.71099	0.75168	1.31132
67	N	1.70801	-0.65917	-0.58415
68	N	-0.83018	1.64967	-0.53145
69	N	1.89421	0.15462	0.51540
70	N	-0.01276	1.88928	0.55500
71	N	-0.98462	-1.09699	0.63789
72	N	-0.30817	-0.37587	1.62477
0				

(X2) TptBu,MeLul2

1	Lu	-0.38842	-1.37835	-0.71130
2	C	-0.83145	0.19850	-5.22549
3	C	1.58187	0.81917	-4.90102
4	C	0.33879	0.22982	-4.22287
5	C	0.62988	-1.19010	-3.76123
6	C	-0.21596	2.47254	-3.00342
7	C	-0.00228	1.10591	-3.03670
8	C	-0.37858	2.83381	-1.68175
9	C	-0.57749	4.18166	-1.08014
10	C	3.52965	-2.03029	-0.96355
11	C	3.56238	-1.83145	0.55852
12	C	5.00888	-1.54420	0.95763
13	C	2.69489	-0.63862	0.94463
14	C	3.08385	-3.09717	1.28535
15	C	-4.34751	-2.81399	1.74951
16	C	-2.99455	2.60946	1.63065
17	C	-2.63902	1.15289	1.62108
18	C	-1.93485	-3.46298	1.75123
19	C	3.04090	0.37594	1.82334
20	C	-2.59770	-1.04166	1.86204
21	C	1.97652	1.24680	1.85798
22	C	-3.33443	0.09617	2.14576
23	C	-2.94484	-2.44683	2.28551
24	C	1.81348	2.48673	2.66340
25	C	-2.98423	-2.48086	3.82512
26	H	-0.57565	-0.32899	-6.01080
27	H	1.85434	0.24086	-5.64397
28	H	-1.04869	1.11345	-5.50230
29	H	1.37511	1.71505	-5.24226
30	H	-1.61472	-0.20876	-4.80101
31	H	0.92032	-1.72966	-4.52653
32	H	2.31194	0.87939	-4.25013
33	H	-0.24371	3.05552	-3.75279
34	H	-0.18149	-1.58219	-3.37548
35	H	1.33890	-1.17456	-3.08554
36	H	-0.63496	4.85270	-1.79219
37	H	3.78091	-1.19469	-1.40810
38	H	4.16145	-2.73602	-1.21409
39	H	2.62568	-2.28735	-1.23978
40	H	-1.40600	4.18772	-0.55725

41	H	0.17901	4.39305	-0.49445
42	H	5.58734	-2.26400	0.62859
43	H	5.29191	-0.69218	0.56517
44	H	-4.34103	-2.77876	0.76975
45	H	-3.21704	2.89791	0.72056
46	H	-1.95233	-3.45604	0.77161
47	H	3.58306	-3.87225	0.95147
48	H	-0.30090	2.46917	0.99400
49	H	2.12798	-3.22671	1.12089
50	H	5.07381	-1.49325	1.93443
51	H	-4.58251	-3.71820	2.04368
52	H	-5.00552	-2.17488	2.09477
53	H	-2.17071	-4.35786	2.07425
54	H	-2.23191	3.12968	1.96070
55	H	1.88814	3.26855	2.07643
56	H	-1.03791	-3.22799	2.06434
57	H	-3.76701	2.75376	2.21629
58	H	3.23980	-2.99799	2.24862
59	H	3.85358	0.45486	2.30798
60	H	-4.15971	0.13640	2.61432
61	H	0.93242	2.48328	3.09244
62	H	2.51131	2.52470	3.34955
63	H	-3.25702	-3.37352	4.12454
64	H	-3.62723	-1.81692	4.15036
65	H	-2.09343	-2.27546	4.17931
66	N	-0.05882	0.62366	-1.77888
67	N	-0.27531	1.69565	-0.93510
68	N	1.44916	-0.42312	0.45758
69	N	1.02931	0.76920	1.02222
70	N	-1.49881	0.67895	1.06503
71	N	-1.46917	-0.70476	1.20141
72	B	-0.26609	1.50754	0.59345
0				

(X3) TptBu,MeLuMeCl

1	Lu	1.02768	-1.26206	-0.37047
2	C	0.26377	-1.67990	-5.04073
3	C	-2.08234	-2.16579	-4.32727
4	C	-0.68345	-1.76956	-3.84333
5	C	-1.26803	0.76841	-3.65946
6	C	-0.76941	-0.43342	-3.16119
7	C	-0.18691	-2.85014	-2.89632
8	C	-1.67850	3.08671	-2.6156
9	C	-1.22631	1.67555	-2.63281
10	C	0.90228	4.24401	0.60089
11	C	1.50114	2.89863	0.76653
12	C	5.18090	0.52510	1.08772
13	C	-1.86682	-3.67515	1.16352
14	C	2.71415	2.55414	1.30373
15	C	2.79114	1.16324	1.27648
16	C	-3.04527	2.16592	1.66406
17	C	3.49788	-1.19776	1.69621
18	C	-2.38643	0.84016	1.61246
19	C	3.86704	0.27103	1.82815
20	C	-1.77370	-1.29520	1.88913
21	C	-2.69332	-0.32891	2.27932
22	C	-1.69019	-2.73269	2.33933
23	C	-0.36764	-3.00287	3.03202
24	C	4.05084	0.58452	3.31679
25	C	-2.81267	-2.99983	3.33606

26	H	-0.07125	-1.01138	-5.67421
27	H	0.31675	-2.55351	-5.48244
28	H	-2.40404	-1.50422	-4.97344
29	H	-2.04215	-3.04683	-4.75379
30	H	1.15746	-1.41725	-4.73136
31	H	-1.57722	0.92910	-4.54285
32	H	-2.69374	-2.20165	-3.56271
33	H	-2.17131	3.28352	-3.43900
34	H	-0.21626	-3.71857	-3.34811
35	H	0.73479	-2.65192	-2.62902
36	H	-0.89937	3.67872	-2.55121
37	H	-0.75981	-2.87561	-2.10113
38	H	-2.26334	3.23363	-1.84139
39	H	0.86460	4.46974	-0.35268
40	H	5.06020	0.33286	0.13281
41	H	-1.04759	2.43180	-0.03442
42	H	-1.13688	-3.53746	0.52382
43	H	-2.72367	-3.49448	0.72587
44	H	-3.41561	2.43404	0.78434
45	H	3.44390	-1.43707	0.74747
46	H	-0.00643	4.24570	0.97150
47	H	1.44831	4.90667	1.07229
48	H	5.44475	1.46216	1.20062
49	H	5.87959	-0.05896	1.45079
50	H	-1.85138	-4.60198	1.48236
51	H	3.37658	3.15054	1.63130
52	H	-2.43789	2.87248	2.00292
53	H	4.18146	-1.74649	2.13297
54	H	2.62963	-1.35567	2.12329
55	H	-3.79887	2.07842	2.30020
56	H	0.36637	-2.86336	2.39739
57	H	-3.62024	-2.83839	2.84777
58	H	-3.40605	-0.45082	2.89504
59	H	4.33207	1.51647	3.42209
60	H	-0.35017	-3.92879	3.35339
61	H	-2.71603	-3.92110	3.59000
62	H	4.73470	-0.00788	3.69251
63	H	3.20315	0.44270	3.78686
64	H	-0.26510	-2.39198	3.79009
65	H	-2.64455	-2.40086	4.06382
66	B	-0.57720	1.55210	-0.09532
67	N	-0.39221	-0.24919	-1.89151
68	N	-0.67842	1.05475	-1.56381
69	N	0.88594	1.75625	0.38592
70	N	1.68545	0.68250	0.69798
71	N	-1.29094	0.57008	0.83067
72	N	-0.89843	-0.75071	0.99095
0				

(X4) TptBu,MeLuMeNeosilyl

1	Lu	0.46224	-0.64746	-1.51707
2	C	-3.35919	0.10084	-4.19683
3	C	-2.39021	-1.83409	-2.94835
4	C	-3.30459	-0.62327	-2.84211
5	C	-4.72361	-1.05992	-2.46255
6	C	4.45556	2.02550	-2.04473
7	C	3.56975	-0.28826	-1.77557
8	C	-2.79601	0.34868	-1.80106
9	C	-3.32923	1.58768	-1.46229
10	C	3.99212	0.96881	-1.03504

11	C	-2.52385	2.09334	-0.47009
12	C	5.14967	0.63262	-0.07633
13	C	2.84354	1.52102	-0.22582
14	C	-0.22928	-4.30341	0.22460
15	C	-2.59833	3.41202	0.22850
16	C	2.82869	2.61478	0.63505
17	C	2.10209	-3.51097	0.75721
18	C	1.55822	2.68319	1.15087
19	C	0.67915	-3.68149	1.28791
20	C	0.12074	-2.32206	1.71620
21	C	0.99681	3.65043	2.13989
22	C	0.74004	-4.61559	2.50884
23	C	-0.74711	-0.63522	2.83970
24	C	-0.38374	-1.95640	2.94656
25	C	-1.31211	0.26780	3.88838
26	H	-3.65813	-0.52448	-4.8904
27	H	-2.46766	0.43698	-4.42426
28	H	-3.98721	0.85139	-4.14164
29	H	-2.77198	-2.47730	-3.58184
30	H	-5.08032	-1.65099	-3.15834
31	H	-1.50741	-1.54860	-3.26385
32	H	5.20902	1.67402	-2.56264
33	H	3.71686	2.24405	-2.65089
34	H	-5.29689	-0.27028	-2.37959
35	H	2.85682	-0.06881	-2.41165
36	H	4.33873	-0.65557	-2.26104
37	H	-2.30303	-2.25512	-2.06714
38	H	-4.09586	2.00170	-1.84050
39	H	4.73537	2.83479	-1.56672
40	H	-4.70127	-1.53883	-1.60760
41	H	3.24148	-0.95095	-1.13256
42	H	5.90641	0.27836	-0.58976
43	H	-0.25298	-3.72354	-0.56475
44	H	-3.34048	3.93582	-0.14087
45	H	0.11858	-5.18391	-0.02692
46	H	2.09099	-2.91748	-0.02236
47	H	-1.75747	3.89900	0.09761
48	H	5.42677	1.44317	0.39892
49	H	2.46146	-4.38525	0.49803
50	H	4.85162	-0.04026	0.57181
51	H	-1.13551	-4.40146	0.58529
52	H	3.55359	3.19861	0.82767
53	H	-2.74627	3.26593	1.18558
54	H	2.66753	-3.12014	1.45591
55	H	0.27390	4.16268	1.72250
56	H	-0.97386	1.86021	1.75286
57	H	1.13150	-5.47405	2.24533
58	H	1.70259	4.26313	2.43489
59	H	-0.16549	-4.76197	2.85411
60	H	0.64546	3.16107	2.91351
61	H	1.29275	-4.20523	3.20731
62	H	-2.09736	0.73301	3.53080
63	H	-0.46427	-2.50776	3.71521
64	H	-0.63470	0.92539	4.15185
65	H	-1.57477	-0.26300	4.66897
66	N	-1.72093	0.09299	-1.04754
67	N	1.63132	0.95084	-0.24800
68	N	-1.55929	1.18349	-0.21079
69	N	0.83542	1.67921	0.61171
70	N	0.06590	-1.28320	0.85474
71	N	-0.47281	-0.23542	1.57648

72	B	-0.58097	1.18349	0.99752
0				

(X5) TptBu,MeLuMeBn_a

1	Lu	0.75370	-1.20483	-0.99685
2	C	-0.42709	0.37569	-5.48758
3	C	-2.71530	0.12917	-4.48492
4	C	-1.20627	0.02921	-4.20309
5	C	-0.88723	-1.39646	-3.79524
6	C	-0.99257	2.38458	-3.10614
7	C	-0.86219	0.99651	-3.10777
8	C	-0.61428	2.81028	-1.85126
9	C	-0.57877	4.20078	-1.30524
10	C	-2.70472	-3.03753	-0.23289
11	C	2.98882	-2.66110	0.78567
12	C	-2.31292	-2.74094	1.23259
13	C	5.04238	-1.54342	1.64921
14	C	-1.96309	-1.28599	1.39952
15	C	2.87938	-0.28417	1.54343
16	C	-1.14817	-3.63450	1.64334
17	C	2.28000	1.85203	1.63714
18	C	3.51778	-1.63264	1.77690
19	C	2.17030	3.31006	1.89780
20	C	-1.95951	0.85151	1.95523
21	C	3.21342	0.94806	2.10128
22	C	-3.32623	-3.15371	2.36276
23	C	-2.57799	-0.34449	2.22715
24	C	-2.23630	2.20571	2.52252
25	C	3.15455	-2.08050	3.21140
26	H	-0.67037	-0.25470	-6.19718
27	H	-0.65199	1.28688	-5.76924
28	H	-2.95012	-0.46988	-5.22245
29	H	0.53456	0.31479	-5.31239
30	H	-2.94031	1.05145	-4.73002
31	H	-1.15453	-2.00911	-4.51312
32	H	-1.28525	2.92847	-3.82726
33	H	-3.21512	-0.12689	-3.68131
34	H	0.07564	-1.48218	-3.63428
35	H	-1.37740	-1.61834	-2.97582
36	H	-0.74834	4.83947	-2.02869
37	H	0.30311	4.37569	-0.91538
38	H	-1.93337	-2.87832	-0.81596
39	H	-1.26637	4.29871	-0.61420
40	H	-3.44190	-2.45022	-0.49999
41	H	-2.98640	-3.97279	-0.31255
42	H	3.16484	-2.35356	-0.12777
43	H	5.27949	-1.29873	0.72976
44	H	3.43965	-3.51820	0.93406
45	H	-0.23440	2.63564	0.82345
46	H	2.02353	-2.77316	0.91311
47	H	2.15935	3.79457	1.04676
48	H	-0.37004	-3.43449	1.08066
49	H	-1.40108	-4.57370	1.52967
50	H	5.44017	-2.41148	1.86892
51	H	-2.47028	2.82136	1.79689
52	H	5.38218	-0.86250	2.26637
53	H	-4.18434	-2.70485	2.21166
54	H	-3.45770	-4.12521	2.34577
55	H	2.93755	3.60482	2.43181
56	H	1.34263	3.49315	2.38790

57	H	-0.92284	-3.46567	2.58219
58	H	3.93973	1.12954	2.68500
59	H	-3.27812	-0.49878	2.85028
60	H	-1.43842	2.53535	2.98607
61	H	-2.98214	2.14932	3.15583
62	H	-2.96816	-2.88846	3.23597
63	H	3.54550	-2.96249	3.38765
64	H	2.17993	-2.13263	3.30093
65	H	3.50809	-1.43263	3.85569
66	B	-0.01389	1.63233	0.40925
67	N	-0.40974	0.58652	-1.91089
68	N	-0.26049	1.71829	-1.12944
69	N	-1.00727	-0.70027	0.65458
70	N	1.79812	-0.14283	0.76810
71	N	1.41980	1.18259	0.82390
72	N	-1.01432	0.63006	1.00957
0				

(X6) TptBu,MeLuMeBn_b

1	Lu	-1.32164	-0.78819	-0.80604
2	C	1.54811	-3.77319	-3.69799
3	C	2.87928	-1.28957	-2.35020
4	C	1.28701	-3.36590	-2.24382
5	C	3.76911	1.10642	-1.93064
6	C	1.69034	-1.92997	-2.00748
7	C	-0.18643	-3.57495	-1.91920
8	C	-4.38105	2.95038	-1.65581
9	C	2.79338	-0.00977	-1.84167
10	C	2.14095	-4.25211	-1.30801
11	C	1.06267	4.25198	-0.75131
12	C	-1.47222	3.72197	-0.67089
13	C	-0.13980	3.37115	-0.64592
14	C	-2.19452	2.53894	-0.52091
15	C	-3.68147	2.36176	-0.41436
16	C	-4.05053	0.89656	-0.28147
17	C	-4.17165	3.10340	0.84114
18	C	-0.37170	-3.41438	2.19345
19	C	1.63161	0.52274	2.33474
20	C	2.76690	1.47442	2.52897
21	C	0.02530	-0.97728	2.55255
22	C	-2.29260	-1.90196	2.88643
23	C	-0.80646	-2.17137	3.02507
24	C	1.08030	-0.36202	3.22924
25	C	-0.75772	-2.15686	4.59825
26	H	0.97883	-3.24141	-4.29349
27	H	2.48954	-3.61346	-3.91752
28	H	1.34239	-4.72423	-3.81306
29	H	3.60467	-1.66052	-2.83742
30	H	4.52350	0.83630	-2.49513
31	H	-4.07077	2.48205	-2.45803
32	H	-0.72964	-2.97281	-2.46900
33	H	3.33330	1.89144	-2.32174
34	H	-0.43342	-4.50354	-2.11051
35	H	-4.16667	3.90372	-1.72917
36	H	-5.35062	2.83973	-1.56748
37	H	3.08957	-4.13656	-1.52388
38	H	1.89082	-5.19255	-1.42982
39	H	1.65866	3.90822	-1.44910
40	H	0.78109	5.16178	-0.98161
41	H	-3.76498	0.41387	-1.08511

42	H	4.09559	1.32743	-1.03436
43	H	-0.34366	-3.38365	-0.97090
44	H	-1.82861	4.59646	-0.76964
45	H	1.98312	-3.99129	-0.37652
46	H	-5.02229	0.81266	-0.17766
47	H	1.53642	4.26309	0.10622
48	H	2.02832	1.88703	0.00636
49	H	-3.60326	0.51793	0.50437
50	H	-3.92147	4.04936	0.77891
51	H	-5.14536	3.02805	0.90559
52	H	-0.64679	-3.29408	1.26010
53	H	-3.75772	2.70728	1.63670
54	H	3.48895	1.25387	1.90435
55	H	-2.51349	-1.79971	1.93471
56	H	0.60153	-3.51369	2.23753
57	H	2.45772	2.38904	2.36110
58	H	-0.79963	-4.21774	2.55867
59	H	-2.79568	-2.65680	3.25666
60	H	-2.52363	-1.08285	3.36665
61	H	3.09824	1.40564	3.44877
62	H	1.36008	-0.52259	4.12268
63	H	0.11141	-2.48569	4.90414
64	H	-1.46911	-2.73137	4.95366
65	H	-0.89236	-1.23873	4.92321
66	B	1.19540	1.17374	-0.14942
67	N	0.90866	-1.08268	-1.32828
68	N	1.58981	0.11204	-1.22037
69	N	-0.06552	2.02553	-0.49625
70	N	-1.34439	1.50314	-0.42227
71	N	0.93707	0.43437	1.17436
72	N	-0.06819	-0.49835	1.29815
0				

(X7) TptBu,MeLuMeNTf2

1	Lu	0.90235	-1.28354	-0.05014
2	C	-2.36375	-2.92884	-3.75077
3	C	3.27280	2.39663	-3.39047
4	C	2.68936	-0.02325	-3.25201
5	C	-0.19201	-3.32403	-2.54801
6	C	-1.70805	-3.24733	-2.39554
7	C	2.80474	1.28131	-2.44158
8	C	-2.24162	-4.59637	-1.90919
9	C	0.75835	2.84340	-2.00323
10	C	1.47195	1.65660	-1.84288
11	C	-2.10217	-2.16580	-1.41904
12	C	3.84135	1.12238	-1.32207
13	C	-0.37014	2.72123	-1.21438
14	C	-1.46400	3.72260	-1.00289
15	C	-3.37656	-1.86076	-0.95704
16	C	-3.23980	-0.75061	-0.15197
17	C	-4.29659	-0.00718	0.59660
18	C	2.89160	-1.52823	2.56317
19	C	-0.80501	1.27454	2.97246
20	C	1.09274	0.12902	3.08339
21	C	-1.99649	2.12418	3.27115
22	C	3.44028	0.69653	3.52674
23	C	2.42658	-0.43823	3.50951
24	C	0.22892	0.92803	3.82141
25	C	2.28893	-1.02597	4.91998
26	H	-2.17849	-3.65482	-4.38255

27	H	2.63743	2.48398	-4.13109
28	H	-1.99846	-2.08949	-4.10103
29	H	2.06166	0.10746	-3.99290
30	H	4.15854	2.17272	-3.74544
31	H	-3.33184	-2.83896	-3.63142
32	H	3.56938	-0.26505	-3.60825
33	H	0.03465	-3.99443	-3.22613
34	H	3.32227	3.24379	-2.89970
35	H	-2.00226	-5.29378	-2.55455
36	H	0.15312	-2.44907	-2.82483
37	H	2.36251	-0.74065	-2.67105
38	H	0.99863	3.58599	-2.54450
39	H	-3.21701	-4.55060	-1.82427
40	H	4.71359	0.90239	-1.71217
41	H	-1.33894	4.47819	-1.61524
42	H	0.20974	-3.57646	-1.69179
43	H	-4.18116	-2.32474	-1.15585
44	H	-2.33131	3.30110	-1.17707
45	H	-1.84678	-4.80851	-1.03745
46	H	3.91045	1.96001	-0.81929
47	H	3.56320	0.40185	-0.71902
48	H	-1.43832	4.04436	-0.07799
49	H	-4.30219	0.93013	0.30895
50	H	-5.17145	-0.40934	0.41318
51	H	-2.13642	1.65421	0.59397
52	H	-4.11000	-0.05279	1.55717
53	H	3.02639	-1.14987	1.66896
54	H	2.21351	-2.23478	2.51924
55	H	3.50475	1.09050	2.63120
56	H	-1.99349	2.90988	2.68529
57	H	3.73587	-1.90540	2.88867
58	H	-2.81484	1.60593	3.11790
59	H	4.31655	0.34853	3.79457
60	H	3.15266	1.38280	4.16487
61	H	-1.96471	2.41537	4.20582
62	H	0.32879	1.18512	4.73035
63	H	1.59110	-1.71542	4.92019
64	H	3.14151	-1.42313	5.19307
65	H	2.04461	-0.31347	5.54750
66	N	0.81501	0.84243	-0.99506
67	N	-1.21870	-1.28777	-0.91280
68	N	-0.33411	1.51721	-0.60733
69	N	-1.93500	-0.39641	-0.13309
70	N	-0.57211	0.70094	1.77351
71	N	0.60878	-0.02060	1.83609
72	B	-1.31765	0.92791	0.42548
0				

(X8) TptBu,MeLuMeOTf_a

1	Lu	-0.13770	-1.42063	0.81601
2	C	0.48602	-3.42979	-3.97813
3	C	-2.36658	1.25386	-3.42774
4	C	-1.46736	-1.19358	-3.45362
5	C	-1.56379	-4.27741	-2.83642
6	C	-1.60676	0.05265	-2.90179
7	C	-0.32408	-3.41136	-2.60896
8	C	-0.78218	-1.95521	-2.52246
9	C	1.62271	3.20566	-1.90035
10	C	0.39127	-3.81291	-1.44354
11	C	1.87938	2.05036	-0.98134

12	C	3.09091	1.61239	-0.46066
13	C	-2.56508	3.57267	0.05492
14	C	3.78819	-1.82002	0.35006
15	C	2.80162	0.46616	0.27385
16	C	5.18377	0.14246	0.94214
17	C	-2.13934	2.43324	0.93046
18	C	3.76268	-0.42662	1.01928
19	C	-2.42844	2.21787	2.25878
20	C	3.34680	-0.55801	2.48596
21	C	-1.79891	1.03497	2.59609
22	C	-0.99960	-0.98085	3.85627
23	C	-1.74906	0.35544	3.93997
24	C	-3.19013	0.12031	4.43249
25	C	-1.03847	1.27393	4.93241
26	H	-0.10255	-3.15508	-4.71090
27	H	-2.70112	1.06060	-4.32863
28	H	0.81836	-4.33625	-4.14776
29	H	-1.77805	-1.47809	-4.30453
30	H	1.24283	-2.81037	-3.91727
31	H	-2.03820	-3.96541	-3.63588
32	H	-1.76945	2.02957	-3.46072
33	H	-1.29144	-5.20947	-2.96033
34	H	-3.12133	1.44775	-2.83407
35	H	1.28861	2.87463	-2.76007
36	H	-2.15607	-4.21010	-2.05916
37	H	2.45561	3.70127	-2.04344
38	H	0.73500	-4.72222	-1.56901
39	H	0.95496	3.80097	-1.49859
40	H	-0.77218	2.19276	-1.46611
41	H	1.13990	-3.19893	-1.29232
42	H	-3.02748	3.22329	-0.73544
43	H	-0.20792	-3.79488	-0.66899
44	H	4.00173	-1.72309	-0.60112
45	H	3.94431	2.01232	-0.58165
46	H	-1.77596	4.08095	-0.22841
47	H	5.49263	0.12598	0.01424
48	H	-3.17099	4.15994	0.55239
49	H	2.90950	-2.24417	0.44536
50	H	4.46782	-2.37775	0.78319
51	H	5.18380	1.06493	1.27131
52	H	5.78207	-0.40093	1.49687
53	H	2.46526	-0.98210	2.53946
54	H	-2.95229	2.76911	2.82692
55	H	4.00235	-1.10832	2.96523
56	H	3.30699	0.33151	2.89571
57	H	-1.46975	-1.58002	3.23934
58	H	-0.08858	-0.82425	3.52993
59	H	-3.63933	-0.51731	3.83860
60	H	-3.68047	0.96997	4.42748
61	H	-0.11450	1.42083	4.63804
62	H	-0.96254	-1.38987	4.74617
63	H	-1.50690	2.13265	4.97586
64	H	-3.17029	-0.23952	5.34455
65	H	-1.03490	0.85720	5.81869
66	N	-1.00374	0.05226	-1.70556
67	N	-0.48903	-1.19843	-1.45596
68	N	0.92497	1.20904	-0.56278
69	N	1.47504	0.21427	0.20593
70	N	-1.36521	1.40146	0.47196
71	N	-1.14334	0.52069	1.52359
72	B	-0.59456	1.29512	-0.85083

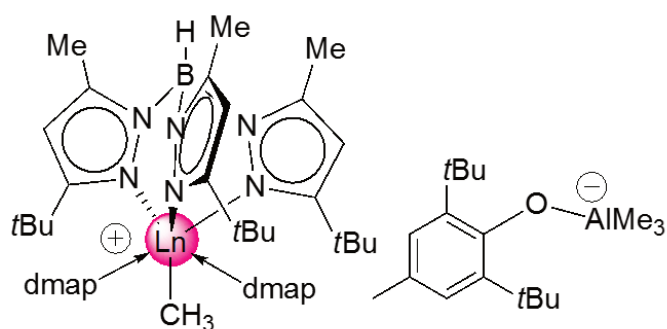
0

(X9) TptBu,MeLuMeOTf_b

1	Lu	-0.10666	-1.62460	0.07682
2	C	-1.39766	0.01065	-5.06482
3	C	0.12502	-1.57515	-3.87519
4	C	-1.05311	-0.61319	-3.70783
5	C	-2.30249	-1.38602	-3.22631
6	C	-0.76229	1.84475	-2.88743
7	C	-0.71862	0.46538	-2.70724
8	C	-0.40267	2.40271	-1.66674
9	C	4.73353	-1.77658	-1.17468
10	C	-0.34866	3.85012	-1.28301
11	C	2.71779	-3.03116	-0.39592
12	C	3.80974	-2.03432	0.01431
13	C	-4.40588	-1.18231	0.53469
14	C	3.21050	-0.72536	0.45905
15	C	3.86143	0.39001	0.95056
16	C	4.64641	-2.61675	1.16987
17	C	2.88276	1.33388	1.16437
18	C	3.03073	2.73064	1.68715
19	C	-2.92384	-2.82177	1.82192
20	C	-3.60804	-1.36412	1.92092
21	C	-2.57137	-0.24717	2.04519
22	C	-1.42678	1.55700	2.58391
23	C	-4.63938	-1.36210	2.99911
24	C	-2.55866	0.84876	2.89098
25	C	-0.84986	2.78288	3.26305
26	H	-1.53278	-0.70133	-5.72496
27	H	-0.66107	0.58735	-5.35489
28	H	-2.21560	0.54065	-4.98278
29	H	-0.09304	-2.24612	-4.55677
30	H	0.91961	-1.07385	-4.15454
31	H	-2.56840	-2.03540	-3.91053
32	H	-0.99268	2.30917	-3.68374
33	H	-3.03677	-0.75689	-3.06899
34	H	0.30472	-2.02393	-3.02306
35	H	-2.09336	-1.85803	-2.39290
36	H	-0.53530	4.40424	-2.06910
37	H	4.21072	-1.41831	-1.92319
38	H	5.15783	-2.61621	-1.44700
39	H	5.42215	-1.12917	-0.91899
40	H	2.18216	-2.64801	-1.12206
41	H	0.54439	4.06405	-0.93893
42	H	3.13490	-3.86384	-0.70133
43	H	-1.01697	4.03217	-0.58980
44	H	-3.79871	-1.35480	-0.21560
45	H	-5.15270	-1.81525	0.50272
46	H	-4.74945	-0.26635	0.47320
47	H	2.14027	-3.21688	0.37389
48	H	5.11336	-3.42260	0.86281
49	H	2.76639	3.37029	0.99267
50	H	4.79264	0.48572	1.10783
51	H	-2.42316	-2.89077	0.98104
52	H	0.42605	2.58406	0.89574
53	H	5.30380	-1.95141	1.46572
54	H	-3.61915	-3.51190	1.84578
55	H	4.05638	-2.84544	1.91861
56	H	3.96379	2.88920	1.93967
57	H	2.45700	2.84868	2.47293

58	H	-5.29957	-2.06262	2.82026
59	H	-2.31168	-2.94870	2.57598
60	H	-0.70692	3.48797	2.59838
61	H	-5.08645	-0.49005	3.02155
62	H	-3.20531	1.06609	3.55139
63	H	-4.20900	-1.53011	3.86419
64	H	0.00463	2.55143	3.68254
65	H	-1.47418	3.10159	3.94827
66	N	-0.34954	0.19180	-1.43571
67	N	-0.14902	1.39969	-0.81615
68	N	1.87445	-0.49793	0.37100
69	N	1.66931	0.79997	0.82296
70	N	-1.50578	-0.19695	1.23397
71	N	-0.80213	0.93422	1.57567
72	B	0.32080	1.51305	0.65551
0				

Mixed Methyl Aryloxy Rare-Earth Metal Complexes Stabilized by a Superbulky Tris(pyrazolyl)borato Ligand



<https://doi.org/10.1021/acs.organomet.9b00631>.

reprinted with permission from

Organometallics, 2019, 38, 4485-4496

Copyright © 2019 American Chemical Society

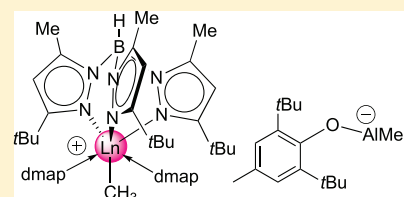
Mixed Methyl Aryloxy Rare-Earth-Metal Complexes Stabilized by a Superbulky Tris(pyrazolyl)borato Ligand

Verena M. Birkelbach, Christoph Stuhl, Cäcilia Maichle-Mössmer,[†] and Reiner Anwander^{*†}

Institut für Anorganische Chemie, Universität Tübingen, Auf der Morgenstelle 18, 72076 Tübingen, Germany

Supporting Information

ABSTRACT: Various mixed methyl aryloxy complexes $\text{Tp}^{\text{tBu,Me}}\text{LnMe}(\text{OAr})$ ($\text{Ln} = \text{Y, Lu}$) were obtained in moderate to high yields according to distinct synthesis protocols dependent on the metal size and sterics of the phenolic proligand. The reaction of $\text{Tp}^{\text{tBu,Me}}\text{LuMe}_2$ and $\text{Tp}^{\text{tBu,Me}}\text{YMe}(\text{AlMe}_4)$ via protonolysis with 1 or 2 equiv $\text{HOC}_6\text{H}_2\text{tBu}_2\text{-2,6-Me-4}$ in *n*-hexane gave the desired complexes $\text{Tp}^{\text{tBu,Me}}\text{LnMe}(\text{OAr})$. Corresponding treatment of $\text{Tp}^{\text{tBu,Me}}\text{LuMe}_2$ with the sterically less demanding $\text{HOC}_6\text{H}_3\text{Me}_2\text{-2,6}$, $\text{HOC}_6\text{H}_3\text{iPr}_2\text{-2,6}$ and $\text{HOC}_6\text{H}_3(\text{CF}_3)_2\text{-3,5}$ led to the formation of the bis(aryloxy) lutetium complexes $\text{Tp}^{\text{tBu,Me}}\text{Lu}(\text{OAr})_2$. Application of a salt-metathesis protocol employing $\text{Tp}^{\text{tBu,Me}}\text{LnMe}(\text{AlMe}_4)$ and the potassium aryloxides KOAr made complexes $\text{Tp}^{\text{tBu,Me}}\text{LnMe}(\text{OAr})$ accessible for the smaller aryloxy ligands as well. All complexes were analyzed by X-ray crystallography to compare the terminal Ln-Me bond lengths and to evaluate the implication of the methyl/aryloxy coordination for the exact cone angles Θ° of the $[\text{Tp}^{\text{tBu,Me}}]$ ancillary ligand. Treatment of $\text{Tp}^{\text{tBu,Me}}\text{LnMe}(\text{AlMe}_4)$ ($\text{Ln} = \text{Lu, Y}$) with $\text{HOC}_6\text{H}_2\text{tBu}_2\text{-2,6-Me-4}$ in the presence of 4-(dimethylamino)pyridine (dmap) produced ion-separated complexes $[\text{Tp}^{\text{tBu,Me}}\text{LnMe}(\text{dmap})_2][\text{Me}_3\text{AlOC}_6\text{H}_2\text{tBu}_2\text{-2,6-Me-4}]$. The thermal instability of $\text{Tp}^{\text{tBu,Me}}\text{LuMe}(\text{OC}_6\text{H}_2\text{tBu}_2\text{-2,6-Me-4})$ was revealed by the formation of $(\text{Tp}^{\text{tBu-H}}/(\text{tBu})_2\text{Me})\text{Lu}(\text{OC}_6\text{H}_2\text{tBu}_2\text{-2,6-Me-4})$ via intramolecular C–H-bond activation.



INTRODUCTION

The quest for methyl compounds has clearly and unmistakably coined the development of organorare-earth-metal (Ln) chemistry.^{1,2} Upon proving their existence, feasibility, and anticipated high reactivity ($[\text{Li}_3\text{LnMe}_6(\text{tmeda})_3]$, Schumann 1978),³ it was the discovery by Watson and Bercaw that $[\text{Ln}]-\text{CH}_3$ moieties ($\text{Ln} = \text{Sc, Y, Lu}$) engage in methane activation^{4,5} that triggered immense research. The synthesis of such highly reactive metallocene derivatives $[\text{Cp}^*\text{LnMe}]_x$ ($x = 1$ for Sc; $x = 2$ for Lu, Y; $x = 3$ for Sm; $\text{Cp}^* = \text{C}_5\text{Me}_5$) from $\text{LnCl}_3(\text{THF})_x$ precursors, however, involves a rather elaborate multistep procedure to ensure the formation of unsolvated, non-ate derivatives.^{4–6} Notwithstanding, cyclopentadienyl ancillary ligands have played a key role in advancing Ln(III) methyl chemistry, and many homometallic $[\text{Cp}^R_2\text{LnMe}(\text{do})_y]_x$ complexes ($y = 0, 1$; $x = 1, 2, 3$) have been structurally characterized.^{4–18} However, the kinetic stabilization of discrete dimethyl Ln(III) derivatives of the type $[(\text{L})\text{LnMe}_2]_x$ proved particularly challenging and depended on the monoanionic ancillary ligand L .^{19–21} Not considering any prevailing ligand redistribution processes, methyl-bridged dimerized and oligomerized species display solid-state structural motifs favored by half-sandwich complexes, e.g., $[\text{Cp}^*\text{YMe}_2]_3$,¹¹ $[\text{Cp}^*\text{ScMe}_2]_2$ ²² or $[\text{Cp}^*\text{LnMe}_2]_3$ ($\text{Ln} = \text{Tm, Lu}$; $\text{Cp}^* = \text{C}_5\text{Me}_4\text{SiMe}_3$).²³ So far, only sterically demanding *N*-coordinating ligands provided access to monometallic complexes $[(\text{L})\text{LnMe}_2]$ (Chart 1), comprising $[(\text{Dipp})\text{NC}(\text{tBu})\text{CHC}(\text{tBu})\text{N}(\text{Dipp})]\text{ScMe}_2$ (I, $\text{Dipp} = \text{C}_6\text{H}_3\text{iPr}_2\text{-2,6}$),²⁴ $[(1\text{-NDipp})\text{-2-(PPh}_2\text{=NDipp)-C}_6\text{H}_4)]\text{ScMe}_2$ (II),²⁵ $\text{Tp}^{\text{tBu,Me}}\text{LnMe}_2$ (III, $\text{Ln} = \text{Ho, Lu}$; $\text{Tp}^{\text{tBu,Me}} = \text{tris}(\text{pyrazolyl-tBu-3-Me-5})\text{borato}$),^{26,27} as well as *N*-

or *P*-donor supported $[2\{\text{N}(\text{Dipp})\text{C}(\text{Ph})\text{N}\}\text{C}_6\text{H}_4\text{CH}=\text{N}(\text{Dipp})]\text{ScMe}_2$ (IV),²⁸ $[\text{MeC}(\text{N}(\text{Dipp}))\text{CHC}(\text{Me})\text{N}(\text{CH}_2)_2\text{N}(\text{Me})(\text{CH}_2)_2\text{NMe}_2]\text{YMe}_2$ (V),²⁹ and $\text{N}[2\text{-PiPr}_2\text{-4-methylphenyl}]\text{ScMe}_2$ (VI).³⁰

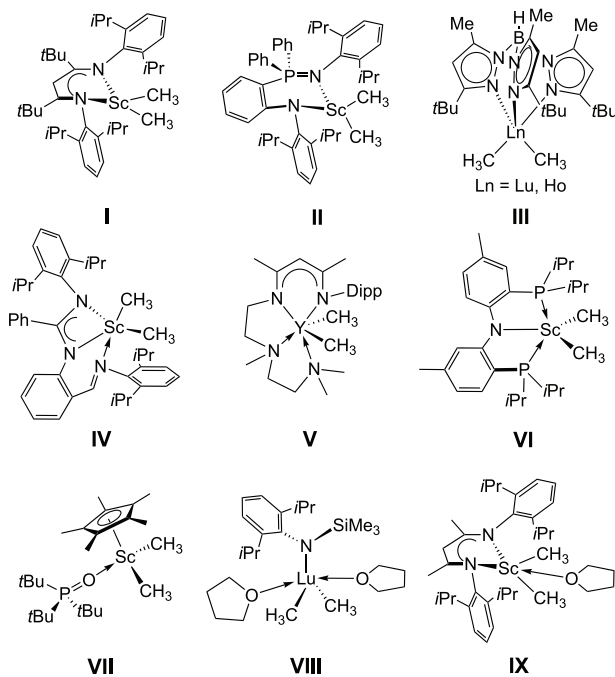
External donor stabilization was exploited for complexes $\text{Cp}^*\text{ScMe}_2(\text{OPtBu}_3)$ (VII),³¹ $[\text{N}(\text{SiMe}_3)(\text{Dipp})]\text{-LuMe}_2(\text{THF})_2$ (VIII),³² and $[(\text{Dipp})\text{NC}(\text{Me})\text{CHC}(\text{Me})\text{N}(\text{Dipp})]\text{ScMe}_2(\text{THF})$ (IX).²⁴

Trofimenko's unique Tp scorpionate ligands^{33,34} seem especially suited for studying the reactivity of such $[(\text{L})\text{-LnMe}_2]$ dimethyl compounds. Only very recently, we reported on a series of different mixed alkyl lutetium complexes $\text{Tp}^{\text{tBu,Me}}\text{LuRMe}$ with R representing alkyl (CH_2SiMe_3 , CH_2Ph) or weakly coordinating groups (chlorido, SO_3CF_3 or $\text{N}(\text{SO}_2\text{CF}_3)_2$).³⁵ The latter complexes were obtained from $\text{Tp}^{\text{tBu,Me}}\text{LuMe}_2$ by applying SiMe_4 -elimination and salt-metathesis protocols.

We were further interested in whether the dimethyl complex $\text{Tp}^{\text{tBu,Me}}\text{LuMe}_2$ ²⁶ or mixed methyl/aluminate complex $\text{Tp}^{\text{tBu,Me}}\text{LnMe}(\text{AlMe}_4)$ ($\text{Ln} = \text{Y, Lu}$)^{36,37} would also engage in selective protonolysis reactions. Aryloxy groups stand out for ease of steric and electronic tunability, chemical robustness, and ready availability.³⁸ Importantly, aryloxy ligands were shown to stabilize half-sandwich hydrocarbyl complexes $[\text{Cp}^*\text{LnR}(\text{OAr})]_x$ ($\text{R} = \text{Me, CH}(\text{SiMe}_3)_2, \text{AlMe}_2$; $\text{Ln} = \text{Sc, Y, La, Ce, Lu}$)^{39–44} and were probed in α -olefin polymerization. To the best of our knowledge, mixed methyl aryloxy

Received: September 17, 2019

Published: November 8, 2019

Chart 1. Structurally Characterized Monometallic Rare-Earth-Metal Dimethyl Complexes (L)LnMe₂

rare-earth-metal complexes have not been characterized by X-ray crystallography to date. Herein, we present the synthesis of various tris(pyrazolyl)borato-stabilized lutetium and yttrium methyl complexes $\text{Tp}^{\text{tBu,Me}}\text{LnMe}(\text{OAr})$ bearing distinct aryloxy ligands. Further exemplary reactivity studies revealed a thermally induced intramolecular C–H-bond activation of the ancillary ligand backbone and a donor (= 4-(dimethylamino)pyridine (dmap))-promoted cationization.

RESULTS AND DISCUSSION

Synthesis of Heteroleptic Bis(aryloxy) and Mixed Me/OAr Ln(III) Complexes. We have shown previously that scorpionate-supported rare-earth-metal methyl complexes $\text{Tp}^{\text{tBu,Me}}\text{LuMe}_2$ and $\text{Tp}^{\text{tBu,Me}}\text{Ln}(\text{AlMe}_4)\text{Me}$ give access to mixed methyl alkyl Ln(III) complexes $\text{Tp}^{\text{tBu,Me}}\text{LuRMe}$ ($\text{R} =$

CH_2SiMe_3 , CH_2Ph).³⁵ Therefore, it was reasoned that the role of these versatile precursors might be expanded to selective protonolyses with phenols as well as salt metatheses with potassium phenolates, respectively. We set out to treat $\text{Tp}^{\text{tBu,Me}}\text{LuMe}_2$, supposedly the most reactive because sterically least hindered, with various alkyl-substituted phenol derivatives HOAr ($\text{HOAr} = \text{HOC}_6\text{H}_3\text{Me}_2$ -2,6, $\text{HOC}_6\text{H}_3\text{iPr}_2$ -2,6, $\text{HOC}_6\text{H}_3(\text{CF}_3)_2$ -3,5, $\text{HOC}_6\text{H}_2\text{tBu}_2$ -2,6-Me-4) (Scheme 1). The reaction of $\text{Tp}^{\text{tBu,Me}}\text{LuMe}_2$ with an equimolar amount of the least bulky $\text{HOC}_6\text{H}_3\text{Me}_2$ -2,6 in *n*-hexane at ambient temperature was indicated by an instant methane evolution. After evaporation of the solvent, crystallization from *n*-hexane afforded colorless crystals identified as bis(aryloxy) derivatives $\text{Tp}^{\text{tBu,Me}}\text{Lu}(\text{OC}_6\text{H}_3\text{Me}_2$ -2,6)₂ (**1-Lu**) and reactant $\text{Tp}^{\text{tBu,Me}}\text{LuMe}_2$ via ¹H NMR spectroscopy. The formation of **1-Lu** (via ligand redistribution or double protonolysis) could not be prevented by performing the reaction at lower temperature (−40 °C). The same behavior was found when carrying out the reaction in toluene. In order to obtain the bis(aryloxy) lutetium complex more efficiently, the reaction was carried out with 2 equiv of the respective phenol. Similarly, protonolysis of $\text{Tp}^{\text{tBu,Me}}\text{LuMe}_2$ with 1 equiv $\text{HOC}_6\text{H}_3\text{iPr}_2$ -2,6 in *n*-hexane led to the bis(aryloxy) derivative $\text{Tp}^{\text{tBu,Me}}\text{Lu}(\text{OC}_6\text{H}_3\text{iPr}_2$ -2,6)₂ (**2-Lu**), even though the sterics of the respective phenol were markedly increased. The ¹H and ¹³C{¹H} NMR spectra of **1-Lu** and **2-Lu** at ambient temperatures showed only one set of signals for the pyrazolyl groups of the $\text{Tp}^{\text{tBu,Me}}$ ligand, similar to that of the starting compound.²⁶

The X-ray diffraction (XRD) analyses of **1-Lu** and **2-Lu** revealed isomorphous structures (Figure S49 and S50). As typically observed for a coordination number CN = 5, the $\text{Tp}^{\text{tBu,Me}}$ ligand adopts a κ^3 -coordination mode, thus accomplishing an environment of the lutetium center that is best described as distorted trigonal bipyramidal.³⁷ This is indicated by the Lu–N(pz) (pz = pyrazolyl) bond lengths, with the axial Lu–N distance being longer than the equatorial ones. Moreover, the Lu–N(pz) bond lengths in **1-Lu** (2.335(2)–2.439(3) Å) are in the same range as those reported for the starting compound $\text{Tp}^{\text{tBu,Me}}\text{LuMe}_2$ (2.339(2)–2.483(2) Å),²⁶ while the ones of **2-Lu** (2.365(1)–2.517(1) Å) appear slightly elongated. This can be attributed to the increased steric bulk of the $[\text{OC}_6\text{H}_3\text{iPr}_2$ -2,6] moieties. Interestingly, the Lu–O distances as well as the Lu–O–C bond angles in **1-Lu** and

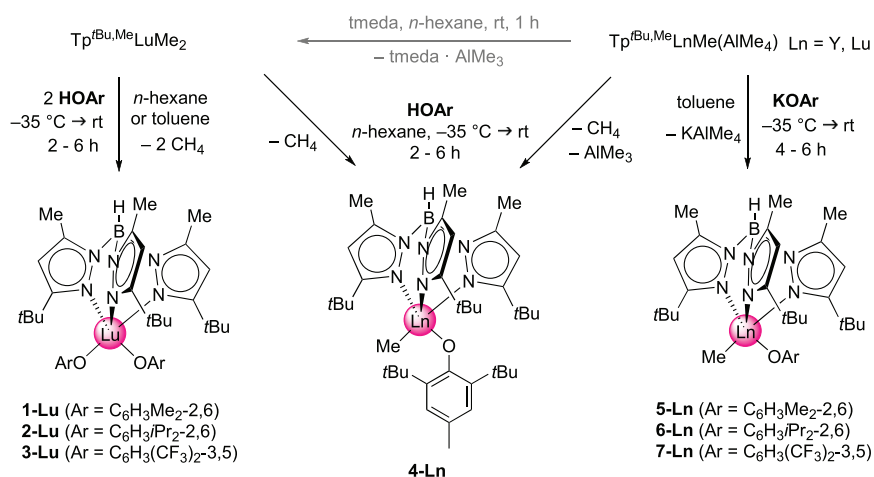
Scheme 1. Synthesis Pathways toward $\text{Tp}^{\text{tBu,Me}}\text{Lu}(\text{OAr})_2$ and Mixed Methyl Aryloxy Ln(III) Complexes $\text{Tp}^{\text{tBu,Me}}\text{LnMe}(\text{OAr})$ 

Table 1. Selected Structural Parameters [\AA , $^\circ$], Chemical Shifts in Benzene- d_6 [ppm], and Mathematically Exact Calculated Cone Angles Θ° [$^\circ$] of Selected $\text{Tp}^{\text{tBu,Me}}\text{Lu}(\text{OAr})_2$ or $\text{Tp}^{\text{tBu,Me}}\text{LuMe}(\text{OAr})^{\text{a}}$

	$\text{Tp}^{\text{tBu,Me}}\text{LuMe}_2^{26}$	1-Lu	2-Lu	3-Lu	4-Lu	5-Lu	6-Lu	7-Lu	8-Lu	9-Lu
Lu1–N(pz)	2.339(2)	2.335(2)	2.365(1)	2.315(2)	2.321(3)	2.328(2)	2.323(1)	2.319(4)	n.a.	2.306(3)
	2.339(2)	2.362(9)	2.370(1)	2.318(2)	2.345(3)	2.334(2)	2.330(1)	2.322(4)		2.380(3)
	2.483(2)	2.439(9)	2.517(1)	2.397(2)	2.626(3)	2.492(2)	2.502(1)	2.442(4)		2.390(3)
Lu1–O1/O2	n.a.	2.052(2)	2.072(1)	2.064(2)	2.092(2)	2.053(2)	2.0548(9)	2.085(3)	n.a.	2.068(2)
		2.06(2)	2.038(1)	2.090(2)						
Lu1–C(Me)	2.364(3)/2.375(2)	n.a.	n.a.	n.a.	2.338(4)	2.358(3)	2.362(1)	2.339(6)	n.a.	2.381(3)
Lu1–O1–C26/25	n.a.	170.9(2)	171.8(1)	145.3(2)	168.2(2)	167.2(2)	168.35(9)	150.9(3)	n.a.	175.9(2)
		174(3)	175.4(1)	147.3(2)						
^1H δ (Lu–Me)	–0.08	n.a.	n.a.	n.a.	0.67	0.55	0.50	0.37	–0.09 ^b	n.a.
^{13}C δ (Lu–Me)	33.0	n.a.	n.a.	n.a.	40.4	32.2	32.1	32.2	26.7 ^b	n.a.
cone angle Θ^{c}	277.1	276.1	272.5	280.4	278.1	276.1	279.2	280.3	n.a.	286.3

^an.a. (not available). ^bMeasured in THF- d_8 . ^cSee the Supporting Information for calculations.

2-Lu are quite similar (Table 1). The treatment of $\text{Tp}^{\text{tBu,Me}}\text{LuMe}_2$ with 2 equiv of the increasingly electron deficient phenol $\text{HOC}_6\text{H}_3(\text{CF}_3)_2\text{-3,5}$ under reaction conditions chosen as for 1-Lu and 2-Lu led to rapid decomposition of the dimethyl complex and a complicated reaction mixture. Therefore, a precooled solution of the reactant $\text{Tp}^{\text{tBu,Me}}\text{LuMe}_2$ in toluene was prepared and the respective phenol was added. Crystallization of the residue from toluene gave the bis(aryloxy) derivative $\text{Tp}^{\text{tBu,Me}}\text{Lu}[\text{OC}_6\text{H}_3(\text{CF}_3)_2\text{-3,5}]_2$ (3-Lu) in good yield. The ^1H NMR spectrum of 3-Lu showed the pyrazolyl signals slightly shifted to higher fields compared to the starting material. Again, the solid-state structure analysis revealed a distorted trigonal bipyramidal coordination geometry, consistent with the aforementioned congeners (Figure S51). The marginally shortened Ln–N(pz) bond lengths compared with 1-Lu and 2-Lu (2.315(2)–2.397(2) \AA for 3-Lu) could be attributed to the decreased steric bulk of 3,5-substituted aryloxy ligand. Striking is the bending of the Lu–O–C linkages (145.3(2) and 147.3(2) $^\circ$), which, however, was found even more pronounced in transition metal complexes, e.g., for $[\text{K}^3\text{-C}_6\text{H}_3\text{-2,6-(CH}_2\text{PtBu}_2)_2\text{Ir}(\text{CH}_3)[\text{OC}_6\text{H}_3(\text{CF}_3)_2\text{-3,5}]$ (131.4(4) $^\circ$)⁴⁵ and $(\text{PPh}_3)_2\text{Ni}[\text{OC}_6\text{H}_3(\text{CF}_3)_2\text{-3,5}]_2$ (122.4(2), 121.0(2) $^\circ$).⁴⁶ Unfortunately, the protonolysis reactions of $\text{Tp}^{\text{tBu,Me}}\text{YMe}(\text{AlMe}_4)$ with 2 equiv HOAr to give the respective bis(aryloxy) yttrium congeners did not give any clean conversion; however, degradation of the ancillary ligand was observed.

The targeted mixed methyl aryloxy Ln(III) complexes could be eventually achieved by utilizing the sterically demanding phenol $\text{HOC}_6\text{H}_2\text{tBu}_2\text{-2,6-Me-4}$. As for the aforementioned syntheses, instant methane evolution, when treating a suspension of $\text{Tp}^{\text{tBu,Me}}\text{LuMe}_2$ in *n*-hexane with the *t*Bu-substituted phenol, indicated a successful protonolysis reaction. The formation of complex $\text{Tp}^{\text{tBu,Me}}\text{LuMe}(\text{OC}_6\text{H}_2\text{tBu}_2\text{-2,6-Me-4})$ (4-Lu) could be confirmed by ^1H and ^{13}C NMR spectroscopy. The proton resonances of the pyrazolyl moieties appeared in the same region as for the precursor. Furthermore, the lutetium-bonded methyl ligand shows one narrow singlet at $\delta = 0.67$ ppm, which is significantly shifted downfield in comparison with the reactant ($\delta = -0.08$ ppm).²⁶ A broad resonance at 1.40 ppm is attributable to the overlapping signals of the *tert*-butyl substituents of the pyrazolyl moieties as well as of the aryloxy ligand. Furthermore, the methyl groups of the pyrazolyl ligand gave one broad singlet at $\delta = 2.08$ ppm (Figure S16 in SI). The aromatic protons of the aryloxy ligand overlap with the signal

of benzene- d_6 but could be unequivocally identified by ^1H – ^1H COSY NMR spectroscopy. The ^{13}C NMR spectroscopic analysis gave a signal for the Lu–Me moiety at $\delta = 40.4$ ppm (Figure S17 in SI). It is noteworthy that an excess of $\text{HOC}_6\text{H}_2\text{tBu}_2\text{-2,6-Me-4}$ (>2 equiv) did not lead to a bis(aryloxy) lutetium complex, mainly attributable to sterics.

The XRD analysis of 4-Lu revealed a monometallic complex with a distorted trigonal bipyramidal coordination geometry of the lutetium center, consistent with the aforementioned complexes (Figure 1). The Ln– $\text{Tp}^{\text{tBu,Me}}$ entity exhibits one

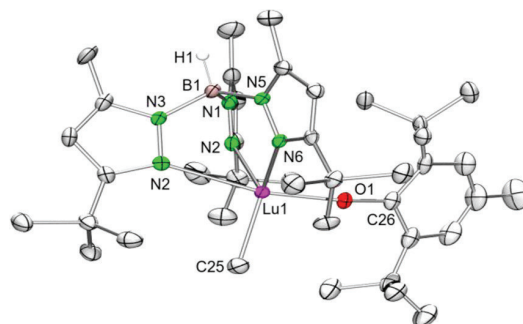


Figure 1. ORTEP representation of the crystal structure of 4-Lu with atomic displacement parameters set at the 50% level. Hydrogen atoms except for BH are omitted for clarity. Selected bond lengths [\AA] and angles [$^\circ$] for 4-Lu are given in Table 1.

significantly elongated Lu–N(pz) bond of 2.626(3) \AA compared to the respective precursor, which nicely displays the coordination flexibility of the scorpionate ligand. The Ln–C(Me) bond length of 2.338(4) \AA of five-coordinate complex 4-Lu compares well with those of similar methyl complexes, e.g., $\text{Tp}^{\text{tBu,Me}}\text{LuMe}_2$ (2.364(3)/2.375(2) \AA),²⁶ but is slightly elongated compared with the methyl triflate complex $\text{Tp}^{\text{tBu,Me}}\text{LuMe}(\text{OTf})$ (2.327(4) \AA),³⁵ as well as $[(\text{DippN})_2\text{C}]_2\text{LuMe}$ (2.314(3) \AA).⁴⁷ Additionally, the Ln–O distance of 2.092(2) \AA of 4-Lu is slightly elongated compared to the range observed for 4-coordinate $\text{Lu}(\text{OC}_6\text{H}_2\text{tBu}_2\text{-2,6})_2(\text{AlMe}_4)$ (1.999(3) and 2.006(3) \AA)⁴³ and homoleptic “3-coordinate” $\text{Lu}(\text{OC}_6\text{H}_2\text{tBu}_2\text{-2,6})_3$ (2.02 \AA).⁴⁸

In order to access mixed methyl aryloxy rare-earth-metal complexes of sterically less demanding aryloxy ligands, we examined complexes $\text{Tp}^{\text{tBu,Me}}\text{LnMe}(\text{AlMe}_4)$ (Ln = Y, Lu) according to salt metathesis reactions. Here, precipitation of KAlMe_4 is considered more advantageous than release of non-

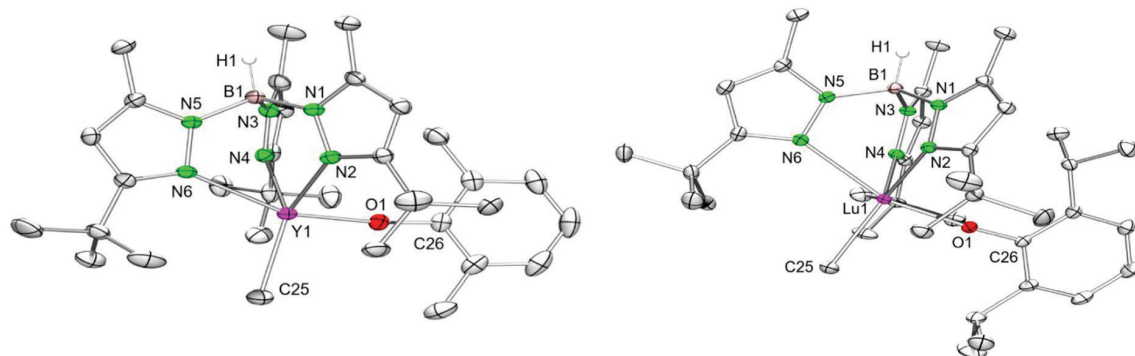


Figure 2. ORTEP representation of the crystal structures of **5-Y** (left) and **6-Lu** (right) with atomic displacement parameters set at the 50% level. Hydrogen atoms except for BH are omitted for clarity. Selected bond lengths [Å] and angles [°] for **5-Y** and **6-Lu** are given in Tables 1 and 2.

innocent AlMe_3 when applying a protonolysis protocol. Initial synthesis attempts with the sterically “most favored” pair $\text{Tp}^{\text{tBu,Me}}\text{YMe}(\text{AlMe}_4)/\text{KOC}_6\text{H}_2\text{tBu}_2\text{-2,6-Me-4}$ toward putative $\text{Tp}^{\text{tBu,Me}}\text{YMe}(\text{OC}_6\text{H}_2\text{tBu}_2\text{-2,6-Me-4})$ (**4-Y**), however, failed in different solvents. To our great surprise, protonolysis of $\text{Tp}^{\text{tBu,Me}}\text{YMe}(\text{AlMe}_4)$ with the respective phenolic proligand instead succeeded under mild reaction conditions (2 h at -35°C ; rapid decomposition of the yttrium complex in solution at ambient temperature) to yield **4-Y** (Scheme 1). Other protonolysis attempts at mixed methyl/aryloxy Ln(III) complexes employing $\text{Tp}^{\text{tBu,Me}}\text{LnMe}(\text{AlMe}_4)$ (Ln = Y, Lu) and less bulky HOAr led to complicated mixtures of products and no clean conversion. Single-crystalline **4-Y** was obtained in good yields from a saturated solution in toluene. The proton NMR spectrum of **4-Y** in toluene- d_8 shows a broad singlet at $\delta = 0.27$ ppm for the terminally bonded Me ligand but no Y–H coupling could be detected (Figure S11 in SI, ^{89}Y : nuclear spin 1/2, natural abundance 100%). Therefore, NMR spectroscopic analyses were performed in THF- d_8 to exclude signal coalescence. Rapid decomposition of **4-Y** in donor solvents, however, required low-temperature experiments. Remarkably, the change of the NMR solvent led to a strong shift of the Y–Me resonance revealing a doublet at $\delta = -0.36$ ppm with $^2J(\text{YH}) = 1.8$ Hz. The ^1H – ^{89}Y HSQC NMR spectrum of **4-Y** at 0°C shows a cross peak at $\delta = 556$ ppm on the ^{89}Y NMR scale (Figure S15 in SI), located highfield compared to the reactant $\text{Tp}^{\text{tBu,Me}}\text{YMe}(\text{AlMe}_4)$ ($\delta = 798$ ppm).²⁷ The $^{13}\text{C}\{^1\text{H}\}$ NMR spectrum displays a doublet at $\delta = 26.8$ ppm for the Y–Me moiety with $^1J(\text{YC}) = 44.6$ Hz. Despite several attempts, single crystals of **4-Y** suitable for an X-ray crystallographic study could not be obtained.

The salt metathesis reactions involving $\text{Tp}^{\text{tBu,Me}}\text{LnMe}(\text{AlMe}_4)$ (Ln = Y, Lu) and the sterically less bulky $\text{KOC}_6\text{H}_3\text{Me}_2\text{-2,6}$ and $\text{KOC}_6\text{H}_3\text{iPr}_2\text{-2,6}$ proceeded as envisaged (Scheme 1). Combining a solution of the rare-earth-metal precursor in toluene and a suspension of the potassium aryloxy in toluene and stirring the mixture for 6 h gave complexes $\text{Tp}^{\text{tBu,Me}}\text{LnMe}(\text{OC}_6\text{H}_3\text{Me}_2\text{-2,6})$ (**5-Ln**; Ln = Y, Lu) or $\text{Tp}^{\text{tBu,Me}}\text{LnMe}(\text{OC}_6\text{H}_3\text{iPr}_2\text{-2,6})$ (**6-Ln**; Ln = Y, Lu) along with insoluble $\text{K}(\text{AlMe}_4)$. Upon separation of the latter via filtration, crystals of **5-Ln** and **6-Ln** could be grown from saturated solutions of toluene in moderate to good yields. The ^1H and $^{13}\text{C}\{^1\text{H}\}$ NMR spectroscopic analyses clearly corroborated the formation of mixed methyl aryloxy Ln(III) complexes. The $\text{Tp}^{\text{tBu,Me}}$ signals of both complexes **5-Ln** and **6-Ln** are very similar and feature only one set of signals, as

already observed for the aforementioned complexes. Also, the resonances of the Ln(III)-bonded methyl group appeared in the same region. Complex **5-Y** shows a doublet for the Y–Me moiety at $\delta = 0.46$ ppm with $^2J(\text{YH}) = 1.8$ Hz (cf., **6-Y**: doublet at $\delta = 0.50$ ppm, $^2J(\text{YH}) = 1.9$ Hz), whereas the terminal methyl group of **5-Lu** is detected at $\delta = 0.55$ ppm (**6-Lu**: singlet at $\delta = 0.50$ ppm), slightly shifted to lower field. For the yttrium congener the respective ^{13}C signal revealed a doublet at $\delta = 22.5$ ppm ($^1J(\text{YC}) = 51.2$ Hz) and the ^1H – ^{89}Y HSQC NMR spectrum shows a cross peak at $\delta = 580$ ppm. As expected, the Lu–Me carbon shift was found at $\delta = 32.2$ ppm, slightly shifted downfield compared with **5-Y**. The carbon resonances of the terminal methyl ligands of complexes **6-Ln** both give a singlet at $\delta = 32.1$ ppm; however, the Y–C coupling for **6-Y** could not be observed. Additionally, the ^1H – ^{89}Y HSQC NMR shows a cross peak at $\delta = 578$ ppm, almost identical to the ^{89}Y resonance of **5-Y**.

Complexes **5-Ln** and **6-Ln** were further analyzed by means of XRD (**5-Y** and **6-Lu**, Figure 2; **5-Lu**, Figure S52 in SI; **6-Y**, Figure S53 in SI). The crystal structures show a distorted trigonal bipyramidal geometry around the rare-earth-metal center as expected. The determined Ln–N(pz) bond lengths are in line with those discussed above and in the respective precursors (e.g., $\text{Tp}^{\text{tBu,Me}}\text{YMe}(\text{AlMe}_4)$: 2.357(2)–2.418(2) Å).³⁷ Furthermore, all complexes nicely demonstrate the scorpionate character of the Tp ligand with two similar Ln–N(pz) bond lengths and the third slightly elongated. Additionally, the Ln–C(Me) distances (**5-Y** 2.409(2) Å; **5-Lu** 2.358(3) Å; **6-Y** 2.404(2) Å; **6-Lu** 2.362(1) Å) and the Ln–O distances (**5-Y** 2.080(1) Å; **5-Lu** 2.053(2) Å; **6-Y** 2.087(1) Å; **6-Lu** 2.0548(9) Å) compare well and reflect the distinct size of the metal centers. For further comparison, the terminal Y–C(CH₃) distances (**5-Y**: 2.409(2) Å, **6-Y**: 2.404(2) Å) are similar to those detected for $\text{Tp}^{\text{tBu,Me}}\text{YMe}(\text{AlMe}_4)$ (2.382(3) Å)³⁷ and $\text{Y}(\text{CH}_3)[(\text{AlMe}_2)\{\text{OSi}(\text{OtBu})_3\}_2][\text{OSi}(\text{OtBu})_3]$ (2.438(2) Å).⁴⁹ Similarly, the Ln–O distances in complexes **5-Ln** and **6-Ln** lie in the expected range, e.g., $\text{Y}(\text{OC}_6\text{H}_2\text{Me}_3\text{-2,4,6})_3(\text{THF})_3$ (Y–O: 2.104(4)–2.114(5) Å),⁵⁰ $[\text{Y}(\mu\text{-OC}_6\text{H}_3\text{Me}_2\text{-2,6})(\text{OC}_6\text{H}_3\text{Me}_2\text{-2,6})_2(\text{THF})_2]$ (Y–O_{terminal}: 2.046(6) Å, 2.075(6) Å),⁵¹ **1-Lu** (2.052(2), 2.06(2) Å), $\text{Ln}(\text{OC}_6\text{H}_3\text{iPr}_2\text{-2,6})_3(\text{THF})_2$ (Y: 2.065(7)–2.086(7) Å⁵² and 2.069(3)–2.086(2) Å; Lu: av. 2.044 Å).⁵⁴ Moreover, the Ln–O–C bond angles on **5-Ln** and **6-Ln** range from 167.2(2) to 168.35(9)°.

The salt-metathesis protocol was also applicable for the pairs $\text{Tp}^{\text{tBu,Me}}\text{LnMe}(\text{AlMe}_4)/\text{KOC}_6\text{H}_3(\text{CF}_3)_2\text{-3,5}$ (Ln = Y, Lu),

subject to certain restrictions. While the synthesis of the lutetium complex $\text{Tp}^{\text{tBu,Me}}\text{LnMe}[\text{OC}_6\text{H}_3(\text{CF}_3)_2\text{-3,5}]$ (**7-Lu**) succeeded in toluene under the reaction conditions previously applied for **5-Ln** and **6-Ln** (Scheme 1), ^1H NMR reaction studies revealed decomposition of the $\text{Tp}^{\text{tBu,Me}}$ ligand for yttrium. Subsequently, milder reaction conditions (4 h at -35°C) were chosen for the effective synthesis of **7-Y**. The ^1H NMR spectra of **7-Lu** and **7-Y** show similar shifts of the Ln–C(Me) moiety at $\delta = 0.37$ and 0.27 ppm (doublet with $^2J(\text{YH}) = 1.8$ Hz). Compared to other Me/OAr congeners a shift to higher fields was observed, which is in accordance with the electron-withdrawing CF_3 groups of the aryloxy ligand. ^{19}F NMR spectroscopy clearly identified both complexes at $\delta = -62.6$ ppm (**7-Y** and **7-Lu**), but unfortunately the expected quartet for the C–F coupling was hardly visible in the $^{13}\text{C}\{^1\text{H}\}$ NMR spectrum (**7-Y**: 132.3 ppm; **7-Lu**: 132.1 ppm) and could also not be detected with longer measurement times due to decomposition of the complexes in solution, especially for **7-Y**. Despite this, Ln–C(Me) carbon resonances were found at $\delta = 22.3$ ppm as a doublet for yttrium ($^1J(\text{YC}) = 50.8$ Hz) and as a singlet for lutetium at $\delta = 32.2$ ppm. The ^1H – ^{89}Y HSQC NMR spectrum shows a cross peak at $\delta = 620$ ppm, considerably shifted downfield compared with complexes **4-Y**, **5-Y**, and **6-Y**.

Suitable crystals for XRD were obtained from saturated solutions in toluene at -35°C (**7-Y**, Figure 3; **7-Lu**, Figure

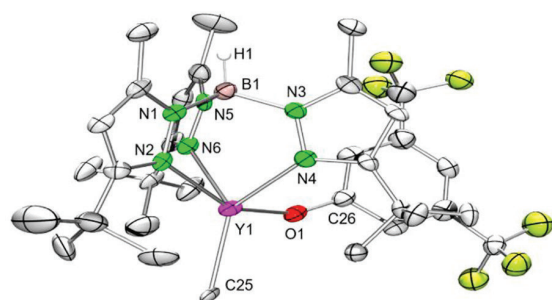


Figure 3. ORTEP representation of the crystal structure of **7-Y** with atomic displacement parameters set at the 50% level. Hydrogen atoms except for BH, the other molecules in the unit cell, and the disorder in one CF_3 group are omitted for clarity. Selected bond lengths [Å] and angles [$^\circ$] for **7-Y** are given in Table 2.

SS4 in SI). In both complexes, the Ln(III) centers adopt the typical distorted trigonal bipyramidal geometry. The Ln–N(pz) bond lengths (**7-Y**: 2.33(1)–2.52(1) Å; **7-Lu**:

2.319(4)–2.442(4) Å) are slightly shortened compared with **5-Ln**, likely reflecting the decreased steric hindrance in the 2- and 6-positions of the aryloxy ligand. The Ln–C(Me) distances of 2.45(1) Å (**7-Y**) and 2.339(6) Å (**7-Lu**) as well as the Ln–O distances of 2.10(1) Å (**7-Y**) and 2.085(3) Å (**7-Lu**) are in the expected range. As already observed for **3-Lu**, the Ln–O–C bond angles (**7-Y**: $148(1)^\circ$, **7-Lu**: $150.9(3)^\circ$) appear strongly bent compared to the complexes bearing other aryloxy ligands.

For better comparability, Table 1 and Table 2 show selected structural parameters, and ^1H and ^{13}C NMR chemical shifts of the important Ln–Me moieties. Furthermore, we were interested in the evaluation of the coordination behavior of the $[\text{Tp}^{\text{tBu,Me}}]$ ancillary ligand in the presence of different sterically demanding coligands. Hence, we calculated the mathematically exact cone angles Θ° (Tables 1 and Table 2) according to a method previously developed by Allen et al.⁵⁵ and implemented by our group for scorpionate ligands.⁵⁶ A noticeable trend was revealed: the cone angles reach a maximum in the presence of the fluorinated aryloxy ligand $[\text{OC}_6\text{H}_3(\text{CF}_3)_2\text{-3,5}]$ (Θ° : **5-Ln** < **6-Ln** < **7-Ln**). Apparently, the CF_3 substituents in the peripheral 3- and 5-positions exhibit the least interactions with the ancillary ligand. Cone angles of similar complexes of lutetium were already reported to range from 277.1° to 280.9° .³⁵ This compares well with the mixed methyl aryloxy rare-earth-metal complexes under study. The calculations also nicely document that the cone angles Θ° of **5-Ln**, **6-Ln**, and **7-Ln** increase with decreasing metal size, as expected for a given ligand set. Comparing only the lutetium complexes, it is interesting to note that the cone angle is marginally larger in the presence of aryloxy ligands with the sterically more demanding *i*Pr and *t*Bu groups in 2- and 6-positions (Θ° : **5-Lu** < **4-Lu** < **6-Lu**).

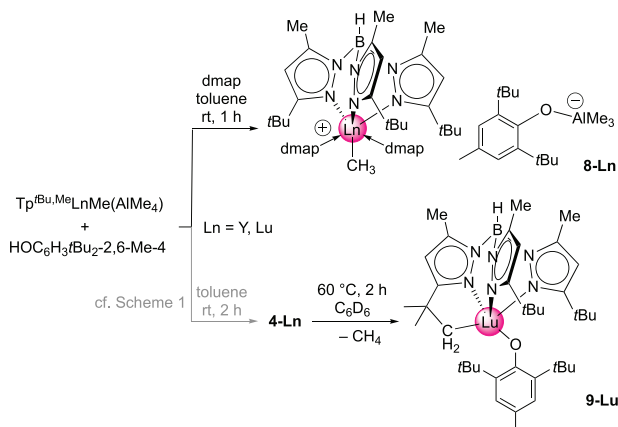
Reactivity Pattern. The overall thermal stability and reactivity toward additional donor molecules was probed exemplarily for methyl aryloxides **4-Ln**. As mentioned before, **4-Y** is temperature-sensitive and hence, expected to be the most reactive derivative. Accordingly, the pairs $\text{Tp}^{\text{tBu,Me}}\text{LnMe}(\text{AlMe}_4)/\text{HOOC}_6\text{H}_2\text{tBu}_2\text{-2,6-Me-4}$ (Ln = Lu, Y) were examined in the presence of dmap (Scheme 2). After 1 h a white precipitate of **8-Ln** had formed, which could be separated and further analyzed. Fortunately, the yttrium congener could be subjected to a crystal structure analysis, which confirmed the formation of ion pairs $[\text{Tp}^{\text{tBu,Me}}\text{LnMe}(\text{dmap})_2][\text{Me}_3\text{Al}(\text{OC}_6\text{H}_2\text{tBu}_2\text{-2,6-Me-4})]$ (Figure 4, left). The formation of ionic homoaluminates in donor solvents is well-known (e.g.,

Table 2. Selected Structural Parameters [Å, $^\circ$], Chemical Shifts, and Coupling Constants in Benzene- d_6 [ppm, Hz], and Mathematically Exact Calculated Cone Angles Θ° [$^\circ$] of Complexes $\text{Tp}^{\text{tBu,Me}}\text{YMe}(\text{OAr})^a$

	$[\text{Tp}^{\text{tBu,Me}}\text{YMe}(\text{AlMe}_4)]^{27,36,37}$	4-Y	5-Y	6-Y	7-Y	8-Y
Y1–N(pz)	2.357(2), 2.361(2)	n.a.	2.381(2), 2.387(2)	2.375(1), 2.384(2)	2.33(1), 2.40(1)	2.407(2), 2.456(2)
	2.418(2)		2.530(2)	2.561(2)	2.52(1)	2.459(2)
Y1–O1	n.a.	n.a.	2.080(1)	2.087(1)	2.10(1)	n.a.
Y1–C(Me)	2.382(3)	n.a.	2.409(2)	2.404(2)	2.45(1)	2.389(2)
Y1–O1–C26	n.a.	n.a.	167.2(1)	176.9(1)	148(1)	n.a.
^1H δ (Y–Me)	0.28/0.25	-0.36^b	0.46	0.50	0.27	-0.09^b
^{13}C δ (Y–Me)	-0.5	26.8^b	22.5	32.1	22.3	26.9^b
$^2J(\text{YH})/^1J(\text{YC})$	n.o./n.o.	1.8/44.6	1.8/51.2	1.9/n.o.	1.8/50.8	n.o./47.4
^1H – ^{89}Y HSQC	798	556^b	580	578	620	555^b
cone angle Θ° ^c	276.1	n.a.	273.9	276.1	278.6	276.8

^an.o. (not observed); n.a. (not available). ^bMeasured in THF- d_8 . ^cSee the Supporting Information for calculations.

Scheme 2. Reactivity of 4-Ln toward DMAP and under Thermolysis Conditions



[YMe₂(THF)₅][AlMe₄],⁵⁷ but solvent-separated heteroaluminate are less common comprising, e.g., amidoaluminate [Li(THF)₂(tmeda)][AlPh₃(tmp)] (tmp = tetramethylpiperido)⁵⁸ or [Ca(THF)₆][AlMe₃(NPh₂)₂].⁵⁹

The ¹H and ¹³C{¹H} NMR spectra of 8-Ln show only one set of signals for the Tp^{tBu,Me} ligand, slightly shifted compared with 4-Ln. The Ln–Me moieties were both found at $\delta = -0.09$ ppm in the ¹H NMR spectrum; however, no Y–H coupling but only a broad signal could be observed. Additionally, ¹³C NMR spectroscopy also revealed almost identical shifts (8-Y: δ , 26.9 ppm, ¹J(YC) = 47.4 Hz); 8-Lu: 26.7 ppm) and the characteristic Y–C coupling. It is noteworthy that ionic 8-Y shows a cross peak at $\delta = 555$ ppm in the ¹H–⁸⁹Y HSQC NMR spectrum (solvent THF-*d*₈), identical to that of Tp^{tBu,Me}YMe(OC₆H₃tBu₂-2,6-Me-4) (4-Y) in THF-*d*₈ (Table 2); however, the shifts in the ¹H NMR spectrum strongly vary (4-Y: -0.36 ppm). Furthermore, the shift of 8-Y in the ¹H–⁸⁹Y HSQC NMR compares well to ionic [YMe₂(THF)₅][AlMe₄] (¹H–⁸⁹Y HMBIC: 535 ppm).⁵⁷ Complexes 8-Ln are stable at ambient temperature, however, undergo B–N bond cleavage at elevated temperature (>50 °C) in THF. The 6-coordinate cationic yttrium center in 8-Y displays a Y–C(Me) distance of 2.389(2) Å, which is significantly shortened compared to those of methyl aryloxy complexes 5-Y, 6-Y, and 7-Y. On the other hand, the Ln–N(pz) distances

(2.407(2)–2.459(2) Å) are markedly elongated. Unfortunately, complex 8-Y did not show any activity in isoprene polymerization.

We were further interested in the thermal stability of such mixed methyl aryloxy rare-earth-metal complexes. As mentioned before, 4-Y is very sensitive toward temperatures above 0 °C and already starts to decompose at ambient temperature after 30 min, indicated by a color change from colorless to yellow. NMR studies indicated extensive degradation of the ancillary ligand and therefore, the formation of an ill-defined mixture of products. In contrast, 4-Lu is stable for days in benzene or toluene solution; however, it shows intramolecular C–H-bond activation of one of the *tert*-butyl groups of the pyrazolyl rings through the terminal methyl group at elevated temperatures (60 °C) (Scheme 2). This is indicated by methane evolution as found in the proton NMR spectrum as well as XRD analysis of suitable crystals (Figure 4, right). This C–H-bond activation for reactive terminal methyl groups was observed before for the [Tp^{tBu,Me}] ligand set; however 9-Lu revealed in accordance with its lower coordination number, Lu–C(CH₃)₂ distances (2.381(3) Å) shorter than in [(Tp^{(tBu-H)2/tBu,Me})Lu(AlMe₃{B(NDippCH)₂})] (2.391(3) Å) and [(Tp^{(tBu-H)2/tBu,Me})Lu(AlMe₃)] (2.418(5) Å) (Tp^{(tBu-H)2/tBu,Me} = hydro(3-Me-5-*t*Bu-pyrazolyl)bis{μ-(3-Me-5-Me₂C–CH₂–pyrazolyl)}borate).⁶⁰ In comparison to 4-Lu, the “sting” Ln–N6(pz) bond length is drastically decreased (4-Lu: 2.626(3) Å; 9-Lu: 2.390(3) Å), and also the Ln–O bond is shorter (4-Lu: 2.092(2) Å; 9-Lu: 2.068(2) Å). Interestingly, the Ln–O–C bond angle is even closer to linear due to the reduced steric bulk around the metal center (4-Lu: 168.2(2)°; 9-Lu: 175.9(2)°).

CONCLUSION

In summary, the monomeric methyl complexes Tp^{tBu,Me}LuMe₂ and Tp^{tBu,Me}LnMe(AlMe₄) (Ln = Lu, Y) provide access for various bis(aryloxy) and mixed methyl aryloxy rare-earth-metal complexes. Applying protonolysis protocols with phenolic proligands HOAr, only the sterically most demanding derivative HOC₆H₃tBu₂-2,6-Me-4 efficiently afforded the desired complexes Tp^{tBu,Me}LnMe(OAr). In contrast, such methane elimination reactions with sterically less hindered phenols reproducibly led to bis(aryloxy) derivatives Tp^{tBu,Me}Lu(OAr)₂. On the other hand complexes Tp^{tBu,Me}LnMe(OAr) with smaller aryloxy ligands can be

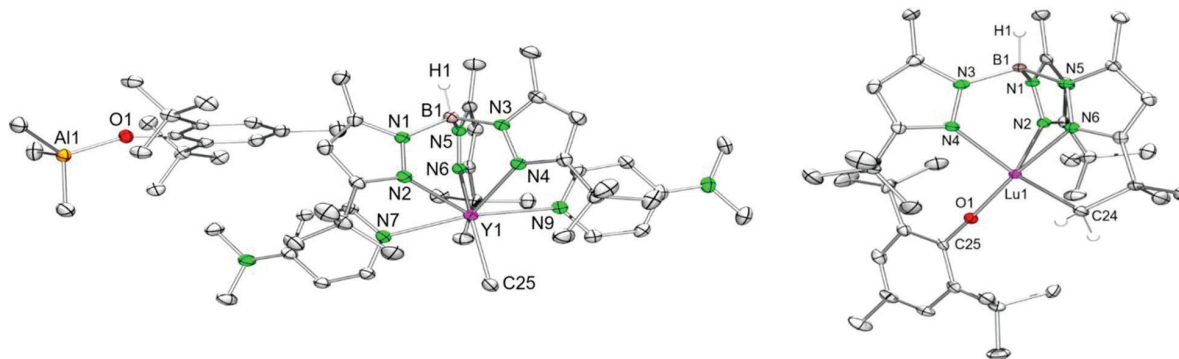


Figure 4. ORTEP representation of the crystal structures of 8-Y (left) and 9-Lu (right) with atomic displacement parameters set at the 50% level. Hydrogen atoms except for BH and CH₂ and the disorder in one *tert*-butyl group are omitted for clarity. Selected bond lengths [Å] and angles [°] for 8-Y and 9-Lu are given in Tables 1 and 2.

readily obtained from $\text{Tp}^{\text{fBu}_2\text{Me}}\text{LnMe}(\text{AlMe}_4)$ via a salt metathesis protocol employing KOAr and generating KAlMe_4 as a coproduct. Examination of the pairs $\text{Tp}^{\text{fBu}_2\text{Me}}\text{LnMe}(\text{AlMe}_4)/\text{HOC}_6\text{H}_2\text{tBu}_2\text{-2,6-Me-4}$ in the presence of the strong neutral donor dmap led to the ion-separated complex $[\text{Tp}^{\text{fBu}_2\text{Me}}\text{LnMe}(\text{dmap})_2][\text{Me}_3\text{Al}(\text{OC}_6\text{H}_2\text{tBu}_2\text{-2,6-Me-4})]$ featuring an anionic heteroaluminato moiety. The proneness of the $[\text{Tp}^{\text{fBu}_2\text{Me}}]$ ancillary ligand for C–H-bond activation in the presence of highly reactive Ln–Me moieties was further revealed by the isolation of complex $[(\text{Tp}^{\text{fBu}_2\text{Me}})/(\text{fBu}_2\text{Me})\text{Lu}(\text{OC}_6\text{H}_2\text{tBu}_2\text{-2,6-Me-4})]$.

EXPERIMENTAL SECTION

General Procedures. All operations were performed with rigorous exclusion of air and water by using standard Schlenk, high-vacuum, and glovebox techniques (MBraun 200B; <0.1 ppm of O_2 , <0.1 ppm of H_2O). Solvents were purified by using Grubbs-type columns (MBraun SPS, solvent purification system) and stored inside a glovebox. Benzene- d_6 and toluene- d_8 were obtained from Sigma-Aldrich and degassed. Benzene- d_6 was dried over NaK alloy for 2 days, and toluene- d_8 was stored over Na. Both were filtered prior to use. THF- d_8 was obtained from Sigma-Aldrich, stirred over NaK alloy and distilled. $\text{HOC}_6\text{H}_3\text{Me}_2\text{-2,6}$, $\text{HOC}_6\text{H}_3\text{iPr}_2\text{-2,6}$, and $\text{HOC}_6\text{H}_3\text{tBu}_2\text{-2,6-Me-4}$ were purchased from Sigma-Aldrich, and $\text{HOC}_6\text{H}_3(\text{CF}_3)_2\text{-3,5}$ and dmap from ABCR and sublimed prior to use. Reagents $\text{KOC}_6\text{H}_3\text{iPr}_2\text{-2,6}$, $\text{KOC}_6\text{H}_3\text{tBu}_2\text{-2,6-Me-4}$, and $\text{KOC}_6\text{H}_3(\text{CF}_3)_2\text{-3,5}$ were prepared from the respective dry phenol and KH in tetrahydrofuran at ambient temperature, and were dried in vacuo prior to use. $\text{Tp}^{\text{fBu}_2\text{Me}}\text{LnMe}(\text{AlMe}_4)$,³⁶ and $\text{Tp}^{\text{fBu}_2\text{Me}}\text{LuMe}_2$ ²⁷ were synthesized according to literature procedures. The NMR spectra of air- and moisture-sensitive compounds were recorded by using J. Young valve NMR tubes on a Bruker AVII+500 spectrometer (^1H , 500.00 MHz, ^{13}C , 125.72 MHz, ^{89}Y 24.496 MHz), a Bruker AVII+400 spectrometer (^1H , 400.13 MHz, ^{13}C , 100.61 MHz, ^{19}F , 376.31 MHz), and a Bruker AVII+250 spectrometer (^1H , 250.00 MHz, ^{11}B , 80.21 MHz, ^{13}C , 62.86 MHz). IR spectra were recorded on a Thermo Fisher Scientific NICOLET 6700 FTIR spectrometer using a DRIFT chamber with dry KBr/sample mixture and KBr windows; IR (DRIFT) data were converted by using the Kubelka–Munk refinement. Elemental analyses were performed on an Elementar Vario MICRO Cube.

$\text{Tp}^{\text{fBu}_2\text{Me}}\text{Lu}(\text{OC}_6\text{H}_3\text{Me}_2\text{-2,6})_2$ (1-Lu). A solution of $\text{HOC}_6\text{H}_3\text{Me}_2\text{-2,6}$ (19.3 mg, 0.158 mmol) in *n*-hexane (5 mL) was added to a suspension of $\text{Tp}^{\text{fBu}_2\text{Me}}\text{LuMe}_2$ (50.0 mg, 0.080 mmol) in *n*-hexane (5 mL) and stirred for 6 h at ambient temperature. The reaction mixture was filtered and the solution was concentrated in vacuo. Crystallization at $-35\text{ }^\circ\text{C}$ yielded compound 1-Lu (62.0 mg, 0.074 mmol, 94%) as colorless crystals. ^1H NMR (250 MHz, benzene- d_6 , $26\text{ }^\circ\text{C}$) δ 7.11 (d, 4H, $^3J(\text{HH}) = 7.2\text{ Hz}$, Ar-H), 6.76 (t, $^3J(\text{HH}) = 14.5\text{ Hz}$, 2H, Ar-H), 5.68 (s, 3H, 4-pz-H), 4.71 (v br d, $^1J(\text{BH}) = 119\text{ Hz}$, 1H, BH), 2.15 (s, 12H, C(CH₃)₂), 2.10 (s, 9H, pz-CH₃), 1.28 (s, 27H, pz-C(CH₃)₃) ppm. $^{13}\text{C}\{^1\text{H}\}$ NMR (63 MHz, benzene- d_6 , $26\text{ }^\circ\text{C}$) δ 166.2 (3-pz-C), 161.5 (Ar-C1), 146.6 (5-pz-C), 128.7 (Ar-C2/6), 126.5 (Ar-C3/5), 117.4 (Ar-C4), 104.9 (4-pz-C), 32.5 (pz-C(CH₃)₃), 30.8 (pz-C(CH₃)₃), 18.1 (C(CH₃)₂), 13.4 (pz-C(CH₃)₃) ppm. $^{11}\text{B}\{^1\text{H}\}$ NMR (80 MHz, benzene- d_6 , $26\text{ }^\circ\text{C}$) δ -8.7 (br s) ppm. IR (KBr) $\tilde{\nu}$ 2959 (m), 2924 (m), 2863 (w), 2560 (vw, B–H), 1590 (w), 1543 (s), 1470 (s), 1426 (vs), 1380 (m), 1373 (m), 1356 (m), 1329 (m), 1292 (vs), 1276 (vs), 1235 (s), 1195 (s), 1178 (s), 1136 (vw), 1093 (m), 1065 (m), 1025 (w), 984 (w), 916 (vw), 875 (m), 840 (w), 809 (w), 793 (w), 783 (m), 769 (m), 759 (m), 742 (w), 729 (w), 709 (w), 680 (vw), 645 (vs), 535 (w), 512 (vw) cm^{-1} . Elemental analysis calcd (%) for $\text{C}_{40}\text{H}_{38}\text{BLuN}_6\text{O}_2$: C 57.15, H 6.95, N 10.00; found C 57.15, H 6.95, N 10.07.

$\text{Tp}^{\text{fBu}_2\text{Me}}\text{Lu}(\text{OC}_6\text{H}_3\text{iPr}_2\text{-2,6})_2$ (2-Lu). A solution of $\text{HOC}_6\text{H}_3\text{iPr}_2\text{-2,6}$ (28.1 mg, 0.158 mmol) in *n*-hexane (5 mL) was added to a suspension of $\text{Tp}^{\text{fBu}_2\text{Me}}\text{LuMe}_2$ (50.0 mg, 0.080 mmol) in *n*-hexane (5 mL) and stirred for 6 h at ambient temperature. The reaction mixture

was filtered and the solution was concentrated in vacuo. Crystallization at $-35\text{ }^\circ\text{C}$ yielded compound 2-Lu (60.0 mg, 0.063 mmol, 80%) as colorless crystals. ^1H NMR (250 MHz, benzene- d_6 , $26\text{ }^\circ\text{C}$) δ 7.12 (s, 4H, Ar-H), 6.90 (t, $^3J(\text{HH}) = 16.2\text{ Hz}$, 2H, Ar-H), 5.62 (s, 3H, 4-pz-H), 4.73 (v br d, $^1J(\text{BH}) = 286\text{ Hz}$, 1H, BH), 3.32 (sept, $^3J(\text{HH}) = 6.8\text{ Hz}$, 4H, CH(CH₃)₂), 2.08 (s, 9H, pz-CH₃), 1.27 (s, 27H, pz-C(CH₃)₃), 1.13 (d, $^3J(\text{HH}) = 7.1\text{ Hz}$, 24H, CH(CH₃)₂) ppm. $^{13}\text{C}\{^1\text{H}\}$ NMR (63 MHz, benzene- d_6 , $26\text{ }^\circ\text{C}$) δ 165.9 (3-pz-C), 158.6 (Ar-C1), 146.3 (5-pz-C), 137.9 (Ar-C2/6), 123.6 (Ar-C3/5), 118.5 (Ar-C4), 105.0 (4-pz-C), 32.1 (pz-C(CH₃)₃), 31.4 (pz-C(CH₃)₃), 26.3 (C(CH₃)₂), 25.5 (C(CH₃)₂), 13.7 (pz-C(CH₃)₃) ppm. $^{11}\text{B}\{^1\text{H}\}$ NMR (80 MHz, benzene- d_6 , $26\text{ }^\circ\text{C}$) δ -8.6 (br s) ppm. IR (KBr) $\tilde{\nu}$ 3051 (vw), 3016 (vw), 2963 (s), 2865 (m), 2576 (vw, B–H), 1589 (w), 1515 (s), 1493 (w), 1461 (s), 1431 (vs), 1380 (s), 1363 (s), 1335 (s), 1321 (s), 1274 (s), 1256 (s), 1201 (vs), 1180 (m), 1115 (w), 1103 (w), 1071 (m), 1064 (m), 1042 (w), 1025 (w), 1018 (w), 985 (w), 934 (vw), 888 (m), 869 (m), 859 (w), 807 (s), 795 (s), 774 (s), 751 (m), 732 (m), 696 (vw), 657 (w), 646 (m), 574 (w), 517 (vw), 464 (vw) cm^{-1} . Elemental analysis calcd (%) for $\text{C}_{48}\text{H}_{74}\text{BLuN}_6\text{O}_2$: C 60.50, H 7.83, N 8.82; found C 61.21, H 8.15, N 8.58. Although these results are outside the range viewed as establishing analytical purity (C: +0.71%), they are provided to illustrate the best values obtained to date.

$\text{Tp}^{\text{fBu}_2\text{Me}}\text{Lu}(\text{OC}_6\text{H}_3(\text{CF}_3)_2\text{-3,5})_2$ (3-Lu). A precooled solution of $\text{HOC}_6\text{H}_2(\text{CF}_3)_2\text{-3,5}$ (36.3 mg, 0.158 mmol) in toluene (5 mL) was added to a precooled solution of $\text{Tp}^{\text{fBu}_2\text{Me}}\text{LuMe}_2$ (50.0 mg, 0.080 mmol) in toluene (5 mL) and stirred for 2 h at $-35\text{ }^\circ\text{C}$. The reaction mixture was filtered and the solution was concentrated in vacuo. Crystallization at $-35\text{ }^\circ\text{C}$ yielded compound 3-Lu (21.0 mg, 0.020 mmol, 37%) as colorless crystals. ^1H NMR (250 MHz, benzene- d_6 , $26\text{ }^\circ\text{C}$) δ 7.35 (s, 2H, Ar-H), 7.03 (s, 4H, Ar-H), 5.54 (s, 3H, 4-pz-H), 4.76 (v br d, 1H, $^1J(\text{BH}) = 140\text{ Hz}$, BH), 2.10 (s, 9H, pz-CH₃), 1.23 (s, 27H, pz-C(CH₃)₃) ppm. $^{13}\text{C}\{^1\text{H}\}$ NMR (63 MHz, benzene- d_6 , $26\text{ }^\circ\text{C}$) δ 165.7 (3-pz-C), 165.2 (Ar-C1), 147.5 (5-pz-C), 133.2 (Ar-CCF₃), 122.4 (Ar-C3/5), 119.4 (Ar-C2/6), 110.7 (Ar-C4), 104.5 (4-pz-C), 32.2 (pz-C(CH₃)₃), 30.4 (pz-C(CH₃)₃), 12.9 (pz-C(CH₃)₃) ppm. ^{13}C NMR resonances for the CF₃ group showed no C–F coupling. $^{11}\text{B}\{^1\text{H}\}$ NMR (80 MHz, benzene- d_6 , $26\text{ }^\circ\text{C}$) δ -8.2 (br s) ppm. $^{19}\text{F}\{^1\text{H}\}$ NMR (376 MHz, benzene- d_6 , $26\text{ }^\circ\text{C}$) δ -62.8 ppm; IR (KBr) $\tilde{\nu}$ 2972 (w), 2935 (vw), 2866 (vw), 2558 (vw, B–H), 1605 (m), 1556 (s), 1533 (vw), 1471 (m), 1466 (m), 1456 (w), 1435 (w), 1399 (s), 1385 (vs), 1360 (m), 1352 (m), 1332 (vw), 1275 (w), 1243 (w), 1204 (w), 1167 (vs), 1128 (vs), 1099 (w), 1084 (w), 1068 (w), 1028 (w), 1016 (w), 997 (m), 964 (s), 893 (w), 883 (w), 878 (vw), 859 (w), 856 (w), 845 (w), 806 (w), 799 (w), 774 (vw), 764 (w), 732 (w), 700 (w), 682 (m), 643 (w), 628 (vw), 613 (vw), 411 (vw) cm^{-1} . Elemental analysis calcd (%) for $\text{C}_{40}\text{H}_{46}\text{BF}_6\text{LuN}_6\text{O}_2$: C 45.47, H 4.39, N 7.95; found C 46.00, H 3.53, N 8.52. Although these results are outside the range viewed as establishing analytical purity (C: +0.53%, H: -0.86%, N: +0.57%), they are provided to illustrate the best values obtained to date. Due to the high F content, no better elemental analysis could be obtained.

$\text{Tp}^{\text{fBu}_2\text{Me}}\text{YMe}(\text{OC}_6\text{H}_2\text{tBu}_2\text{-2,6-Me-4})$ (4-Y). A precooled solution of $\text{HOC}_6\text{H}_2\text{tBu}_2\text{-2,6-Me-4}$ (18.0 mg, 0.082 mmol) in *n*-hexane (5 mL) was added to a precooled suspension of $\text{Tp}^{\text{fBu}_2\text{Me}}\text{YMe}(\text{AlMe}_4)$ (50.0 mg, 0.081 mmol) in *n*-hexane (5 mL) at $-35\text{ }^\circ\text{C}$. The suspension was stirred for 2 h at $-35\text{ }^\circ\text{C}$. The reaction mixture was evaporated to dryness in vacuo and washed with *n*-hexane (3 × 2 mL). Crystallization from toluene yielded compound 4-Y (47 mg, 0.063 mmol, 78%). ^1H NMR (500 MHz, toluene- d_8 , $26\text{ }^\circ\text{C}$) δ 7.17 (s, 2H, Ar-H), 5.50 (s, 3H, 4-pz-H), 4.55 (v br d, $^1J(\text{BH}) = 100\text{ Hz}$, 1H, BH), 2.39 (s, 3H, C(CH₃)₃), 1.99 (br s, 9H, pz-CH₃), 1.55 (s, 18H, C(CH₃)₃), 1.29 (s, 27H, pz-C(CH₃)₃), 0.27 (br s, 3H, YCH₃) ppm. ^1H NMR (500 MHz, THF- d_8 , $0\text{ }^\circ\text{C}$) δ 6.70 (s, 2H, Ar-H), 6.20 (s, 3H, 4-pz-H), 4.74 (v br d, $^1J(\text{BH}) = 100\text{ Hz}$, 1H, BH), 2.44 (s, 3H, C(CH₃)₃), 2.09 (br s, 9H, pz-CH₃), 1.43 (s, 18H, C(CH₃)₃), 1.37 (s, 27H, pz-C(CH₃)₃), -0.36 (d, 3H, $^2J(\text{YH}) = 1.8\text{ Hz}$, YCH₃) ppm. $^{13}\text{C}\{^1\text{H}\}$ NMR (101 MHz, THF- d_8 , $0\text{ }^\circ\text{C}$) δ 165.2 (3-pz-C), 159.6 (Ar-C1), 149.2 (5-pz-C), 138.6 (Ar-C2/6), 124.8 (Ar-C3/5), 119.9

(Ar-C4), 105.8 (4-pz-C), 35.4 (Ar-C(CH₃)₃), 32.9 (pz-C(CH₃)₃), 31.5 (Ar-C(CH₃)₃), 31.1 (pz-C(CH₃)₃), 26.8 (d, ¹J(YC) = 44.6 Hz, YCH₃), 21.5 (Ar-C(CH₃)₃), 13.6 (pz-C(CH₃)₃) ppm. ¹¹B{¹H} NMR (80 MHz, benzene-*d*₆, 26 °C) δ -8.8 (br s) ppm. ⁸⁹Y NMR (from ¹H-⁸⁹Y HSQC, 25 MHz, THF-*d*₈, 0 °C) δ 556 ppm; IR (KBr) $\tilde{\nu}$ 2957 (s), 2931 (m), 2857 (m), 2566 (vw, B-H), 1539 (s), 1489 (vw), 1473 (m), 1464 (m), 1458 (m), 1426 (vs), 1382 (w), 1354 (m), 1348 (m), 1325 (w), 1286 (s), 1261 (vw), 1240 (vw), 1184 (m), 1161 (vs), 1135 (w), 1071 (m), 1062 (w), 1028 (w), 984 (vw), 888 (vw), 866 (m), 859 (m), 859 (w), 847 (m), 812 (w), 804 (w), 788 (w), 779 (w), 760 (s), 730 (vw), 682 (m), 675 (m), 659 (m), 644 (m), 590 (vw), 575 (vw), 548 (w), 524 (w), 472 (vw), 439 (vw), 426 (m) cm⁻¹. Elemental analysis calcd (%) for C₄₀H₆₆BN₆OY: C 64.34, H 8.91, N 11.25; found C 63.65, H 8.43, N 10.38. Although these results are outside the range viewed as establishing analytical purity (C: -0.79%, N: -0.87%), they are provided to illustrate the best values obtained to date. Due to fast decomposition at ambient temperature no better elemental analysis could be obtained.

Tp^{tBu,Me}LuMe(OC₆H₂tBu₂-2,6-Me-4) (4-Lu). A solution of HOC₆H₂tBu₂-2,6-Me-4 (35.0 mg, 0.159 mmol) in *n*-hexane (5 mL) was added to a suspension of Tp^{tBu,Me}LuMe₂ (100 mg, 0.158 mmol) in *n*-hexane (5 mL) and stirred for 6 h at ambient temperature. The solution was filtered and concentrated in vacuo. Crystallization at -35 °C yielded compound 4-Lu (100 mg, 0.121 mmol, 77%) as colorless crystals. ¹H NMR (400 MHz, benzene-*d*₆, 26 °C) δ 7.17 (s, 2H, Ar-H), 5.66 (s, 3H, 4-pz-H), 4.66 (v br d, ¹J(BH) = 100 Hz, 1H, BH), 2.30 (s, 3H, C(CH₃)₃), 2.08 (br s, 9H, pz-CH₃), 1.40 (br s, 45H, C(CH₃)₃), 0.67 (s, 3H, LuCH₃) ppm. ¹³C{¹H} NMR (101 MHz, benzene-*d*₆, 26 °C) δ 166.0 (3-pz-C), 162.5 (Ar-C1), 138.6 (5-pz-C), 126.1 (Ar-C3/5), 124.1 (Ar-C4), 120.4 (Ar-C2/6), 104.9 (4-pz-C), 40.4 (Lu-CH₃), 32.5 (Ar-C(CH₃)₃), 31.0 (C(CH₃)₃), 21.3 (Ar-C(CH₃)₃), 13.4 (pz-C(CH₃)₃) ppm. ¹¹B{¹H} NMR (80 MHz, benzene-*d*₆, 26 °C) δ -8.1 (br s) ppm; IR (KBr) $\tilde{\nu}$ 3067 (vw), 3026 (vw), 2961 (vs), 2928 (s), 2865 (m), 2563 (w, B-H), 1544 (vs), 1464 (m), 1428 (vs), 1409 (s), 1353 (s), 1328 (m), 1264 (vs), 1232 (vs), 1217 (vs), 1198 (s), 1170 (m), 1155 (w), 1129 (w), 1121 (w), 1070 (m), 1055 (m), 1025 (m), 1017 (m), 1004 (w), 984 (w), 889 (vw), 861 (vw), 849 (m), 823 (m), 808 (m), 793 (m), 779 (m), 767 (m), 731 (w), 679 (w), 646 (w), 639 (w), 525 (m), 512 (w), 503 (w), 438 (w), 404 (w) cm⁻¹. Elemental analysis calcd (%) for C₄₀H₆₆BLuN₆O: C 57.69, H 7.99, N 10.09; found C 58.27, H 8.19, N 9.86. Although these results are outside the range viewed as establishing analytical purity (C: +0.58%), they are provided to illustrate the best values obtained to date.

Tp^{tBu,Me}YMe(OC₆H₃Me₂-2,6) (5-Y). A suspension of KOC₆H₃Me₂-2,6 (26.1 mg, 0.163 mmol) in toluene (5 mL) was added to a solution of Tp^{tBu,Me}YMe(AlMe₄) (100 mg, 0.163 mmol) in toluene (5 mL). The reaction mixture was stirred for 6 h at ambient temperature. The precipitate was removed by filtration and the solution was concentrated in vacuo. Crystallization at -35 °C yielded compound 5-Y (62.0 mg, 0.096 mmol, 59%) as colorless crystals. ¹H NMR (250 MHz, benzene-*d*₆, 26 °C) δ 7.01 (d, 2H, ³J(HH) = 7.3 Hz, Ar-H), 6.66 (t, ³J(HH) = 14.4 Hz, 1H, Ar-H), 5.57 (s, 3H, 4-pz-H), 4.72 (v br d, 1H, ¹J(BH) = 130 Hz, BH), 2.12 (s, 9H, pz-CH₃), 1.82 (s, 6H, C(CH₃)₃), 1.36 (s, 27H, pz-C(CH₃)₃), 0.46 (d, 3H, ²J(YH) = 1.8 Hz, YCH₃) ppm. ¹³C{¹H} NMR (63 MHz, benzene-*d*₆, 26 °C) δ 165.1 (3-pz-C), 161.9 (Ar-C1), 146.3 (5-pz-C), 128.2 (Ar-C2/6), 126.8 (Ar-C3/5), 116.8 (Ar-C4), 103.8 (4-pz-C), 32.6 (pz-C(CH₃)₃), 31.0 (pz-C(CH₃)₃), 22.5 (d, YCH₃, ²J(YC) = 51.2 Hz), 17.1 (Ar-C(CH₃)₃), 13.4 (pz-C(CH₃)₃) ppm. ¹¹B{¹H} NMR (80 MHz, benzene-*d*₆, 26 °C) δ -8.9 (br s) ppm. ⁸⁹Y NMR (from ¹H-⁸⁹Y HSQC, 25 MHz, benzene-*d*₆, 26 °C) δ 580 ppm; IR (KBr) $\tilde{\nu}$ 3002 (vw), 2961 (vs), 2927 (m), 2862 (m), 2569 (vw, B-H), 1589 (w), 1541 (s), 1464 (vs), 1425 (vs), 1381 (w), 1359 (s), 1348 (m), 1336 (vw), 1308 (vs), 1284 (s), 1238 (s), 1197 (vs), 1173 (m), 1119 (w), 1090 (m), 1074 (m), 1063 (m), 1026 (m), 1013 (w), 986 (w), 876 (w), 862 (w), 848 (vw), 802 (s), 787 (m), 766 (m), 756 (s), 757 (s), 745 (w), 730 (w), 708 (w), 657 (vw), 657 (m), 645 (m), 537 (w), 514 (vw), 478 (vw), 464 (w), 420 (w) cm⁻¹. Elemental analysis calcd

(%) for C₃₃H₅₂BN₆OY: C 61.12, H 8.08, N 12.96; found C 61.43, H 8.15, N 12.78.

Tp^{tBu,Me}LuMe(OC₆H₃Me₂-2,6) (5-Lu). A suspension of KOC₆H₃Me₂-2,6 (23.0 mg, 0.144 mmol) in toluene (5 mL) was added to a solution of Tp^{tBu,Me}LuMe(AlMe₄) (100 mg, 0.143 mmol) in toluene (5 mL). The reaction mixture was stirred for 6 h at ambient temperature. The precipitate was removed by filtration and the solution was concentrated in vacuo. Crystallization at -35 °C yielded compound 5-Lu (51.0 mg, 0.069 mmol, 48%) as colorless crystals. ¹H NMR (250 MHz, benzene-*d*₆, 26 °C) δ 7.02 (d, 2H, ³J(HH) = 7.4 Hz, Ar-H), 6.66 (t, ³J(HH) = 13.4 Hz, 1H, Ar-H), 5.62 (s, 3H, 4-pz-H), 4.69 (v br d, 1H, ¹J(BH) = 150 Hz, BH), 2.12 (s, 9H, pz-CH₃), 1.82 (s, 6H, C(CH₃)₃), 1.39 (s, 27H, pz-C(CH₃)₃), 0.55 (s, 3H, Lu-CH₃) ppm. ¹³C{¹H} NMR (63 MHz, benzene-*d*₆, 26 °C) δ 165.8 (3-pz-C), 161.9 (Ar-C1), 146.3 (5-pz-C), 128.3 (Ar-C2/6), 127.0 (Ar-C3/5), 116.8 (Ar-C4), 104.0 (4-pz-C), 32.5 (pz-C(CH₃)₃), 32.2 (Lu-CH₃), 31.1 (pz-C(CH₃)₃), 17.1 (Ar-C(CH₃)₃), 13.3 (pz-C(CH₃)₃) ppm. ¹¹B{¹H} NMR (80 MHz, benzene-*d*₆, 26 °C) δ -8.5 ppm. IR (KBr) $\tilde{\nu}$ 3002 (vw), 2962 (s), 2909 (m), 2863 (w), 2863 (vw), 2571 (vw, B-H), 1589 (vw), 1542 (s), 1465 (s), 1435 (vs), 1360 (s), 1351 (m), 1338 (w), 1307 (vw), 1288 (vs), 1239 (m), 1198 (s), 1174 (vs), 1132 (w), 1090 (w), 1075 (m), 1062 (m), 1027 (w), 1013 (w), 987 (w), 877 (w), 863 (w), 849 (vw), 804 (w), 788 (s), 768 (s), 757 (s), 745 (w), 731 (vw), 708 (w), 676 (vw), 657 (vw), 645 (m), 537 (w), 516 (w), 487 (vw), 401 (m) cm⁻¹. Elemental analysis calcd (%) for C₃₃H₅₂BLuN₆O: C 53.96, H 7.14, N 11.44; found C 53.88, H 6.99, N 11.37.

Tp^{tBu,Me}YMe(OC₆H₃iPr₂-2,6) (6-Y). A suspension of KOC₆H₃iPr₂-2,6 (35.3 mg, 0.163 mmol) in toluene (5 mL) was added to a solution of Tp^{tBu,Me}YMe(AlMe₄) (100 mg, 0.163 mmol) in toluene (5 mL). The reaction mixture was stirred for 6 h at ambient temperature. The precipitate was removed by filtration and the solution was concentrated in vacuo. Crystallization at -35 °C yielded compound 6-Y (64.0 mg, 0.091 mmol, 56%) as colorless crystals. ¹H NMR (250 MHz, benzene-*d*₆, 26 °C) δ 7.13 (d, ³J(HH) = 7.6 Hz, Ar-H), 6.85 (t, ³J(HH) = 15.1 Hz, 1H, Ar-H), 5.60 (s, 3H, 4-pz-H), 4.73 (v br d, ¹J(BH) = 286 Hz, 1H, BH), 3.09 (br s, 2H, CH(CH₃)₂), 2.13 (s, 9H, pz-CH₃), 1.39 (s, 27H, pz-C(CH₃)₃), 1.12 (d, ³J(HH) = 7.0 Hz, 12H, CH(CH₃)₂), 0.50 (d, 3H, ²J(YH) = 1.9 Hz, YCH₃) ppm. ¹³C{¹H} NMR (63 MHz, benzene-*d*₆, 26 °C) δ 165.3 (3-pz-C), 158.7 (Ar-C1), 146.3 (5-pz-C), 138.0 (Ar-C2/6), 123.0 (Ar-C3/5), 117.7 (Ar-C4), 104.3 (4-pz-C), 32.3 (pz-C(CH₃)₃), 32.1 (Y-CH₃), 31.1 (pz-C(CH₃)₃), 25.8 (Ar-CH(CH₃)₂), 24.5 (Ar-CH(CH₃)₂), 13.3 (pz-C(CH₃)₃) ppm. ¹¹B{¹H} NMR (80 MHz, benzene-*d*₆, 26 °C) δ -8.5 (br s) ppm. ⁸⁹Y NMR (from ¹H-⁸⁹Y HSQC, 25 MHz, benzene-*d*₆, 26 °C) δ 578 ppm; IR (KBr) $\tilde{\nu}$ 3017 (vw), 2960 (s), 2862 (w), 2558 (vw, B-H), 1587 (vw), 1540 (s), 1458 (m), 1433 (s), 1379 (w), 1354 (m), 1335 (s), 1274 (s), 1241 (w), 1209 (m), 1194 (m), 1175 (m), 1119 (vw), 1074 (w), 1011 (vw), 984 (vw), 888 (w), 866 (w), 798 (m), 766 (m), 750 (m), 730 (w), 695 (w), 679 (w), 660 (w), 646 (w), 570 (vw), 515 (vw), 464 (vw), 437 (vw), 403 (w) cm⁻¹. Elemental analysis calcd (%) for C₃₇H₆₀BN₆OY: C 63.07, H 8.58, N 11.93; found C 62.74, H 8.49, N 11.67.

Tp^{tBu,Me}LuMe(OC₆H₃iPr₂-2,6) (6-Lu). A suspension of KO-C₆H₃iPr₂-2,6 (31.1 mg, 0.144 mmol) in toluene (5 mL) was added to a solution of Tp^{tBu,Me}LuMe(AlMe₄) (100 mg, 0.143 mmol) in toluene (5 mL). The reaction mixture was stirred for 6 h at ambient temperature. The precipitate was removed by filtration and the solution was concentrated in vacuo. Crystallization at -35 °C yielded compound 6-Lu (80.0 mg, 0.101 mmol, 71%) as colorless crystals. ¹H NMR (250 MHz, benzene-*d*₆, 26 °C) δ 7.11 (d, ³J(HH) = 7.5 Hz, 2H, Ar-H), 6.85 (t, ³J(HH) = 15.1 Hz, 1H, Ar-H), 5.60 (s, 3H, 4-pz-H), 4.70 (v br d, ¹J(BH) = 150 Hz, 1H, BH), 3.08 (br s, 2H, CH(CH₃)₂), 2.12 (s, 9H, pz-CH₃), 1.38 (s, 27H, pz-C(CH₃)₃), 1.11 (br s, 12H, CH(CH₃)₂), 0.50 (s, 3H, Lu-CH₃) ppm. ¹³C{¹H} NMR (63 MHz, benzene-*d*₆, 26 °C) δ 165.5 (3-pz-C), 158.6 (Ar-C1), 146.3 (5-pz-C), 137.7 (Ar-C2/6), 122.9 (Ar-C3/5), 117.8 (Ar-C4), 104.3 (4-pz-C), 32.4 (pz-C(CH₃)₃), 32.1 (Lu-CH₃), 31.1 (pz-C(CH₃)₃), 25.8 (Ar-CH(CH₃)₂), 24.5 (Ar-CH(CH₃)₂), 13.3 (pz-C(CH₃)₃) ppm. ¹¹B{¹H} NMR (80 MHz, benzene-*d*₆, 26 °C) δ -8.5 (br s)

ppm; IR (KBr) $\tilde{\nu}$ 2964 (s), 2863 (w), 2564 (vw, B–H), 1542 (s), 1488 (vw), 1472 (w), 1463 (m), 1456 (m), 1435 (vs), 1380 (vw), 1355 (m), 1339 (s), 1277 (m), 1241 (w), 1210 (w), 1194 (m), 1174 (m), 1139 (vw), 1099 (vw), 1073 (m), 1061 (w), 1043 (vw), 1028 (w), 1013 (vw), 989 (vw), 892 (w), 870 (w), 848 (vw), 805 (w), 790 (s), 766 (m), 747 (m), 696 (vw), 677 (vw), 661 (vw), 646 (w), 640 (w), 572 (vw), 517 (w), 491 (vw), 421 (vw), 401 (w) cm^{-1} . Elemental analysis calcd (%) for $\text{C}_7\text{H}_6\text{BLuN}_6\text{O}$: C 56.20, H 7.65, N 10.63; found C 56.50, H 7.64, N 10.68.

$\text{Tp}^{\text{tBu,Me}^y\text{Me}}[\text{OC}_6\text{H}_3(\text{CF}_3)_2\text{-3,5}]$ (7-Y). A precooled solution of $\text{KOC}_6\text{H}_3(\text{CF}_3)_2\text{-3,5}$ (40.1 mg, 0.150 mmol) in toluene (5 mL) was added to a precooled suspension of $\text{Tp}^{\text{tBu,Me}^y\text{Me}}(\text{AlMe}_4)$ (75.0 mg, 0.122 mmol) in toluene (5 mL) at -35°C . The suspension was stirred for 4 h at -35°C . The precipitate was removed by filtration and the solution was concentrated in vacuo. Crystallization at -35°C yielded compound 7-Y (79.0 mg, 0.104 mmol, 69%) as colorless crystals. ^1H NMR (250 MHz, benzene- d_6 , 26°C) δ 6.98 (s, 1H, Ar-H), 6.36 (s, 2H, Ar-H), 5.53 (s, 3H, 4-pz-H), 4.73 (v br d, 1H, $^1\text{J}(\text{BH}) = 150\text{ Hz}$, BH), 2.12 (s, 9H, pz- CH_3), 1.32 (s, 27H, pz- $\text{C}(\text{CH}_3)_3$), 0.27 (d, 3H, $^2\text{J}(\text{YH}) = 1.8\text{ Hz}$, Y- CH_3) ppm. $^{13}\text{C}\{^1\text{H}\}$ NMR (63 MHz, benzene- d_6 , 26°C) δ 165.0 (Ar-C1), 164.8 (3-pz-C), 147.0 (5-pz-C), 132.2 (Ar-CCF $_3$), 121.2 (Ar-C4), 119.4 (Ar-C2/6), 109.3 (Ar-C3/5), 103.7 (4-pz-C), 32.4 (pz- $\text{C}(\text{CH}_3)_3$), 31.1 (pz- $\text{C}(\text{CH}_3)_3$), 22.3 (d, $^2\text{J}(\text{YC}) = 50.8\text{ Hz}$, Y- CH_3), 13.1 (pz- $\text{C}(\text{CH}_3)_3$) ppm. ^{13}C NMR resonances for the CF_3 groups showed no C–F coupling. $^{11}\text{B}\{^1\text{H}\}$ NMR (80 MHz, benzene- d_6 , 26°C) δ -7.9 (br s) ppm. $^{19}\text{F}\{^1\text{H}\}$ NMR (376 MHz, benzene- d_6 , 26°C) δ -62.6 ppm. ^{89}Y NMR (from ^1H – ^{89}Y HSQC, 25 MHz, benzene- d_6 , 26°C) δ 620 ppm; IR (KBr) $\tilde{\nu}$ 2966 (m), 2933 (w), 2907 (w), 2861 (w), 2559 (w, B–H), 1601 (w), 1558 (vw), 1541 (vs), 1506 (vw), 1471 (s), 1458 (s), 1447 (m), 1435 (s), 1392 (vs), 1359 (s), 1351 (m), 1334 (w), 1311 (vw), 1273 (vs), 1252 (w), 1242 (w), 1205 (m), 1194 (m), 1170 (vs), 1123 (vs), 1100 (w), 1073 (m), 1064 (m), 1027 (m), 1013 (w), 996 (w), 986 (w), 963 (s), 882 (w), 876 (w), 866 (w), 843 (w), 802 (s), 765 (s), 731 (w), 681 (m), 658 (w), 643 (m), 622 (w), 612 (m), 569 (vw), 516 (w), 472 (w), 464 (w), 442 (w), 409 (s) cm^{-1} . Elemental analysis calcd (%) for $\text{C}_{33}\text{H}_{46}\text{BF}_6\text{N}_6\text{OY}$: C 52.40, H 6.13, N 11.11; found C 52.78, H 6.25, N 11.21.

$\text{Tp}^{\text{tBu,Me}^y\text{LuMe}}[\text{OC}_6\text{H}_3(\text{CF}_3)_2\text{-3,5}]$ (7-Lu). A suspension of $\text{KOC}_6\text{H}_3(\text{CF}_3)_2\text{-3,5}$ (38.2 mg, 0.142 mmol) in toluene (5 mL) was added to a solution of $\text{Tp}^{\text{tBu,Me}^y\text{LuMe}}(\text{AlMe}_4)$ (100 mg, 0.142 mmol) in toluene (5 mL). The reaction mixture was stirred for 6 h at ambient temperature. The precipitate was removed by filtration and the solution was concentrated in vacuo. Crystallization at -35°C yielded compound 7-Lu (80.0 mg, 0.095 mmol, 67%) as colorless crystals. ^1H NMR (250 MHz, benzene- d_6 , 26°C) δ 7.03 (s, 1 H, Ar-H), 6.34 (s, 2H, Ar-H), 5.57 (s, 3H, 4-pz-H), 4.66 (v br d, 1H, $^1\text{J}(\text{BH}) = 120\text{ Hz}$, BH), 2.12 (s, 9H, pz- CH_3), 1.35 (s, 27H, pz- $\text{C}(\text{CH}_3)_3$), 0.37 (s, 3H, Lu- CH_3) ppm. $^{13}\text{C}\{^1\text{H}\}$ NMR (63 MHz, benzene- d_6 , 26°C) δ 165.7 (3-pz-C), 165.5 (Ar-C1), 147.0 (5-pz-C), 132.1 (Ar-CCF $_3$), 126.9 (Ar-C4), 119.5 (Ar-C2/6), 109.2 (Ar-C3/5), 104.2 (4-pz-C), 32.3 (pz- $\text{C}(\text{CH}_3)_3$), 32.2 (Lu- CH_3), 31.0 (pz- $\text{C}(\text{CH}_3)_3$), 13.0 (pz- $\text{C}(\text{CH}_3)_3$) ppm. ^{13}C NMR resonances for the CF_3 group showed no C–F coupling. $^{11}\text{B}\{^1\text{H}\}$ NMR (80 MHz, benzene- d_6 , 26°C) δ -8.3 (br s) ppm. $^{19}\text{F}\{^1\text{H}\}$ NMR (376 MHz, benzene- d_6 , 26°C) δ -62.6 ppm; IR (KBr) $\tilde{\nu}$ 2963 (m), 2936 (m), 2910 (w), 2862 (w), 2560 (w, B–H), 1601 (m), 1541 (s), 1470 (s), 1433 (m), 1391 (vs), 1357 (m), 1334 (w), 1310 (vw), 1273 (vs), 1251 (w), 1242 (w), 1195 (m), 1169 (vs), 1125 (vs), 1099 (w), 1071 (m), 1062 (m), 1028 (w), 1015 (w), 996 (w), 986 (w), 963 (m), 881 (w), 866 (w), 843 (w), 802 (m), 765 (m), 731 (w), 704 (w), 680 (m), 658 (vw), 643 (w), 612 (w), 516 (vw), 410 (w), 403 (w) cm^{-1} . Elemental analysis calcd (%) for $\text{C}_{33}\text{H}_{46}\text{BF}_6\text{LuN}_6\text{O}$: C 47.04, H 5.50, N 9.97; found C 47.52, H 5.42, N 10.11.

$[\text{Tp}^{\text{tBu,Me}^y\text{Me}}(\text{dmap})_2][\text{Me}_3\text{Al}(\text{OC}_6\text{H}_2\text{tBu}_2\text{-2,6-Me-4})]$ (8-Y). A solution of $\text{HOC}_6\text{H}_2\text{tBu}_2\text{-2,6-Me-4}$ (35.9 mg, 0.163 mmol) in toluene (5 mL) was added to a solution of $\text{Tp}^{\text{tBu,Me}^y\text{Me}}(\text{AlMe}_4)$ (100 mg, 0.163 mmol) in toluene (5 mL). A solution of dmap (29.8 mg, 0.243 mmol) in *n*-hexane (1 mL) was added to the solution and the reaction mixture was stirred for 1 h at ambient temperature. The precipitate

was allowed to settle and washed with cold toluene ($3 \times 2\text{ mL}$). The precipitate was dried in vacuo and gave 8-Y as white solid (80.0 mg, 0.075 mmol, 46%). Crystals suitable for XRD analysis could be obtained by performing the reaction under the same conditions without stirring. ^1H NMR (500 MHz, THF- d_8 , 0°C) δ 7.70 (br s, 4H, dmap), 6.70 (s, 2H, Ar-H), 6.44 (s br, 4H, dmap), 6.03 (s, 3H, 4-pz-H), 4.93 (v br d, $^1\text{J}(\text{BH}) = 100\text{ Hz}$, 1H, BH), 2.95 (s br, 12H, dmap, N(CH_3) $_2$), 2.50 (s, 9H, pz- CH_3), 2.08 (s, 3H, C(CH_3) $_3$), 1.37 (s, 18H, C(CH_3) $_3$), 1.09 (s, 27H, pz- $\text{C}(\text{CH}_3)_3$), -0.09 (s br, 3H, YCH $_3$), -1.01 (s, 9H, AlCH $_3$) ppm. $^{13}\text{C}\{^1\text{H}\}$ NMR (101 MHz, THF- d_8 , 26°C) δ 165.2 (3-pz-C), 159.9 (Ar-C1), 155.7 (C3, dmap), 149.7 (5-pz-C), 148.4 (C1, dmap), 138.8 (Ar-C2/6), 124.8 (Ar-C3/5), 120.8 (Ar-C4), 107.2 (4-pz-C), 105.8 (C2, dmap), 38.8 (NCH $_3$, dmap), 35.4 (Ar-C(CH_3) $_3$), 32.7 (pz- $\text{C}(\text{CH}_3)_3$), 31.7 (pz- $\text{C}(\text{CH}_3)_3$), 30.9 (Ar-C(CH_3) $_3$), 26.9 (d, $^2\text{J}(\text{YC}) = 47.4\text{ Hz}$, Y- CH_3), 21.5 (Ar-C(CH_3) $_3$), 13.6 (pz- $\text{C}(\text{CH}_3)_3$), -2.7 (AlCH $_3$) ppm. $^{11}\text{B}\{^1\text{H}\}$ NMR (80 MHz, THF- d_8 , 26°C) δ -8.7 ppm. ^{89}Y NMR (from ^1H – ^{89}Y HSQC, 25 MHz, THF- d_8 , 26°C) δ 555 ppm; IR (KBr) $\tilde{\nu}$ 3057 (vw), 3016 (w), 2958 (s), 2915 (m), 2863 (w), 2723 (vw), 2561 (vw, B–H), 1640 (m), 1616 (s), 1557 (m), 1539 (vs), 1456 (m), 1436 (m), 1418 (s), 1386 (m), 1355 (m), 1313 (w), 1286 (w), 1265 (m), 1236 (s), 1200 (m), 1160 (w), 1132 (w), 1120 (w), 1066 (m), 1037 (vw), 1023 (w), 1004 (s), 985 (w), 949 (w), 887 (vw), 861 (w), 833 (m), 819 (m), 806 (m), 792 (w), 781 (m), 760 (w), 729 (w), 689 (w), 646 (w), 614 (vw), 533 (w), 520 (w), 502 (vw), 458 (vw), 439 (vw), 419 (vw), 412 (vw) cm^{-1} . Elemental analysis calcd (%) for $\text{C}_{37}\text{H}_{95}\text{AlBN}_6\text{OY}$: C 64.40, H 9.01, N 13.17, found C 64.91, H 8.54, N 13.74. Although these results are outside the range viewed as establishing analytical purity (C: +0.51%, N: +0.57%), they are provided to illustrate the best values obtained to date.

$[\text{Tp}^{\text{tBu,Me}^y\text{LuMe}}(\text{dmap})_2][\text{Me}_3\text{Al}(\text{OC}_6\text{H}_2\text{tBu}_2\text{-2,6-Me-4})]$ (8-Lu). A solution of $\text{HOC}_6\text{H}_2\text{tBu}_2\text{-2,6-Me-4}$ (15.7 mg, 0.071 mmol) in toluene (5 mL) was added to a solution of $\text{Tp}^{\text{tBu,Me}^y\text{LuMe}}(\text{AlMe}_4)$ (50.0 mg, 0.071 mmol) in toluene (5 mL). A solution of dmap (26.1 mg, 0.214 mmol) in *n*-hexane (1 mL) was added to the solution and the reaction mixture was stirred for 1 h at ambient temperature. The precipitate was allowed to settle and washed with cold toluene ($3 \times 2\text{ mL}$). The solid was dried in vacuo and gave 8-Lu as white solid (25.0 mg, 0.022 mmol, 31%). Crystals could be obtained by performing the reaction under the same conditions without stirring. ^1H NMR (500 MHz, THF- d_8 , 26°C) δ 7.82 (br s, 4H, dmap), 6.70 (s, 2H, Ar-H), 6.45 (s br, 4H, dmap), 6.04 (s, 3H, 4-pz-H), 4.94 (v br d, $^1\text{J}(\text{BH}) = 100\text{ Hz}$, 1H, BH), 2.95 (s br, 12H, dmap, N(CH_3) $_2$), 2.50 (s, 9H, pz- CH_3), 2.10 (s, 3H, C(CH_3) $_3$), 1.38 (s, 18H, C(CH_3) $_3$), 1.12 (s, 27H, pz- $\text{C}(\text{CH}_3)_3$), -0.09 (s br, 3H, YCH $_3$), -1.01 (s, 9H, AlCH $_3$) ppm. $^{13}\text{C}\{^1\text{H}\}$ NMR (101 MHz, THF- d_8 , 26°C) δ 165.1 (3-pz-C), 159.8 (Ar-C1), 155.8 (C3, dmap), 149.6 (5-pz-C), 148.3 (C1, dmap), 138.7 (Ar-C2/6), 124.8 (Ar-C3/5), 120.8 (Ar-C4), 107.1 (4-pz-C), 105.7 (C2, dmap), 38.8 (NCH $_3$, dmap), 35.4 (Ar-C(CH_3) $_3$), 32.7 (pz- $\text{C}(\text{CH}_3)_3$), 31.6 (pz- $\text{C}(\text{CH}_3)_3$), 30.9 (Ar-C(CH_3) $_3$), 26.7 (Lu- CH_3), 21.4 (Ar-C(CH_3) $_3$), 13.6 (pz- $\text{C}(\text{CH}_3)_3$) ppm. ^{13}C NMR resonances for the AlCH $_3$ group could not be detected. $^{11}\text{B}\{^1\text{H}\}$ NMR (80 MHz, THF- d_8 , 26°C) δ -8.8 ppm. IR (KBr) $\tilde{\nu}$ 2959 (m), 2909 (m), 2812 (vw), 2563 (vw, B–H), 1616 (vs), 1543 (vs), 1506 (w), 1487 (w), 1457 (m), 1422 (s), 1393 (m), 1351 (m), 1327 (w), 1288 (m), 1267 (vw), 1238 (s), 1195 (m), 1182 (m), 1168 (m), 1117 (w), 1063 (m), 1023 (w), 1003 (vs), 986 (w), 949 (vw), 888 (vw), 862 (w), 848 (m), 818 (m), 809 (m), 798 (m), 782 (w), 770 (w), 761 (vw), 728 (vw), 681 (s), 642 (w), 612 (w), 554 (w), 537 (w), 511 (w), 480 (vw), 442 (vw), 412 (w) cm^{-1} . Elemental analysis calcd (%) for $\text{C}_{37}\text{H}_{95}\text{AlBLuN}_6\text{O}$: C 59.57, H 8.33, N 12.19, found C 60.09, H 8.21, N 12.41. Although these results are outside the range viewed as establishing analytical purity (C: +0.52%), they are provided to illustrate the best values obtained to date.

Thermal Activation of 4-Lu (9-Lu). In a glovebox, compound 4-Lu was dissolved in benzene- d_6 and placed in a J. Young valve NMR tube. The NMR tube was heated to 60°C for 2 h, and a color change from colorless to slight yellow was observed. The deuterated solvent was evaporated, and few crystals suitable for XRD could be obtained from a saturated solution of 9-Lu in toluene at -35°C .

X-ray Crystallography and Crystal Structure Determinations. Single crystals of 1-Lu, 2-Lu, 3-Lu, 4-Lu, 5-Ln, 6-Ln, 7-Ln, 8-Y, and 9-Lu were grown by standard techniques from saturated solutions in *n*-hexane, toluene, or THF at $-35\text{ }^{\circ}\text{C}$ as stated in the [Experimental Section](#). Suitable crystals were collected in a glovebox and coated with Parabar 10312 (previously known as Paratone N, Hampton Research) and fixed on a nylon loop/glass fiber. X-ray data for all compounds were collected on a Bruker APEX II DUO instrument equipped with an $I\mu\text{S}$ microfocus sealed tube and QUAZAR optics for $\text{MoK}\alpha$ ($\lambda = 0.71073\text{ \AA}$) and $\text{CuK}\alpha$ ($\lambda = 1.54184\text{ \AA}$) radiation. The data collection strategy was determined using COSMO⁶¹ employing ω -scans. Raw data were processed using APEX⁶² and SAINT,⁶³ corrections for absorption effects were applied using SADABS.⁶⁴ The structures were solved by direct methods and refined against all data by full-matrix least-squares methods on F^2 using SHELXTL⁶⁵ and ShelXle.⁶⁶ Disorder models were calculated using DSR, a program for refining structures in ShelXl.⁶⁷ Compound 7-Y was refined as a twin, using hklf4 format. Restraints were given (RIGU/ISOR) because the complex showed additional disorder. 7-Lu was also twinned, and refinement in hklf5 format decreased the $wR2$ from 0.48 to 0.085. Restraints were given for the disordered CF_3 groups. All graphics were produced employing ORTEP-3⁶⁸ and POV-Ray.⁶⁹ Further details of the refinement and crystallographic data are listed in [Table S1](#) (SI) and in the CIF files (CCDC depositions 1952857–1952868).

■ ASSOCIATED CONTENT

Supporting Information

The Supporting Information is available free of charge on the ACS Publications website at DOI: [10.1021/acs.organomet.9b00631](https://doi.org/10.1021/acs.organomet.9b00631).

NMR spectra and crystallographic data for compounds 1-Lu, 2-Lu, 3-Lu, 4-Lu, 5-Ln, 6-Ln, 7-Ln, 8-Y, and 9-Lu, as well as cone angle calculations (PDF)

Structure data (XYZ)

Accession Codes

CCDC 1952857–1952868 contain the supplementary crystallographic data for this paper. These data can be obtained free of charge via www.ccdc.cam.ac.uk/data_request/cif, or by emailing data_request@ccdc.cam.ac.uk, or by contacting The Cambridge Crystallographic Data Centre, 12 Union Road, Cambridge CB2 1EZ, UK; fax: +44 1223 336033.

■ AUTHOR INFORMATION

Corresponding Author

*E-mail: reiner.anwander@uni-tuebingen.de.

ORCID

Cäcilia Maichle-Mössmer: 0000-0001-7638-1610

Reiner Anwander: 0000-0002-1543-3787

Notes

The authors declare no competing financial interest.

■ ACKNOWLEDGMENTS

We are grateful to the German Science Foundation for financial support (Grant: AN 238/15-2).

■ REFERENCES

- (1) Mingos, D. M. P.; Carabtree, R. H. *Comprehensive Organometallic Chemistry III*; Elsevier Science, 2006; Vol. 4.01.
- (2) Zimmermann, M.; Anwander, R. Homoleptic rare-earth metal complexes containing Ln-C sigma-bonds. *Chem. Rev.* **2010**, *110*, 6194–6259.

- (3) Schumann, H.; Müller, J. Tris[(N,N,N',N'-tetramethylethylenediamin)lithium]-hexamethylberbat(III) und -lutetat(III). *Angew. Chem.* **1978**, *90*, 307–308.

- (4) Watson, P. L. Methane exchange reactions of lanthanide and early-transition-metal methyl complexes. *J. Am. Chem. Soc.* **1983**, *105*, 6491–6493.

- (5) Thompson, M. E.; Baxter, S. M.; Bulls, A. R.; Burger, B. J.; Nolan, M. C.; Santarsiero, B. D.; Schaefer, W. P.; Bercaw, J. E. σ -Bond metathesis for carbon-hydrogen bonds of hydrocarbons and Sc-R (R = H, alkyl, aryl) bonds of permethylscandocene derivatives. Evidence for noninvolvement of the π system in electrophilic activation of aromatic and vinylic C-H bonds. *J. Am. Chem. Soc.* **1987**, *109*, 203–219.

- (6) Evans, W. J.; Perotti, J. M.; Ziller, J. W. Synthetic utility of $[(\text{C}_3\text{Me}_3)_2\text{Ln}][(\mu\text{-Ph})_2\text{BPh}]$ in accessing $[(\text{C}_3\text{Me}_3)_2\text{Ln}]_x$ unsolvated alkyl lanthanide metallocenes, complexes with high C-H activation reactivity. *J. Am. Chem. Soc.* **2005**, *127*, 3894–3909.

- (7) Thompson, M. E.; Bercaw, J. E. Some aspects of the chemistry of alkyl and hydride derivatives of permethylscandocene. *Pure Appl. Chem.* **1984**, *56*, 1–11.

- (8) Ziegler, T.; Folga, E.; Berces, A. A density functional study on the activation of hydrogen-hydrogen and hydrogen-carbon bonds by $\text{Cp}_2\text{Sc-H}$ and $\text{Cp}_2\text{Sc-CH}_3$. *J. Am. Chem. Soc.* **1993**, *115*, 636–646.

- (9) Watson, P. L.; Parshall, G. W. Organolanthanides in catalysis. *Acc. Chem. Res.* **1985**, *18*, 51–56.

- (10) Sadow, A. D.; Tilley, T. D. Homogeneous catalysis with methane. A strategy for the hydromethylation of olefins based on the nondegenerate exchange of alkyl groups and sigma-bond metathesis at scandium. *J. Am. Chem. Soc.* **2003**, *125*, 7971–7977.

- (11) Dietrich, H. M.; Grove, H.; Tömmros, K. W.; Anwander, R. Multiple C-H bond activation in group 3 chemistry: synthesis and structural characterization of an yttrium-aluminum-methine cluster. *J. Am. Chem. Soc.* **2006**, *128*, 1458–1459.

- (12) Holton, J.; Lappert, M. F.; Ballard, D. G. H.; Pearce, R.; Atwood, J. L.; Hunter, W. E. Alkyl-bridged complexes of the d- and f-block elements. Part 2. Bis[bis(η -cyclopentadienyl)methylmetal(III)] complexes, and the crystal and molecular structure of the yttrium and ytterbium species. *J. Chem. Soc., Dalton Trans.* **1979**, 54–61.

- (13) Davidson, P. J.; Lappert, M. F.; Pearce, R. Metal σ -hydrocarbyls, MRn Stoichiometry, structures, stabilities, and thermal decomposition pathways. *Chem. Rev.* **1976**, *76*, 219–242.

- (14) Shen, Q.; Cheng, Y.; Lin, Y. Preparation and molecular structure of methylbis(*t*-butyl-cyclopentadienyl)neodymium and -gadolinium. *J. Organomet. Chem.* **1991**, *419*, 293–298.

- (15) Stults, S. D.; Andersen, R. A.; Zalkin, A. Preparation of $(\text{Me}_3\text{CC}_3\text{H}_5)_4\text{M}_2(\mu\text{-Me})_2$ (M = Ce or U) and the crystal structure of the cerium derivative. *J. Organomet. Chem.* **1993**, *462*, 175–182.

- (16) Voskoboynikov, A. Z.; Parshina, I. N.; Shestakova, A. K.; Butin, K. P.; Beletskaya, I. P.; Kuz'mina, L. A. G.; Howard, J. A. K. Reactivity of Lanthanide and Yttrium Hydrides and Hydrocarbyls toward Organosilicon Hydrides and Related Compounds. *Organometallics* **1997**, *16*, 4041–4055.

- (17) Schumann, H.; Keitsch, M. R.; Demtschuk, J.; Molander, G. A. Organometallic compounds of the lanthanides. *J. Organomet. Chem.* **1999**, *582*, 70–82.

- (18) Satoh, Y.; Ikitake, N.; Nakayama, Y.; Okuno, S.; Yasuda, H. Syntheses of bis- and tetra(trimethylsilyl) substituted lanthanocene methyl complexes and their catalyses for polymerizations of methyl methacrylate, ϵ -caprolactone and *l*-lactide. *J. Organomet. Chem.* **2003**, *667*, 42–52.

- (19) Edelmann, F. T.; Freckmann, D. M. M.; Schumann, H. Synthesis and Structural Chemistry of Non-Cyclopentadienyl Organolanthanide Complexes. *Chem. Rev.* **2002**, *102*, 1851–1896.

- (20) Piers, W. Non-cyclopentadienyl ancillaries in organogroup 3 metal chemistry: a fine balance in ligand design. *Coord. Chem. Rev.* **2002**, *233–234*, 131–155.

- (21) Arndt, S.; Okuda, J. Mono(cyclopentadienyl) Complexes of the Rare-Earth Metals. *Chem. Rev.* **2002**, *102*, 1953–1976.

- (22) Robert, D.; Spaniol, T. P.; Okuda, J. Neutral and Monocationic Half-Sandwich Methyl Rare-Earth Metal Complexes: Synthesis, Structure, and 1,3-Butadiene Polymerization Catalysis. *Eur. J. Inorg. Chem.* **2008**, 2801–2809.
- (23) Zhang, W. X.; Wang, Z.; Nishiura, M.; Xi, Z.; Hou, Z. Ln₄(CH₂)₄ cubane-type rare-earth methylidene complexes consisting of “(C₅Me₄SiMe₃)LnCH₂” units (Ln = Tm, Lu). *J. Am. Chem. Soc.* **2011**, 133, 5712–5715.
- (24) Hayes, P. G.; Piers, W. E.; Lee, L. W. M.; Knight, L. K.; Parvez, M.; Elsegood, M. R. J.; Clegg, W. Dialkylscandium Complexes Supported by β-Diketiminato Ligands: Synthesis, Characterization, and Thermal Stability of a New Family of Organoscandium Complexes. *Organometallics* **2001**, 20, 2533–2544.
- (25) Conroy, K. D.; Piers, W. E.; Parvez, M. Synthesis and thermal behavior of dimethyl scandium complexes featuring anilido-phosphinimine ancillary ligands. *J. Organomet. Chem.* **2008**, 693, 834–846.
- (26) Zimmermann, M.; Litlabø, R.; Törnroos, K. W.; Anwender, R. “Metastable” Lu(GaMe₄)₃ Reacts Like Masked [LuMe₃]: Synthesis of an Unsolvated Lanthanide Dimethyl Complex. *Organometallics* **2009**, 28, 6646–6649.
- (27) Schädle, D.; Maichle-Mössmer, C.; Schädle, C.; Anwender, R. Rare-earth-metal methyl, amide, and imide complexes supported by a superbulky scorpionate ligand. *Chem. - Eur. J.* **2015**, 21, 662–670.
- (28) Zhou, J.; Xiang, L.; Guo, J.; Leng, X.; Chen, Y. Formation and Reactivity of a C-P-N-Sc Four-Membered Ring: H₂, O₂, CO, Phenylsilane, and Pinacolborane Activation. *Chem. - Eur. J.* **2017**, 23, 5424–5428.
- (29) Zhou, J.; Chu, J.; Zhang, Y.; Yang, G.; Leng, X.; Chen, Y. An yttrium hydride-silane complex as a structural model for a sigma-bond metathesis transition state. *Angew. Chem., Int. Ed.* **2013**, 52, 4243–4246.
- (30) Scott, J.; Fan, H.; Wicker, B. F.; Fout, A. R.; Baik, M. H.; Mindiola, D. J. Lewis acid stabilized methylidene and oxoscandium complexes. *J. Am. Chem. Soc.* **2008**, 130, 14438–9.
- (31) Henderson, L. D.; MacInnis, G. D.; Piers, W. E.; Parvez, M. A new family of monocyclopentadienyl organoscandium bis-alkyls supported by a bulky trialkylphosphine oxide ancillary. *Can. J. Chem.* **2004**, 82, 162–165.
- (32) Schädle, D.; Meermann-Zimmermann, M.; Maichle-Mössmer, C.; Schädle, C.; Törnroos, K. W.; Anwender, R. Rare-earth metal methylidene complexes with Ln₃(μ³-CH₂)(μ³-Me)(μ²-Me)₃ core structure. *Dalton Trans* **2015**, 44, 18101–18110.
- (33) Trofimenko, S. Recent advances in poly(pyrazolyl)borate (scorpionate) chemistry. *Chem. Rev.* **1993**, 93, 943–980.
- (34) Marques, N.; Sella, A.; Takats, J. Chemistry of the Lanthanides Using Pyrazolylborate Ligands. *Chem. Rev.* **2002**, 102, 2137–2160.
- (35) Birkelbach, V. M.; Thim, R.; Stuhl, C.; Maichle-Mössmer, C.; Anwender, R. Potential Precursors for Terminal Methylidene Rare-Earth-Metal Complexes Supported by a Superbulky Tris(pyrazolyl)-borato Ligand. *Chem. - Eur. J.* **2019**, DOI: 10.1002/chem.201903606.
- (36) Zimmermann, M.; Takats, J.; Kiel, G.; Törnroos, K. W.; Anwender, R. Ln(III) methyl and methylidene complexes stabilized by a bulky hydrotris(pyrazolyl)borate ligand. *Chem. Commun.* **2008**, 612–614.
- (37) Litlabø, R.; Zimmermann, M.; Saliu, K.; Takats, J.; Törnroos, K. W.; Anwender, R. A rare-earth metal variant of the Tebbe reagent. *Angew. Chem., Int. Ed.* **2008**, 47, 9560–9564.
- (38) Boyle, T. J.; Ottey, L. A. Advances in structurally characterized lanthanide alkoxide, aryloxy, and silyloxy compounds. *Chem. Rev.* **2008**, 108, 1896–1917.
- (39) Heeres, H. J.; Meetsma, A.; Teuben, J. H.; Rogers, R. D. Mono(pentamethylcyclopentadienyl) complexes of cerium(III). Synthesis, molecular structure, thermal stability, and reactivity of (C₅Me₅)CeX₂ (X = 2,6-di-tert-butylphenoxy, CH(SiMe₃)₂, and N(SiMe₃)₂) complexes. *Organometallics* **1989**, 8, 2637–2646.
- (40) Piers, W. E.; Bunel, E. E.; Bercau, J. E. Synthesis and characterization of mono-(pentamethylcyclopentadienyl)-alkoxy scandium alkyl derivatives, (η⁵-C₅Me₅)(OR)ScR'. *J. Organomet. Chem.* **1991**, 407, 51–60.
- (41) Schaverien, C. J. Alkoxides as ancillary ligands in organo-lanthanide chemistry: synthesis of, reactivity of, and olefin polymerization by the μ-hydride-μ-alkyl compounds [Y(C₅Me₅)(OC₆H₃tBu₂)₂](μ-H)(μ-alkyl). *Organometallics* **1994**, 13, 69–82.
- (42) Klooster, W. T.; Brammer, L.; Schaverien, C. J.; Budzelaar, P. H. M. C-H Bonds Are Not Elongated by Coordination to Lanthanide Metals: Single-Crystal Neutron Diffraction Structures of (C₅Me₅)Y(OC₆H₃tBu₂)CH(SiMe₃)₂ at 20 K and (C₅Me₅)La{CH(SiMe₃)₂}₂ at 15 K. *J. Am. Chem. Soc.* **1999**, 121, 1381–1382.
- (43) Fischbach, A.; Herdtweck, E.; Anwender, R.; Eickerling, G.; Scherer, W. Reactivity of Trimethylaluminum with Lanthanide Aryloxides: Adduct and Tetramethylaluminate Formation. *Organometallics* **2003**, 22, 499–509.
- (44) Fischbach, A.; Herdtweck, E.; Anwender, R. Synthesis and derivatization of half-lanthanidocene aryl(alk)oxide complexes. *Inorg. Chim. Acta* **2006**, 359, 4855–4864.
- (45) Choi, J.; Choliy, Y.; Zhang, X.; Emge, T. J.; Krogh-Jespersen, K.; Goldman, A. S. Cleavage of sp³ C-O bonds via oxidative addition of C-H bonds. *J. Am. Chem. Soc.* **2009**, 131, 15627–9.
- (46) Kim, M.; Zakharov, L. N.; Rheingold, A. L.; Doerrer, L. H. Synthesis and structural characterization of Groups 10 and 11 mononuclear fluoroaryloxy complexes. *Polyhedron* **2005**, 24, 1803–1812.
- (47) Jende, L. N.; Maichle-Mössmer, C.; Anwender, R. Rare-earth metal formamidate complexes from [(C₅Me₅)LnMe₂]₃ and [LnMe₃]_n precursors. *J. Organomet. Chem.* **2018**, 857, 138–144.
- (48) Steele, L. A. M.; Boyle, T. J.; Kemp, R. A.; Moore, C. The selective insertion of carbon dioxide into a lanthanide(III) 2,6-di-*t*-butyl-phenoxy bond. *Polyhedron* **2012**, 42, 258–264.
- (49) Dettenrieder, N.; Dietrich, H. M.; Maichle-Mössmer, C.; Anwender, R. Yttrium Siloxide Complexes Bearing Terminal Methyl Ligands: Molecular Models for Ln-CH₃ Terminated Silica Surfaces. *Chem. - Eur. J.* **2016**, 22, 13189–13200.
- (50) Deacon, G. B.; Junk, P. C.; Moxey, G. J. Mono-, di-, tri- and tetranuclear rare earth complexes obtained using a moderately bulky aryloxy ligand. *Chem. - Asian J.* **2009**, 4, 1717–1728.
- (51) Evans, W. J.; Olofson, J. M.; Ziller, J. W. Utility of the 2,6-dimethylphenoxy ligand in providing chloride- and oxide-free yttrium [Y(OR)₃(solvent)_a]_b complexes with accessible coordination sites. *Inorg. Chem.* **1989**, 28, 4308–4309.
- (52) Hamidi, S.; Deacon, G. B.; Junk, P. C.; Neumann, P. Direct reaction of iodine-activated lanthanoid metals with 2,6-diisopropylphenol. *Dalton Trans* **2012**, 41, 3541–3552.
- (53) Cornish, A. D.; Mills, D. P.; Lewis, W.; Blake, A. J.; Liddle, S. T. Reactions of alkali metal and yttrium alkyls with a sterically demanding bis(aryloxysilyl)methane: Formation of aryloxy complexes by Si-O bond cleavage. *C. R. Chim.* **2010**, 13, 593–602.
- (54) Barnhart, D. M.; Clark, D. L.; Gordon, J. C.; Huffman, J. C.; Vincent, R. L.; Watkin, J. G.; Zwick, B. D. Synthesis, Properties, and X-ray Structures of the Lanthanide η⁶-Arene-Bridged Aryloxy Dimers Ln₂(O-2,6-*i*-Pr₂C₆H₃)₆ and Their Lewis Base Adducts Ln(O-2,6-*i*-Pr₂C₆H₃)₃(THF)₂ (Ln = Pr, Nd, Sm, Gd, Er, Yb, Lu). *Inorg. Chem.* **1994**, 33, 3487–3497.
- (55) Bilbrey, J. A.; Kazez, A. H.; Locklin, J.; Allen, W. D. Exact ligand cone angles. *J. Comput. Chem.* **2013**, 34, 1189–1197.
- (56) Stuhl, C.; Maichle-Mössmer, C.; Anwender, R. Magnesium Stung by Nonclassical Scorpionate Ligands: Synthesis and Cone-Angle Calculations. *Chem. - Eur. J.* **2018**, 24, 14254–14268.
- (57) Nieland, A.; Mix, A.; Neumann, B.; Stammmler, H.-G.; Mitzel, N. W. Lanthanoid Tetramethylaluminates and Their Paramagnetic NMR Parameters. *Eur. J. Inorg. Chem.* **2014**, 51–57.
- (58) Langer, J.; Kriek, S.; Görls, H.; Kreisel, G.; Seidel, W.; Westerhausen, M. Organic heterobimetallic complexes of the alkaline earth metals (Ae = Ca, Sr, Ba) with tetrahedral metallate anions of three-valent metals (M = B, Al, Ga, and V). *New J. Chem.* **2010**, 34, 1667.

- (59) Krieck, S.; Görls, H.; Westerhausen, M. Synthesis and molecular structure of hexakis(tetrahydrofuran)calcium bis-[trimethyl-(diphenylamino)Alanate]. *Inorg. Chem. Commun.* **2008**, *11*, 911–913.
- (60) Bonath, M.; Hollfelder, C. O.; Schädle, D.; Maichle-Mössmer, C.; Sirsch, P.; Anwender, R. C-H Bond Activation and Isoprene Polymerization by Lutetium Alkylaluminum/gallate Complexes Bearing a Peripheral Boryl and a Bulky Hydrotris(pyrazolyl)borate Ligand. *Eur. J. Inorg. Chem.* **2017**, 4683–4692.
- (61) COSMO v. 1.61; Bruker AXS Inc.: Madison, WI, 2012.
- (62) APEX 3 v. 2017.3–0; Bruker AXS Inc.: Madison, WI, 2017.
- (63) SAINT v. 8.38A; Bruker AXS Inc.: Madison, WI, 2017.
- (64) Krause, L.; Herbst-Irmer, R.; Sheldrick, G. M.; Stalke, D. *J. Appl. Crystallogr.* **2015**, *48*, 3–10.
- (65) Sheldrick, G. Crystal structure refinement with SHELXL. *Acta Crystallogr., Sect. C: Struct. Chem.* **2015**, *71*, 3–8.
- (66) Hübschle, C. B.; Sheldrick, G. M.; Dittrich, B. ShelXle: a Qt graphical user interface for SHELXL. *J. Appl. Crystallogr.* **2011**, *44*, 1281–1284.
- (67) Kratzert, D.; Holstein, J. J.; Krossing, I. DSR: enhanced modelling and refinement of disordered structures with SHELXL. *J. Appl. Crystallogr.* **2015**, *48*, 933–938.
- (68) Farrugia, L. WinGX and ORTEP for Windows: an update. *J. Appl. Crystallogr.* **2012**, *45*, 849–854.
- (69) POV-Ray v. 3.6; Persistence of Vision Raytracer Pty. Ltd.: Williamstown, Australia, 2004; <http://www.povray.org>.

Supporting Information

Mixed Methyl Aryloxy Rare-Earth Metal Complexes Stabilized by a Superbulky Tris(pyrazolyl)borato Ligand

Verena M. Birkelbach, Christoph Stuhl, Cäcilia Maichle-Mössmer, and Reiner Anwander*

Institut für Anorganische Chemie, Eberhard Karls Universität Tübingen, Auf der
Morgenstelle 18, 72076 Tübingen (Germany)

* to whom correspondence should be addressed: E-Mail reiner.anwander@uni-tuebingen.de

Table of contents

NMR spectroscopy

^1H NMR, $^{13}\text{C}\{^1\text{H}\}$ NMR, $^{11}\text{B}\{^1\text{H}\}$ NMR spectra of complex 1-Lu	Pages S3-S4
^1H NMR, $^{13}\text{C}\{^1\text{H}\}$ NMR, $^{11}\text{B}\{^1\text{H}\}$ NMR spectra of complex 2-Lu	Pages S4-S5
^1H NMR, $^{13}\text{C}\{^1\text{H}\}$ NMR, $^{11}\text{B}\{^1\text{H}\}$ NMR, $^{19}\text{F}\{^1\text{H}\}$ NMR spectra of complex 3-Lu	Pages S6-S7
^1H NMR, $^{13}\text{C}\{^1\text{H}\}$ NMR, $^{11}\text{B}\{^1\text{H}\}$ NMR, ^1H - ^{89}Y HSQC NMR spectra of complex 4-Y	Pages S8-S10
^1H NMR, $^{13}\text{C}\{^1\text{H}\}$ NMR, $^{11}\text{B}\{^1\text{H}\}$ NMR spectra of complex 4-Lu	Pages S10-S11
^1H NMR, $^{13}\text{C}\{^1\text{H}\}$ NMR, $^{11}\text{B}\{^1\text{H}\}$ NMR, ^1H - ^{89}Y HSQC NMR spectra of complex 5-Y	Pages S12-S13
^1H NMR, $^{13}\text{C}\{^1\text{H}\}$ NMR, $^{11}\text{B}\{^1\text{H}\}$ NMR spectra of complex 5-Lu	Pages S14-S15
^1H NMR, $^{13}\text{C}\{^1\text{H}\}$ NMR, $^{11}\text{B}\{^1\text{H}\}$ NMR, ^1H - ^{89}Y HSQC NMR spectra of complex 6-Y	Pages S15-S17
^1H NMR, $^{13}\text{C}\{^1\text{H}\}$ NMR, $^{11}\text{B}\{^1\text{H}\}$ NMR spectra of complex 6-Lu	Pages S17-S18
^1H NMR, $^{13}\text{C}\{^1\text{H}\}$ NMR, $^{11}\text{B}\{^1\text{H}\}$ NMR, $^{19}\text{F}\{^1\text{H}\}$ NMR, ^1H - ^{89}Y HSQC NMR spectra of complex 7-Y	Pages S19-S21
^1H NMR, $^{13}\text{C}\{^1\text{H}\}$ NMR, $^{11}\text{B}\{^1\text{H}\}$ NMR, $^{19}\text{F}\{^1\text{H}\}$ NMR spectra of complex 7-Lu	Pages S21-S23
^1H NMR, $^{13}\text{C}\{^1\text{H}\}$ NMR, $^{11}\text{B}\{^1\text{H}\}$ NMR, ^1H - ^{89}Y HSQC NMR spectra of complex 8-Y	Pages S24-S25
^1H NMR, $^{13}\text{C}\{^1\text{H}\}$ NMR, $^{11}\text{B}\{^1\text{H}\}$ NMR spectra of complex 8-Lu	Pages S26-S26

X-ray structure analyses

ORTEP representation of the molecular structure for compounds 1-Lu , 2-Lu , 3-Lu , 5-Lu , 6-Y , and 7-Lu	Pages S27-S28
Comprehensive crystallographic data for compounds 1-Lu , 2-Lu , 3-Lu , 4-Lu , 5-Ln , 6-Ln , 7-Ln , 8-Y , and 9-Lu	Pages S29-S31

Cone angle analyses

Cone angle calculations	Pages S32-S36
-------------------------	---------------

NMR spectroscopy

The solvent residual peaks are marked with an asterisk (*).

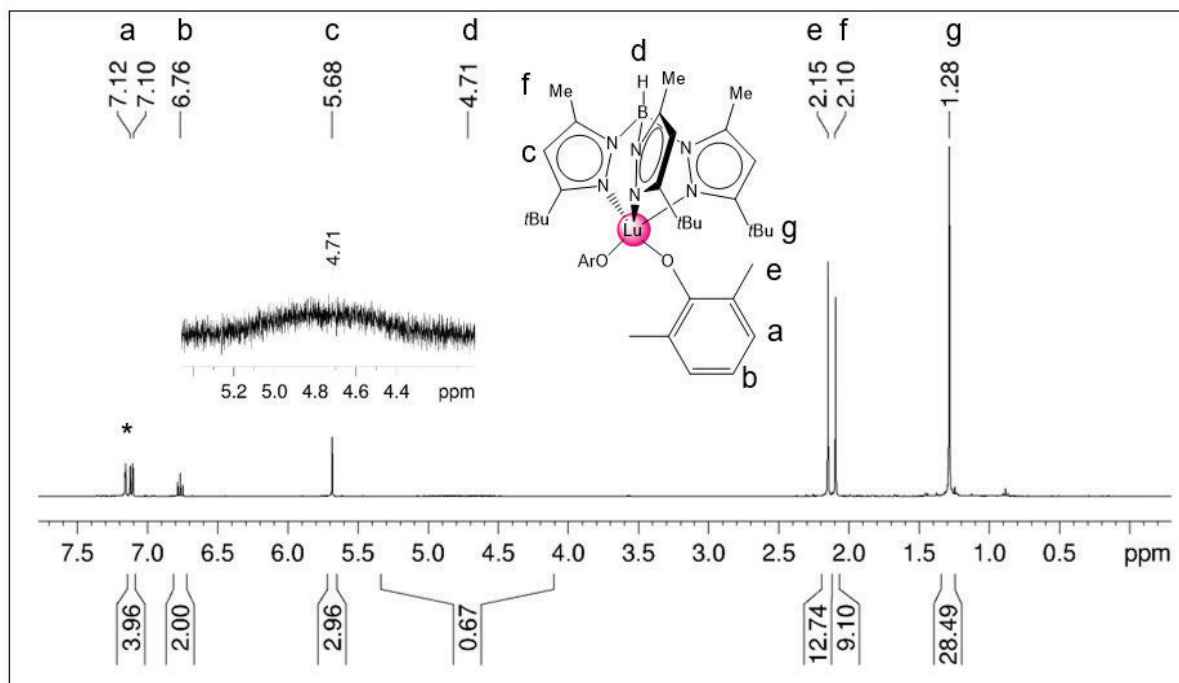


Figure S1. ^1H NMR spectrum (250 MHz, $[\text{D}_6]\text{benzene}$) of complex $\text{Tp}^{\text{tBu,Me}}\text{Lu}(\text{OC}_6\text{H}_3\text{Me}_2\text{-2,6})_2$ (**1-Lu**) at 26 °C.

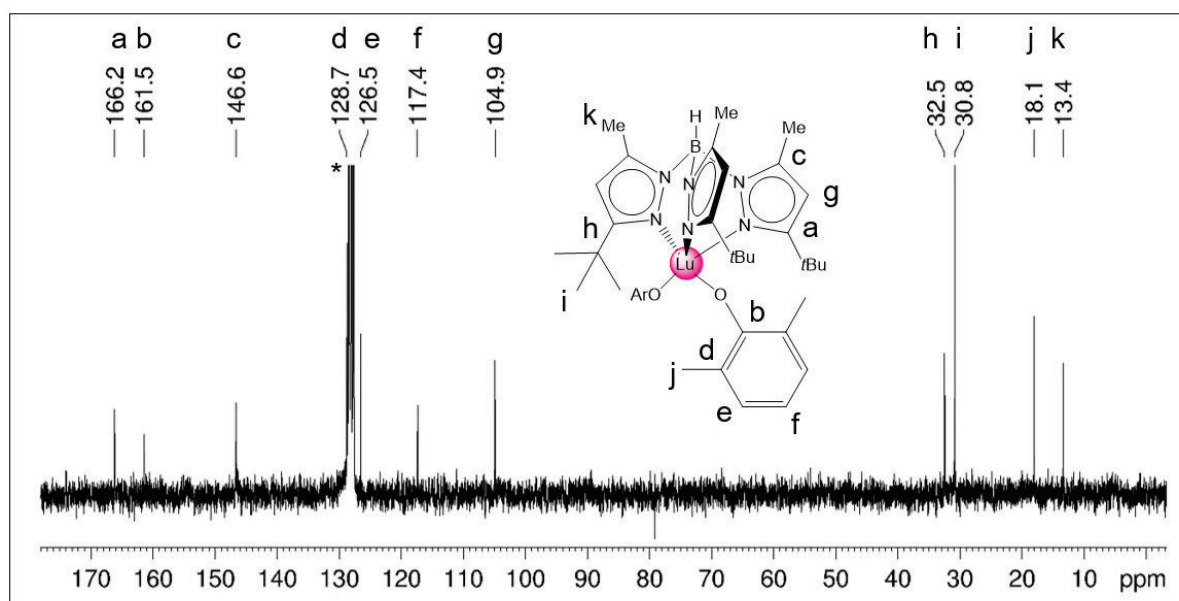


Figure S2. $^{13}\text{C}\{^1\text{H}\}$ NMR spectrum (63 MHz, $[\text{D}_6]\text{benzene}$) of complex $\text{Tp}^{\text{tBu,Me}}\text{Lu}(\text{OC}_6\text{H}_3\text{Me}_2\text{-2,6})_2$ (**1-Lu**) at 26 °C.

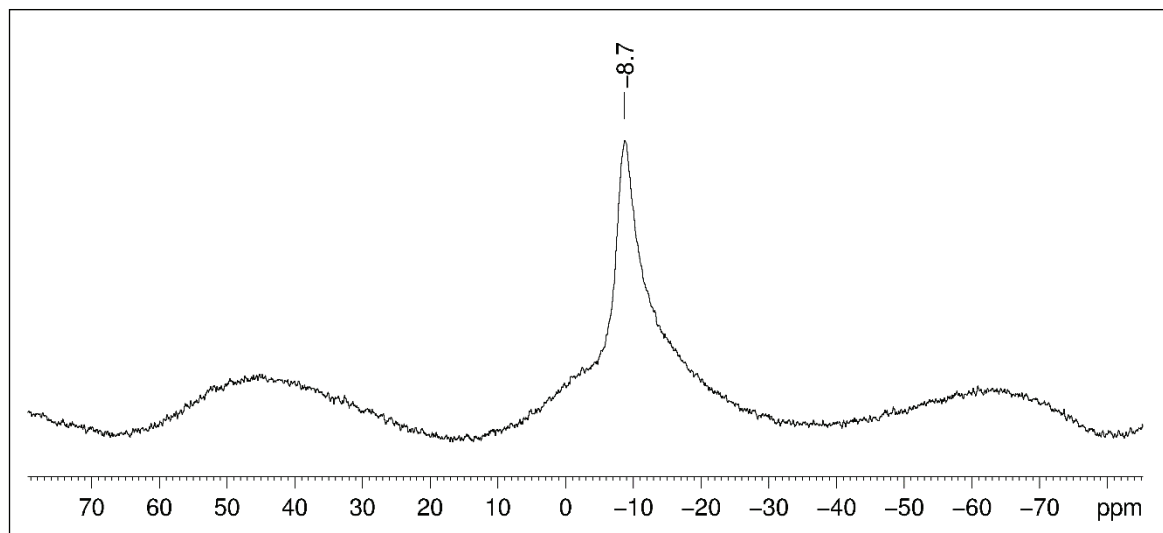


Figure S3. $^{11}\text{B}\{^1\text{H}\}$ NMR spectrum (80 MHz, $[\text{D}_6]$ benzene) of complex $\text{Tp}^{\text{fBu,Me}}\text{Lu}(\text{OC}_6\text{H}_3\text{Me}_2\text{-}2,6)_2$ (**1-Lu**) at 26 °C.

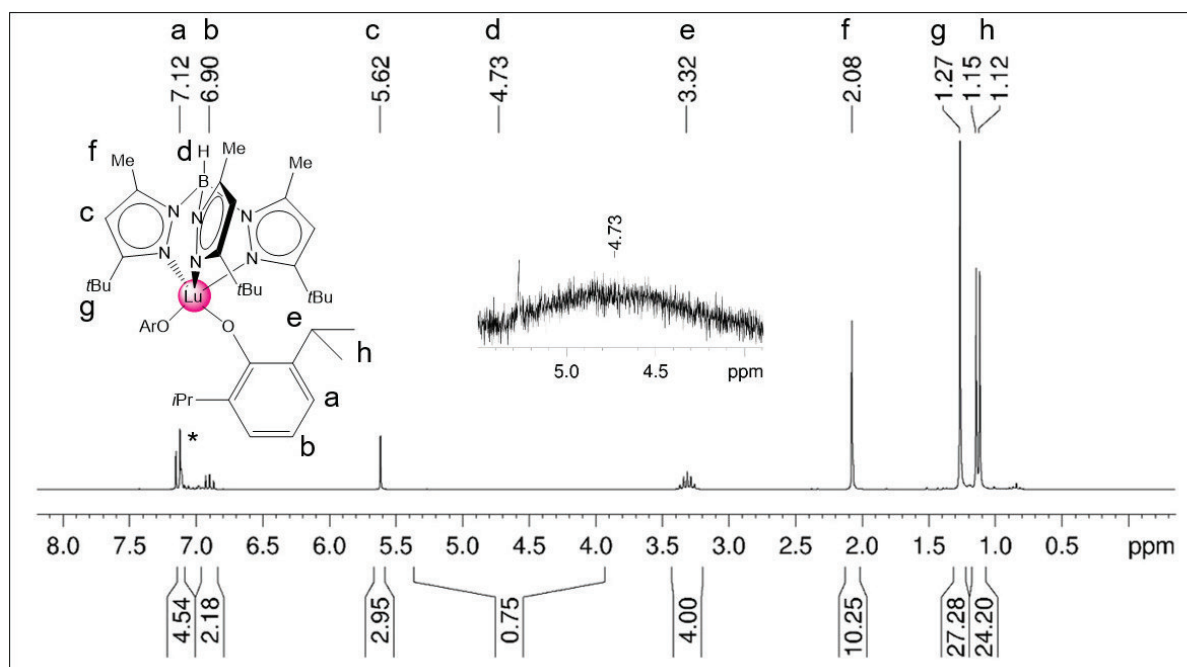


Figure S4. ^1H NMR spectrum (250 MHz, $[\text{D}_6]$ benzene) of complex $\text{Tp}^{\text{fBu,Me}}\text{Lu}(\text{OC}_6\text{H}_3\text{iPr}_2\text{-}2,6)_2$ (**2-Lu**) at 26 °C.

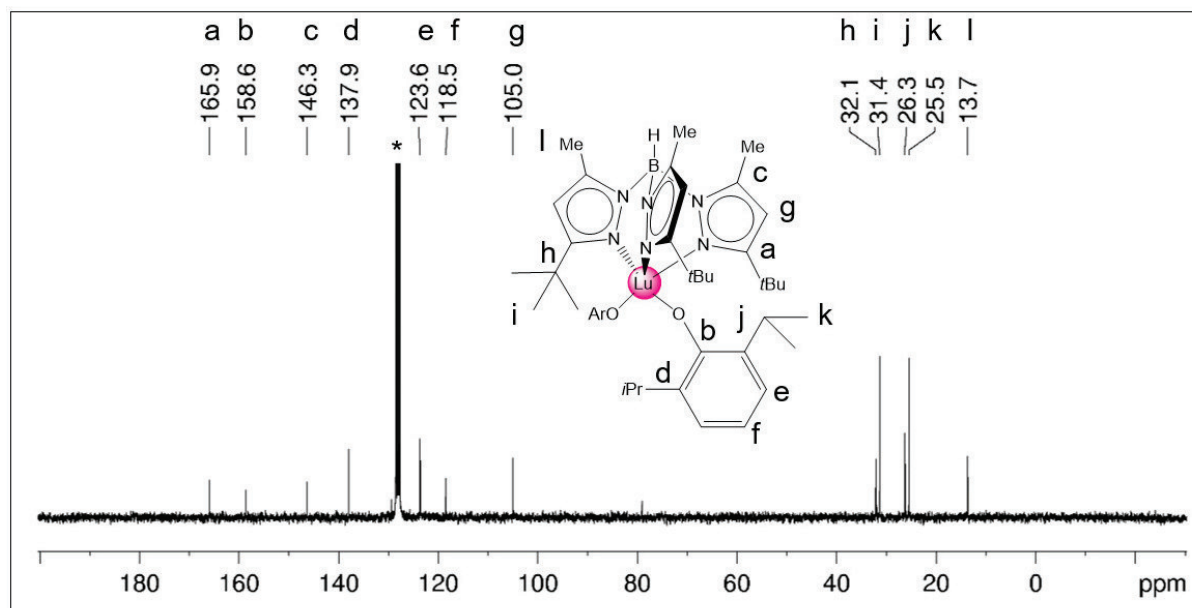


Figure S5. $^{13}\text{C}\{^1\text{H}\}$ NMR spectrum (63 MHz, $[\text{D}_6]$ benzene) of complex $\text{Tp}^{\text{fBu,Me}}\text{Lu}(\text{OC}_6\text{H}_3i\text{Pr}_2-2,6)_2$ (**2-Lu**) at 26 °C.

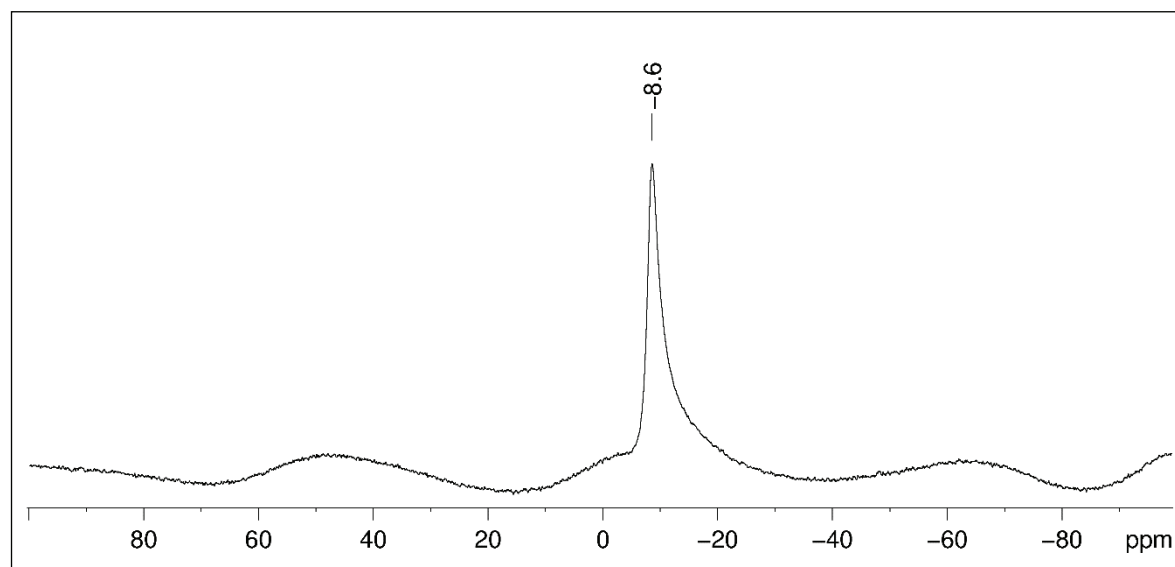


Figure S6. $^{11}\text{B}\{^1\text{H}\}$ NMR spectrum (80 MHz, $[\text{D}_6]$ benzene) of complex $\text{Tp}^{\text{fBu,Me}}\text{Lu}(\text{OC}_6\text{H}_3i\text{Pr}_2-2,6)_2$ (**2-Lu**) at 26 °C.

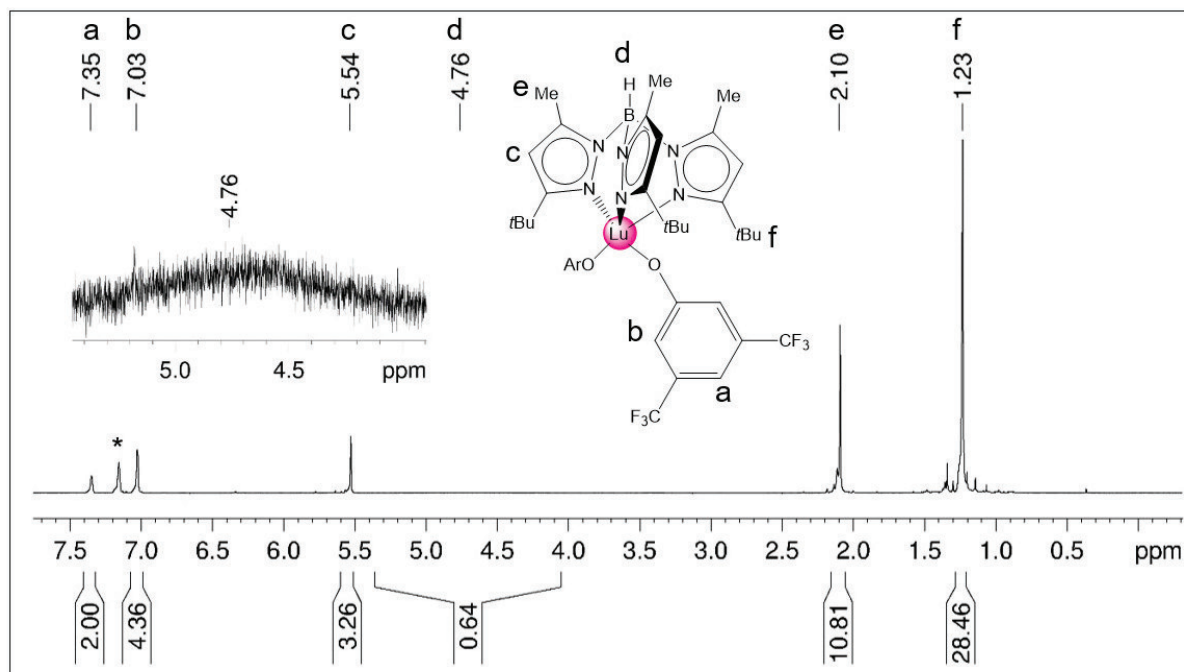


Figure S7. ^1H NMR spectrum (250 MHz, $[\text{D}_6]\text{benzene}$) of complex $\text{Tp}^{\text{tBu,Me}}\text{Lu}[\text{OC}_6\text{H}_3(\text{CF}_3)_2\text{-3,5}]_2$ (**3-Lu**) at 26 °C.

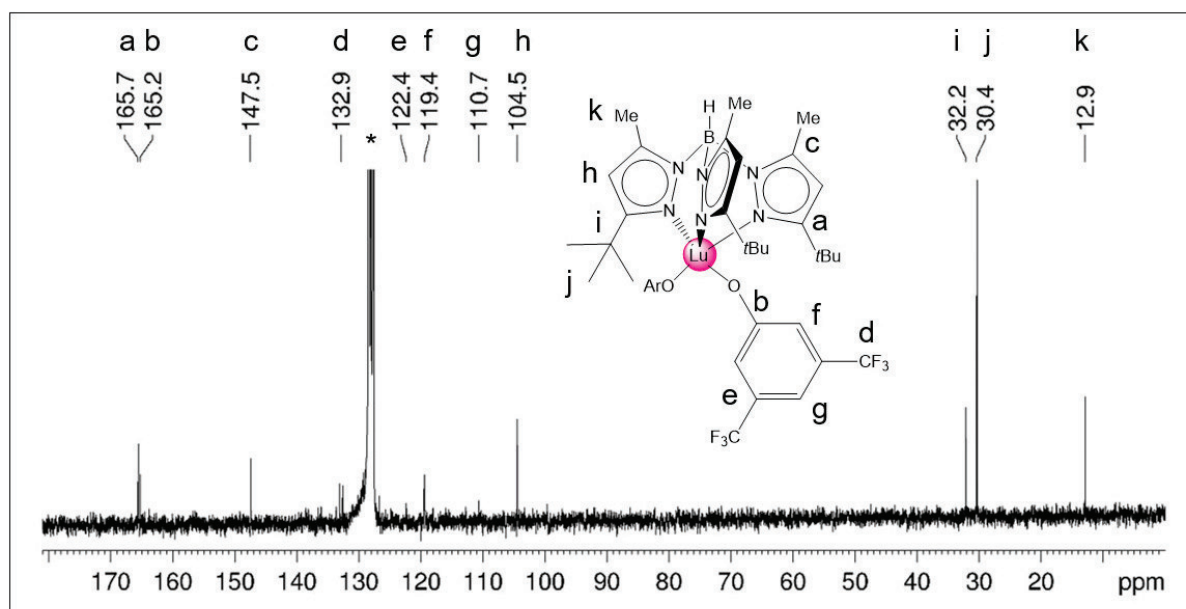


Figure S8. $^{13}\text{C}\{^1\text{H}\}$ NMR spectrum (63 MHz, $[\text{D}_6]\text{benzene}$) of complex $\text{Tp}^{\text{tBu,Me}}\text{Lu}[\text{OC}_6\text{H}_3(\text{CF}_3)_2\text{-3,5}]_2$ (**3-Lu**) at 26 °C.

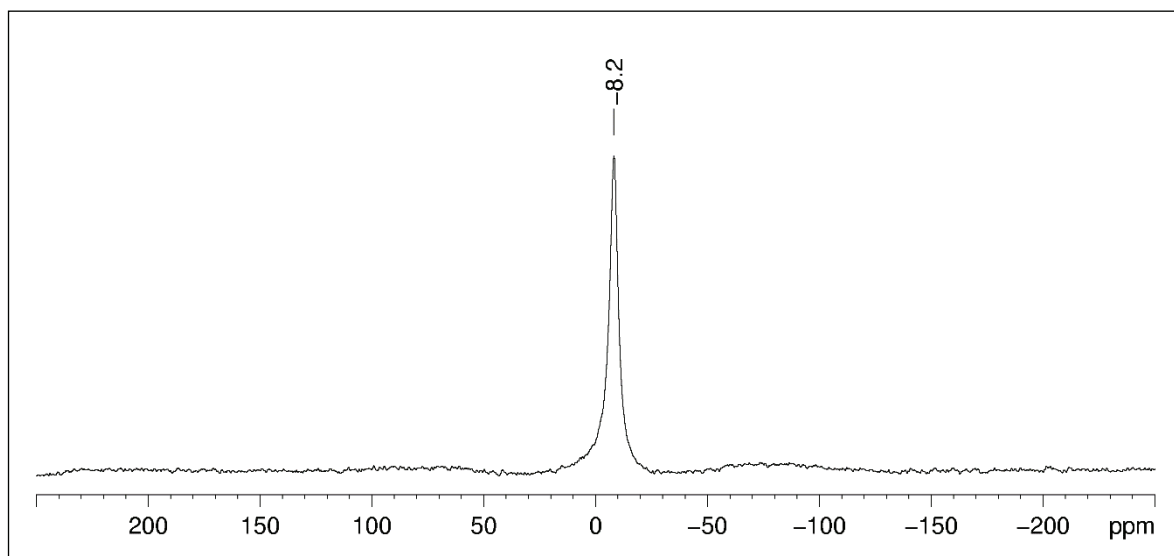


Figure S9. $^{11}\text{B}\{^1\text{H}\}$ NMR spectrum (80 MHz, $[\text{D}_6]$ benzene) of complex $\text{Tp}^{t\text{Bu,Me}}\text{Lu}[\text{OC}_6\text{H}_3(\text{CF}_3)_2\text{-3,5}]_2$ (**3-Lu**) at 26 °C.

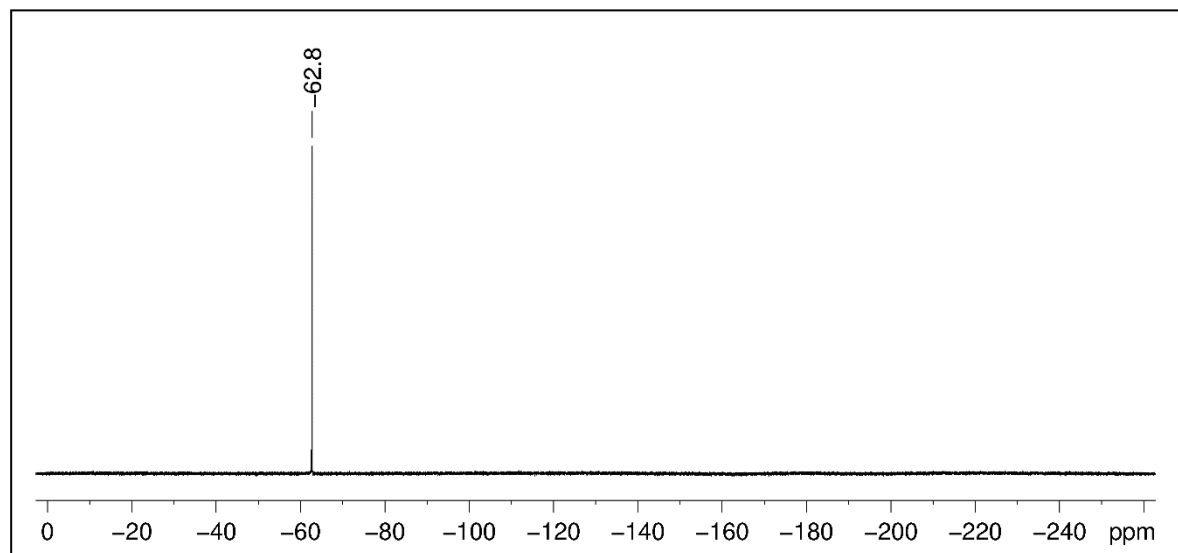


Figure S10. $^{19}\text{F}\{^1\text{H}\}$ NMR spectrum (376 MHz, $[\text{D}_6]$ benzene) of complex $\text{Tp}^{t\text{Bu,Me}}\text{Lu}[\text{OC}_6\text{H}_3(\text{CF}_3)_2\text{-3,5}]_2$ (**3-Lu**) at 26 °C.

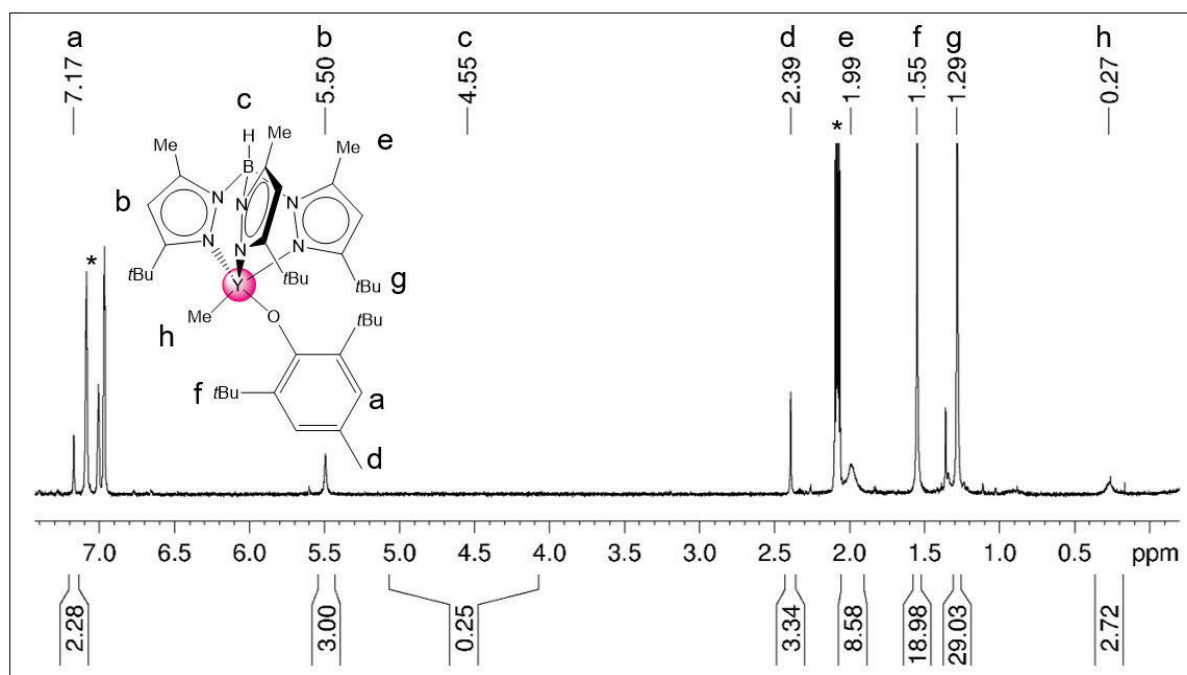


Figure S11. ^1H NMR spectrum (500 MHz, $[\text{D}_8]\text{toluene}$) of complex $\text{Tp}^{\text{tBu,Me}}\text{YMe}(\text{OC}_6\text{H}_2\text{tBu}_2\text{-2,6-Me-4})$ (**4-Y**) at 26°C .

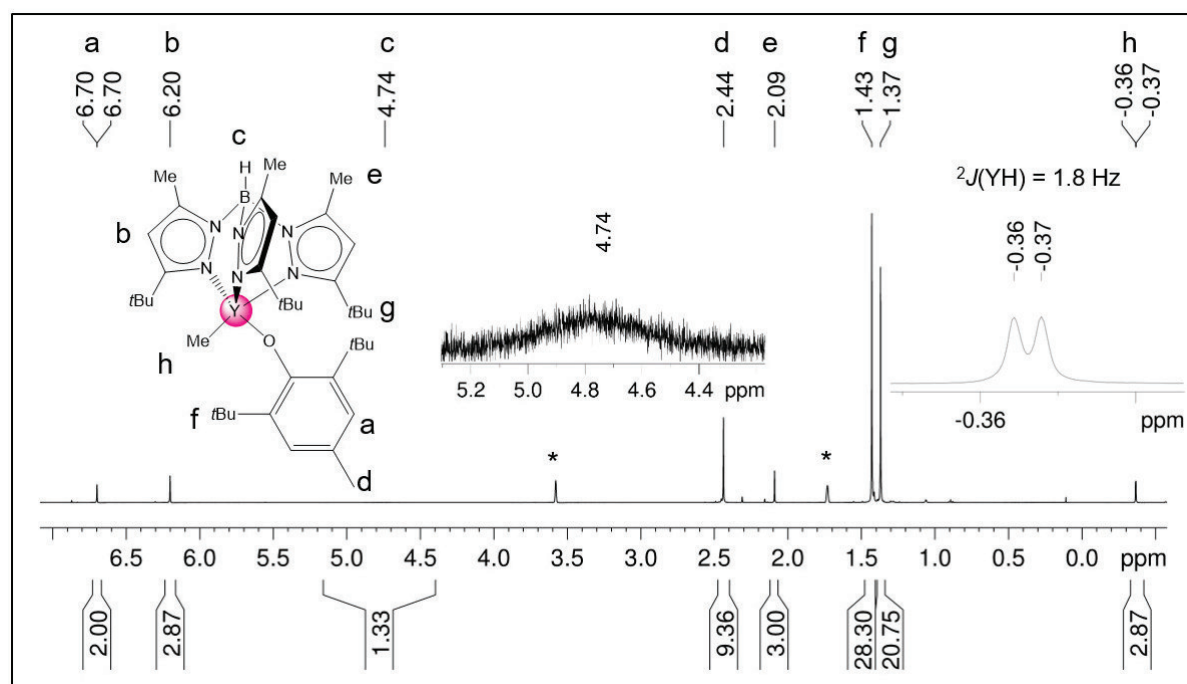


Figure S12. ^1H NMR spectrum (500 MHz, $[\text{D}_8]\text{thf}$) of complex $\text{Tp}^{\text{tBu,Me}}\text{YMe}(\text{OC}_6\text{H}_2\text{tBu}_2\text{-2,6-Me-4})$ (**4-Y**) at 0°C .

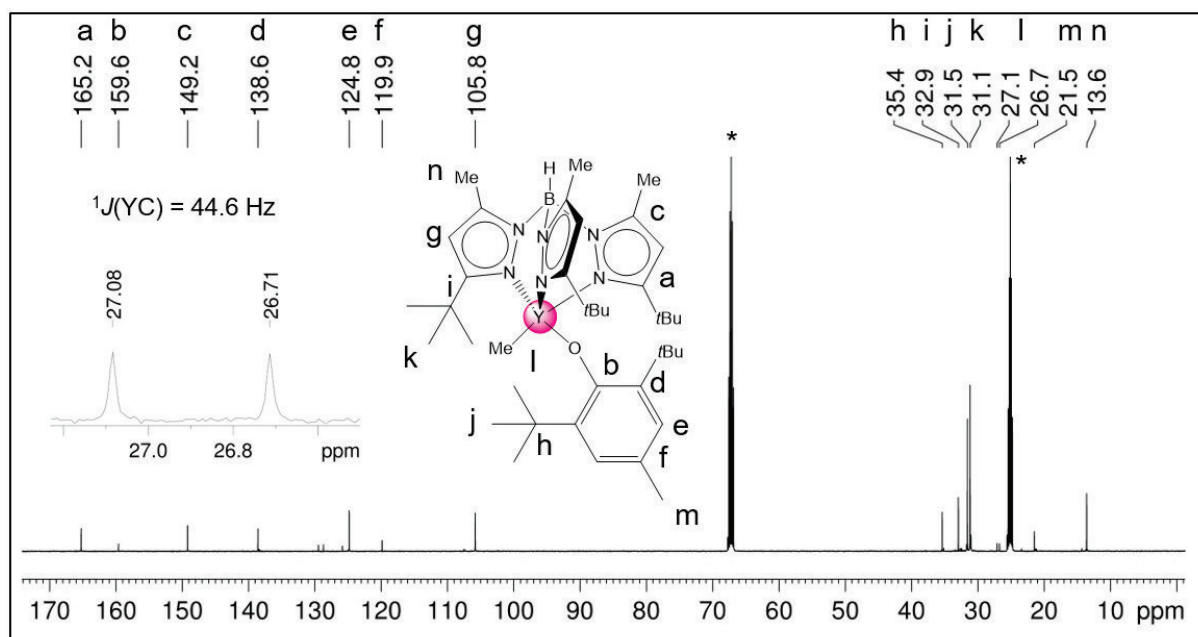


Figure S13. $^{13}\text{C}\{^1\text{H}\}$ NMR spectrum (126 MHz, $[\text{D}_8]\text{thf}$) of complex $\text{Tp}^{\text{tBu,Me}}\text{YMe}(\text{OC}_6\text{H}_2\text{tBu}_2\text{-2,6-Me-4})$ (**4-Y**) at 0 °C

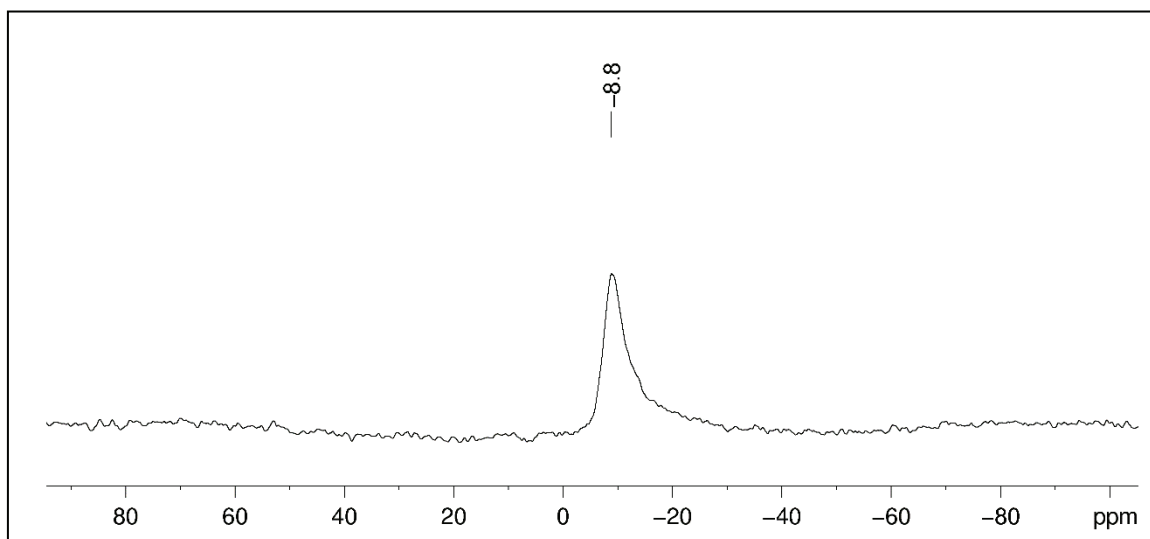


Figure S14. $^{11}\text{B}\{^1\text{H}\}$ NMR spectrum (80 MHz, $[\text{D}_8]\text{toluene}$) of complex $\text{Tp}^{\text{tBu,Me}}\text{YMe}(\text{OC}_6\text{H}_2\text{tBu}_2\text{-2,6-Me-4})$ (**4-Y**) at 26 °C.

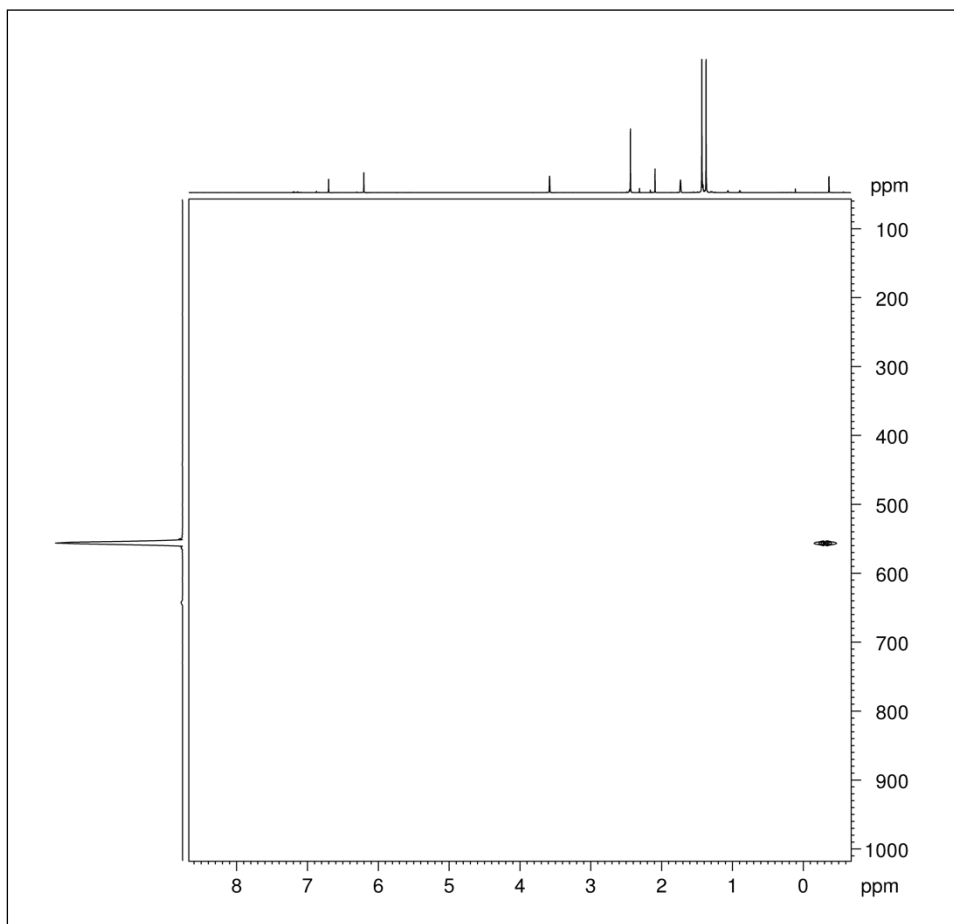


Figure S15. ^1H - ^{89}Y HSQC NMR spectrum (25 MHz, $[\text{D}_8]\text{thf}$) of complex $\text{Tp}^{\text{tBu,Me}}\text{YMe}(\text{OC}_6\text{H}_2\text{tBu}_2\text{-2,6-Me-4})$ (**4-Y**) at 0°C .

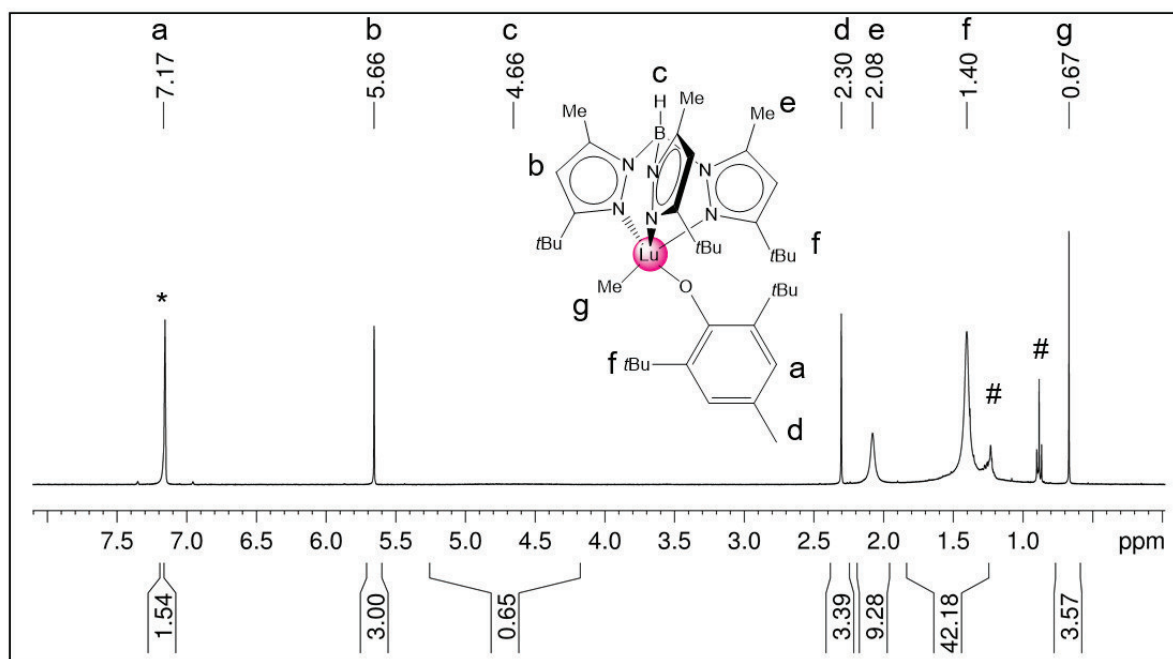


Figure S16. ^1H NMR spectrum (400 MHz, $[\text{D}_6]\text{benzene}$) of complex $\text{Tp}^{\text{tBu,Me}}\text{LuMe}(\text{OC}_6\text{H}_2\text{tBu}_2\text{-2,6-Me-4})$ (**4-Lu**) at 26°C with traces of *n*-hexane (#).

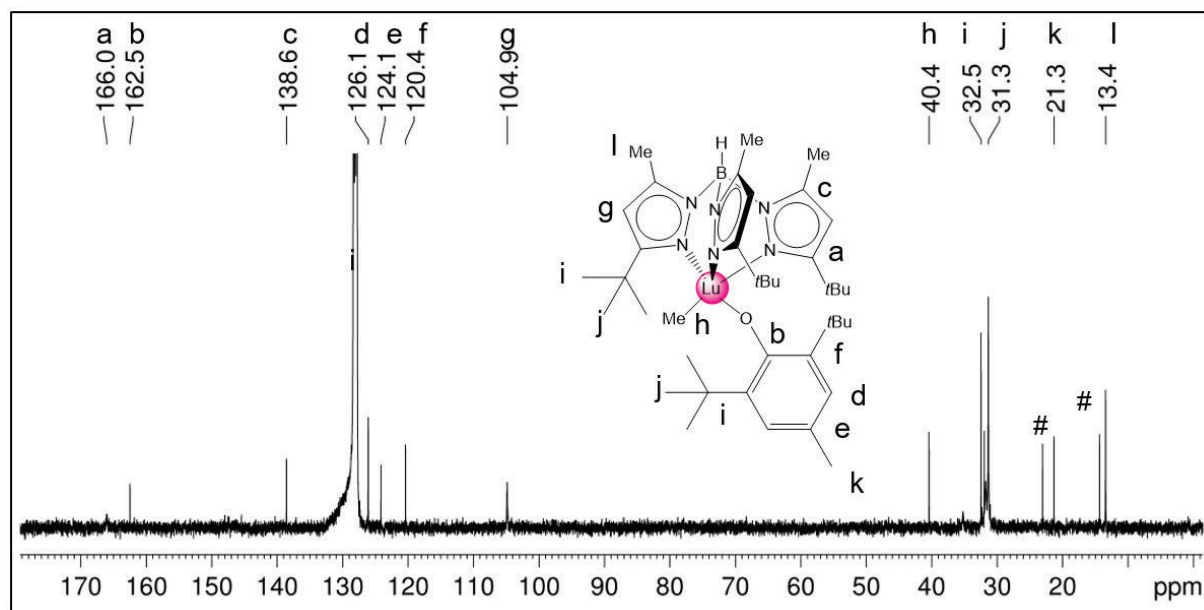


Figure S17. $^{13}\text{C}\{^1\text{H}\}$ NMR spectrum (101 MHz, $[\text{D}_6]$ benzene) of complex $\text{Tp}^{\text{tBu,Me}}\text{LuMe}(\text{OC}_6\text{H}_2\text{tBu}_2\text{-2,6-Me-4})$ (4-Lu) at 26 °C with traces of *n*-hexane (#).

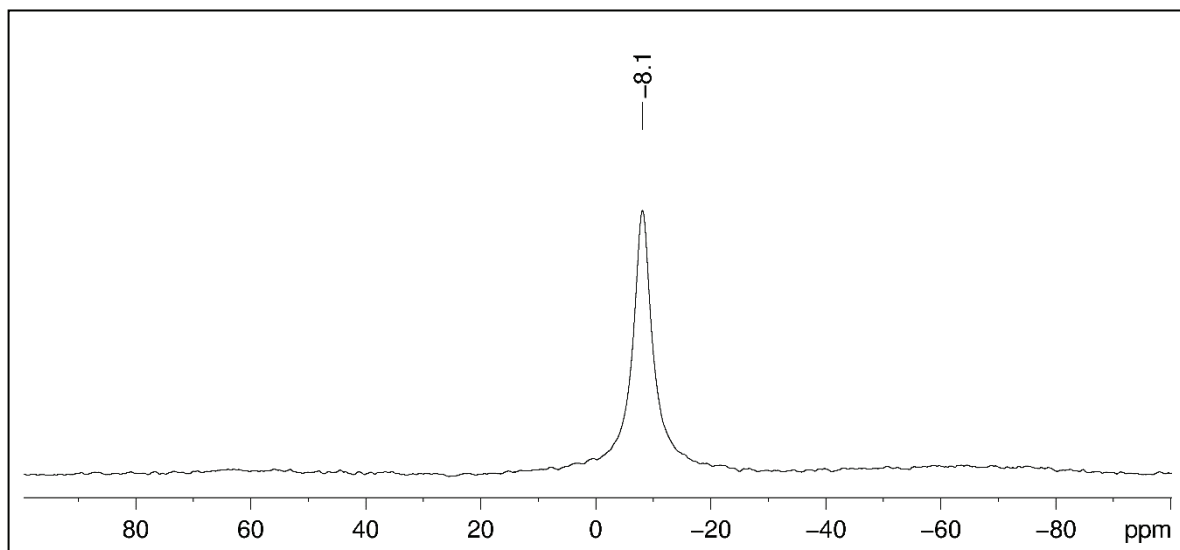


Figure S18. $^{11}\text{B}\{^1\text{H}\}$ NMR spectrum (80 MHz, $[\text{D}_6]$ benzene) of complex $\text{Tp}^{\text{tBu,Me}}\text{LuMe}(\text{OC}_6\text{H}_2\text{tBu}_2\text{-2,6-Me-4})$ (4-Lu) at 26 °C.

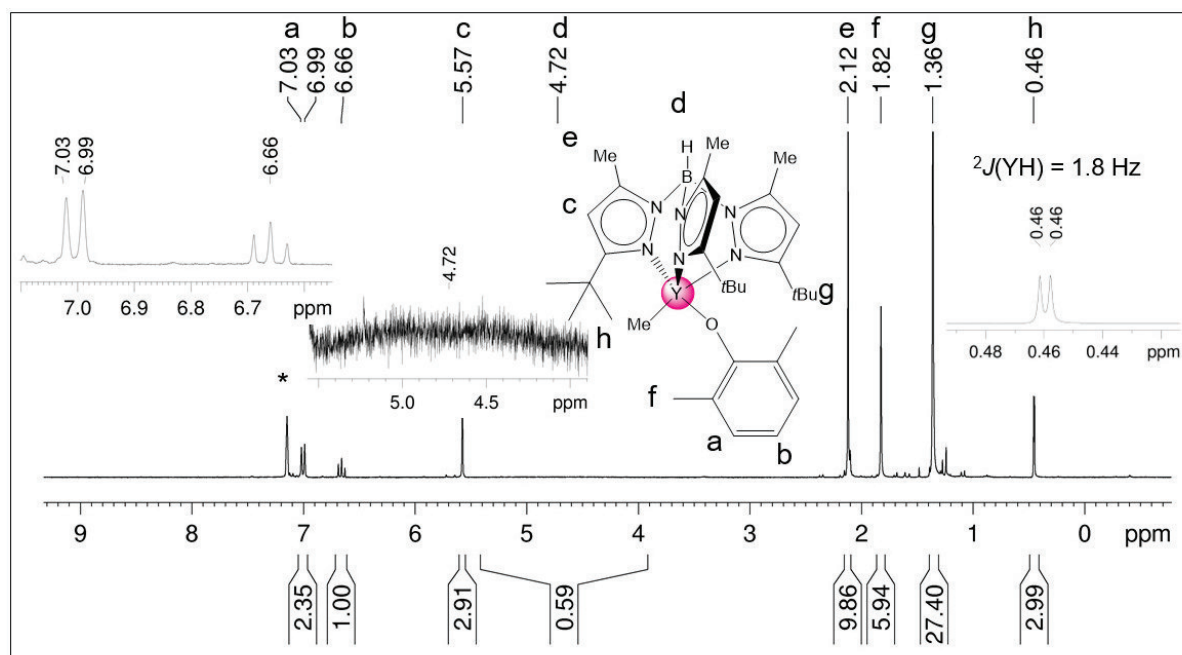


Figure S19. ^1H NMR spectrum (250 MHz, $[\text{D}_6]$ benzene) of complex $\text{Tp}^{\text{tBu,Me}}\text{YMe}(\text{OC}_6\text{H}_3\text{Me}_2\text{-}2,6)$ (**5-Y**) at 26 °C.

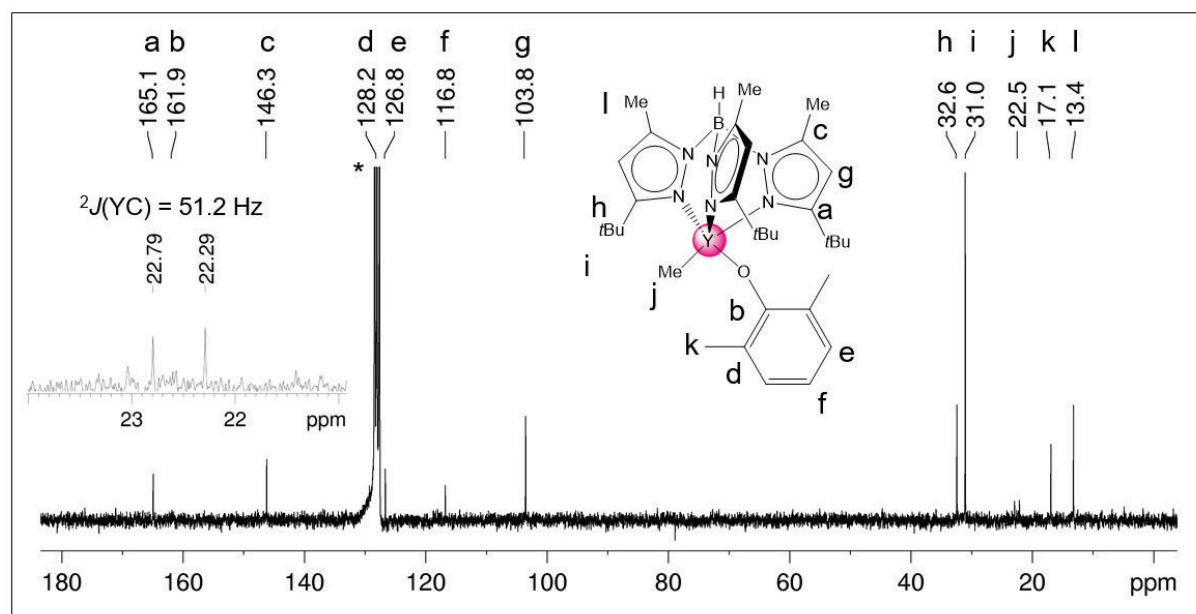


Figure S20. $^{13}\text{C}\{^1\text{H}\}$ NMR spectrum (63 MHz, $[\text{D}_6]$ benzene) of complex $\text{Tp}^{\text{tBu,Me}}\text{YMe}(\text{OC}_6\text{H}_3\text{Me}_2\text{-}2,6)$ (**5-Y**) at 26 °C.

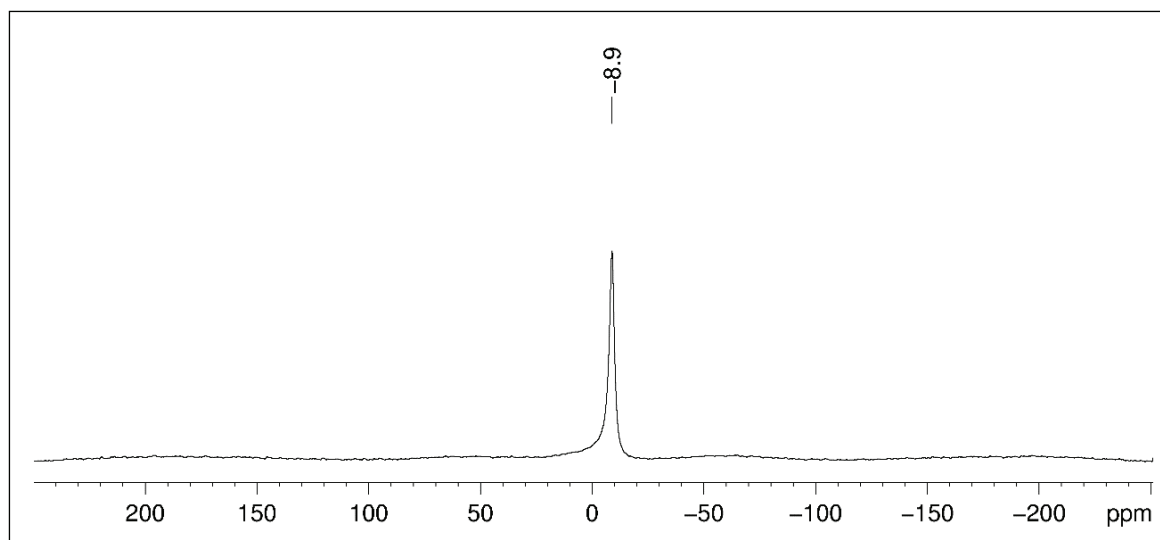


Figure S21. $^{11}\text{B}\{^1\text{H}\}$ NMR spectrum (80 MHz, $[\text{D}_6]$ benzene) of complex $\text{Tp}^{\text{tBu,Me}}\text{YMe}(\text{OC}_6\text{H}_3\text{Me}_2\text{-2,6})$ (**5-Y**) at 26 °C.

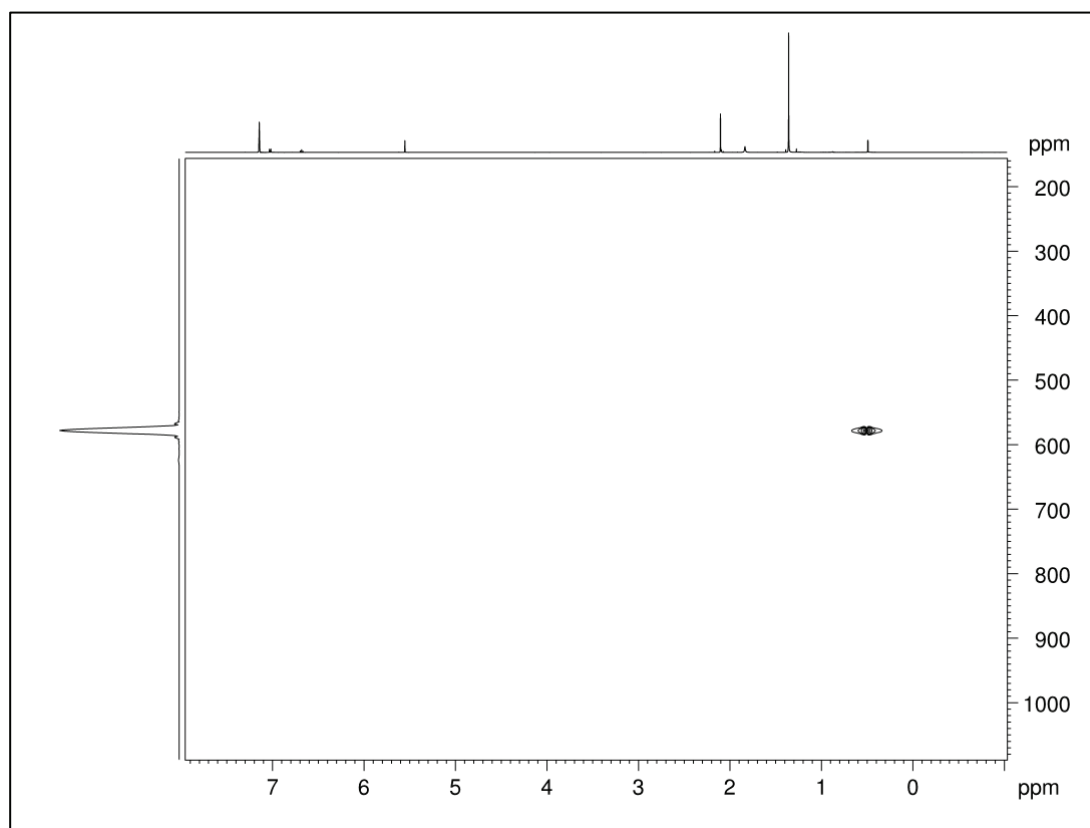


Figure S22. ^1H - ^{89}Y HSQC NMR spectrum (25 MHz, $[\text{D}_6]$ benzene) of complex $\text{Tp}^{\text{tBu,Me}}\text{YMe}(\text{OC}_6\text{H}_3\text{Me}_2\text{-2,6})$ (**5-Y**) at 26 °C.

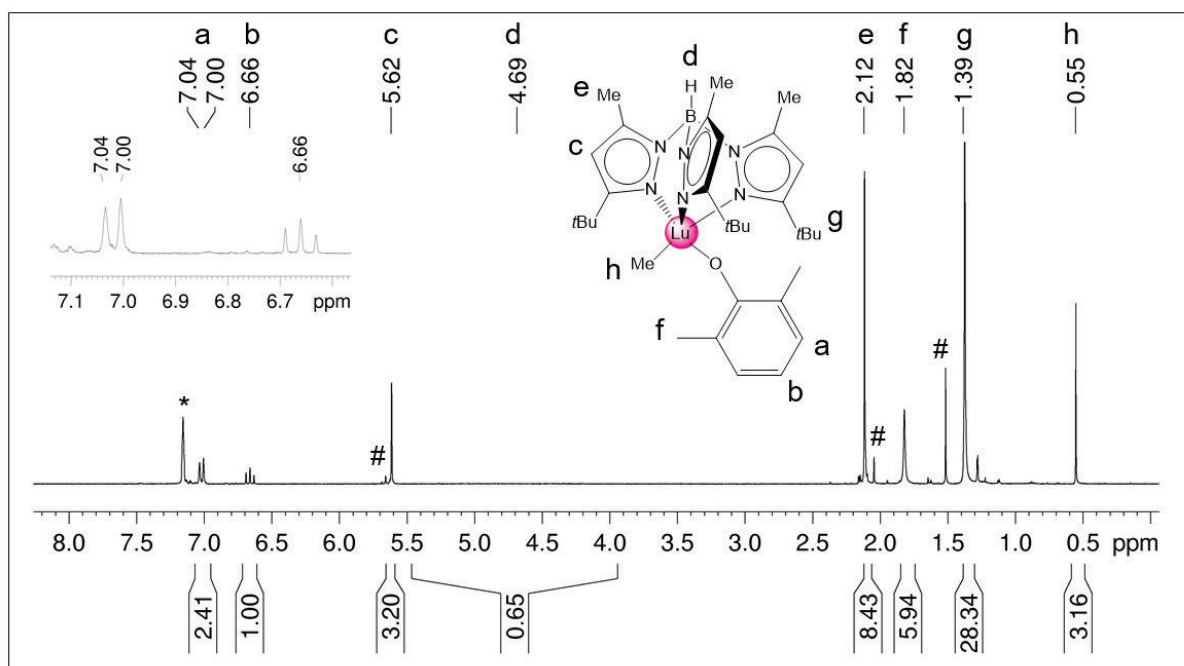


Figure S23. ^1H NMR spectrum (250 MHz, $[\text{D}_6]$ benzene) of complex $\text{Tp}^{\text{fBu,Me}}\text{LuMe}(\text{OC}_6\text{H}_3\text{Me}_2\text{-2,6})$ (**5-Lu**) at 26 °C with traces of $\text{Tp}^{\text{fBu,Me}}\text{LuMe}(\text{AlMe}_4)$ (#).

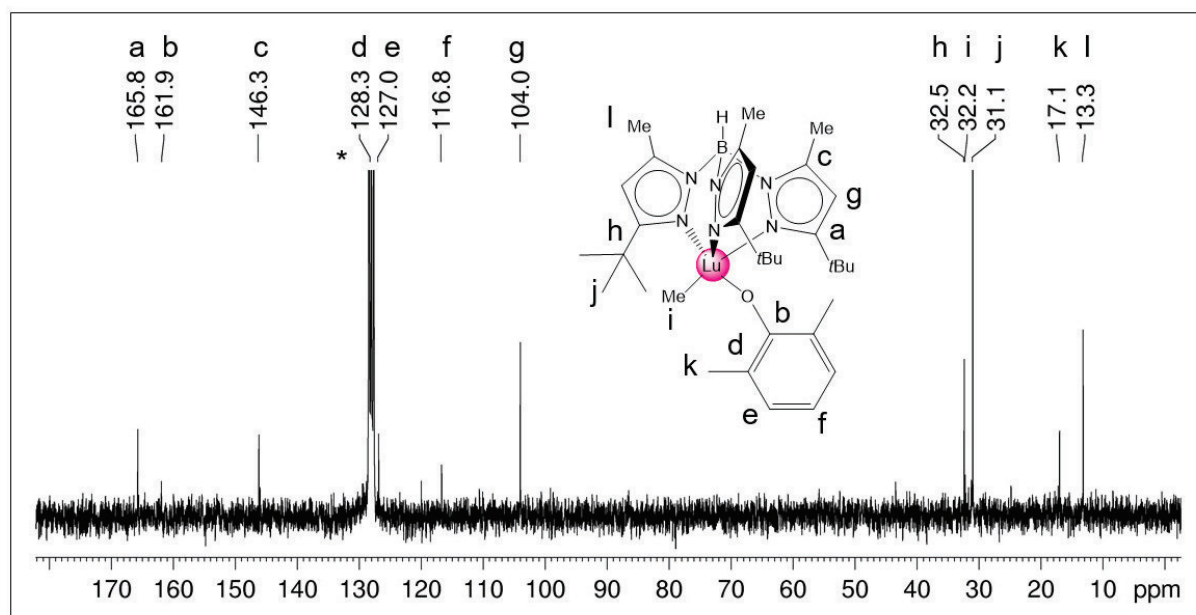


Figure S24. $^{13}\text{C}\{^1\text{H}\}$ NMR spectrum (63 MHz, $[\text{D}_6]$ benzene) of complex $\text{Tp}^{\text{fBu,Me}}\text{LuMe}(\text{OC}_6\text{H}_3\text{Me}_2\text{-2,6})$ (**5-Lu**) at 26 °C.

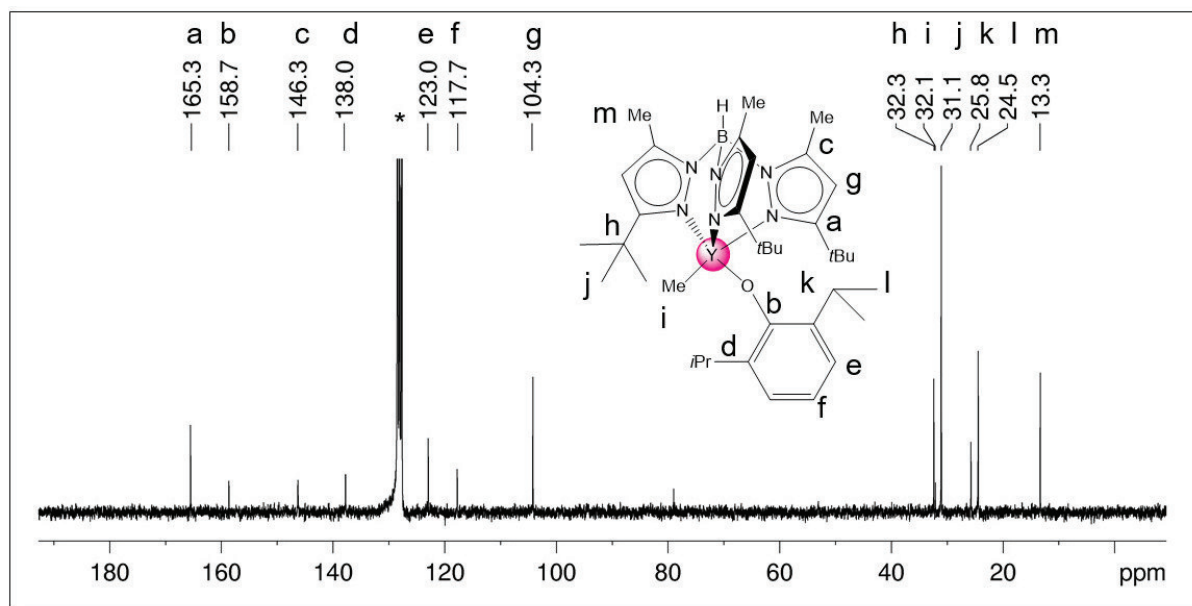


Figure S27. $^{13}\text{C}\{^1\text{H}\}$ NMR spectrum (63 MHz, $[\text{D}_6]$ benzene) of complex $\text{Tp}^{\text{tBu,Me}}\text{YMe}(\text{OC}_6\text{H}_3\text{iPr}_2\text{-2,6})$ (**6-Y**) at 26 °C, no Y-C coupling was observed.

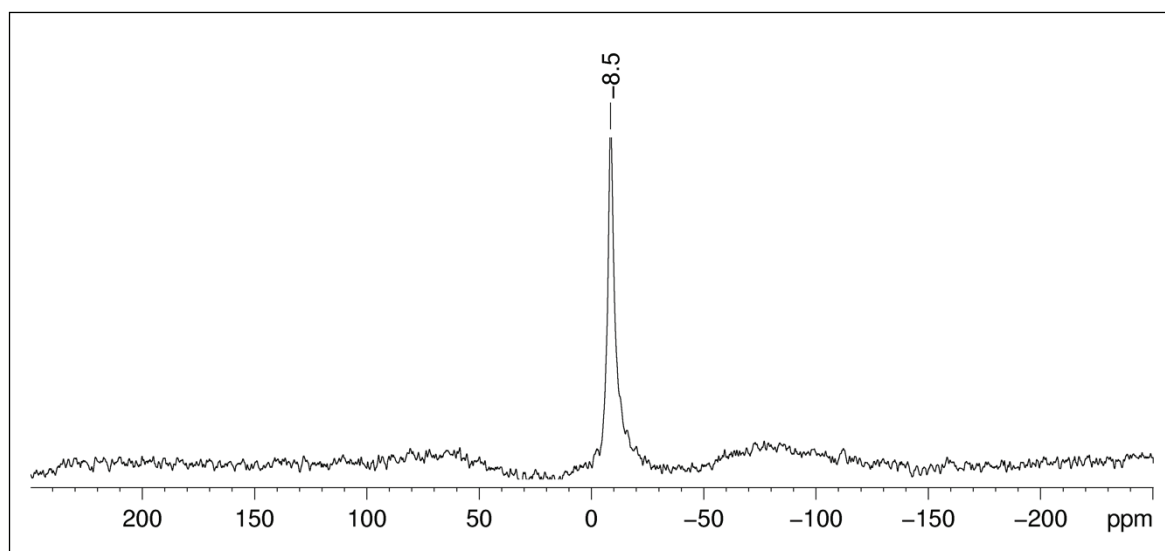


Figure S28. $^{11}\text{B}\{^1\text{H}\}$ NMR spectrum (80 MHz, $[\text{D}_6]$ benzene) of complex $\text{Tp}^{\text{tBu,Me}}\text{YMe}(\text{OC}_6\text{H}_3\text{iPr}_2\text{-2,6})$ (**6-Y**) at 26 °C.

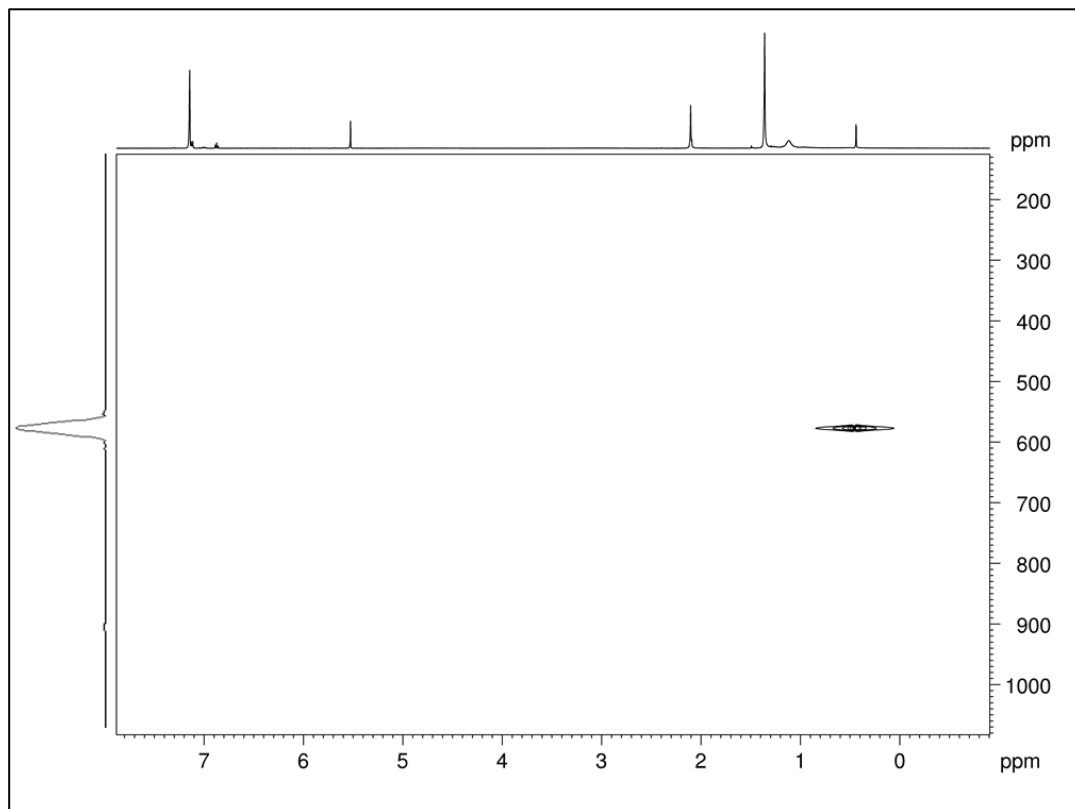


Figure S29. ^1H - ^{89}Y HSQC NMR spectrum (25 MHz, $[\text{D}_6]$ benzene) of complex $\text{Tp}^{\text{fBu,Me}}\text{YMe}(\text{OC}_6\text{H}_3/\text{Pr}_2\text{-2,6})$ (**6-Y**) at 26 °C.

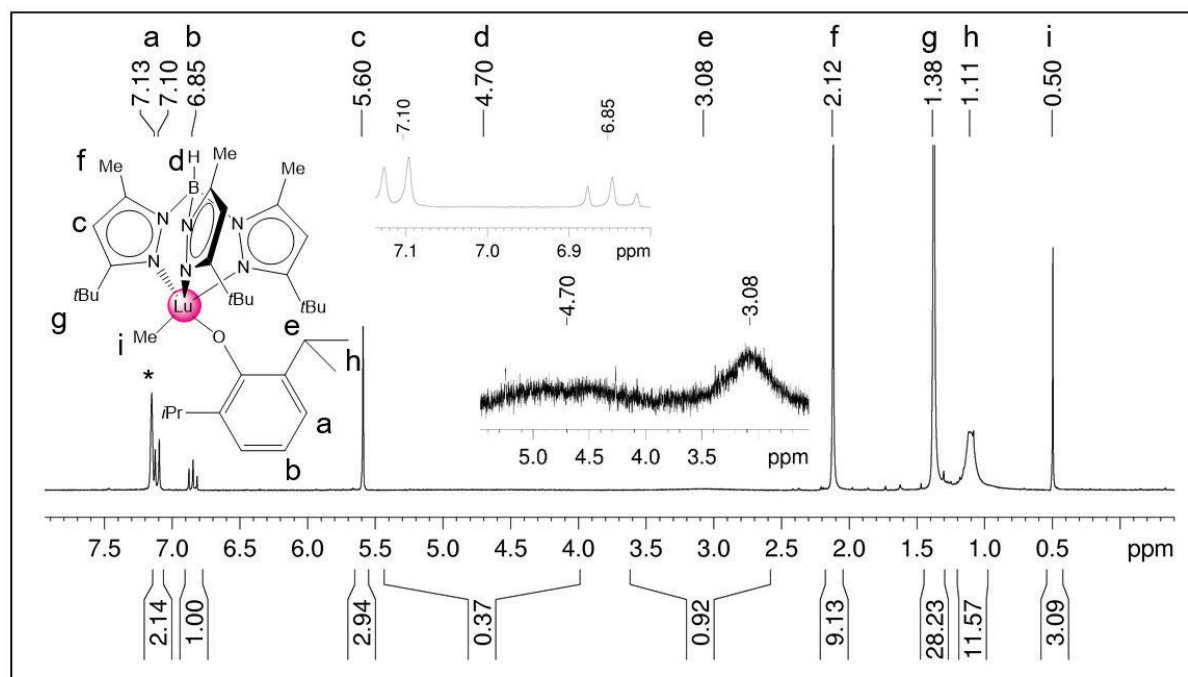


Figure S30. ^1H NMR spectrum (250 MHz, $[\text{D}_6]$ benzene) of complex $\text{Tp}^{\text{fBu,Me}}\text{LuMe}(\text{OC}_6\text{H}_3/\text{Pr}_2\text{-2,6})$ (**6-Lu**) at 26 °C.

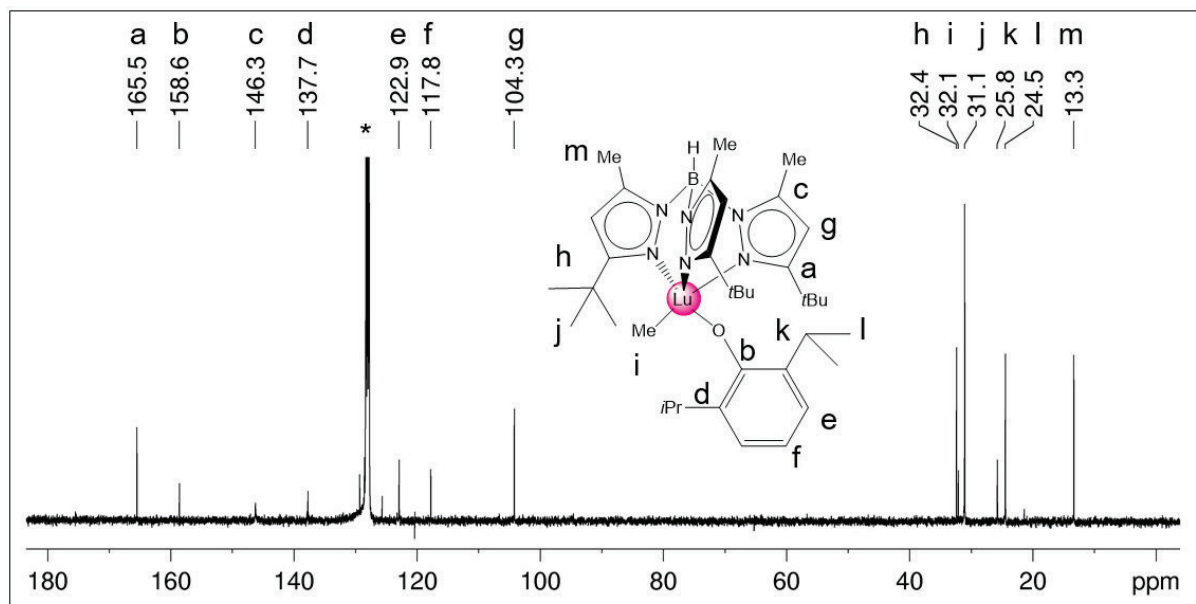


Figure S31. $^{13}\text{C}\{^1\text{H}\}$ NMR spectrum (63 MHz, $[\text{D}_6]$ benzene) of complex $\text{Tp}^{\text{tBu,Me}}\text{LuMe}(\text{OC}_6\text{H}_3i\text{Pr}_2\text{-2,6})$ (**6-Lu**) at 26 °C.

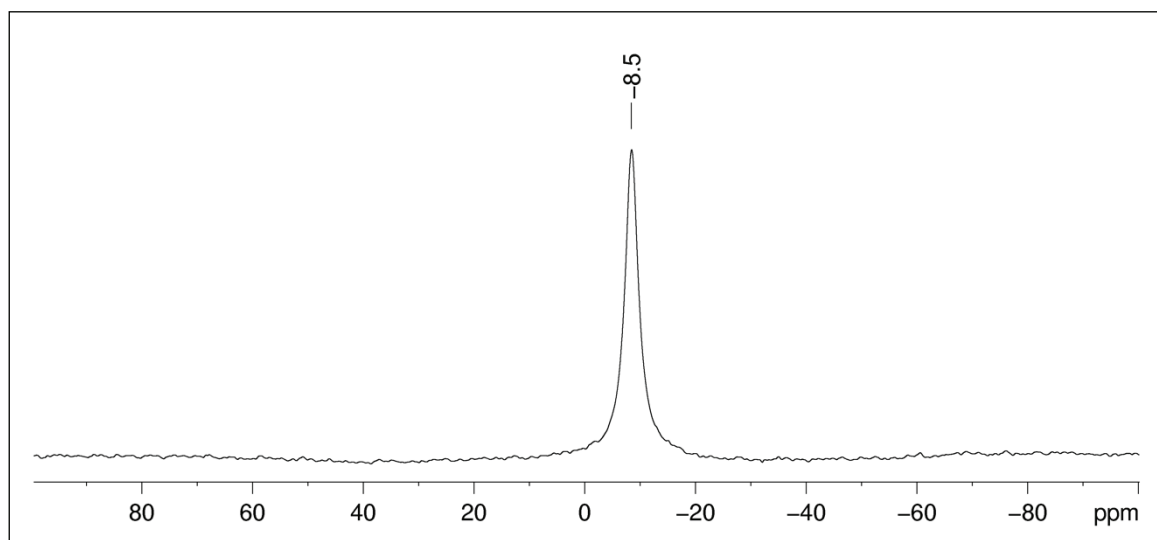


Figure S32. $^{11}\text{B}\{^1\text{H}\}$ NMR spectrum (80 MHz, $[\text{D}_6]$ benzene) of complex $\text{Tp}^{\text{tBu,Me}}\text{LuMe}(\text{OC}_6\text{H}_3i\text{Pr}_2\text{-2,6})$ (**6-Lu**) at 26 °C.

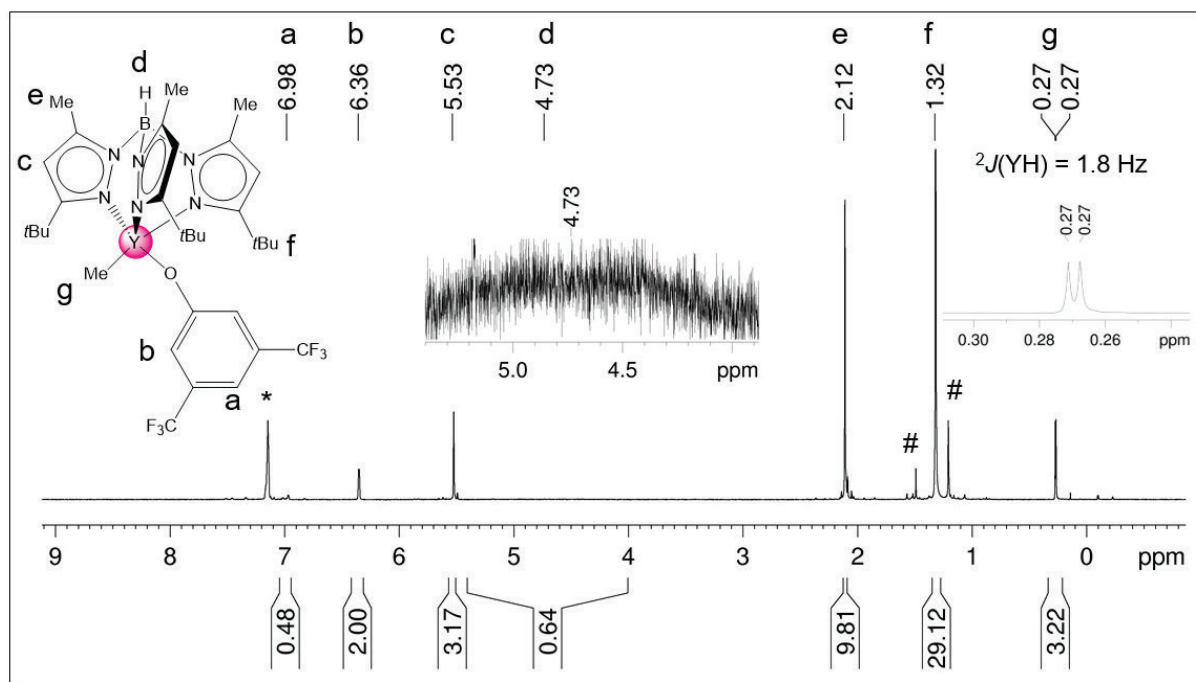


Figure S33. ^1H NMR spectrum (250 MHz, $[\text{D}_6]$ benzene) of complex $\text{Tp}^{\text{tBu,Me}}\text{YMe}[\text{OC}_6\text{H}_3(\text{CF}_3)_2\text{-3,5}]$ (**7-Y**) at 26 °C and traces of decomposition products (#).

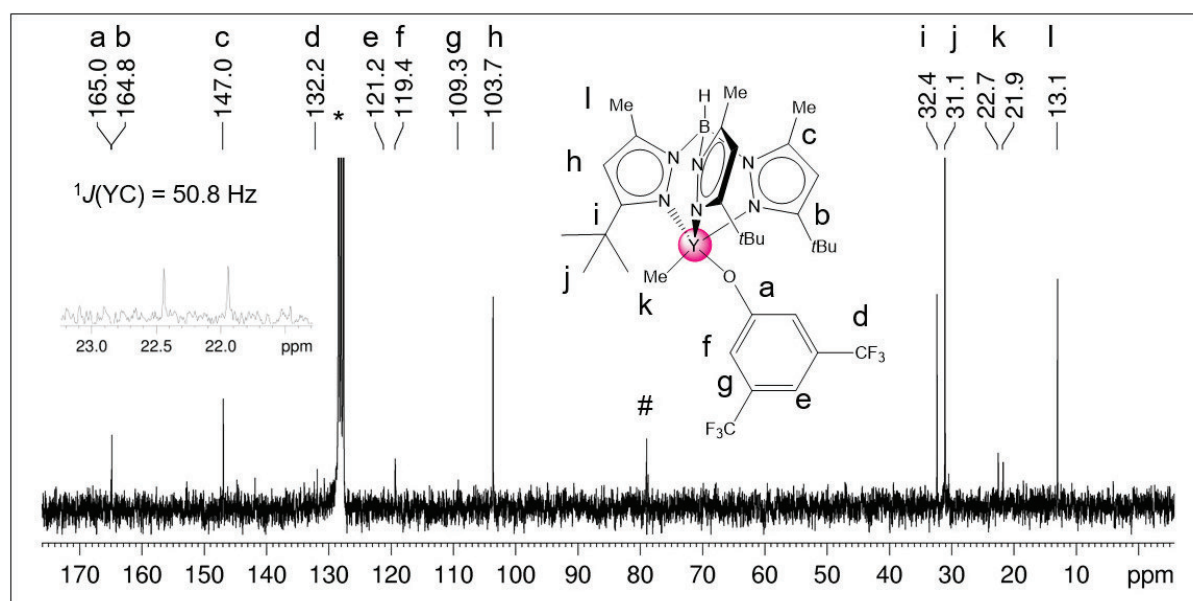


Figure S34. $^{13}\text{C}\{^1\text{H}\}$ NMR spectrum (63 MHz, $[\text{D}_6]$ benzene) of complex $\text{Tp}^{\text{tBu,Me}}\text{YMe}[\text{OC}_6\text{H}_3(\text{CF}_3)_2\text{-3,5}]$ (**7-Y**) at 26 °C and traces of decomposition products (#).

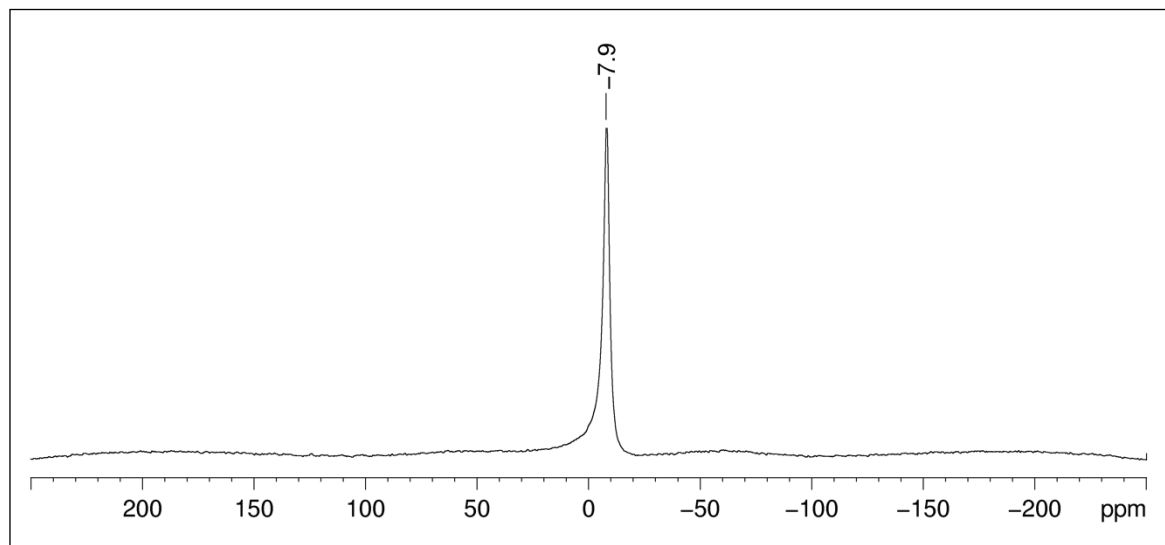


Figure S35. $^{11}\text{B}\{^1\text{H}\}$ NMR spectrum (80 MHz, $[\text{D}_6]$ benzene) of complex $\text{Tp}^{\text{tBu,Me}}\text{YMe}[\text{OC}_6\text{H}_3(\text{CF}_3)_2\text{-3,5}]$ (**7-Y**) at 26 °C.

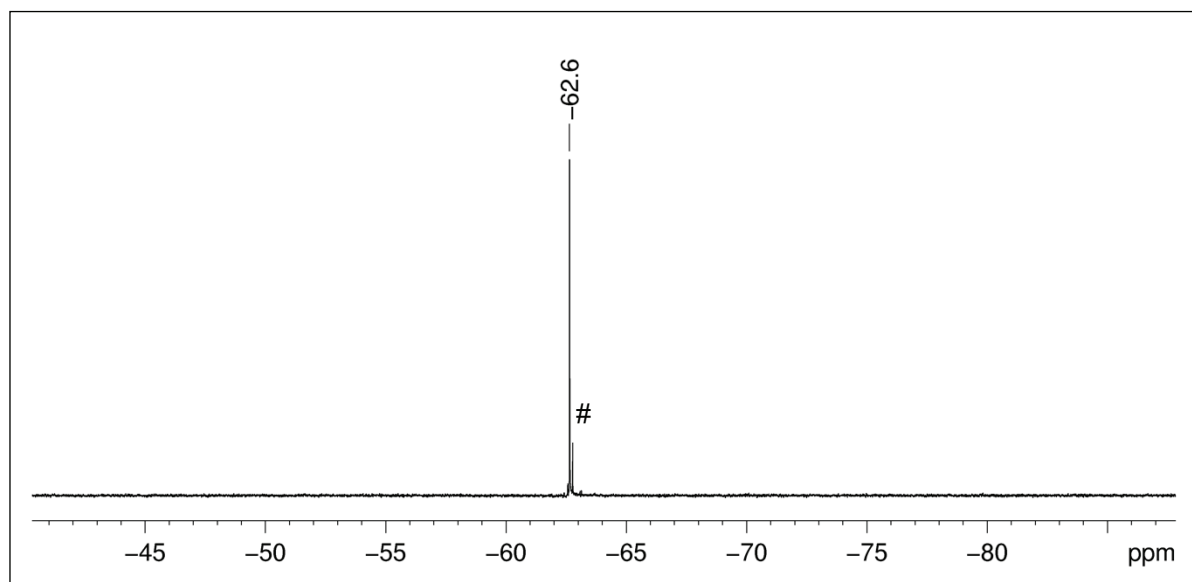


Figure S36. $^{19}\text{F}\{^1\text{H}\}$ NMR spectrum (376 MHz, $[\text{D}_6]$ benzene) of complex $\text{Tp}^{\text{tBu,Me}}\text{YMe}[\text{OC}_6\text{H}_3(\text{CF}_3)_2\text{-3,5}]$ (**7-Y**) at 26 °C and traces of decomposition products (#).

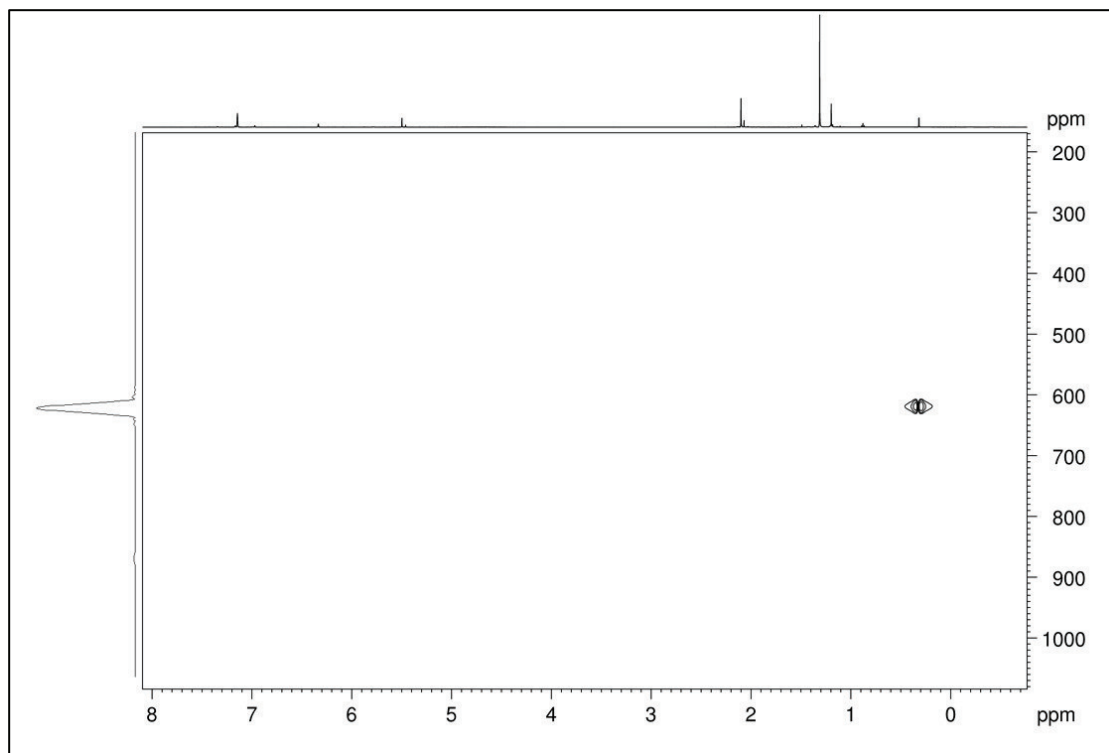


Figure S37. ^1H - ^{89}Y HSQC NMR spectrum (25 MHz, $[\text{D}_6]$ benzene) of complex $\text{Tp}^{\text{tBu,Me}}\text{YMe}[\text{OC}_6\text{H}_3(\text{CF}_3)_2\text{-3,5}]$ (**7-Y**) at 26 °C.

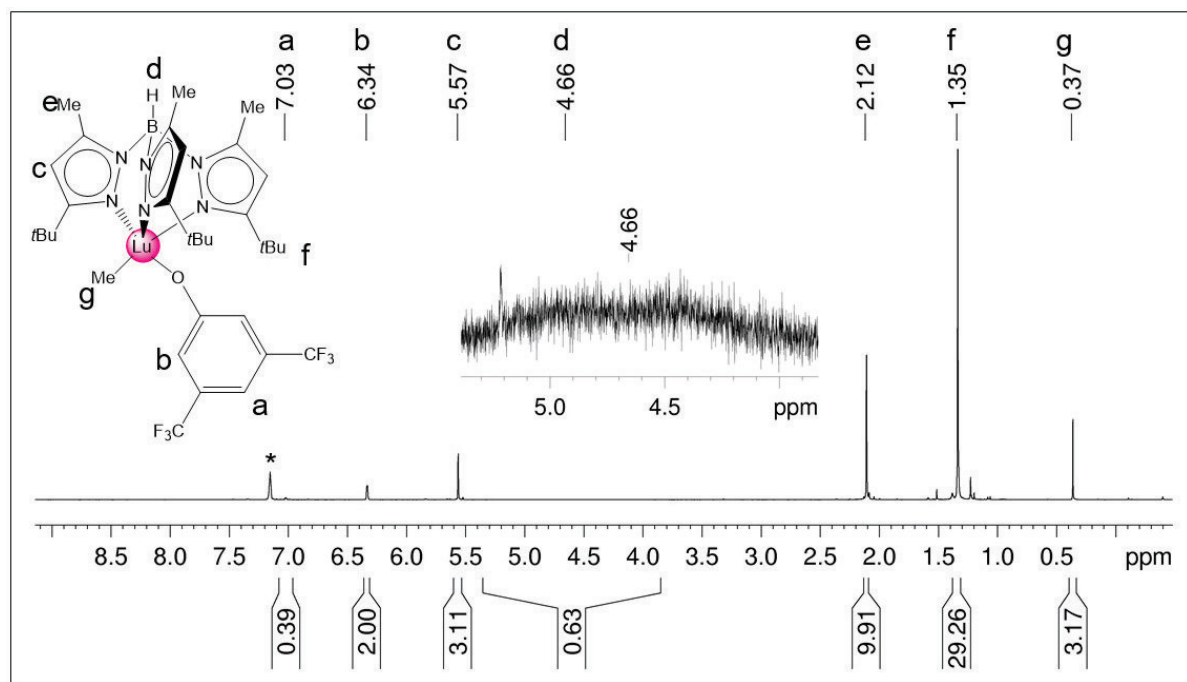


Figure S38. ^1H NMR spectrum (250 MHz, $[\text{D}_6]$ benzene) of complex $\text{Tp}^{\text{tBu,Me}}\text{LuMe}[\text{OC}_6\text{H}_3(\text{CF}_3)_2\text{-3,5}]$ (**7-Lu**) at 26 °C.

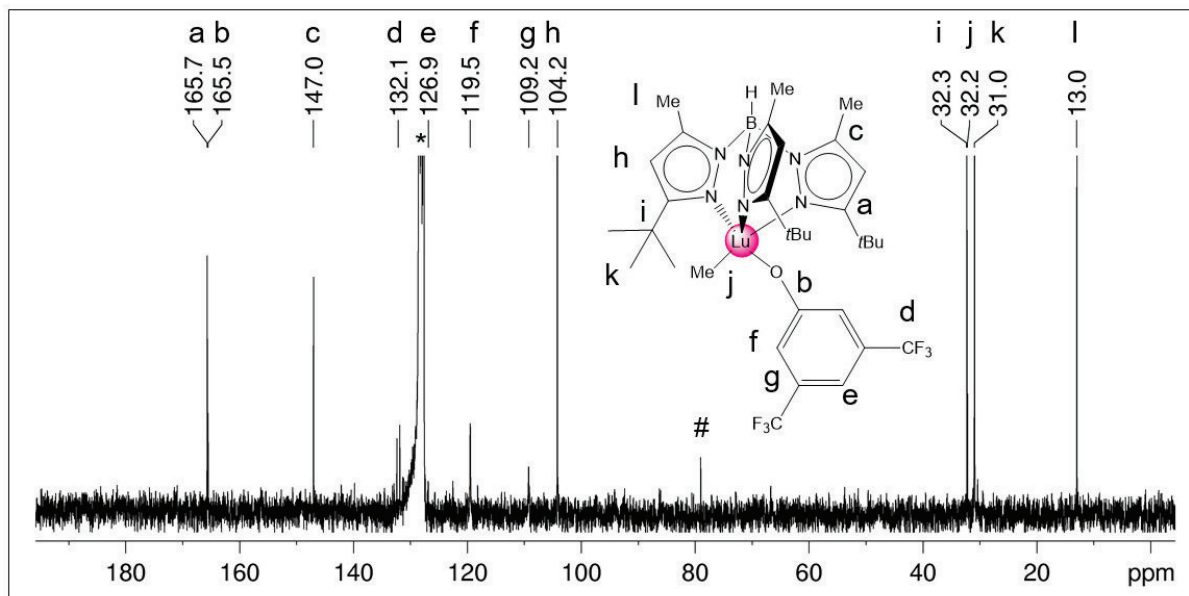


Figure S39. $^{13}\text{C}\{^1\text{H}\}$ NMR spectrum (63 MHz, $[\text{D}_6]$ benzene) of complex $\text{Tp}^{\text{tBu,Me}}\text{LuMe}[\text{OC}_6\text{H}_3(\text{CF}_3)_2\text{-3,5}]$ (**7-Lu**) at 26 °C and traces of decomposition products (#).

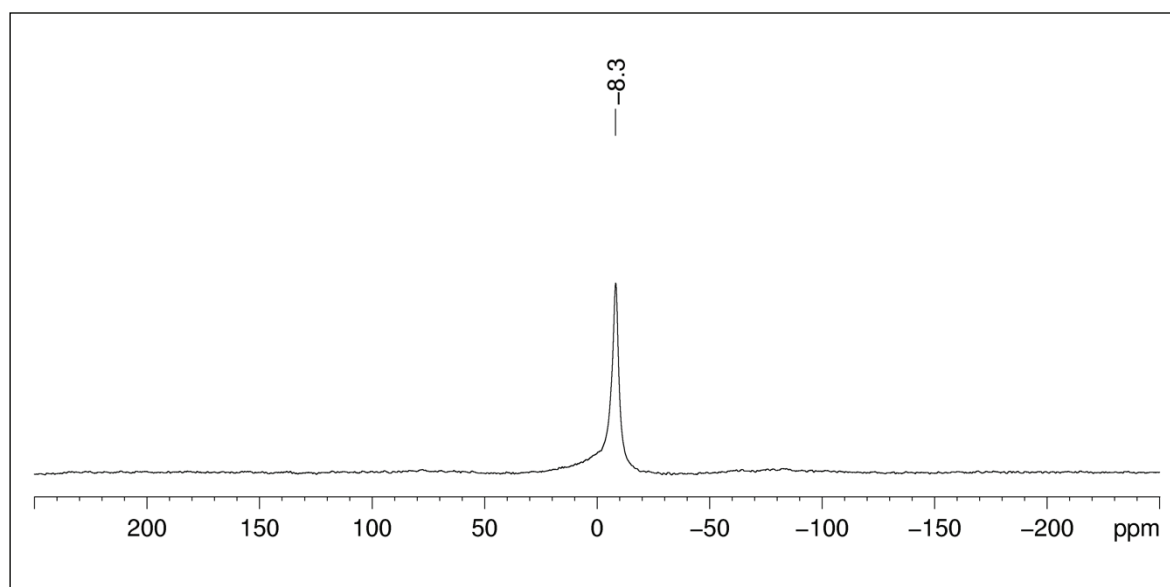


Figure S40. $^{11}\text{B}\{^1\text{H}\}$ NMR spectrum (80 MHz, $[\text{D}_6]$ benzene) of complex $\text{Tp}^{\text{tBu,Me}}\text{LuMe}[\text{OC}_6\text{H}_3(\text{CF}_3)_2\text{-3,5}]$ (**7-Lu**) at 26 °C.

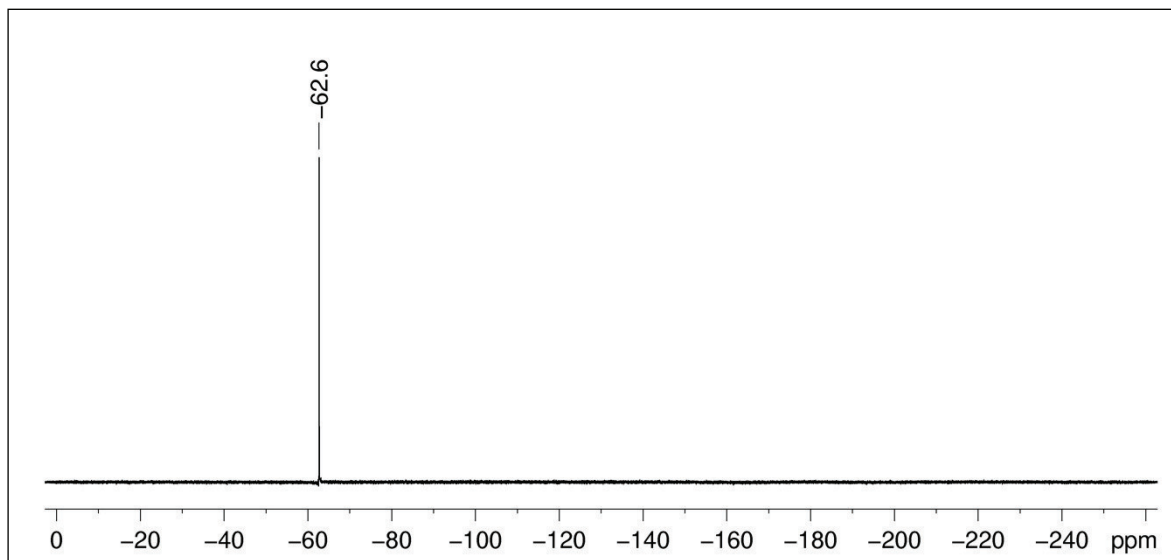


Figure S41. $^{19}\text{F}\{^1\text{H}\}$ NMR spectrum (376 MHz, $[\text{D}_6]$ benzene) of complex $\text{Tp}^{\text{tBu,Me}}\text{LuMe}[\text{OC}_6\text{H}_3(\text{CF}_3)_2\text{-3,5}]$ (**7-Lu**) at 26 °C.

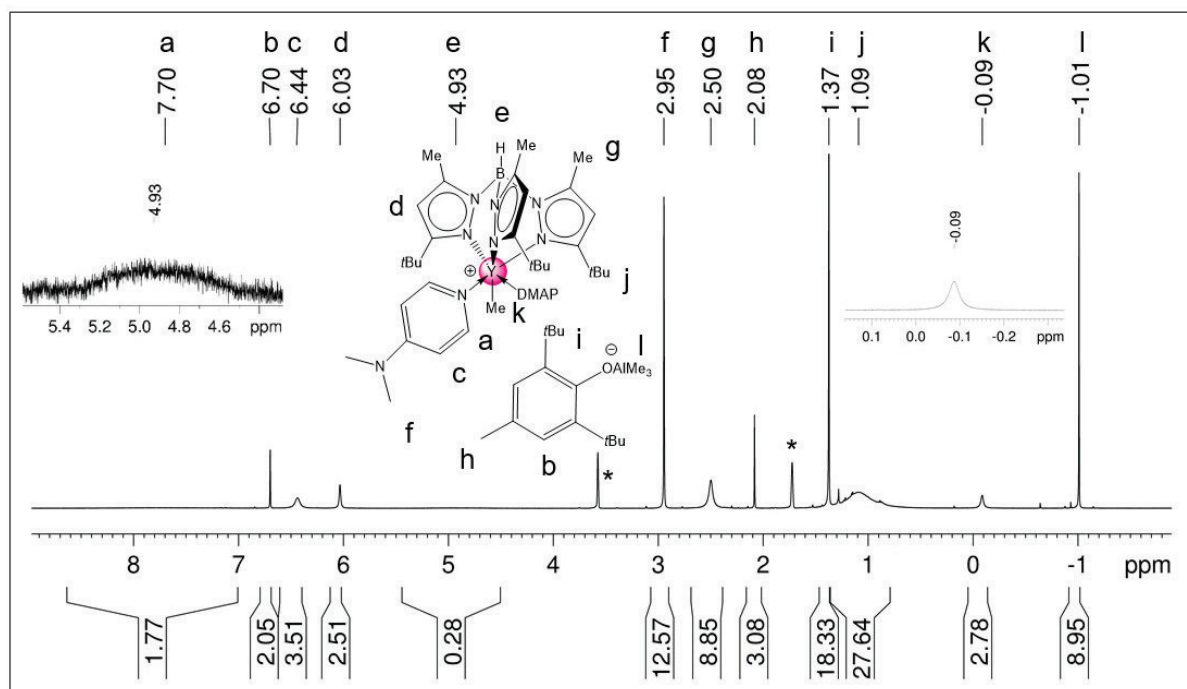


Figure S42. ^1H NMR spectrum (500 MHz, $[\text{D}_8]$ thf) of complex $[\text{Tp}^{\text{tBu,Me}}\text{YMe}(\text{dmap})_2][\text{Me}_3\text{Al}(\text{OC}_6\text{H}_2\text{tBu}_2\text{-2,6-Me-4})]$ (**8-Y**) at 0 °C, no Y-H coupling was observed.

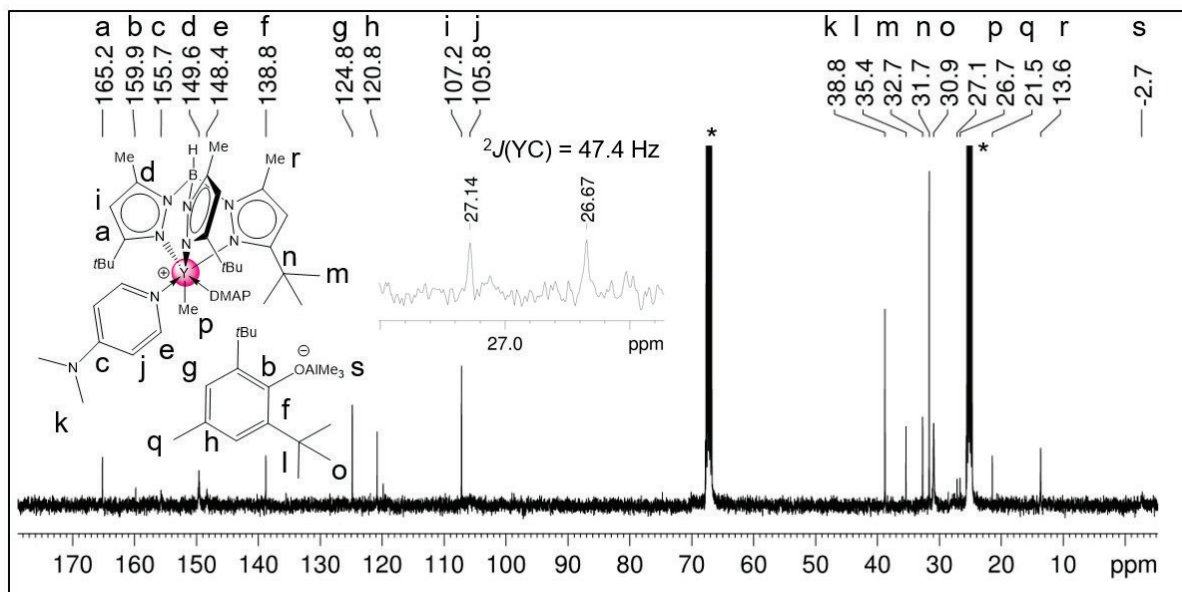


Figure S43. $^{13}\text{C}\{^1\text{H}\}$ NMR spectrum (101 MHz, $[\text{D}_8]\text{thf}$) of complex $[\text{Tp}^{\text{tBu,Me}}\text{YMe}(\text{dmap})_2][\text{Me}_3\text{Al}(\text{OC}_6\text{H}_2\text{tBu}_2\text{-2,6-Me-4})]$ (**8-Y**) at 26 °C.

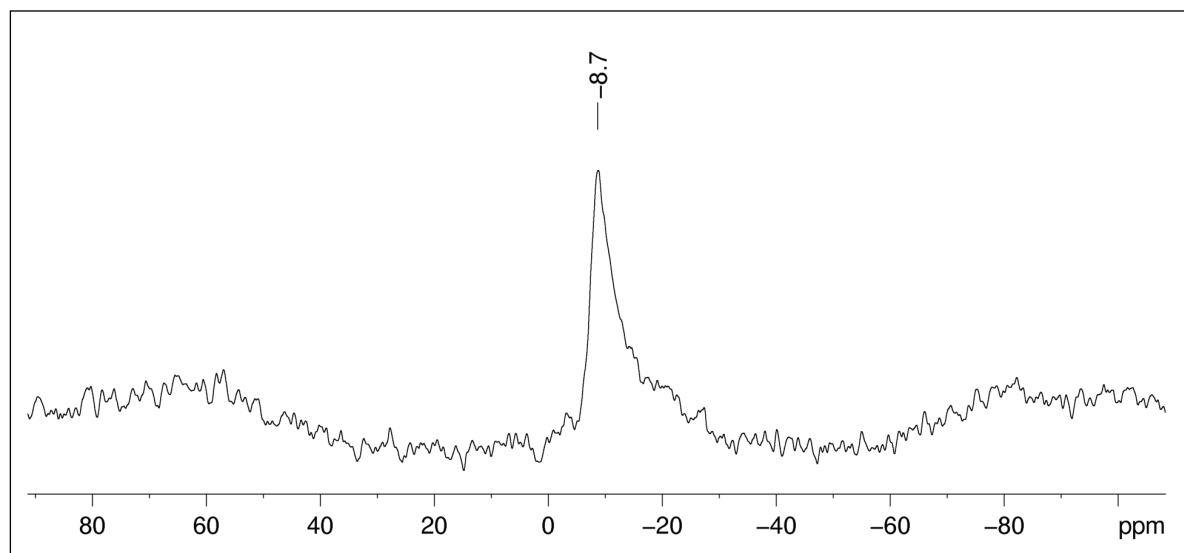


Figure S44. $^{11}\text{B}\{^1\text{H}\}$ NMR spectrum (80 MHz, $[\text{D}_8]\text{thf}$) of complex $[\text{Tp}^{\text{tBu,Me}}\text{YMe}(\text{dmap})_2][\text{Me}_3\text{Al}(\text{OC}_6\text{H}_2\text{tBu}_2\text{-2,6-Me-4})]$ (**8-Y**) at 26 °C.

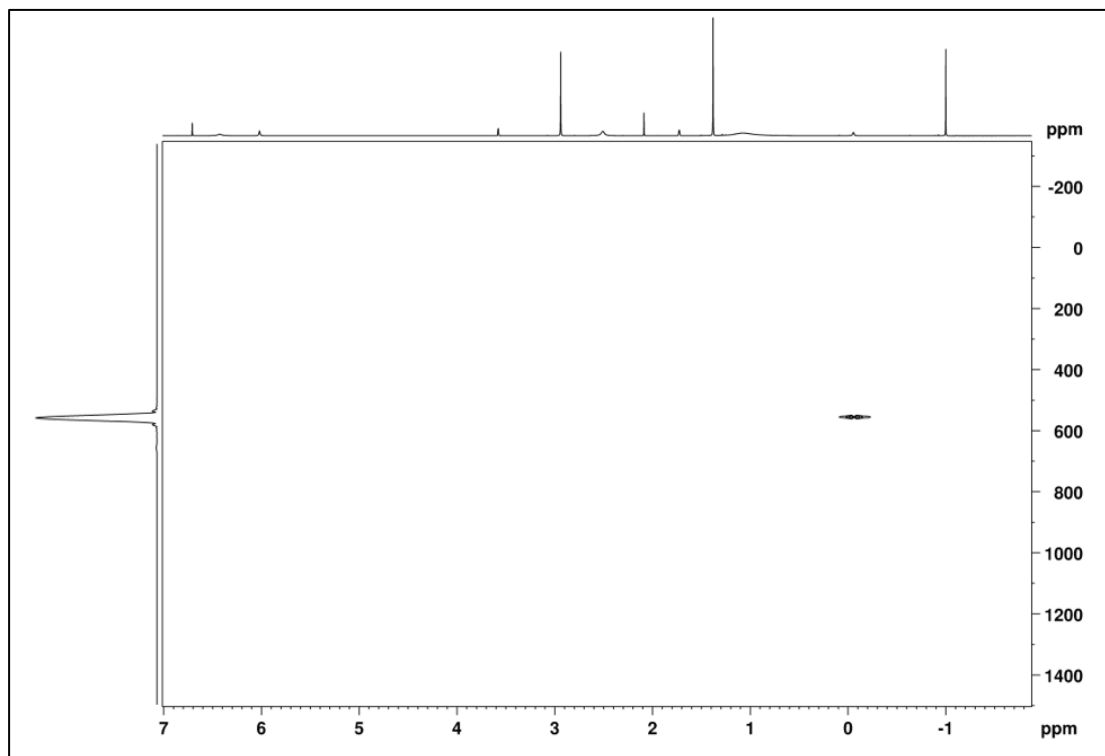


Figure S45. ^1H - ^{89}Y HSQC NMR spectrum (25 MHz, $[\text{D}_6]\text{thf}$) of complex $[\text{Tp}^{\text{tBu,Me}}\text{YMe}(\text{dmap})_2][\text{Me}_3\text{Al}(\text{OC}_6\text{H}_2\text{tBu}_2\text{-2,6-Me-4})]$ (**8-Y**) at 0°C .

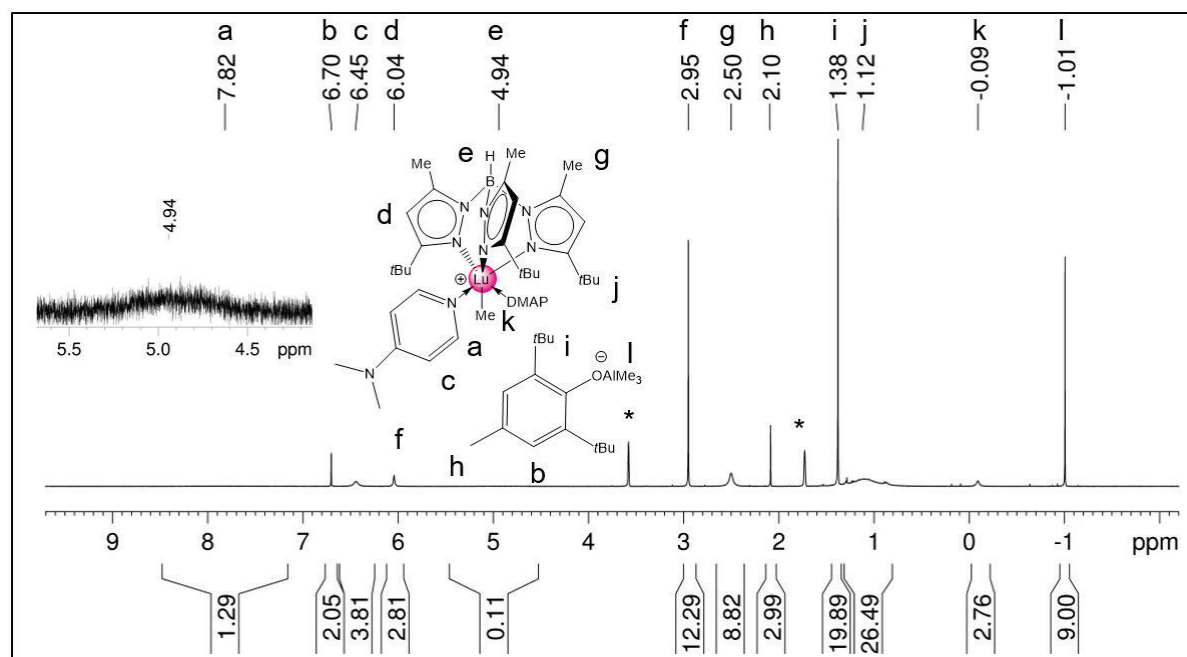


Figure S46. ^1H NMR spectrum (500 MHz, $[\text{D}_8]\text{thf}$) of complex $[\text{Tp}^{\text{tBu,Me}}\text{LuMe}(\text{dmap})_2][\text{Me}_3\text{Al}(\text{OC}_6\text{H}_2\text{tBu}_2\text{-2,6-Me-4})]$ (**8-Lu**) at 26°C .

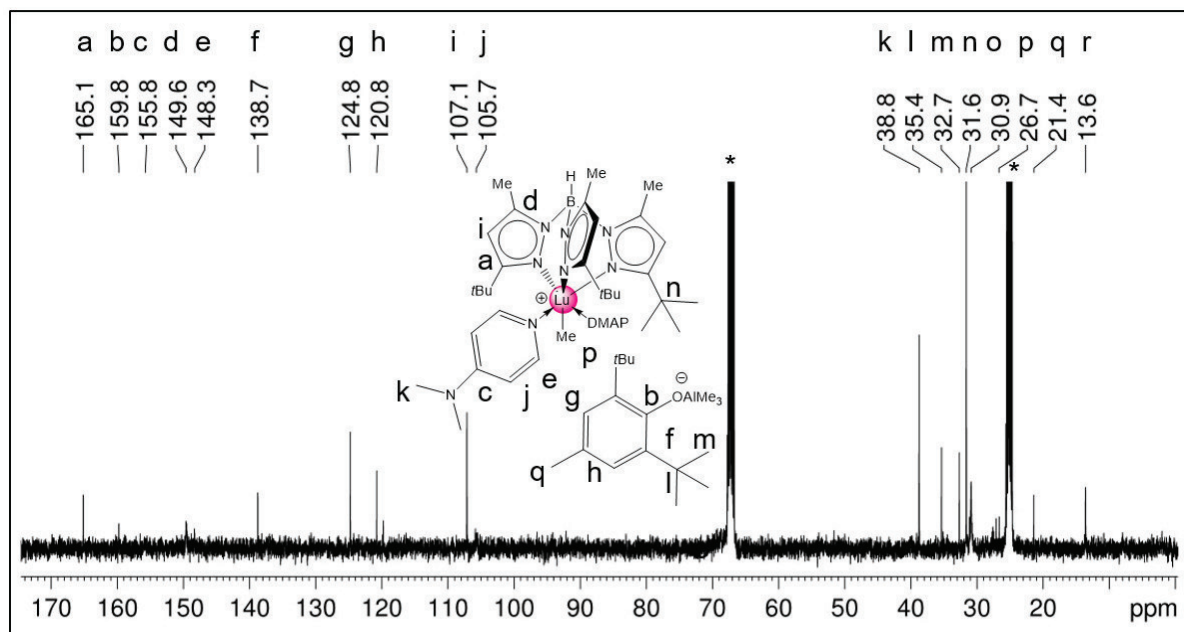


Figure S47. $^{13}\text{C}\{^1\text{H}\}$ NMR spectrum (101 MHz, $[\text{D}_3]\text{thf}$) of complex $[\text{Tp}^{\text{fBu,Me}}\text{LuMe}(\text{dmap})_2][\text{Me}_3\text{Al}(\text{OC}_6\text{H}_2\text{fBu}_2\text{-2,6-Me-4})]$ (**8-Lu**) at 26 °C.

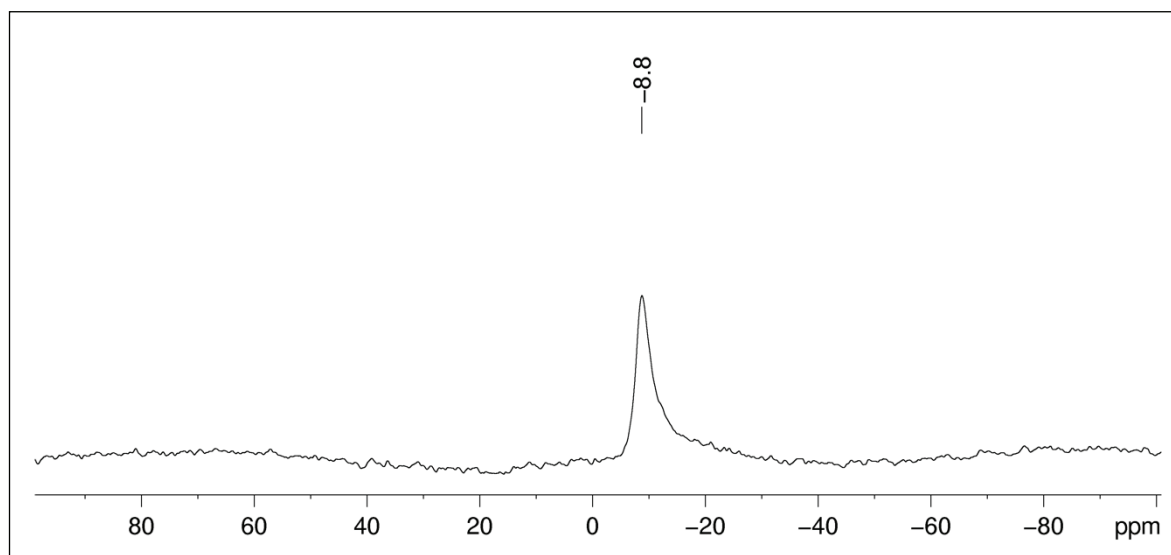
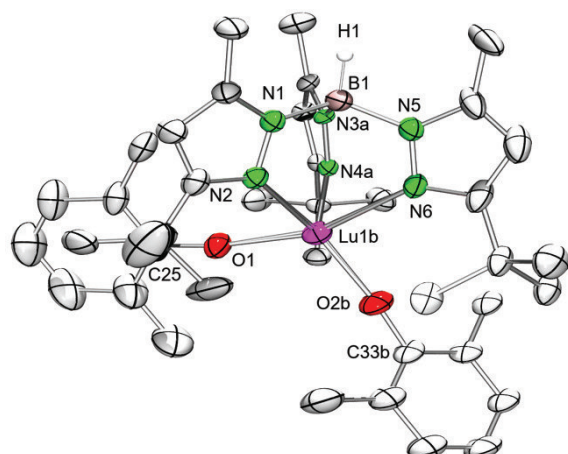


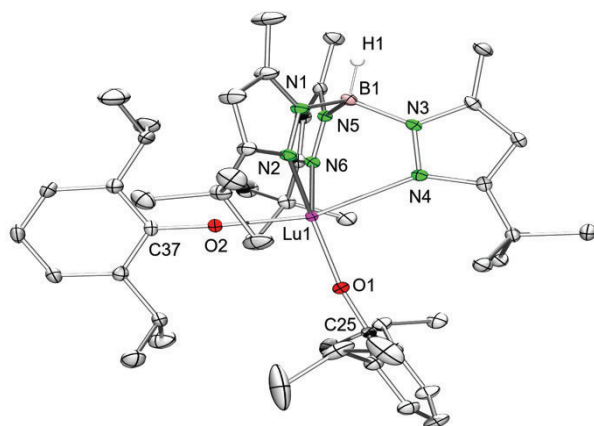
Figure S48. $^{11}\text{B}\{^1\text{H}\}$ NMR spectrum (80 MHz, $[\text{D}_3]\text{thf}$) of complex $[\text{Tp}^{\text{fBu,Me}}\text{LuMe}(\text{dmap})_2][\text{Me}_3\text{Al}(\text{OC}_6\text{H}_2\text{fBu}_2\text{-2,6-Me-4})]$ (**8-Lu**) at 26 °C.

X-ray structure analyses



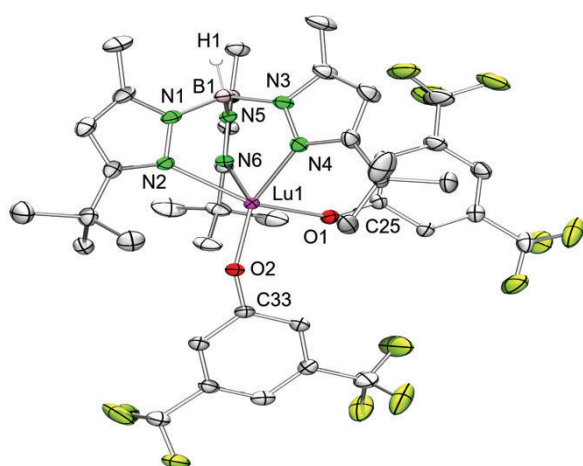
1-Lu	Selected bond lengths and angles [Å, °]
Lu1b–N2	2.335(2)
Lu1b–N4	2.362(9)
Lu1b–N6	2.439(3)
Lu1b–O1	2.052(2)
Lu1b–O2b	2.06(2)
Lu1b–O1–C25	170.9(2)
Lu1b–O2b–C33b	174(3)

Figure S49. ORTEP representation of the crystal structure of **1-Lu** with atomic displacement parameters set at the 50% level. Hydrogen atoms except for BH and the disorder in the *tert*-butyl groups, one aryloxy ligand, and one pyrazolyl ligand are omitted for clarity.



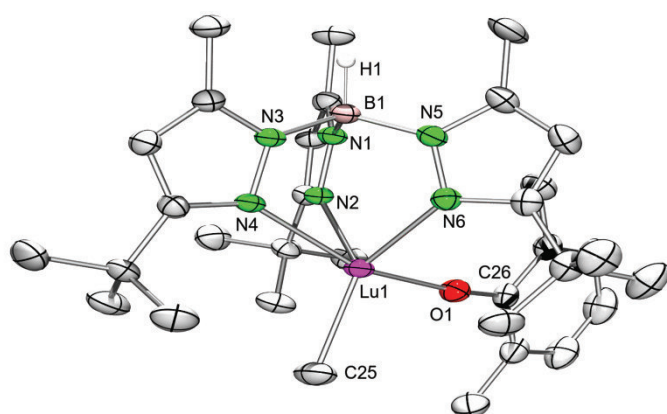
2-Lu	Selected bond lengths and angles [Å, °]
Lu1–N2	2.365(1)
Lu1–N4	2.517(1)
Lu1–N6	2.370(1)
Lu1–O1	2.072(1)
Lu1–O2	2.038(1)
Lu1–O1–C25	171.8(1)
Lu1–O2–C37	175.4(1)

Figure S50. ORTEP representation of the crystal structure of **2-Lu** with atomic displacement parameters set at the 50% level. Hydrogen atoms except for BH, the second molecule in the unit cell and solvents are omitted for clarity.



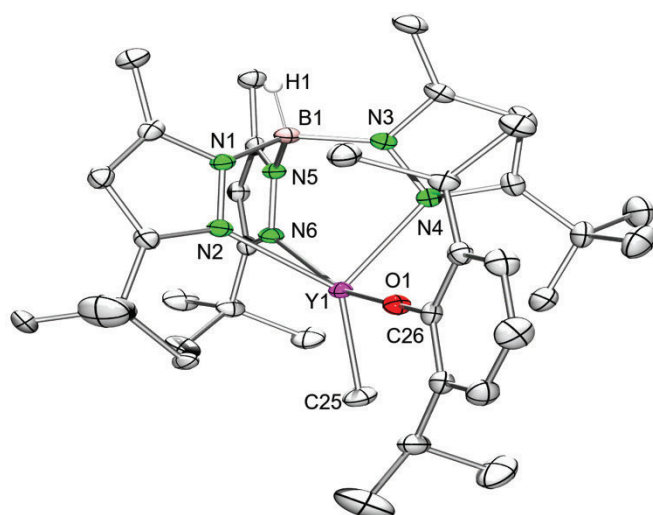
3-Lu	Selected bond lengths and angles [Å, °]
Lu1–N2	2.397(2)
Lu1–N4	2.318(2)
Lu1–N6	2.315(2)
Lu1–O1	2.090(2)
Lu1–O2	2.064(2)
Lu1–O1–C25	145.3(2)
Lu1–O2–C33	147.3(2)

Figure S51. ORTEP representation of the crystal structure of **3-Lu** with atomic displacement parameters set at the 50% level. Hydrogen atoms except for BH and the disorder in one CF₃ group are omitted for clarity.



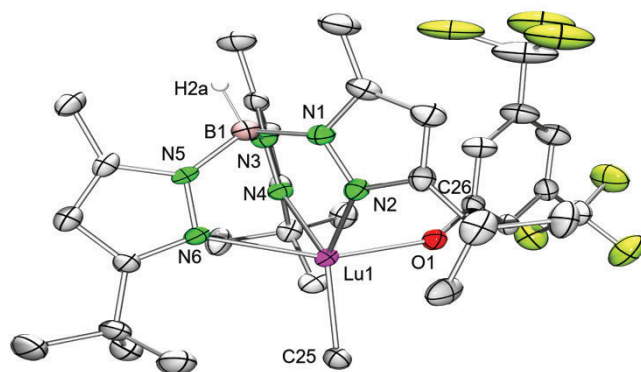
5-Lu	Selected bond lengths and angles [Å, °]
Lu1–N2	2.334(2)
Lu1–N4	2.492(2)
Lu1–N6	2.328(2)
Lu1–O1	2.053(2)
Lu1–C25	2.358(3)
Lu1–O1–C26	167.2(2)

Figure S52. ORTEP representation of the crystal structure of **5-Lu** with atomic displacement parameters set at the 50% level. Hydrogen atoms except for BH are omitted for clarity.



6-Y	Selected bond lengths and angles [Å, °]
Y1–N2	2.375(1)
Y1–N4	2.384(2)
Y1–N6	2.561(2)
Y1–O1	2.087(1)
Y1–C25	2.404(2)
Y1–O1–C26	176.9(1)

Figure S53. ORTEP representation of the crystal structure of **6-Y** with atomic displacement parameters set at the 50% level. Hydrogen atoms except for BH, the disorder in one *tert*-butyl group and solvent molecules are omitted for clarity.



7-Lu	Selected bond lengths and angles [Å, °]
Lu1–N2	2.319(4)
Lu1–N4	2.322(4)
Lu1–N6	2.442(4)
Lu1–O1	2.085(3)
Lu1–C25	2.339(6)
Lu1–O1–C26	150.9(3)

Figure S54. ORTEP representation of the crystal structure of **7-Lu** with atomic displacement parameters set at the 50% level. Hydrogen atoms except for BH, the second molecule in the unit cell and the disorder in one CF₃ group are omitted for clarity.

Table S1. Comprehensive crystallographic data for compounds **1-Lu**, **2-Lu**, **3-Lu**, and **4-Lu**

	1-Lu	2-Lu	3-Lu	4-Lu
CCDC	1952866	1952862	1952859	1952861
formula	C ₄₀ H ₅₈ BLuN ₆ O ₂	C ₄₈ H ₇₄ BLuN ₆ O ₂ • ½ C ₇ H ₈	C ₄₀ H ₄₆ BF ₁₂ LuN ₆ O ₂	C ₄₀ H ₆₆ BLuN ₆ O
M [g mol ⁻¹]	839.69	998.97	1056.61	832.76
crystal system	triclinic	triclinic	monoclinic	monoclinic
space group	<i>P</i> $\bar{1}$	<i>P</i> $\bar{1}$	<i>P</i> 2 ₁ /c	<i>P</i> 2 ₁ /c
a [Å]	13.2578(12)	10.0205(6)	11.2564(8)	19.301(2)
b [Å]	14.1925(13)	22.1089(14)	21.3657(14)	9.9326(11)
c [Å]	14.9775(14)	23.8154(15)	18.8036(13)	22.217(2)
α [°]	90.420(2)	76.770(2)	90	90
β [°]	109.7010(10)	78.528(2)	96.4670(10)	104.378(2)
γ [°]	103.9910(10)	84.220(2)	90	90
V [Å ³]	2562.3(4)	5025.0(5)	4493.5(5)	4125.8(8)
Z	2	4	4	4
T [K]	102(2)	100(2)	100(2)	100(2)
ρ _{calcd} [g cm ⁻³]	1.090	1.320	1.562	1.341
μ [mm ⁻¹]	1.958	2.008	2.287	2.429
F (000)	864	2084	2112	1728
Θ range [°]	1.486 to 27.483	1.786 to 29.130	2.055 to 29.117	1.893 to 27.200
total reflns	56923	195002	65376	87459
unique reflns	11737	27049	12066	9184
R _{int}	0.0478	0.0440	0.0432	0.0623
observed reflns (I > 2σ)	10141	23803	10379	8005
Data/restraints/parameter	11737 / 741 / 727	27049 / 29 / 1169	12066 / 55 / 632	9184 / 0 / 466
R1/wR2 (I > 2σ) ^[a]	0.0290 / 0.0613	0.0205 / 0.0470	0.0279 / 0.0635	0.0323 / 0.0610
R1/wR2 (all data) ^[a]	0.0392 / 0.0643	0.0260 / 0.0491	0.0352 / 0.0667	0.0402 / 0.0628
GOF ^[a]	1.073	1.028	1.036	1.193
largest diff. peak and hole [e Å ⁻³]	1.120 and -0.823	1.107 and -0.714	1.545 and -0.705	1.459 and -1.855

[a] R1 = $\Sigma(|F_0| - |F_c|) / \Sigma|F_0|$, F₀ > 4s(F₀). wR2 = $\{\Sigma[w(F_0^2 - F_c^2)^2] / \Sigma[w(F_0^2)^2]\}^{1/2}$.

Table S1 continued.Comprehensive crystallographic data for compounds **5-Y**, **5-Lu**, **6-Y**, and **6-Lu**

	5-Y	5-Lu	6-Y	6-Lu
CCDC	1952865	1952858	1952868	1952860
formula	C ₃₃ H ₅₂ BN ₆ OY	C ₃₃ H ₅₂ BLuN ₆ O	C ₄₄ H ₆₈ BN ₆ OY	C ₄₄ H ₆₈ BLuN ₆ O
M [g mol ⁻¹]	648.52	734.58	796.76	882.82
crystal system	monoclinic	monoclinic	monoclinic	triclinic
space group	<i>P2₁/n</i>	<i>P2₁/n</i>	<i>P2₁/n</i>	<i>P$\bar{1}$</i>
a [Å]	11.8874(2)	11.8831(5)	20.0903(12)	10.6560(5)
b [Å]	19.2010(3)	19.2344(8)	10.2628(6)	12.6363(5)
c [Å]	15.5311(3)	15.4889(7)	22.1377(13)	17.0849(7)
α [°]	90	90	90	76.3380(10)
β [°]	96.7110(10)	96.3300(10)	104.0960(10)	82.3050(10)
γ [°]	90	90	90	87.5710(10)
V [Å ³]	3520.68(11)	3518.6(3)	4427.0(5)	2215.16(16)
Z	4	4	4	2
T [K]	160(2)	180(2)	99(2)	100(2)
ρ _{calcd} [g cm ⁻³]	1.224	1.387	1.195	1.324
μ [mm ⁻¹]	1.689	2.838	1.356	2.267
F (000)	1376	1504	1704	916
Θ range [°]	1.693 to 27.875	1.694 to 30.119	1.897 to 27.099	1.659 to 30.538
total reflns	44128	62037	79010	99941
unique reflns	8401	10339	9763	13480
R _{int}	0.0371	0.0476	0.0777	0.0362
observed reflns (I > 2σ)	6562	8229	7940	12838
Data/restraints/parameter	8401 / 0 / 398	10339 / 0 / 398	9763 / 333 / 584	13480 / 0 / 500
R1/wR2 (I > 2σ) ^[a]	0.0365 / 0.0755	0.0273 / 0.0581	0.0333 / 0.0765	0.0172 / 0.0407
R1/wR2 (all data) ^[a]	0.0583 / 0.0821	0.0406 / 0.0637	0.0480 / 0.0826	0.0186 / 0.0413
GOF ^[a]	1.017	1.025	1.006	1.055
largest diff. peak and hole [e Å ⁻³]	0.536 and -0.704	2.338 and -0.919	0.384 and -0.335	2.016 and -0.752

[a] $R1 = \frac{\sum(|F0| - |Fc|)}{\sum|F0|}$, $F0 > 4s(F0)$. $wR2 = \{\frac{\sum[w(F02 - Fc2)^2]}{\sum[w(F02)^2]}\}^{1/2}$.

Table S1 continued.Comprehensive crystallographic data for compounds **7-Y**, **7-Lu**, **8-Y**, and **9-Lu**

	7-Y	7-Lu	8-Y	9-Lu
CCDC	1952863	1952857	1952867	1952864
Formula	C ₃₃ H ₄₆ BF ₆ N ₆ OY	C ₃₃ H ₄₆ BF ₆ LuN ₆ O	C ₅₇ H ₉₅ AIBN ₁₀ OY	C ₃₉ H ₆₂ BLuN ₆ O
M [g mol ⁻¹]	756.48	842.54	1063.12	816.72
Crystal system	monoclinic	monoclinic	triclinic	monoclinic
Space group	P 2 ₁	P 2 ₁ /c	P $\bar{1}$	P 2 ₁ /c
a [Å]	20.8816(15)	20.8123(15)	16.8784(16)	17.0580(12)
b [Å]	21.1727(15)	21.1757(15)	20.723(2)	11.9100(9)
c [Å]	18.8326(13)	18.8646(14)	20.752(2)	20.5209(15)
α [°]	90	90	61.930(2)	90
β [°]	116.7770(10)	116.879(2)	72.578(3)	110.9950(10)
γ [°]	90	90	79.844(3)	90
V [Å ³]	7433.4(9)	7415.7(9)	6105.6(10)	3892.3(5)
Z	2	8	4	4
T [K]	100(2)	100(2)	100(2)	100(2)
ρ _{calcd} [g cm ⁻³]	1.352	1.509	1.157	1.394
μ [mm ⁻¹]	1.633	2.727	1.014	2.574
F (000)	3136	3392	2288	1688
Θ range [°]	1.211 to 28.282	1.097 to 30.032	1.477 to 30.184	1.338 to 27.483
total reflns	148707	21614	265056	68987
unique reflns	36898	21614	35933	8921
R _{int}	0.0836	0.061	0.1098	0.0928
observed reflns (I > 2σ)	27179	18206	24681	6770
Data/restraints/parameter	36898 / 3181 / 1908	21614 / 69 / 919	35933 / 0 / 1341	8921 / 36 / 485
R1/wR2 (I > 2σ) ^[a]	0.0508 / 0.1086	0.0386 / 0.0863	0.0475 / 0.0946	0.0284 / 0.0555
R1/wR2 (all data) ^[a]	0.0834 / 0.1225	0.0509 / 0.0923	0.0900 / 0.1088	0.0491 / 0.0617
GOF ^[a]	1.021	1.073	1.018	1.017
largest diff. peak and hole [e Å ⁻³]	1.776 and -0.366	5.899 and -1.015	0.639 and -0.541	0.558 and -0.681

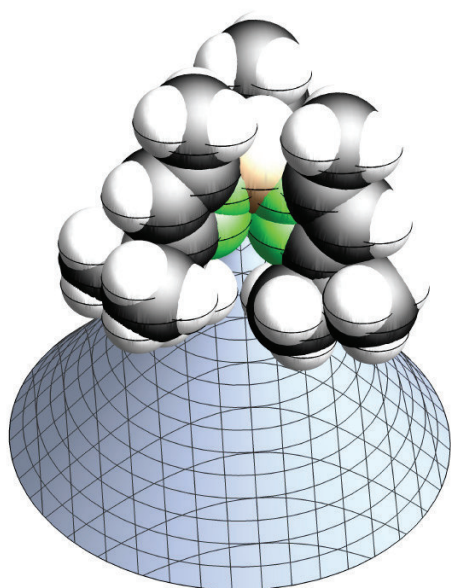
[a] R1 = $\Sigma(|F_0| - |F_c|) / \Sigma|F_0|$, F₀ > 4s(F₀). wR2 = $\{\Sigma[w(F_0 - F_c)^2] / \Sigma[w(F_0)^2]\}^{1/2}$.

Cone angle calculations

To calculate the mathematically exact cone angles a series of .xyz files was generated from the final .cif files with ORTEP. The Mathematica package was downloaded free of charge from <http://www.ccqc.uga.edu/references/software.php>.

The supplemental file [cone angle data.xyz] contains the computed Cartesian coordinates of all of the molecules reported in this study. The file may be opened as a text file to read the coordinates, or opened directly by a molecular modeling program such as Mercury (version 3.3 or later, <http://www.ccdc.cam.ac.uk/pages/Home.aspx>) for visualization and analysis.

The adopted van der Waals radii were $r = 1.20, 1.70, 1.55, 1.52, 1.92 \text{ \AA}$ for H, C, N, O, B in this order.



$\text{Tp}^{\text{tBu,Me}}\text{YMe}(\text{AlMe}_4)_a$

Ligand atoms forming cone = {19, 40, 57}

Cone angle (deg) = 280.65

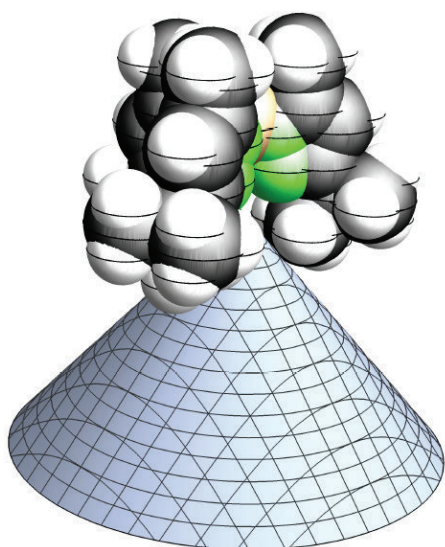
Cone axis = {0.547789, 0.180831, -0.81684}

$\text{Tp}^{\text{tBu,Me}}\text{YMe}(\text{AlMe}_4)_b$ (cone depicted)

Ligand atoms forming cone = {29, 45, 68}

Cone angle (deg) = 276.12

Cone axis = {0.446285, 0.195798, -0.873208}

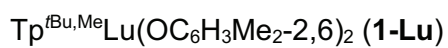
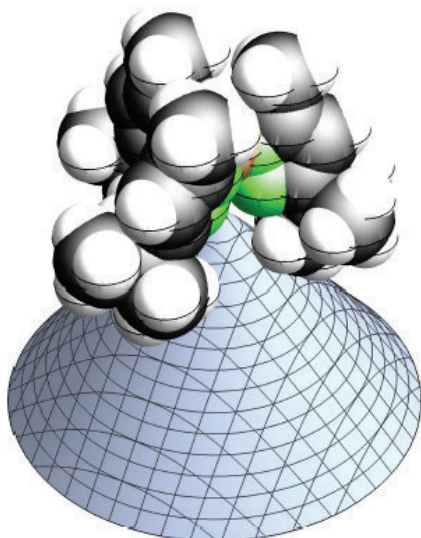


$\text{Tp}^{\text{tBu,Me}}\text{LuMe}_2$

Ligand atoms forming cone = {25, 38, 63}

Cone angle (deg) = 277.06

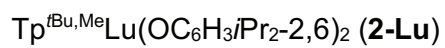
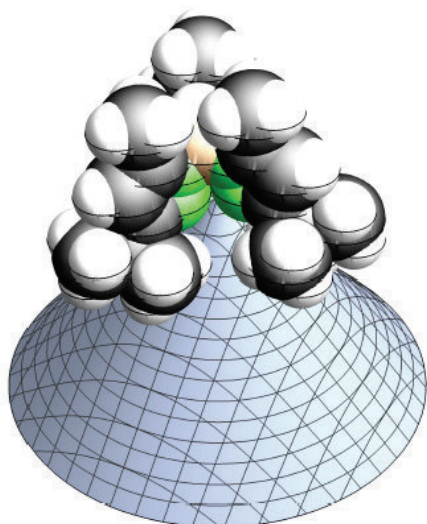
Cone axis = { -0.894711, -6.37622 $\times 10^{-17}$, -0.446646}



Ligand atoms forming cone = {8, 48, 55}

Cone angle (deg) = 276.07

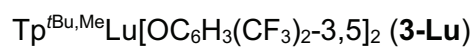
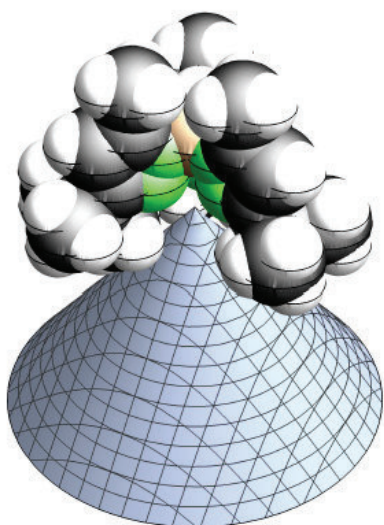
Cone axis = {-0.225924, 0.939593, 0.257144}



Ligand atoms forming cone = {19, 31, 53}

Cone angle (deg) = 272.526

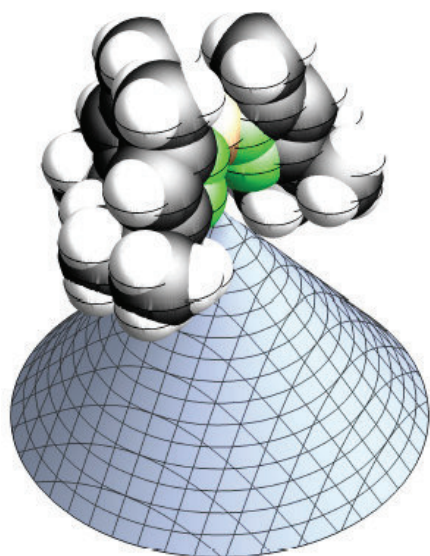
Cone axis = {-0.166388, 0.92943, 0.329356}



Ligand atoms forming cone = {20, 26, 54}

Cone angle (deg) = 280.424

Cone axis = {-0.71205, -0.687129, 0.144353}

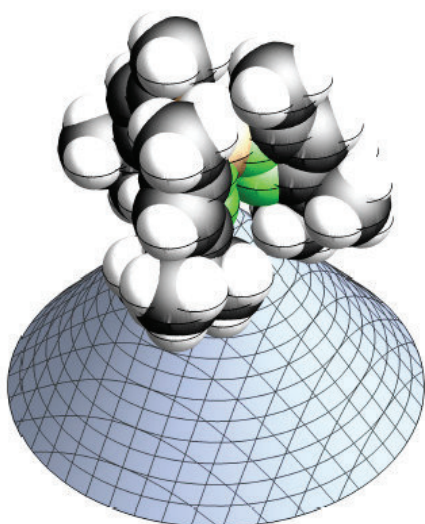


$\text{Tp}^{\text{tBu,Me}}\text{LuMe}(\text{OC}_6\text{H}_2\text{tBu}_2\text{-2,6-Me-4})$ (**4-Lu**)

Ligand atoms forming cone = {21, 43, 44}

Cone angle (deg) = 278.118

Cone axis = {-0.165494, 0.984032, -0.0655229}

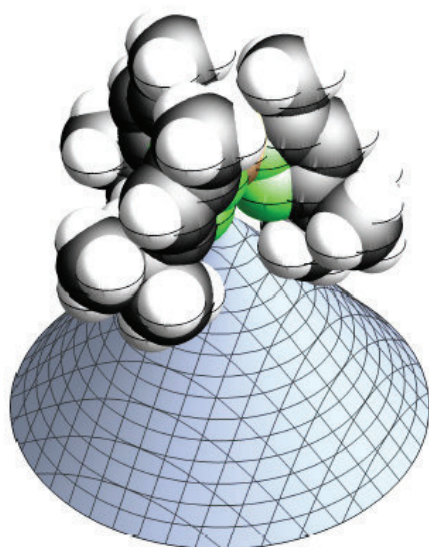


$\text{Tp}^{\text{tBu,Me}}\text{YMe}(\text{OC}_6\text{H}_3\text{Me}_2\text{-2,6})$ (**5-Y**)

Ligand atoms forming cone = {23, 39, 57}

Cone angle (deg) = 273.902

Cone axis = {0.696277, -0.00548779, -0.717752}

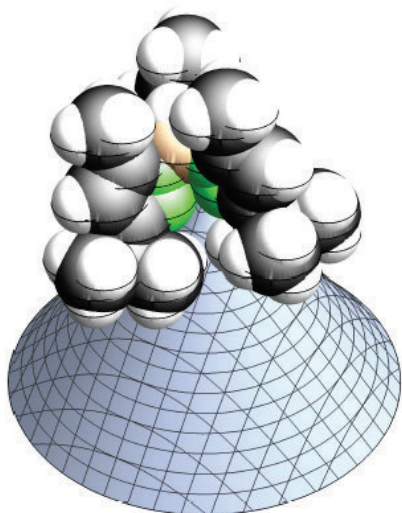


$\text{Tp}^{\text{tBu,Me}}\text{LuMe}(\text{OC}_6\text{H}_3\text{Me}_2\text{-2,6})$ (**5-Lu**)

Ligand atoms forming cone = {8, 48, 55}

Cone angle (deg) = 276.07

Cone axis = {-0.225924, 0.939593, 0.257144}

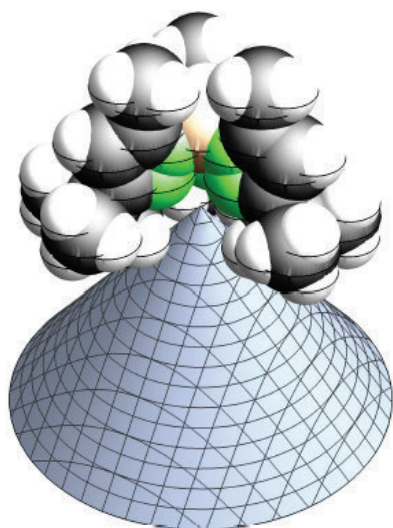


$\text{Tp}^{\text{tBu,Me}}\text{YMe}(\text{OC}_6\text{H}_3\text{iPr}_2\text{-2,6})$ (**6-Y**)

Ligand atoms forming cone = {13, 46, 67}

Cone angle (deg) = 276.057

Cone axis = {-0.76823, -0.250027, -0.589329}

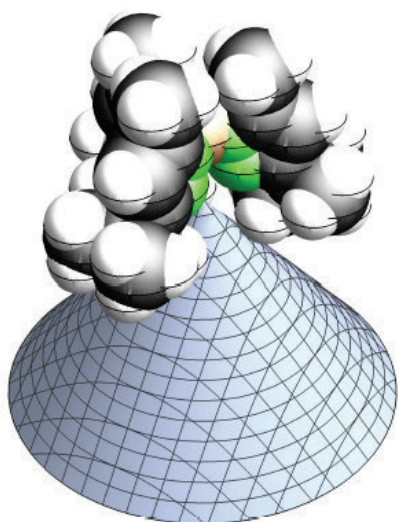


$\text{Tp}^{\text{tBu,Me}}\text{LuMe}(\text{OC}_6\text{H}_3\text{iPr}_2\text{-2,6})$ (**6-Lu**)

Ligand atoms forming cone = {23, 35, 60}

Cone angle (deg) = 279.236

Cone axis = {-0.999597, -0.0067429, -0.0275751}

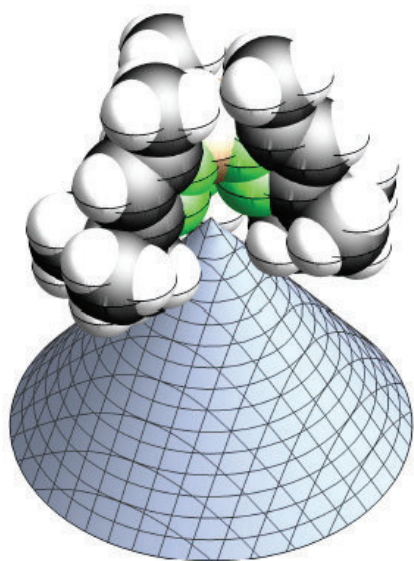


$\text{Tp}^{\text{tBu,Me}}\text{YMe}[\text{OC}_6\text{H}_3(\text{CF}_3)_2\text{-3,5}]$ (**7-Y**)

Ligand atoms forming cone = {23, 34, 58}

Cone angle (deg) = 278.637

Cone axis = {-0.205908, 0.616546, -0.759917}

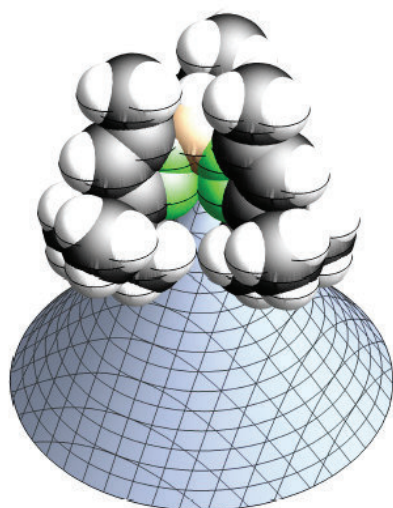


$\text{Tp}^{\text{tBu,Me}}\text{LuMe}[\text{OC}_6\text{H}_3(\text{CF}_3)_2\text{-3,5}]$ (**7-Lu**)

Ligand atoms forming cone = {26, 46, 65}

Cone angle (deg) = 280.343

Cone axis = {-0.627792, -0.76852, 0.123506}

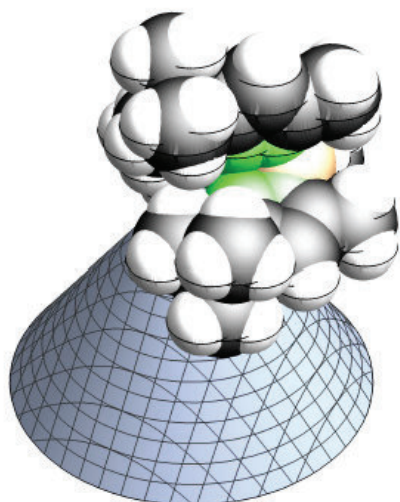


$[\text{Tp}^{\text{tBu,Me}}\text{YMe}(\text{dmap})_2][\text{Me}_3\text{AlOC}_6\text{H}_2\text{tBu}_2\text{-2,6-Me-4}]$ (**8-Y**)

Ligand atoms forming cone = {20, 40, 58}

Cone angle (deg) = 276.798

Cone axis = {0.185673, -0.952331, -0.242058}



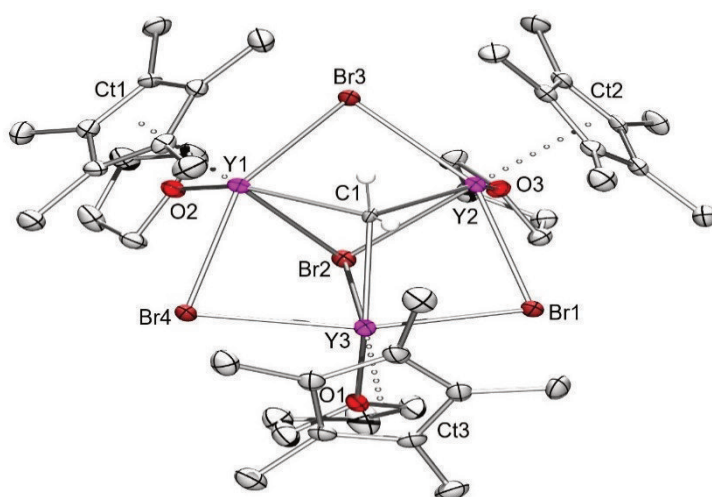
$\text{Tp}^{\text{tBu,Me}}\text{Lu}(\text{BHT})_{\text{activated}}$ (**9-Lu**)

Ligand atoms forming cone = {22, 43, 66}

Cone angle (deg) = 286.297

Cone axis = {0.992352, -0.119976, 0.0290265}

**Elucidation of
Cyclopentadienyl-Supported
Rare-Earth-Metal Methylidene
Complexes: Scope of Coligands
and Tebbe olefination**



Elucidation of Cyclopentadienyl-Supported Rare-Earth-Metal Methylidene Complexes: Scope of Coligands and Tebbe Olefination

Verena M. Birkelbach, H. Martin Dietrich, Christoph Stuhl, Cécilia Maichle-Mössmer, and Reiner Anwander*^[a]

[a] V. M. Birkelbach, Dr. H. M. Dietrich, Dr. C. Stuhl, Dr. C. Maichle-Mössmer, Prof. Dr. R. Anwander, Institut für Anorganische Chemie, Eberhard Karls Universität Tübingen, Auf der Morgenstelle 18, 72076 Tübingen (Germany)

E-mail: reiner.anwander@uni-tuebingen.de

Supporting Information Placeholder

ABSTRACT: A series of different mixed halogenido/tetramethylaluminato rare-earth metal compounds with the general formula $[\text{Cp}^R\text{Ln}(\text{AlMe}_4)_x(\text{X})_y]_z$ were synthesized from cyclopentadienyl-based bis(aluminato) rare-earth-metal precursors by utilizing mild halogenido transfer reagents SiMe_3X ($\text{X} = \text{Cl}, \text{Br}, \text{I}$). Further donor-induced aluminato cleavage generated the mixed halogenido/methylidene rare-earth metal complexes. Treatment of various half-sandwich $\text{Cp}^R\text{Ln}(\text{AlMe}_4)_2$ complexes ($\text{Cp}^R = \text{C}_5\text{Me}_5, \text{C}_5\text{Me}_4\text{SiMe}_3, \text{Ln} = \text{Y}, \text{La}, \text{Lu}$) with the mild halogenido transfer reagents SiMe_3X ($\text{X} = \text{Cl}, \text{Br}, \text{I}$) resulted in efficient and selective halogenido/tetramethylaluminato exchange. Depending on the size of the rare-earth metal, dimeric $[\text{Cp}^R\text{Ln}(\text{AlMe}_4)(\mu\text{-X})_2]$ ($\text{Ln} = \text{Y}, \text{Lu}$) and decametallate $[\text{Cp}^R_3\text{La}_3(\text{AlMe}_4)_2(\mu\text{-X})_4]_2$ could be obtained. Donor(THF)-induced tetramethylaluminato cleavage gave access to new mixed “methyl-free” halogenido/methylidene complexes $\text{Cp}^R_3\text{Ln}(\mu\text{-X})_3(\mu_3\text{-X})(\mu_3\text{-CH}_2)(\text{THF})_3$ for yttrium and lanthanum in good yields. Additionally, mixed halogenido/methylidene Y(III) complexes could be obtained *via* methyl/halogenido exchange employing $(\text{C}_5\text{Me}_5)_3\text{Y}(\mu\text{-Me})_3(\mu_3\text{-Me})(\mu_3\text{-CH}_2)(\text{THF})_3$ and SiMe_3X *via* tetramethylsilane elimination. All methylidene complexes were probed in Tebbe olefination reactions and found to react as efficient Schrock-type nucleophilic carbenes with ketones and aldehydes affording the respective terminal alkenes. Such reactivity is as high as of the prominent Tebbe reagent, but less tolerant toward sterically demanding and functionalized substrates (like esters).

INTRODUCTION: The seminal discoveries by Schrock and Tebbe of discrete $\text{Cp}_2\text{Ta}(\text{CH}_2)(\text{CH}_3)^{+2}$ and $\text{Cp}_2\text{Ti}(\mu\text{-CH}_2)(\mu\text{-Cl})\text{Al}(\text{CH}_3)_2$,³ respectively, in the mid 70's marked a true breakthrough in molecular transition-metal alkylidene chemistry. The feasibility/stability of such “Schrock”-type nucleophilic carbenes and their applicability/superb performance in fundamental organic transformations such as olefin metathesis⁴⁻⁶ and carbonyl methylenation (Wittig-type reactivity)^{4, 7} triggered immense research activities.^{5, 8-9} Tebbe's compound $\text{Cp}_2\text{Ti}(\mu\text{-CH}_2)(\mu\text{-Cl})\text{Al}(\text{CH}_3)_2$, also termed

Tebbe reagent, involving a Lewis acid ($\text{LA} = \text{AlClMe}_2$)-stabilized $[\text{Ti}=\text{CH}_2]$ moiety,^{3, 10} has featured a most efficient (rapid $\text{C}=\text{O}$ to $\text{C}=\text{CH}_2$ conversion at ambient temperatures) and hence prominent carbonyl methylenation reagent in organic syntheses ever since.¹¹⁻¹⁴ Crucially, in natural product synthesis the Tebbe reagent often outperforms the Wittig reagent CH_2PMe_3 due to its enhanced functional group tolerance (e.g., ester or acetal) or the Petasis reagent $\text{Cp}_2\text{Ti}(\text{CH}_3)_2$ which requires elevated temperatures (65 °C) to form the $[\text{Ti}=\text{CH}_2]$ moiety *via* methane elimination.¹⁵⁻²⁰ Drawbacks of the Tebbe reagent are its moisture-sensitivity, the co-formation of Ti(III) species when Cp_2TiCl_2 is reacted with “reducing” agent AlMe_3 , and the viability of methylenation only.²¹⁻²² On the other hand reduced titanium species such as obtained from the ternary system $\text{CH}_2\text{Br}_2/\text{TiCl}_4/\text{Zn}$ and $\text{CH}_2\text{Br}_2/\text{TiCl}_4/\text{Mg}$ have been employed according to the Takai-Lombardo reaction for the mild methylenation of ketones counteracting enolization (thus counteracting any epimerization of α -chiral centers; also high functional group tolerance).²³⁻²⁴ Moreover, excess of divalent $\text{Cp}_2\text{Ti}[\text{P}(\text{OEt})_3]_2$ (*via* $\text{Cp}_2\text{TiCl}_2/\text{Mg}/\text{P}(\text{OEt})_3$) is successfully used in the olefination of thioacetals with carbonyl compounds (Takeda reaction, characterized by a wide substrate scope).²⁵ Switching to group 6 reagents, the iodo-methylidene Cr(III) complex $\text{Cr}_2\text{Cl}_4(\text{CHI})(\text{THF})_4$ (Takai-olefination reagent) has been employed successfully to convert aldehydes to *E*-iodido-functionalized olefins accessible to further derivatization.²⁶⁻²⁹

Despite this eminent performance of early transition-metal-based alkylidene complexes in olefination reactions, rare-earth-metal (Ln) variants showing this extraordinary reactivity came in the focus only recently. As with the Tebbe reagent, Lewis acids (mainly AlMe_3) were shown to exert a stabilizing effect on increasingly ionic rare-earth metal methylidene compounds.³⁰⁻³² Most of such LA-stabilized Ln(III) complexes, featuring $[\text{Ln}(\mu\text{-CH}_2)(\mu\text{-CH}_3)\text{Al}]$ moieties, have revealed promising reactivity in methylidene transfer reactions, however, the bridging methyl groups can further engage in Ln(III)-size dependent

carbonyl alkylation reactions forming alkoxy compounds as well.^{30, 33} To obtain and ensure the unique and clean Wittig-type reactivity, homometallic compounds devoid of alkylating LAs seem necessary. So far, two structural motifs of rare-earth metal methylidene complexes were utilized in methylidene transfer reactions, comprising cubane-like tetrametallic $[(L)Ln(CH_2)]_4$ (I; Ln = smaller-sized expensive rare-earth metals only) and trimetallic complexes $(L)Ln(\mu-X)_3(\mu_3-CH_2)(THF)_n$ (II-VI) with L as a monoanionic ligand

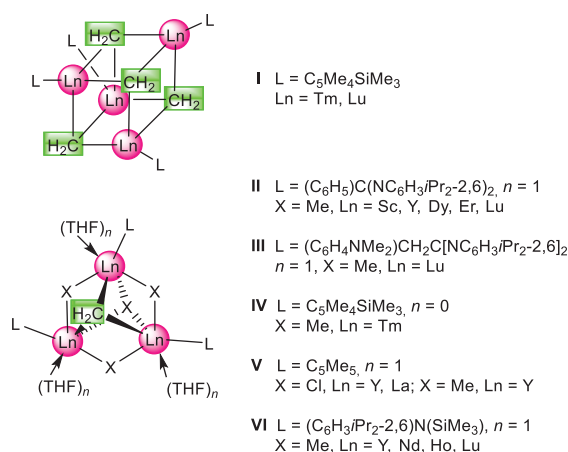
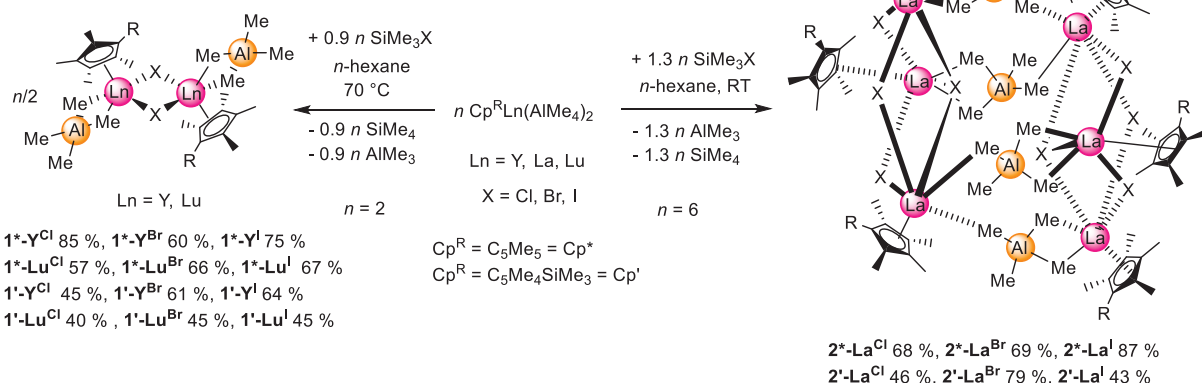


Figure 1. Different types of tetra- and trimetallic rare-earth metal methylidene complexes shown to be active in methylidene transfer reactions.

and X either methyl or halogenido moieties (Figure 1). Key step for the synthesis of these rare-earth-metal methylidene complexes is the intermediate formation of very reactive Ln–Me moieties. For example, the generation of the cubane-like lutetium complex stabilized by the electron rich cyclopentadienyl ligand $C_5Me_4SiMe_3$ (Cp^*), was



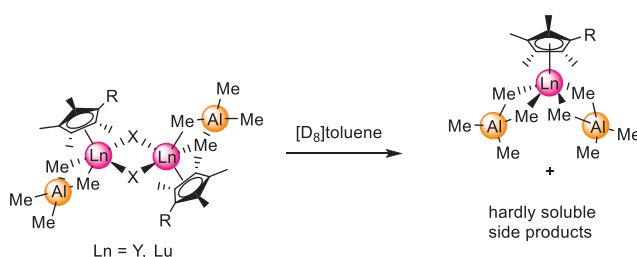
Scheme 1. Synthesis pathway toward different heterobimetallic complexes $[Cp^RLn(AlMe_4)(\mu-X)]_2$, and $[Cp^R_3La_3(AlMe_4)_2(\mu-X)_4]_2$.

achieved by C–H bond activation of the dimethyl precursor $[Cp^*Lu(CH_3)_2]_2$ via release of CH_4 .³⁴ Another method for the generation of the Ln–Me moiety is the reaction of a LA with the precursor $[(L)Ln(R)]_2$ (II: R = $CH_2C_6H_4NMe_2$, L = $PhC(NC_6H_3iPr_{2-2,6})_2$ for Ln = Sc, Y, Er, Lu; III: L = $(C_6H_4NMe_2)CH_2C(NC_6H_3iPr_{2-2,6})_2$ for Ln = Lu; IV: R = CH_2SiMe_3 , L = $C_5Me_4SiMe_3$, Ln = Tm)³⁴⁻³⁷ or through donor-induced cleavage of organoaluminum stabilized “alkyls in disguise” $(L)Ln(AlMe_4)_2$ (V^Y : L = C_5Me_5 , Ln = Y; VI: L = $N(C_6H_3iPr_{2-2,6})(SiMe_3)$, Ln = Y, Nd, Ho, Lu; II: L = $PhC(NC_6H_3iPr_{2-2,6})_2$, Ln = Sc, Lu) for bridging methyl groups^{33, 35, 38-39} or $[(L)Ln(AlMe_4)_x(Cl)_y]_z$ (V: L = C_5Me_5 , Ln = Y with $x = y$, $z = 2$, La with $2x = y$, $z = 6$) for bridging chlorido units,⁴⁰ in all cases followed by inter- or intramolecular C–H activation. To selectively achieve clean conversion of carbonylic substrates into terminal alkenes, the bridging positions need to carry unreactive ligands such as halogenido, as in $(C_5Me_5)_3Ln_3(\mu-Cl)_3(\mu_3-CH_2)(THF)_3$ (V: Ln = Y, La).⁴⁰ Herein, we present a full account of the synthesis of complexes of the type $Cp^R_3Ln_3(\mu-X)_3(\mu_3-CH_2)(THF)_3$ giving consideration to effective synthesis protocols, scope of the bridging ligand X, implications of the Ln(III) size, and application in methylidene transfer reactions. For the latter olefination reactions, comparison is drawn to the illustrious Tebbe reagent.⁴¹

RESULTS AND DISCUSSION

Mixed Ligand $AlMe_4/X$ Precursor Synthesis: Scope and Molecular Composition. Recently, we reported on a convenient method for the synthesis of mixed chlorido/tetramethylaluminato heterobimetallic rare-earth-metal complexes of different nuclearity depending on the size of the Ln(III) center.⁴² This procedure required the treatment of half-sandwich complexes $(C_5Me_5)Ln(AlMe_4)_2$ with the chlorido transfer reagent Me_2AlCl at low temperatures. In

search of milder and adjustable halogenido transfer reagents, we opt for trimethylsilyl halide reagents, inspired by the work of Orpen *et al.* on SiMe₃I (TMSI)-promoted alkyl/iodido exchange reactions.⁴³ We anticipated/envisaged that these increasingly versatile reagents SiMe₃X could reveal the impact of less electronegative halogens (X) not only on the heterobimetallic cluster synthesis but also (if the latter succeed) on the olefination reactions. To probe any Ln(III)-size and “cyclopentadienyl” effects we chose Cp^RLn(AlMe₄)₂ (Cp^R = C₅Me₅, C₅Me₄SiMe₃; Ln = Y, La, Lu) as representative precursors. As found earlier for the chlorido derivative [(C₅Me₅)Y(AlMe₄)(μ-Cl)]₂, treatment of the bis(alkylaluminato) half-sandwich complexes containing the smaller-sized rare-earth metals yttrium and lutetium with 0.9 equiv. or less of the halogenido transfer reagent led to the successful single AlMe₄⁻/X exchange and the formation of dimeric complexes [Cp^RLn(AlMe₄)(μ-X)]₂ in good yields (**1**-Ln^X, Scheme 1, left).^{42, 44}



Scheme 2. Ligand redistribution of complexes **1***-Ln^X and **1**'-Ln^X over time in aromatic solvents identified with NMR spectroscopy.

Elemental analyses and crystal structural analyses confirmed the general composition, however, the NMR data showed two different sets of signal, one belonging to unreacted Cp^RLn(AlMe₄)₂. A closer look at this apparent discrepancy between solid-state analytics and NMR measurements indicated the occurrence of ligand redistribution in aromatic solvents over time (Scheme 2). Such intermolecular ligand exchange would involve the co-formation of putative [Cp^RLnX₂], but the hardly soluble byproducts were not further characterized. Furthermore, the true nature of the composition of the complexes **1**-Ln was validated with elemental analysis as well as various cell checks confirming the product crystallized from the mother liquor in *n*-hexane as exclusive product when not being re-dissolved in aromatic solvents. The ambient temperature ¹H NMR spectra of all complexes [(C₅Me₅)Ln(AlMe₄)(μ-X)]₂ clearly display one signal for the Cp-CH₃ groups as well as one for the AlMe₄ moieties as expected from the C_i symmetry of the complexes, and further one set of signals of (C₅Me₅)Ln(AlMe₄)₂ due to the afore mentioned behavior in solution (spectra shown in the ESI). For all compounds, a clear trend was found for the Cp-CH₃ signals with a shift downfield for each respective metal from Cl to I (**1***-Y^{Cl}: 1.89 ppm, **1***-Y^{Br}: 1.92 ppm, **1***-Y^I: 1.98 ppm; **1***-Lu^{Cl}: 1.93 ppm, **1***-Lu^{Br}: 1.96 ppm, **1***-Lu^I: 2.00 ppm) as well as for the Ln-Me signals (**1***-Y^{Cl}: -0.20 ppm, **1***-Y^{Br}: -0.18 ppm, **1***-Y^I: -0.15 ppm; **1***-Lu^{Cl}: -0.05 ppm, **1***-Lu^{Br}: -0.00 ppm, **1***-Lu^I: 0.04 ppm). Furthermore, the signals compare well with those of the starting compounds (C₅Me₅)Ln(AlMe₄)₂ (Y: 1.72 ppm, -

0.33 ppm; Lu: 1.75 ppm, -0.18 ppm). Exactly the same Cl-to-I trend was observed for all complexes [(C₅Me₄SiMe₃)Ln(AlMe₄)(μ-X)]₂. The proton NMR spectra show four different signals, two for the Cp-Me moieties (**1**'-Y^{Cl}: 2.15/1.85 ppm, **1**'-Y^{Br}: 2.17/1.86 ppm, **1**'-Y^I: 2.22/1.93 ppm; **1**'-Lu^{Cl}: 2.17/1.87 ppm, **1**'-Lu^{Br}: 2.19/1.88 ppm, **1**'-Lu^I: 2.23/1.86 ppm), one for the Si-Me unit and one for the Al-Me moieties (**1**'-Y^{Cl}: -0.18 ppm, **1**'-Y^{Br}: -0.15 ppm, **1**'-Y^I: -0.13 ppm; **1**'-Lu^{Cl}: -0.05 ppm, **1**'-Lu^{Br}: 0.01 ppm, **1**'-Lu^I: 0.01 ppm). Again, the signals compare well with those of the starting compounds (C₅Me₄SiMe₃)Ln(AlMe₄)₂ (Y: 2.00/1.75 ppm, -0.31 ppm; Lu: 1.99/1.75 ppm, -0.14 ppm). For the yttrium half-sandwich complexes, a doublet for the AlMe₄ signal with a ³J(YH) coupling constant around 2.3 Hz was observed, except for **1***-Y^{Cl} indicating a highly fluxional nature. The respective Lu complexes display very broad signals for the Lu-Me moiety, indicating a less pronounced dynamic behavior of the bridging and terminal Me groups in solution as expected for the smaller-sized Lu(III) center. The ¹³C NMR spectra clearly shows the same trend of the halogenido ligands on the ¹³C chemical shift and, as expected, two signals for C₅Me₅ and six signals for C₅Me₄SiMe₃, respectively. For most of the complexes, the Al-CH₃ signals could not be detected, due to their low solubility as well as the relatively fast ligand redistribution process, which is consistent with literature.⁴² The ⁸⁹Y NMR resonances from ¹H-⁸⁹Y HSQC measurements revealed also highfield-shifted signals in the presence of the more electron-withdrawing halogenido ligand (e.g., **1***-Y^{Cl}: 208 ppm versus **1***-Y^{Br}: 246 ppm), but only a marginal effect of the cyclopentadienyl ligand (e.g., **1***-Y^{Cl}: 208 ppm versus **1**'-Y^{Cl}: 206 ppm). For comparison, the starting compounds Cp^RY(AlMe₄)₂ display ⁸⁹Y NMR resonances at 175 ppm (Cp^R = C₅Me₅) and 170 ppm (Cp^R = C₅Me₄SiMe₃). Due to solubility issues, long measurement periods, and rapid ligand redistribution, ¹H-⁸⁹Y HSQC spectra could not be obtained for **1***-Y^I and **1**'-Y^I (detection of precursors only). X-ray diffraction (XRD) analyses were performed on **1***-Y^{Br}, **1***-Y^I, and **1***-Lu^{Br} (Figures 2, S59 and S60). The mentioned [(C₅Me₅)Ln(AlMe₄)(μ-X)]₂ complexes revealed the dimeric solid-state structure with seven-coordinate Ln centers: the monoanionic Cp ligand occupies three coordination sites and the methyl groups as well as the bridging halogenido ligands occupy two each. The crystal structures are isostructural to **1***-Y^{Cl}.⁴² The Y-C(Me) distance appears slightly decreased for the heavier halide complexes **1***-Y^{Br} and **1***-Y^I as an impact of the changed halogen electronegativity (**1***-Y^{Cl}: av. 2.573 Å,⁴² **1***-Y^{Br}: 2.531(2)/2.566(2) Å, **1***-Y^I: 2.529(4)/2.563(4) Å), but compare well with the reactant (C₅Me₅)Y(AlMe₄)₂ (2.549(3)-2.655(3) Å).⁴⁵ As expected, the Lu-C(Me) bond lengths in **1***-Lu^{Br} are shortened (2.486(3)/2.529(3) Å) compared to **1***-Y^{Br}, reflecting the smaller Ln(III) size. This is further supported by the differences in the Ln-Br distances (**1***-Y^{Br}: 2.8493(8)/2.8687(10) Å, **1***-Lu^{Br}: 2.7961(7)/2.8257(8) Å) as well as the Ln...Al interatomic distances (**1***-Y^{Cl}: 3.0584(12) Å,⁴² **1***-Y^{Br}: 3.0970(10) Å, **1***-Lu^{Br}: 3.0434(10) Å). Only few complexes with bromido ligands bridging two rare-earth-metal centers are known including dimeric 3-(2,6-*i*Pr₂C₆H₃)-1-[2-(1

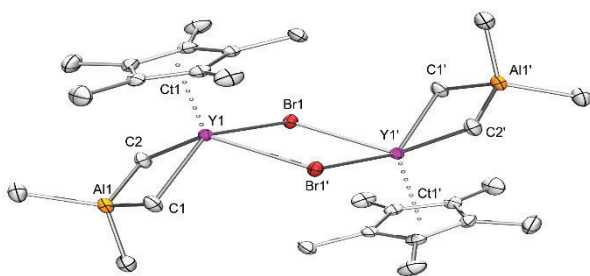


Figure 2. ORTEP representation of the crystal structure of 1^*-Y^{Br} with atomic displacement parameters set at the 50 % level. Hydrogen atoms are omitted for clarity. Selected bond lengths [Å] and angles [°] for 1^*-Y^{Br} : Y1-Br1 2.8493(8), Y1-Br1' 2.8687(10), Y1-C1 2.531(2), Y1-C2 2.566(2), Y1...Al1 3.0970(10), Y1...Ct1 2.310, Al1-C1 2.073(2), Al1-C2 2.079(2), Al1-C3 1.981(2), Al1-C4 1.969(2); Br1-Y-Br1' 79.54(3), Y1-Br1-Y1' 100.46(3), C1-Y1-C2 83.26(8), Y1-C1-Al1 83.90(8), Y1-C2-Al1 82.92(8).

-(4,7-Me₂)indenyl)propyl]imidazol-2-ylidene(trimethylsilylmethyl)-bromido yttrium (Y-Br bond lengths: 2.8645(7) and 2.8747(7) Å,⁴⁶ [Y(η⁵-Me₂C₃H₃)₂Br]₂ (2.857(1) and 2.868(1) Å,⁴⁷ and [(η⁵,η⁵-Cp-CMe₂-fluorenyl)Y(μ-Br)]₂ (2.8055(13)/2.8065(12) Å)⁴⁸ the latter showing shorter Y-Br distances compared to 1^*-Y^{Br} .

The tetramethylaluminato/halogenido exchange was also probed for the lanthanum complexes Cp^RLa(AlMe₄)₂. Treatment of the respective bis(tetramethylaluminato) half-sandwich complexes with 1.3 equiv. of TMSX resulted in the formation of hexalanthanum clusters of the general composition [Cp^R₃La₃(AlMe₄)₂(μ-X)]₄. All reactions yielded colorless crystals from resting *n*-hexane solutions at ambient temperatures, and XRD analyses were carried out exemplarily for $2^*-\text{La}^{\text{Br}}$ and $2'-\text{La}^{\text{Cl}}$ (Figures S61 and 3). Due to the insolubility of all complexes $2-\text{La}$ in non-polar and aromatic NMR solvents, solution NMR spectroscopic analysis was not accessible. The crystal structures of $2^*-\text{La}^{\text{Br}}$ and $2'-\text{La}^{\text{Cl}}$ with formally 8-coordinate La(III) centers are isostructural to the previously reported complex (C₅Me₅)₆La₆{(μ-Me)₃AlMe₃}(μ₃-Cl)₂(μ-Cl)₆ ($2^*-\text{La}^{\text{Cl}}$).⁴² Two La₃Al₂ subunits, related by C₂-symmetry feature distinctly coordinating halogenido ligands (μ₂, μ₃) and a strand of (μ-η²-Me₂)Al(Me)(μ-η¹-Me)-interconnecting aluminato ligands. Striking is the Ln:X ratio of 1:1.3 which is different from that of the dimeric yttrium and lutetium complexes in this work (1:1). Unsurprisingly, the La-X bond lengths of 2^*-La^{I} (3.2323(4)-3.3455(4) Å) are elongated compared to $2^*-\text{La}^{\text{Cl}}$ (La-Cl: 2.8049(9)-3.0708(9) Å),⁴² while the La-C(Me) bond lengths as well as the La...Al distance appear slightly shortened ($2^*-\text{La}^{\text{Cl}}$: La-C(Me) 2.774(4)-2.955(3) Å; La...Al 3.3150(11)-3.3534(11) Å,⁴² 2^*-La^{I} : La-C(Me) 2.771(4)-2.777(4) Å, La...Al 3.3159(12)-3.3192(12) Å). For further comparison, the precursor (C₅Me₅)La(AlMe₄)₂⁴⁹ displays La-C(Me) bond lengths (2.694(3)-2.802(4) Å) as well as La...Al distances (3.0141(9)-3.2687(9) Å) which are shorter than in $2^*-\text{La}^{\text{Cl}}$ and 2^*-La^{I} . Overall, the different Cp^R ligand in $2'-\text{La}^{\text{Cl}}$ has only a small impact on the molecular structure,

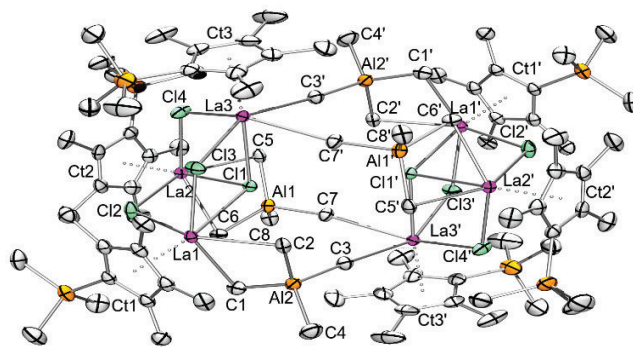
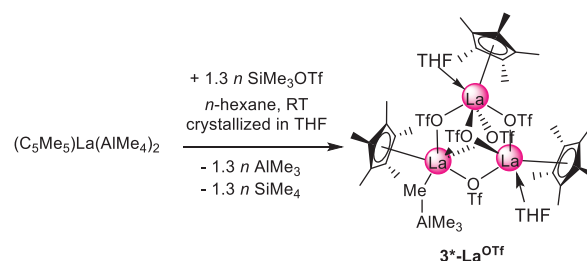


Figure 3. ORTEP representation of the crystal structure of $2'-\text{La}^{\text{Cl}}$ with atomic displacement parameters set at the 50 % level. Hydrogen atoms are omitted for clarity. Selected bond lengths [Å] and angles [°] for $2'-\text{La}^{\text{Cl}}$: La1-Cl1 3.0787(6), La1-Cl2 2.8382(7), La1-Cl3 2.8298(7), La2-Cl1 3.0725(7), La2-Cl2 2.8421(7), La2-Cl4 2.8395(7), La3-Cl1 3.0111(6), La3-Cl3 2.8101(7), La3-Cl4 2.8087(7), La1-C1 2.809(3), La1-C2 2.774(3), La2-C5 2.742(3), La2-C6 2.764(3), La3-C3' 2.947(3), La3-C7' 2.970(3), La1...Ct1 2.507, La2...Ct2 2.507, La3...Ct3 2.501, La1...Al2 3.3371(9), La2...Al1 3.2849(9); La1-Cl1-La2 100.878(19), La1-Cl1-La3 100.870(18), La1-Cl2-La2 113.20(2), La1-Cl3-La3 112.70(2), La2-Cl1-La3 100.579(19), La2-Cl4-La3 111.91(2), La1-C1-Al2 85.28(10), La1-C2-Al2 86.40(10), La2-C5-Al1 85.40(10), La2-C6-Al1 84.78(10), C1-La1-C2 75.19(9), C5-La2-C6 76.58(9), C3'-La3-C7' 77.39(9).

but the bond lengths become significantly elongated from $2^*-\text{La}^{\text{Cl}}$ to $2'-\text{La}^{\text{Cl}}$ (La-Cl, 2.8087(7) to 3.0787(6) Å; La-C(Me), 2.742(3)-2.970(3) Å; La...Al, 3.2849(9)-3.3371(9) Å).

The introduction of electron-withdrawing pseudo-halogenido ligands such as triflate (OTf) proved more difficult but was successful for the system (C₅Me₅)La(AlMe₄)₂/SiMe₃OTf yielding crystalline heterobimetallic complex (C₅Me₅)₃La₃(AlMe₄)(μ-OTf)₃(μ₃-OTf)₂(THF)₂ ($3^*-\text{La}^{\text{OTf}}$) (Scheme 3). The solubility of this complex in non-polar and aromatic solvents is limited, while decomposition to several C-F bond cleavage products occurred in THF over time (monitored with ¹H NMR spectroscopy), if not prevented by lower temperatures.

Scheme 3. Reactivity of (C₅Me₅)La(AlMe₄)₂ toward pseudo-halogenido-transfer reagent SiMe₃OTf.



An XRD analysis of $3^*-\text{La}^{\text{OTf}}$ (crystallized from THF) revealed a tetrametallic complex with three μ₂- and two μ₃-

bridging triflate ligands. The core structure can be best described as a 12-membered ring consisting of three [La–O–S–O] units with two μ_3 -coordinating triflate caps. An eight-fold coordination of the lanthanum centers is accomplished by the peripheral cyclopentadienyl rings, two THF

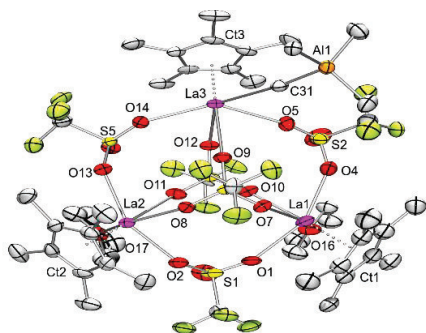
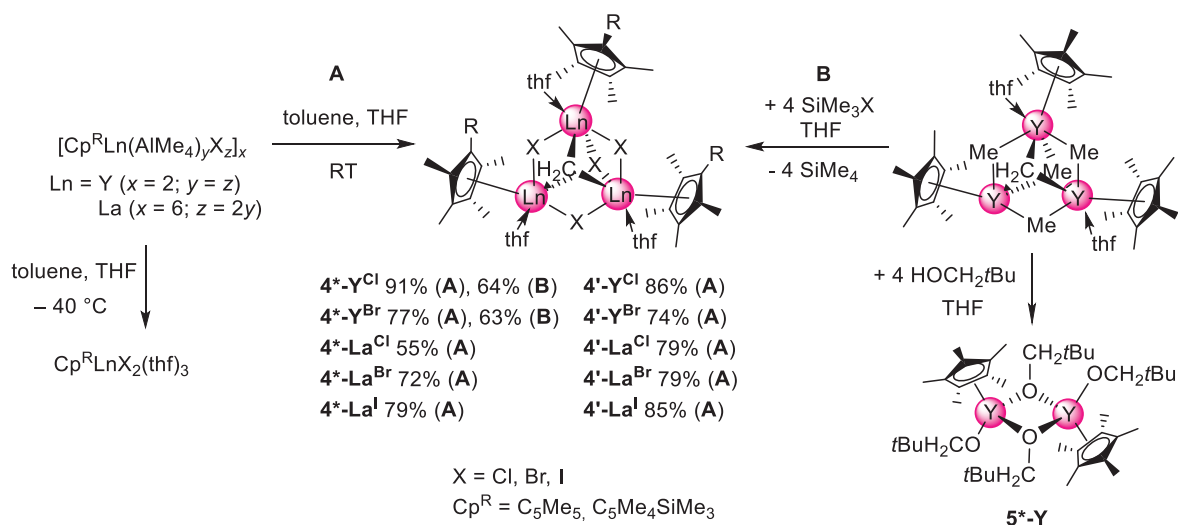


Figure 4. ORTEP representation of the crystal structure of 3^* -La^{OTf} with atomic displacement parameters set at the 50 % level. Hydrogen atoms and the disorder in the Cp rings as well as the CF₃ groups are omitted for clarity. Selected bond lengths [Å] for 3^* -La^{OTf}: La1...Ct1 2.564, La2...Ct2 2.463, La3...Ct3 2.498, La–C31 2.942(7), La1–O1 2.477(5), La1–O4 2.441(6), La1–O7 2.520(5), La1–O10 2.496(5), La2–O2 2.490(5), La2–O8 2.529(5), La2–O11 2.553(5), La2–O13 2.436(5), La3–O5 2.591(5), La3–O9 2.601(4), La2–O12 2.575(4), La2–O14 2.584(5), La3–C31 2.942(7), La3...Al1 4.971.

molecules, and one remaining AlMe₄[−] ligand, which coordinates one lanthanum center in a η^1 -fashion. The La...Ct distances (2.463–2.564 Å) match those detected in the other 2 -La. Further, the La–O distances range between 2.436(5) and 2.591(5) Å for μ_2 -bridging triflate ligands and 2.496(5) to 2.575(4) for μ_3 -bridging triflate moieties. The La–C(Me) distance of 2.942(7) Å is located in the upper range of complexes 2 -La.

Donor-Induced Methylidene Formation from Mixed Ligand AlMe₄/X Ln(III) Complexes. We communicated previously that mixed ligand complexes [(C₅Me₅)Ln(AlMe₄)_x(Cl)_y]_z (Ln = Y with $x = y$, $z = 2$, La with $2x = y$, $z = 6$) can selectively undergo donor(THF)-promoted alkylaluminate cleavage (separation of AlMe₃(THF)) and engage in subsequent C–H-bond activation of the emerging terminal Ln–CH₃ moiety. Accordingly, complexes **1** and **2** were suspended in toluene and treated with excess of THF at ambient temperature (Scheme 4, Path A). As found earlier for the pentamethylcyclopentadienyl ancillary ligand and the chlorido coligand, the yttrium and lanthanum reactions formed trimetallic rare-earth-metal methylidene complexes derivatives complexes Cp^RLn(μ -X)₃(μ_3 -X)(μ_3 -CH₂)(THF)₃ (3^* -Ln^X and $3'$ -Ln^X; Ln = Y, La) for all halogenido ligands

Despite major efforts, the respective lutetium methylidene complexes could not be synthesized *via* this protocol (presumably Lu(III) is too small). Furthermore, the combination of Y/I/CH₂ could not be achieved, most likely because of another Ln(III)/halogenido size mismatch (Y(III) middle-sized, I[−] too big). ¹H NMR spectroscopic studies revealed the formation of methyl/iodido species [Cp^RYMeI(THF)_x]_n and di(iodido) complexes [Cp^RYI₂(THF)_x]_n upon addition of THF to 1^* -Y^I and $1'$ -Y^I, but any cluster formation was not observed. For all probed methylidene clusters, their formation is strongly dependent on the chosen reaction conditions. More precisely, if the synthesis is carried out below ambient temperatures, Cp-stabilized di(halogenido) Ln(III) complexes Cp^RLnX₂(THF)₃ could be isolated, which is exemplarily evidenced by the crystal structure of (C₅Me₅)LaI₂(THF)₃ (Figure S62). In addition, while the formation of the lanthanum methylidene derivatives follows a stoichiometrically correct pathway ($8 X^- + 4 AlMe_4^- \rightarrow 2[4 X^- + CH_2^{2-} + 2 AlMe_3 + CH_4]$), there is an obvious stoichiometric mismatch for the yttrium reactions ($1.5 [2 X^- + 2 AlMe_4^-] \rightarrow 3 X^- + CH_2^{2-} + 2 AlMe_3 + CH_4$), clearly indicating a shortage of



Scheme 4. Different synthesis pathways for the generation of mixed halogenido/methylidene rare-earth-metal complexes.

halogenido ligands. Although the formation of the targeted methyl-free complexes **4**-**Y** seems favored under the chosen crystallization conditions, halogenido-deficient mixed methyl/halogenido/methylene Ln(III) complexes of the type $\text{Cp}^R_3\text{Y}_3(\mu_2\text{-CH}_3)_x(\mu_2\text{-X})_y(\mu_3\text{-X})(\mu_3\text{-CH}_2)(\text{THF})_3$ ($x+y=3$) can be identified and isolated as well (Figure S58 Supporting Information). Spurred by these obvious drawbacks, we implemented an alternative synthesis protocol.

Methyl/Methylidene to X/Methylidene Transformation. Having in mind the very rigid methylidene cluster entities (as evidenced by NMR spectroscopy, *vide infra*), we envisaged the mixed methyl/methylidene cluster complex $(\text{C}_5\text{Me}_5)_3\text{Y}_3(\mu\text{-Me})_3(\mu_3\text{-Me})(\mu_3\text{-CH}_2)(\text{THF})_2$ **V**^Y as potential precursor for **4**-type complexes. Compound **V**^Y can be readily obtained from $(\text{C}_5\text{Me}_5)\text{Y}(\text{AlMe}_2)_2$.³⁹ Much to our delight treatment of **V**^Y with **4** equiv. of halogenido transfer reagent SiMe_3X in THF gave the desired complexes **4**^{*}-**Y**^{Cl} and **4**^{*}-**Y**^{Br} *via* tetramethylsilane elimination. However, once again, the yttrium methylidene complex with bridging iodido moieties, that is putative **4**^{*}-**Y**^I was not feasible, and only degradation of the inner core and an ill-defined product mixture were found. It is noteworthy, that protonolyses of complex **V**^Y are more difficult to control. For example the reaction of **V**^Y with **4** equiv. of neopentanol was rather unselective and afforded the bis(alkoxy) yttrium half-sandwich complex $[(\text{C}_5\text{Me}_5)\text{Y}(\text{OCH}_2t\text{Bu})(\mu\text{-OCH}_2t\text{Bu})]_2$ **5**^{*}-**Y** (Scheme 4, crystal structure is depicted in Figure S63), involving the alcoholysis of both the methyl and methylidene ligands.

Characterization of Methylidene Complexes 4-Ln. The ambient temperature ¹H NMR spectra of all crystalline compounds $\text{Cp}^R_3\text{Ln}_3(\mu\text{-X})_3(\mu_3\text{-X})(\mu_3\text{-CH}_2)(\text{THF})_3$ recorded in [D₈]THF show one set of signals for the ancillary Cp ligands, in accordance with their symmetry in the solid state (spectral data pictured in the ESI). As detected for the precursors **1**^{*}-**Y**^X and **1**'-**Y**^X, the shift of the CH₂ group is significant for each introduced halogenido ligand and shows a clear trend from Cl⁻ to I⁻ for the respective ligand set. The methylidene signal of all yttrium complexes features a quartet due to the coupling with the three ⁸⁹Y nuclei (**4**^{*}-**Y**^{Cl}: -0.35 ppm, **4**^{*}-**Y**^{Br}: -0.33 ppm, **4**'-**Y**^{Cl}: -0.42 ppm, **4**'-**Y**^{Br}: -0.42 ppm), while shifted to higher field compared to that in **V**^Y (-0.31 ppm).³⁹ It is noteworthy, that complex **4**'-**Y**^{Br} showed decomposition in THF after 30 minutes. For all lanthanum compounds, the methylidene signal exhibits a singlet markedly shifted to higher field compared to the yttrium congeners. As indicated by the same shift range (**4**^{*}-**La**^{Cl}: -0.93 ppm, **4**^{*}-**La**^{Br}: -0.93 ppm, **4**^{*}-**La**^I: -0.97 ppm; **4**'-**La**^{Cl}: -0.96 ppm, **4**'-**La**^{Br}: -0.97 ppm, **4**'-**La**^I: -0.96 ppm), the halogenido ligand exerts only a minor influence on lanthanum-bound CH₂²⁻ group. As expected, the ¹³C NMR spectra show one set of signals for the respective Cp ligand, however the ¹³C signal for the CH₂ group could not be detected even after 18 h of measuring time. Moreover, ¹H-⁸⁹Y HSQC NMR spectra reinforce the dependency of the ⁸⁹Y shift on the halogenido ligand (**4**^{*}-**Y**^{Cl}: 163 ppm, **4**^{*}-**Y**^{Br}: 196 ppm; **4**'-**Y**^{Cl}: 150 ppm, **4**'-**Y**^{Br}: 183 ppm) and clearly display a high-field shift compared to the respective starting compounds.

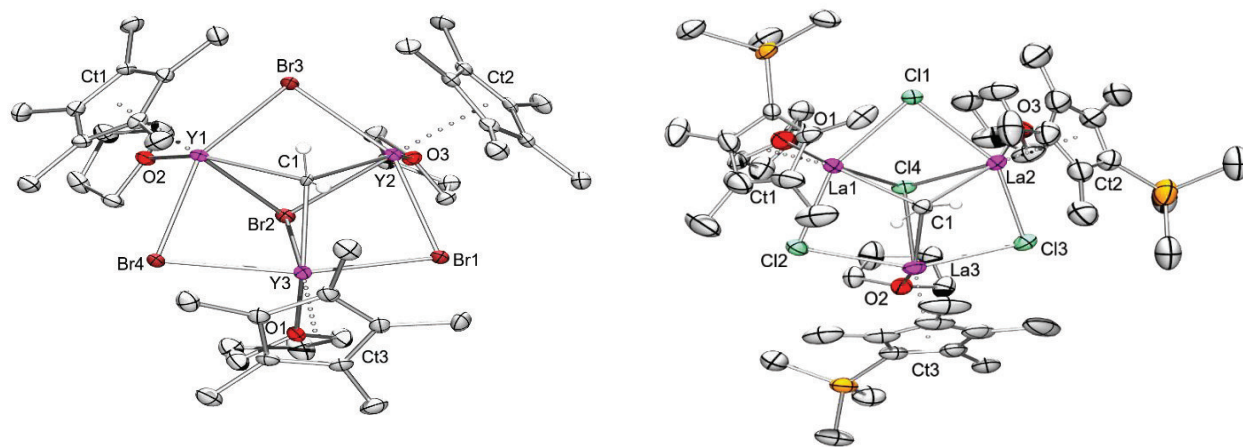
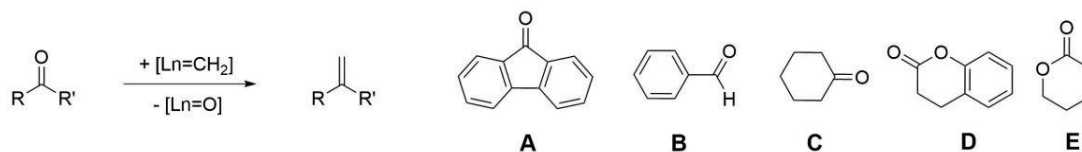


Figure 5. ORTEP representation of the molecular structure of **4**^{*}-**Y**^{Br} (left) and **4**'-**La**^{Cl} (right) with atomic displacement parameters set at the 50 % level. Hydrogen atoms except for the CH₂ group and lattice solvent as well as the disorder in the Cp-rings are omitted for clarity. Selected bond lengths [Å] and angles [°] for **4**^{*}-**Y**^{Br}: Y1–C1 2.484(3), Y2–C1 2.532(3), Y3–C1 2.431(3), Y1–Br3 3.0807(5), Y1–Br2 2.8870(5), Y1–Br4 2.8699(5), Y2–Br1 2.8538(5), Y2–Br2 3.0609(5), Y2–Br3 2.8757(5), Y3–Br1 2.8853(5), Y3–Br2 3.0578(5), Y3–Br4 2.8781(5), Y1…Ct1 2.388, Y2…Ct2 2.387, Y3…Ct3 2.400, Y1–O2 2.420(3), Y2–O3 2.406(3), Y3–O1 2.460(3); Y1–C1–Y2 100.45(13), Y2–C1–Y3 98.12(12), Y1–C1–Y3 97.44(12), Y1–Br3–Y2 83.984(14), Y1–Br4–Y3 79.971(14), Y2–Br1–Y3 81.585(13), Y1–Br2–Y2 77.770(13), Y1–Br2–Y3 73.985(13), Y2–Br2–Y3 75.585(13); Selected bond lengths [Å] and angles [°] for **4**'-**La**^{Cl}: La1–C1 2.572(3), La2–C1 2.580(3), La3–C1 2.576(3), La1–Cl1 2.8796(7), La1–Cl2 2.8782(8), La1–Cl4 3.0325(8), La2–Cl1 2.8906(7), La2–Cl3 2.8828(8), La2–Cl4 3.0314(8), La3–Cl2 2.8783(8), La3–Cl3 2.8834(9), La2–Cl4 3.0226(7), La1…Ct1 2.533, La2…Ct2 2.449, La3…Ct3 2.544, La1–O1 2.527(13), La2–O2 2.593(3), La3–O3 2.611(2), La1–C1–La2 98.63(10), La2–C1–La3 98.03(10), La1–C1–La3 98.60(10), La1–Cl1–La2 85.24(2), La1–Cl1–La3 84.93(2), La2–Cl3–La3 85.36(2), La1–Cl4–La2 80.234(19), La1–Cl4–La3 79.859(19), La2–Cl4–La3 80.434(18).

Crystallization of the obtained methylidene complexes could be achieved from saturated solutions in a mixture of toluene and THF at $-40\text{ }^{\circ}\text{C}$. XRD analyses were carried out for 4^*-Y^{Br} , $4^*\text{-La}^{\text{Br}}$ as well as $4'\text{-La}^{\text{Cl}}$ and the obtained crystal structures are depicted in Figure 5 and Figure S64 for $4^*\text{-La}^{\text{Br}}$. As detected previously for $4^*\text{-Ln}^{\text{Cl}}$ ($\text{Ln} = \text{Y}, \text{La}$), the three Ln(III) centers adopt a distorted pseudooctahedral geometry involving one shielding C_5Me_5 site, one μ_3 -bridging and three μ_2 -halogenido ligands, THF donor ligands, as well as the μ_3 -bridging methylidene moiety, protruding from the Ln_3X_3 plane. Comparison of 4^*-Y^{Cl} with 4^*-Y^{Br} revealed elongated bond lengths for both Y-X (4^*-Y^{Cl} : μ_2 : $2.7028(6)$ - $2.72787(6)$ Å, μ_3 : $2.8522(5)$ - $2.8897(5)$ Å;⁴⁰ 4^*-Y^{Br} : μ_2 : $2.8538(5)$ - $2.8870(5)$ Å; μ_3 : $3.0578(5)$ - $3.0807(5)$ Å) and $\text{Y-C}(\text{CH}_2)$ (4^*-Y^{Cl} : $2.424(2)$ - $2.450(2)$ Å;⁴⁰ 4^*-Y^{Br} : $2.431(3)$ - $2.532(3)$ Å) of the bromido derivative. The same trend can be found for the distances of $4^*\text{-La}^{\text{Cl}}$ and $4^*\text{-La}^{\text{Br}}$ comparing La-X ($4^*\text{-La}^{\text{Cl}}$: μ_2 : $2.8614(8)$ - $2.8929(8)$ Å, μ_3 : $3.0014(7)$ - $3.0334(7)$ Å;⁴⁰ $4^*\text{-La}^{\text{Br}}$: μ_2 : $3.0047(5)$ - $3.0385(5)$ Å; μ_3 : $3.1670(4)$ - $3.2074(4)$ Å) and $\text{La-C}(\text{CH}_2)$ ($4^*\text{-La}^{\text{Cl}}$: $2.537(3)$ - $2.635(3)$ Å;⁴⁰ $4^*\text{-La}^{\text{Br}}$: $2.553(3)$ - $2.646(4)$ Å). $4'\text{-La}^{\text{Cl}}$ ($2.572(3)$ - $2.580(3)$ Å) showed slightly shortened $\text{La-C}(\text{CH}_2)$ bond lengths compared to $4'\text{-La}^{\text{Cl}}$ however, similar La-Cl bond lengths (μ_2 : $2.8782(8)$ - $2.8906(7)$ Å; μ_3 : $3.0226(7)$ - $3.0325(8)$ Å). As μ_3 bridging methylidene complexes of lanthanum are still elusive, comparison can be drawn to the tris(pyrazolyl)borato-supported rare-earth-metal variant of the Tebbe reagent $\text{Tp}^{\text{tBu,Me}}\text{La}(\text{CH}_2)(\text{AlMe}_3)_2$ with a $\text{La-C}(\text{CH}_2)$ bond length of $2.519(2)$ Å.³⁰ The $\text{Y-C}(\text{CH}_2)$ distances in complexes 4-Y can be compared to complex VI^{Y} (see Figure 1, $2.345(5)$ - $2.424(4)$ Å,³³ V^{Y} ($2.283(4)$ - $2.477(3)$ Å)³⁹ and $(\text{NCN}^{\text{dipp}})_3\text{Y}_3(\mu\text{-Me})_3(\mu_3\text{-CH}_2)(\mu_3\text{-CCTMS})$ ($2.382(6)$ - $2.418(6)$ Å),³⁷ which tend to be shorter. Overall, trimetallic rare-earth metal methylidene complexes mentioned above in Figure 1 show similar average $\text{Ln-C}(\text{CH}_2)$ bond lengths considering the different ionic radii of the rare-earth metal centers, e.g. II^{Sc} 2.367 Å,³⁵ II^{Er} 2.388 Å,³⁷ II^{Lu} 2.376 Å,³⁵ IV^{Tm} 2.346 Å,³⁴ VI^{Nd} 2.475 Å,³⁸ VI^{Ho} 2.391 Å,³⁸ and VI^{Lu} 2.347 Å.³³

Methylidene-Transfer Reactions: Carbonyl Methylation and Lacton Polymerization. Naturally, we were interested in the reactivity of these new methylidene complexes to enlighten any Ln(III) size effect and impact of the halogenido ligand. With addition of carbonylic substrates, it was demonstrated previously that the methylidene complexes under study act as Schrock-type nucleophilic carbenes. Accordingly, reactivity studies were carried out by monitoring the transformations of 2 equiv. of cyclohexanone, benzaldehyde, 9-fluorenone, and dihydrocoumarin with methylidene complexes 4-Ln in $[\text{D}_8]\text{THF}$ at ambient temperature. The yields were determined after 15 minutes (exact procedure recorded in the ESI). For comparison, the established Tebbe reagent was tested under the same conditions in $[\text{D}_6]\text{benzene}$ (Tebbe reagent decomposes in THF). The sole formation of the respective olefinic product in decent to excellent yields revealed the intended suppression of undesired methylated side products (Table 1). Strikingly, complexes bearing bridging iodides (4^*-La^{I} and $4'\text{-La}^{\text{I}}$) are not capable of converting sterically demanding 9-fluorenone (entry A) even after prolonged reaction time (> 12 h), likely attributable to the decreased accessibility of the CH_2 moiety, less protruding being efficiently shielded by the bulky iodide ligands. Despite this, the yttrium complexes convert all tested ketones and aldehydes in very good yields, equaling the performance of the Tebbe reagent $\text{Cp}_2\text{Ti}(\mu\text{-CH}_2)(\mu\text{-Cl})\text{AlMe}_2$. The lanthanum-based methylidene complexes also convert the carbonyl functionalities in good yields and reactivity increases from the chlorido to bromido derivatives, however, the conversion decreases again with the introduction of iodido ligands in the bridging positions. The conversion of cyclohexanone (entry C) proceeds in good yields for all complexes. Furthermore, the presence of the silyl-substituted Cp ancillary ligand does not only increase the solubility of these complexes, but even increased all yields, except for $4'\text{-La}^{\text{Br}}$ with 9-fluorenone (entry A), possibly due to the increased steric bulk implied by SiMe_3 substituents. Unfortunately, no reaction

Table 1. Methylidene-transfer reactivity of rare-earth metal complexes 4^*-Ln and $4'\text{-Ln}$ in $[\text{D}_8]\text{THF}$, probed for 9-fluorenone (A), benzaldehyde (B), cyclohexanone (C), dihydrocoumarin (D), δ -valerolactone (E).



	4^*-Y^{Cl}	4^*-Y^{Br}	$4'\text{-Y}^{\text{Cl}}$	$4'\text{-Y}^{\text{Br}}$	$4^*\text{-La}^{\text{Cl}}$	$4^*\text{-La}^{\text{Br}}$	4^*-La^{I}	$4'\text{-La}^{\text{Cl}}$	$4'\text{-La}^{\text{Br}}$	$4'\text{-La}^{\text{I}}$	Tebbe ^[a]
A	>99 %	>99 %	>99 %	>99 %	62 %	95 %	0 %	62 %	44 %	0 %	>99 %
B	>99 %	>99 %	>99 %	>99 %	53 %	57 %	59 %	64 %	72 %	78 %	>99 %
C	>99 %	>99 %	>99 %	>99 %	62 %	85 %	55 %	>99 %	>99 %	>99 %	>99 %
D	0 %	0 %	0 %	0 %	0 %	0 %	0 %	0 %	0 %	0 %	67 %
E	76 % ^[P]	86 % ^[P]	60 % ^[P]	51 % ^[P]	67 % ^[P]	87 % ^[P]	23 % ^[P]	88 % ^[P]	85 % ^[P]	70 % ^[P]	>99 %

^[a] in C_6D_6 , ^[P] polymerization

was observed for dihydrocoumarin (entry **D**) as it was shown for the Tebbe reagent. Interestingly, the reaction of cyclic esters as δ -valerolactone with the mixed halogenide/methylidene complexes showed polymerization in moderate to good yields contrary to the methylidene transfer performed by the Tebbe reagent (the exact procedure for the polymerization is given in the ESI). Additionally, the reactivity of complexes **3-La** was tested for their capability for *in situ* methylidene transfer, however Tebbe-like olefination was not observed.

Re-visiting the Tebbe Reagent. It was only recently that Mindiola and coworkers reported on the complicated but successful structural elucidation of the prominent Tebbe reagent.²¹ They could show, that the Tebbe reagent favorably co-crystallizes from a mixture of *n*-pentane and toluene, with the trivalent decomposition product $\text{Cp}_2\text{Ti}(\mu\text{-Cl})_2\text{AlMe}_2$ (site occupancy 0.38). Similar to their results, we obtained crystals of it from a saturated solution of a mixture of *n*-pentane and toluene but the crystal structure analysis revealed only a minor amount (site occupancy 0.06) of side product $\text{Cp}_2\text{Ti}(\mu\text{-Cl})_2\text{AlMe}_2$. Not surprisingly, the Ti–C(CH₂) bond lengths of Mindiola's and our studies differ significantly (this work: 2.058(3) Å, Mindiola's work: 2.095(5) Å),²¹ and further, also the Ti–Cl bond lengths vary (this work: 2.455 and 2.456(7) Å, Mindiola's work: 2.5585(7) Å),²¹ which can only be attributed to the different quantities of side product present in the crystal.

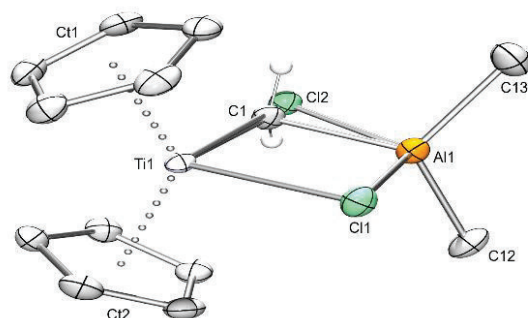


Figure 6. ORTEP representation of the crystal structure of the Tebbe reagent $\text{Cp}_2\text{Ti}(\mu\text{-CH}_2)(\mu\text{-Cl})\text{AlMe}_2$ (94 %) and $\text{Cp}_2\text{Ti}(\mu\text{-Cl})_2\text{AlMe}_2$ (6 %) with atomic displacement parameters set at the 50 % level. Hydrogen atoms except for the CH₂ group and lattice toluene are omitted for clarity. Selected bond lengths [Å] for $\text{Cp}_2\text{Ti}(\mu\text{-CH}_2)(\mu\text{-Cl})\text{AlMe}_2$: Ti1–C1 2.058(3), Ti1–Cl1 2.455, Ti1–Cl2 2.456(7), Ti1...Ct1 2.054, Ti1...Ct2 2.061, Al1–CH2 2.067(2), Al1–Cl1 2.3090(5), Al1–Cl2 2.074(8).

CONCLUSION

In summary, treatment of the half-sandwich precursors $\text{Cp}^R\text{Ln}(\text{AlMe}_4)_2$ with mild halogenido transfer reagents SiMe_3X led to the formation of various mixed tetramethylaluminato/halogenido rare-earth-metal cluster compounds $[(\text{Cp}^R)\text{Ln}(\text{AlMe}_4)_x(\text{Cl})_y]_z$ stabilized by sterically and

electronically distinct cyclopentadienyl ligands. The nuclearity of these clusters could be identified with XRD measurements and revealed isostructural behavior to their chlorido analogues. Interestingly, the cluster nuclearity is strongly dependent on the rare-earth-metal size, however, the impact of the varying cyclopentadienyl and halogenido ligands on the solid-state structure showed solely minor influence. Further work will be carried out for the better understanding of the fluxional behavior of the smaller cluster compounds in aromatic solvents. The transformation of such mixed tetramethylaluminato/halogenido Ln(III) half-sandwich complexes into methylidene complexes $\text{Cp}^R_3\text{Ln}_3(\mu\text{-X})_3(\mu_3\text{-X})(\mu_3\text{-CH}_2)(\text{THF})_3$ is (a) temperature dependent (< ambient temperatures mainly give bis(halogenido) Ln(III) complexes $\text{Cp}^R\text{LnX}_2(\text{THF})_3$), (b) Ln(III)-size dependent (respective Lu(III) methylidene were not obtained), and (c) halogenido-size dependent ($\text{Cp}^R_3\text{Y}_3(\mu\text{-I})_3(\mu_3\text{-I})(\mu_3\text{-CH}_2)(\text{THF})_3$ were not obtained). Furthermore, a silane elimination protocol starting from $(\text{C}_5\text{Me}_5)_3\text{Y}_3(\mu\text{-Me})_3(\mu_3\text{-Me})(\mu_3\text{-CH}_2)(\text{THF})_2$ was implemented for the synthesis of the respective halogenido/methylidene complex. Such rare-earth-metal methylidene complexes can be fine-tuned (*via* Ln(III) and the halogenido ligand) to match the performance of the Tebbe reagent in methylation reactions of ketones and aldehydes. However, the “ $\text{Ln}_3(\text{CH}_2)$ ” moieties are less tolerant toward bulky and functionalized substrates, as evidenced for the polymerization of δ -valerolactone.

EXPERIMENTAL SECTION

All operations were performed with rigorous exclusion of air and water by using standard Schlenk, high-vacuum, and glovebox techniques (MBraun 200B; <0.1 ppm O₂, <0.1 ppm H₂O). Solvents were purified by using Grubbs columns (MBraun SPS, solvent purification system) and stored inside a glovebox. [D₆]benzene, [D₈]toluene, and [D₈]THF were obtained from Sigma-Aldrich, degassed, and [D₆]benzene and [D₈]THF were dried over NaK alloy for two days, [D₈]toluene was stored over Na. Both were filtered prior to use. SiMe_3Cl , SiMe_3Br , and SiMe_3OTf were purchased from Sigma Aldrich and used as received. SiMe_3I was purchased from ABCR and filtered prior to use. Neopentanol was purchased from Alfa Aesar and sublimed. Trimethylaluminum was purchased from ABCR and used as received. Cp_2TiCl_2 was purchased from Sigma Aldrich and sublimed prior to use. 9-fluorenone was purchased from Sigma Aldrich and sublimed, benzaldehyde and cyclohexanone was purchased from Acros Organics and distilled, dihydrocoumarin was purchased from TCI and distilled. $(\text{C}_5\text{Me}_5)\text{Ln}(\text{AlMe}_4)_2$,⁴⁹ $(\text{C}_5\text{Me}_4\text{SiMe}_3)\text{Ln}(\text{AlMe}_4)_2$,⁴⁴ and $(\text{C}_5\text{Me}_5)_3\text{Y}_3(\mu\text{-Me})_3(\mu_3\text{-Me})(\mu_3\text{-CH}_2)(\text{THF})_2$ ³⁹ were synthesized according to literature procedures. The NMR spectra of air- and moisture-sensitive compounds were recorded by using J. Young valve NMR tubes on a Bruker AVII+400 spectrometer (¹H, 400.13 MHz, ¹³C, 100.61 MHz), and on a Bruker AVII+500 spectrometer (¹H, 500.13 MHz, ¹³C, 125.76 MHz, ⁸⁹Y, 24.51 MHz). IR spectra were recorded on a

Thermo Fisher Scientific NICOLET 6700 FTIR spectrometer using a DRIFT chamber with dry KBr/sample mixture and KBr windows; IR (DRIFT) data were converted by using the Kubelka-Munk refinement Elemental analyses were performed on an Elementar Vario MICRO Cube.

General procedure for the synthesis of $[\text{Cp}^{\text{R}}\text{Ln}(\text{AlMe}_4)(\mu\text{-X})]_2$ (Ln = Y, Lu; X = Cl, Br, I; $\text{Cp}^{\text{R}} = \text{C}_5\text{Me}_5, \text{C}_5\text{Me}_4\text{SiMe}_3$)

A solution of 0.9 equiv. SiMe_3X in *n*-hexane (2 mL) was added to a solution of $(\text{C}_5\text{Me}_5)_2\text{Ln}(\text{AlMe}_4)_2$ in *n*-hexane (2 mL). The reaction mixture was heated to 70 °C for 1 h. The mixture was allowed to cool to ambient temperatures and crystals suitable for XRD were grown within 2-4 days at ambient temperatures. Stirring the crystals shortly in cold toluene and decanting of the solution can remove potential impurities of the starting compound.

$[(\text{C}_5\text{Me}_5)_2\text{Y}(\text{AlMe}_4)(\mu\text{-Cl})]_2$ (1^*-Y^{Cl}): Following the procedure described above, SiMe_3Cl (49.1 mg, 452 μmol) and $(\text{C}_5\text{Me}_5)_2\text{Y}(\text{AlMe}_4)_2$ (200 mg, 502 μmol) yielded 1^*-Y^{Cl} as white powder (148 mg, 213 μmol , 85 %). ^1H NMR (500 MHz, $[\text{D}_8]\text{toluene}$, 26 °C): δ 1.89 (s, 30H, Cp- CH_3), -0.20 (d, $^2J(\text{YH}) = 2.3$ Hz, 24H, Al- CH_3) ppm. $^{13}\text{C}\{^1\text{H}\}$ NMR (101 MHz, $[\text{D}_8]\text{toluene}$, 26 °C): δ 123.0 (d, $^1J(\text{YC}) = 1.7$ Hz, C_5Me_5), 12.0 (Cp- CH_3) ppm; ^{13}C resonances for the AlMe_4 groups could not be detected. ^{89}Y NMR (from ^1H - ^{89}Y HSQC, 25 MHz, $[\text{D}_8]\text{toluene}$, 26 °C): δ 208 ppm. IR (KBr): $\tilde{\nu} = 2948$ (s), 2907 (s), 2859 (m), 1488 (w), 1454 (m), 1433 (m), 1387 (w), 1379 (m), 1194 (w), 1065 (vw), 1024 (w), 803 (vw), 705 (vs), 690 (s), 592 (vw), 576 (w), 401 (m) cm^{-1} ; elemental analysis calcd (%) for $\text{C}_{28}\text{H}_{54}\text{Al}_2\text{Cl}_2\text{Y}_2$: C 48.50, H 7.85; found C 48.32, H 7.30. The analytical data were consistent with those previously published.⁴²

$[(\text{C}_5\text{Me}_5)_2\text{Y}(\text{AlMe}_4)(\mu\text{-Br})]_2$ (1^*-Y^{Br}): Following the procedure described above, SiMe_3Br (69.2 mg, 452 μmol) and $(\text{C}_5\text{Me}_5)_2\text{Y}(\text{AlMe}_4)_2$ (200 mg, 502 μmol) yielded 1^*-Y^{Br} as white powder (104 mg, 150 μmol , 60 %). ^1H NMR (400 MHz, $[\text{D}_8]\text{toluene}$, 26 °C): δ 1.92 (s, 30H, Cp- CH_3), -0.18 (d, $^2J(\text{YH}) = 2.3$ Hz, 24H, Al- CH_3) ppm. $^{13}\text{C}\{^1\text{H}\}$ NMR (101 MHz, $[\text{D}_8]\text{toluene}$, 26 °C): δ 123.5 (d, $^1J(\text{YC}) = 1.5$ Hz, C_5Me_5), 12.3 (Cp- CH_3) ppm; ^{13}C resonances for the AlMe_4 groups could not be detected. ^{89}Y NMR (from ^1H - ^{89}Y HSQC, 25 MHz, $[\text{D}_8]\text{toluene}$, 26 °C): δ 246 ppm. IR (KBr): $\tilde{\nu} = 2929$ (m), 2914 (m), 2888 (w), 2863 (w), 2823 (w), 2789 (vw), 1487 (vw), 1446 (w), 1234 (w), 1419 (w), 1434 (vw), 1380 (w), 1219 (m), 1188 (w), 1022 (vw), 801 (vw), 715 (vs), 697 (vs), 608 (w), 587 (s), 482 (w), 457 (w), 422 (w) cm^{-1} ; elemental analysis calcd (%) for $\text{C}_{28}\text{H}_{54}\text{Al}_2\text{Br}_2\text{Y}_2$: C 42.99, H 6.96; found C 42.66, H 7.30.

$[(\text{C}_5\text{Me}_5)_2\text{Y}(\text{AlMe}_4)(\mu\text{-I})]_2$ (1^*-Y^{I}): Following the procedure described above, SiMe_3I (90.4 mg, 452 μmol) and $(\text{C}_5\text{Me}_5)_2\text{Y}(\text{AlMe}_4)_2$ (200 mg, 502 μmol) yielded 1^*-Y^{I} as white powder (165 mg, 188 μmol , 75 %). ^1H NMR (400 MHz, $[\text{D}_8]\text{toluene}$, 26 °C): δ 1.98 (s, 30H, Cp- CH_3), -0.15 (br s,

24H, Al- CH_3) ppm. $^{13}\text{C}\{^1\text{H}\}$ NMR (101 MHz, $[\text{D}_8]\text{toluene}$, 26 °C): δ 124.1 (C_5Me_5), 11.4 (Cp- CH_3) ppm; ^{13}C resonances for the AlMe_4 groups could not be detected. IR (KBr): $\tilde{\nu} = 2968$ (w), 2917 (m), 2885 (m), 2862 (w), 2823 (w), 2731 (vw), 1683 (vw), 1669 (vw), 1575 (w), 1568 (w), 1532 (vw), 1520 (w), 1506 (vw), 1472 (w), 1455 (w), 1446 (w), 1435 (w), 1418 (w), 1394 (vw), 1379 (w), 1218 (w), 1188 (m), 1063 (vw), 1022 (w), 800 (vw), 714 (vs), 697 (vs), 691 (vs), 604 (w), 580 (s), 536 (vw), 527 (vw), 518 (vw), 482 (w), 479 (w), 458 (w), 419 (vw), 401 (w) cm^{-1} ; elemental analysis calcd (%) for $\text{C}_{28}\text{H}_{54}\text{Al}_2\text{I}_2\text{Y}_2$: C 38.38, H 6.21; found C 38.19, H 6.07.

$[(\text{C}_5\text{Me}_5)_2\text{Lu}(\text{AlMe}_4)(\mu\text{-Cl})]_2$ ($1^*\text{-Lu}^{\text{Cl}}$): Following the procedure described above, SiMe_3Cl (21.0 mg, 193 μmol) and $(\text{C}_5\text{Me}_5)_2\text{Lu}(\text{AlMe}_4)_2$ (100 mg, 212 μmol) yielded $1^*\text{-Lu}^{\text{Cl}}$ as white powder (52.0 mg, 60.1 μmol , 57 %). ^1H NMR (400 MHz, $[\text{D}_8]\text{toluene}$, 26 °C): δ 1.93 (s, 30H, Cp- CH_3), -0.05 (br s, 24H, Al- CH_3) ppm. $^{13}\text{C}\{^1\text{H}\}$ NMR (101 MHz, $[\text{D}_8]\text{toluene}$, 26 °C): δ 121.4 (C_5Me_5), 12.1 (Cp- CH_3) ppm; ^{13}C resonances for the AlMe_4 groups could not be detected. IR (KBr): $\tilde{\nu} = 3013$ (vw), 2975 (w), 2916 (m), 2888 (m), 2840 (w), 2823 (w), 2736 (vw), 1558 (vw), 1539 (vw), 1520 (vw), 1506 (w), 1488 (vw), 1455 (w), 1435 (w), 1418 (w), 1379 (vw), 1374 (vw), 1219 (w), 1192 (m), 1021 (vw), 800 (vw), 715 (vs), 700 (vs), 693 (vs), 668 (m), 582 (s), 471 (m), 457 (m), 419 (vw) cm^{-1} ; elemental analysis calcd (%) for $\text{C}_{28}\text{H}_{54}\text{Al}_2\text{Cl}_2\text{Lu}_2$: C 38.86, H 6.29; found C 38.91, H 6.27.

$[(\text{C}_5\text{Me}_5)_2\text{Lu}(\text{AlMe}_4)(\mu\text{-Br})]_2$ ($1^*\text{-Lu}^{\text{Br}}$): Following the procedure described above, SiMe_3Br (29.2 mg, 191 μmol) and $(\text{C}_5\text{Me}_5)_2\text{Lu}(\text{AlMe}_4)_2$ (100 mg, 212 μmol) yielded $1^*\text{-Lu}^{\text{Br}}$ as white powder (67.0 mg, 70.2 μmol , 66 %). ^1H NMR (400 MHz, $[\text{D}_8]\text{toluene}$, 26 °C): δ 1.96 (s, 30H, Cp- CH_3), 0.00 (br s, 24H, Al- CH_3) ppm. $^{13}\text{C}\{^1\text{H}\}$ NMR (101 MHz, $[\text{D}_8]\text{toluene}$, 26 °C): δ 121.8 (C_5Me_5), 12.3 (Cp- CH_3) ppm; ^{13}C resonances for the AlMe_4 groups could not be detected. IR (KBr): $\tilde{\nu} = 3014$ (w), 2976 (w), 2917 (s), 2887 (m), 2841 (m), 2824 (w), 2734 (vw), 1556 (vw), 1486 (vw), 1435 (w), 1418 (w), 1391 (vw), 1379 (vw), 1219 (m), 1192 (m), 1022 (w), 800 (vw), 713 (vs), 697 (vs), 613 (m), 578 (s), 473 (m), 459 (m), 413 (vw) cm^{-1} ; elemental analysis calcd (%) for $\text{C}_{28}\text{H}_{54}\text{Al}_2\text{Br}_2\text{Lu}_2$: C 35.24, H 5.70; found C 35.22, H 5.51.

$[(\text{C}_5\text{Me}_5)_2\text{Lu}(\text{AlMe}_4)(\mu\text{-I})]_2$ (1^*-Lu^{I}): Following the procedure described above, SiMe_3I (38.1 mg, 190 μmol) and $(\text{C}_5\text{Me}_5)_2\text{Lu}(\text{AlMe}_4)_2$ (100 mg, 212 μmol) yielded 1^*-Lu^{I} as white powder (74.0 mg, 70.6 μmol , 67 %). ^1H NMR (400 MHz, $[\text{D}_8]\text{toluene}$, 26 °C): δ 2.00 (s, 30H, Cp- CH_3), 0.04 (br s, 24H, Al- CH_3) ppm. $^{13}\text{C}\{^1\text{H}\}$ NMR (101 MHz, $[\text{D}_8]\text{toluene}$, 26 °C): δ 122.6 (C_5Me_5), 13.1 (Cp- CH_3) ppm; ^{13}C resonances for the AlMe_4 groups could not be detected. IR (KBr): $\tilde{\nu} = 2969$ (w), 2915 (m), 2886 (m), 2862 (w), 1444 (w), 1433 (w), 1419 (w), 1379 (w), 1226 (w), 1190 (w), 1022 (vw), 712 (vs), 696 (vs), 580 (s), 480 (w), 473 (w), 459 (w), 402 (w) cm^{-1} ; elemental analysis calcd (%) for $\text{C}_{28}\text{H}_{54}\text{Al}_2\text{I}_2\text{Lu}_2$: C 32.08, H 5.19; found C 31.94, H 5.01.

[(C₅Me₄SiMe₃)Y(AlMe₄)(μ-Cl)]₂ (1'-Y^{Cl}): Following the procedure described above, SiMe₃Cl (21.4 mg, 197 μmol) and (C₅Me₄SiMe₃)Y(AlMe₄)₂ (100 mg, 219 μmol) yielded 1'-Y^{Cl} as white powder (40.0 mg, 49.4 μmol, 45 %). ¹H NMR (400 MHz, [D₈]toluene, 26 °C): δ 2.15 (s, 12H, Cp-CH₃-2,5), 1.85 (s, 12H, Cp-CH₃-3,4), 0.32 (s, 18H, Si-CH₃), -0.18 (d, ²J(YH) = 2.4 Hz, 24H, Al-CH₃) ppm. ¹³C{¹H} NMR (101 MHz, [D₈]toluene, 26 °C): δ 132.3 (2,5-C₅Me₄SiMe₃), 128.4 (3,4-C₅Me₄SiMe₃), 120.3 (1-C₅Me₄SiMe₃), 15.7 (Cp-CH₃), 11.9 (Cp-CH₃), 2.1 (Si-Me), 0.3 (br, Al-Me) ppm. ⁸⁹Y NMR (from ¹H-⁸⁹Y HSQC, 25 MHz, [D₈]toluene, 26 °C): δ 206 ppm. IR (KBr): $\tilde{\nu}$ = 2948 (m), 2918 (m), 2892 (m), 2826 (w), 2794 (vw), 1456 (w), 1448 (w), 1436 (vw), 1429 (vw), 1419 (vw), 1406 (vw), 1322 (w), 1248 (m), 1219 (w), 1187 (w), 1019 (vw), 846 (vs), 838 (vs), 756 (m), 715 (vs), 697 (vs), 633 (w), 608 (w), 583 (s), 481 (w), 459 (vw), 425 (w) cm⁻¹; elemental analysis calcd (%) for C₃₂H₆₆Al₂Cl₂Lu₂Si₂: C 47.47, H 8.22; found C 47.58, H 7.94. The analytical data were consistent with those previously published.⁴⁴

[(C₅Me₄SiMe₃)Y(AlMe₄)(μ-Br)]₂ (1'-Y^{Br}): Following the procedure described above, SiMe₃Br (30.2 mg, 197 μmol) and (C₅Me₄SiMe₃)Y(AlMe₄)₂ (100 mg, 219 μmol) yielded 1'-Y^{Br} as white powder (60.0 mg, 66.8 μmol, 61 %). ¹H NMR (400 MHz, [D₈]toluene, 26 °C): δ 2.17 (s, 12H, Cp-CH₃-2,5), 1.86 (s, 12H, Cp-CH₃-3,4), 0.33 (s, 18H, Si-CH₃), -0.15 (d, ²J(YH) = 2.4 Hz, 24H, Al-CH₃) ppm. ¹³C{¹H} NMR (101 MHz, [D₈]toluene, 26 °C): δ 132.8 (2,5-C₅Me₄SiMe₃), 128.3 (3,4-C₅Me₄SiMe₃), 120.5 (1-C₅Me₄SiMe₃), 15.8 (Cp-CH₃), 12.3 (Cp-CH₃), 2.8 (br, Al-Me), 2.2 (Si-Me) ppm. ⁸⁹Y NMR (from ¹H-⁸⁹Y HSQC, 25 MHz, [D₈]toluene, 26 °C): δ 240 ppm. IR (KBr): $\tilde{\nu}$ = 2955 (w), 2918 (m), 2892 (w), 2824 (w), 2790 (vw), 1482 (vw), 1448 (vw), 1408 (vw), 1388 (vw), 1377 (vw), 1344 (vw), 1321 (w), 1248 (m), 1219 (w), 1190 (w), 1128 (vw), 1019 (vw), 846 (vs), 838 (vs), 756 (m), 716 (vs), 697 (vs), 633 (w), 611 (w), 582 (w), 482 (w), 460 (w), 426 (m) cm⁻¹; elemental analysis calcd (%) for C₃₂H₆₆Al₂Br₂Lu₂Si₂: C 42.77, H 7.40; found C 42.81, H 7.34.

[(C₅Me₄SiMe₃)Y(AlMe₄)(μ-I)]₂ (1'-Y^I): Following the procedure described above, SiMe₃I (39.4 mg, 197 μmol) and (C₅Me₄SiMe₃)Y(AlMe₄)₂ (100 mg, 219 μmol) yielded 1'-Y^I as white powder (70.0 mg, 70.5 μmol, 64 %). ¹H NMR (400 MHz, [D₈]toluene, 26 °C): δ 2.22 (s, 12H, Cp-CH₃-2,5), 1.93 (s, 12H, Cp-CH₃-3,4), 0.37 (s, 18H, Si-CH₃), -0.13 (s, 24H, Al-CH₃) ppm. ¹³C{¹H} NMR (101 MHz, [D₈]toluene, 26 °C): δ 133.3 (2,5-C₅Me₄SiMe₃), 129.4 (3,4-C₅Me₄SiMe₃), 121.4 (1-C₅Me₄SiMe₃), 16.3 (Cp-CH₃), 13.2 (Cp-CH₃), 3.7 (br, Al-Me), 2.1 (Si-Me) ppm. IR (KBr): $\tilde{\nu}$ = 2948 (m), 2898 (m), 2870 (w), 2736 (vw), 1504 (vw), 1481 (vw), 1454 (w), 1447 (w), 1417 (w), 1404 (vw), 1388 (vw), 1374 (vw), 1345 (vw), 1321 (w), 1263 (w), 1253 (m), 1246 (m), 1216 (w), 1194 (w), 1127 (vw), 1020 (w), 987 (vw), 848 (s), 836 (vs), 755 (m), 736 (w), 707 (vs), 698 (vs), 693 (s), 687 (s), 638 (w), 630 (w), 601 (w), 579 (w), 559 (w), 526 (vw), 515 (w), 508 (vw), 496 (vw), 472 (vw), 457 (vw), 421 (m), 405 (vw) cm⁻¹; elemental analysis calcd (%) for C₃₂H₆₆Al₂I₂Lu₂Si₂: C 38.72, H 6.70; found C 38.58, H 6.64.

[(C₅Me₄SiMe₃)Lu(AlMe₄)(μ-Cl)]₂ (1'-Lu^{Cl}): Following the procedure described above, SiMe₃Cl (18.0 mg, 166 μmol) and (C₅Me₄SiMe₃)Lu(AlMe₄)₂ (100 mg, 184 μmol) yielded 1'-Lu^{Cl} as white powder (36.1 mg, 36.7 μmol, 40 %). ¹H NMR (400 MHz, [D₈]toluene, 26 °C): δ 2.17 (s, 12H, Cp-CH₃-2,5), 1.87 (s, 12H, Cp-CH₃-3,4), 0.32 (s, 18H, Si-CH₃), -0.05 (br s, 24H, Al-CH₃) ppm. ¹³C{¹H} NMR (101 MHz, [D₈]toluene, 26 °C): δ 130.9 (2,5-C₅Me₄SiMe₃), 126.8 (3,4-C₅Me₄SiMe₃), 118.4 (1-C₅Me₄SiMe₃), 15.8 (Cp-CH₃), 11.8 (Cp-CH₃), 2.1 (Si-CH₃) ppm; ¹³C resonances for the AlMe₄ groups could not be detected. IR (KBr): $\tilde{\nu}$ = 2949 (vw), 2887 (w), 2771 (w), 2730 (vw), 1485 (vw), 1448 (w), 1327 (vw), 1243 (w), 1185 (m), 1131 (w), 1107 (vw), 845 (w), 758 (m), 687 (s), 630 (m), 505 (s), 459 (m), 445 (m), 418 (vw) cm⁻¹; elemental analysis calcd (%) for C₃₂H₆₆Al₂Cl₂Lu₂Si₂: C 39.15, H 6.78; found C 39.22, H 6.86.

[(C₅Me₄SiMe₃)Lu(AlMe₄)(μ-Br)]₂ (1'-Lu^{Br}): Following the procedure described above, SiMe₃Br (25.4 mg, 166 μmol) and (C₅Me₄SiMe₃)Lu(AlMe₄)₂ (100 mg, 184 μmol) yielded 1'-Lu^{Br} as white powder (44.0 mg, 41.1 μmol, 45 %). ¹H NMR (400 MHz, [D₈]toluene, 26 °C): δ 2.19 (s, 12H, Cp-CH₃-2,5), 1.88 (s, 12H, Cp-CH₃-3,4), 0.34 (s, 18H, Si-CH₃), 0.01 (br s, 24H, Al-CH₃) ppm. ¹³C{¹H} NMR (101 MHz, [D₈]toluene, 26 °C): δ 131.4 (2,5-C₅Me₄SiMe₃), 127.1 (3,4-C₅Me₄SiMe₃), 120.4 (1-C₅Me₄SiMe₃), 15.9 (Cp-CH₃), 12.2 (Cp-CH₃), 2.2 (Si-CH₃) ppm; ¹³C resonances for the AlMe₄ groups could not be detected. IR (KBr): $\tilde{\nu}$ = 3014 (w), 2970 (m), 2947 (m), 2920 (m), 2892 (m), 2825 (w), 2740 (vw), 1484 (vw), 1447 (w), 1433 (w), 1408 (w), 1388 (vw), 1377 (vw), 1371 (vw), 1344 (w), 1321 (m), 1248 (s), 1227 (w), 1188 (w), 1129 (vw), 1020 (vw), 846 (vs), 837 (vs), 756 (s), 715 (vs), 701 (vs), 633 (m), 613 (m), 582 (s), 530 (w), 476 (w), 463 (w), 425 (w), 405 (vw) cm⁻¹; elemental analysis calcd (%) for C₃₂H₆₆Al₂Br₂Lu₂Si₂: C 35.90, H 6.21; found C 35.68, H 5.95.

[(C₅Me₄SiMe₃)Lu(AlMe₄)(μ-I)]₂ (1'-Lu^I): Following the procedure described above, SiMe₃I (33.2 mg, 166 μmol) and (C₅Me₄SiMe₃)Lu(AlMe₄)₂ (100 mg, 184 μmol) yielded 1'-Lu^I as white powder (48.0 mg, 41.2 μmol, 45 %). ¹H NMR (400 MHz, [D₈]toluene, 26 °C): δ 2.23 (br s, 12H, Cp-CH₃-2,5), 1.86 (s, 12H, Cp-CH₃-3,4), 0.33 (s, 18H, Si-CH₃), 0.01 (br s, 24H, Al-CH₃) ppm. ¹³C{¹H} NMR (101 MHz, [D₈]toluene, 26 °C): δ 132.1 (2,5-C₅Me₄SiMe₃), 127.6 (3,4-C₅Me₄SiMe₃), 123.0 (1-C₅Me₄SiMe₃), 16.2 (Cp-CH₃), 12.6 (Cp-CH₃), 1.7 (Si-CH₃) ppm; ¹³C resonances for the AlMe₄ groups could not be detected. IR (KBr): $\tilde{\nu}$ = 2973 (w), 2948 (w), 2905 (w), 2860 (w), 2731 (vw), 1575 (w), 1485 (vw), 1455 (w), 1436 (w), 1436 (w), 1428 (w), 1418 (w), 1405 (w), 1386 (vw), 1374 (vw), 1345 (vw), 1321 (m), 1249 (m), 1129 (vw), 1085 (vw), 1021 (w), 989 (vw), 952 (vw), 847 (vs), 839 (vs), 756 (m), 688 (w), 668 (vw), 630 (w), 570 (vw), 424 (m), 404 (w) cm⁻¹; elemental analysis calcd (%) for C₃₂H₆₆Al₂I₂Lu₂Si₂: C 33.00, H 5.71; found C 33.64, H 5.67.

General procedure for the synthesis of [Cp^R₃La₃(AlMe₄)₂(μ-X)]₂ (X = Cl, Br, I; Cp^R = C₅Me₅, C₅Me₄SiMe₃)

A solution of 1.3 equiv. SiMe_3X in *n*-hexane (2 mL) was added to a solution of $(\text{C}_5\text{Me}_5)_3\text{La}(\text{AlMe}_2)_2$ in *n*-hexane (2 mL). The reaction was stirred overnight at ambient temperatures. The precipitate was allowed to settle, washed with *n*-hexane (3 x 1 mL), and dried *in vacuo*. Crystals can be obtained by performing the reaction under the same conditions without stirring. Due to poor solubility any meaningful NMR spectra could not be obtained.

$[(\text{C}_5\text{Me}_5)_3\text{La}_3(\text{AlMe}_2)_4(\mu\text{-Cl})_4]_2$ ($2^*\text{-La}^{\text{Cl}}$): Following the procedure described above, SiMe_3Cl (63.0 mg, 580 μmol) and $(\text{C}_5\text{Me}_5)_3\text{La}(\text{AlMe}_2)_2$ (200 mg, 446 μmol) yielded $2^*\text{-La}^{\text{Cl}}$ as white powder (119 mg, 50.4 μmol , 68 %). IR (KBr): $\tilde{\nu} = 2911$ (s), 2858 (m), 1488 (vw), 1439 (w), 1379 (vw), 1190 (m), 1043 (w), 1027 (w), 763 (w), 696 (vs), 623 (m), 587 (m), 531 (w) cm^{-1} ; elemental analysis calcd for $\text{C}_{76}\text{H}_{138}\text{Al}_4\text{Cl}_8\text{La}_6 \times \text{C}_6\text{H}_{14}$: C 41.68, H 6.48; found C 41.46, H 6.50. The analytical data were consistent with those previously published.⁴²

$[(\text{C}_5\text{Me}_5)_3\text{La}_3(\text{AlMe}_2)_4(\mu\text{-Br})_4]_2$ ($2^*\text{-La}^{\text{Br}}$): Following the procedure described above, SiMe_3Br (88.8 mg, 580 μmol) and $(\text{C}_5\text{Me}_5)_3\text{La}(\text{AlMe}_2)_2$ (200 mg, 446 μmol) yielded $2^*\text{-La}^{\text{Br}}$ as white powder (139 mg, 51.1 μmol , 69 %). IR (KBr): $\tilde{\nu} = 2954$ (m), 2912 (s), 2858 (m), 1449 (w), 1436 (w), 1420 (w), 1379 (w), 1193 (w), 1039 (m), 1026 (m), 768 (w), 700 (vs), 621 (s), 585 (m), 558 (w), 530 (w) cm^{-1} ; elemental analysis calcd for $\text{C}_{76}\text{H}_{138}\text{Al}_4\text{Br}_8\text{La}_6 \times \text{C}_6\text{H}_{14}$: C 36.23, H 5.64; found C 36.60, H 5.54.

$[(\text{C}_5\text{Me}_5)_3\text{La}_3(\text{AlMe}_2)_4(\mu\text{-I})_4]_2$ (2^*-La^{I}): Following the procedure described above, SiMe_3I (116 mg, 580 μmol) and $(\text{C}_5\text{Me}_5)_3\text{La}(\text{AlMe}_2)_2$ (200 mg, 446 μmol) yielded 2^*-La^{I} as white powder (200 mg, 64.6 μmol , 87 %). IR (KBr): $\tilde{\nu} = 2954$ (s), 2915 (s), 2857 (m), 1487 (w), 1454 (m), 1436 (m), 1419 (w), 1388 (vw), 1378 (w), 1195 (m), 1037 (m), 1026 (m), 768 (w), 698 (vs), 616 (s), 583 (m), 555 (w), 523 (w) cm^{-1} ; elemental analysis calcd for $\text{C}_{76}\text{H}_{138}\text{Al}_4\text{I}_8\text{La}_6 \times \text{C}_6\text{H}_{14}$: C 31.83, H 4.95; found C 32.26, H 4.76.

$[(\text{C}_5\text{Me}_4\text{SiMe}_3)_3\text{La}_3(\text{AlMe}_2)_4(\mu\text{-Cl})_4]_2$ ($2'\text{-La}^{\text{Cl}}$): Following the procedure described above, SiMe_3Cl (55.8 mg, 514 μmol) and $(\text{C}_5\text{Me}_4\text{SiMe}_3)_3\text{La}(\text{AlMe}_2)_2$ (200 mg, 395 μmol) yielded $2'\text{-La}^{\text{Cl}}$ as white powder (80.0 mg, 34.7 μmol , 46 %). IR (KBr): $\tilde{\nu} = 2950$ (w), 2906 (w), 2861 (w), 1482 (vw), 1452 (w), 1431 (vw), 1386 (vw), 1375 (vw), 1344 (vw), 1325 (w), 1261 (w), 1247 (m), 1195 (w), 1124 (vw), 1043 (w), 1029 (w), 1019 (w), 847 (vs), 836 (vs), 755 (m), 704 (m), 627 (m), 584 (w), 532 (w), 418 (m) cm^{-1} ; elemental analysis calcd for $\text{C}_{88}\text{H}_{174}\text{Si}_6\text{Al}_4\text{Cl}_8\text{La}_6$: C 40.25, H 6.68; found C 40.40, H 6.64.

$[(\text{C}_5\text{Me}_4\text{SiMe}_3)_3\text{La}_3(\text{AlMe}_2)_4(\mu\text{-Br})_4]_2$ ($2'\text{-La}^{\text{Br}}$): Following the procedure described above, SiMe_3Br (78.6 mg, 513 μmol) and $(\text{C}_5\text{Me}_4\text{SiMe}_3)_3\text{La}(\text{AlMe}_2)_2$ (200 mg, 395 μmol) yielded $2'\text{-La}^{\text{Br}}$ as white powder (160 mg, 52.2 μmol , 79 %). IR (KBr): $\tilde{\nu} = 2951$ (w), 2906 (w), 1482 (vw), 1451 (w), 1430 (vw), 1406 (vw), 1387 (vw), 1375 (vw), 1344 (vw), 1324 (w), 1260 (w), 1247 (m), 1195 (w), 1123 (vw), 1039 (w), 1022 (w), 844 (vs), 836 (vs), 755 (m), 701 (m), 626 (m), 585 (w), 533

(vw), 418 (w) cm^{-1} ; elemental analysis calcd for $\text{C}_{88}\text{H}_{174}\text{Si}_6\text{Al}_4\text{Br}_8\text{La}_6 \times \text{C}_6\text{H}_{14}$: C 36.80, H 6.18; found C 36.46, H 6.09.

$[(\text{C}_5\text{Me}_4\text{SiMe}_3)_3\text{La}_3(\text{AlMe}_2)_4(\mu\text{-I})_4]_2$ ($2'\text{-La}^{\text{I}}$): Following the procedure described above, SiMe_3I (103 mg, 515 μmol) and $(\text{C}_5\text{Me}_4\text{SiMe}_3)_3\text{La}(\text{AlMe}_2)_2$ (200 mg, 395 μmol) yielded $2'\text{-La}^{\text{I}}$ as white powder (100 mg, 28.3 μmol , 43 %). IR (KBr): $\tilde{\nu} = 2954$ (m), 2904 (m), 2861 (w), 1485 (w), 1454 (w), 1387 (vw), 1375 (w), 1344 (w), 1323 (m), 1249 (m), 1196 (w), 1123 (vw), 1037 (w), 1018 (w), 847 (vs), 836 (vs), 754 (s), 697 (s), 618 (m), 585 (w), 554 (w), 519 (w), 420 (w) cm^{-1} ; elemental analysis calcd for $\text{C}_{88}\text{H}_{174}\text{Si}_6\text{Al}_4\text{I}_8\text{La}_6 \times 2 \text{C}_6\text{H}_{14}$: C 34.03, H 5.77; found C 33.92, H 5.84.

$(\text{C}_5\text{Me}_5)_3\text{La}_3(\text{AlMe}_2)_4(\mu\text{-OTf})_3(\mu_3\text{-OTf})_2$ ($3^*\text{-La}^{\text{OTf}}$): Following the procedure described for 2-La , SiMe_3OTf (64.4 mg, 290 μmol) and $(\text{C}_5\text{Me}_5)_3\text{La}(\text{AlMe}_2)_2$ (100 mg, 223 μmol) yielded $3^*\text{-La}^{\text{OTf}}$ as white powder (105 mg, 58.9 μmol , 79 %). IR (KBr): $\tilde{\nu} = 2919$ (w), 2872 (w), 1505 (vw), 1455 (w), 1446 (w), 1436 (w), 1380 (w), 1325 (w), 1312 (vs), 1287 (vs), 1260 (s), 1245 (s), 1227 (s), 1209 (s), 1195 (s), 1104 (vw) 1043 (vs), 941 (vw), 771 (w), 763 (w), 719 (m), 694 (m), 687 (m), 668 (w), 636 (s), 631 (s), 588 (w), 582 (w), 559 (w), 518 (m), 509 (m), 490 (vw) cm^{-1} ; elemental analysis calcd (%) for $\text{C}_{47}\text{H}_{58}\text{AlF}_{15}\text{La}_3\text{O}_{17}\text{S}_5$: C 31.64, H 3.28; found C 32.71, H 4.49. Due to the high F and S content no better elemental analysis could be obtained. The yield is determined in relation to the metal.

General procedure for the synthesis of $\text{Cp}^R\text{Y}_3(\mu\text{-X})_3(\mu_3\text{-X})(\mu_3\text{-CH}_2)(\text{THF})_3$ ($\text{X} = \text{Cl}, \text{Br}, \text{I}$, $\text{Cp}^R = \text{C}_5\text{Me}_5, \text{C}_5\text{Me}_4\text{SiMe}_3$)

$(\text{C}_5\text{Me}_5)_3\text{Y}_3(\mu\text{-X})_3(\mu_3\text{-X})(\mu_3\text{-CH}_2)(\text{THF})_3$ (4-Y^{X}):

Route A: $[\text{Cp}^R\text{Y}(\text{AlMe}_2)(\mu\text{-X})]_2$ 1-Y^{X} was suspended in toluene (1 mL) and THF (2 mL) was added. The reaction was shaken several times, filtered and allowed to stand at ambient temperatures for 3-4 days. A color change to yellow-orange occurred, the mixture was concentrated and stored at -40°C to yield crystalline material. The yield was determined in relation to the halogenido content.

Route B: A solution of 4 equiv. of SiMe_3X in THF (1 mL) were added to a solution of $(\text{C}_5\text{Me}_5)_3\text{Y}_3(\mu\text{-Me})_3(\mu_3\text{-Me})(\mu_3\text{-CH}_2)(\text{THF})_2$ V^{Y} in THF (4 mL). The solution was allowed to stir for 46 h at ambient temperature. Removal of the solvent and washing with *n*-hexane gave the products as white powder. Crystals were obtained from saturated solutions in THF at -40°C .

$(\text{C}_5\text{Me}_5)_3\text{Y}_3(\mu\text{-Cl})_3(\mu_3\text{-Cl})(\mu_3\text{-CH}_2)(\text{THF})_3$ (4^*-Y^{Cl}):

Following route A described above, 1^*-Y^{Cl} (0.100 mg, 144 μmol) yielded 4^*-Y^{Cl} as colorless crystals (68.0 mg, 65.2 μmol , 91 %).

Following route B described above, SiMe_3Cl (48.8 mg, 449 μmol), and V^{Y} (100 mg, 112 μmol) yielded 4^*-Y^{Cl} as white powder (70.0 mg, 67.0 μmol , 64 %). ^1H NMR (400 MHz, $[\text{D}_8]\text{THF}$, 26 $^\circ\text{C}$): δ 3.61 (m, 12H, THF), 1.98 (s, 45H, Cp- CH_3), 1.77 (m, 12H, THF), -0.35 (q, $^3J(\text{YH}) = 4.4$ Hz, 2H, Y- CH_2) ppm. ^{13}C NMR (101 MHz, $[\text{D}_8]\text{THF}$, 26 $^\circ\text{C}$): δ 118.0 (C₅Me₅), 67.4 (THF), 25.3 (THF), 12.2 (Cp- CH_3) ppm; ^{13}C resonances for the CH_2 group could not be detected. ^{89}Y NMR (from ^1H - ^{89}Y HSQC, 25 MHz, $[\text{D}_8]\text{THF}$, 26 $^\circ\text{C}$): δ 163 ppm. IR (KBr): $\tilde{\nu} = 2967$ (s), 2930 (vs), 2896 (vs), 2856 (vs), 2751 (w), 2719 (w), 1484 (w), 1450 (s), 1374 (m), 1344 (w), 1313 (w), 1295 (w), 1248 (w), 1176 (w), 1065 (m), 1024 (vs), 920 (m), 878 (s), 804 (w), 661 (m), 635 (m), 594 (m), 505 (s), 438 (s), 428 (s), 415 (s), 407 (s) cm^{-1} ; elemental analysis calcd (%) for C₄₃H₇₁Cl₄Y₃O₃: C 49.44, H 6.85; found C 49.19, H 6.81. The analytical data is inconsistent to those previously published.⁴⁰

(C₅Me₅)₃Y₃(μ -Br)₃(μ_3 -Br)(μ_3 -CH₂)(THF)₃ (4^{*}-Y^{Br}):

Following route A described above, 1^*-Y^{Br} (0.100 mg, 128 μmol) yielded 4^*-Y^{Br} as colorless crystals (60.0 mg, 49.1 μmol , 77 %).

Following route B described above, SiMe_3Br (68.7 mg, 44.9 μmol), and V^{Y} (100 mg, 112 μmol) yielded 4^*-Y^{Br} as white powder (80.0 mg, 65.4 μmol , 63 %). ^1H NMR (400 MHz, $[\text{D}_8]\text{THF}$, 26 $^\circ\text{C}$): δ 3.62 (m, 12H, THF), 2.01 (s, 45H, Cp- CH_3), 1.77 (m, 12H, THF), -0.33 (q, $^3J(\text{YH}) = 4.4$ Hz, 2H, Y- CH_2) ppm. ^{13}C NMR (101 MHz, $[\text{D}_8]\text{THF}$, 26 $^\circ\text{C}$): δ 118.7 (C₅Me₅), 67.4 (THF), 25.2 (THF), 12.7 (Cp- CH_3) ppm; ^{13}C resonances for the CH_2 group could not be detected. ^{89}Y NMR (from ^1H - ^{89}Y HSQC, 25 MHz, $[\text{D}_8]\text{THF}$, 26 $^\circ\text{C}$): δ 196 ppm. IR (KBr): $\tilde{\nu} = 2968$ (s), 2937 (s), 2892 (s), 2853 (s), 2719 (vw), 1568 (vw), 1557 (vw), 1539 (vw), 1506 (vw), 1520 (vw), 1471 (w), 1455 (m), 1436 (m), 1374 (w), 1343 (vw), 1314 (vw), 1295 (vw), 1246 (vw), 1185 (vw), 1063 (w), 1020 (vs), 921 (m), 874 (vs), 667 (m), 594 (w), 499 (m), 484 (m), 471 (m), 458 (m), 437 (m), 419 (vs), 412 (s) cm^{-1} ; elemental analysis calcd (%) for C₄₃H₇₁Br₄Y₃O₃: C 42.25, H 5.85; found C 42.74, H 5.89.

(C₅Me₄SiMe₃)₃Y₃(μ -Cl)₃(μ_3 -Cl)(μ_3 -CH₂)(THF)₃ (4^{*}-Y^{Cl}):

Following route A described above, 1^*-Y^{Cl} (0.100 mg, 123 μmol) yielded 4^*-Y^{Cl} as colorless crystals (64.0 mg, 53.0 μmol , 86 %). ^1H NMR (400 MHz, $[\text{D}_8]\text{THF}$, 26 $^\circ\text{C}$): δ 3.61 (m, 12H, THF), 2.11 (s, 18H, Cp- CH_3 -2,5), 2.06 (s, 18H, Cp- CH_3 -3,4), 1.77 (m, 12H, THF), 0.24 (s, 27H, Si-Me), -0.42 (q, $^3J(\text{YH}) = 4.4$ Hz, 2H, Y- CH_2) ppm. ^{13}C NMR (101 MHz, $[\text{D}_8]\text{THF}$, 26 $^\circ\text{C}$): δ 127.6 (2,5-C₅Me₄SiMe₃), 123.8 (3,4-C₅Me₄SiMe₃), 113.9 (1-C₅Me₄SiMe₃), 67.5 (THF), 25.2 (THF), 15.2 (Cp- CH_3), 13.0 (Cp- CH_3), 2.8 (Si-Me) ppm; ^{13}C resonances for the CH_2 group could not be detected. ^{89}Y NMR (from ^1H - ^{89}Y HSQC, 25 MHz, $[\text{D}_8]\text{THF}$, 26 $^\circ\text{C}$): δ 150 ppm. IR (KBr): $\tilde{\nu} = 2979$ (m), 2948 (s), 2894 (s), 2861 (m), 2360 (vw), 1558 (w), 1539 (w), 1520 (w), 1506 (w), 1496 (w), 1488 (w), 1472 (w), 1456 (m), 1447 (m), 1436 (m), 1418 (w), 1404 (w), 1386 (vw), 1373 (vw), 1326 (m), 1245 (m), 1186 (vw), 1130

(w), 1106 (vw), 1020 (m), 917 (w), 847 (vs), 834 (vs), 752 (s), 684 (s), 668 (s), 641 (m), 628 (m), 571 (w), 559 (w), 518 (w), 502 (w), 489 (w), 473 (w), 457 (m), 435 (w), 419 (m) cm^{-1} ; elemental analysis calcd (%) for C₄₉H₇₇Cl₄O₃Si₃Y₃: C 48.76, H 6.43; found C 48.90, H 7.22.

(C₅Me₄SiMe₃)₃Y₃(μ -Br)₃(μ_3 -Br)(μ_3 -CH₂)(THF)₃ (4^{*}-Y^{Br}):

Following route A described above, 1^*-Y^{Br} (0.100 mg, 111 μmol) yielded 4^*-Y^{Br} as colorless crystals (56.9 mg, 41.1 μmol , 74 %). ^1H NMR (400 MHz, $[\text{D}_8]\text{THF}$, 26 $^\circ\text{C}$): δ 3.62 (m, 12H, THF), 2.14 (s, 18H, Cp- CH_3 -2,5), 2.10 (s, 18H, Cp- CH_3 -3,4), 1.78 (m, 12H, THF), 0.25 (s, 27H, Si-Me), -0.42 (q, $^3J(\text{YH}) = 4.4$ Hz, 2H, Y- CH_2) ppm. ^{13}C NMR (101 MHz, $[\text{D}_8]\text{THF}$, 26 $^\circ\text{C}$): δ 128.3 (2,5-C₅Me₄SiMe₃), 124.5 (3,4-C₅Me₄SiMe₃), 115.1 (1-C₅Me₄SiMe₃), 67.6 (THF), 25.4 (THF), 15.7 (Cp- CH_3), 13.7 (Cp- CH_3), 2.9 (Si-Me) ppm; ^{13}C resonances for the CH_2 group could not be detected. ^{89}Y NMR (from ^1H - ^{89}Y HSQC, 25 MHz, $[\text{D}_8]\text{THF}$, 26 $^\circ\text{C}$): δ 183 ppm. IR (KBr): $\tilde{\nu} = 2980$ (m), 2949 (m), 2894 (m), 2727 (vw), 1494 (vw), 1454 (w), 1405 (vw), 1384 (vw), 1372 (vw), 1344 (w), 1324 (m), 1243 (m), 1183 (vw), 1130 (vw), 1081 (vw), 1019 (m), 916 (w), 875 (m), 845 (vs), 834 (vs), 754 (s), 729 (m), 694 (w), 684 (w), 640 (w), 628 (m), 573 (vw), 511 (w), 499 (vw), 491 (vw), 476 (w), 466 (w), 451 (m), 422 (m), 410 (w) cm^{-1} ; elemental analysis calcd (%) for C₄₉H₇₇Br₄O₃Si₃Y₃ x OC₄H₈: C 43.70, H 5.88; found C 43.59, H 5.86.

General procedure for the synthesis of Cp^R₃La₃(μ -X)₃(μ_3 -X)(μ_3 -CH₂)(THF)₃ (4^{*}-La^X): (X = Cl, Br, I, Cp^R = C₅Me₅, C₅Me₄SiMe₃)

$[\text{Cp}^{\text{R}}_3\text{La}_3(\text{AlMe}_2)_2(\mu\text{-X})_4]_2$ 2-La^X was suspended in toluene (1 mL) and THF (2 mL) was added. The reaction was shaken several times, filtered and allowed to stand at ambient temperatures for 3-4 days. A color change to yellow-orange occurred, the mixture was concentrated and stored at -40 $^\circ\text{C}$ to yield crystalline material.

(C₅Me₅)₃La₃(μ -Cl)₃(μ_3 -Cl)(μ_3 -CH₂)(THF)₃ (4^{*}-La^{Cl}): Following the procedure described above, $2^*\text{-La}^{\text{Cl}}$ (200 mg, 84.6 μmol) yielded $4^*\text{-La}^{\text{Cl}}$ as light yellow powder (27.8 mg, 23.3 μmol , 55 %). ^1H NMR (400 MHz, $[\text{D}_8]\text{THF}$, 26 $^\circ\text{C}$): δ 3.65 (m, 12H, THF), 2.09 (s, 45H, Cp- CH_3), 1.81 (m, 12H, THF), -0.93 (s 2H, La- CH_2) ppm. ^{13}C NMR (101 MHz, $[\text{D}_8]\text{THF}$, 26 $^\circ\text{C}$): δ 117.2 (C₅Me₅), 67.3 (THF), 25.3 (THF), 10.8 (Cp- CH_3) ppm; ^{13}C resonances for the CH_2 group could not be detected. IR (KBr): $\tilde{\nu} = 2981$ (s), 2890 (vs), 2803 (m), 2729 (vw), 1488 (w), 1437 (m), 1420 (w), 1376 (w), 1172 (m), 1023 (s), 992 (s), 920 (w), 870 (m), 840 (w), 717 (vs), 671 (s), 595 (m), 565 (s), 544 (s), 462 (vw), 451 (vw), 434 (vw), 419 (vw), 405 (vw) cm^{-1} ; elemental analysis calcd (%) for C₄₃H₇₁Cl₄La₃O₃: C 43.23, H 5.99; found C 43.77, H 6.10. The analytical data were consistent with those previously published.⁴⁰

(C₅Me₅)₃La₃(μ -Br)₃(μ_3 -Br)(μ_3 -CH₂)(THF)₃ (4^{*}-La^{Br}): Following the procedure described above, $2^*\text{-La}^{\text{Br}}$ (200 mg,

73.6 μmol) yielded $4^*\text{-La}^{\text{Br}}$ as light yellow powder (36.4 mg, 26.5 μmol , 72 %). ^1H NMR (400 MHz, $[\text{D}_8]\text{THF}$, 26 $^\circ\text{C}$): δ 3.66 (m, 12H, THF), 2.10 (s, 45H, Cp- CH_3), 1.81 (m, 12H, THF), -0.93 (s, 2H, La- CH_2) ppm. ^{13}C NMR (101 MHz, $[\text{D}_8]\text{THF}$, 26 $^\circ\text{C}$): δ 120.8 (C_5Me_5), 67.3 (THF), 25.2 (THF), 12.0 (Cp- CH_3) ppm; ^{13}C resonances for the CH_2 group could not be detected. IR (KBr): $\tilde{\nu}$ = 2961 (s), 2891 (vs), 2856 (vs), 2752 (w), 2723 (w), 1558 (w), 1532 (vw), 1506 (w), 1495 (w), 1488 (w), 1471 (w), 1456 (m), 1447 (m), 1436 (m), 1375 (w), 1344 (vw), 1247 (vw), 1185 (vw), 1061 (vw), 1021 (vs), 916 (w), 875 (s), 729 (vw), 694 (w), 667 (w), 633 (w), 623 (w), 590 (w), 550 (vw), 517 (vw), 501 (vw), 457 (w), 423 (w), 418 (m), 405 (s) cm^{-1} ; elemental analysis calcd (%) for $\text{C}_{43}\text{H}_{71}\text{Br}_4\text{La}_3\text{O}_3$: C 37.63, H 5.21; found C 37.70, H 5.68.

$(\text{C}_5\text{Me}_5)_3\text{La}_3(\mu\text{-I})_3(\mu_3\text{-I})(\mu_3\text{-CH}_2)(\text{THF})_3$ (4^*-La^{I}): Following the procedure described above, 2^*-La^{I} (200 mg, 64.6 μmol) yielded 4^*-La^{I} as light yellow powder (39.7 mg, 25.5 μmol , 79 %). ^1H NMR (400 MHz, $[\text{D}_8]\text{THF}$, 26 $^\circ\text{C}$): δ 3.62 (m, 12H, THF), 2.14 (s, 45H, Cp- CH_3), 1.77 (m, 12H, THF), -0.97 (s, 2H, La- CH_2) ppm. ^{13}C NMR (101 MHz, $[\text{D}_8]\text{THF}$, 26 $^\circ\text{C}$): δ 123.2 (C_5Me_5), 67.3 (THF), 25.2 (THF), 13.2 (Cp- CH_3) ppm; ^{13}C resonances for the CH_2 group could not be detected. IR (KBr): $\tilde{\nu}$ = 2975 (m), 2934 (m), 2890 (s), 1487 (w), 1455 (m), 1432 (w), 1377 (vw), 1367 (vw), 1343 (vw), 1294 (vw), 1243 (w), 1176 (w), 1062 (vw), 1035 (s), 1012 (vs), 949 (w), 920 (m), 912 (m), 854 (vs), 839 (s), 834 (s), 665 (w) cm^{-1} ; elemental analysis calcd (%) for $\text{C}_{43}\text{H}_{71}\text{I}_4\text{La}_3\text{O}_3$: C 33.10, H 4.59; found C 33.69, H 4.75.

$(\text{C}_5\text{Me}_4\text{SiMe}_3)_3\text{La}_3(\mu\text{-Cl})_3(\mu_3\text{-Cl})(\mu_3\text{-CH}_2)(\text{THF})_3$ ($4^*\text{-La}^{\text{Cl}}$): Following the procedure described above, $2^*\text{-La}^{\text{Cl}}$ (200 mg, 73.7 μmol) yielded $4^*\text{-La}^{\text{Cl}}$ as light yellow powder (40.0 mg, 29.2 μmol , 79 %). ^1H NMR (400 MHz, $[\text{D}_8]\text{THF}$, 26 $^\circ\text{C}$): δ 3.62 (m, 12H, THF), 2.19 (s, 18H, Cp- CH_3 -2,5), 2.14 (s, 18H, Cp- CH_3 -3,4), 1.77 (m, 12H, THF), 0.25 (s, 27H, Si-Me), -0.96 (s, 2H, La- CH_2) ppm. ^{13}C NMR (101 MHz, $[\text{D}_8]\text{THF}$, 26 $^\circ\text{C}$): δ 129.5 (2,5- $\text{C}_5\text{Me}_4\text{SiMe}_3$), 126.0 (3,4- $\text{C}_5\text{Me}_4\text{SiMe}_3$), 117.2 (1- $\text{C}_5\text{Me}_4\text{SiMe}_3$), 67.4 (THF), 25.3 (THF), 14.5 (Cp- CH_3 -2,5), 12.5 (Cp- CH_3 -3,4), 2.7 (Si-Me) ppm; ^{13}C resonances for the CH_2 group could not be detected. IR (KBr): $\tilde{\nu}$ = 2969 (m), 2949 (m), 2889 (m), 2858 (m), 2757 (vw), 1558 (w), 1539 (vw), 1520 (w), 1506 (vw), 1489 (w), 1472 (w), 1456 (m), 1447 (w), 1435 (w), 1418 (w), 1404 (w), 1385 (vw), 1373 (vw), 1326 (m), 1243 (m), 1128 (vw), 1025 (m), 916 (w), 871 (m), 835 (vs), 754 (m), 730 (w), 685 (m), 668 (w), 629 (w), 417 (s), 403 (m) cm^{-1} ; elemental analysis calcd (%) for $\text{C}_{49}\text{H}_{89}\text{Cl}_4\text{La}_3\text{O}_3\text{Si}_3$ x $\text{C}_4\text{H}_8\text{O}$: C 44.63, H 6.73; found C 44.66, H 6.76.

$(\text{C}_5\text{Me}_4\text{SiMe}_3)_3\text{La}_3(\mu\text{-Br})_3(\mu_3\text{-Br})(\mu_3\text{-CH}_2)(\text{THF})_3$ ($4^*\text{-La}^{\text{Br}}$): Following the procedure described above, $2^*\text{-La}^{\text{Br}}$ (200 mg, 65.2 μmol) yielded $4^*\text{-La}^{\text{Br}}$ as light yellow powder (40.0 mg, 25.9 μmol , 79 %). ^1H NMR (400 MHz, $[\text{D}_8]\text{THF}$, 26 $^\circ\text{C}$): δ 3.61 (m, 12H, THF), 2.22 (s, 18H, Cp- CH_3 -2,5), 2.18 (s, 18H, Cp- CH_3 -3,4), 1.77 (m, 12H, THF), 0.26 (s, 27H, Si-Me), -0.97 (s, 2H, La- CH_2) ppm. ^{13}C NMR (101 MHz, $[\text{D}_8]\text{THF}$, 26 $^\circ\text{C}$): δ 130.1 (2,5- $\text{C}_5\text{Me}_4\text{SiMe}_3$), 126.6 (3,4- $\text{C}_5\text{Me}_4\text{SiMe}_3$), 118.0 (1- $\text{C}_5\text{Me}_4\text{SiMe}_3$), 67.3 (THF), 25.2 (THF), 15.0 (Cp- CH_3 -2,5),

13.1 (Cp- CH_3 -3,4), 2.8 (Si-Me) ppm; ^{13}C resonances for the CH_2 group could not be detected. IR (KBr): $\tilde{\nu}$ = 2976 (w), 2971 (w), 2951 (w), 2890 (w), 2860 (w), 1456 (w), 1447 (w), 1436 (w), 1343 (vw), 1326 (w), 1242 (m), 1021 (m), 914 (vw), 870 (m), 848 (vs), 835 (vs), 754 (m), 684 (w), 668 (vw), 638 (vw), 628 (w), 442 (vw), 420 (w), 408 (w), 403 (w) cm^{-1} ; elemental analysis calcd (%) for $\text{C}_{49}\text{H}_{89}\text{Br}_4\text{La}_3\text{O}_3\text{Si}_3$: C 38.05, H 5.80; found C 38.09, H 5.72.

$(\text{C}_5\text{Me}_4\text{SiMe}_3)_3\text{La}_3(\mu\text{-I})_3(\mu_3\text{-I})(\mu_3\text{-CH}_2)(\text{THF})_3$ (4^*-La^{I}): Following the procedure described above, 2^*-La^{I} (200 mg, 56.7 μmol) yield 4^*-La^{I} as light yellow powder (47.9 mg, 27.7 μmol , 85 %). ^1H NMR (400 MHz, $[\text{D}_8]\text{THF}$, 26 $^\circ\text{C}$): δ 3.62 (m, 12H, THF), 2.19 (s, 18H, Cp- CH_3 -2,5), 2.19 (s, 18H, Cp- CH_3 -3,4), 1.77 (m, 12H, THF), 0.36 (s, 27H, Si-Me), -0.96 (s, 2H, La- CH_2) ppm. ^{13}C NMR (101 MHz, $[\text{D}_8]\text{THF}$, 26 $^\circ\text{C}$): δ 131.3 (2,5- $\text{C}_5\text{Me}_4\text{SiMe}_3$), 128.7 (3,4- $\text{C}_5\text{Me}_4\text{SiMe}_3$), 120.7 (1- $\text{C}_5\text{Me}_4\text{SiMe}_3$), 67.3 (THF), 25.2 (THF), 15.3 (Cp- CH_3 -2,5), 13.8 (Cp- CH_3 -3,4), 3.3 (Si-Me) ppm; ^{13}C resonances for the CH_2 group could not be detected. IR (KBr): $\tilde{\nu}$ = 2973 (w), 2950 (w), 2893 (w), 1481 (vw), 1471 (w), 1454 (vw), 1447 (w), 1405 (vw), 1386 (vw), 1375 (vw), 1324 (w), 1246 (m), 1124 (vw), 1013 (w), 948 (vw), 914 (vw), 847 (vs), 837 (vs), 754 (w), 686 (w), 636 (vw), 627 (w), 422 (w) cm^{-1} ; elemental analysis calcd (%) for $\text{C}_{49}\text{H}_{89}\text{I}_4\text{La}_3\text{O}_3\text{Si}_3$: C 33.92, H 5.17; found C 34.20, H 5.67.

$[(\text{C}_5\text{Me}_5)\text{Y}(\text{OCH}_2\text{tBu})(\mu\text{-OCH}_2\text{tBu})_2]$ (5^*-Y): Following route **B** described for 4-Y , HOCH_2tBu (36.6 mg, 41.5 μmol) and $[(\text{C}_5\text{Me}_5)_3\text{Y}_3(\mu\text{-Me})_3(\mu_3\text{-Me})(\mu_3\text{-CH}_2)(\text{THF})_2]$ (100 mg, 112 μmol) yielded 5^*-Y as white powder (49.0 mg, 61.5 μmol , 30 %). The yield is determined in relation to HOCH_2tBu . ^1H NMR (400 MHz, $[\text{D}_8]\text{THF}$, 26 $^\circ\text{C}$): δ 3.69 (s, 4H, CH_2), 3.49 (s, 4H, CH_2), 2.15 (s, 30H, Cp- CH_3), 0.99 (s, 18H, CH_3), 0.91 (s, 18H, CH_3) ppm. ^{13}C NMR (101 MHz, $[\text{D}_8]\text{THF}$, 26 $^\circ\text{C}$): δ 117.7 (C_5Me_5), 78.6 (CH_2), 76.6 (CH_2), 33.7 ($\text{C}(\text{CH}_3)_3$), 33.1 ($\text{C}(\text{CH}_3)_3$), 27.1 ($\text{C}(\text{CH}_3)_3$), 26.6 ($\text{C}(\text{CH}_3)_3$), 11.4 (Cp- CH_3) ppm. ^{89}Y NMR (from ^1H - ^{89}Y HSQC, 25 MHz, $[\text{D}_8]\text{THF}$, 26 $^\circ\text{C}$): δ 1021 ppm. IR (KBr): $\tilde{\nu}$ = 2948 (vs), 2906 (s), 2862 (s), 2812 (m), 2726 (vw), 2695 (w), 1506 (vw), 1478 (m), 1457 (m), 1437 (w), 1418 (vw), 1392 (w), 1361 (w), 1256 (vw), 1132 (vs), 1047 (s), 1017 (s), 933 (w), 898 (w), 752 (vw), 615 (s), 559 (m), 440 (m), 420 (s), 411 (m) cm^{-1} ; elemental analysis calcd (%) for $\text{C}_{40}\text{H}_{74}\text{O}_4\text{Y}_2$: C 60.29, H 9.36; found C 59.63, H 8.63.

$\text{Cp}_2\text{Ti}(\mu\text{-Cl})(\mu\text{-CH}_2)\text{AlMe}_2$: Cp_2TiCl_2 (500 mg, 2.01 mmol), was dissolved in toluene (15 mL) and a solution of AlMe_3 (290 mg, 4.02 mmol) in *n*-hexane (5 mL) was added. The solution turned dark red within 5 min. The solution was allowed to rest at ambient temperatures for 48 h. The solvent was removed *in vacuo*. The remaining oily solid was extracted with *n*-pentane (3 x 5 mL). The solution was concentrated and toluene (1 mL) was added for better crystallization. Red crystals grew from a saturated solution at -40 $^\circ\text{C}$ within one day. ^1H NMR (400 MHz, $[\text{D}_6]$ benzene, 26 $^\circ\text{C}$): δ 8.28 (s, 2H, CH_2), 5.60 (s, 10H, Cp- H), -0.26 (s, 6H, AlCH_3) ppm.

X-ray Crystallography and Crystal Structure Determinations

Single crystals of $1^*-\text{Ln}^{\text{Br}}$, 1^*-Y^{I} , 2^*-La^{I} , $2'-\text{La}^{\text{Cl}}$, $3^*-\text{La}^{\text{OTf}}$, $4^*-\text{Ln}^{\text{Br}}$, 5^*-Y , $(\text{C}_5\text{Me}_5)\text{LaI}_2(\text{THF})_3$, and $\text{Cp}_2\text{Ti}(\mu\text{-CH}_2)(\mu\text{-Cl})\text{AlMe}_2$ were grown by standard techniques from saturated solutions in *n*-hexane, toluene or THF at -35°C as stated in the experimental section. Suitable crystals were collected in a glovebox and coated with Parabar 10312 (previously known as Paratone N, Hampton Research) and fixed on a nylon loop/glass fiber.

X-ray data for compounds of $1^*-\text{Ln}^{\text{Br}}$, 1^*-Y^{I} , 2^*-La^{I} , $2'-\text{La}^{\text{Cl}}$, $3^*-\text{La}^{\text{OTf}}$, $4^*-\text{Ln}^{\text{Br}}$, 5^*-Y , $(\text{C}_5\text{Me}_5)\text{LaI}_2(\text{THF})_3$, and $\text{Cp}_2\text{Ti}(\mu\text{-CH}_2)(\mu\text{-Cl})\text{AlMe}_2$ were collected on a Bruker APEX II DUO instrument equipped with an $\text{I}\mu\text{S}$ microfocus sealed tube and QUAZAR optics for $\text{MoK}\alpha$ ($\lambda = 0.71073 \text{ \AA}$) and $\text{CuK}\alpha$ ($\lambda = 1.54184 \text{ \AA}$) radiation. The data collection strategy was determined using COSMO⁵⁰ employing ω -scans. Raw data were processed using APEX,⁵¹ and SAINT,⁵² corrections for absorption effects were applied using SADABS.⁵³ The structures were solved by direct methods and refined against all data by full-matrix least-squares methods on F₂ using SHELXTL⁵⁴ and ShelXle.⁵⁵ Disorder models are calculated using DSR, a program for refining structures in ShelXl.⁵⁶ All graphics were produced employing ORTEP-3⁵⁷ and POV-Ray.⁵⁸ Further details of the refinement and crystallographic data are listed in Table S1 (ESI) and in the CIF files. CCDC depositions xxx contain all the supplementary crystallographic data for this paper. These data can be obtained free of charge from The Cambridge Crystallographic Data Centre via www.ccdc.cam.ac.uk/structures/.

ASSOCIATED CONTENT

Supporting Information

The Supporting Information is available free of charge on the ACS Publications website.

AUTHOR INFORMATION

Corresponding Author

to whom correspondence should be addressed: E-mail: reiner.anwander@uni-tuebingen.de

ACKNOWLEDGMENT

We are grateful to the German Science Foundation for support (grant: AN 238/15-2).

REFERENCES

- Guggenberger, L. J.; Schrock, R. R., Structure of bis(cyclopentadienyl)methylmethylene tantalum and the estimated barrier to rotation about the tantalum-methylene bond. *J. Am. Chem. Soc.* **1975**, *97*, 6578-6579.
- Schrock, R. R., Alkylidene complexes of niobium and tantalum. *Acc. Chem. Res.* **2002**, *12*, 98-104.
- Tebbe, F. N.; Parshall, G. W.; Reddy, G. S., Olefin homologation with titanium methylene compounds. *J. Am. Chem. Soc.* **1978**, *100*, 3611-3613.
- Meinhart, J. D.; Anslyn, E. V.; Grubbs, R. H., Synthesis, reactivity and kinetic studies of bis(η^5 -cyclopentadienyl)titanium methylenephosphine complexes. *Organometallics* **1989**, *8*, 583-589.
- Grubbs, R. H., Olefin metathesis. *Tetrahedron* **2004**, *60*, 7117-7140.
- Astruc, D., The metathesis reactions: from a historical perspective to recent developments. *New. J. Chem.* **2005**, *29*, 42.
- Petasis, N. A.; Bzowej, E. I., Titanium-mediated carbonyl olefinations. 1. Methylenations of carbonyl compounds with dimethyltitanocene. *J. Am. Chem. Soc.* **1990**, *112*, 6392-6394.
- Holton, J.; Lappert, M. F.; Pearce, R.; Yarrow, P. I. W., Bridged hydrocarbyl or hydrocarbon binuclear transition metal complexes: classification, structures, and chemistry. *Chem. Rev.* **1983**, *83*, 135-201.
- Schrock, R. R.; Hoveyda, A. H., Molybdenum and tungsten imido alkylidene complexes as efficient olefin-metathesis catalysts. *Angew. Chem. Int. Ed.* **2003**, *42*, 4592-633. *Angew. Chem.* **2003**, *115*, 38, 4740-4782.
- Kickham, J. E.; Guérin, F.; Stephan, D. W., Divergent Pathways of C-H Bond Activation: Reactions of (*t*-Bu₃PN)₂TiMe₂ with Trimethylaluminum. *J. Am. Chem. Soc.* **2002**, *124*, 11486-11494.
- Howard, T. R.; Lee, J. B.; Grubbs, R. H., Titanium metallacarbene-metallacyclobutane reactions: stepwise metathesis. *J. Am. Chem. Soc.* **1980**, *102*, 6876-6878.
- Cannizzo, L. F.; Grubbs, R. H., Reactions of "Cp₂Ti=CH₂" sources with acid anhydrides and imides. *J. Org. Chem.* **1985**, *50*, 2316-2323.
- Pine, S. H.; Shen, G. S.; Hoang, H., Ketone Methylenation Using the Tebbe and Wittig Reagents - A Comparison. *Synthesis* **1991**, *1991*, 165-167.
- Hartley, R. C.; McKiernan, G. J., Titanium reagents for the alkylidenation of carboxylic acid and carbonic acid derivatives. *J. Chem. Soc., Perkin Trans. 1* **2002**, 2763-2793.
- Crowther, D. J.; Baenziger, N. C.; Jordan, R. F., Group 4 metal dicarbollide chemistry. Synthesis, structures, and reactivity of electrophilic alkyl complexes (Cp*)(C₂B₉H₁₁)M(R), M = Hf, Zr. *J. Am. Chem. Soc.* **1991**, *113*, 1455-1457.
- Petasis, N. A.; Lu, S. P.; Bzowej, E. I.; Fu, D. K.; Staszewski, J. P.; Akritopoulou-Zanze, I.; Patane, M. A.; Hu, Y. H., Organotitanium compounds in organic synthesis. *Pure Appl. Chem.* **1996**, *68*, 667-670.
- Scoles, L.; Minhas, R.; Duchateau, R.; Jubb, J.; Gambarotta, S., Synthesis and Characterization of Novel Titanium(III) and -(IV) Alkyls and Carbenes Supported by Amide Ligands. Crystal Structure of [(Cy₂N)₂Ti(μ -CH₂)₂]. *Organometallics* **1994**, *13*, 4978-4983.
- Scholl, M.; Ding, S.; Lee, C. W.; Grubbs, R. H., Synthesis and Activity of a New Generation of Ruthenium-Based Olefin Metathesis Catalysts Coordinated with 1,3-Dimesityl-4,5-dihydroimidazol-2-ylidene Ligands. *Org. Lett.* **1999**, *1*, 953-956.
- Hogenbirk, M.; Schat, G.; Akkerman, Otto S.; Bickelhaupt, F.; Schottek, J.; Albrecht, M.; Fröhlich, R.; Kehr,

- G.; Erker, G.; Kooijman, H.; Spek, Anthony L., (μ -Methylene)bis(methylzirconocene): Preparation, Molecular Structure, and Thermal Disproportionation. *Eur. J. Inorg. Chem.* **2004**, *2004*, 1175-1182.
20. Grant, L. N.; Ahn, S.; Manor, B. C.; Baik, M. H.; Mendiola, D. J., Structural elucidation of a mononuclear titanium methylidene. *Chem. Commun.* **2017**, *53*, 3415-3417.
21. Thompson, R.; Nakamaru-Ogiso, E.; Chen, C.-H.; Pink, M.; Mendiola, D. J., Structural Elucidation of the Illustrious Tebbe Reagent. *Organometallics* **2013**, *33*, 429-432.
22. Ott, K. C.; De Boer, E. J. M.; Grubbs, R. H., An investigation of the reaction of bis(cyclopentadienyl)titanium dichlorides with trimethylaluminum. Mechanism of an α -hydrogen abstraction reaction. *Organometallics* **1984**, *3*, 223-230.
23. Takai, K.; Hotta, Y.; Oshima, K.; Nozaki, H., Effective methods of carbonyl methylenation using CH_2I_2 -Zn-Me₃Al and CH_2Br_2 -Zn-TiCl₄ system. *Tetrahedron Letters* **1978**, *19*, 2417-2420.
24. Lombardo, L., Methylenation of carbonyl compounds with $\text{Zn}(\text{CH}_2\text{Br})_2/\text{TiCl}_4$. Application to gibberellins. *Tetrahedron Letters* **1982**, *23*, 4293-4296.
25. Horikawa, Y.; Watanabe, M.; Fujiwara, T.; Takeda, T., New Carbonyl Olefination Using Thioacetals. *J. Am. Chem. Soc.* **1997**, *119*, 1127-1128.
26. Takai, K.; Nitta, K.; Utimoto, K., Simple and selective method for aldehydes (RCHO) to (E)-haloalkenes (RCH=CHX) conversion by means of a haloform-chromous chloride system. *J. Am. Chem. Soc.* **1986**, *108*, 7408-7410.
27. Okazoe, T.; Takai, K.; Utimoto, K., (E)-Selective olefination of aldehydes by means of gem-dichromium reagents derived by reduction of gem-diiodoalkanes with chromium(II)chloride. *J. Am. Chem. Soc.* **1987**, *109*, 951-953.
28. Murai, M.; Taniguchi, R.; Hosokawa, N.; Nishida, Y.; Mimachi, H.; Oshiki, T.; Takai, K., Structural Characterization and Unique Catalytic Performance of Silyl-Group-Substituted Geminal Dichromiummethane Complexes Stabilized with a Diamine Ligand. *J. Am. Chem. Soc.* **2017**, *139*, 13184-13192.
29. Werner, D.; Anwender, R., Unveiling the Takai Olefination Reagent via Tris(tert-butoxy)siloxy Variants. *J. Am. Chem. Soc.* **2018**, *140*, 14334-14341.
30. Litlabø, R.; Zimmermann, M.; Saliu, K.; Takats, J.; Törnroos, K. W.; Anwender, R., A rare-earth metal variant of the Tebbe reagent. *Angew. Chem. Int. Ed.* **2008**, *47*, 9560-9564. *Angew. Chem.* **2008**, *120*, 9702-9706.
31. Scott, J.; Fan, H.; Wicker, B. F.; Fout, A. R.; Baik, M. H.; Mendiola, D. J., Lewis acid stabilized methylidene and oxoscandium complexes. *J. Am. Chem. Soc.* **2008**, *130*, 14438-9.
32. Bojer, D.; Neumann, B.; Stammler, H. G.; Mitzel, N. W., Subtle Size Effects in C-H Activation Reactions of Lanthanum and Praseodymium Tetramethylaluminates by Neutral Trinitrogen Bases. *Eur. J. Inorg. Chem.* **2011**, 3791-3796.
33. Zimmermann, M.; Rauschmaier, D.; Eichele, K.; Törnroos, K. W.; Anwender, R., Amido-stabilized rare-earth metal mixed methyl methylidene complexes. *Chem. Commun.* **2010**, 46, 5346-8.
34. Zhang, W. X.; Wang, Z.; Nishiura, M.; Xi, Z.; Hou, Z., $\text{Ln}_4(\text{CH}_2)_4$ cubane-type rare-earth methylidene complexes consisting of " $(\text{C}_5\text{Me}_4\text{SiMe}_3)\text{LnCH}_2$ " units (Ln = Tm, Lu). *J. Am. Chem. Soc.* **2011**, *133*, 5712-5715.
35. Hong, J.; Zhang, L.; Yu, X.; Li, M.; Zhang, Z.; Zheng, P.; Nishiura, M.; Hou, Z.; Zhou, X., Syntheses, structures, and reactivities of homometallic rare-earth-metal multimethyl methylidene and oxo complexes. *Chem. Eur. J.* **2011**, *17*, 2130-7.
36. Hong, J.; Zhang, L.; Wang, K.; Zhang, Y.; Weng, L.; Zhou, X., Methylidene rare-earth-metal complex mediated transformations of C=N, N=N and N-H bonds: new routes to imido rare-earth-metal clusters. *Chem. Eur. J.* **2013**, *19*, 7865-73.
37. Hong, J.; Li, Z.; Chen, Z.; Weng, L.; Zhou, X.; Zhang, L., Small molecule activation by mixed methyl/methylidene rare earth metal complexes. *Dalton Trans.* **2016**, *45*, 6641-9.
38. Schädle, D.; Meermann-Zimmermann, M.; Maichle-Mössmer, C.; Schädle, C.; Törnroos, K. W.; Anwender, R., Rare-earth metal methylidene complexes with $\text{Ln}_3(\mu^3\text{-CH}_2)(\mu^3\text{-Me})(\mu^2\text{-Me})_3$ core structure. *Dalton Trans.* **2015**, *44*, 18101-18110.
39. Hollfelder, C. O.; Jende, L. N.; Dietrich, H. M.; Eichele, K.; Maichle-Mössmer, C.; Anwender, R., 1,3-Diene Polymerization Promoted by Half-Sandwich Rare-Earth-Metal Dimethyl Complexes: Active Species Clustering and Cationization/Deactivation Processes. *Chem. Eur. J.* **2019**, *25*, 7298-7302.
40. Dietrich, H. M.; Törnroos, K. W.; Anwender, R., "Ionic carbenes": synthesis, structural characterization, and reactivity of rare-earth metal methylidene complexes. *J. Am. Chem. Soc.* **2006**, *128*, 9298-9.
41. Scott, J.; Mendiola, D. J., A tribute to Frederick Nye Tebbe. Lewis acid stabilized alkylidyne, alkylidene, and imides of 3d early transition metals. *Dalton Trans.* **2009**, 8463-8472.
42. Dietrich, H. M.; Schuster, O.; Törnroos, K. W.; Anwender, R., Heterobimetallic half-lanthanidocene clusters: novel mixed tetramethylaluminato/chloro coordination. *Angew. Chem. Int. Ed.* **2006**, *45*, 4858-63. *Angew. Chem.* **2006**, *118*, 4977.
43. Van der Heijden, H.; Schaverien, C. J.; Orpen, A. G., The first salt- and solvent-free monocyclopentadienyl lanthanide dialkyl complex. X-ray structure determinations of $\text{La}(\eta^5\text{-C}_5\text{Me}_5)[\text{CH}(\text{SiMe}_3)_2]_2$ and of its tetrahydrofuran adduct: compounds containing agostic silicon-carbon bonds. *Organometallics* **1989**, *8*, 255-258.
44. Zimmermann, M.; Törnroos, K. W.; Sitzmann, H.; Anwender, R., Half-sandwich bis(tetramethylaluminato) complexes of the rare-earth metals: synthesis, structural chemistry, and performance in isoprene polymerization. *Chem. Eur. J.* **2008**, *14*, 7266-77.
45. Dietrich, H. M.; Törnroos, K. W.; Herdtweck, E.; Anwender, R., Tetramethylaluminato and Tetramethylgallate Coordination in Rare-Earth Metal Half-Sandwich and Metallocene Complexes. *Organometallics* **2009**, *28*, 6739-6749.
46. Downing, S. P.; Guadaño, S. C.; Pugh, D.; Danopoulos, A. A.; Bellabarba, R. M.; Hanton, M.; Smith, D.; Tooze, R. P., Indenyl- and Fluorenyl-Functionalized N-Heterocyclic Carbene Complexes of Titanium, Zirconium, Vanadium, Chromium, and Yttrium. *Organometallics* **2007**, *26*, 3762-3770.

47. Kunze, M. R.; Steinborn, D.; Merzweiler, K.; Wagner, C.; Sieler, J.; Taube, R., Synthese, Struktur und Reaktivität von Tris-, Bis- und Mono(2,4-dimethylpentadienyl)-Komplexen des Neodyms, Lanthans und des Yttriums. *Z. Anorg. Allg. Chem.* **2007**, *633*, 1451-1463.
48. Kirillov, E.; Lehmann, C. W.; Razavi, A.; Carpentier, J.-F., Synthesis, Structure, and Polymerization Activity of Neutral Halide, Alkyl, and Hydrido Yttrium Complexes of Isopropylidene-Bridged Cyclopentadienyl-Fluorenyl Ligands. *Organometallics* **2004**, *23*, 2768-2777.
49. Dietrich, H. M.; Zapilko, C.; Herdtweck, E.; Anwender, R., Ln(AlMe₄)₃ as New Synthetic Precursors in Organolanthanide Chemistry: Efficient Access to Half-Sandwich Hydrocarbyl Complexes. *Organometallics* **2005**, *24*, 5767-5771.
50. COSMO v. 1.61; Bruker AXS Inc.: Madison, WI, **2012**.
51. APEX 3 v. 2017.3-0; Bruker AXS Inc.: Madison, WI, **2017**.
52. SAINT v. 8.38A; Bruker AXS Inc.: Madison, WI, **2017**.
53. Krause, L.; Herbst-Irmer, R.; Sheldrick, G. M.; Stalke, D., *J. Appl. Cryst.* **2015**, *48*, 3-10.
54. Sheldrick, G., Crystal structure refinement with SHELXL. *Acta Crystallogr. Sect. C: Cryst. Struct. Commun.* **2015**, *71*, 3-8.
55. Hübschle, C. B.; Sheldrick, G. M.; Dittrich, B., ShelXle: a Qt graphical user interface for SHELXL. *J. Appl. Crystallogr.* **2011**, *44*, 1281-1284.
56. Kratzert, D.; Holstein, J. J.; Krossing, I., DSR: enhanced modelling and refinement of disordered structures with SHELXL. *J. Appl. Cryst.* **2015**, *48*, 933-938.
57. Farrugia, L., WinGX and ORTEP for Windows: an update. *J. Appl. Crystallogr.* **2012**, 849-854.
58. POV-Ray v. 3.6; Persistence of Vision Raytracer Pty. Ltd.: Williamstown, Australia, 2004; <http://www.povray.org>.

Supporting Information

Elucidation of Cyclopentadienyl-Supported Rare-Earth-Metal Methylidene Complexes: Scope of Coligands and Tebbe Olefination

Verena M. Birkelbach, H. Martin Dietrich, Christoph Stuhl, Cäcilia Maichle-Mössmer, and Reiner Anwander*

Institut für Anorganische Chemie, Eberhard Karls Universität Tübingen, Auf der Morgenstelle 18, 72076 Tübingen (Germany)

* to whom correspondence should be addressed: E-Mail reiner.anwander@uni-tuebingen.de

Table of contents

NMR spectroscopy

^1H , $^{13}\text{C}\{^1\text{H}\}$, and ^1H - ^{89}Y HSQC NMR spectra of complex 1*-Y^{Cl}	Page S3-S4
^1H , $^{13}\text{C}\{^1\text{H}\}$, and ^1H - ^{89}Y HSQC NMR spectra of complex 1*-Y^{Br}	Page S4-SS5
^1H , and $^{13}\text{C}\{^1\text{H}\}$ NMR spectra of complex 1*-Y^I	Page S6
^1H , and $^{13}\text{C}\{^1\text{H}\}$ NMR spectra of complex 1*-Lu^{Cl}	Page S7
^1H , and $^{13}\text{C}\{^1\text{H}\}$ NMR spectra of complex 1*-Lu^{Br}	Page S8
^1H , and $^{13}\text{C}\{^1\text{H}\}$ NMR spectra of complex 1*-Lu^I	Page S9
^1H , $^{13}\text{C}\{^1\text{H}\}$, and ^1H - ^{89}Y HSQC NMR spectra of complex 1'-Y^{Cl}	Page S10-S11
^1H , $^{13}\text{C}\{^1\text{H}\}$, and ^1H - ^{89}Y HSQC NMR spectra of complex 1'-Y^{Br}	Page S11-S13
^1H , and $^{13}\text{C}\{^1\text{H}\}$ NMR spectra of complex 1'-Y^I	Page S13-S14
^1H , and $^{13}\text{C}\{^1\text{H}\}$ NMR spectra of complex 1'-Lu^{Cl}	Page S14-S15
^1H , and $^{13}\text{C}\{^1\text{H}\}$ NMR spectra of complex 1'-Lu^{Br}	Page S15-S16
^1H , and $^{13}\text{C}\{^1\text{H}\}$ NMR spectra of complex 1'-Lu^I	Page S16-S17
^1H , and $^{13}\text{C}\{^1\text{H}\}$, ^1H - ^{89}Y HSQC NMR spectra of complex 4*-Y^{Cl}	Page S17-S18
^1H , and $^{13}\text{C}\{^1\text{H}\}$, ^1H - ^{89}Y HSQC NMR spectra of complex 4*-Y^{Br}	Page S19-S20
^1H , $^{13}\text{C}\{^1\text{H}\}$, and ^1H - ^{89}Y HSQC NMR spectra of complex 4'-Y^{Cl}	Page S20-S21
^1H , $^{13}\text{C}\{^1\text{H}\}$, and ^1H - ^{89}Y HSQC NMR spectra of complex 4'-Y^{Br}	Page S22-S23
^1H , and $^{13}\text{C}\{^1\text{H}\}$ NMR spectra of complex 4*-La^{Cl}	Page S23-S24
^1H , and $^{13}\text{C}\{^1\text{H}\}$ NMR spectra of complex 4*-La^{Br}	Page S24-S25
^1H , and $^{13}\text{C}\{^1\text{H}\}$ NMR spectra of complex 4*-La^I	Page S25-S26
^1H , and $^{13}\text{C}\{^1\text{H}\}$ NMR spectra of complex 4'-La^{Cl}	Page S26-S27
^1H , and $^{13}\text{C}\{^1\text{H}\}$ NMR spectra of complex 4'-La^{Br}	Page S27-S28
^1H , and $^{13}\text{C}\{^1\text{H}\}$ NMR spectra of complex 4'-La^I	Page S28-S29
^1H , $^{13}\text{C}\{^1\text{H}\}$, and ^1H - ^{89}Y HSQC NMR spectra of complex 5*-Y	Page S29-S30
^1H NMR spectrum of the Tebbe reagent Cp₂Ti(μ-CH₂)(μ-Cl)AlMe₂	Page S31
^1H NMR spectrum of (C₅Me₅)₃Y₃(μ-CH₃)(μ-Cl)₂(μ_3-Cl)(μ_3-CH₂)(thf)₃	Page S31

Reactivity studies and Polymerization

General procedure for methylenide transfer Page S32

General procedure for the polymerization of δ -valerolactone Page S33

X-ray structure analyses

ORTEP representation of the molecular structure for compounds **1^{*}-Y^I**, **1^{*}-Lu^{Br}**, **2^{*}-La^I**, **(C₅Me₅)LaI₂(thf)₃**, and **5^{*}-Y** Page S34-35

Comprehensive crystallographic data for compounds **1^{*}-Y^{Br}**, **1^{*}-Y^I**, **1^{*}-Lu^{Br}**, **2^{*}-La^I**, **2^{*}-La^{Cl}**, **3^{*}-La^{OTf}**, **4^{*}-Y^{Br}**, **4^{*}-La^{Br}**, **4^{*}-La^{Cl}**, **(C₅Me₅)LaI₂(thf)₃**, and **5^{*}-Y** Page S36-S38

NMR spectroscopy

The solvent residual peaks are marked with an asterisk (*)

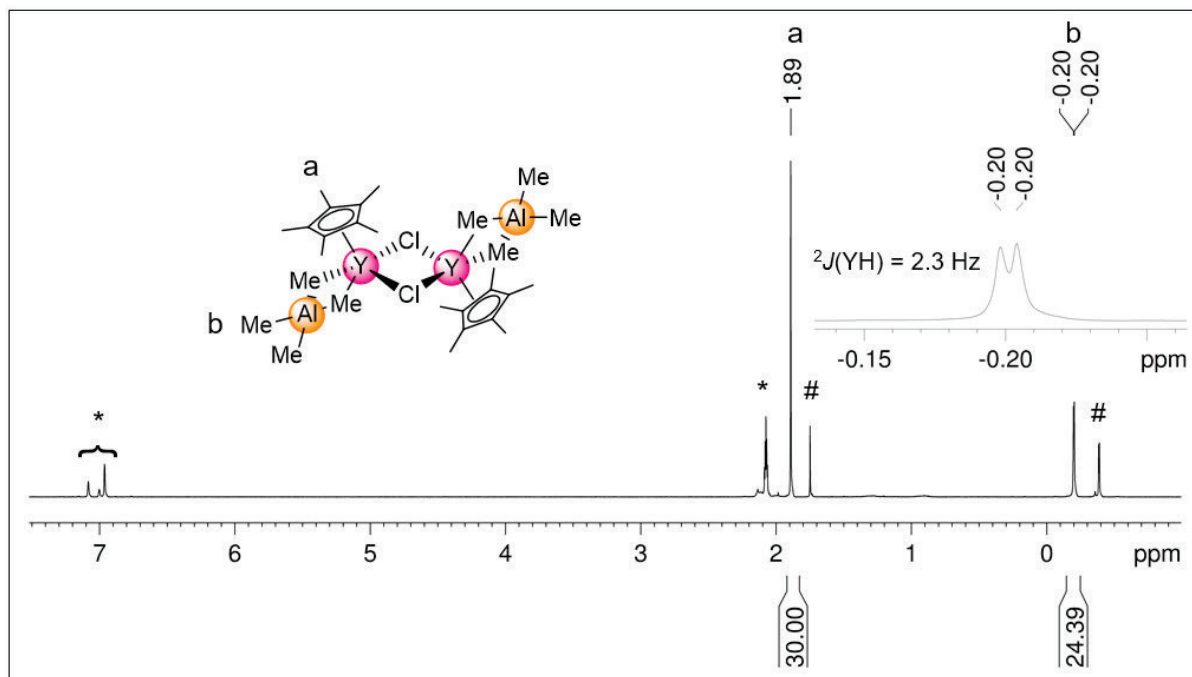


Figure S1. ^1H NMR spectrum (400 MHz, $[\text{D}_8]\text{toluene}$) of complex 1^*-Y^{Cl} at 26 °C and $[(\text{C}_5\text{Me}_5)\text{Y}(\text{AlMe}_4)_2]$ (#), formed upon dissolving *via* ligand redistribution.

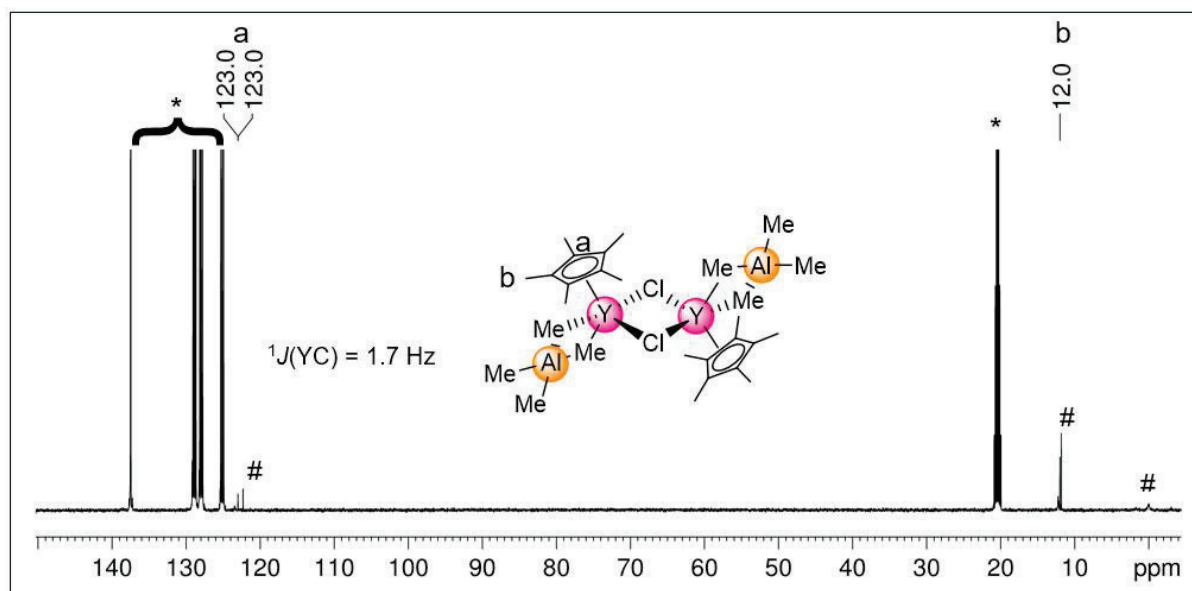


Figure S2. $^{13}\text{C}\{^1\text{H}\}$ NMR spectrum (101 MHz, $[\text{D}_8]\text{toluene}$) of complex 1^*-Y^{Cl} at 26 °C and $[(\text{C}_5\text{Me}_5)\text{Y}(\text{AlMe}_4)_2]$ (#), formed upon dissolving *via* ligand redistribution. The ^{13}C NMR signal for the Al-Me groups could not be detected.

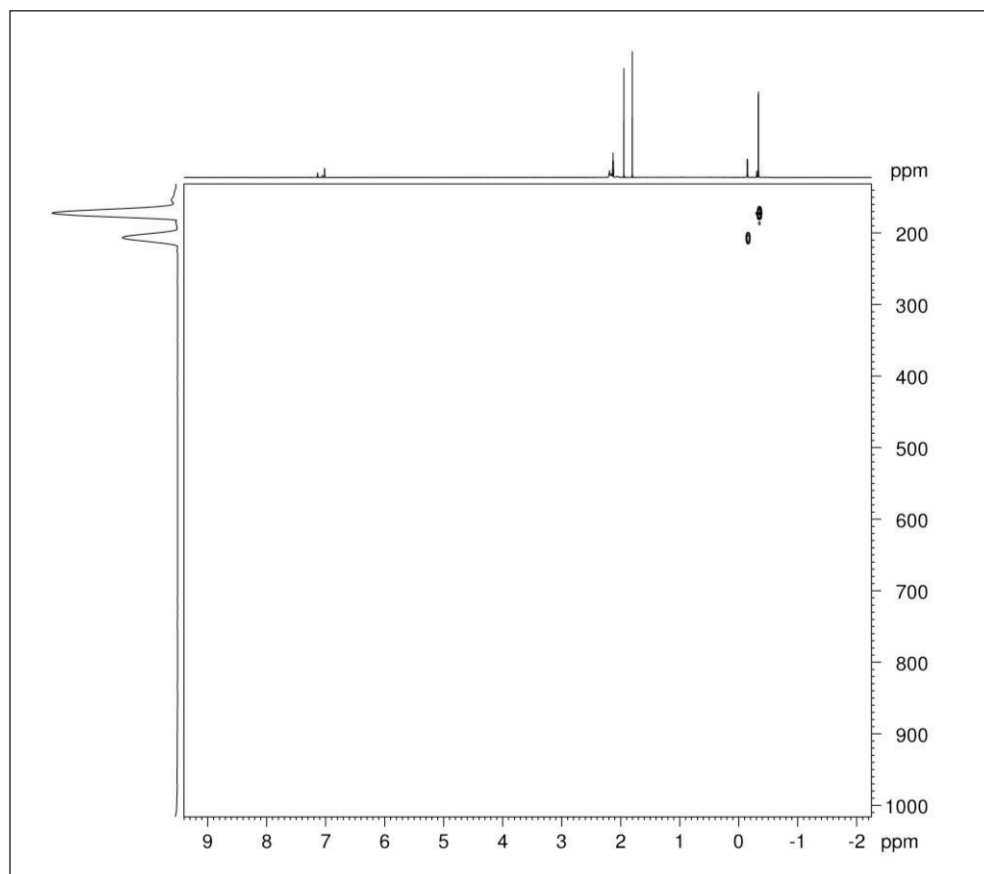


Figure S3. ^1H - ^{89}Y HSQC NMR spectrum (25 MHz, $[\text{D}_8]$ toluene) of complex 1^*-Y^{Cl} at 26 °C and $[(\text{C}_5\text{Me}_5)\text{Y}(\text{AlMe}_4)_2]$ (175 ppm), formed upon dissolving *via* ligand redistribution.

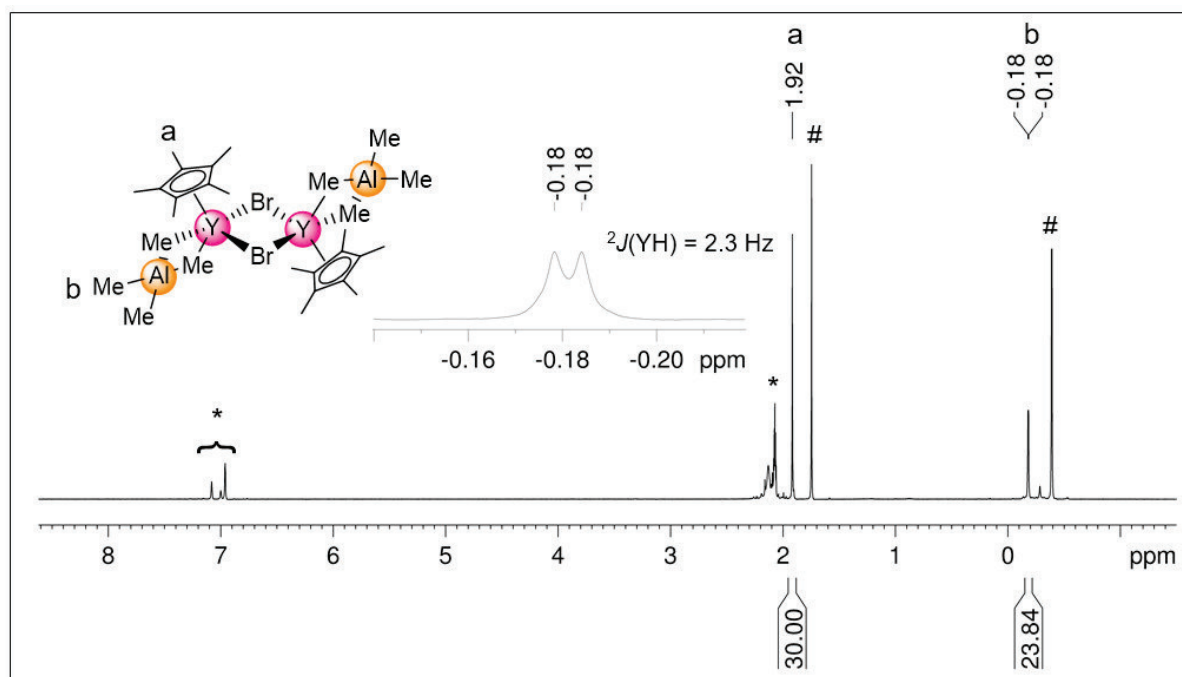


Figure S4. ^1H NMR spectrum (400 MHz, $[\text{D}_8]$ toluene) of complex 1^*-Y^{Br} at 26 °C and $[(\text{C}_5\text{Me}_5)\text{Y}(\text{AlMe}_4)_2]$ (#), formed upon dissolving *via* ligand redistribution.

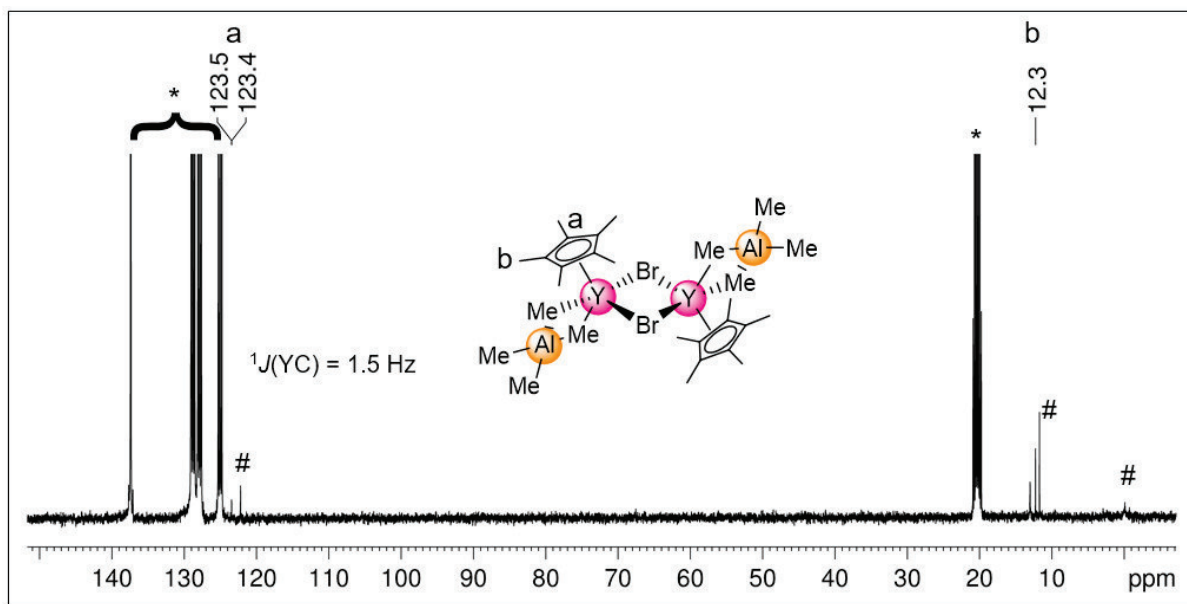


Figure S5. $^{13}\text{C}\{^1\text{H}\}$ NMR spectrum (101 MHz, $[\text{D}_8]\text{toluene}$) of complex 1^*-Y^{Br} at 26 °C and $[(\text{C}_5\text{Me}_5)\text{Y}(\text{AlMe}_4)_2]$ (#), formed upon dissolving *via* ligand redistribution. The ^{13}C NMR signal for the Al-Me groups could not be detected.

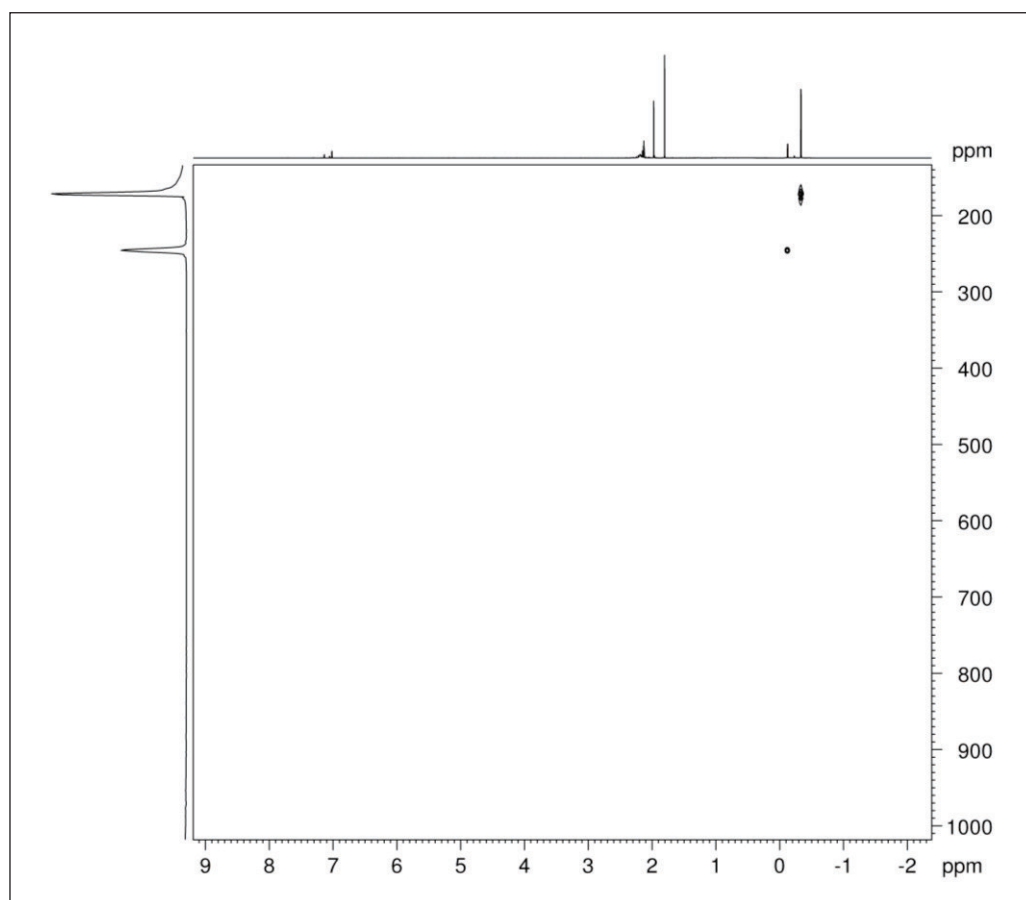


Figure S6. $^1\text{H}-^{89}\text{Y}$ HSQC NMR spectrum (25 MHz, $[\text{D}_8]\text{toluene}$) of complex 1^*-Y^{Br} at 26 °C and $[(\text{C}_5\text{Me}_5)\text{Y}(\text{AlMe}_4)_2]$ (175 ppm), formed upon dissolving *via* ligand redistribution.

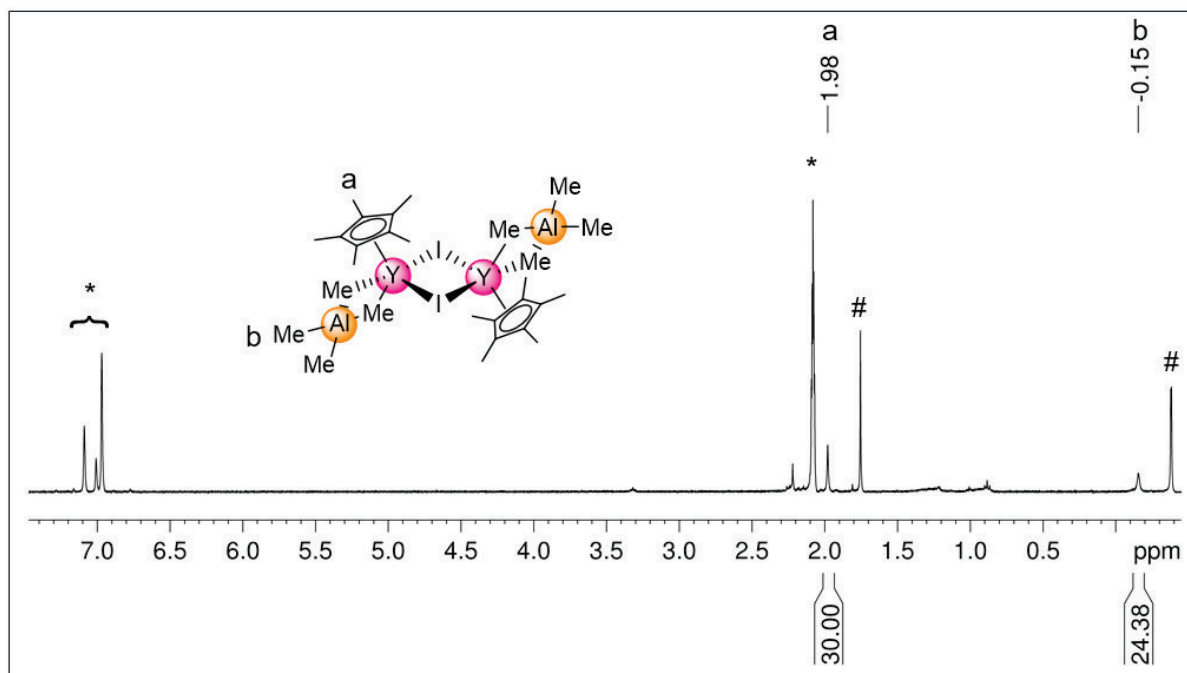


Figure S7. ^1H NMR spectrum (400 MHz, $[\text{D}_8]$ toluene) of complex 1^*-Y^{I} at 26 °C and $[(\text{C}_5\text{Me}_5)\text{Y}(\text{AlMe}_4)_2]$ (#), formed upon dissolving *via* ligand redistribution.

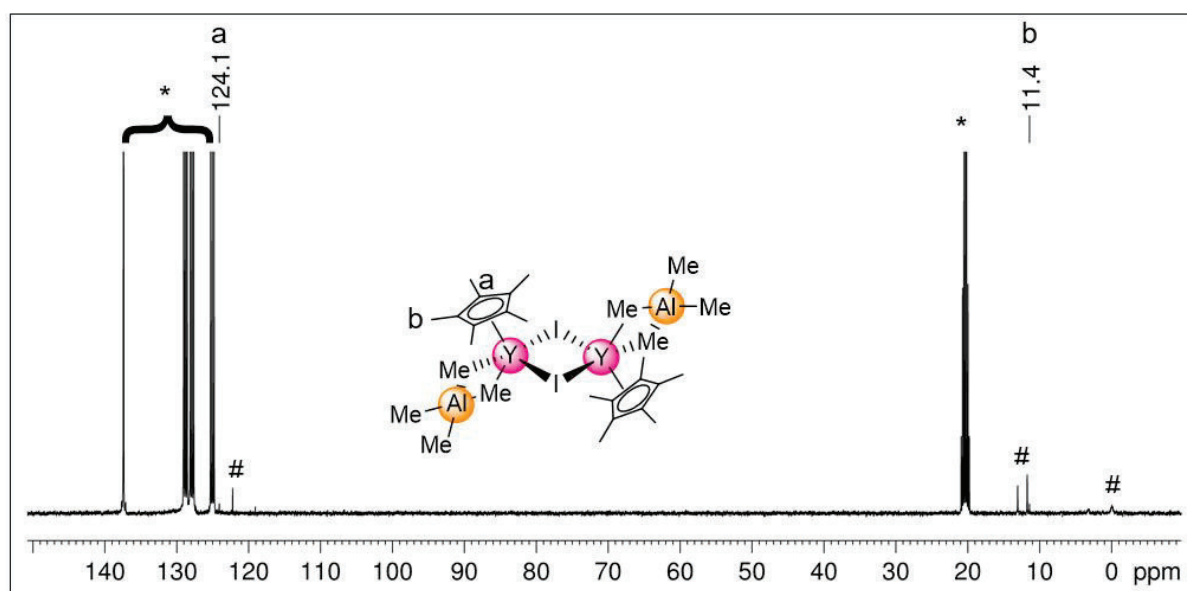


Figure S8. $^{13}\text{C}\{^1\text{H}\}$ NMR spectrum (101 MHz, $[\text{D}_8]$ toluene) of complex 1^*-Y^{I} at 26 °C and $[(\text{C}_5\text{Me}_5)\text{Y}(\text{AlMe}_4)_2]$ (#), formed upon dissolving *via* ligand redistribution.

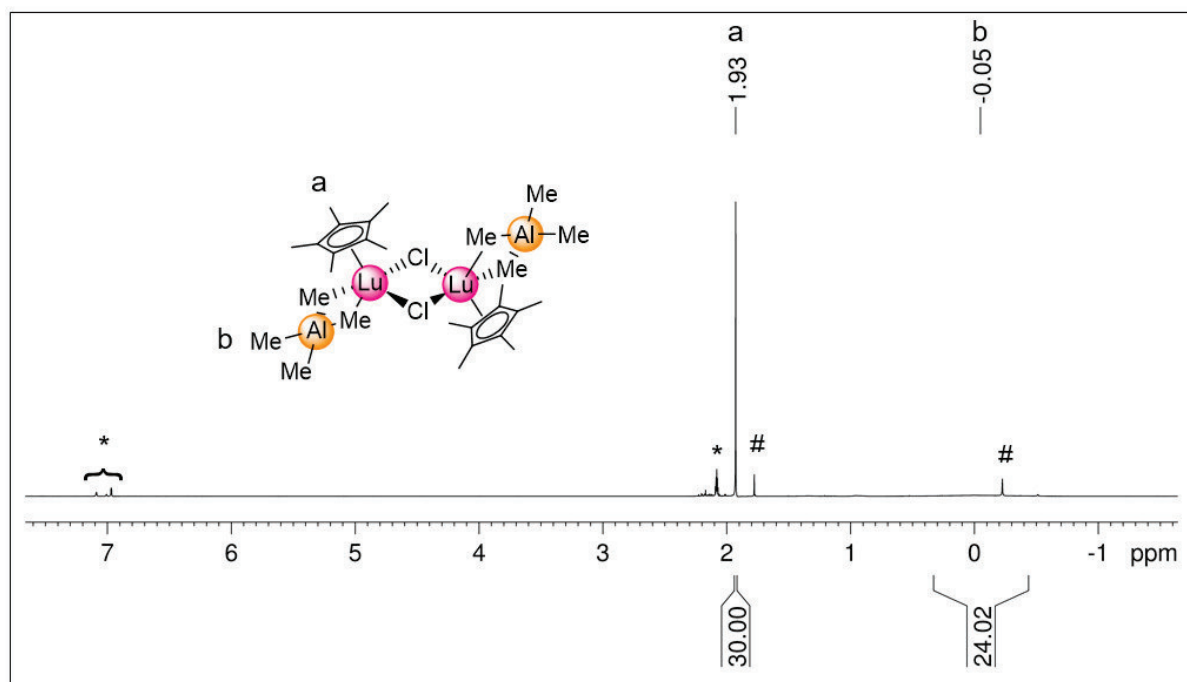


Figure S9. ^1H NMR spectrum (400 MHz, $[\text{D}_8]$ toluene) of complex $1^*\text{-Lu}^{\text{Cl}}$ at 26 °C and $[(\text{C}_5\text{Me}_5)\text{Lu}(\text{AlMe}_4)_2]$ (#), formed upon dissolving *via* ligand redistribution.

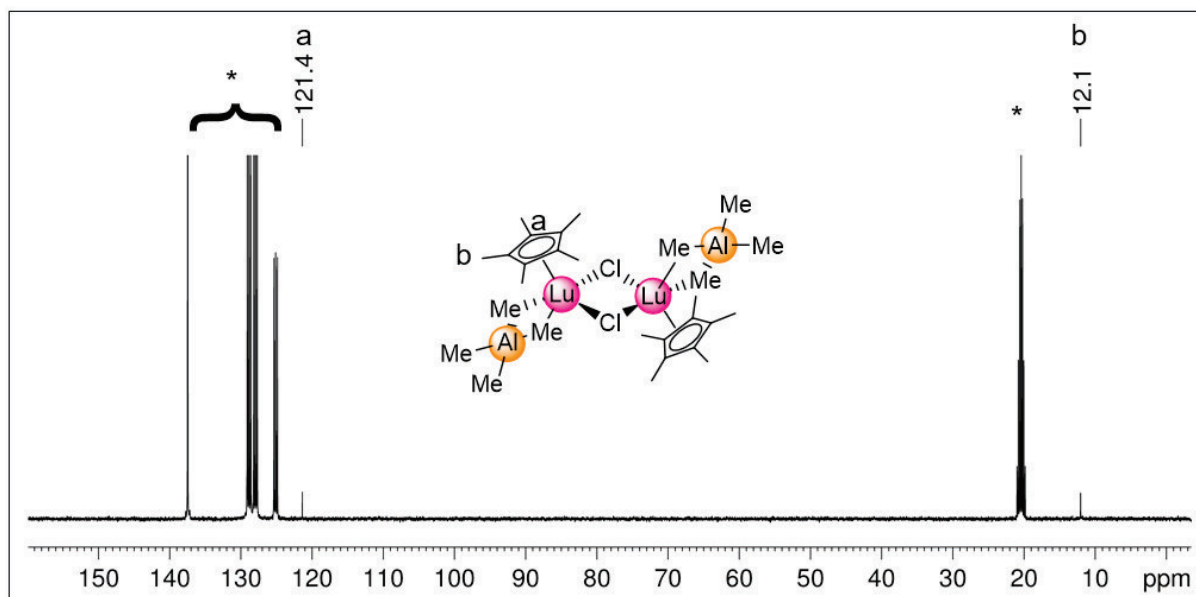


Figure S10. $^{13}\text{C}\{^1\text{H}\}$ NMR spectrum (101 MHz, $[\text{D}_8]$ toluene) of complex $1^*\text{-Lu}^{\text{Cl}}$ at 26 °C. The ^{13}C NMR signal for the Al–Me groups could not be detected.

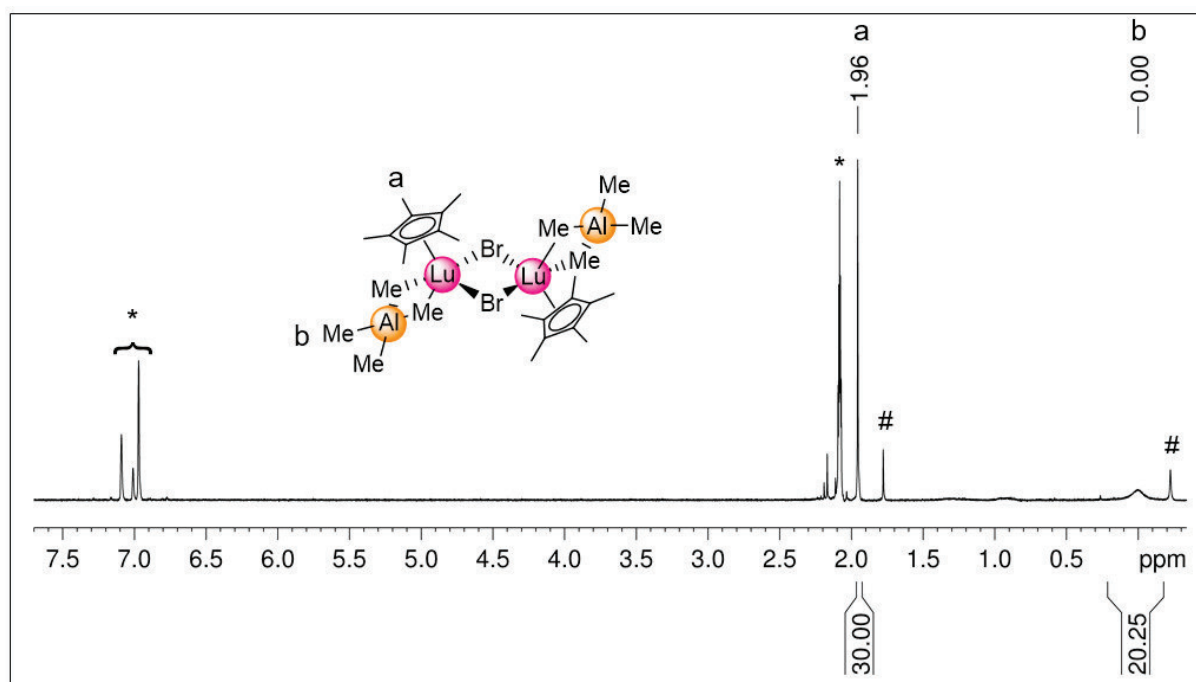


Figure S11. ^1H NMR spectrum (400 MHz, $[\text{D}_8]$ toluene) of complex $1^*\text{-Lu}^{\text{Br}}$ at 26 °C and $[(\text{C}_5\text{Me}_5)\text{Lu}(\text{AlMe}_4)_2]$ (#), formed upon dissolving *via* ligand redistribution.

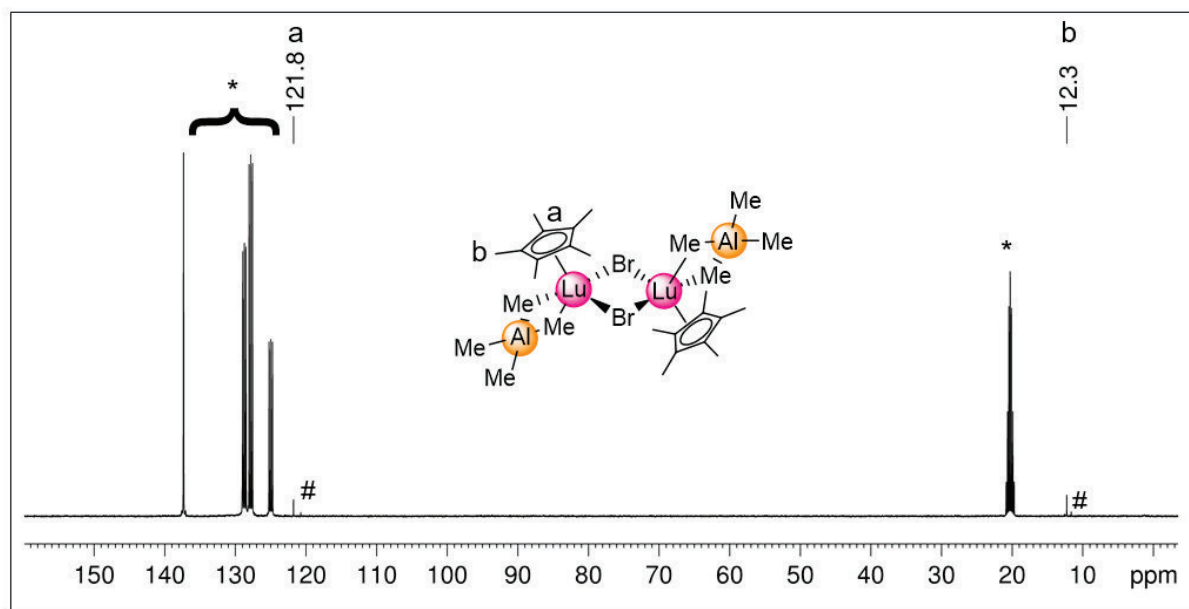


Figure S12. $^{13}\text{C}\{^1\text{H}\}$ NMR spectrum (101 MHz, $[\text{D}_8]$ toluene) of complex $1^*\text{-Lu}^{\text{Br}}$ at 26 °C and $[(\text{C}_5\text{Me}_5)\text{Lu}(\text{AlMe}_4)_2]$ (#), formed upon dissolving *via* ligand redistribution. The ^{13}C signal for the Al–Me groups could not be detected.

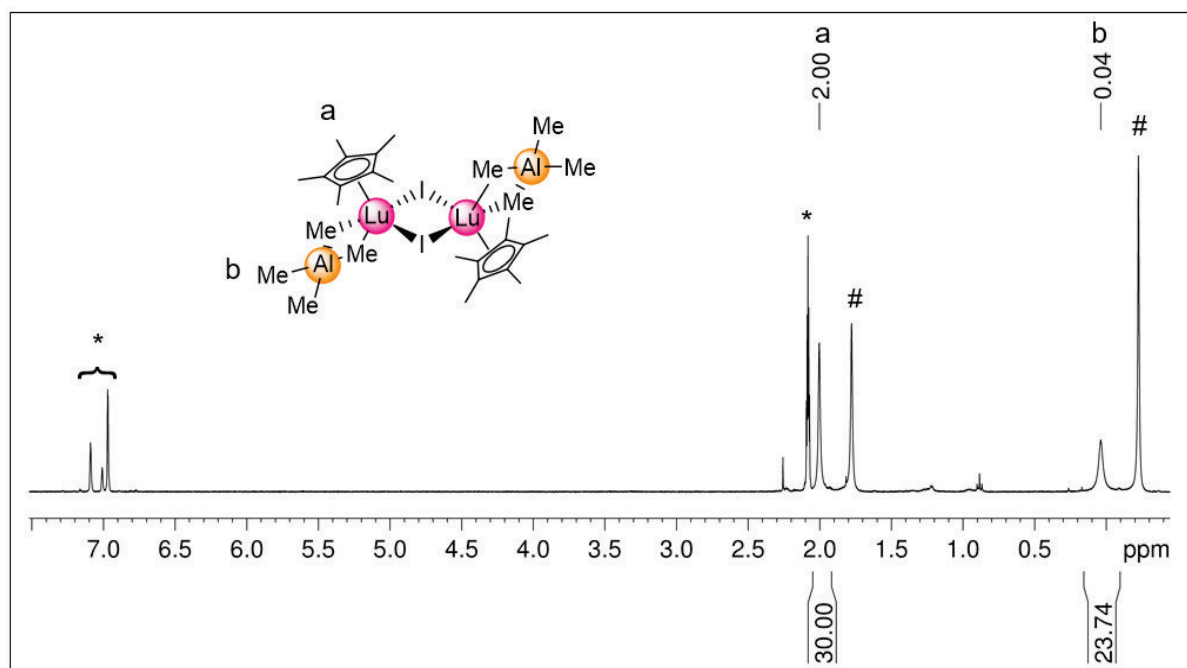


Figure S13. ^1H NMR spectrum (400 MHz, $[\text{D}_8]$ toluene) of complex 1^*-Lu^{I} at 26 °C and $[(\text{C}_5\text{Me}_5)\text{Lu}(\text{AlMe}_2)_2]$ (#), formed upon dissolving *via* ligand redistribution.

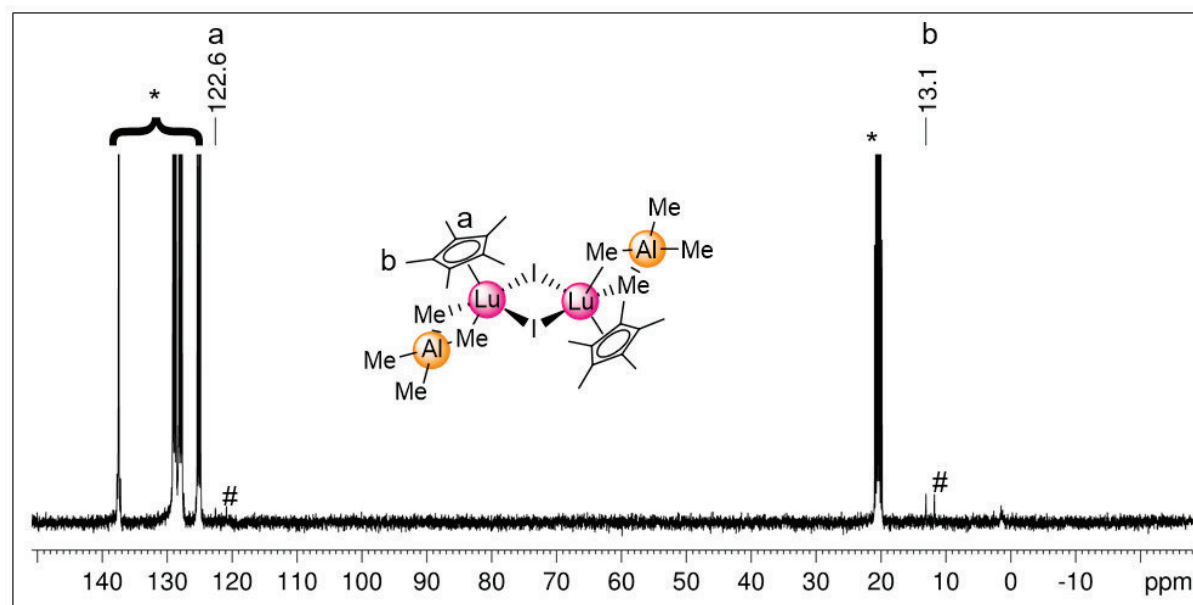


Figure S14. $^{13}\text{C}\{^1\text{H}\}$ NMR spectrum (101 MHz, $[\text{D}_8]$ toluene) of complex 1^*-Lu^{I} at 26 °C and $[(\text{C}_5\text{Me}_5)\text{Lu}(\text{AlMe}_2)_2]$ (#), formed upon dissolving *via* ligand redistribution. The ^{13}C signal for the Al–Me groups could not be detected.

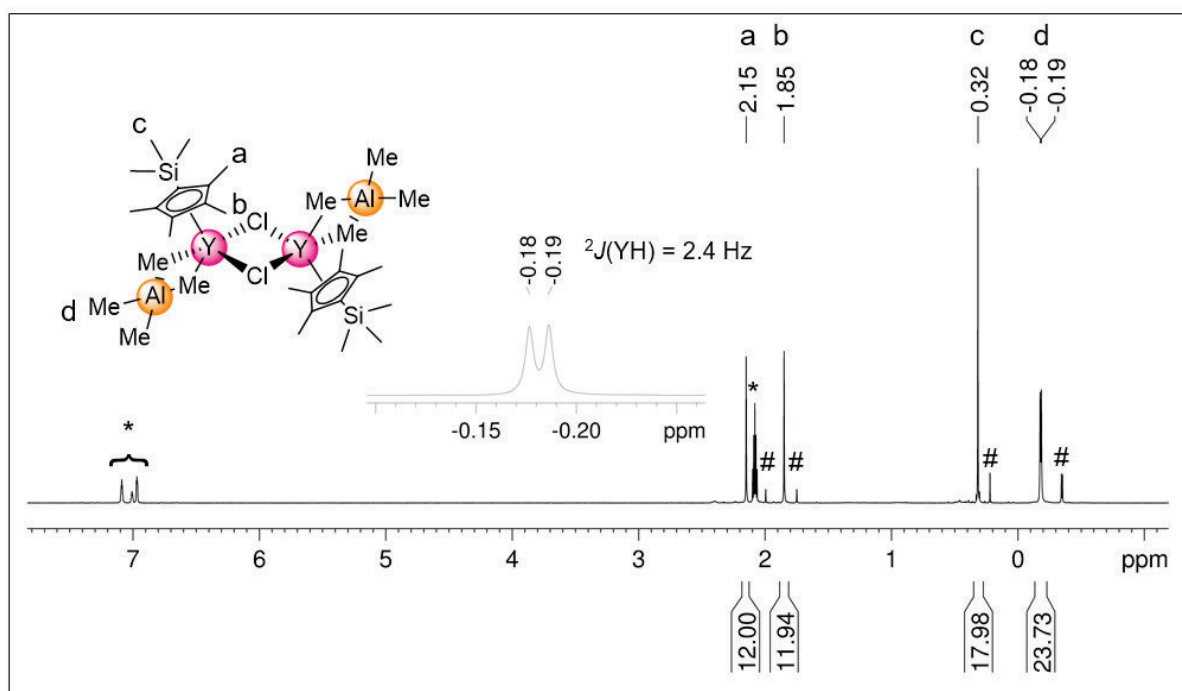


Figure S15. ^1H NMR spectrum (400 MHz, $[\text{D}_8]$ toluene) of complex $1'\text{-Y}^{\text{Cl}}$ at 26 °C and $[(\text{C}_5\text{Me}_4\text{SiMe}_3)\text{Y}(\text{AlMe}_4)_2]$ (#), formed upon dissolving *via* ligand redistribution.

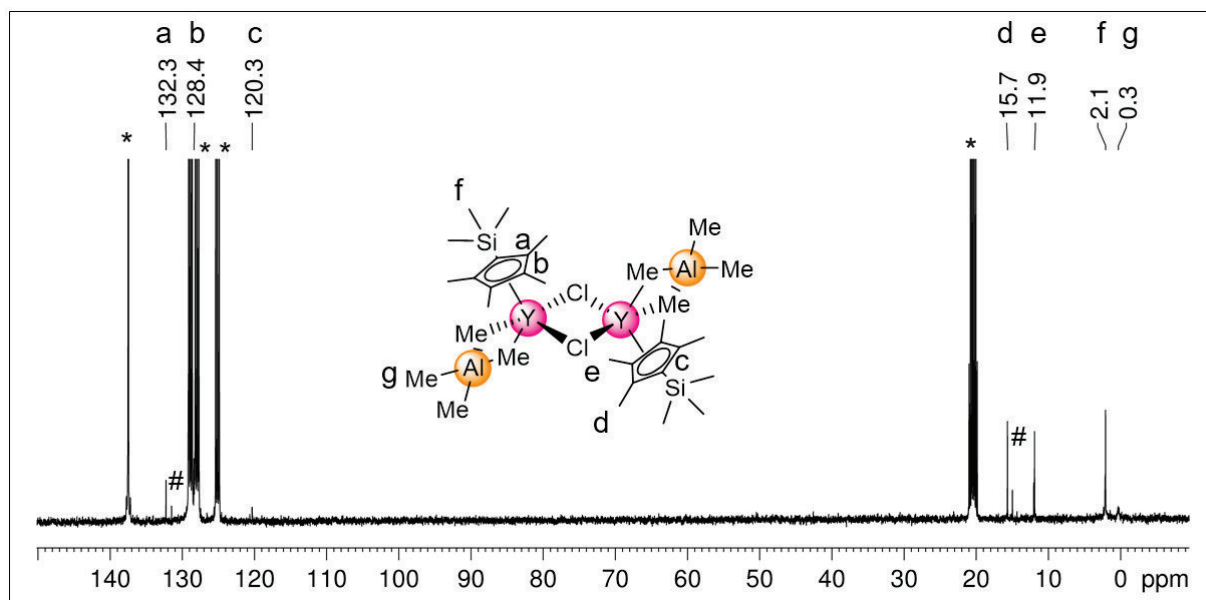


Figure S16. $^{13}\text{C}\{^1\text{H}\}$ NMR spectrum (101 MHz, $[\text{D}_8]$ toluene) of complex $1'\text{-Y}^{\text{Cl}}$ at 26 °C and $[(\text{C}_5\text{Me}_4\text{SiMe}_3)\text{Y}(\text{AlMe}_4)_2]$ (#), formed upon dissolving *via* ligand redistribution.

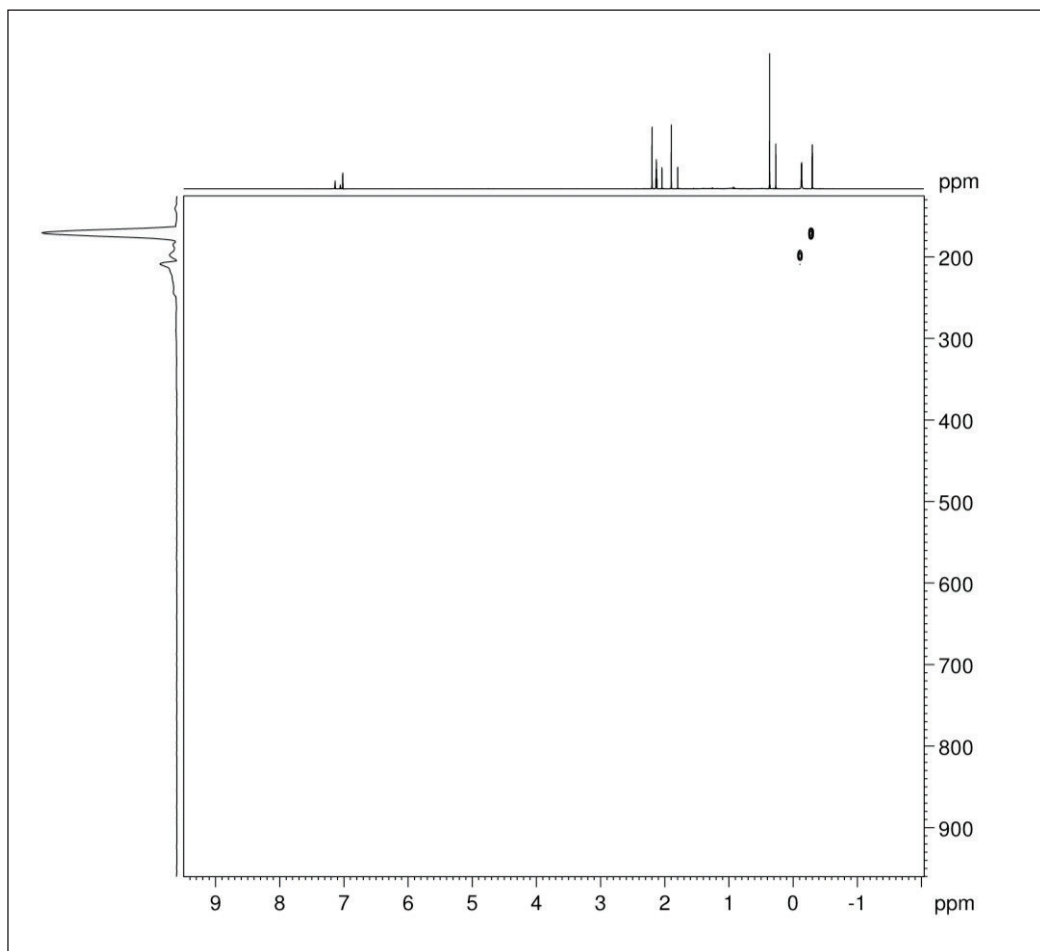


Figure S17. ^1H - ^{89}Y HSQC NMR spectrum (25 MHz, $[\text{D}_8]$ toluene) of complex $\mathbf{1}^{\text{-Y}^{\text{Cl}}}$ at 26 °C and $[(\text{C}_5\text{Me}_4\text{SiMe}_3)\text{Y}(\text{AlMe}_4)_2]$ (170 ppm), formed upon dissolving *via* ligand redistribution.

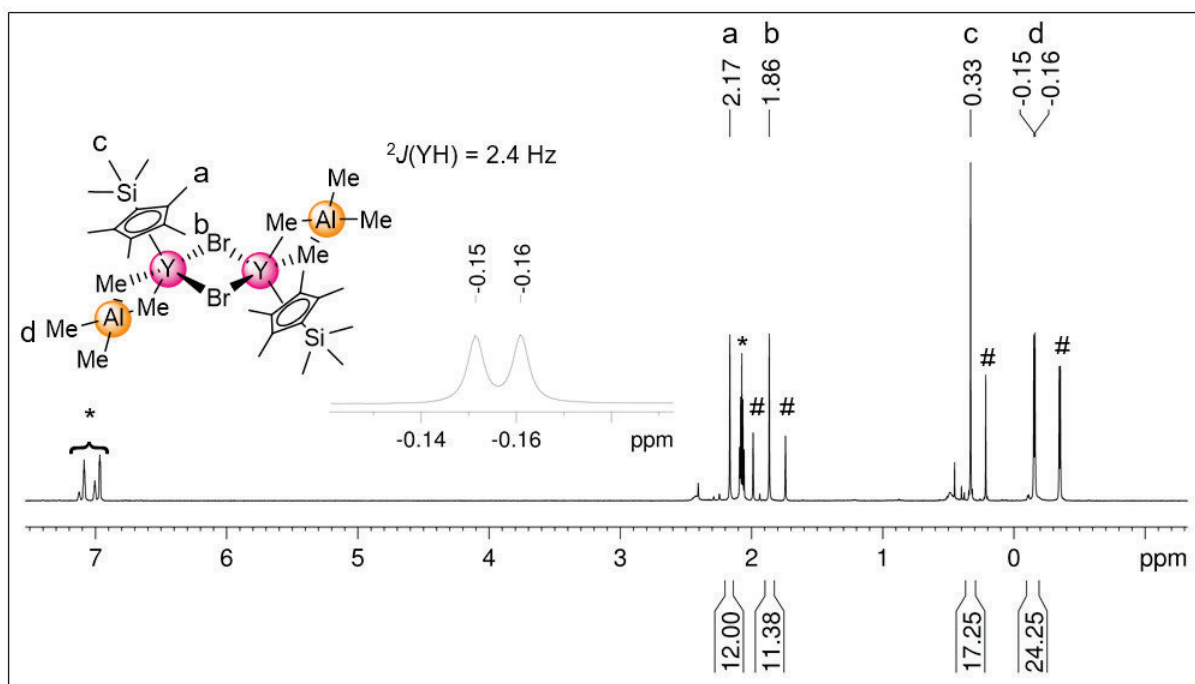


Figure S18. ^1H NMR spectrum (400 MHz, $[\text{D}_8]$ toluene) of complex $\mathbf{1}^{\text{-Y}^{\text{Br}}}$ at 26 °C and $[(\text{C}_5\text{Me}_4\text{SiMe}_3)\text{Y}(\text{AlMe}_4)_2]$ (#), formed upon dissolving *via* ligand redistribution.

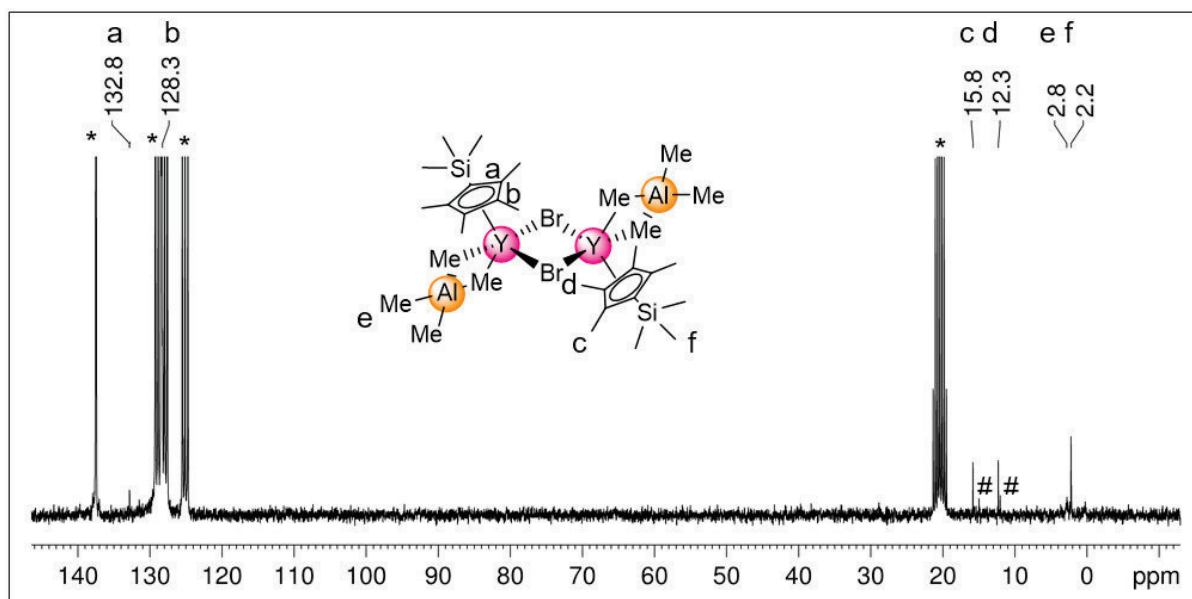


Figure S19. $^{13}\text{C}\{^1\text{H}\}$ NMR spectrum (101 MHz, $[\text{D}_8]$ toluene) of complex $1'\text{-Y}^{\text{Br}}$ at 26 °C and $[(\text{C}_5\text{Me}_4\text{SiMe}_3)\text{Y}(\text{AlMe}_4)_2]$ (#), formed upon dissolving *via* ligand redistribution. The signal of the C-SiMe_3 unit is detected in $^1\text{H-}^{13}\text{C}$ HMBC (Figure S20).

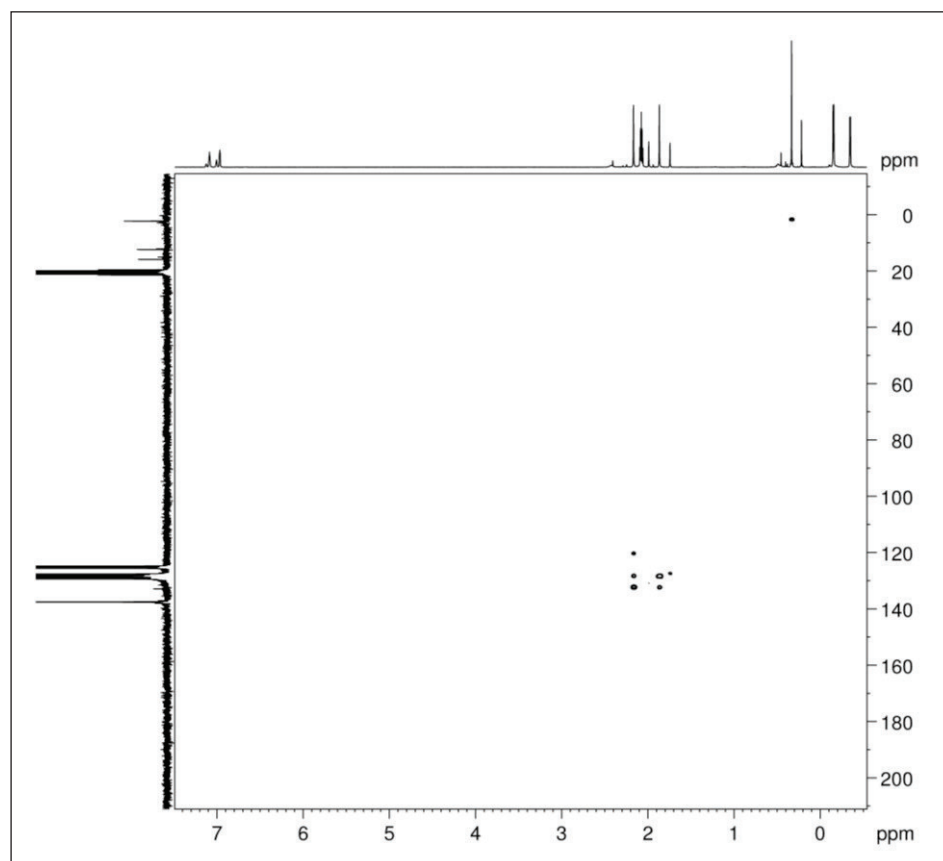


Figure S20. $^1\text{H-}^{13}\text{C}$ HMBC NMR spectrum (101 MHz, $[\text{D}_8]$ toluene) of complex $1'\text{-Y}^{\text{Br}}$ at 26 °C.

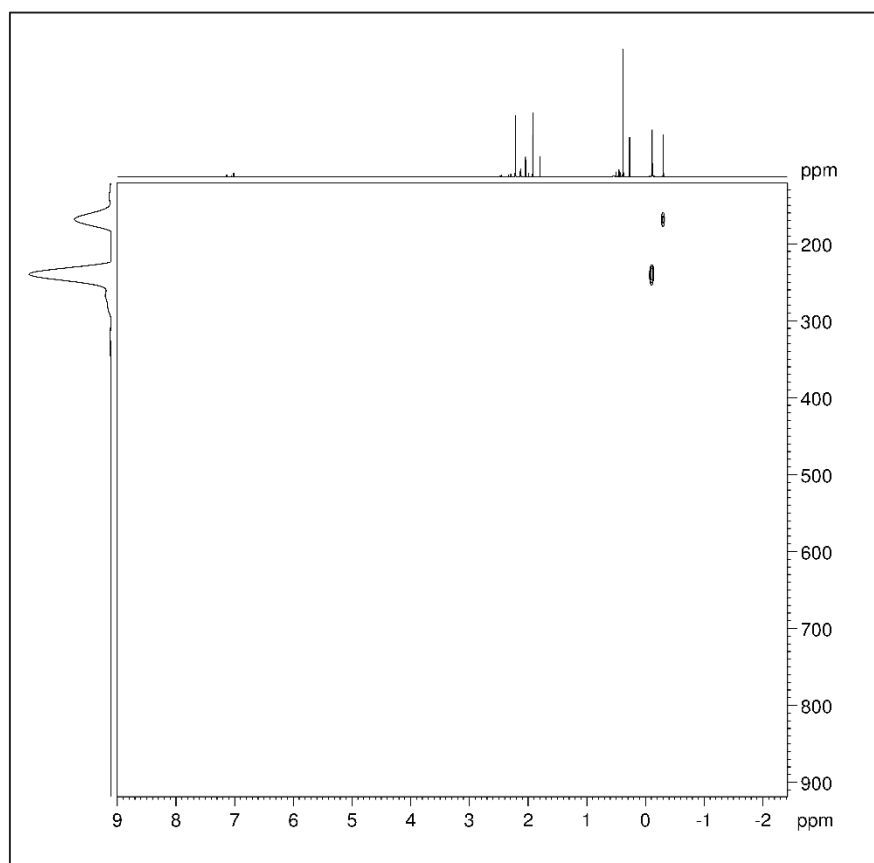


Figure S21. ^1H - ^{89}Y HSQC NMR spectrum (25 MHz, $[\text{D}_8]$ toluene) of complex $\mathbf{1}'\text{-Y}^{\text{Br}}$ at 26 °C and $[(\text{C}_5\text{Me}_4\text{SiMe}_3)\text{Y}(\text{AlMe}_4)_2]$ (170 ppm), formed upon dissolving *via* ligand redistribution.

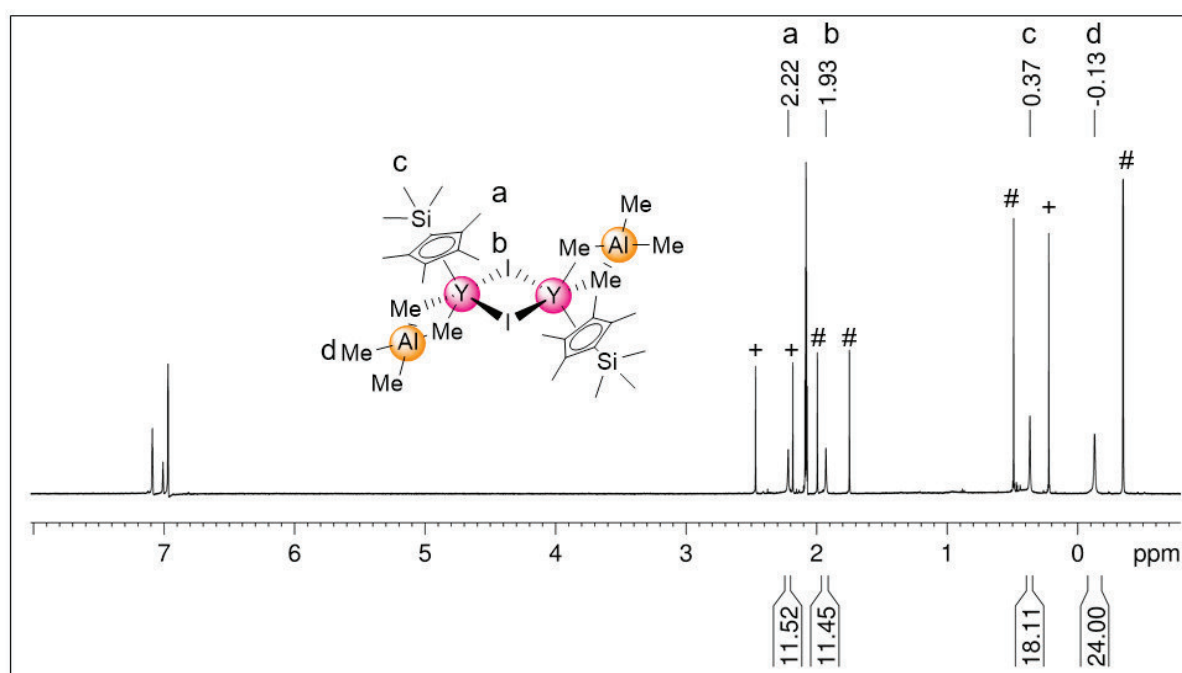


Figure S22. ^1H NMR spectrum (400 MHz, $[\text{D}_8]$ toluene) of complex $\mathbf{1}'\text{-Y}^{\text{I}}$ at 26 °C and $[(\text{C}_5\text{Me}_4\text{SiMe}_3)\text{Y}(\text{AlMe}_4)_2]$ (#) and other dissolution products (+), formed upon dissolving *via* ligand redistribution.

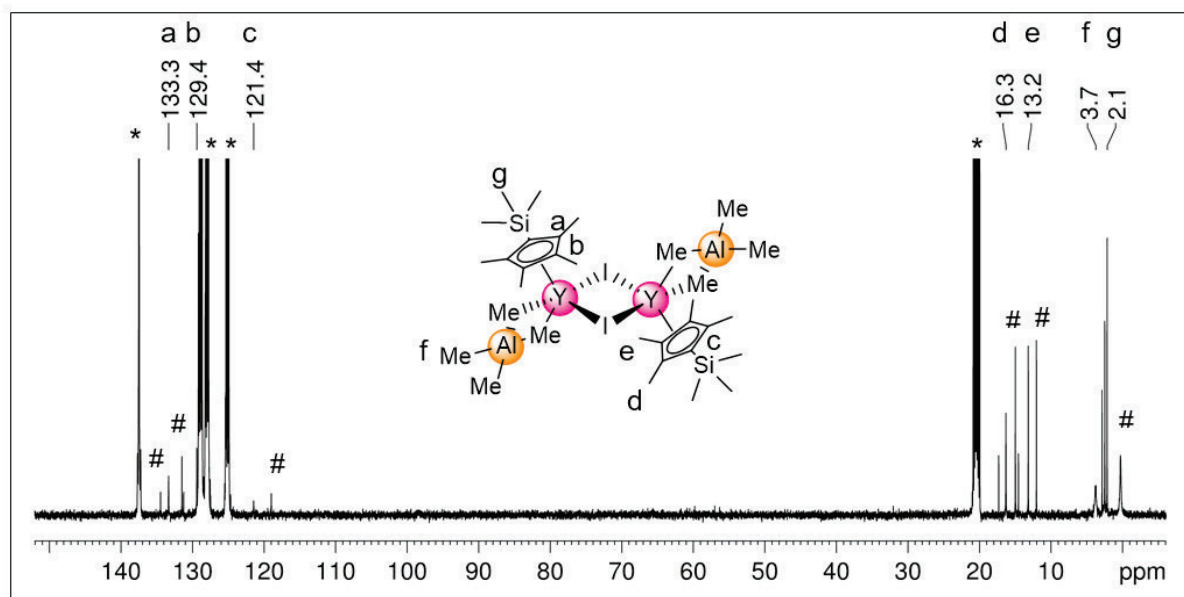


Figure S23. $^{13}\text{C}\{^1\text{H}\}$ NMR spectrum (101 MHz, $[\text{D}_8]\text{toluene}$) of complex $1'\text{-Y}^{\text{I}}$ at 26°C and $[(\text{C}_5\text{Me}_4\text{SiMe}_3)\text{Y}(\text{AlMe}_4)_2]$ (#), formed upon dissolving *via* ligand redistribution.

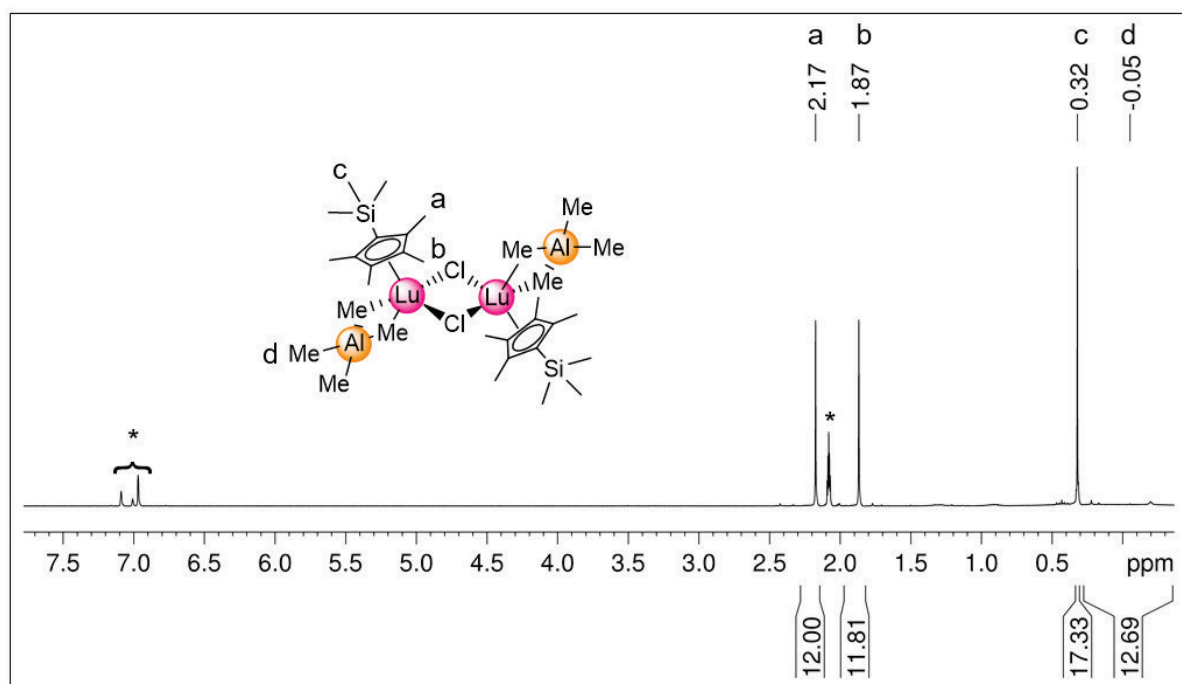


Figure S24. ^1H NMR spectrum (400 MHz, $[\text{D}_8]\text{toluene}$) of complex $1'\text{-Lu}^{\text{Cl}}$ at 26°C .

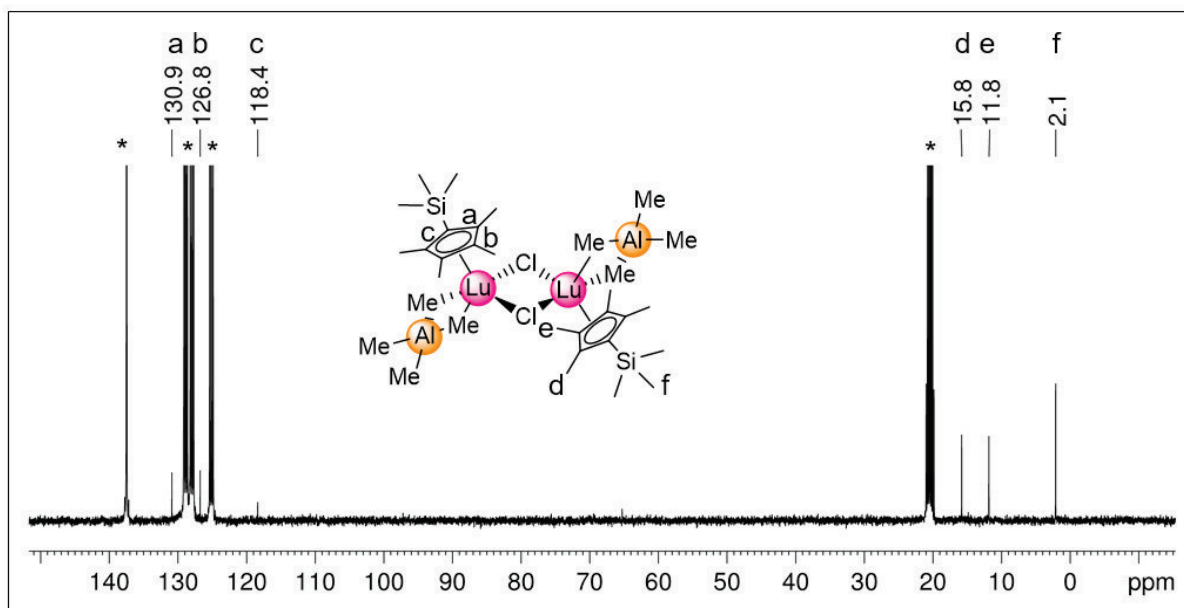


Figure S25. $^{13}\text{C}\{^1\text{H}\}$ NMR spectrum (101 MHz, $[\text{D}_8]$ toluene) of complex $1'\text{-Lu}^{\text{Cl}}$ at 26 °C. ^{13}C resonances for the AlMe_4 groups could not be detected.

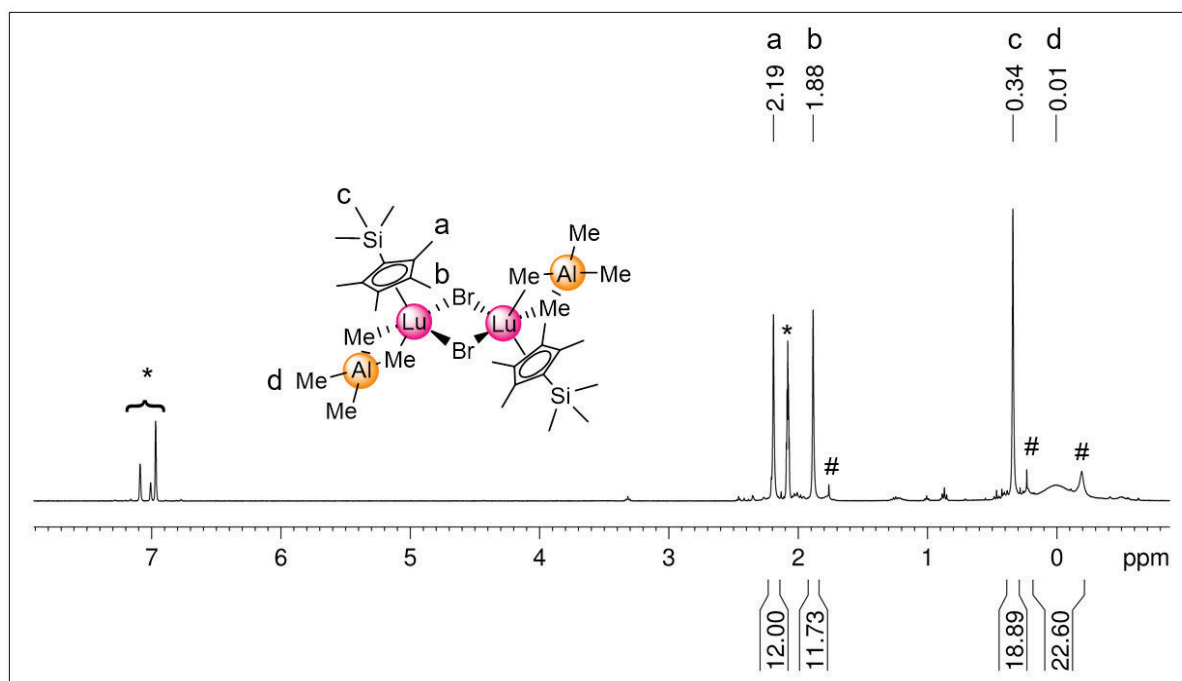


Figure S26. ^1H NMR spectrum (400 MHz, $[\text{D}_8]$ toluene) of complex $1'\text{-Lu}^{\text{Br}}$ at 26 °C and $[(\text{C}_5\text{Me}_4\text{SiMe}_3)\text{Lu}(\text{AlMe}_4)_2]$ (#), formed upon dissolving *via* ligand redistribution.

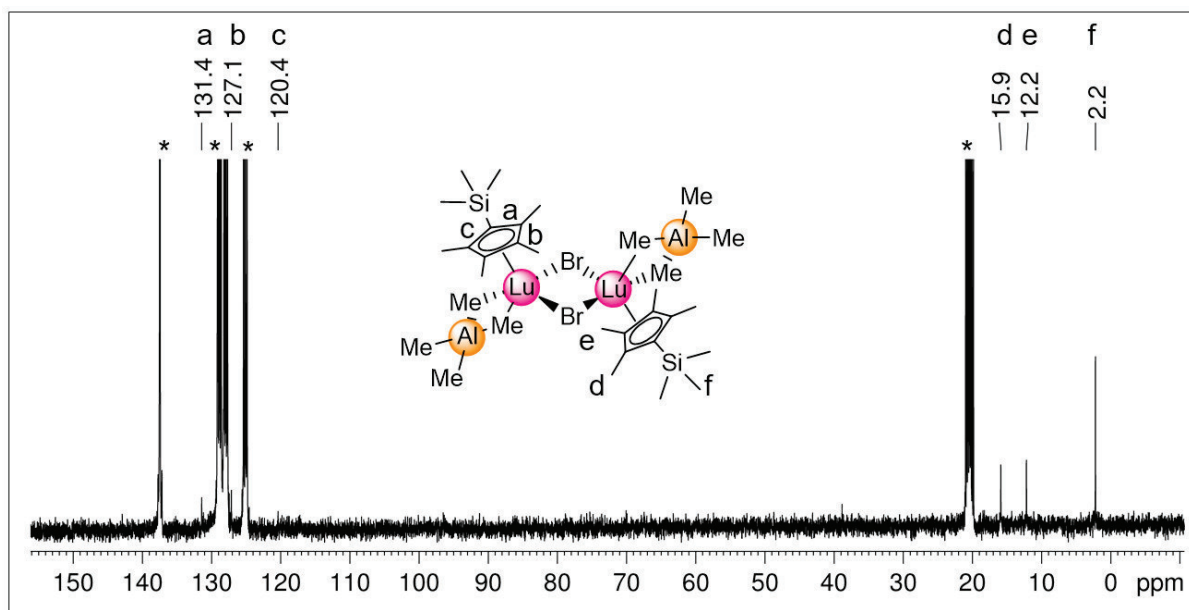


Figure S27. $^{13}\text{C}\{^1\text{H}\}$ NMR spectrum (101 MHz, $[\text{D}_8]$ toluene) of complex $1'\text{-Lu}^{\text{Br}}$ at 26 °C and $[(\text{C}_5\text{Me}_4\text{SiMe}_3)\text{Lu}(\text{AlMe}_4)_2]$ (#), formed upon dissolving *via* ligand redistribution. ^{13}C resonances for the AlMe_4 groups could not be detected.

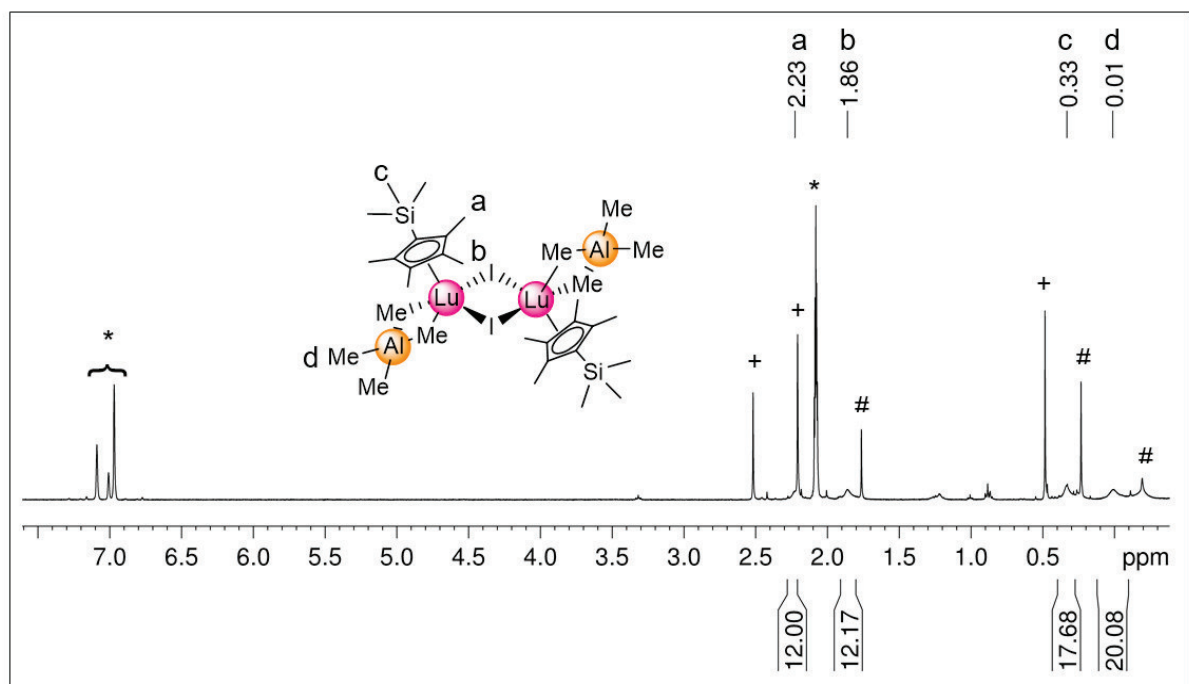


Figure S28. ^1H NMR spectrum (400 MHz, $[\text{D}_8]$ toluene) of complex $1'\text{-Lu}^{\text{I}}$ at 26 °C and $[(\text{C}_5\text{Me}_4\text{SiMe}_3)\text{Lu}(\text{AlMe}_4)_2]$ (#) and other dissolution products (+), formed upon dissolving *via* ligand redistribution.

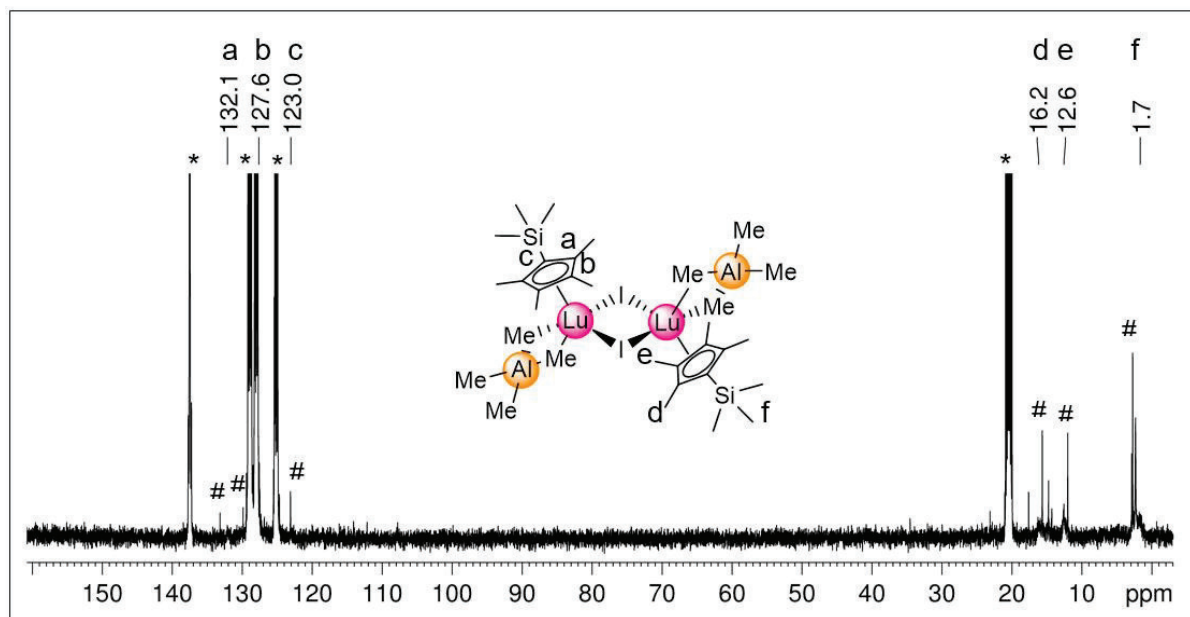


Figure S29. $^{13}\text{C}\{^1\text{H}\}$ NMR spectrum (101 MHz, $[\text{D}_8]\text{toluene}$) of complex **1'-Lu^I** at 26 °C and $[(\text{C}_5\text{Me}_4\text{SiMe}_3)\text{Lu}(\text{AlMe}_4)_2]$ (#), formed upon dissolving *via* ligand redistribution. ^{13}C resonances for the AlMe_4 groups could not be detected.

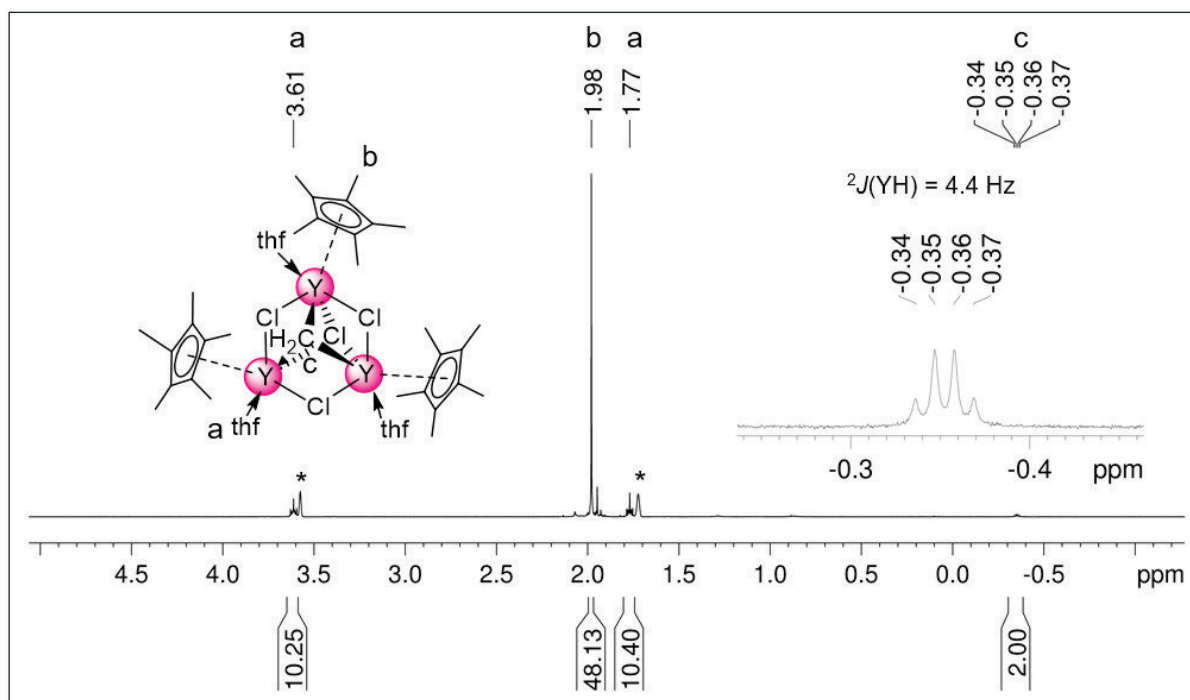


Figure S30. ^1H NMR spectrum (400 MHz, $[\text{D}_8]\text{thf}$) of complex **4*-Y^{Cl}** at 26 °C.

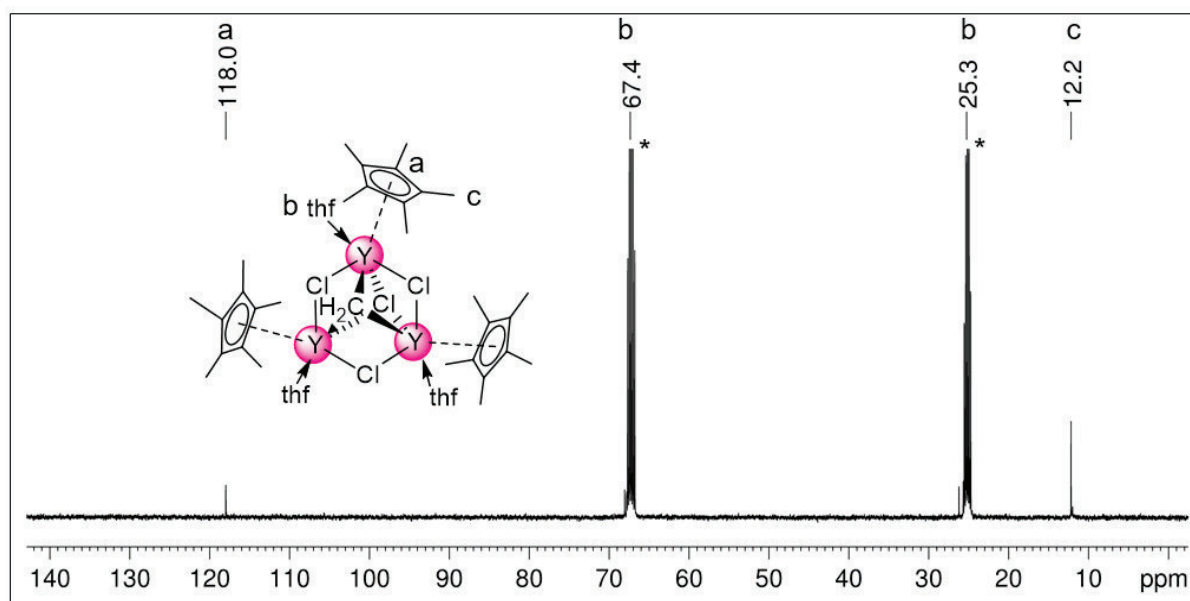


Figure S31. $^{13}\text{C}\{^1\text{H}\}$ NMR spectrum (101 MHz, $[\text{D}_8]\text{thf}$) of complex 4^*-Y^{Cl} at 26 °C. ^{13}C resonances for the CH_2 group could not be detected.

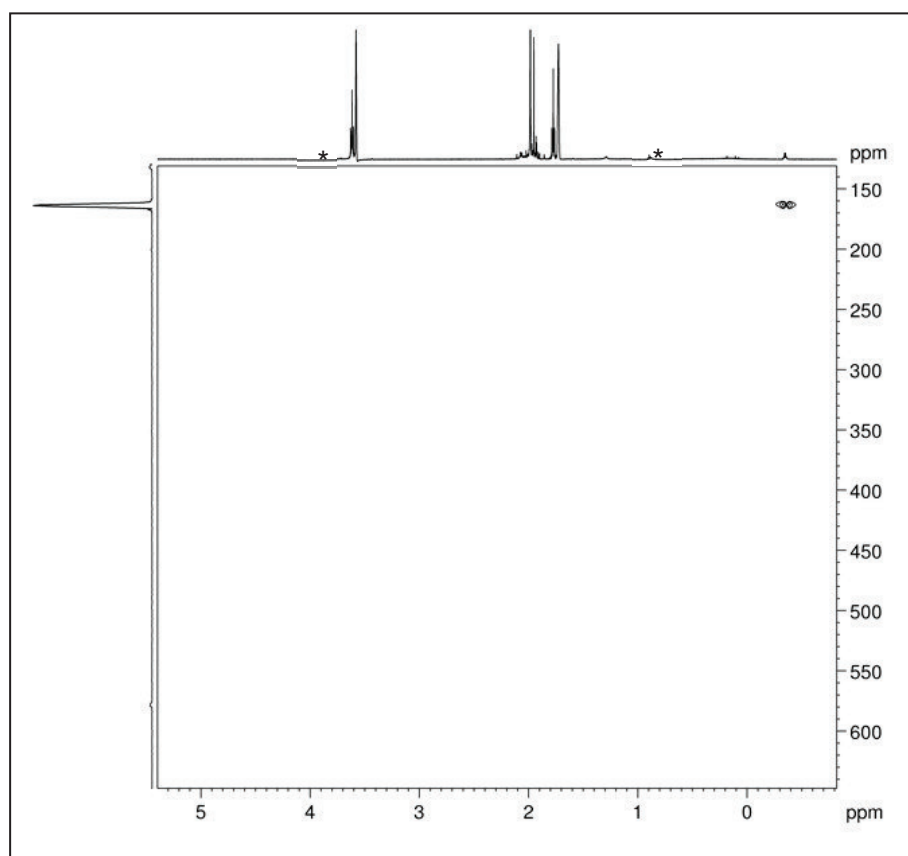


Figure S32. $^1\text{H}-^{89}\text{Y}$ HSQC NMR spectrum (25 MHz, $[\text{D}_8]\text{thf}$) of complex 4^*-Y^{Cl} at 26 °C.

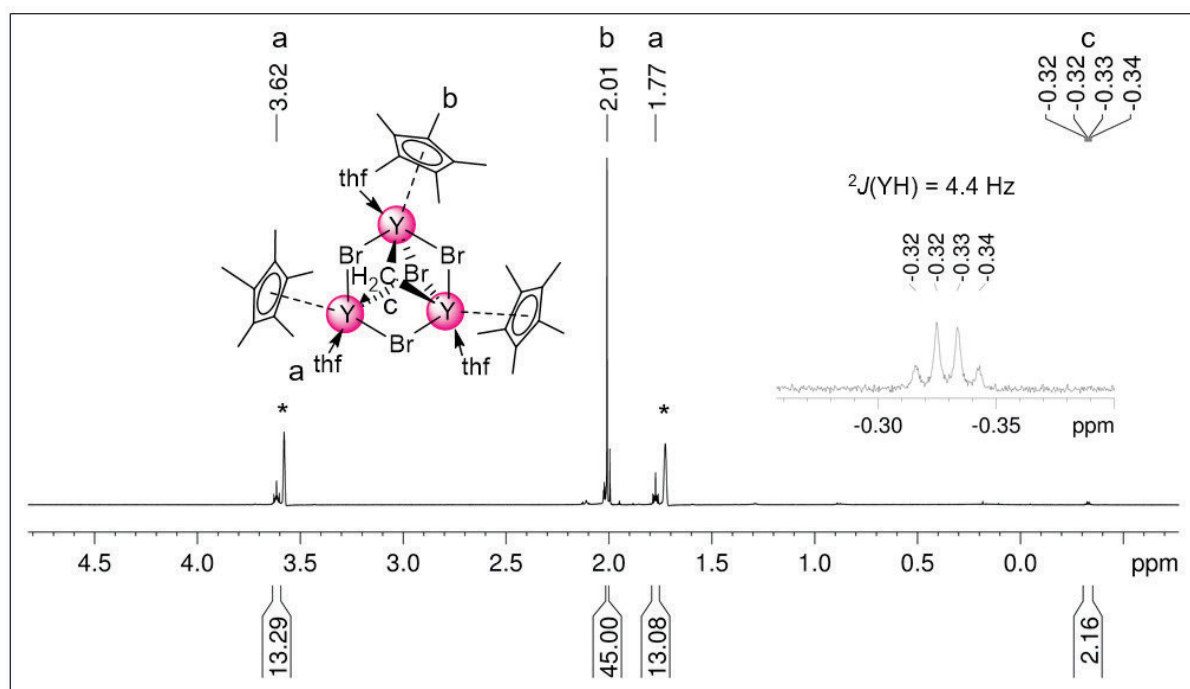


Figure S33. ^1H NMR spectrum (400 MHz, $[\text{D}_8]\text{thf}$) of complex 4^*-Y^{Br} at 26 $^\circ\text{C}$.

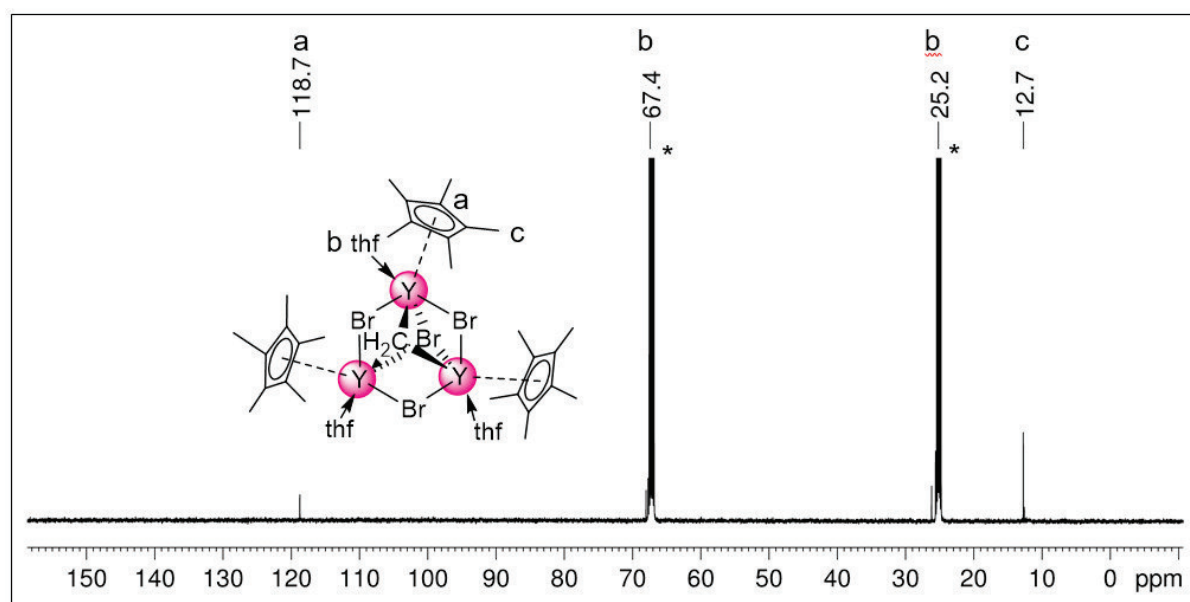


Figure S34. $^{13}\text{C}\{^1\text{H}\}$ NMR spectrum (101 MHz, $[\text{D}_8]\text{thf}$) of complex 4^*-Y^{Br} at 26 $^\circ\text{C}$. ^{13}C resonances for the CH_2 group could not be detected.

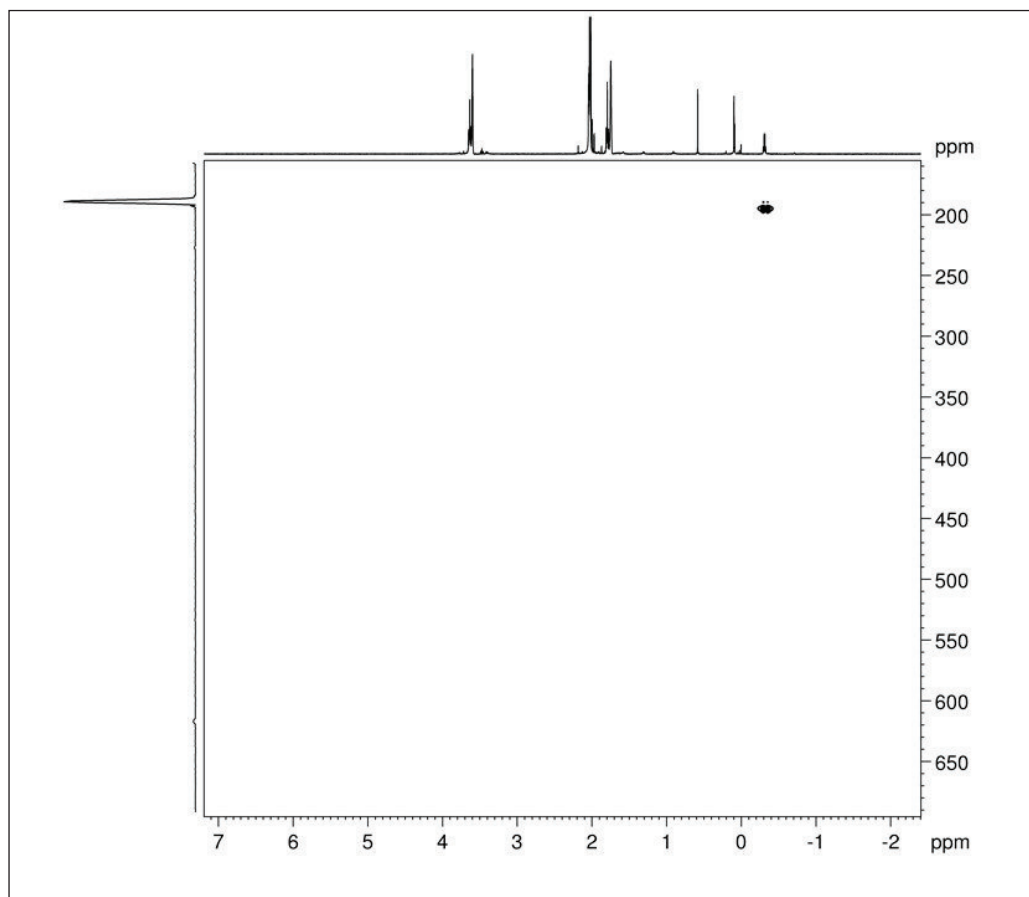


Figure S35. ^1H - ^{89}Y HSQC NMR spectrum (25 MHz, $[\text{D}_8]\text{thf}$) of complex 4^*-Y^{Br} at 26 °C.

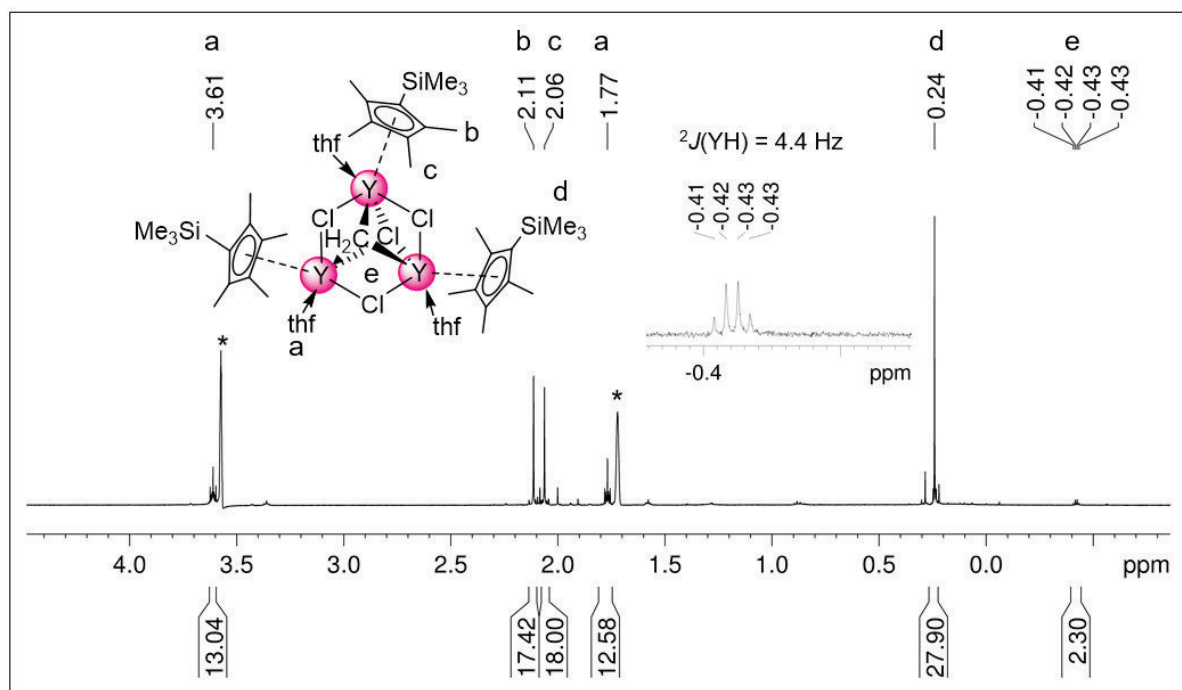


Figure S36. ^1H NMR spectrum (400 MHz, $[\text{D}_8]\text{thf}$) of complex $4'-\text{Y}^{\text{Cl}}$ at 26 °C.

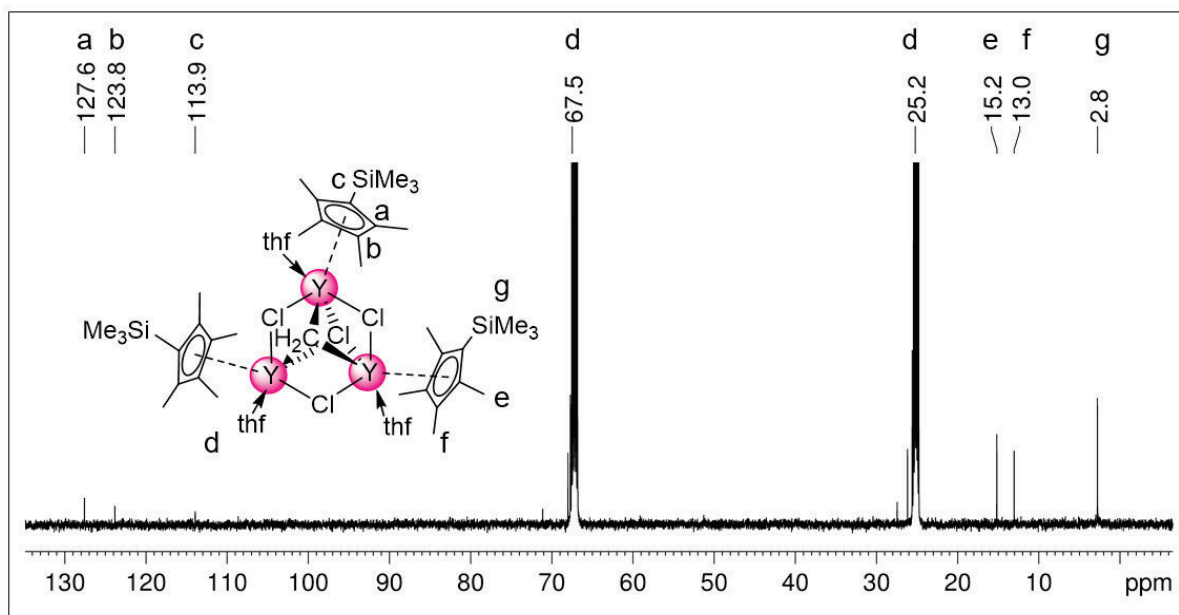


Figure S37. $^{13}\text{C}\{^1\text{H}\}$ NMR spectrum (101 MHz, $[\text{D}_8]\text{thf}$) of complex $4'\text{-Y}^{\text{Cl}}$ at 26 °C. ^{13}C resonances for the CH_2 group could not be detected.

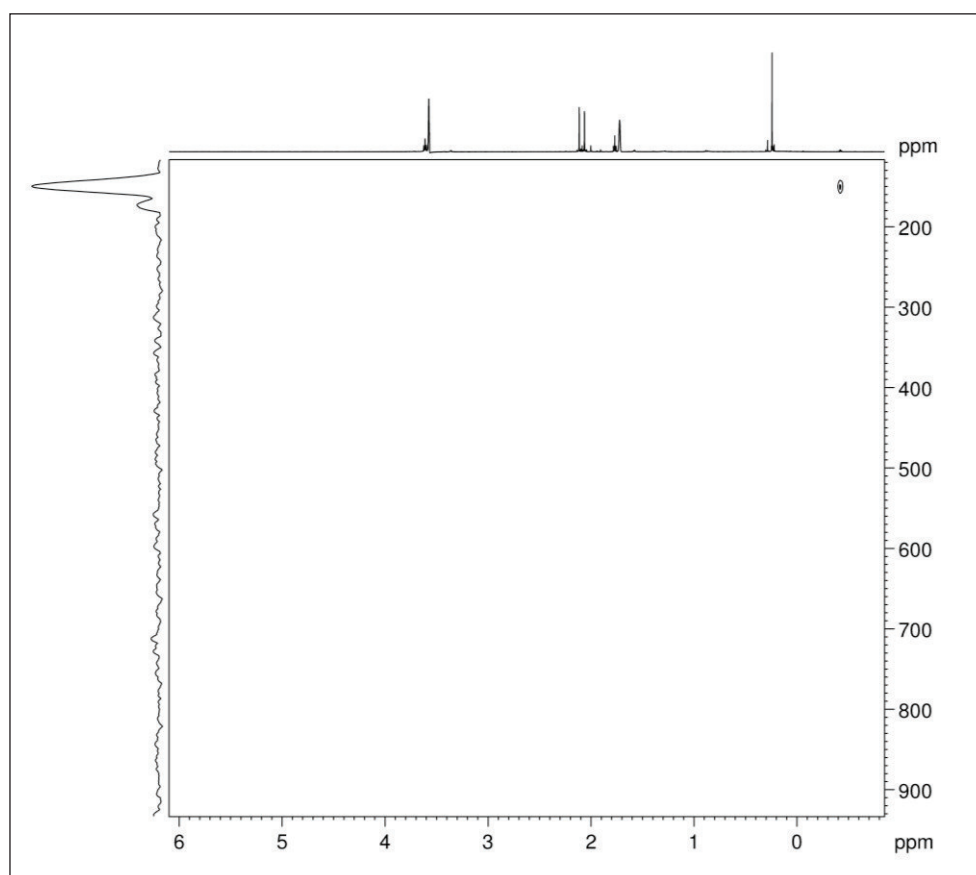


Figure S38. $^1\text{H}\text{-}^{89}\text{Y}$ HSQC NMR spectrum (25 MHz, $[\text{D}_8]\text{thf}$) of complex $4'\text{-Y}^{\text{Cl}}$ at 26 °C.

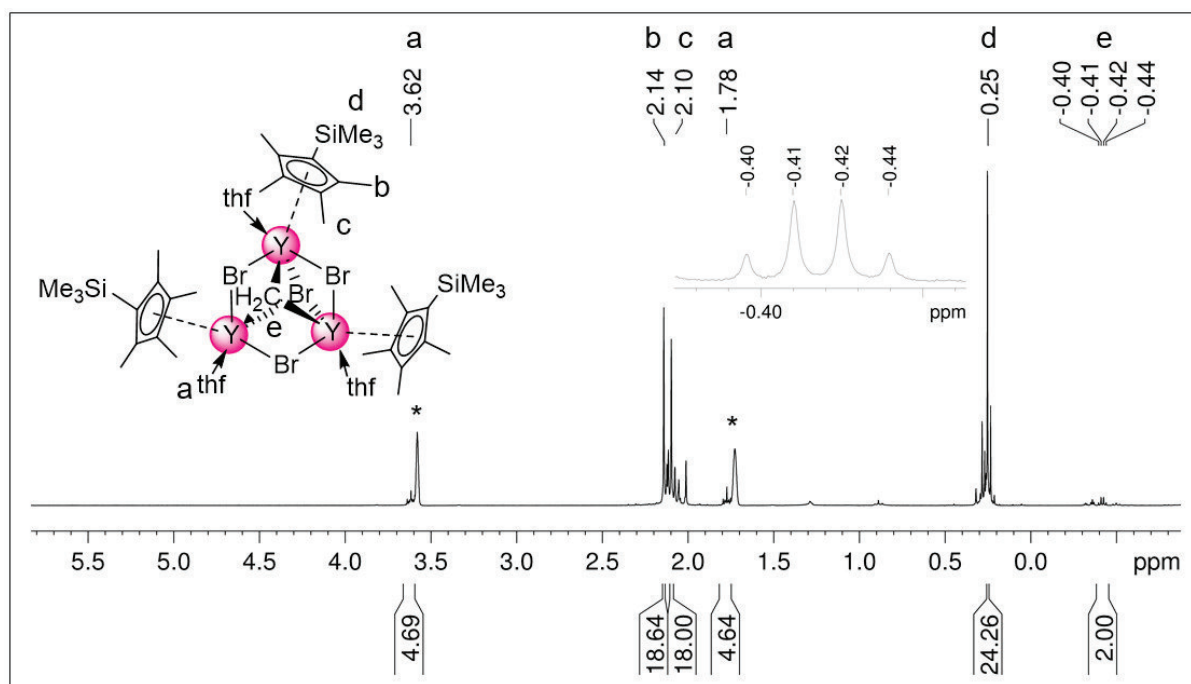


Figure S39. ^1H NMR spectrum (400 MHz, $[\text{D}_8]\text{thf}$) of complex $4'\text{-Y}^{\text{Br}}$ at 26 $^\circ\text{C}$.

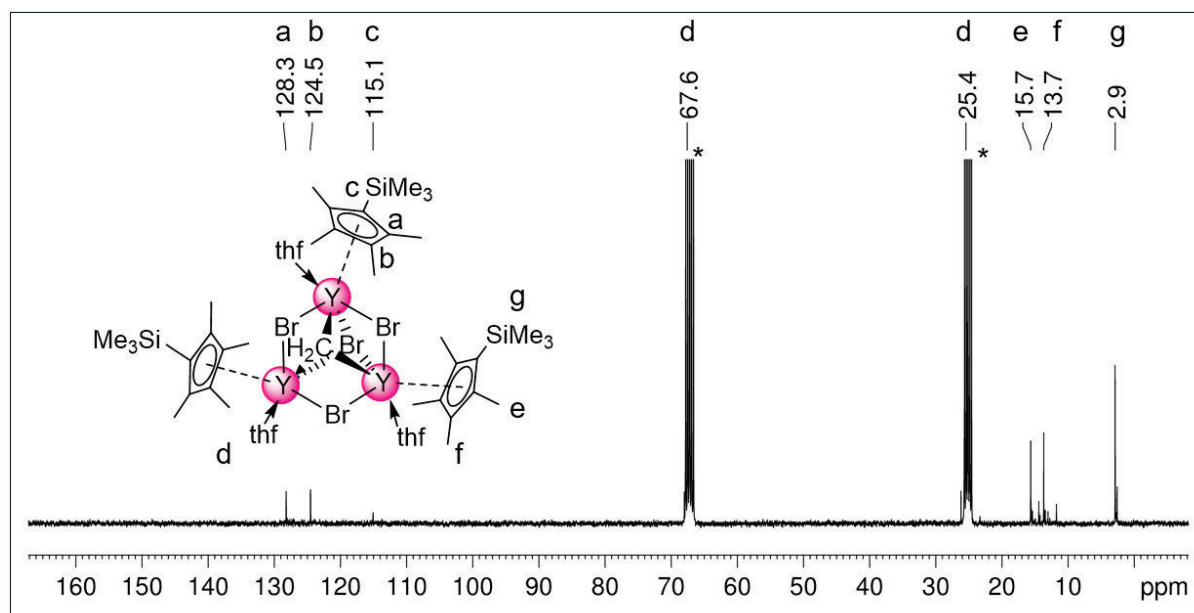


Figure S40. $^{13}\text{C}\{^1\text{H}\}$ NMR spectrum (101 MHz, $[\text{D}_8]\text{thf}$) of complex $4'\text{-Y}^{\text{Br}}$ at 26 $^\circ\text{C}$. ^{13}C resonances for the CH_2 group could not be detected.

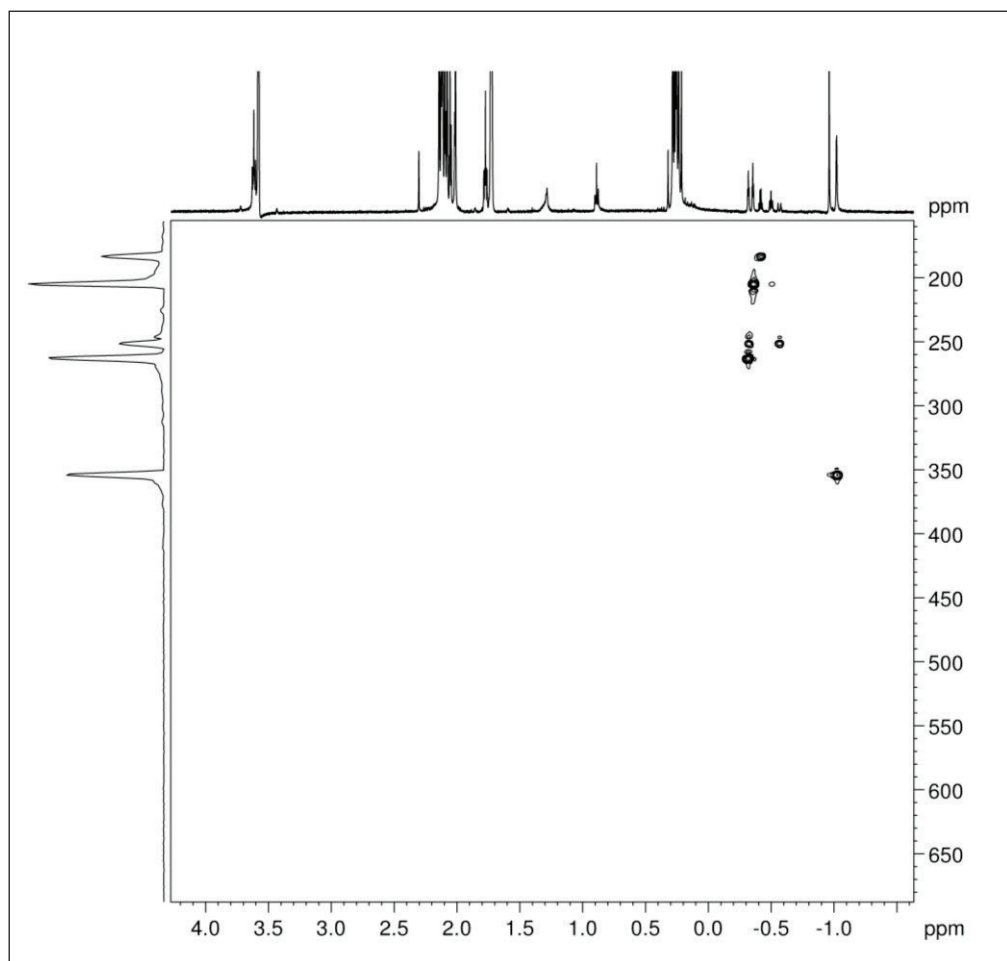


Figure S41. ^1H - ^{89}Y HSQC NMR spectrum (25 MHz, $[\text{D}_8]\text{thf}$) of complex $4'\text{-Y}^{\text{Br}}$ at 26 °C with decomposition products.

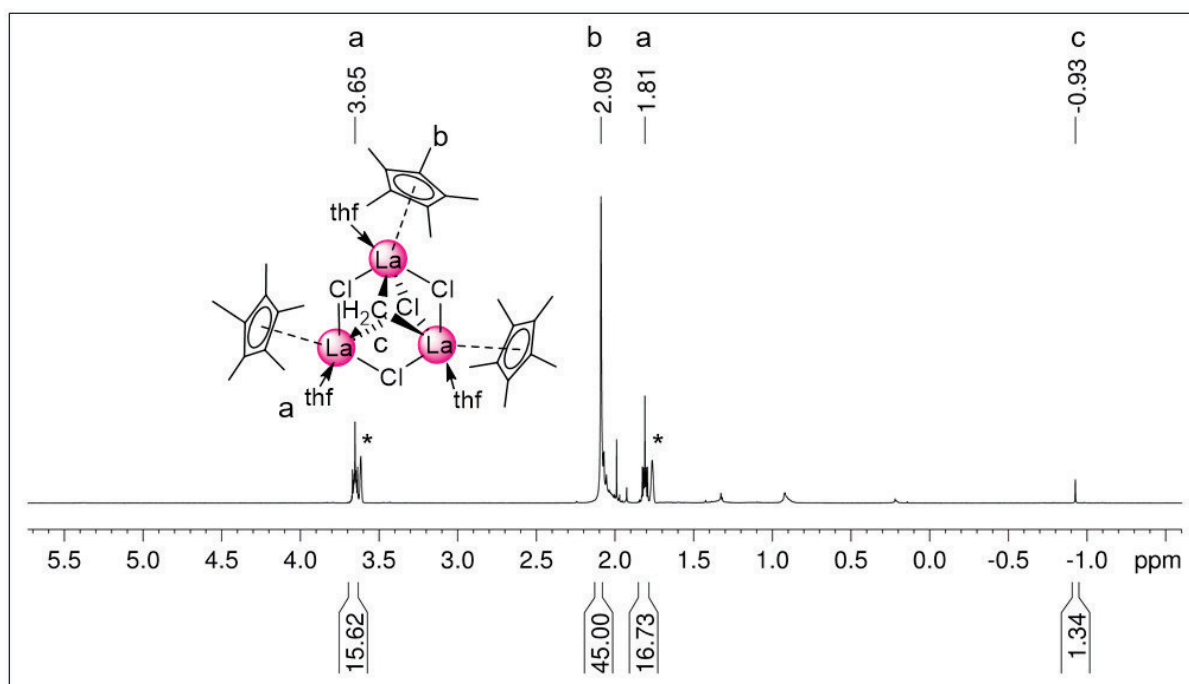


Figure S42. ^1H NMR spectrum (400 MHz, $[\text{D}_8]\text{thf}$) of complex $4'\text{-La}^{\text{Cl}}$ at 26 °C.

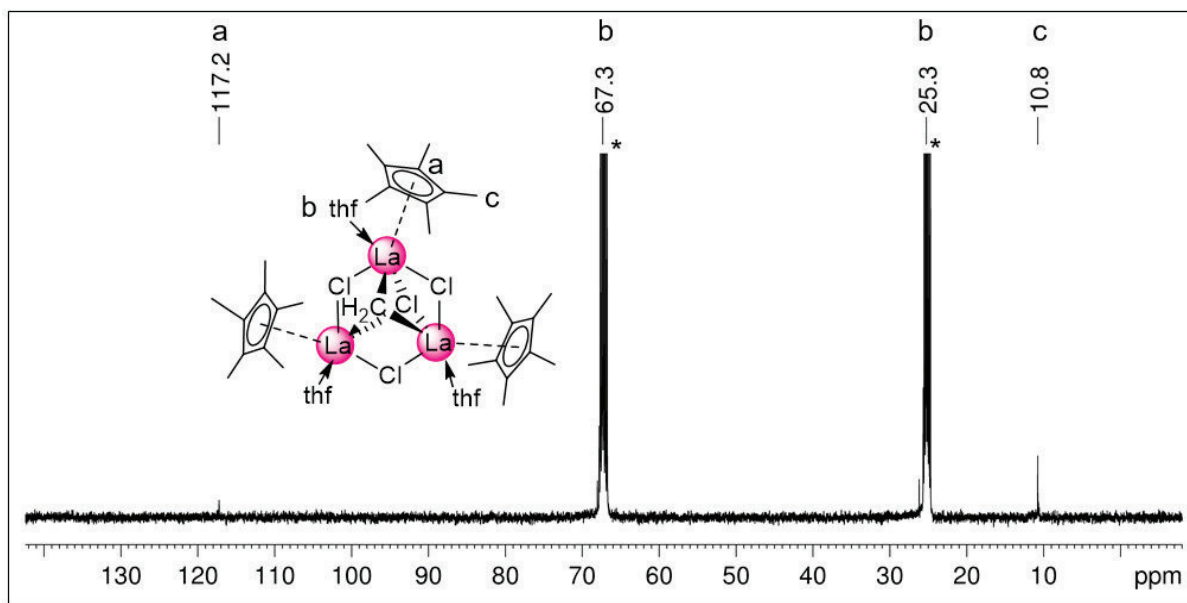


Figure S43. $^{13}\text{C}\{^1\text{H}\}$ NMR spectrum (101 MHz, $[\text{D}_8]\text{thf}$) of complex $4^*\text{-La}^{\text{Cl}}$ at 26 °C. ^{13}C resonances for the CH_2 group could not be detected.

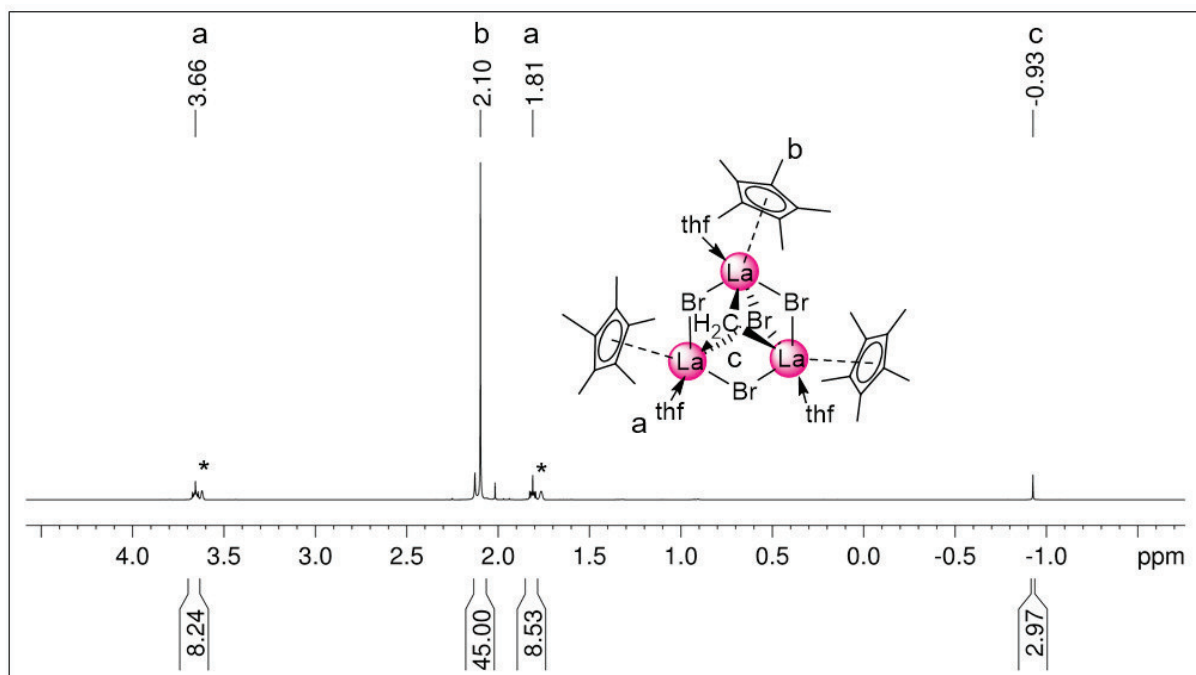


Figure S44. ^1H NMR spectrum (400 MHz, $[\text{D}_8]\text{thf}$) of complex $4^*\text{-La}^{\text{Br}}$ at 26 °C.

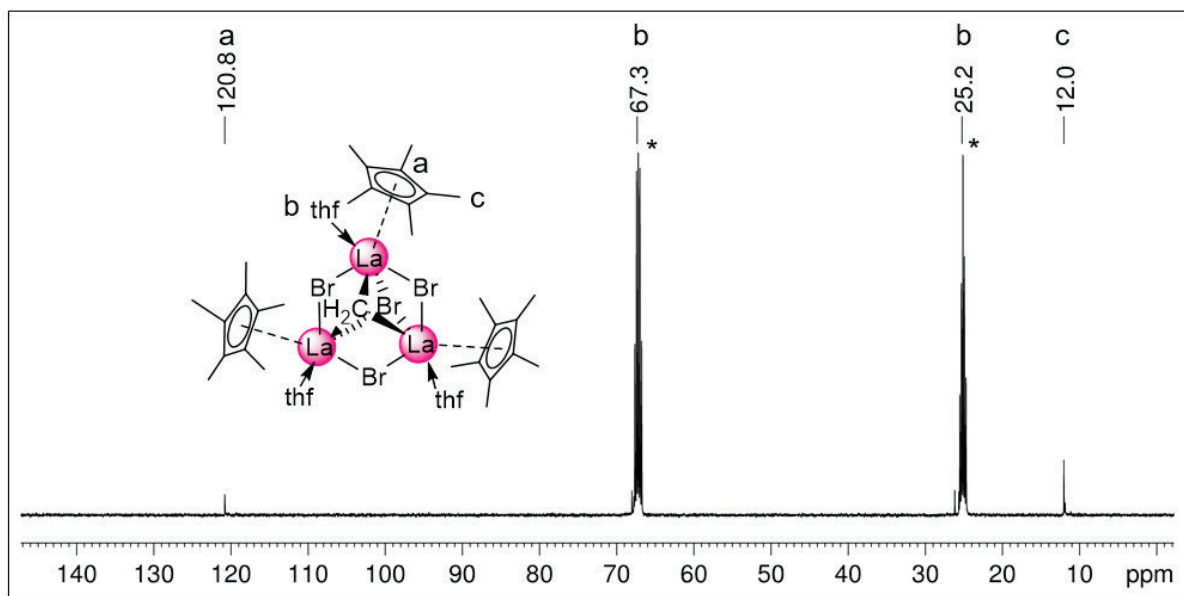


Figure S45. $^{13}\text{C}\{^1\text{H}\}$ NMR spectrum (101 MHz, $[\text{D}_8]\text{thf}$) of complex $4^*\text{-La}^{\text{Br}}$ at 26 °C. ^{13}C resonances for the CH_2 group could not be detected.

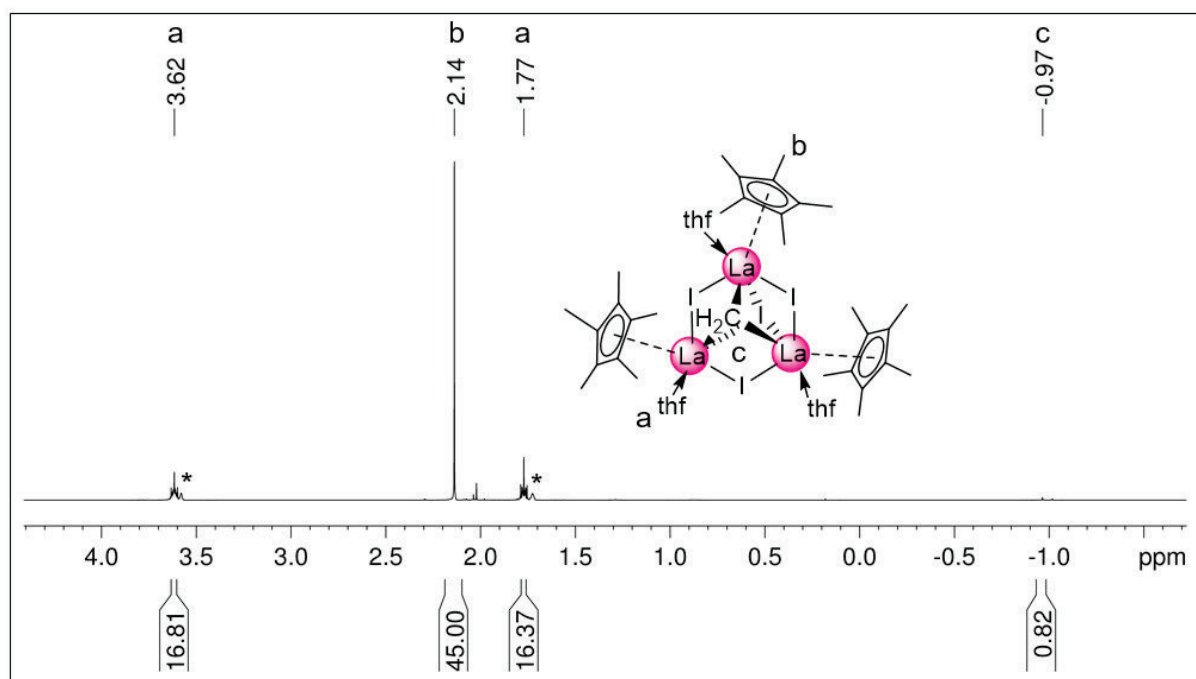


Figure S46. ^1H NMR spectrum (400 MHz, $[\text{D}_8]\text{thf}$) of complex 4^*-La^{I} at 26 °C.

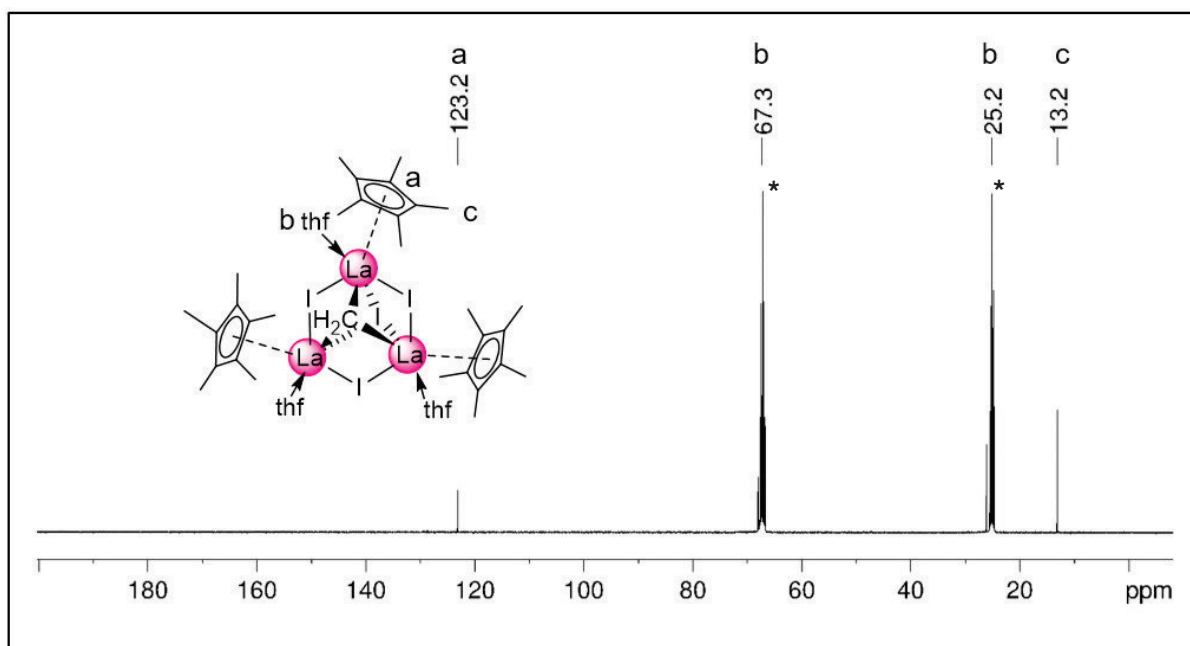


Figure S47. $^{13}\text{C}\{^1\text{H}\}$ NMR spectrum (101 MHz, $[\text{D}_8]\text{thf}$) of complex 4^*-La^{I} at 26 °C. ^{13}C resonances for the CH_2 group could not be detected.

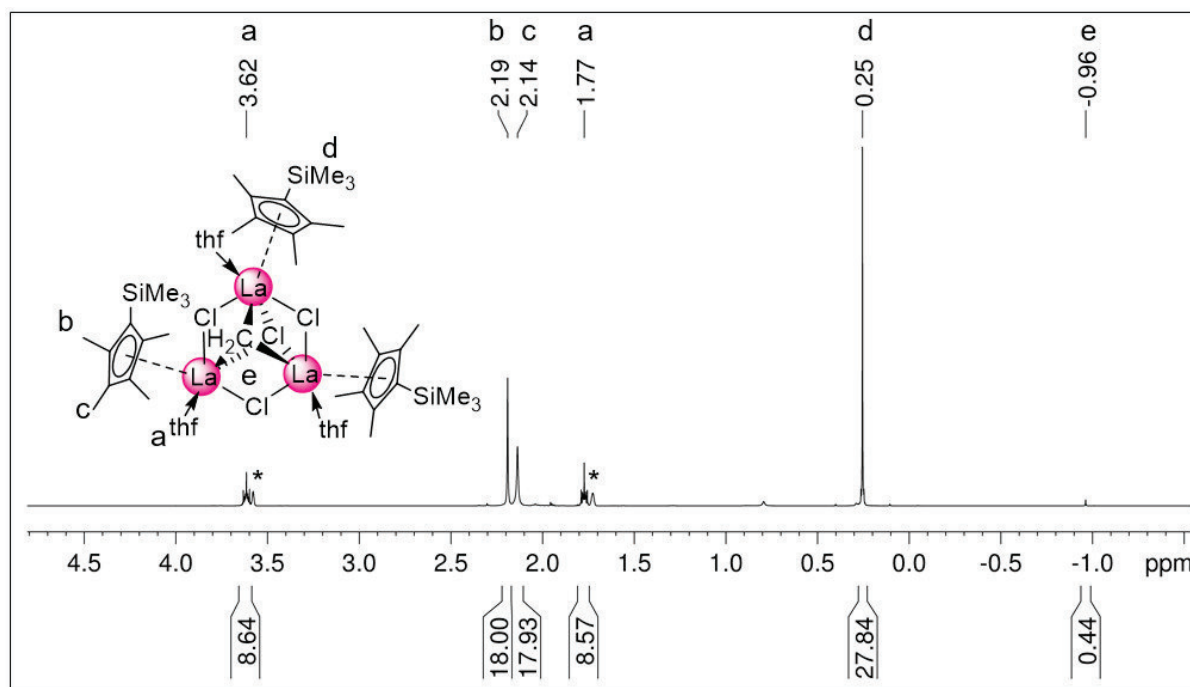


Figure S48. ^1H NMR spectrum (400 MHz, $[\text{D}_8]\text{thf}$) of complex $4^{\prime}\text{-La}^{\text{Cl}}$ at 26 °C.

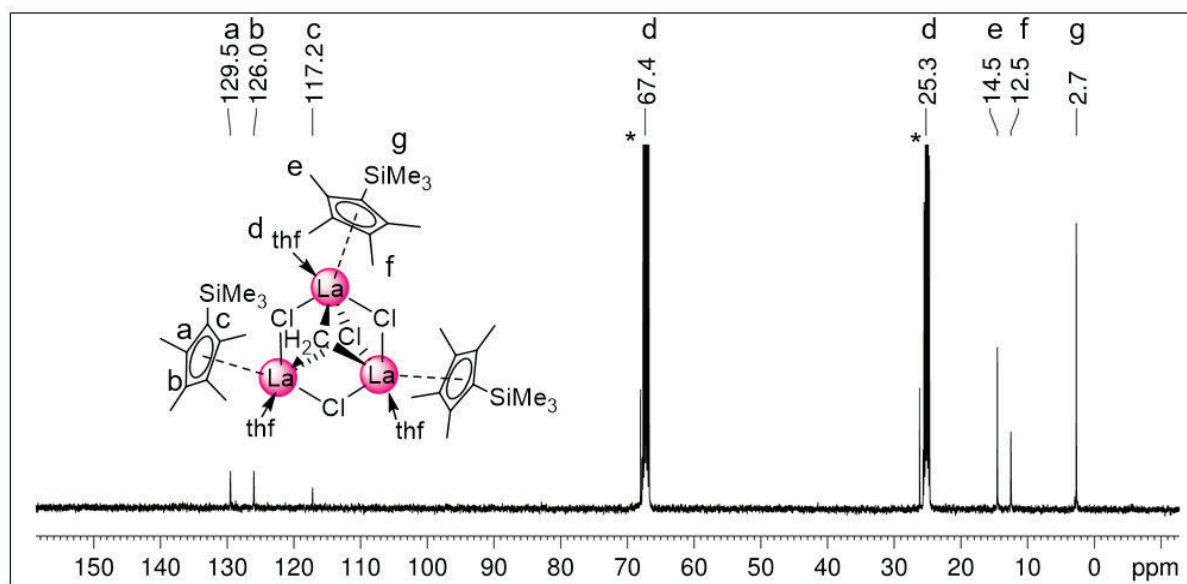


Figure S49. $^{13}\text{C}\{^1\text{H}\}$ NMR spectrum (101 MHz, $[\text{D}_8]\text{thf}$) of complex $4'\text{-La}^{\text{Cl}}$ at 26 °C. ^{13}C resonances for the CH_2 group could not be detected.

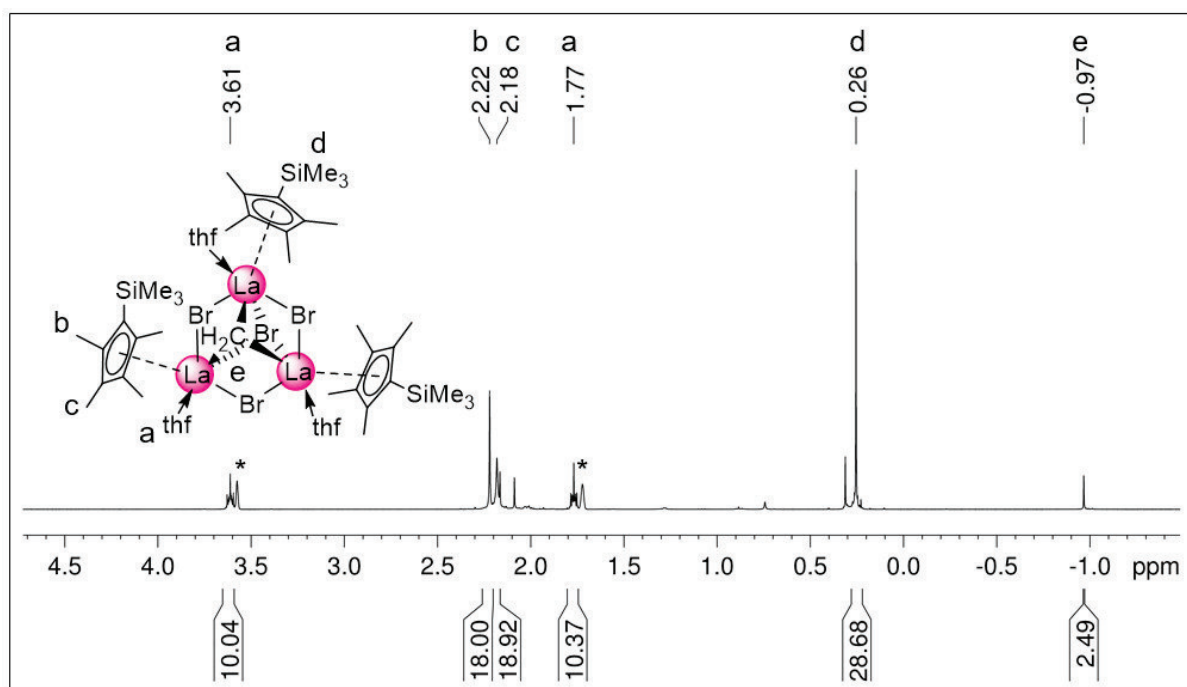


Figure S50. ^1H NMR spectrum (400 MHz, $[\text{D}_8]\text{thf}$) of complex $4'\text{-La}^{\text{Br}}$ at 26 °C.

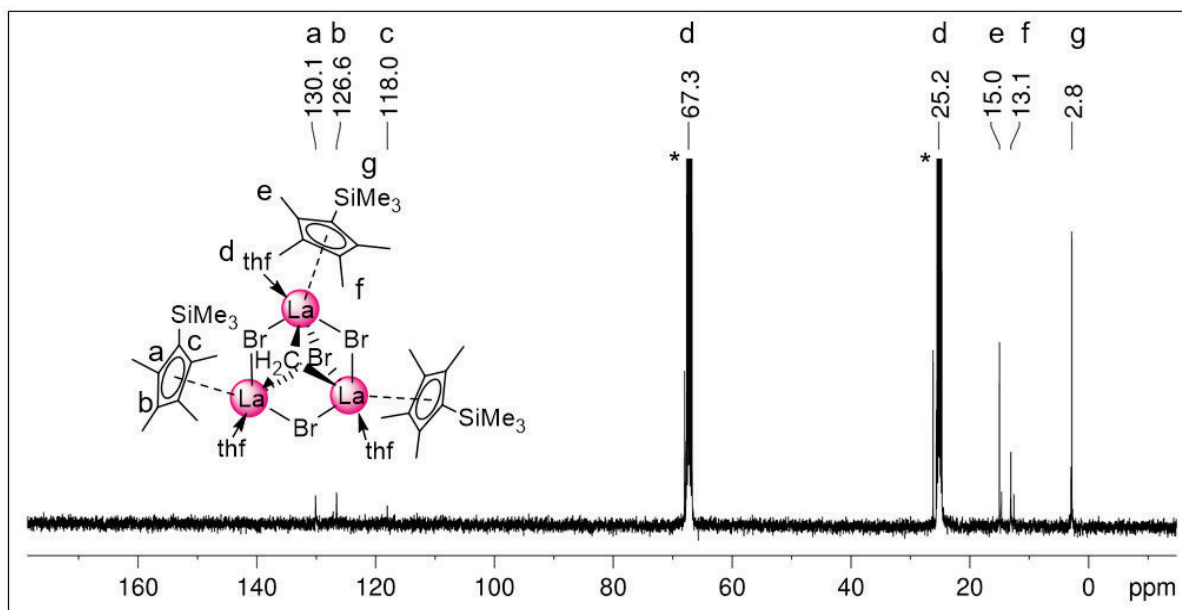


Figure S51. $^{13}\text{C}\{^1\text{H}\}$ NMR spectrum (101 MHz, $[\text{D}_8]\text{thf}$) of complex $4'\text{-La}^{\text{Br}}$ at 26 °C. ^{13}C resonances for the CH_2 group could not be detected.

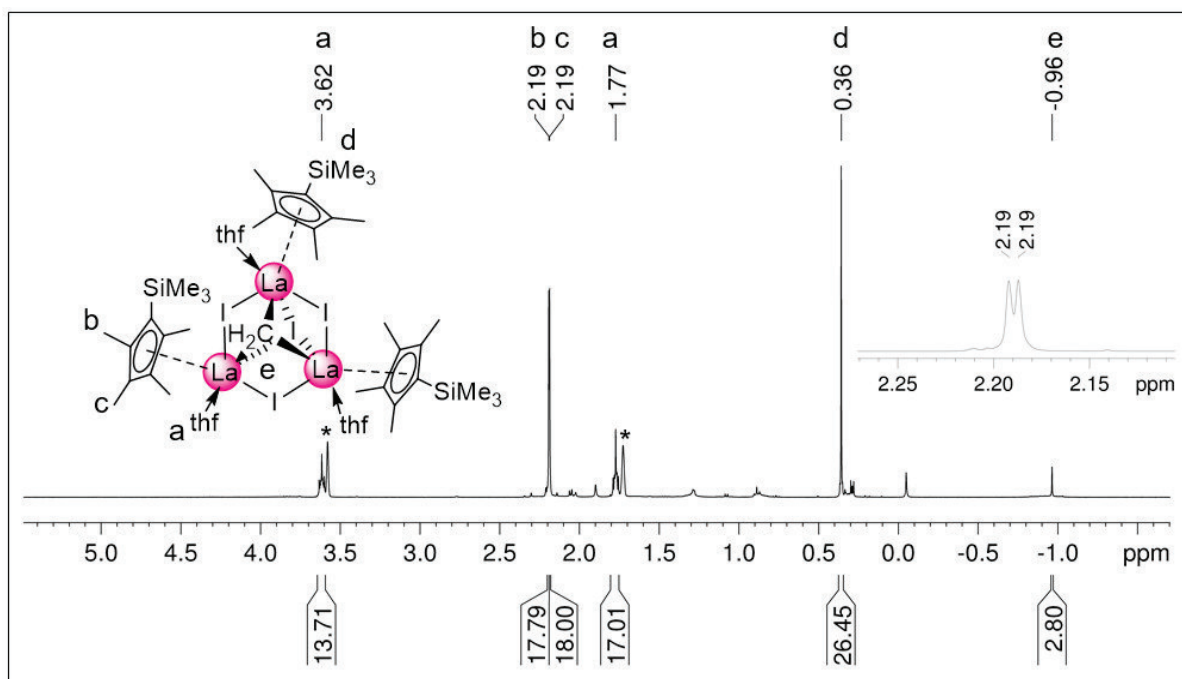


Figure S52. ^1H NMR spectrum (400 MHz, $[\text{D}_8]\text{thf}$) of complex $4'\text{-La}^{\text{I}}$ at 26 °C.

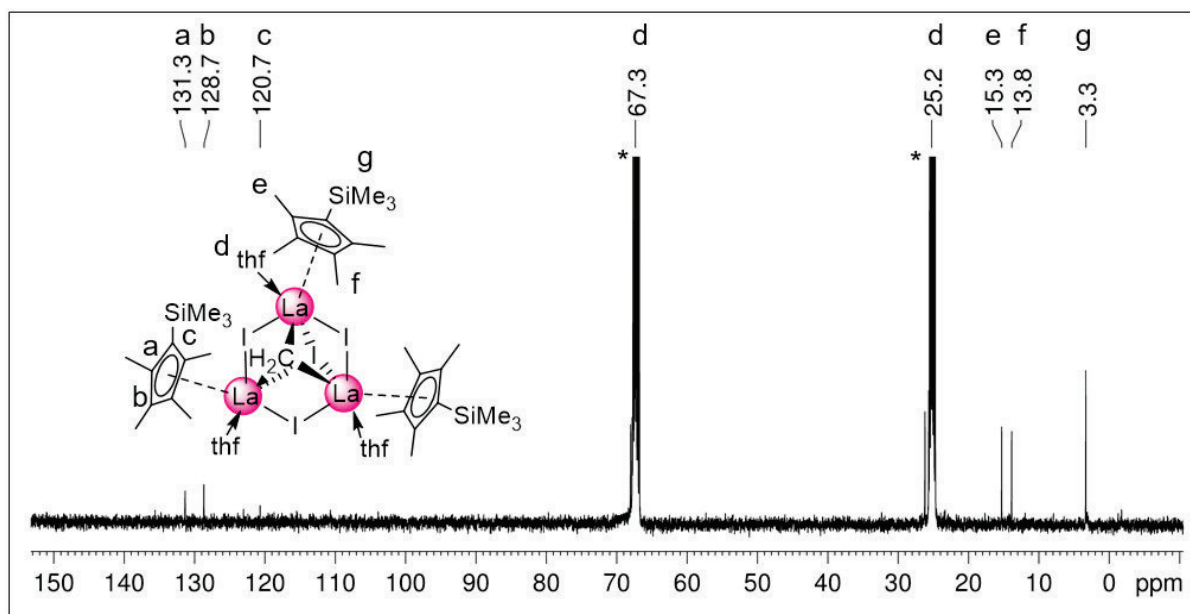


Figure S53. $^{13}\text{C}\{^1\text{H}\}$ NMR spectrum (101 MHz, $[\text{D}_3]\text{thf}$) of complex **4'-La^I** at 26 °C. ^{13}C resonances for the CH_2 group could not be detected.

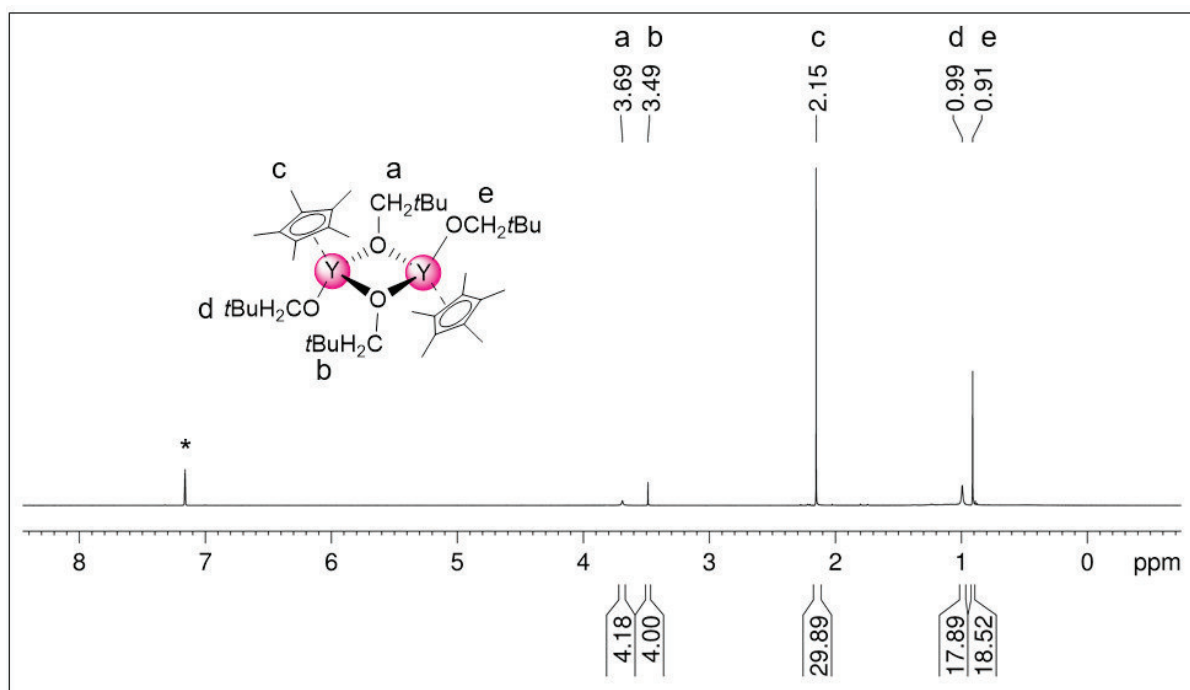


Figure S54. ^1H NMR spectrum (500 MHz, $[\text{D}_6]\text{benzene}$) of complex **5*-Y** at 26 °C.

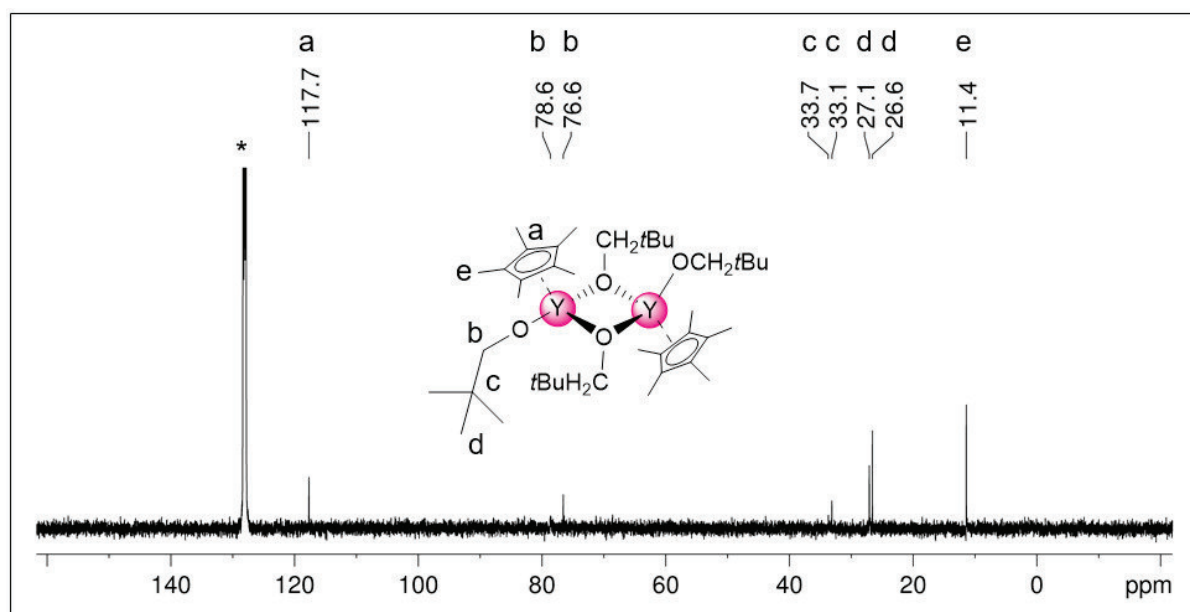


Figure S55. $^{13}\text{C}\{^1\text{H}\}$ NMR spectrum (101 MHz, $[\text{D}_6]$ benzene) of complex 5^*-Y at 26 °C.

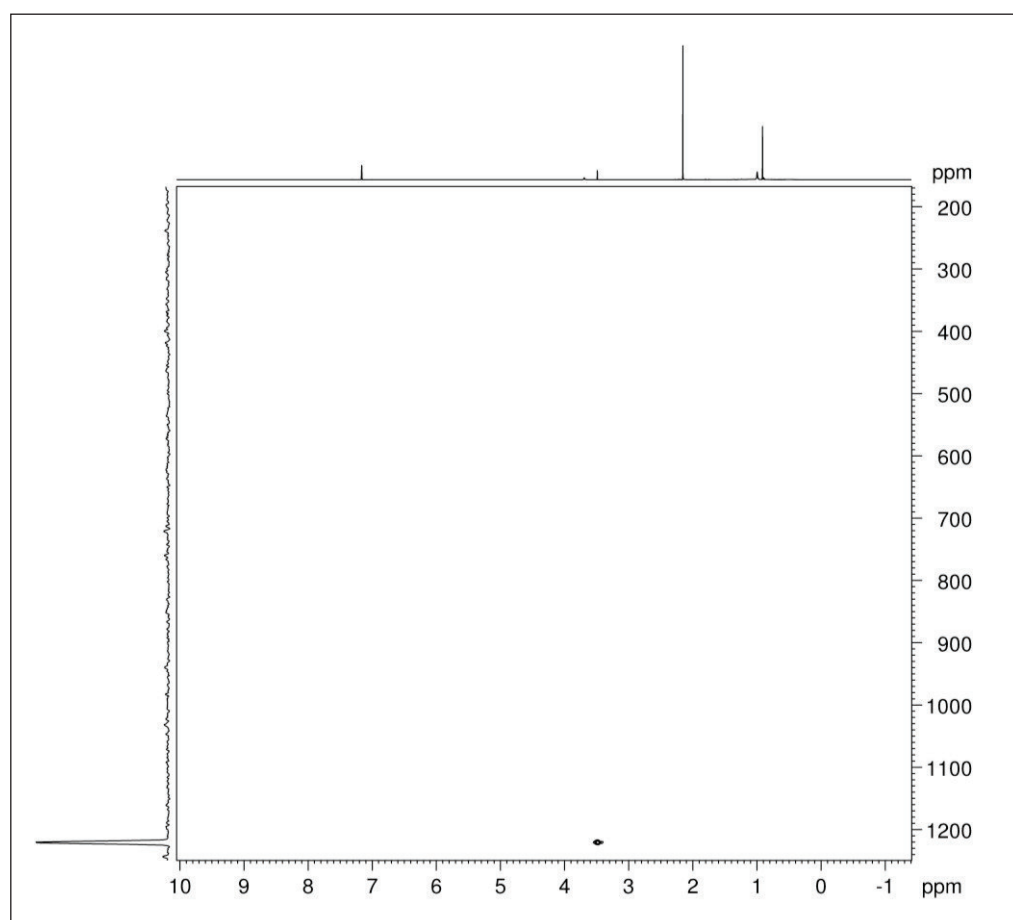


Figure S56. $^1\text{H}\text{-}^{89}\text{Y}$ HSQC NMR spectrum (25 MHz, $[\text{D}_6]$ benzene) of complex 5^*-Y at 26 °C.

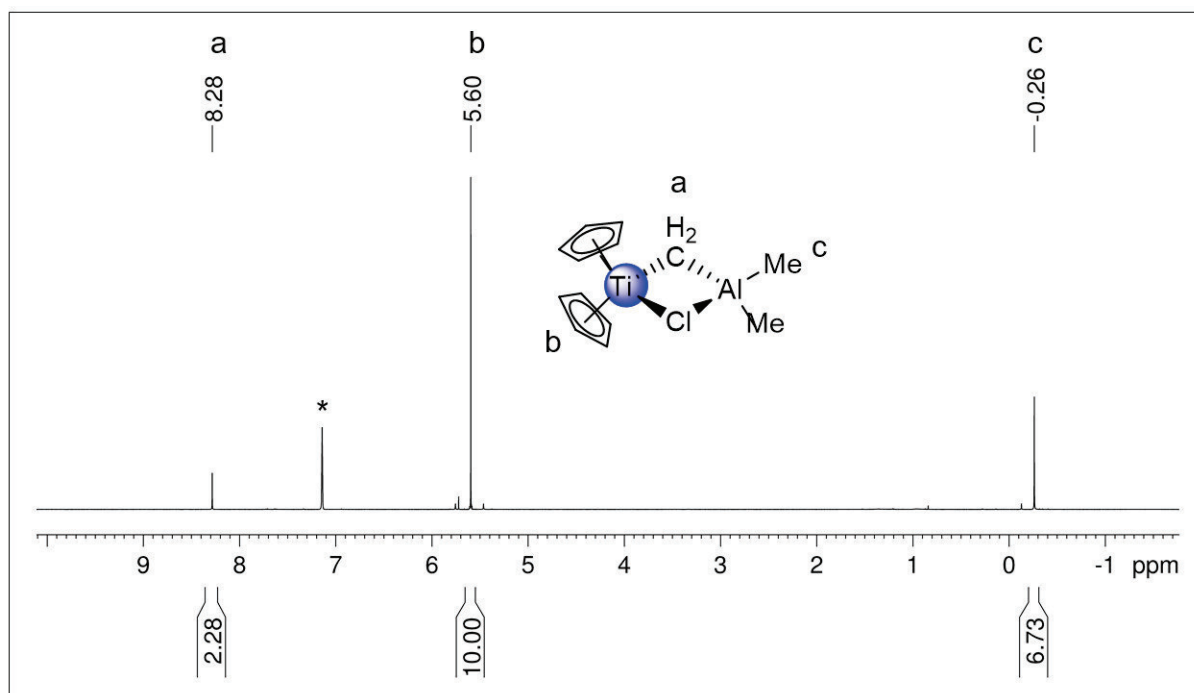


Figure S57. ^1H NMR spectrum (400 MHz, $[\text{D}_6]$ benzene) of the **Tebbe reagent** at 26 $^\circ\text{C}$.

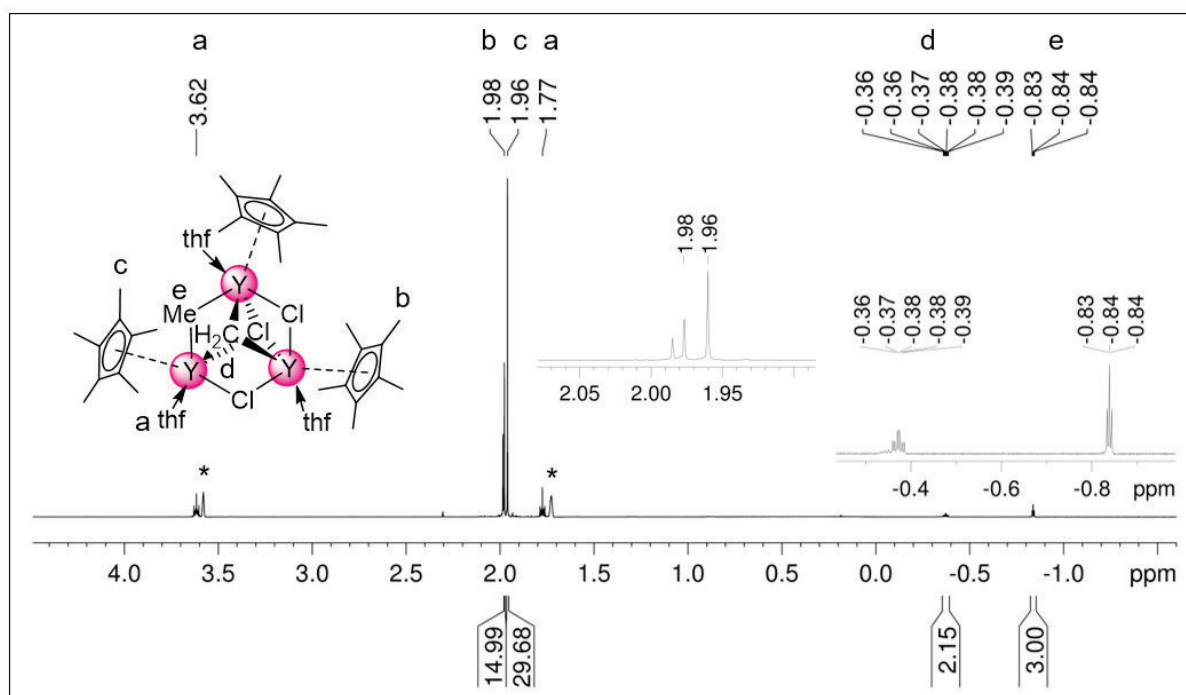


Figure S58. ^1H NMR spectrum (400 MHz, $[\text{D}_6]$ thf) of complex $(\text{C}_5\text{Me}_5)_3\text{Y}_3(\mu\text{-CH}_3)(\mu\text{-Cl})_2(\mu_3\text{-Cl})(\mu_3\text{-CH}_2)(\text{thf})_3$ at 26 $^\circ\text{C}$.

Reactivity studies

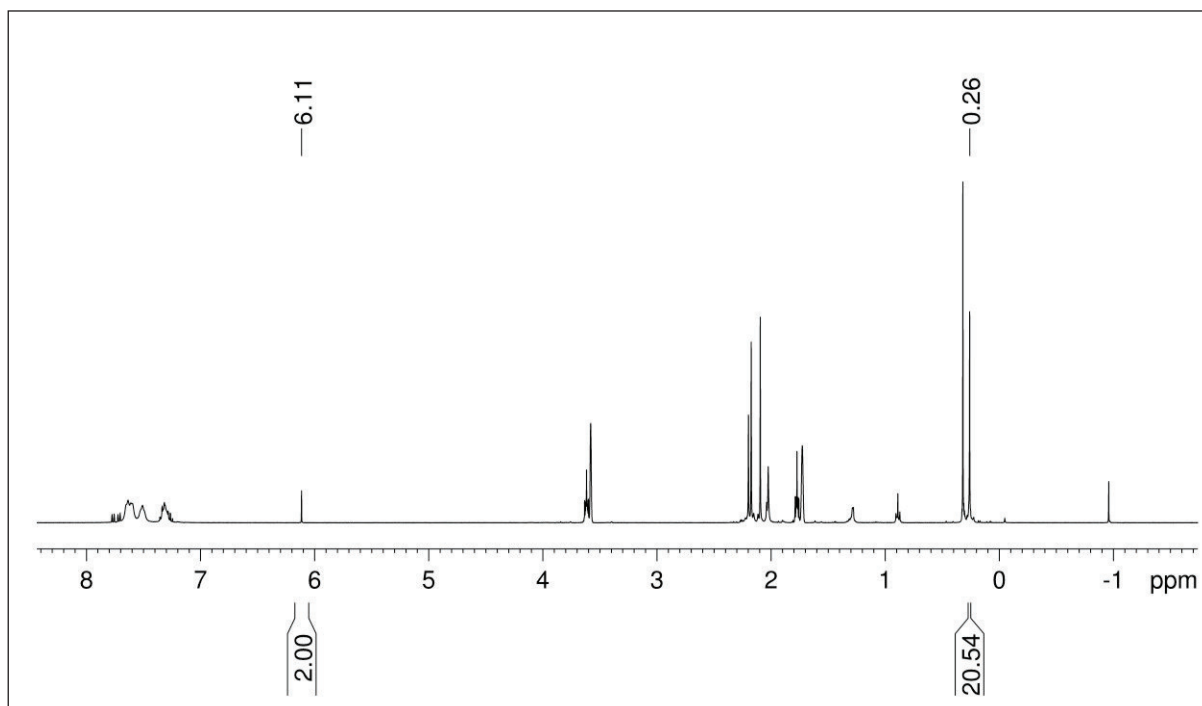
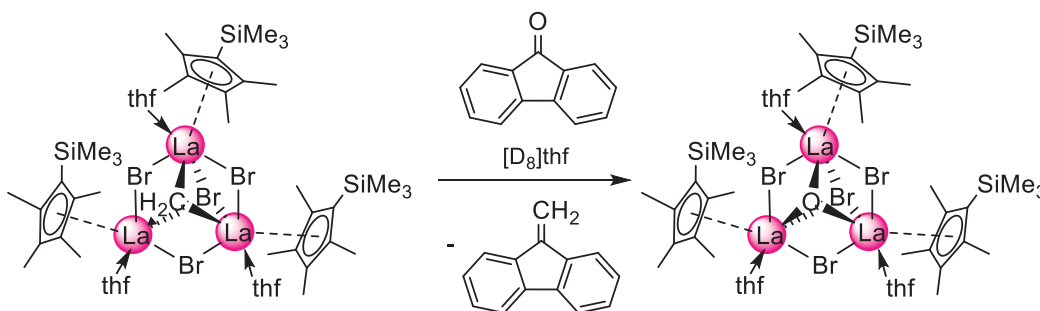
Methylidene transfer:

All reactions were monitored *via* ^1H NMR spectroscopy and performed according to the following protocol:

The respective methylidene complex (5 mg) was dissolved in 0.3 ml of $[\text{D}_8]\text{thf}$ in a J.Young-valved NMR tube. Two equivalents of the carbonylic reagent dissolved in 0.2 ml of $[\text{D}_8]\text{thf}$ were added. The NMR tube was shaken several times within 15 min and then a Proton NMR was immediately recorded. The yields of all reactions were calculated from the integral ratio olefinic functionality/ Cp^{R} ($\text{CH}_2/\text{Cp}-\text{Me}$ or $\text{CH}_2/\text{SiMe}_3$) or from the integral ratio olefinic functionality/ $\text{Y}-\text{CH}_2$ depending on the accessibility of the respective signals.

The reactivity studies with the Tebbe reagent were performed under the same conditions except the solvent. For the Tebbe reagent $[\text{D}_6]\text{benzene}$ was chosen, concerning its decomposition in thf.

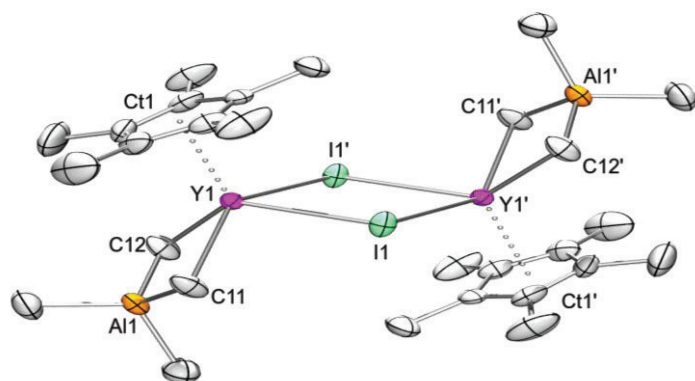
Exemplary, the reactivity of $4^{\text{r}}\text{-La}^{\text{Br}}$ with 9-fluorenone for the generation of 9-methylidene-fluorene is shown in the following.



Polymerization of δ -valerolactone:

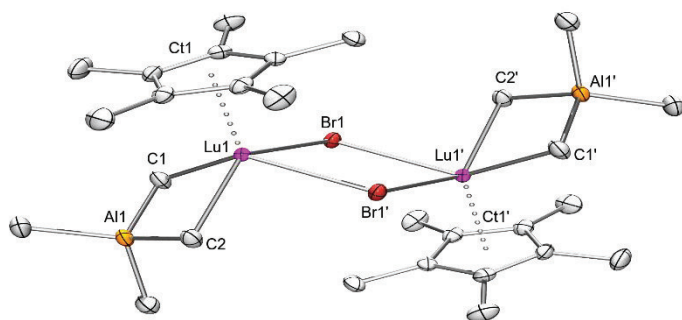
In a glovebox the respective methylidene complex (0.005 mmol) was weighed into a vial, dissolved in 2 mL of THF and δ -valerolactone (5 mmol) in 2 mL THF was added. The mixture was allowed to stir for 15 minutes. Then the vial was exposed to air and quenched with 10 ml of *n*-hexane. The mixture was allowed to stir for 30 minutes and the solvent decanted. The formed polymer was washed with *n*-hexane (3 x 5 mL) and dried. The crude poly-valerolactone (PVL) was characterized as a THF solution for GPC measurements.

X-ray structure analyses



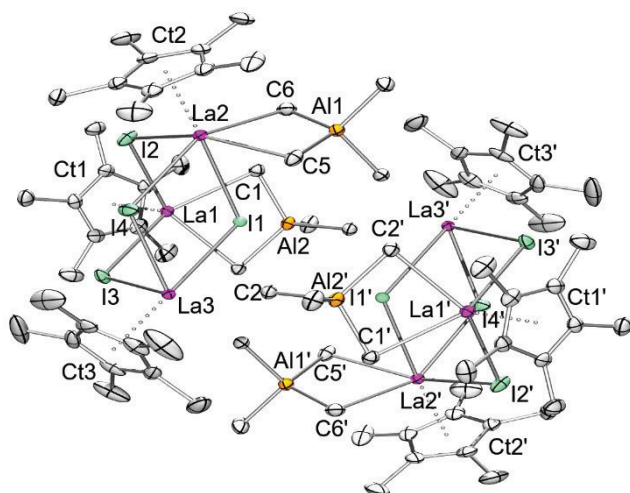
1*-Y^I	Selected bond lengths [Å]
Y1–I1/I1'	3.0695(4)/3.1016(4)
Y1–C11/C12	2.563(4)/2.529(4)
Y1–Al1	3.0902(11)
Y1–Ct1	2.305

Figure S59. ORTEP representation of the crystal structure of **1*-Lu^{Br}** with atomic displacement parameters set at the 50% level. Hydrogen atoms are omitted for clarity.



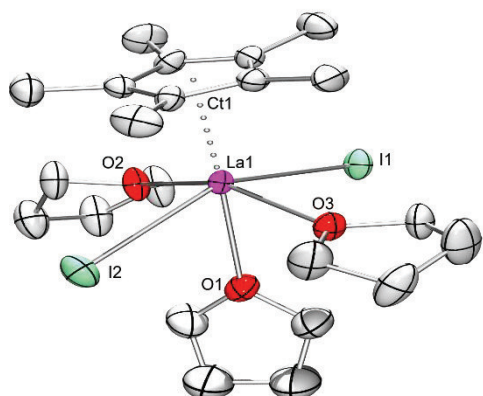
1*-Lu^{Br}	Selected bond lengths [Å]
Lu1–Br1/Br1'	2.7961(7)/2.8257(8)
Lu1–C1/C2	2.529(3)/2.486(3)
Lu1–Al1	3.0434(10)
Lu1–Ct1	2.258

Figure S60. ORTEP representation of the crystal structure of **1*-Lu^{Br}** with atomic displacement parameters set at the 50% level. Hydrogen atoms are omitted for clarity.



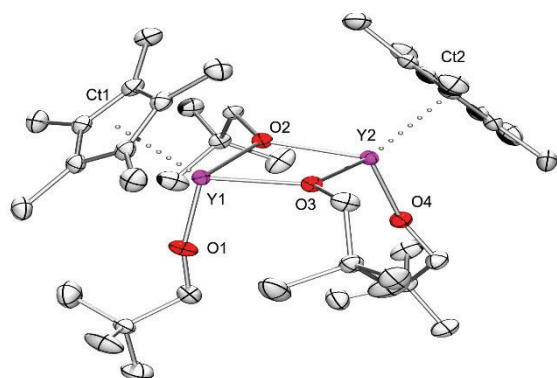
2*-La^I	Selected bond lengths [Å]
La1–I1/I2/I3	3.4366(4)/3.2327(4)/3.2470(4)
La2–I1/I2/I4	3.3981(4)/3.2379(4)/3.2605(4)
La3–I1/I3/I4	3.3455(4)/3.2323(4)/3.2096(4)
La–Ct	2.512/2.509/2.503
La1–C1/C2	2.773(4)/2.771(4)
La2–C5/C6	2.777(4)/2.771(4)
La1–Al2	3.3192(12)
La2–Al1	3.3159(12)
La3–C3'/C7'	2.954(4)/ 2.966(3)

Figure S61. ORTEP representation of the crystal structure of **2*-La^I** with atomic displacement parameters set at the 50% level. Hydrogen atoms and lattice *n*-hexane are omitted for clarity.



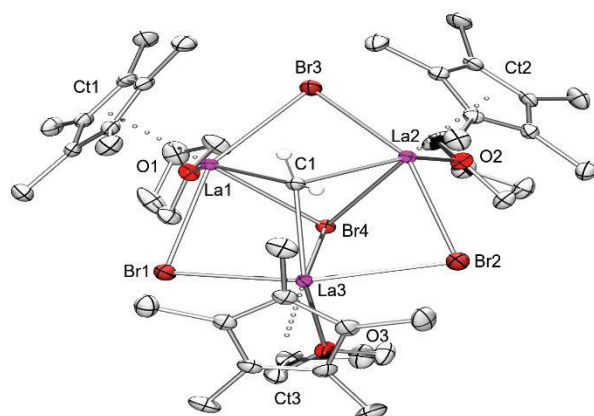
[(C₅Me₅)LaI₂(thf)₃]	Selected bond lengths [Å]
La1–I1/I2	3.1974(9)/3.2453(7)
La1–Ct1	2.540
La1–O1/O2/O3	2.629(6)/2.546(4)/2.533(4)

Figure S62. ORTEP representation of the crystal structure of **[(C₅Me₅)LaI₂(thf)₃]** with atomic displacement parameters set at the 50% level. Hydrogen atoms and the disorder in one thf molecule are omitted for clarity.



5*-Y	Selected bond lengths [Å]
Y–Ct	2.353, 2.377
Y–O1/O4	2.027(2), 2.029(2)
Y–O2/O3	2.2316(19), 2.2383(19), 2.2451(19), 2.2538(19)

Figure S63. ORTEP representation of the crystal structure of **5*-Y** with atomic displacement parameters set at the 50% level. Hydrogen atoms are omitted for clarity.



4*-La^{Br}	Selected bond lengths [Å]
La1–Br1/3/4	3.0307(5)/3.0279(4)/3.2074(4)
La2–Br2/3/4	3.0047(5)/3.0274(4)/3.1670(4)
La3–Br1/2/4	3.0307(4)/3.0385(5)/3.1849(4)
La1/2/3–CH ₂	2.572(3)/2.646(4)/2.553(3)

Figure S64. ORTEP representation of the crystal structure of **4*-La^{Br}** with atomic displacement parameters set at the 50% level. Hydrogen atoms except for CH₂ and solvent toluene are omitted for clarity.

Table S1. Comprehensive crystallographic data for compounds **1*-Y^{Br}**, **1*-Y^I**, **1*-Lu^{Br}**, and **2*-La^I**

	1*-Y^{Br}	1*-Y^I	1*-Lu^{Br}	2*-La^I
CCDC				
Formula	C ₂₈ H ₅₄ Al ₂ Br ₂ Y ₂	C ₂₈ H ₅₄ Al ₂ I ₂ Y ₂	C ₂₈ H ₅₄ Al ₂ Br ₂ Lu ₂	C ₈₈ H ₁₆₆ Al ₄ I ₈ La ₆
M [g mol ⁻¹]	782.31	876.29	954.43	3180.78
Crystal system	orthorhombic	orthorhombic	orthorhombic	triclinic
Space group	<i>Pbca</i>	<i>Pbca</i>	<i>Pbca</i>	<i>P</i>
a [Å]	9.649(4)	9.6420(3)	9.716(3)	15.1879(17)
b [Å]	14.704(6)	15.1683(4)	14.542(5)	15.4891(18)
c [Å]	25.105(10)	25.5125(7)	24.882(8)	15.6522(18)
α [°]	90	90	90	103.083(3)
β [°]	90	90	90	118.426(2)
γ [°]	90	90	90	104.865(3)
V [Å ³]	3562(2)	3731.27(18)	3515.8(19)	2854.7(6)
Z	4	4	4	1
T [K]	100(2)	100(2)	100(2)	100(2)
ρ _{calcd} [g cm ⁻³]	1.459	1.560	1.803	1.850
μ [mm ⁻¹]	5.549	4.811	7.920	4.423
F (000)	1584	1728	1840	1512
Θ range [°]	1.622-29.125	1.596-28.275	2.651-28.274	1.491-30.077
total reflns	35167	43739	65293	122186
unique reflns	4777	4630	4362	16728
R _{int}	0.0560	0.0427	0.0440	0.0781
observed reflns (I > 2σ)	3864	3858	3893	14086
Data/restraints/parameter	4777/185/0	4630/0/185	4362/185/0	16728/615/259
R1/wR2 (I > 2σ) [a]	0.0257/0.0517	0.0331/0.0609	0.0222/0.0405	0.0329/0.0798
R1/wR2 (all data) [a]	0.0401/0.0554	0.0480/0.0652	0.0177/0.0388	0.0417/0.0861
GOF [a]	1.011	1.106	1.098	1.064
largest diff. peak and hole [e Å ⁻³]	0.604 and – 0.341	0.878 and – 0.760	1.075 and – 0.626	2.204 and – 1.147

[a] R1 = $\Sigma(|F_o| - |F_c|) / \Sigma|F_o|, F_o > 4\sigma(F_o)$. wR2 = $\{\Sigma[w(F_o^2 - F_c^2)^2] / \Sigma[w(F_o^2)^2]\}^{1/2}$.

Table S1 continued. Comprehensive crystallographic data for compounds **2'-La^{Cl}**, **3*-La^{OTf}**, **4*-Y^{Br}**, and **4*-La^{Br}**.

	2'-La^{Cl}	3*-La^{OTf}	4*-Y^{Br}	4*-La^{Br}
CCDC				
Formula	C ₈₈ H ₁₇₄ Al ₄ Cl ₈ La ₆ Si ₆	C ₉₄ H ₁₄₆ Al ₂ F ₃₀ La ₆ O ₃₄ S ₁₀	C _{60.50} H ₉₁ Br ₄ Y ₃ O ₃	C _{60.50} H ₉₁ Br ₄ La ₃ O ₃
M [g mol ⁻¹]	2625.78	3598.12	1452.70	1602.70
Crystal system	monoclinic	triclinic	triclinic	triclinic
Space group	<i>C</i> 2/ <i>c</i>	<i>P</i> -1	<i>P</i>	<i>P</i>
a [Å]	34.9606(16)	14.6570(15)	14.1530(6)	14.3915(7)
b [Å]	13.4774(6)	14.9347(15)	15.8798(7)	16.0503(8)
c [Å]	26.2883(12)	18.1390(19)	16.5355(6)	16.7132(8)
α [°]	90	102.5380(10)	102.7230(10)	102.5370(10)
β [°]	106.8900(10)	103.4360(10)	114.0310(10)	114.2580(10)
γ [°]	90	96.6000(10)	105.3420(10)	104.6900(10)
V [Å ³]	11852.2(9)	3712.2(7)	3037.8(2)	3170.7(3)
Z	4	1	2	2
T [K]	150(2)	100(2)	100(2)	100(2)
ρ _{calcd} [g cm ⁻³]	1.472	1.610	1.588	1.679
μ [mm ⁻¹]	2.421	1.940	5.514	4.545
F (000)	5264	1780	1470	1578
Θ range [°]	1.217-30.172	2.954-27.103	1.433-28.282	1.408-29.209
total reflns	251615	16328	83784	130276
unique reflns	17537	16328	15065	17141
Rint	0.0653		0.0921	0.0397
observed reflns (I>2σ)	14294	12846	10729	15187
Data/restraints/parameter	17537/534/0	16328/624/1051	15065/693/95	17141/693/64
R1/wR2 (I>2σ) [a]	0.0310/0.0645	0.0461/0.0913	0.0408/0.0821	0.0385/0.0940
R1/wR2 (all data) [a]	0.0461/0.0722	0.0763/0.1084	0.0744/0.0935	0.0323/0.0904
GOF [a]	1.108	1.077	1.023	1.054
largest diff. peak and hole [e Å ⁻³]	1.314 and -0.695	2.227 and -1.955	1.566 and -0.913	1.366 and -2.902

[a] R1 = $\Sigma(|F_o| - |F_c|) / \Sigma|F_o|, F_o > 4\sigma(F_o)$. wR2 = $\{\Sigma[w(F_o^2 - F_c^2)^2] / \Sigma[w(F_o^2)^2]\}^{1/2}$.

Table S1 continued. Comprehensive crystallographic data for compounds **4'-La^{Cl}**, **[(C₅Me₅)LaI₂(thf)₃]**, **5*-Y**, and the **Tebbe reagent**.

	4'-La^{Cl}	[(C₅Me₅)LaI₂(thf)₃]	5*-Y	Tebbe reagent
CCDC				
Formula	C _{60.50} H ₉₁ Cl _{2.50} La ₃ O _{1.50} Si ₂	C ₂₂ H ₃₉ I ₂ LaO ₃	C ₄₀ H ₇₄ O ₄ Y ₂	C _{32.85} H _{43.70} Al ₂ Cl _{2.15} Ti ₂
M [g mol ⁻¹]	592.55	744.24	796.81	664.55
Crystal system	triclinic	trigonal	monoclinic	monoclinic
Space group	<i>P</i> -1	<i>R</i> -3:H	<i>P</i> 21/ <i>c</i>	<i>C</i> 2/ <i>c</i>
a [Å]	15.2944(6)	42.437(13)	11.8884(13)	22.2702(13)
b [Å]	16.6590(7)	42.437	17.8190(18)	11.8790(7)
c [Å]	16.8144(7)	9.155(3)	20.366(2)	15.1179(17)
α [°]	119.0030(10)	90	90	90
β [°]	91.5250(10)	90	99.491(2)	125.5250(10)
γ [°]	108.6950(10)	120	90	90
V [Å ³]	3462.5(2)	14278(10)	4255.2(8)	3255.0(5)
Z	2	18	4	4
T [K]	100(2)	160(2)	100(2)	100(2)
ρ _{calcd} [g cm ⁻³]	0.568	1.558	1.244	1.356
μ[mm ⁻¹]	1.939	3.307	2.748	0.742
F (000)	515	6444	1696	1389
Θ range [°]	1.643-28.282	0.960-25.022	2.079-26.411	2.186 to 30.072
total reflns	152989	24793	82006	38797
unique reflns	17172	5617	8700	4771
R _{int}	0.0319	0.1211	0.1141	0.0413
observed reflns (I>2σ)	15005	3643	5897	4340
Data/restraints/parameter	17172/1978/810	5617/494/304	8700/0/437	4771/0/193
R1/wR2 (I>2σ) [a]	0.0353/0.0866	0.0353/0.0639	0.0382/0.0754	0.0294/0.0762
R1/wR2 (all data)[a]	0.0426/0.0939	0.0669/0.0713	0.0763/0.0888	0.0326/0.0790
GOF[a]	1.038	0.803	1.004	1.041
largest diff. peak and hole [e Å ⁻³]	2.331 and -2.279	0.712 and -0.760	0.427 and -0.426	0.429 and -0.288

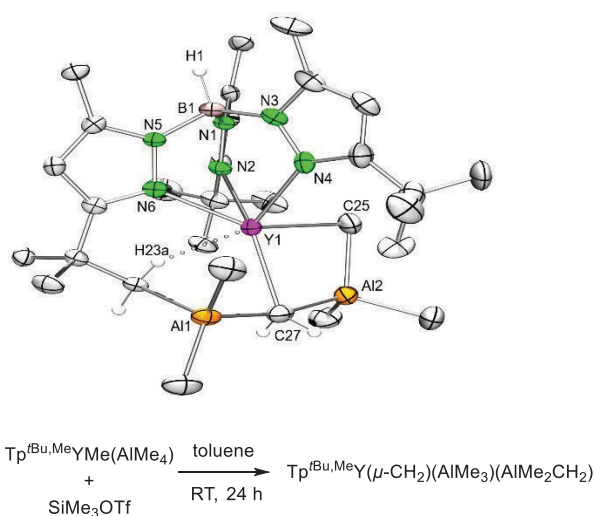
[a] R1 = $\Sigma(|F_o| - |F_c|) / \Sigma|F_o|, F_o > 4\sigma(F_o)$. wR2 = $\{\Sigma[w(F_o^2 - F_c^2)^2] / \Sigma[w(F_o^2)^2]\}^{1/2}$.

F

Appendix

Appendix

Analytical data of compounds not included in the main results or manuscripts



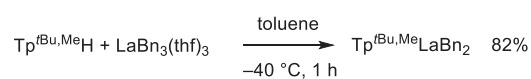
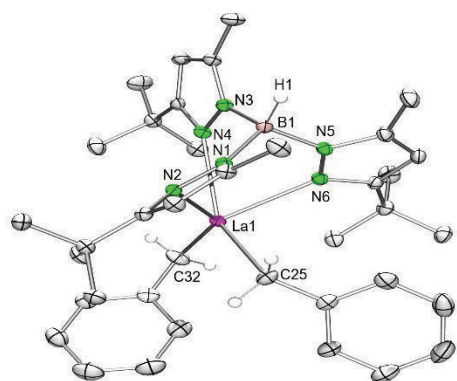
$\text{Tp}^{\text{tBu,Me}}\text{Y}(\mu\text{-CH}_2)(\text{AlMe}_3)(\text{AlMe}_2\text{CH}_2)$ VB-324A
Serendipitous finding

$R_1[\text{I} > \sigma(\text{I})]$ 5.80%, $wR_2(\text{all data})$ 13.39%

$a = 12.0899(17) \text{ \AA}$, $\alpha = 90^\circ$

$b = 35.475(5) \text{ \AA}$, $\beta = 109.581(3)^\circ$

$c = 10.1556(14) \text{ \AA}$, $\gamma = 90^\circ$



$\text{Tp}^{\text{tBu,Me}}\text{LaBn}_2$ VB-328

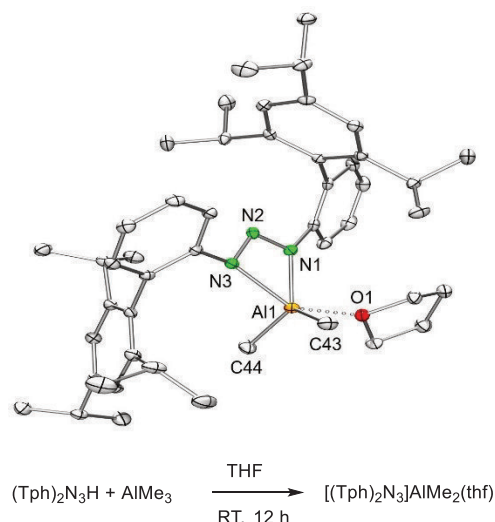
$R_1[\text{I} > \sigma(\text{I})]$ 3.05%, $wR_2(\text{all data})$ 7.68%

$a = 17.275(2) \text{ \AA}$, $\alpha = 90^\circ$

$b = 11.4136(13) \text{ \AA}$, $\beta = 105.182(2)^\circ$

$c = 19.647(2) \text{ \AA}$, $\gamma = 90^\circ$

Additional analyses: ^1H NMR, ^{11}B NMR



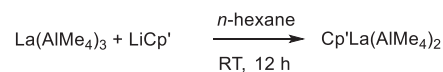
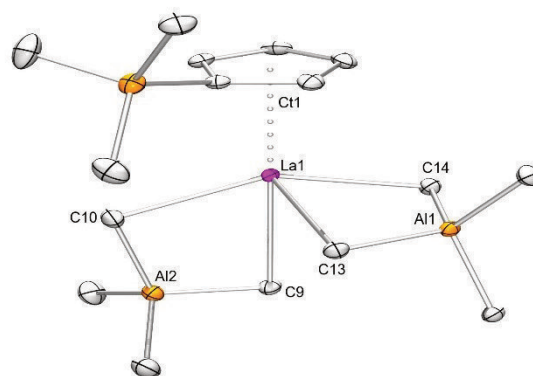
$[(\text{Tph})_2\text{N}_3]\text{AlMe}_2(\text{thf})$ VB-51

$R_1[\text{I} > \sigma(\text{I})]$ 3.92%, $wR_2(\text{all data})$ 10.05%

$a = 9.0383(2) \text{ \AA}$, $\alpha = 92.453(2)^\circ$

$b = 10.7498(3) \text{ \AA}$, $\beta = 95.5340(10)^\circ$

$c = 26.6079(7) \text{ \AA}$, $\gamma = 111.3010(10)^\circ$



$\text{Cp}'\text{La}(\text{AlMe}_4)_2$ VB-118

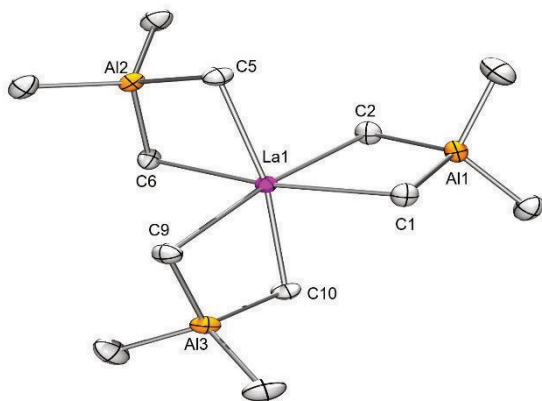
$R_1[\text{I} > \sigma(\text{I})]$ 1.65%, $wR_2(\text{all data})$ 3.91%

$a = 9.490(3) \text{ \AA}$, $\alpha = 90^\circ$

$b = 20.227(7) \text{ \AA}$, $\beta = 110.153(6)^\circ$

$c = 12.819(4) \text{ \AA}$, $\gamma = 90^\circ$

Additional analyses: ^1H NMR, ^{13}C NMR



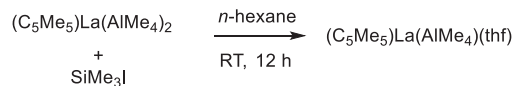
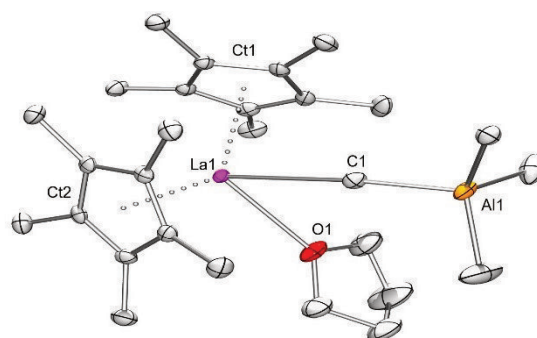
La(AlMe₄)₃ VB-84

R₁[I>sigma(I)] 1.85%, wR₂(all data) 4.20%

a = 17.7818(18) Å, α = 90°

b = 18.2278(18) Å, β = 108.3444(13)°

c = 13.7359(14) Å, γ = 90°



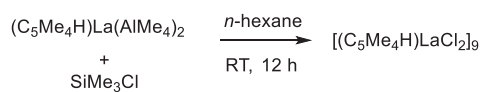
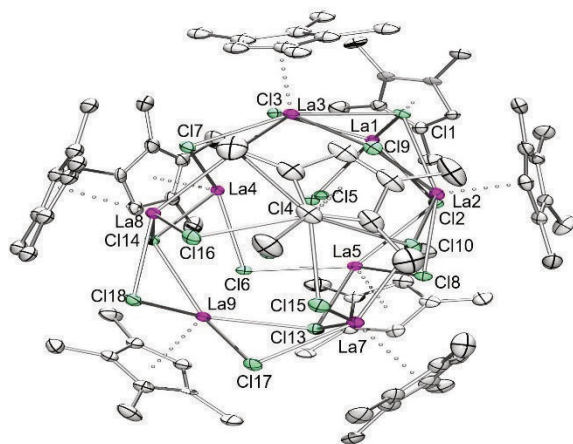
(C₅Me₅)La(AlMe₄)(thf) VB-100_2
Serendipitous finding

R₁[I>sigma(I)] 2.74%, wR₂(all data) 5.53%

a = 18.808(16) Å, α = 90°

b = 8.677(7) Å, β = 113.609(11)°

c = 19.029(16) Å, γ = 90°



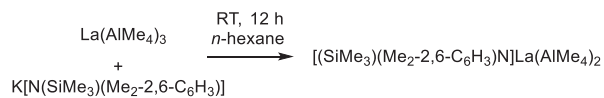
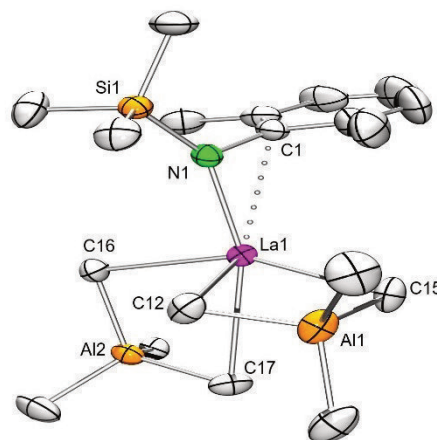
[(C₅Me₄H)LaCl₂]₉ VB-143

R₁[I>sigma(I)] 5.72%, wR₂(all data) 16.77%

a = 44.546(2) Å, α = 90°

b = 14.9053(8) Å, β = 90°

c = 25.5401(13) Å, γ = 90°



[(SiMe₃)(Me₂-2,6-C₆H₃)N]La(AlMe₄)₂ VB-63_02

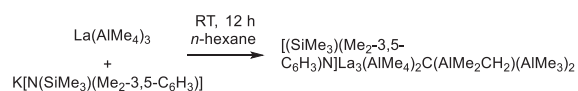
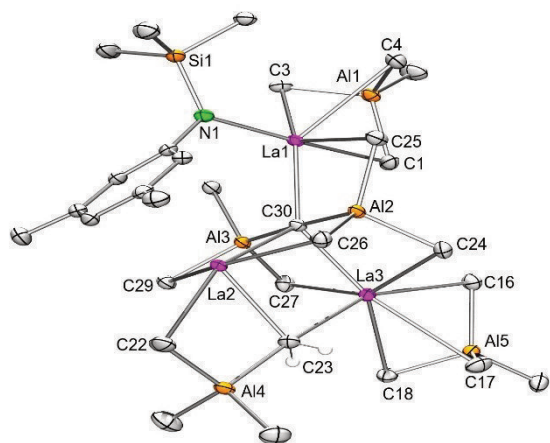
R₁[I>sigma(I)] 1.99%, wR₂(all data) 4.83%

a = 10.132(3) Å, α = 90°

b = 12.890(3) Å, β = 102.684(5)°

c = 20.586(5) Å, γ = 90°

Additional analyses: ¹H NMR, EA



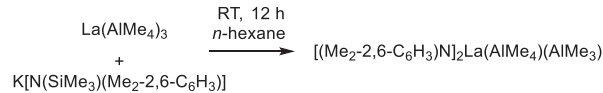
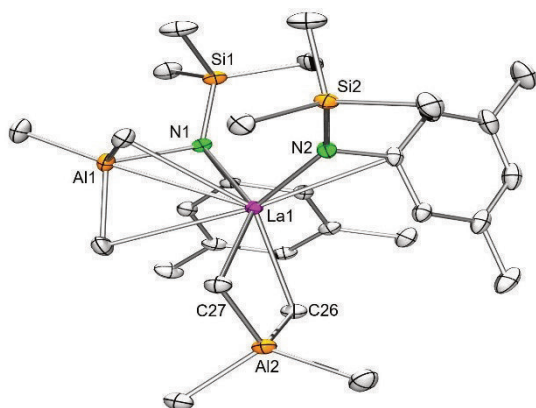
VB 169_01 $[(\text{SiMe}_3)(\text{Me}_2\text{-}3,5\text{-C}_6\text{H}_3)\text{N}]_2\text{La}_3(\text{AlMe}_4)_2\text{C}(\text{AlMe}_2\text{CH}_2)(\text{AlMe}_3)_2$
Serendipitous finding

$R_1[\text{I} > \sigma(\text{I})]$ 2.35%, $wR_2(\text{all data})$ 5.25%

$a = 10.639(3) \text{ \AA}$, $\alpha = 91.553(6)^\circ$

$b = 14.127(4) \text{ \AA}$, $\beta = 106.460(7)^\circ$

$c = 16.197(5) \text{ \AA}$, $\gamma = 105.528(9)^\circ$



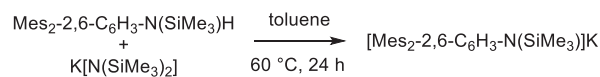
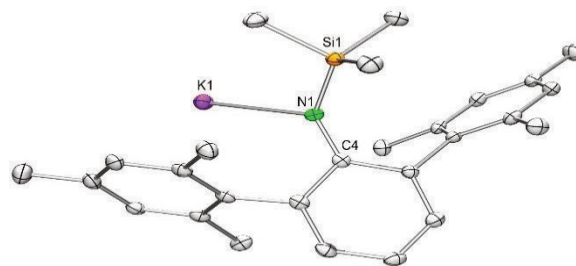
$[(\text{Me}_2\text{-}2,6\text{-C}_6\text{H}_3)\text{N}]_2\text{La}(\text{AlMe}_4)(\text{AlMe}_3)$ VB-169_02
Serendipitous finding

$R_1[\text{I} > \sigma(\text{I})]$ 1.53%, $wR_2(\text{all data})$ 3.87%

$a = 12.5093(4) \text{ \AA}$, $\alpha = 90^\circ$

$b = 17.8012(5) \text{ \AA}$, $\beta = 91.7610(10)^\circ$

$c = 16.2480(5) \text{ \AA}$, $\gamma = 90^\circ$



$[\text{Mes}_2\text{-}2,6\text{-C}_6\text{H}_3\text{N}(\text{SiMe}_3)]\text{K}$ VB-188

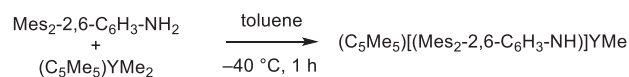
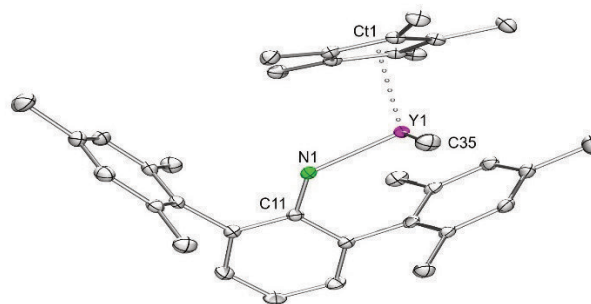
$R_1[\text{I} > \sigma(\text{I})]$ 3.61%, $wR_2(\text{all data})$ 8.12%

$a = 25.3050(18) \text{ \AA}$, $\alpha = 90^\circ$

$b = 6.9947(5) \text{ \AA}$, $\beta = 90^\circ$

$c = 13.7134(10) \text{ \AA}$, $\gamma = 90^\circ$

Additional analyses: ^1H NMR, ^{29}Si NMR



$(\text{C}_5\text{Me}_5)[\text{Mes}_2\text{-}2,6\text{-C}_6\text{H}_3\text{N}(\text{SiMe}_3)]\text{YMe}$ VB-317

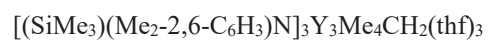
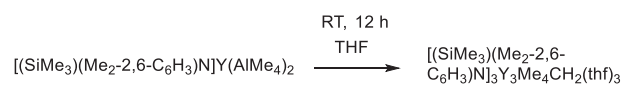
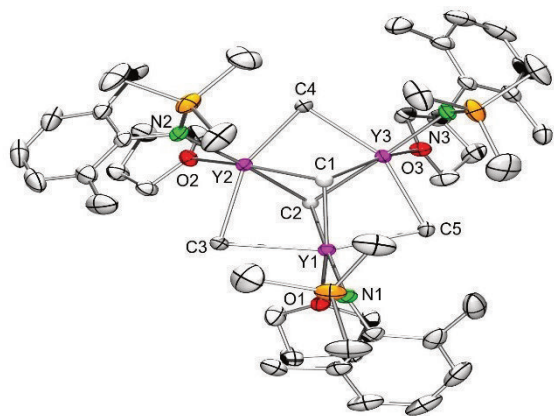
$R_1[\text{I} > \sigma(\text{I})]$ 2.88%, $wR_2(\text{all data})$ 7.45%

$a = 10.1825(16) \text{ \AA}$, $\alpha = 90^\circ$

$b = 20.765(3) \text{ \AA}$, $\beta = 91.466(3)^\circ$

$c = 14.084(2) \text{ \AA}$, $\gamma = 90^\circ$

Additional analyses: ^1H NMR



VB-170

R₁[I>sigma(I)] 2.14%, wR₂(all data) 4.93%

a = 21.1598(16) Å, α = 90°

b = 21.1598(16) Å, β = 90°

c = 11.3203(9) Å, γ = 120°

Additional analyses: ¹H NMR, EA

Curriculum Vitae

Personal Details

Name: Verena Margareta Birkelbach

Date of Birth: November 06, 1991

Place of Birth: Forchheim, Germany

Nationality: German

Education

Nov. 2015 – Nov. 2019 PhD studies
Eberhard Karls Universität Tübingen

Sep. 2013 – Sep. 2015 Study of Chemistry (Master of Science)
Friedrich-Alexander Universität Erlangen
Master thesis: “Well-defined Molecular Alumoxanes: Modeling
Structural Aspects of MAO”
Supervisor: Prof. Dr. Sjoerd Harder

May 2011 – Aug. 2013 Study of Chemistry (Bachelor of Science)
Regular Progress of Semesters 3-6
Fast track 2in1 Bachelor studies of Semesters 1 and 2
Bachelor thesis: “Synthetische und Sensorische
Charakterisierung von Terpenithioethern”
Supervisor: Prof. Dr. Andrea Büttner

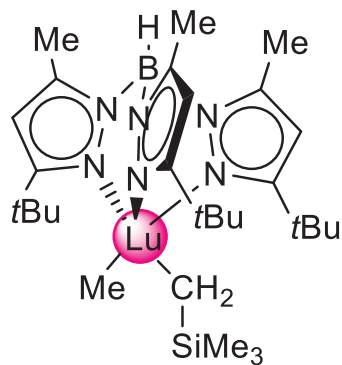
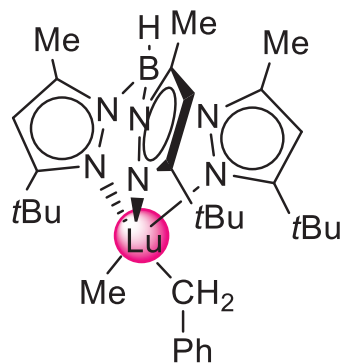
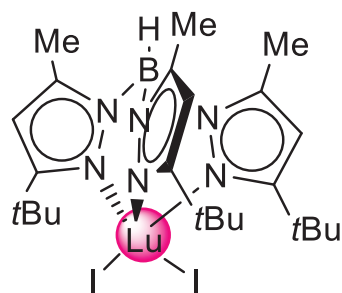
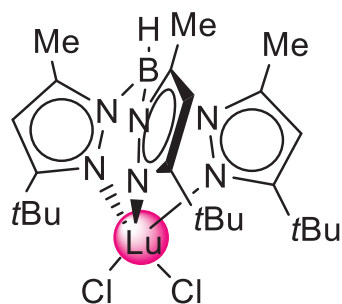
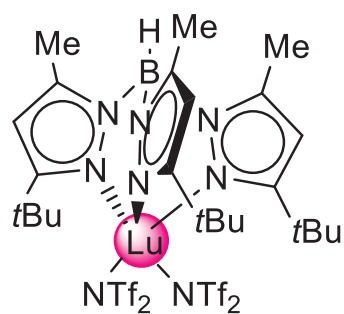
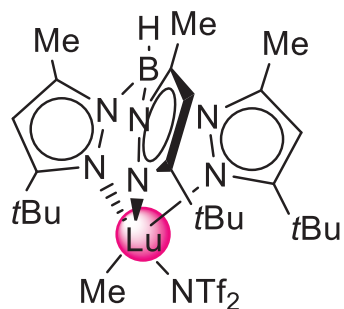
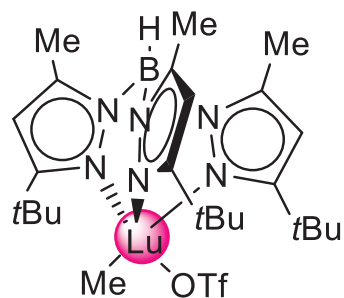
Sep. 2002 – May 2011 Ehrenbürg Gymnasium Forchheim
Allgemeine Hochschulreife

Sep. 1998 – Jul. 2002 Anna-Grundschule Forchheim

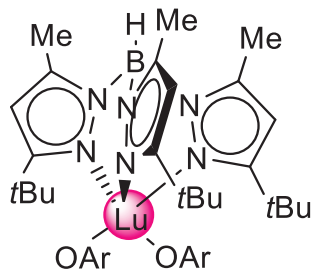
Structurally characterized complexes

On the following pages all X-ray structurally characterized compounds are listed as *ChemDraw* sketches.

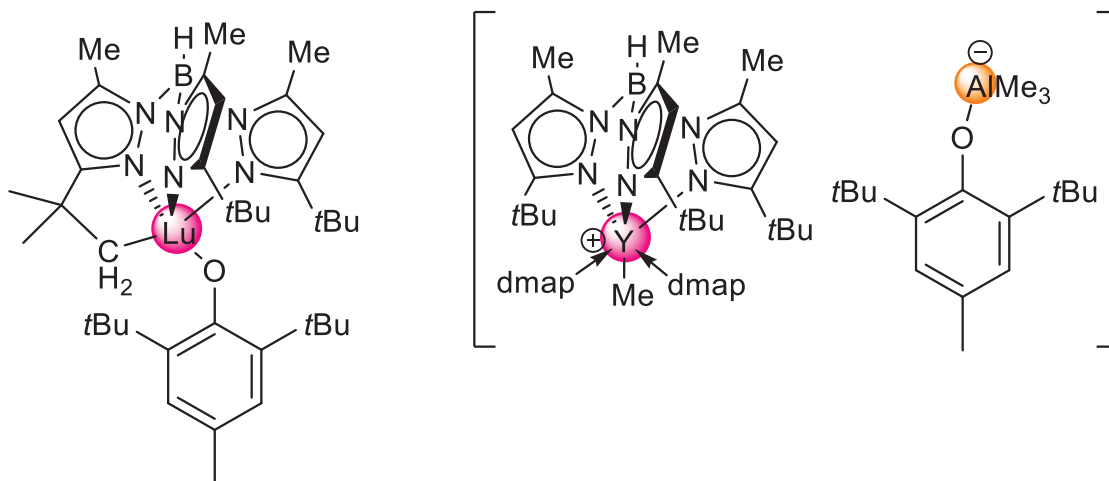
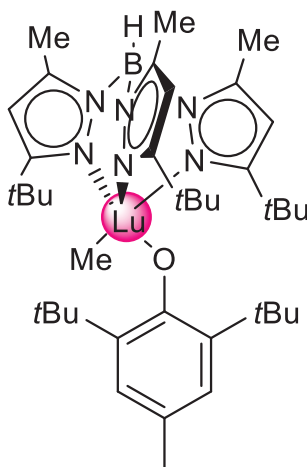
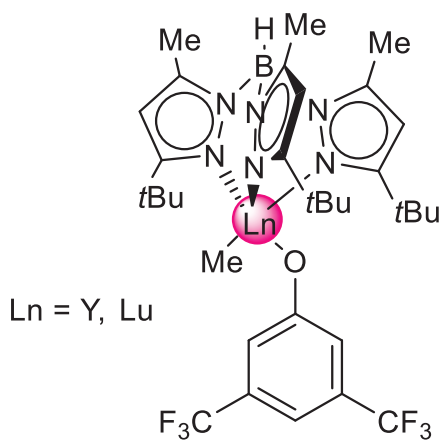
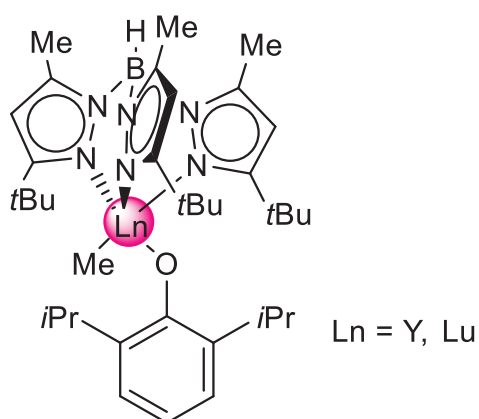
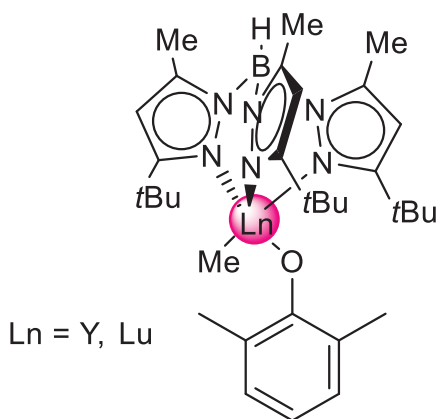
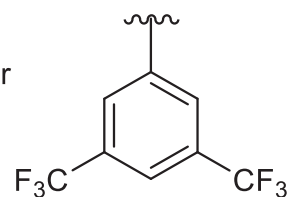
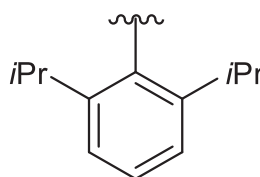
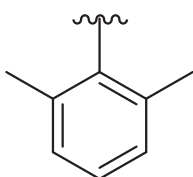
$\text{Tp}^{\text{tBu,Me}}$ -supported rare-earth-metal complexes



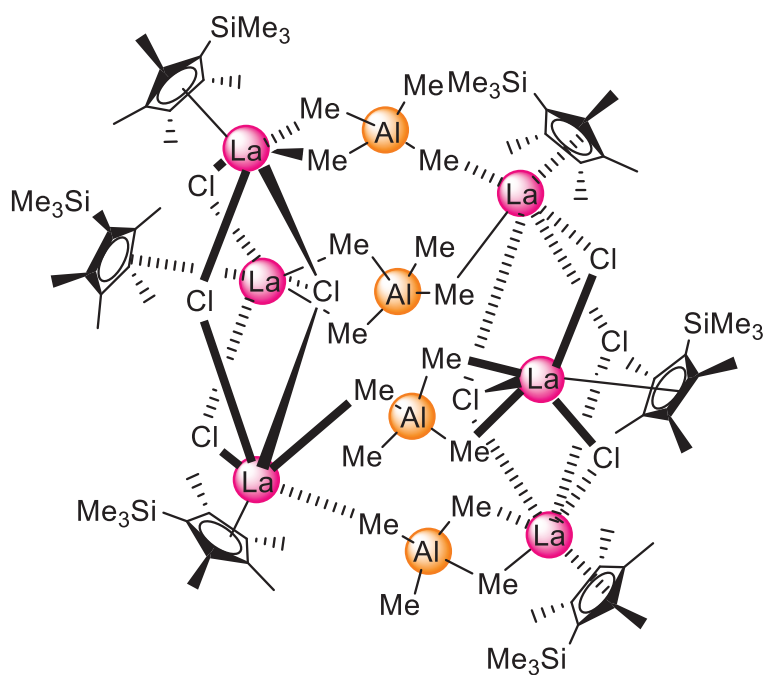
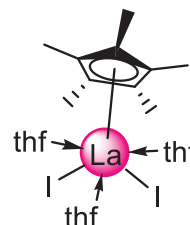
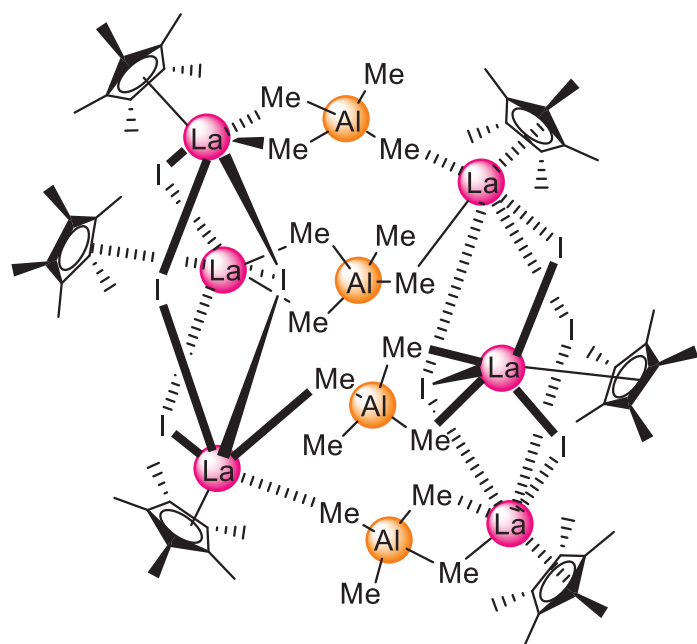
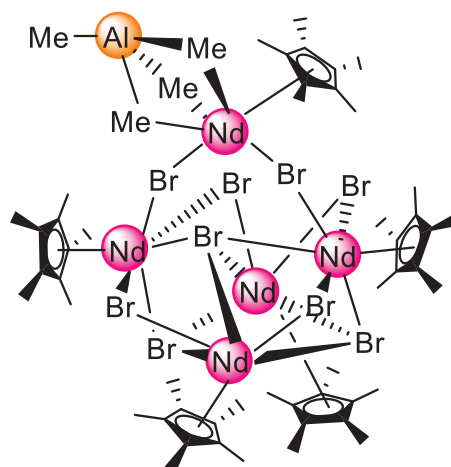
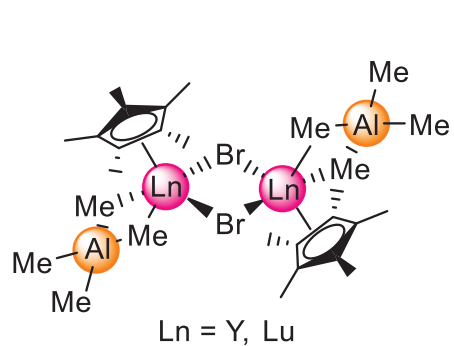
Tp^{tBu,Me}-supported rare-earth-metal complexes



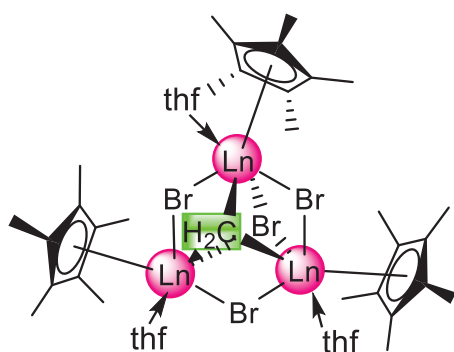
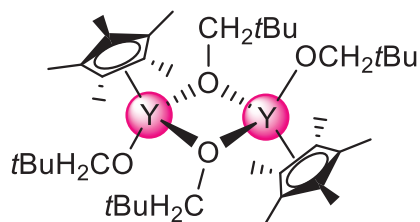
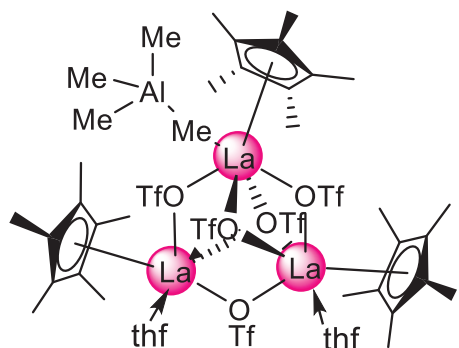
Ar:



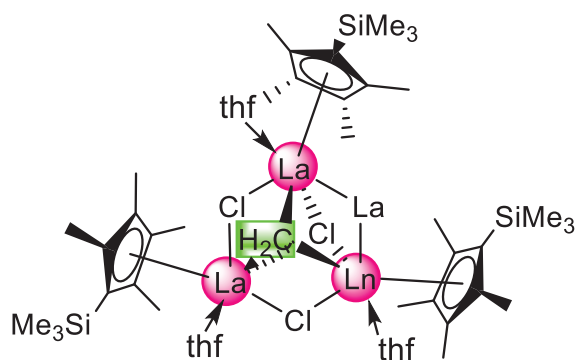
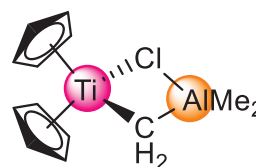
Cyclopentadienyl-ligand supported rare-earth-metal complexes



Cyclopentadienyl-ligand supported rare-earth-metal complexes and TEBBE reagent



Ln = Y, La



Silylamido-supported rare-earth-metal complexes (unpublished)

